

Diss. ETH No. 8283

**STABLE ISOTOPE INVESTIGATIONS OF FLUID - ROCK
INTERACTION DURING METAMORPHISM AND EXHUMATION
OF ECLOGITE-FACIES ROCKS: CASE STUDIES FROM THE
SWISS AND ITALIAN ALPS**

A dissertation submitted to the
SWISS FEDERAL INSTITUTE OF TECHNOLOGY ZURICH

for the degree of
Doctor of Natural Sciences

presented by
Gretchen Lieuana Früh-Green
Dipl. Petrogr. Univ. Zürich

born June 5, 1956

citizen of Mogelsberg SG and
California, USA

accepted on the recommendation of

Prof. A.B. Thompson, examiner
Dr. C.M. Graham, co-examiner
Prof. S.M. Schmid, co-examiner

1987

TABLE OF CONTENTS

Summary

Zusammenfassung

Acknowledgements

CHAPTER 1: GENERAL INTRODUCTION

1.1.	Purpose and Scope of the Work	1
1.2.	Stable Isotope Geochemistry	3
1.2.1.	General Theory and Terminology	3
1.2.2.	Oxygen Isotope Equilibration During Metamorphism	6
1.2.2.1.	Large-scale Equilibrium: Pervasive Isotopic Exchange	7
1.2.2.2.	Local Equilibrium	7
1.2.3.	Mechanisms of Isotopic Exchange	9
1.2.4.	Controls on Oxygen Isotopic Compositions	11
1.2.5.	Models of Fluid-Rock Interaction Using Oxygen Isotope Data	13
1.2.5.1.	Mass-Balance Calculations of Isotopic Exchange	13
1.3.	Constraints on Fluid Flow	15

CHAPTER 2: ADULA-CIMA LUNGA NAPPE

2.1.	Geological Setting	17
2.2.	Cima di Gagnone: General Geology and Lithologic Units	17
2.2.1.	Cima di Gagnone: Metamorphic Evolution	22
2.2.1.1.	Eclogite-facies Metamorphism	22
2.2.1.2.	Amphibolite-facies Overprinting	22
2.3.	Outcrop Relations and Petrography: Outcrop CH 271	23
2.3.1.	Mineralogy and Petrography of Mafic Rocks	23
2.3.1.1.	Deformation/Recrystallization Relations and Mechanisms in the Mafic Rocks	25
2.3.1.2.	Summary of Observations and Interpretations of the Mafic Rocks	28
2.3.2.	Mineralogy and Petrography of Pelitic Rocks	29
2.3.2.1.	Kyanite-free Schists: Equilibrium Textures (Cl 12, CL 13, CL 9)	29
2.3.2.2.	Kyanite-free Schists: Disequilibrium Textures (Cl 4a)	31
2.3.2.3.	Kyanite-bearing Schists: Equilibrium Textures (CH 40, CH 99)	31

2.3.2.4.	Kyanite-bearing Schists: Disequilibrium Textures (CH 278, CL 11a)	31
2.3.2.5.	Summary of Key Observations on the Pelitic Rocks	32
2.3.	Veins	32
2.4.	Mineral Chemistry and Cation-Exchange Geothermometry	33
2.4.1.	Garnets	33
2.4.2.	Biotites	36
2.4.3.	Garnet-biotite Mg-Fe Exchange Thermometry	39
2.4.4.	Summary	41

CHAPTER 3: STABLE ISOTOPE DATA AND MODELS OF FLUID-ROCK INTERACTION

3.0.	Sample Preparation and Analytical Methods	43
3.1.	Oxygen Isotope Data	43
3.1.1.	Metabasites	43
3.1.2.	Metapelites	44
3.1.3.	Discussion	44
3.2.	Hydrogen Isotope Data	50
3.3.	Eclogite-facies Fluid-Rock Interaction Event (A1-->E)	51
3.3.1.	A Model of Rayleigh Distillation and Dehydration of Amphibolite	51
3.3.1.1.	Computation Method for Rayleigh Distillation	54
3.3.2.	Results of Rayleigh Distillation Computations in Metabasites	56
3.3.2.1.	Initial Parameters	56
3.3.2.2.	Fluid-Rock Ratios	56
3.3.2.3.	Modal Changes and Isotopic Effects of Dehydration and Rayleigh Distillation in Metabasites	57
3.3.2.4.	Summary	59
3.3.2.5.	Discussion	59
3.3.3.	A Model of Eclogite-Facies Fluid Infiltration in Metapelites	61
3.3.3.1.	Initial Parameters	62
3.3.3.2.	Upper Limit: Maximum Amount of P2-->P1 which can be Shifted	62
3.3.3.3.	Lower Limit: Minimum Amount of P2-->P1 which can be Shifted	63
3.3.3.4.	Summary and Discussion	64
3.4.	Amphibolite Facies Fluid-Rock Interaction Event (E-->A2)	65
3.4.1.	A Model of Rayleigh Distillation and Dehydration of Metapelites	66

3.4.1.1.	Initial Parameters	67
3.4.1.2.	Fluid-Rock Ratios	67
3.4.1.3.	Modal Changes and Isotopic Effects of Rayleigh Distillation and Dehydration of Metapelites	68
3.4.2.	A Model of Amphibolite-Facies Fluid Infiltration into Metabasites	70
3.4.2.1.	Initial Parameters	71
3.4.2.2.	Isotopic Effects of Fluid Infiltration and Hydration of Eclogites	71
3.4.2.3.	Summary	72
3.5.	Attainment of Oxygen Isotopic Equilibrium in Metamorphic Rocks	73
3.5.1.	Equilibrium-Disequilibrium Relations in the Metabasites	75
3.5.2.	Equilibrium-Disequilibrium Relations in the Metapelites	77
3.5.2.1.	Local Equilibrium	77
3.5.2.2.	Large-Scale Equilibrium	80
3.6.	Summary and Conclusions	82
3.6.1.	A Philosophical Discussion of the Production and Consumption of Hydrous Fluids in Polymetamorphic Terrains	84

CHAPTER 4: MONTE MUCRONE (SEZIA-LANZO ZONE): GENERAL GEOLOGY, PETROGRAPHY AND MICROFABRICS

4.1.	Brief Description of the Sesia-Lanzo Zone	87
4.1.1.	Tectonic Units	87
4.2.	Monte Mucrone Metagranitoids	88
4.2.1.	General Overview	89
4.2.1.1.	Nomenclature	90
4.2.2.	Previous Work: Metamorphic Evolution of the Metagranitoids at the Monte Mucrone	93
4.3.	Monte Mucrone: Unfoliated Meta-Quartz Diorite	93
4.3.1.	Mineralogy, Petrology and Mineral Chemistry	94
4.3.1.1.	Na-Pyroxene (Pseudomorphing Plagioclase)	94
4.3.1.2.	Biotite	97
4.3.1.3.	Garnet	97
4.3.1.4.	Phengitic White Mica	97
4.3.1.5.	Quartz	101
4.3.1.6.	K-feldspar	102
4.3.2.	Deformation and Retrograde Overprinting in the Meta-Quartz Diorite	102
4.3.3.	Summary and Discussion	102

4.4.	Eclogitic Mylonites in Ductile Shear Zones (samples Mu1-1, 1-2. 4-2. 17b, R185, R17/3)	103
4.4.1.	Eclogitic Mylonites: Petrology, Mineral Chemistry and Microfabrics	105
4.4.1.1.	Na-pyroxene	107
4.4.1.1.1.	Pyroxene Chemistry	109
4.4.1.1.2.	Textural Evolution of Na-pyroxene	111
4.4.1.2.	Garnet	115
4.4.1.2.1.	Garnet Chemistry	117
4.4.1.2.2.	Chemical and Textural Evolution of Garnet	119
4.4.1.3.	White Mica	119
4.4.1.3.1.	White Mica Chemistry	121
4.4.1.3.2.	Textural Evolution of the White Mica	121
4.4.1.4.	Quartz	122
4.4.1.4.1.	Quartz Microfabrics	124
4.4.2.	Summary and Discussion	125
4.4.2.1.	Jadeite-Garnet Mylonites	125
4.4.2.2.	Overprinted Mylonites	126
4.5.	Veins Associated with Ductile Shear Zones	127
4.5.1.	Vein Petrology, Mineral Chemistry and Microfabrics	128
4.5.1.1.	Zoisite	128
4.5.1.2.	Garnet	129
4.5.1.3.	Quartz	129
4.5.1.4.	Na-pyroxene	129
4.5.2.	Wallrock Petrology, Mineral Chemistry and Microfabric	132
4.5.2.1.	Jadeite-Garnet Fels	132
4.5.2.1.1.	Garnet Chemistry	132
4.5.2.1.2.	Pyroxene Chemistry	133
4.5.2.1.3.	Mica Chemistry	133
4.5.2.1.4.	Discussion	133
4.5.2.2.	Overprinted Jadeite-Garnet Fels	134
4.5.3.	Summary and Discussion	134
4.6.	Completely Recrystallized Omphacite-Garnet Orthogneiss	135
4.6.1.	Mineralogy, Petrology and Phase chemistry (Samples R 82/1, R 191)	135
4.6.2.	Crystallization and Reaction History	136
4.7.	Greenschist-Facies Deformation and Recrystallization	139

**CHAPTER 5: MONTE MUCRONE METAGRANITOIDS:
ECLOGITE-FACIES GEOCHEMICAL AND
REACTION HISTORY**

5.1.	Possible Reactions in the Mte. Mucrone Metagranitoids	144
5.1.1.	Possible Reactions in the Unfoliated Meta-Quartz Diorites	145
5.1.2.	Possible Reactions in the Mylonites	148
5.1.2.1.	Jadeite-Garnet Mylonites	148
5.1.2.2.	Overprinted Mylonites	150
5.1.3.	Possible Reactions in the Omphacite-Garnet Orthogneisses	151
5.2.	Bulk Rock and Stable Isotope Geochemistry of the Mte. Mucrone Metagranitoids	154
5.2.1.	Bulk Rock and Stable Isotope Geochemistry of the Unfoliated Meta-Quartz Diorites	154
5.2.2.	Bulk Rock and Stable Isotope Geochemistry of the Jadeite-Garnet Mylonites	154
5.2.3.	Bulk Rock and Stable Isotope Geochemistry of the Overprinted Mylonites	161
5.2.4.	Bulk Rock and Stable Isotope Geochemistry of the Omphacite-Garnet Orthogneisses	163
5.3.	Pressure-Temperature Considerations for the Eclogite-Facies Metamorphism of Mte. Mucrone Metagranitoids	166
5.3.1.	Pressure Estimates	166
5.3.2.	Cation-Exchange Geothermometry	166
5.3.3.	Oxygen Isotope Fractionation Geothermometry	167
5.4.	Mechanisms of Oxygen Isotope Exchange	170
5.4.1.	A Discussion	170
5.4.2.	Oxygen Isotope Exchange Mechanisms in the Formation of the Mte. Mucrone Metagranitoids	172
5.5.	Discussion: The Role of Hydrous Fluids in the Mineralogical and Deformational History of the Mte. Mucrone Metagranitoids	175
5.5.1.	Stable Isotope Constraints	175
5.5.2.	Meta- Quartz Diorite Formation	176
5.5.3.	Fluid Infiltration and Mylonite Formation	177
5.5.3.1.	Jadeite-Garnet Mylonites	177
5.5.3.2.	Overprinted Mylonites	177
5.5.4.	Fluid Infiltration and Vein Formation	178
5.5.5.	Fluid Infiltration and Omphacite-Garnet Orthogneiss Formation	180

5.5.6.	A Model of Fluid-Rock Interaction During The Eclogite-Facies Evolution of the Mte. Mucrone Ductile Shear Zones	181
5.6.	Source and Amount of External Fluid	184
5.7.	Summary and Discussion	190
CHAPTER 6: GENERAL SUMMARY AND CONCLUSIONS		193
	References	194
	Appendix	
	Curriculum Vitae	

SUMMARY

Although stable isotope geochemistry has mainly been used in the past to estimate metamorphic temperatures, it is widely becoming a useful tool to determine the nature and extent of fluid-rock interaction during metamorphism. In this study, stable isotope geochemical methods have been applied to determine the scales and mechanisms of fluid interaction and motion during metamorphism and uplift of eclogite-facies rocks. In addition, the relationship between fluids and deformation, and the extent to which isotopic equilibrium is attained in high-grade metamorphic rocks is investigated. Two areas have been chosen where petrologic and chemical evidence point to fluid involvement during their evolution.

Cima di Gagnone

Chapters 2 and 3 concern the production and extent of fluid migration during eclogite-facies metamorphism and subsequent amphibolite-facies overprinting of pelitic and mafic rocks at the Cima di Gagnone area of the Cima Lunga Nappe, the southwestern extension of the Adula Nappe. The central alpine Adula-Cima Lunga Nappe is a slice of pre-Mesozoic continental basement consisting predominantly of metagranitic and metapelitic gneiss and schist. Less abundant mafic and carbonate rocks, as well as ultramafics in the southern Cima Lunga Nappe, occur as lenses and layers in the polymetamorphic metasediments. Two phases of alpine metamorphism, accompanied by varying degrees of deformation, have affected these rocks. High pressure mineral assemblages (inferred to be Early Alpine by Van de Plas, 1959) are older than nappe emplacement and are overprinted by an Oligocene Barrovian-style regional metamorphism. High-pressure mineral assemblages are mainly preserved in mafic lenses and record a continuous increase in P-T conditions from 12-15 Kb / 500-600 °C in the north of the Adula nappe to more than 20Kb / 800 °C in the south (Heinrich, 1983). A distinct decrease in pressure characterizes the Tertiary Barrovian-style metamorphism which varies from greenschist facies in the north to upper amphibolite-facies (sillimanite grade) in the south.

The *Early Alpine eclogite-facies* metamorphism is characterized by *dehydration of amphibolite* (A1-->E), which produced nearly anhydrous kyanite-eclogite containing $\text{Omp} + \text{Gar} + \text{Qtz} + \text{Kyn} + \text{Hbl} + \text{Zoi} \pm \text{Ilm} \pm \text{Rut}$ (Heinrich, 1986, see Table 1.1. for abbreviations). Simultaneous *hydration* reactions in neighbouring *pelitic* rocks may have acted as sinks for the hydrous fluid produced by the dehydrating amphibolites. The subsequent *Tertiary, amphibolite-facies* metamorphic event is marked by

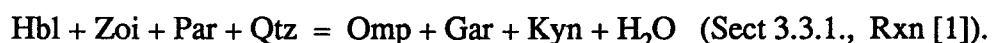
re-hydration of the kyanite-eclogites (E-->A2). Fluid infiltration-fronts are indicated by a systematic mineralogical transition from eclogite in the cores of competent lenses to symplectite (Plg ± Bio ± Hbl) to fine-grained amphibolite, forming rims along contacts to pelitic country rocks. Simultaneous deformation and grain coarsening resulted in the formation of amphibolite tails parallel to the schistosity in the neighbouring metapelites. Based on relict corona textures, Heinrich (1982, 1983) has suggested that the hydrous fluid was produced by dehydration reactions in the metapelites (now containing Qtz + Plg + Bio + Gar ± Mus ± Kyn ± Sta ± Ksp).

Detailed sampling for isotopic analyses has been made at outcrop CH271, which has been described by Heinrich (1979, 1982, 1983). Sample locations are shown in detail in Fig 2.3., isotopic compositions are given in Table 3.1. and are shown graphically in Figs. 3.1 and 3.3. The metapelites form two isotopically distinct groups. Those in the immediate vicinity of the mafic lens represent an isotopically "light" group, classified as P₁-pelites, in which $\delta^{18}\text{O}_{\text{WR}}$ varies between 6.0 ‰ and 7.0 ‰. $\delta^{18}\text{O}_{\text{Qz}}$ in this group ranges from 8.6‰ to 9.4‰. In contrast, the metapelites which are located at least 30m away from the mafic rock (classified as P₂-pelite) have $\delta^{18}\text{O}_{\text{WR}}$ and $\delta^{18}\text{O}_{\text{Qz}}$ -compositions which range from 8.4 ‰ to 10 ‰ and 10.4-11.8 ‰, respectively.

$\delta^{18}\text{O}_{\text{Qz}}$ from the eclogitic core of the mafic lense, Qtz segregation veins and symplectite lie within a narrow range from 7.8‰ to 8.2‰, with a relatively constant $\delta^{18}\text{O}_{\text{WR}}$ of 5.5‰. The amphibolites form two distinct groups. The fine-grained amphibolites along the rims of the lens have compositions similar to the eclogitic core, whereas coarse-grained amphibolite layers which form the tails have consistent $\delta^{18}\text{O}_{\text{WR}}$ and $\delta^{18}\text{O}_{\text{Plg}}$ compositions of 6.5‰ and 7.9-8.4‰, respectively.

Although the isotopic compositions of the mafic rocks lie within the range of those known for basalts and some eclogites, the values for the P₁-pelitic rocks are depleted in ¹⁸O relative to known metasediments of similar metamorphic grade (see Fig 3.2.). The isotopic compositions of the P₂-pelites are similar to those of isotopically constant pre-Mesozoic rocks from the Central Alps reported by Hoernes and Friedrichson (1980), who attribute the depletion in ¹⁸O and large-scale homogenization to pervasive interaction with magmatic fluids during a pre-Alpine (Hercynian or older) metamorphic event. The possibility that these low-¹⁸O pelites were derived from igneous or meta-igneous rocks is discussed in Section 3.3.2. Assuming that prior to Alpine metamorphism, all the pelitic rocks in the Gagnone area had relatively similar chemical and isotopic compositions, the depletion in ¹⁸O in the P₁-metapelites, relative to the P₂-pelites, suggest that further fluid-rock interaction occurred during alpine metamorphism and may be related to the dehydration of amphibolite during the A₁-->E metamorphic event.

Based on a Rayleigh Distillation mechanism of fluid-rock interaction as presented by Rumble (1979, 1982), isotopic fractionation during dehydration of amphibolite (A1-->E) to form eclogite has been modelled for the simple reaction:



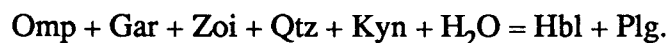
The results of the model have shown that fluid production during eclogite-facies dehydration would not be sufficient to cause the observed isotopic signatures in the surrounding P1-metapelites by a mechanism of exchange by fluid flow. Thus, the low $\delta^{18}\text{O}$ -values may represent low ^{18}O -source rocks, or may be the result of fluid-rock interaction and isotopic exchange with other fluids not locally derived from the dehydration of the amphibolites. The relative position of the ^{18}O depleted P1-pelites to the mafic lens suggests that, if fluid flow is considered as the mechanism of isotope exchange, the contact between the relatively massive mafic rocks and the foliated metapelites may have acted as a preferential pathway for fluid flow. However, due to the polymetamorphic nature of these rocks, the timing of a possible infiltration event, involving an external fluid, remains uncertain.

In contrast to a model of isotopic exchange by fluid flow, the hydrous fluid produced during the A1->E dehydration event may have remained in the system (due to low permeabilities and/or a low $P_{\text{H}_2\text{O}}$ - pressure gradient ?) as a static, grain-boundary film. In this case, the exchange mechanism may have been by oxygen diffusion between the two rock reservoirs, mafic rocks and pelites (i.e. rock-rock interaction), resulting in the $\delta^{18}\text{O}$ -compositions observed in the P1-pelites.

Re-hydration of the eclogites and complete recrystallization of the metapelites during uplift and Tertiary regional metamorphism (E-->A2) is discussed in section 3.4. A quantitative model of dehydration and Rayleigh Distillation in the metapelites is presented for the simplified reaction



(Sect. 3.4.1. Rxn [2]; see also Heinrich 1982). The predicted isotopic composition of the hydrous fluid produced by the reaction above has been used to model simultaneous fluid infiltration and hydration of the mafic lense for the simplified reaction:



The results of these models have shown that the fine-grained amphibolites which comprise the rim of the mafic lens at outcrop CH271 may represent limited fluid-rock interaction (low fluid/rock ratios, <0.1:1); whereby only enough hydrous fluid was able to permeate the rock to cause complete amphibolitisation but no isotopic shift. The isotopic shift observed in the recrystallized tails of the mafic lens requires only local interaction with fluids produced by dehydration reactions in the immediately

surrounding metapelites. Amphibolite-facies deformation may have been instrumental in increasing permeability of these otherwise impermeable mafic rocks allowing higher F/R ratios and fluid flow. The increased amount of fluid during deformation may have enhanced the growth rates of the hornblende and plagioclase aggregates in the tails of the lens, resulting in the coarse-grained amphibolites and the strong foliation now observed (see also Section 2.3.1.1).

Comparison of the variations in mineral fractionations and isotopic temperature estimated for the metapelites indicates that local equilibrium within single layers was in general not achieved in these rocks. The temperature distributions suggest that garnet, ilmenite and rutile may have retained their eclogite-facies isotopic compositions. Lower isotopic temperatures are indicated for the amphibolite-facies metamorphism (350 - 500°C) than those estimated by cation-exchange geothermometry (460-670°C). Samples of comparable grain sizes and mineral modes exhibit variabilities which cannot be explained purely by diffusion and redistribution of oxygen upon cooling. The data may indicate the presence of differing, small amounts of an intergranular hydrous fluid, resulting in local (on a mm-scale) oxygen isotope redistribution between those minerals which are more easily reset to lower temperatures (e.g. plagioclase and mica). There is no correlation between the degree of isotopic equilibrium and the degree of recrystallization and/or deformation observed in these rocks.

Mte. Mucrone

Chapters 4 and 5 deal with the role of fluids in processes of metamorphism and ductile deformation during the eclogite-facies evolution of metagranitoids from the Monte Mucrone in the Sesia Zone. Previous geological and petrological work has suggested that prior to deformation, restricted chemical communication resulted in local equilibrium domains and then gradually, in the later stages of deformation, large-scale equilibrium was approached. Fluids may have been important in the development of the orthogneiss as well as acting as a catalyst in the approach towards chemical equilibrium. Detailed mineralogical, textural and stable isotope studies have been made on ductile shear zones in the relatively undeformed rocks at the east face of the Mte. Mucrone in order to determine the role of fluids in deformation and recrystallization during the eclogite-facies metamorphism of these rocks.

The petrological, geochemical and microstructural data presented in this study indicate large variations in the degree of eclogite-facies recrystallization and deformation recorded in the Mte. Mucrone metagranitoids. At least two *main phases of eclogite-facies recrystallization* are evident in these rocks and can be directly related to

the *timing and degree of deformation*. An *initial pre-kinematic Jadeite Phase* resulted in the formation of fine-grained aggregates of jadeite + quartz + zoisite as pseudomorphs after the primary igneous plagioclase. Plagioclase breakdown reactions may have accompanied or have been subsequent to biotite breakdown reactions which produced garnet and phengitic white-mica. The progress of biotite breakdown may have been limited by the supply of alumina and calcium from plagioclase domains, as is indicated by chemically distinct corona textures of garnet and phengitic white-mica around biotite in the meta-quartz diorites. Incomplete reaction, resulting in the corona textures, may have been due to slow diffusion rates and/or a paucity of intergranular fluid during the initial stages of eclogite-facies metamorphism.

An *initial high strain deformation event* resulted in superplastically-deformed pyroxene layers, grain coarsening and partial chemical homogenization. Enlargement of equilibrium domains may have resulted in the completion of the biotite reaction and produced the assemblage jadeite + garnet + phengite + quartz, characteristic of the mylonitic rocks. Bulk rock geochemical and stable isotope data indicate that infiltration of an external hydrous fluid phase is associated with deformation and recrystallization in the jadeite-garnet mylonites. Local changes in the activities of sodium, potassium and H₂O could have produced the assemblages observed in the deformed rocks.

The *duration and timing* of fluid infiltration relative to *high strain deformation* appears to have been crucial to the mineralogical evolution of the Mte. Mucrone granitoids, resulting in the chemical and microstructural differences recorded in these rocks. A model has been presented for the formation of the ductile shear zones at the Mte. Mucrone. It has been suggested that subsequent to the formation of fine-grained aggregates of Jad + Zoi + Qtz, as pseudomorphs after igneous plagioclase, an initial stage of fluid infiltration occurred along fractures or faults, catalysing diffusive mass transfer and grain growth rates and resulting in the formation of coarser-grained, 1-5 cm wide, reaction zones. Fluid-induced reaction and grain coarsening may have acted as a hardening mechanism and resulted in the concentration of subsequent high strain deformation, and the formation of the mylonites, along these zones.

The jadeite-garnet mylonites, characterized by nearly homogeneous phase compositions and coarser grain-sizes of jadeite, garnet and phengite (relative to the unfoliated meta-quartz diorites), may represent syn-deformational recrystallization and limited fluid infiltration. Preserved chemical zoning in garnet, heterogeneous mica compositions, and inclusion-rich pyroxene grains in some mylonite samples (i.e. in overprinted mylonites) indicate local anhydrous deformation; whereby localized post-kinematic infiltration along these deformation zones resulted in new growth of omphacitic pyroxene and a second generation of more grossular-rich garnet. Limited permeabilities in some of

these mylonite zones may have resulted in an excess of fluid pressure during post-kinematic infiltration and led to fracturing into the less deformed wallrocks and the formation of the zoisite-garnet veins.

Complete recrystallization and formation of omphacite-garnet orthogneiss may have resulted from progressive syn-kinematic infiltration and longer deformation periods. The presence of omphacite and paragonite, characteristic of the orthogneiss, may be due to original variations in bulk rock chemistries and/or may be related to a decrease in Na-, K- and H₂O-activities during deformation and fluid infiltration.

The microfabrics of the deformed rocks, combined with stable isotope and bulk rock geochemical data suggests that fluid infiltration may not have been continuous but rather occurred in pulses and was channelized along zones of increased permeabilities due to high strain deformation. High-strain deformation continued during exhumation and may have been accompanied by further pulses of fluid activity.

Rudimentary, isotopic mass-balance modelling of the infiltration event suggests that the hydrous fluid was ¹⁶O-rich and may have been *produced locally* by dehydration reactions in the neighbouring metapelitic and metabasic rocks. However, comparison with the isotopic study of Desmons and O'Neil (1978) indicates a lack of large-scale isotopic exchange between the granitic rocks and the neighbouring eclogitic mica schist complex. Minimum fluid to rock ratios, based on depletions in ¹⁸O in the deformed rocks, have been estimated to range from approximately 1.0 to 0.75 for equilibration with fluids with isotopic compositions of 6.0 to 6.5‰ and at a temperature of 500 °C. Stable isotope profiles perpendicular to the ductile shear zones indicate a decrease in W/R-ratios to values of less than 0.1 at distances of approximately 30 cm from the centers of these zones.

The evidence for metasomatic alteration, associated with deformation and formation of the mylonites and Omp-Gar orthogneisses, suggests that isotopic exchange occurred through a surface-controlled mechanism of chemical transformation and was driven by disequilibrium relationships between metagranitoid and the infiltrating fluid. Discordant calculated isotopic temperatures, as well as apparent discrepancies between a predicted order of recorded temperature and that determined may reflect the presence of intergranular, static fluid, resulting in diffusive oxygen exchange between quartz, phengite and Na- pyroxene upon cooling.

The results of this study suggest that under eclogite-facies metamorphic conditions, diffusion and growth rates may be extremely slow in nearly anhydrous rocks, and may directly hinder complete reaction and recrystallization. Both deformation and an external fluid appear to be determining factors in the metamorphic evolution of the Mte. Mucrone granitic body. However, an access of limited amounts of hydrous fluid appears to have

been determinant to the attainment of chemical homogenization of garnet and pyroxene.

The rheological properties of the primary quartz diorite may have been such that the rock was highly resistant to deformation during the early stages of metamorphism and became more deformable after the formation of the fine-grained plagioclase pseudomorphs (reaction enhanced ductility). At the onset of eclogite-facies metamorphism, a paucity of grain boundary fluid, and as a result slow intercrystalline diffusion, caused local chemical and textural domains and an overall state of disequilibrium. High strain deformation may have enhanced intra- and intercrystalline diffusion rates and may have increased permeabilities such as to allow infiltration of an external hydrous fluid into the previously dry system.

ZUSAMMENFASSUNG

Diese Studie untersucht mit Hilfe stabiler Isotopen den Umfang und die Mechanismen der Gesteins-Fluid Wechselwirkungen während eclogitfazieller und folgender retrograder Metamorphosen. Zusätzlich wurde die Wechselwirkung zwischen Fluiden und Deformation untersucht und der Umfang, in welchen Isotopengleichgewicht in hochgradigmetamorphen Gesteinen erreicht wurden. Dazu wurden zwei Gebiete ausgewählt, in denen petrologische und chemische Daten auf einen Einfluss von Fluiden während der metamorphen Entwicklung hindeuten.

In den Kapiteln 2 und 3 wird der Einfluss von Fluiden während der eclogitfaziellen und darauffolgenden amphibolitfaziellen Metamorphose in pelitischen und mafischen Gesteine der Cima-Lunga Decke diskutiert. Die Frühalpine eclogitfazielle Metamorphose ist durch Entwässerung von Amphibolit charakterisiert (A1->E), wodurch die nahezu H₂O-freie Paragenese Omp + Gar + Qtz + Dis + Hbl + Zoi ± Ilm ± Rut produziert wird. Gleichzeitig ablaufende Hydratationsreaktionen in benachbarten pelitischen Gesteinen können die bei der Dehydratation der Amphibolite freigewordenen H₂O-reichen Fluide aufgenommen haben. Die darauf folgende tertiäre amphibolitfazielle Metamorphose ist gekennzeichnet durch die Rehydratation der Disthen-Eclogite (E->A2). Die Front der Fluidbewegung ist markiert durch die randliche Umwandlung der Eclogitlinsen in Symplektit (Dio + Plg ± Hbl), gefolgt von feinkörnigem Amphibolit (Plg + Hbl ± Gra ± Qtz), der seinerseits an den Enden der Linsen in grobkörnigen Amphibolit (Plg + Hbl ± Bio ± Tit) übergeht. Aufgrund von reliktschen Corona-Strukturen kann gezeigt werden, dass die wässrigen Fluide durch Dehydrationsreaktionen der Pelite erzeugt sind.

Die Isotopenanalysen der Metapelite fallen in zwei Kategorien: Die in der unmittelbaren Umgebung der mafischen Linsen (P1-Pelite) sind $\delta^{16}\text{O}$ -reich, wobei das $\delta^{18}\text{O}_{\text{WR}}$ (Gesamtgestein) zwischen 6.0 und 7.6‰ variiert und das Quarz- $\delta^{18}\text{O}$ zwischen 8.6 und 9.4‰. Im Gegensatz dazu haben die Metapelite ca. 30m entfernt von den mafischen Linsen (P2-Pelite) Gesamtgesteins- $\delta^{18}\text{O}$ -werte zwischen 8.4 and 10.0‰; $\delta^{18}\text{O}_{\text{Qz}}$ liegt zwischen 10.4 und 11.8‰. Die $\delta^{18}\text{O}_{\text{Qz}}$ -werte der eclogitischen Kerne, sowie der Quarzadern und der Symplektite liegen zwischen 7.8 und 8.2‰, mit konstantem $\delta^{18}\text{O}_{\text{WR}}$ von 5.5‰. Die Amphibolite zerfallen ebenfalls in zwei Gruppen: Die feinkörnigen Ränder der Linsen haben $\delta^{18}\text{O}_{\text{WR}}$ -Werte ähnlich den eclogitischen Kernen, während die grobkörnigen Enden jeweils $\delta^{18}\text{O}_{\text{WR}}$ -Werte von 6.5‰ zeigen.

Modellrechnungen zeigen, dass die Isotopenverhältnisse der P1-Pelite nicht durch lokalen Fluid-Austausch während A1->E erklärt werden können, sondern dass das System für externen Fluide austausch offen gewesen sein muss. Ein quantitatives Dehydratationsmodell und Rayleigh-Fraktionierung in den Metapeliten wird vorgestellt für

die vereinfachte Reaktion



Die vorausgesagte Isotopenzusammensetzung der durch diese Reaktion erzeugten Fluide wird verwendet für die Modellierung gleichzeitiger Fluidinfiltration und Hydratation der mafischen Linsen.

Die Ergebnisse dieser Modelle zeigen, dass die feinkörnigen Amphibolitränder der Eclogitlinsen eine begrenzte Wechselwirkung zwischen Fluid und Gestein darstellen (bei niedrigem Fluid/Gesteinsverhältnis = < 0.1). Die beobachtete Veränderung im Isotopenverhältnis in den rekristallisierten Enden der mafischen Linsen erfordert lediglich eine lokale Wechselwirkung mit Fluiden, die durch Dehydratation in den unmittelbar angrenzenden Metapeliten erzeugt werden. Der Vergleich der Isotopenfraktionierung zwischen Mineralpaaren mit den Isotopentemperaturabschätzungen in Metapeliten zeigt, dass lokales Gleichgewicht in einzelnen Lagen im allgemeinen nicht erreicht wird. Die Temperaturverteilung deutet darauf hin, dass Granat, Ilmenit und Rutil ihre eclogitfaziellen Isotopenzusammensetzungen beibehalten können.

Für die amphibolitfazielle Metamorphose werden niedrigere Isotopentemperaturen angezeigt (350 - 500 °C) als die mit Kationaustauschgeothermometrie erhaltenen (460 - 670 °C). Diese Diskrepanzen deuten auf die Anwesenheit lokal verschiedener, geringer Mengen intergranularer Fluide hin, was eine lokale (im mm-Bereich) Sauerstoffisotopenunverteilung zwischen solchen Mineralen erzeugt, bei denen sich leicht eine Verschiebung zu niedrigeren Temperaturisotopenverhältnissen einstellt (z.B. Biotit und Plagioklas). Es existiert keine Korrelation zwischen dem Mass der Isotopen-equilibrierung und dem Mass der Rekristallisation und/oder Deformation in diesen Gesteinen.

Gegenstand der Kapitel 4 und 5 ist die Rolle der Fluide in Metagranitoiden des Monte Mucrone (Sesia Zone) während der Metamorphose und der duktilen Deformation bei der Entwicklung der Eklogitfazies. Frühere geologische und petrologische Untersuchungen ließen vermuten, daß vor der Deformation in begrenzten Gleichgewichtsdomänen beschränkter chemischer Ausgleich erfolgte. In einer späteren Phase der Deformation wurde dann graduell eine Annäherung zu einem umfassenden Gleichgewicht erreicht, wobei Fluide vermutlich als Katalysator wirkten.

Um die Wichtigkeit der Fluide bei der Deformation und der Rekristallisation während der eklogitfaziellen Metamorphose zu ermitteln, wurden an der Ostseite des Monte Mucrone an duktilen Scherzonen innerhalb relativ undeformierter Gesteine Proben entnommen, an welchen detaillierte mineralogische, texturale und isotopengeologische (stabile Isotopen) Untersuchungen durchgeführt wurden.

Die in dieser Arbeit dargestellten petrologischen, geochemischen und mikrostrukturellen Daten des Metagranitoides des Monte Mucrone spiegeln eine große

Variationsbreite des Rekristallisationsgrades und der Deformation unter eklogitfaziellen Bedingungen wider. Dabei korrelieren mindestens 2 Phasen einer eklogitfaziellen Rekristallisation zeitlich und intensitätsmäßig mit der Deformation. Während einer initialen präkinematischen Jadeit-Phase bildete sich ein feinkörniges Aggregat bestehend aus Jadeit + Quarz + Zoisit pseudomorph nach primärem magmatischen Plagioklas. Diese Zersetzungsreaktion wurde begleitet/oder gefolgt von einem fortschreitenden Zerfall des Biotites zugunsten der Bildung von Granat und phengitischem Hellglimmer. Corona-Texturen, bestehend aus Granat und phengitischem Hellglimmer, welche den Biotit in den Metagranitoiden umgeben, deuten darauf hin, daß die Biotitzersetzungsreaktion möglicherweise auf die Zufuhr von Al und Ca aus Plagioklasdomänen beschränkt war. Die Corona-Texturen sind Hinweise für unvollständig abgelaufene Reaktionen, welche Folge einer zu langsamen Diffusionsrate und/oder einer zu geringen Menge von intergranularem Fluid zu Beginn dieser Metamorphose sein könnten.

Ein erstes Deformationsereignis mit großen Verformungsbeträgen ("high strain") hatte superplastisch verformte Pyroxenlagen, Kornvergrößerung und partielle chemische Homogenisierung zur Folge. Eine Vergrößerung der Gleichgewichtsdomänen ließ die Biotitreaktion unter Bildung der für die Mylonite charakteristischen Mineralparagenese Jadeit + Granat + Phengit + Quarz vollständig ablaufen.

Geochemische Gesamtgesteinsanalysen und Werte stabiler Isotope zeigen, daß in den Jadeit-Granat-Myloniten mit der Deformation und der Rekristallisation eine Zufuhr einer wässrigen fluiden Lösung verbunden ist. Lokale Änderungen der Aktivitäten von Na, K und H₂O kann zu den beobachteten Paragenesen in den deformierten Gesteinen geführt haben.

Dauer und Zeitpunkt des Eindringens der Fluide in bezug zur "High-Strain" Deformation scheint für die mineralogische Entwicklung der Granitoide des Monte Mucrone von entscheidender Bedeutung zu sein und äußert sich in chemischen und mikrostrukturellen Unterschieden in diesen Gesteinen. Es wird ein Modell für die Bildung der duktilen Scherzonen des Monte Mucrone vorgestellt. Dabei wird angenommen, daß unmittelbar nach der Bildung des feinkörnigen Aggregates von Jad + Zoi + Qtz - als Pseudomorphose nach magmatischem Plagioklas - entlang von Rissen und Spalten erste Fluide zugeführt wurden. Diese Fluidzufuhr hatte eine katalysierende Wirkung auf den diffusiven Massentransport und die Kornwachstumsraten, welche die Bildung von gröberkörnigen, 1-5 cm breiten Reaktionssäumen zur Folge hatte. Fluid-induzierte Reaktionen und Kornvergrößerung wirkten wahrscheinlich als Verhärtungsmechanismus und bewirkten entlang dieser Zonen eine Konzentration subsequenter "High-Strain" Deformation und die Bildung von Myloniten.

Die Jadeit-Granat-Mylonite, charakterisiert durch fast homogene Phasenzusammensetzung und gröbere Korngröße von Jadeit, Granat und Phengit (bezogen auf die

ungeschieferten Metaquarzdiorite), deuten auf synkinematische Rekristallisation und beschränkte Fluidzufuhr hin. Erhaltene chemische Zonierungen in Granat, heterogene Glimmerzusammensetzung und einschlußreiche Pyroxenkristalle in manchen Mylonitproben (d.h. in überprägten Myloniten) zeigen lokal eine Deformation ohne Wasserzufuhr. Lokale postkinematische Infiltration entlang dieser Scherzonen führte hingegen zur Neubildung von omphacitischem Pyroxen und einer 2. Generation von grossularreicherem Granat. Begrenzte Permeabilität könnte nach der Bildung dieser Mylonitzonen einen Überschuß an Fluid-P während dieser postkinematischen Infiltrationsphase bewirkt haben und zu kleineren Brüchen in den weniger deformierten umgebenden Gesteinen und zur Bildung von Zoi-Ga-Adern geführt haben.

Vollkommene Rekristallisation und Bildung von Omphacit-Granat-Orthogneissen können das Ergebnis einer progressiven synkinematischen Infiltration und längerer Deformationsperioden sein. Die Anwesenheit von Omphacit und Paragonit - charakteristisch in diesen Orthogneissen - läßt sich durch ursprüngliche Schwankungen des Gesamtgesteinschemismus und/oder durch eine Abnahme der Na-, K- und H₂O-Aktivitäten während der Deformation und der Fluidzufuhr erklären.

Die Mikrostrukturen der deformierten Gesteine, Werte stabiler Isotopen und geochemische Gesamtgesteinsanalysen lassen vermuten, daß die Fluidzufuhr nicht kontinuierlich war, sondern daß sie pulsierend erfolgte und entlang von Zonen mit wachsender Permeabilität infolge von "High-Strain" Deformation kanalisiert wurde. Die "High-Strain" Verformung dauerte während der Hebung des Gebirges an und wurde wahrscheinlich von weiteren Stößen fluidier Aktivität begleitet.

Rudimentäre Isotopenmassenbilanzmodelle der Infiltration zeigen, daß das wässrige Fluid in ¹⁶O angereichert war und lokal durch Entwässerungsreaktionen in dem Nebengestein (Metapelite und Metabasite) gebildet worden sein könnte. Vergleiche aber mit Isotopenuntersuchungen von DESMONS und O'NEIL (1975) zeigen einen fehlenden großräumigen Isotopenaustausch zwischen granitischen Gesteinen und dem benachbarten Eklogit-Glimmerschieferkomplex. Beruhend auf ¹⁸O-Abreicherung in den deformierten Gesteinen wurde die Variation der minimalen "fluid to rock ratio" (W/R) auf 1.0-0.75 geschätzt für die Equilibrierung der Fluide mit einer Isotopenzusammensetzung von 6.0-6.5 ‰ und bei Temperaturen von 500°C. Daten stabiler Isotopen, gemessen an Proben, welche senkrecht zu der duktilen Scherzone entnommen wurden, zeigen eine Abnahme des W/R-Verhältnisses zu Werten <0.1 bei einer Distanz von ca. 30 cm von der Mitte der Scherzone.

Der Beweis für metasomatische Veränderung, Deformation und Bildung von Myloniten und Omp-Gra-Orthogneissen läßt vermuten, daß der Isotopenaustausch durch chemische Veränderung - bedingt durch oberflächenkontrollierende Mechanismen - erfolgte und durch Ungleichgewichte zwischen Metagranitoiden und dem

infiltrierenden Fluid gelenkt wurde. Sowohl diskordante berechnete Isotopentemperaturen als auch scheinbare Unterschiede zwischen einer vorhergesagten Größenordnung überlieferter Temperaturen könnten die Anwesenheit von intergranularem statischen Fluid widerspiegeln, welches eventuell diffusiven O-Austausch zwischen Quarz, Phengit und Na-Pyroxen nach der Abkühlung bewirkte.

Diese Untersuchung ergibt, daß unter eklogitfaziellen metamorphen Bedingungen die Diffusions- und Wachstumsraten in wasserfreien Gesteinen sehr langsam sind und möglicherweise direkt eine vollkommene Reaktion und Rekristallisation verhindern. Sei es Deformation wie auch externe Fluide scheinen entscheidende Faktoren in der metamorphen Entwicklung des Granitkörpers des Mte. Mucrone zu sein. Jedoch scheint eine beschränkte Menge von wässriger Lösung (Fluid) entscheidend für die chemische Homogenisierung von Granat und Pyroxen zu sein.

Die rheologischen Eigenschaften des primären Quarzdiorites waren vermutlich so, daß das Gestein während der frühen Phase der Metamorphose sehr großen Widerstand gegen Deformation leistete und nach der Bildung der feinkörnigen Plagioklas-Pseudomorphosen besser deformierbar wurde (die Reaktion förderte die Duktilität). Am Beginn der eklogitfaziellen Metamorphose verursachte geringes Angebot an Korngrenzfluid - und als dessen Ergebnis langsame interkristalline Diffusion - die Bildung von lokal begrenzten chemischen und textuellen Domänen und ein generelles Ungleichgewicht. "High-Strain" Deformation hat möglicherweise intra- und interkristalline Diffusionsraten erhöht und die Permeabilität gesteigert, so daß ein Eindringen von externen wässrigen Fluiden in das ursprünglich trockene System möglich wurde.

ACKNOWLEDGEMENTS

At many stages during the course of this thesis work I felt as if I were immersed in an exercise of self-punishment. Often I had to ask myself - why are you doing this? The answer must lie in an inexplicable drive and thirst for knowledge. The opportunity to learn and to push myself one step further has motivated me the most during these seemingly endless years of my university life. My teachers have been innumerable; they range from the highest "popes" in the various fields of the Earth Sciences to the first year diploma students, who have indirectly taught me how to teach them. I feel fortunate to have been able to study and work at the ETH in Zürich and to have had the opportunity to come into contact with so many wonderful teachers - no matter how painful it may have all been.

First of all, I would sincerely like to thank my advisor, Alan Thompson, for his generous moral and financial support. Alan has continually kept me in a schizophrenic state of elation, confusion, commitment, frustration and determination throughout the last five years that I have worked with him. He pushed me when I needed pushing; he encouraged me when I needed encouraging; and maybe he even confused me to make me think. Although we differ greatly in our academic character - he, the thinker, and I, the observer, I have thoroughly enjoyed working with the "King of triangles and back-of-the-envelope calculations".

Through Alan, I have had the opportunity to get to know Colin Graham in Edinburgh, Scotland and the dismal, little town of East Kilbride, where I spent many (happy/not so happy) hours doing the stable isotope analytical work at the Scottish Universities Research and Reactor Centre (SURRC). Tony Fallack taught me the techniques of oxygen extraction from silicates and patiently guided me through the "Jungle Gym" of valves, diffusion pumps and nitrogen traps, and introduced me to the principles of mass spectrometry. Terry Donnelley quietly answered my persistent questions and kindly carried out the isotope analyses on samples that I left behind or sent to him. Colin, Toni, Terry and many others at the University of Edinburgh and the SURRC left me with the lovely Scottish lilt ringing in my ears and a special affection for Scotland and the Scottish people.

I feel fortunate to have been able to go back "home" to California for a good dose of sunshine and a visit with my family, while working with James O'Neil at the USGS in Menlo Park. I would like to acknowledge Jim's help and the work that his technicians Rob Brigham, Matt Stairs and Lanny did for me during and after my visits.

Judith McKenzie and Helmut Weissert are to be "blamed" and thanked for introducing me to the world of stable isotope geochemistry. Although I have drifted

away to lower sections of the earth's crust, both Helmi and Daniel Bernoulli have continually kept me interested in ophiolites and oceanic processes. I appreciate their constant support and friendship. Carol Simpson and Stefan Schmid sparked my interest in rock deformation and led me through the microscopic realm of dislocation creep and dynamic recrystallization. Both Carol and Stefan have reinforced an early lesson I was taught in Santa Barbara - never be afraid to ask questions. Stefan's inquisitive nature and constructive criticism have taught me to observe things I would have passed over and to recognize inconsistencies in an argument.

The most rewarding and valuable part of my thesis work has been the exchange of ideas, the discussions at five o'clock beer, and the friendships that my fellow doctoral students have given me. Among the many people that have helped me throughout my studies at the ETH, I would especially like to mention and thank E. Reusser, P. Ulmer, P. Brack, M. Amgwerd, K. Diethelm, L. Diamond, J. Ganguin, H. Hansmann, H. Stünitz, R. Panozzo-Stünitz, P. Nievergelt, R. Schmid, A. Stäubli, U. Rösli, U. Sonderegger, M. Schenk, Ch. Heinrich, C. Gerber, S. Girsberger, V. Trommsdorff, and V. Dietrich - the list could go on and on. I have also benefited greatly by discussions with the numerous post-docs and academic guests which have passed through Zürich. In particular, I would like to thank J. Ridley, Ch. Hy, B. Yardley, M. Engi, and D. Rubie for their help and interest.

I feel particularly fortunate to have shared an office with Eric Reusser and Peter Ulmer. They are responsible for my hate-love relationship with computers and the electron microprobe, and both have cleared away much of the confusion associated with phase petrology. Without Eric's constant help and amazing ability to explain complicated mathematics in a way that even I understand, many of the ideas and results in this thesis would not have been developed. I would also like to thank Jurg Sommerauer, who cheerfully instructed me in the use of the microprobe and was always available for discussion and to remedy the problems when the wrong button was pushed. Dr. Douglas Rumble III kindly provided the original version of the computer output which was used to calculate the models of fluid-rock interaction in Chapter 3.

I would like to thank Tony Willy for promptly preparing (the last) thin sections, and R. Aubert and W. Wittwer for instructing me in mineral separation techniques and helping with the tedious task of separation. A very special thank-you goes to Mona Jakobsson for her year-long friendliness and help with all the administrative problems. In addition, I would like to express my appreciation to Frau H. Boedecker for her help with locating publications and for tending to all the special requests associated with the library. Financial support from the Swiss Nationalfonds and the ETH Forschungscredit is gratefully acknowledged.

Ernst Lutz, Kurt Eugster and Ruedi Früh, and his family, Urs and Vre Früh, made it possible for me to come to Switzerland and have become my second family. They have contributed greatly to my understanding of the Swiss culture and to making Switzerland my second "Heimat". I would like to thank them all not only for their financial, but especially for their moral support and friendship during my studies at the ETH.

This thesis would not have come to completion without the endless help of my personal "rock of stability", Stefano Bernasconi. Stefano carried out the difficult task of typing, correcting, hunting down references and juggling files between four different computer systems. He is directly responsible for producing the final version of this "Mac Thesis". Stefano has constantly motivated and encouraged me, and his composed character has acted as a personal tranquilizer during the stressful months of writing this thesis. If I could patent his serenity and patience, I would be a rich woman and would have no need to worry about the few drops of water that flowed through the Sesia Zone 120 million years ago!

Lastly, I would like to sincerely thank my parents, Donald and Margaret Green, for instilling in me the value of education and for giving me the opportunity to study at a university. As a sign of my appreciation for their continual support, I would like to dedicate this thesis to them.

CHAPTER 1

GENERAL INTRODUCTION

1.1 PURPOSE AND SCOPE OF THE WORK

In contrast to some processes such as sedimentation and volcanism, many processes including metamorphism, are not directly observable. However, it is the physical and the chemical changes that have taken place in metamorphic rocks which allow an insight into the natural processes which have occurred during the evolution of the earth's crust. Traditionally metamorphic petrology has aimed at estimating the conditions of pressure, temperature and the fluid composition by which mineral assemblages in a rock approach or have achieved equilibrium. The application of experimental and thermodynamic methods to the study of mineral-fluid phase equilibria (e.g. Kerrick, 1974; Greenwood, 1975; Ferry, 1976, 1983, 1986; Ferry and Burt, 1982), as well as structural data on the controls of fluid flow (e.g. Etheridge et al., 1983a,b; Rutter and Brodie, 1985) have greatly increased our understanding of compositions, origins and behaviour of metamorphic fluids. In addition, fluid inclusion studies (e.g. Touret, 1977; Roedder, 1984; Crawford and Hollister, 1986) and the application of stable isotope techniques have provided further valuable information about the compositions and origins of metamorphic fluids and have put better constraints on the extent and mechanisms of fluid-rock interaction during metamorphism (e.g. Garlick and Epstein, 1967; Rice et al, 1976; Rumble et al, 1982; Ferry, 1983; Graham et al., 1983).

Although stable isotope geochemistry was originally used to determine temperature at which mineral assemblages equilibrate (Urey, 1947), it has widely become a useful tool in many aspects of metamorphic petrology. Due to isotopic fractionations which accompany many natural processes, stable isotope techniques, combined with petrologic data, can be used in metamorphic studies to:

- estimate temperatures of formation;
- determine the nature, extent and mechanism of fluid-rock interaction, and to deduce the source and direction of flow of metamorphic fluids;
- document equilibrium/disequilibrium relationships of mineral assemblages; and
- deduce the source of materials of metamorphic rocks.

In recent years many stable isotope studies have investigated fluid-rock interaction in hydrothermally altered areas around igneous intrusions (e.g. Ferry, 1978; Norton and Taylor, 1979; Lattanzi et al, 1980). Other studies have characterized fluid flow associated with devolatilization reactions in carbonate and mafic rocks (e.g. Rumble et al, 1982; Ferry, 1976b; Graham et al, 1983; Baumgartner, 1986). Fewer studies deal with fluid-rock interactions in carbonate-free metamorphic terrains (Frey et al, 1976) or are aimed at documenting isotopic equilibrium/disequilibrium relationships during metamorphism (e.g. Deines, 1977; Rumble and Spear, 1983). The intent of this study is to use stable isotope geochemistry to determine the scales and mechanisms of fluid interaction and motion in various metamorphic environments, as well as to investigate the relationship between fluids and deformation and the extent to which isotopic equilibrium is attained in metamorphic rocks. Two areas have been chosen where petrologic and chemical evidence indicates fluid involvement during their metamorphic evolutions.

Chapters 2 and 3 are concerned with the extent of fluid migration during eclogite-facies dehydration reactions and the subsequent amphibolite-facies overprinting during Tertiary metamorphism of mafic and pelitic rocks from the Cima di Gagnone area (Cima Lunga - Adula Nappe). This study is a continuation of investigations by Ch. Heinrich (1982, 1983, 1986) who has studied the amphibolitisation of eclogite lenses and layers enclosed in pelitic schists and has suggested that the fluid responsible for the hydration of the mafic eclogites was produced by dehydration reactions in the metapelites and only travelled distances less than a metre. The hydration of eclogite to symplectite (Hbl + Di + Plag) and amphibolite occurred at the same time as the dehydration of muscovite in the enclosing metapelites (now containing Qtz + Plag + Bio + Gar). The petrological and chemical changes associated with the amphibolite-facies overprinting on the eclogite mafic and pelitic rocks is discussed in Chapter 2. Models of Rayleigh distillation and fluid infiltration during the earlier eclogite-facies metamorphic event and during subsequent amphibolite-facies recrystallization are presented in Chapter 3. In addition, stable isotope evidence for the scales of fluid-rock interaction and isotopic exchange and equilibrium are discussed.

Chapters 4 and 5 deal with the role of fluids in processes of metamorphism and ductile deformation during the eclogite-facies evolution of metagranitoids from the Monte Mucrone in the Sesia Zone. Previous geological and petrological work has been carried out by P.O. Koons and D. Rubie, who have suggested that prior to deformation, restricted chemical communication resulted in local equilibrium domains and then gradually, in the later stages of deformation, large-scale equilibrium was approached. Fluids may have been important in the development of the orthogneiss as

well as acting as a catalyst in the approach towards chemical equilibrium (Koons, Rubie and Früh-Green, in review). Detailed mineralogical, textural and stable isotope studies have been made on ductile shear zones in the relatively undeformed rocks at the east face of the Mte. Mucrone in order to determine the role of fluids in deformation and recrystallization during the eclogite-facies metamorphism of these rocks.

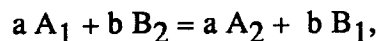
1.2. STABLE ISOTOPE GEOCHEMISTRY

The following sections are intended as a general introduction and review of the application of stable isotope geochemical methods to problems of fluid-rock interaction during metamorphism. Further and more detailed information may be obtained in the recently published book "Stable Isotopes in High Temperature Geological Processes", edited by J.W. Valley, H.P. Taylor and J.R. O'Neil (1986).

1.2.1. GENERAL THEORY AND TERMINOLOGY

Modern stable isotope geochemistry began with a classic paper on the isotopic fractionation between simple gaseous molecules by H. Urey in 1947, and was quickly proven to be of valuable use to geologists (Craig, 1953; Epstein and Mayeda, 1953; Emiliani, 1955). Stable isotope geology deals with the fractionation of the stable isotopes by physical and chemical reactions occurring in nature. The group of elements whose isotopes are especially susceptible to natural isotope fractionation includes H, C, N, O and S. These are among the most abundant elements in the earth and are intimately associated with the biosphere, the hydrosphere and the lithosphere. Consequently, the study of their isotopes provides information on a variety of geological processes occurring in different geological environments.

Isotope exchange reactions involve a redistribution of isotopes of an element among different molecules which contain that element. Such an exchange reaction can be written in terms of general chemical equilibrium:



where:

1 = light isotope

of the species A and B

2 = heavy isotope

The equilibrium constant of such a reaction is expressed as:

$$K = [A_2 / A_1]^a / [B_2 / B_1]^b$$

Concentrations are used rather than activities or fugacities because ratios of activity coefficients for isotopically substituted molecules are equal to unity. When there is more than one atom of the isotopic element in the chemical formula, for example $\text{Si } ^{18}\text{O}_2$ or CD_4 , all atoms in the substance are the isotope indicated. Using methods of statistical mechanics, the isotope equilibrium constant can be expressed in terms of the partition function Q , between the two molecules $A_1 + A_2$ or $B_1 + B_2$. Thus,

$$K = Q_{A_2} / Q_{A_1} / Q_{B_2} / Q_{B_1}.$$

Q is defined by the following equation:

$$Q = \sum_n g_n \cdot e^{-E_n / kT}$$

where g_n is the statistical weight of the n^{th} allowed energy level E_n , k is the Boltzmann constant and T is the temperature in Kelvin.

It is thus seen that isotope exchange reactions are temperature dependent. At different temperatures different isotope ratios will be present. As temperatures approach 0°K , the equilibrium constant tends towards zero and corresponds to complete isotope separation (i.e. no isotope exchange). As temperature increases (approaching infinity), there is less isotope exchange, and isotope fractionation approaches the value of 1.

The evaluation of partition function ratios becomes quite complicated when solid phases are considered. It is more customary to consider fractionation factors rather than equilibrium constants. Fractionation factors may be determined from direct laboratory measurements, from semi-empirical calculations, or from regularities in samples which formed during well understood geological processes. The fractionation factor α is simply expressed in terms of the ratio R of the numbers of any two isotopes found in the chemical compounds involved:

$$\alpha_{A-B} = R_A / R_B$$

and α is related to the equilibrium constant in the following way:

$$\alpha = (K)^{1/n}$$

where n is the number of atoms exchanged.

Isotope data are always given in terms of difference in absolute isotope ratios between two substances, and are expressed in δ -notation as defined below:

$$\delta = [R_{\text{sample}} / R_{\text{standard}} - 1] \times 1000 \text{ (‰)}$$

where R is the ratio of the heavy (rare) isotope to the light (common) isotope, e.g. $^{18}\text{O}/^{16}\text{O}$, $^{13}\text{C}/^{12}\text{C}$, D/H , etc.

simply signifies the enrichment or depletion of ^{18}O in a sample relative to a standard. Absolute isotopic abundances are not used because they cannot be measured as precisely as relative differences. There are two internationally accepted reference standards for oxygen: PDB (Pee Dee Belemnite) and SMOW (Standard Mean Ocean Water). The PDB Standard is normally used in paleotemperature studies of carbonate rocks; whereas SMOW is more common in isotopic studies of metamorphic rocks (see Friedman and O' Neil, 1977 for further discussion of the various standards used in stable isotope analysis).

The measured δ -value is related to the fractionation factor α by:

$$\alpha_{\text{A-B}} = 1 + \delta_{\text{A}} / 1000 / 1 + \delta_{\text{B}} / 1000.$$

Using the mathematical relationship:

$$10^3 \ln (1.0 X) \approx X ,$$

a useful approximation can be obtained by taking the natural logarithm of both sides of the previous equation so that:

$$\ln \alpha_{\text{A-B}} = \ln (1 + \delta_{\text{A}} / 1000) - \ln (1 + \delta_{\text{B}} / 1000)$$

since $\delta/1000$ is always less than 1.0, the following approximation can be written:

$$\ln (1 + \delta_{\text{A}} / 1000) \approx \delta_{\text{A}} / 1000 \quad \text{and} \quad \ln (1 + \delta_{\text{B}} / 1000) \approx \delta_{\text{B}} / 1000 .$$

Thus, by substitution:

$$\delta_{\text{A}} - \delta_{\text{B}} \approx 1000 \ln \alpha_{\text{A-B}} .$$

The quantity $1000 \ln \alpha_{\text{A-B}}$ is referred to as the "per mil fractionation" and will be independent of the standard used (Friedman and O' Neil, 1977). The quantity $(\delta_{\text{A}} - \delta_{\text{B}})$ can be replaced by the Δ -value, so that a general relationship between α , δ and Δ can be defined:

$$\Delta_{\text{A-B}} = \delta_{\text{A}} - \delta_{\text{B}} \approx 1000 \ln \alpha_{\text{A-B}}$$

For a discussion of the accuracy and limitations of this approximation see Friedman and O' Neil (1977,p. KK2).

In stable isotope geochemistry, the logarithm function $1000 \ln \alpha$, has an important significance. Early calculations by Bigeleisen and Mayer (1947) have shown that for perfect gases $\ln \alpha$ varies as a function of $1/T^2$ at high temperatures and $1/T$ at low temperatures. In addition, theoretical calculations (Bottinga and Javoy, 1973, 1975) and laboratory experiments (see App. V) have shown that there is often a linear relationship between $1000 \ln \alpha$ and temperature. Both theoretical and experimentally determined fractionation factors of oxygen isotopic exchange can be described by the relationship:

fractionation factors of oxygen isotopic exchange can be described by the relationship:

$$1000 \ln \alpha_{A-B} = a \cdot 10^6 T^{-2} + b \approx \delta_A - \delta_B = \Delta_{A-B}$$

where a and b are constants and A and B are any two species which attain isotopic equilibrium. This relationship forms the basis for oxygen isotope geothermometry (for comprehensive reviews see Javoy, 1977; Clayton, 1981, O'Neil, 1986). An example of empirical fractionation curves, calculated by Kieffer (1982) for various common silicate minerals are shown in Fig. 1.1.

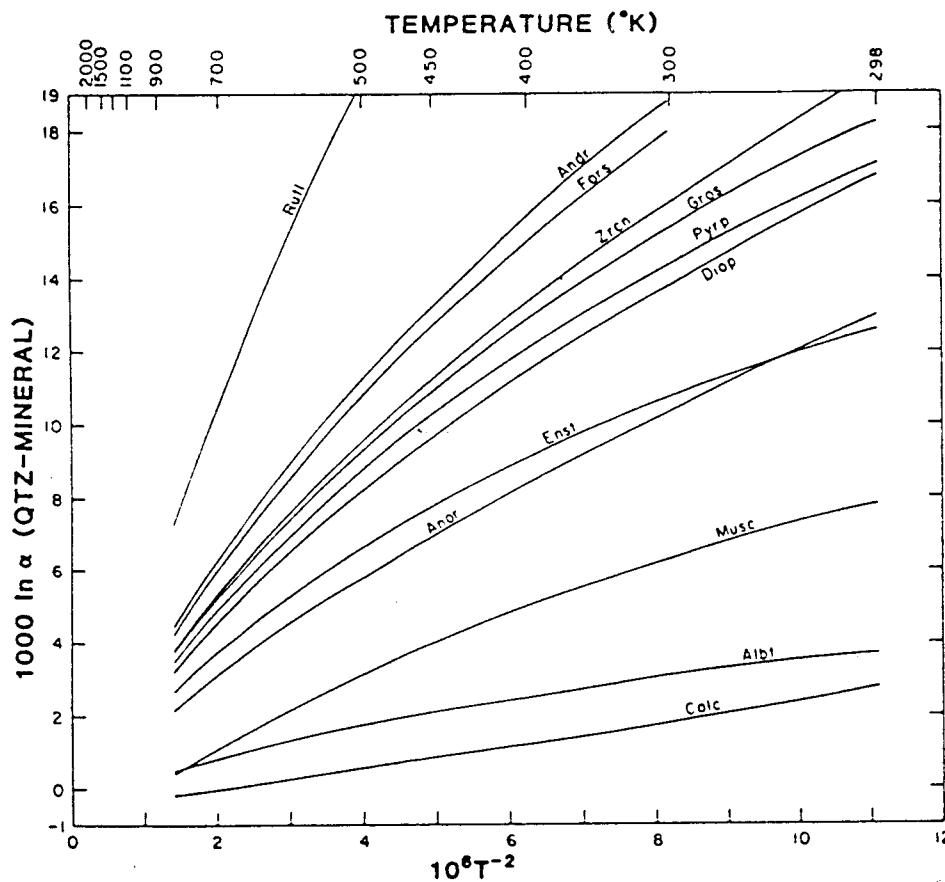


Fig. 1.1: Fractionation factors between quartz and the minerals indicated. The mineral abbreviations are: Qtz (quartz), Calc (calcite), Albt (albite), Musc (muscovite), Enst (clinoenstatite), Anor (anorthite), Diop (diopside), Pyrp (pyrope), Gros (grossular), Zrcn (zircon), Fors (forsterite), Andr (andradite), Rut (rutile). From Kieffer (1982).

1.2.2. OXYGEN ISOTOPE EQUILIBRATION DURING METAMORPHISM

The application of oxygen isotope geochemistry to petrological problems of fluid-rock interaction generally assumes that isotopic equilibrium has been achieved and

that it is frozen in at - or close to - the temperature of formation of the mineral assemblages present. Any discussion of the attainment of oxygen isotopic equilibrium needs to include both the criteria used to test for equilibrium and the scale at which equilibrium is thought to have occurred.

1.2.2.1. Large-scale equilibrium: pervasive isotopic exchange.

Some isotope studies of metamorphic rocks have shown that isotopic homogenisation can occur over distances of kilometers and within interbedded rocks of varying original chemical and isotopic compositions (Taylor et al, 1963; Garlick and Epstein, 1967; Rumble et al, 1982; Rumble and Spear, 1983; Wickham 1985).

Various mechanisms are thought to be responsible for such pervasive isotopic exchange: (1) self-diffusion of oxygen-bearing molecules through static pore fluids; (2) infiltration and fluid flow through interconnected pore space (Nagy and Parmentier, 1982; Rumble and Spear, 1983); (3) volume diffusion through solid grains (Taylor, 1974; Friedrichson and Hoernes, 1980; Matthews et al, 1983); or (4) solution - reprecipitation (i.e. recrystallization) of individual mineral grains. (See also discussion in Section 1.2.3 and 5.4).

Large-scale isotopic exchange and homogenisation can be determined by measuring similar minerals from various rock types, whose original isotopic compositions are known to be different. If the minerals have uniform isotopic compositions regardless of their original difference prior to metamorphism, large-scale isotopic equilibrium can be assumed.

1.2.2.2. Local equilibrium

In contrast to equilibrium on an outcrop scale and in the presence of a pervasive fluid, local grain-to-grain equilibrium may be attained between adjacent mineral grains in a single rock type or layer. Thus, isotope exchange occurs over a distance equal to or greater than the grain sizes in the rock but less than the thickness of the bedding or layering. A test of local exchange equilibrium may be made by analysing at least two mineral pairs from various rock types and determine whether the isotopic fractionations are consistent (Javoy et al., 1970; Deines, 1977). Since isotopic fractionation is temperature dependent, uniform fractionation between mineral pairs, despite variations in bulk isotopic composition, should yield concordant temperature estimates and would indicate attainment of local isotopic equilibrium. The identification of concordant temperatures as evidence for isotopic equilibrium assumes that the calibration factors are

absolutely accurate and that temperatures represent peak metamorphic conditions with no retrograde isotopic exchange. Concordant temperatures may also result from either (a) similarities in grain-sizes and diffusional parameters of the coexisting (analyzed) phases and/or (b) loss of hydrous fluid from the rock, yielding a concordant closure temperature (see also Deines, 1977 and discussion in Gilletti, 1986).

Table 1.1

Sequence of minerals in the order (bottom to top) of increasing tendency to concentrate ^{18}O during equilibrium isotopic exchange (modified from Taylor, 1967, p. 128). The δ -values are fully hypothetical, but show reasonable variations between coexisting minerals in low- to middle-grade pelitic schists. The relative order of the minerals in parentheses are not as well known as the other, more abundant minerals.

Minerals	δ Value
Quartz (tridymite)	15.0
Dolomite	14.2
K-feldspar, albite	13.0
Calcite	12.8
Na-rich plagioclase	12.5
Ca-rich plagioclase (kyanite)	11.5
Muscovite, paragonite, (Na-pyroxene)	11.3
Augite, orthopyroxene, diopside, (glaucophane)	10.5
Hornblende (sphene, lawsonite)	10.5
Olivine, garnet (zircon, apatite)	9.5
Biotite	8.5
Chlorite	8.0
Ilmenite	5.5
Magnetite, hematite	4.5

Another basic indication of isotopic equilibrium is the relative order of ^{18}O - enrichment in coexisting mineral phases. Quartz tends to concentrate ^{18}O relative to the other common minerals, whereas minerals such as magnetite, ilmenite and rutile tend to be the most ^{16}O -rich. A list of minerals and their relative tendency to incorporate ^{18}O is shown in Table 1.1 (taken from Taylor, 1967, p.128; see also Garlick and Epstein, 1967, p. 197). This sequence of decreasing ^{18}O -content is due to crystal-chemical effects. Since the vibrational frequencies are directly related to the bond strength and cation mass, the minerals which have the most strongly bonded oxygen and/or have oxygen bonded cations of low atomic weight will be more enriched in ^{18}O . More highly

polymerized silicates and those with the highest vibrational frequencies (e.g. quartz) tend to concentrate ^{18}O . Although the correct sequence of ^{18}O -concentrations does not guarantee isotopic equilibrium, reversals in the order of ^{18}O -enrichment clearly indicates conditions of disequilibrium or may be evidence for retrograde exchange or unusual fluid-rock interaction during metamorphism.

1.2.3. MECHANISMS OF ISOTOPIC EXCHANGE

There have been few studies in stable isotope geochemistry which have been directly aimed at determining the mechanisms by which oxygen isotopes exchange and reach equilibrium. In general, oxygen isotope exchange is considered to result from two basic mechanisms: (1) surface reactions and (2) diffusion of oxygen-bearing species through crystals, either along lattice planes or crystal defects. Surface reactions can include dissolution/reprecipitation mechanisms, recrystallisation of a pre-existing mineral or transformation of one mineral into another (e.g. Matthews et al, 1983; Cole et al, 1983).

Most experiments on isotopic exchange are aimed at determining fractionation factors in mineral-fluid systems. In their experimental study on the effect of cation exchange on oxygen isotopic exchange in feldspars, O' Neil and Taylor (1967) suggested that the oxygen exchange occurred by a fine-scale dissolution/reprecipitation-front moving through the crystals. Based on these experiments as well as many others which showed a similar phenomenon of solution-recrystallisation, Cole et al (1983, and references therein) calculated rates of oxygen isotopic exchange for many of the most common rock-forming minerals. Their calculations showed that under the same conditions (temperature, grain size, fluid/mineral ratios), diffusion-controlled rates of isotopic exchange are several orders of magnitude less than those accompanying surface reactions. They concluded that oxygen isotopic exchange occurs primarily through surface-controlled mechanisms when the minerals and fluids are out of chemical equilibrium, and through diffusion once the minerals and fluids have reached chemical equilibrium (see also discussion in Section 5.4).

The dominant mechanism of oxygen isotope exchange may vary depending on the mineral species involved. Based on stereological and scanning electron microscopic (SEM) analyses, combined with a three-isotope method of determining isotope exchange (see also Matsuhisa et al., 1978), Matthews et al. (1983) have shown that two different mechanisms of isotopic exchange dominate during mineral-water interactions for the minerals quartz and plagioclase at elevated pressures and temperatures. Quartz-water isotopic exchange ($T = 250\text{ }^{\circ}\text{C}$ to $600\text{ }^{\circ}\text{C}$; $P_{\text{H}_2\text{O}} = 1$ to 22

kbar) seems to be *initially* dominated by a recrystallization mechanism of 'Oswald ripening', in which recrystallized grains of quartz form faceted overgrowths on original grains that have been rounded by solution processes. As recrystallization proceeds (with an increasing degree of exchange), the specific surface area of the quartz grains decreases and thus reduces the amount of surface free energy as the thermodynamic driving force for recrystallization. As a result, recrystallization is retarded and further isotopic exchange becomes more and more dominated by diffusional mechanisms. Matthews et al envision the diffusional mechanism to be similar to that of 'hydraulic weakening' described by Griggs (1967), in which oxygen in Si-O-Si bridges are hydrolyzed by migrating water molecules.

In contrast to mechanisms of quartz-water interactions, and contrary to the interpretation of O'Neil and Taylor (1967) discussed above, substantial recrystallization was not observed by Matthews et al (1983) in isotopic exchange experiments on albite- and anorthite-water at $T = 500\text{ }^{\circ}\text{C}$ to $600\text{ }^{\circ}\text{C}$ and $P_{\text{H}_2\text{O}} = 2$ to 15 kbar. Matthews et al propose that oxygen isotope exchange during plagioclase-water interactions is dominated by a diffusional mechanism in which H_2O penetrates the plagioclase grains and reactively exchanges with oxygen atoms which share (Al, Si) O_4 - tetrahedra.

At high water pressures (above 4 Kbar) dissolution/reprecipitation may be the more dominant mechanism of isotopic exchange (Matsuhisa et al, 1979; Yund and Anderson, 1978). However, Matthews et al (1983) have emphasized the fact that their observations are applicable to systems of mineral-water exchange between loose grains and *abundant* fluid (i.e. high fluid to mineral ratios). It may thus be unwise to directly apply the observed results to processes in natural systems in which fluid/rock ratios are low and the fluid phase is mainly concentrated along grain boundaries, crystal defects, voids etc. Natural environments may tend to inhibit recrystallization, except possibly during processes of metamorphism which involve increases in permeability (i.e. through devolatilization reactions and/or during brittle deformation). Evidence for a diffusional mechanism of oxygen isotope exchange in plagioclase has been observed by Taylor, (1974) from the San Juan volcanic field, Colorado and by Friedrichson and Hoernes (1980) for plagioclase phenocrysts in hydrothermally altered ocean-floor basalts. However, evidence for a similar mechanism of recrystallization as that observed in the experiments of Matthews et al (1983) have not been substantiated in natural systems.

Theoretically, isotopic exchange can take place in fluid-absent systems directly through diffusion between mineral grains in mutual contact. The rates of exchange will be controlled by temperature, grain dimensions, activation energies and diffusivities and will be orders of magnitude slower than diffusion in the presence of water (e.g. Yund and Anderson, 1974, 1978; Gilletti et al, 1978; Graham 1981).

Hydrogen diffusion studies by Graham et al (1980) and Graham (1981) have shown that rates and mechanisms of hydrogen isotopic exchange with minerals are greatly dependent on the presence of a hydrous phase. Furthermore, Graham (1981) argues that isotopic exchange of both hydrogen and oxygen will continue during cooling in metamorphic and hydrothermal systems if a hydrous fluid phase is present and will directly affect the temperature at which isotopic exchange ceases. If hydrous intergranular fluid is effectively lost from the system before cooling, isotope exchange will slow down drastically and possibly the maximum temperature of metamorphism will be recorded in the rock. These conclusions of Graham's have direct implications for the evaluation and determination of isotopic equilibrium, for the interpretation of the cooling history in metamorphic rocks, and for correlation with other thermometers (e.g. cation exchange).

1.2.4. CONTROLS ON OXYGEN ISOTOPIC COMPOSITIONS

Systems of oxygen isotopic exchange can be regarded in the same way as any other mass-transfer system. Oxygen isotopic fractionation between mineral phases in a rock will occur as temperature and mineral modes change and/or as new minerals are formed during metamorphic reactions. In a *closed system*, in which the isotopic and chemical compositions of the rocks are originally homogeneous, changes in temperature and pressure during metamorphism will influence mineral reactions and can result in changes in the isotopic compositions of the coexisting mineral phases, but the overall whole-rock ^{18}O -budget will remain constant. This is analogous to the behaviour of bulk rock chemistry in a closed system. Cation-redistribution can take place and mineral modes may change through mineral reactions during metamorphism, but the whole rock chemical composition will remain the same.

If changes in the whole rock isotopic and chemical compositions are observed, the system can no longer be regarded as closed: something must have been added or taken away. In *open systems* of fluid-rock or rock-rock interaction, shifts in ^{18}O away from the original isotopic composition will be primarily controlled by:

- the relative difference between the *initial* composition of the rock ($\delta^i \text{}^{18}\text{O}_{\text{WR}}$) and that of fluid phase ($\delta^i \text{}^{18}\text{O}_{\text{Fl}}$) which either enters or leaves the system;
- the relative difference between $\delta^i \text{}^{18}\text{O}_{\text{WR}}$ of two rock reservoirs which are interconnected via a fluid phase;
- the total amount of oxygen in the initial fluid (X_{Fl}^i) relative to the total amount of oxygen in the rock (X_{WR}^i);
- the mechanism of fluid-rock interaction.

The mechanisms of fluid-rock interaction, such as Rayleigh distillation (see below) during devolatilization reactions, and/or infiltration of an externally-derived fluid phase, will affect both the amount of oxygen and the isotopic composition of the system and will control the amount of shift in $^{18}\text{O}_{\text{WR}}$ (see Rumble, 1979, 1982; Rumble et al, 1982; Taylor, 1977, 1979; Rye et al, 1976).

Rayleigh distillation is a process in which a fluid is derived internally during devolatilization reactions. Once the fluid is produced it is expelled and does not react with the rock again. Numerical modelling by Rumble (1979, 1980, 1982) of Rayleigh distillation during simultaneous decarbonation and dehydration reactions in calc-silicate rocks has shown that only small shifts (1-2‰) in ^{18}O of minerals and whole rock result, whereas shifts in ^{13}C are much larger. The difference in behaviour between carbon and oxygen isotopes is explained by the fact that, compared to the amount of oxygen lost from the rock as H_2O , much more, if not all, carbon atoms are strongly partitioned into the fluid phase and thus leave the system, resulting in large fractionations of ^{13}C in any residual carbonate-bearing mineral.

Rumble mentions that similar modelling by Lattanzi et al (1980) resulted in much larger depletions in ^{18}O . The difference between the two models is that the minerals involved in the devolatilization reactions do not exchange isotopically in the Lattanzi-model, and more oxygen atoms are lost from the system through the fluid phase. This model can be tested by measuring the residual of the phase which produces volatiles (e.g. calcite in a carbonate system or muscovite in a hydrous system) as well as all coexisting mineral phases to determine whether or not isotopic exchange equilibrium between any of all the phases has been attained. Applications of the Rumble-type distillation model are presented in Chapter 3.

In contrast to small shifts in ^{18}O during Rayleigh distillation, Rumble's modelling of infiltration and combined infiltration/Rayleigh distillation show that greater shifts in ^{18}O can result. His models and the resulting shifts in ^{18}O depend greatly on F/R ratios and on the chemical and isotopic composition of the infiltrating fluid. The greatest shifts in ^{18}O will result in systems with high F/R (>1:1) and with fluids which are extremely out of isotopic equilibrium with the rock being infiltrated (Rumble, 1982, p. 345-346). In these models there is little difference in results between pure infiltration, in which only isotopic exchange with an external fluid occurs without accompanying devolatilization reactions, and infiltration accompanied by devolatilization reactions and Rayleigh distillation. This is to be expected since results of the Rayleigh distillation model produced only minimal changes. Rumble has also shown that for isothermal, isobaric infiltration and reaction, oxygen isotopic equilibrium between the rock and the infiltrating fluid may not be attained; whereas under isobaric, polythermal conditions, isotopic

equilibrium is approached more closely and earlier in the progress of the reaction.

It is also important to remember that a lack of shift in ^{18}O does not necessarily mean that no infiltration occurred during the metamorphic history of a rock. If an externally-derived fluid is in isotopic equilibrium with the rock it infiltrates, no isotopic exchange will result. In such a case, other methods of evaluating fluid-rock interaction must be relied upon.

1.2.5 MODELS OF FLUID / ROCK INTERACTION USING OXYGEN ISOTOPE DATA

Several models of isotopic exchange as a result of fluid/rock interaction are found in the literature. Examples of numerical modelling of fluid transport and isotopic exchange in hydrothermal systems, based on the principles of transport theory, are presented by Norton & Taylor (1982); Cathles (1983) and Baumgartner & Rumble (1986). Alternative approaches in monitoring isotopic exchange and fluid-rock interaction are offered by mass balance calculations as presented by Taylor (1977), Rumble (1982) and Blattner (1985).

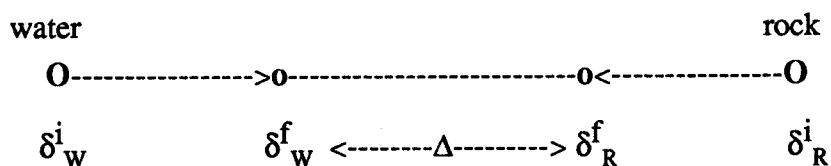
Any model which uses stable isotopes as an indication for fluid-rock ratios will only determine minimal values, since once the fluid is in isotopic equilibrium with a rock, no evidence of the amount of water which has subsequently gone through the rock will be left behind.

1.2.5.1. Mass-balance calculations of isotopic exchange

If a fluid phase is initially out of isotopic equilibrium with the solid phase, the isotopes will be redistributed between all the phases in the system which the fluid infiltrates, and is to an extent dependent on the exchange mechanism. Stable isotope exchange can be considered the same as any mass transfer system. Water-rock interaction in a closed system can be described by the basic mass-balance equation:

$$W \delta_{\text{W}}^{\text{i}} + R \delta_{\text{R}}^{\text{i}} = W \delta_{\text{W}}^{\text{f}} + R \delta_{\text{R}}^{\text{f}}, \quad (1.1)$$

where W, R are the atomic per cent of oxygen in the water and rock, respectively, relative to the total oxygen in the system, and δ_{W} , δ_{R} are the oxygen isotopic compositions of water and rock before exchange (i = initial) and after exchange (f = final). This isotopic relationship for water-rock interaction is represented schematically in the following bar graph:



whereby Δ is simply defined as $\delta_{\text{R}}^{\text{f}} - \delta_{\text{W}}^{\text{f}}$, and will be a function of the temperature at which exchange takes place.

Equation (1.1) can be rearranged to define a ratio of water oxygen to rock oxygen, W/R,

$$W/R = \delta_{\text{R}}^{\text{f}} - \delta_{\text{R}}^{\text{i}} / \delta_{\text{W}}^{\text{f}} - \delta_{\text{W}}^{\text{i}} \quad (1.2).$$

Using the above definition of Δ , equation (1.2) becomes :

$$W/R = \delta_{\text{R}}^{\text{f}} - \delta_{\text{R}}^{\text{i}} / \delta_{\text{W}}^{\text{i}} - (\delta_{\text{R}}^{\text{f}} - \Delta) \quad (1.3)$$

(Taylor, 1977).

In an open-system in which each increment of water makes only a single pass through the system, the integrated W/R ratio has been calculated by Taylor (1977) to be:

$$\begin{aligned}
 W/R &= \ln \left[(\delta_{\text{W}}^{\text{f}} + \Delta - \delta_{\text{R}}^{\text{i}}) / (\delta_{\text{W}}^{\text{i}} - (\delta_{\text{R}}^{\text{f}} - \Delta)) \right] \\
 &= \ln \left[(W/R)_{\text{closed system}} + 1 \right] \quad (1.4)
 \end{aligned}$$

W/R ratios calculated by this equation are similar to those calculated by Rumble (1982) for stepwise fluid infiltration and isotopic exchange. In Rumble's models, infinitesimally small increments of fluid infiltration and isotopic re-equilibration produce small isotopic changes in the components of the system. These changes are then summed over all the increments and the overall fluid-rock interaction ($\delta^{18}\text{O}$ -shift) is determined. Modal compositions of the fluid and the rock, as well as porosity, temperature and pressure, can be changed after each step of calculation. In all of these mass-balance calculation models, no constraints are placed on the mechanisms by which the isotopes exchange (i.e. diffusion-controlled or surface reactions), nor on the permeability of the rock.

Baumgartner and Rumble (1986) point out the drawbacks in these types of mass-balance, isotopic exchange models. These models can essentially be regarded as one-dimensional with no time constraints and no possibility to monitor the spatial evolution of the mass transport system. However, anyone familiar with the complexities of numerical modelling and transport theory will appreciate the simplicity and first approximation that mass-balance calculation models allow.

1.3. CONSTRAINTS ON FLUID FLOW

The mechanism by which fluid escapes from a rock will be determined by the amount that fluid pressure (P_f) deviates from the stable lithostatic pressure (P_l). Such a deviation will be directly influenced by the permeability of the rock in which a fluid phase is produced and the permeability of the surrounding rock pile which the fluid must pass through. Rock permeability is controlled by a number of factors which include: (1) number, distribution and orientation of fractures; (2) applied stress; (3) porosity; (4) pore-fluid pressure; (5) precipitation of secondary minerals by pore fluids; (6) dissolution of minerals by pore fluids (e.g. Brace, 1968, 1972, 1980; Morrow et al., 1981); and (7) reactions taking place in the rocks. Very little is actually known about in-situ permeability of medium to high grade metamorphic rocks. In a comparison of laboratory-determined permeabilities and in-situ permeabilities of various rock types, Brace (1980) pointed out that permeabilities can vary greatly for any group of rocks and will depend greatly on the presence and spacing of fractures. In general, the range of in-situ permeabilities appear to be consistent with those estimated in laboratory studies (Brace, 1980, 1984). Measured permeabilities of crystalline rocks in drill holes range from 10^{-18} to 10^{-13} m², whereas the least permeable rocks in this group are comparable to those of argillaceous rocks (10^{-21} to 10^{-17} m²). Brace (1984) concluded that the permeability of basalts may be the most variable of any common rock type, covering a range of nearly 9 orders of magnitude (10^{-20} to 10^{-10} m²).

As fluids are released during devolatilization reactions, both P_f and the rocks permeability will initially increase (Brace, 1980). In addition, such metamorphic reactions tend to increase the rock's porosity because the volume of the mineral products in the rock after devolatilization will generally be less than that of the reacting phases (Fyfe et al., 1978; Rumble et al., 1982, see also Chapter 3). A steady state will result if permeability increases such that the rate of fluid loss is equal to the rate of fluid production. However, since tensile strength of a rock at metamorphic conditions is very small, once fluid pressure exceeds lithostatic pressure, the rock will eventually fail, resulting in fractures (hydraulic fracturing) and/or shear zones (shear failure) (e.g. Brace, 1968; Secor, 1968; Fyfe et al., 1978; Etheridge et al., 1984; Rutter and Brodie, 1985).

The presence of extensive veins in metamorphic rocks is commonly interpreted as rock failure due to an excess of fluid pressure in which the resulting fractures act as channelways for fluid flow (e.g. Walter and Orville, 1982; Rumble and Spear, 1983; Yardley, 1982, 1986; Wood and Walter, 1986; Heinrich, 1986). In contrast, veining in some metamorphic terrains may be completely absent or scarce. Larger scale isotopic

exchange without apparent fracturing or veining is often interpreted as indicating steady-state conditions of fluid flow during metamorphism (e.g. Garlick and Epstein, 1967; Taylor et al., 1963; Rumble et al, 1963; Rumble and Spear, 1983; Ferry 1983b, 1984; Graham et al., 1983). The critical factors which will directly control fluid pressure and determine whether or not a rock will fail, and veins will form, are the rates of fluid production, or fluid influx, and the pervasive permeability of the rocks.

CHAPTER 2

ADULA - CIMA LUNGA NAPPE

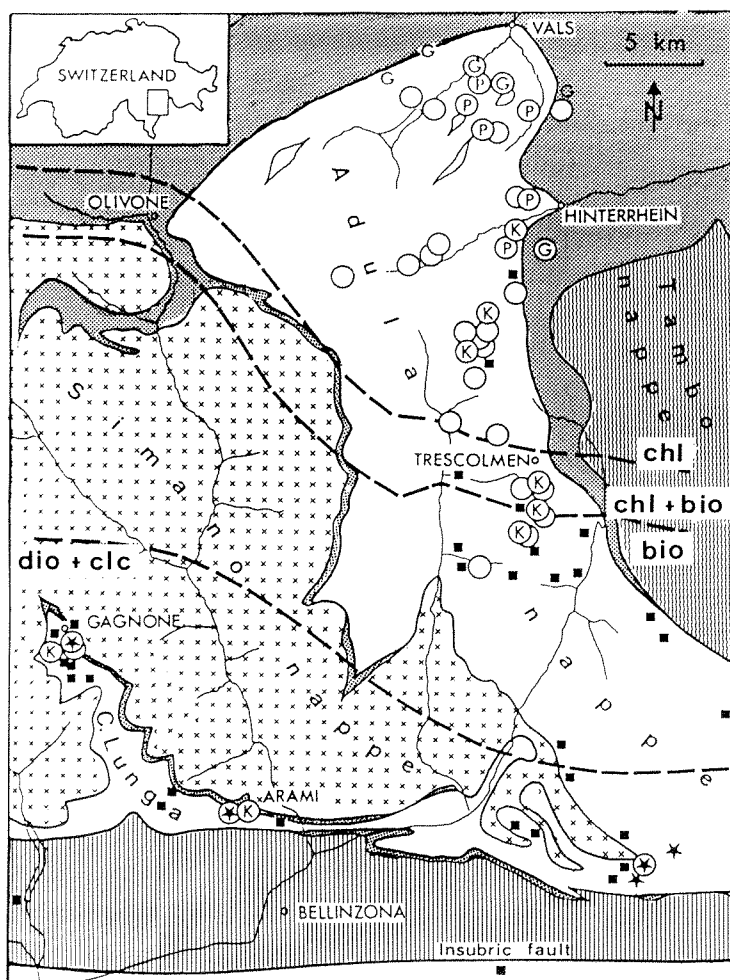
2.1. GEOLOGICAL SETTING

The central alpine Adula-Cima Lunga Nappe is a slice of pre-Mesozoic continental basement consisting predominantly of metagranitic and metapelitic gneiss and schist. Less abundant mafic and carbonate rocks, as well as ultramafics in the southern Cima Lunga Nappe, occur as lenses and layers in the polymetamorphic metasediments. Two phases of alpine metamorphism, accompanied by varying degrees of deformation, have affected these rocks. Mesozoic or lower Tertiary high pressure mineral assemblages are older than nappe emplacement and are overprinted by an Oligocene Barrovian-style regional metamorphism. High-pressure mineral assemblages are mainly preserved in mafic lenses and record a continuous increase in P-T conditions from 12-15 Kb / 500-600 °C in the north of the Adula nappe to more than 20Kb / 800 °C in the south (Heinrich, 1983). A distinct decrease in pressure characterizes the Tertiary Barrovian-style metamorphism which varies from greenschist facies in the north to upper amphibolite-facies (sillimanite grade) in the south.

The rocks of the Adula-Cima Lunga Nappe have undergone a complicated structural and polymetamorphic history. A pre-alpine, high temperature metamorphic event is indicated by Carboniferous Rb/Sr and K/Ar age determinations on some micas from the northern Adula nappe (Jäger et al, 1967; Jäger et al, 1969; Frey et al, 1974). In addition, whole rock Rb/Sr data indicates a late Carboniferous age for migmatites in the southern Adula nappe, with some local remobilisation during the Tertiary amphibolite-facies metamorphism (Hänny et al, 1975).

2.2. CIMA DI GAGNONE : GENERAL GEOLOGY AND LITHOLOGIC UNITS

The Cima di Gagnone area, southeast of Frasco in Val Verzasca TI (Fig. 2.1), occupies the northeastern corner of the Cima Lunga Nappe, which is the southern extension of the Adula nappe. A metacarbonate zone of possibly Mesozoic age separates the Cima Lunga Nappe from the underlying, rather monotonous metagranitic gneisses of the Simano Nappe. The exact nappe boundary is difficult to trace in most areas because it is isoclinally folded (Codoni, 1981). These folds have amplitudes up to several hundred meters. The axial planes are nearly horizontal at the Cima di Gagnone area and become progressively steeper southwards towards the narrow east-west trending "Wurzel Zone" along the insubric line.



Mesozoic sediments and mafic+ultramafic igneous rocks



Pre-Mesozoic basement rocks in 'nappe cores'



Tambo



Adula-
Cima Lunga



Simano



Maggia &
Bellinzona -
Zones

○ eclogite with omphacite + garnet preserved

■ completely amphibolitized eclogite

minerals in textural equilibrium with garnet+omphacite+quartz:

K kyanite G blue amphibole P albitic plagioclase

⊗ garnet lherzolite

★ completely chloritized garnet lherzolite

○ location

Fig. 2.1

Tectonic map of the Eastern Central Alps of Switzerland, modified from Heinrich (1982, Figure 1 and references there in). The Adula-Cima Lunga Nappe, which overlies the Simano Nappe and is overlain by the Tambo Nappe, is a pre-Mesozoic continental basement complex consisting predominantly of metagranitic gneisses and schists with less abundant metacarbonates, metabasites and metaperidotites (only in the south). Mineral assemblages in rocks of mafic and ultramafic compositions, occurring as discontinuous layers and lenses, record early-Alpine eclogite-facies metamorphic conditions which are older than nappe emplacement, a Tertiary Barrovian-style regional metamorphism overprints the high pressure mineral assemblages and ranges from greenschist-facies in the north to upper amphibolite-facies (sillimanite-grade) in the south. Nappe boundaries are cut by mineral isogrades surfaces of the syn- to post-tectonic Tertiary metamorphism. Data shown are from Heinrich (1982) and references there in.

The Cima di Gagnone area is one of the best studied areas in the Cima Lunga-Adula Nappe. A detailed summary of the most pertinent studies in the area is given in Heinrich, 1983 p. 25. Extensive structural mapping (Heinrich, 1978; Stäubli, 1978; Schläpfer, 1978; Zingg, 1978) has shown that intensive deformation and isoclinal folding occurred simultaneously with the Tertiary upper amphibolite-facies metamorphism. This latest stage of metamorphism has essentially obliterated most of the earlier structures and mineral assemblages in the metapelitic to metagranitic gneisses and schists which comprise most of the area. Relict eclogite-facies mineral assemblages have only been preserved in boudins and lenses in areas of low strain (Heinrich 1978, 1982). With the exception of one outcrop of garnet peridotite south of Passo Scaiee (Trommsdorff, 1980, Stop 28, p. 313; Evans and Trommsdorff, 1978) and corona textures in one sample of metapelite (CH 200, Heinrich 1982, 1983), these relict eclogite-facies assemblages (Qtz + Omp + Gar + Kyn; see Table 2.1 for an explanation of the abbreviations used in this study) occur exclusively in rocks of mafic composition. Structures in the eclogite and garnet lherzolite relicts are rotated and truncated by those in the amphibolite-facies pelitic country rocks.

Table 2.1

List of abbreviations of mineral names used throughout this study.

Alb	= albite	Mus	= muscovite
Alm	= almandine	Omp	= ompacite
An	= anorthite	Par	= paragonite
And	= andradite	Phe	= phengite
Bio	= biotite	Plg	= plagioclase
Chl	= chlorite	Pyr	= pyrope
Dio	= diopside	Qtz	= quartz
Gar	= garnet	Rut	= rutile
Gro	= grossular	Sil	= sillimanite
Hbl	= hornblende	Spe	= spessartine
Ilm	= ilmenite	Sph	= sphene
Jad	= jadeite	Sta	= staurolite
Ksp	= K-feldspar	Zoi	= zoisite
Kyn	= kyanite		

Based on the most predominant rock-type present, Heinrich (1978) divided the Cima di Gagnone-Val Motto area into three lithological zones (Fig. 2.2).

Biotite-Hornblende Gneiss forms the tectonically lowest lithological unit and lies directly over the granitic gneiss of the Simano Nappe. This gneiss contains biotite, hornblende, plagioclase, quartz, sphene and garnet and is intercalated with coarse-grained massive amphibolite. The amphibolite occurs as several meters thick boudins and discontinuous layers. In contrast to the rocks of similar composition and

character in the tectonically higher units, no textural relicts of eclogite-facies minerals have yet been found in these amphibolites.

The biotite-hornblende zone is overlain by an approximately 100m thick *Kyanite Gneiss Zone* of semi-pelitic to pelitic composition. The interlayered biotite gneiss and kyanite-bearing garnet gneisses and schists are well foliated and form a large-scale, nearly flat-lying, isoclinal fold. These rocks contain varying amounts of biotite, muscovite, kyanite, garnet, quartz and plagioclase with less abundant staurolite, tourmaline, rutile and ilmenite. 20 cm thick quartz lenses, with up to 10 cm long kyanite crystals, are common in this zone. These lenses are nearly always oriented parallel to foliation, and the kyanites are commonly bent and slightly altered to muscovite.

Nearly round, 1-2m in diameter mafic boudins, lenses and pods occur throughout the kyanite-gneiss zone. These boudins and lenses have a characteristic zoning pattern in which relict eclogite-facies mineral assemblages of kyanite + omphacite + garnet + quartz are found solely in the centers and grade into fine-grained symplectite (Dio+ Plg) with fine-grained amphibolite forming along the rims. The petrology, evolution and significance of these eclogites and meta-eclogites have been described in detail by Heinrich (1979, 1982, 1983, 1986) and are the basis for the present study. Their relationships will be discussed more thoroughly in a subsequent section.

A *Biotite-Augengneiss Zone* forms the tectonically highest unit in the Cima di Gagnone area. These rocks are more granitic in composition and are characterized by porphyroblastic augen (up to 1 cm long) of plagioclase and quartz. Biotite, plagioclase and quartz are the main constituents in the matrix with less abundant and varying amounts of muscovite, K-feldspar and garnet. Kyanite is rare in this zone. As in the kyanite-gneiss zone, mafic rocks with relict eclogite-facies mineralogy occur in isolated lenses. 1m to 200m large lenses of ultramafic rocks are distributed throughout the biotite-augengneiss zone. These rocks have undergone a complicated metamorphic and metasomatic history and have been the subject of many intensive petrological and geochemical studies (eg. Trommsdorff et al, 1975; Evans and Trommsdorff, 1974, 1978; Evans et al, 1979, 1981; Pfeiffer, 1978, 1981). Spectacular occurrences of eclogites, meta-eclogites and metarodingites are often associated with the ultramafic lenses and are described in detail by Evans et al (1979).

With the exception of one outcrop containing a relict garnet peridotite core, the ultramafic rocks are composed of olivine + talc + chlorite + tremolite \pm Mg-amphibole (Mg-cummingtonite or anthophyllite) or olivine + enstatite + tremolite + chlorite (Evans and Trommsdorff, 1978). Continuous fluid activity is indicated by various generations of veins, and metasomatic reactions which have produced talc- and magnesite-rich alteration zones (Pfeiffer, 1978, 1981). On the basis of petrological and geochemical data, the ultramafic and mafic rock association have been interpreted by Trommsdorff et

al (1975) and Evans et al (1979,1981) as an oceanic complex of peridotite and tholeiitic basalt which underwent differing degrees of serpentinisation and rodingitisation prior to an early-alpine eclogite-facies metamorphism with subsequent amphibolite-facies metamorphism and metasomatic alteration.

Silica-rich metacarbonates and metadolomites are rare in the biotite-augengneiss and kyanite-gneiss zones. They occur as thin layers and are often associated with the ultramafic lenses.

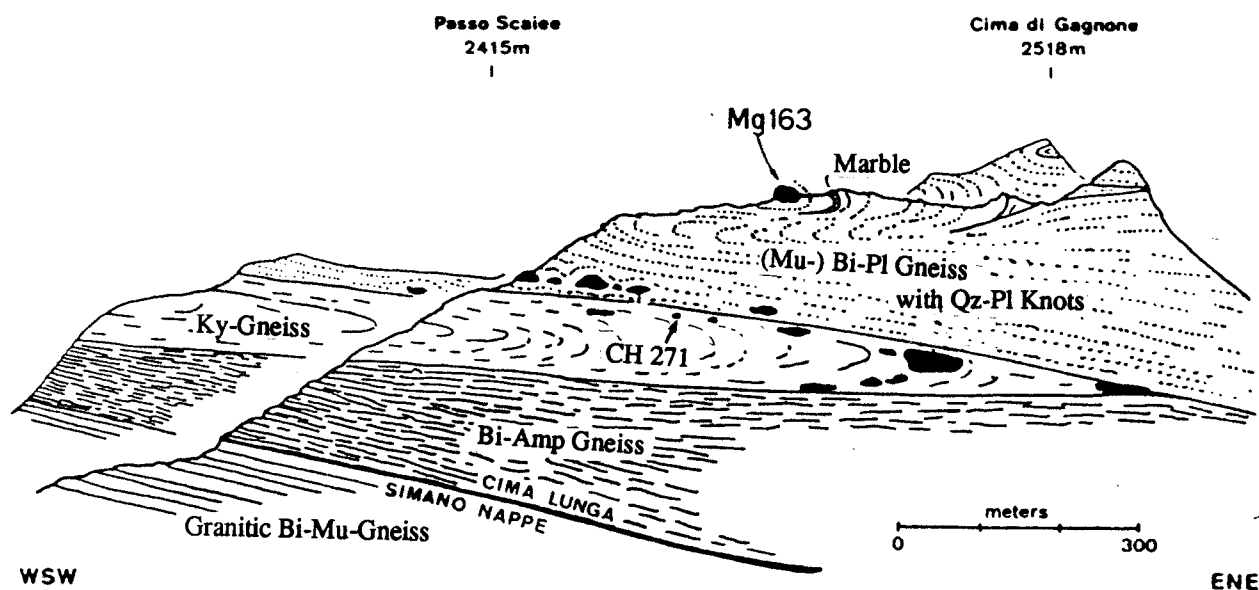


Fig. 2.2. Schematic profile of the Cima di Gagnone area from Heinrich (1978,1983; see references there in). Ultramafic rocks (garnet peridotite, Mg 160, and chlorite peridotite Mg 163, see Evans and Trommsdorff, 1978) as well as eclogites occur as discontinuous layers and lenses in distinct horizons in the biotite augengneiss- and kyanite gneiss-zones.

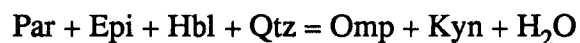
Preliminary results from oxygen isotope analyses on the mafic rocks at outcrop MG163 (see Evans and Trommsdorff, 1974; 1978) indicate distinctly different oxygen isotopic values for mineral separates and whole rocks than those for the mafic lenses in the kyanite gneiss zone (see Chapter 3). Whole rock and quartz values for both fresh eclogites and amphibolites at outcrop MG163 show constant $\delta^{18}\text{O}$ of 3.0‰ - 3.5‰ and 6.3‰ - 6.4‰, respectively. These values are at least 2‰ lower than those for normal ultramafic rocks (e.g. Taylor, 1968; Javoy, 1978; Kyser et al., 1981, 1982; see also Figs. 3.1 and 3.2), for normal basaltic rocks (e.g. Taylor and Epstein, 1962; Garlick and Epstein, 1967; Gregory and Taylor, 1981) and for some eclogites (e.g. Vogel and Garlick, 1970; Javoy, 1971; Arginier et al., 1985). These preliminary oxygen isotope data indicate either unusually ^{18}O -depleted source materials for the mafic rocks or large-scale isotopic exchange with ^{16}O -rich fluids. Without further

oxygen data and especially hydrogen isotope data, an interpretation of these results or a determination of possible sources for the interacting fluid cannot be conclusively determined. However, comparison of these data with data from outcrop CH271 (discussed in detail in Chapter 3) suggests that all of the mafic rocks from the Cima di Gagnone area may not have been derived from the same source material (e.g. subducted oceanic crust), or that outcrop MG163 experienced very local, ^{18}O -depleted fluid activity during its metamorphic evolution.

2.2.1. CIMA DI GAGNONE: METAMORPHIC EVOLUTION

2.2.1.1. Eclogite-Facies Metamorphism

Based on detailed petrological and textural studies, Heinrich (1983, 1986) has suggested that the kyanite-bearing eclogites from the Cima di Gagnone area evolved by prograde dehydration reactions from hydrous pre-Alpine mafic precursors. The presence of primary hydrous minerals (Hbl + Zoi) coexisting with, and as inclusions in, the stable eclogite-facies assemblages of Omp + Kyn + Gar + Qtz, together with theoretical Schreinemaker's analysis and thermobarometry, allowed Heinrich to propose a generalized dehydration "isograd" reaction:



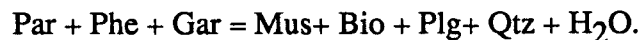
(reaction 12, Heinrich, 1986)

This reaction was interpreted as marking the regional transition from fluid-absent metamorphism in the north to fluid-present metamorphism in the south at pressures and temperatures over 12-15 Kb and 500-600 °C. Numerous veins containing Qtz + Kyn + Omp strongly suggest that a free fluid phase locally coexisted with the kyanite eclogites some time during prograde eclogite-facies metamorphism. Heinrich (1986, p. 150) interprets these veins as a result of hydraulic fracturing and suggests that the H_2O -bearing fluid phase was local and temporary in occurrence.

2.2.1.2. Amphibolite-Facies overprinting

Despite a common metamorphic history, the rocks at the Cima di Gagnone area exhibit contrasting degrees of overprinting during the Tertiary amphibolite-facies metamorphism. The metapelitic to metagranitic country rocks have *completely recrystallized* in the amphibolite facies and now contain assemblages of Qtz + Bio + Plg + Mus + Gar. Some mica-poor, pelitic rocks contain relict kyanite and garnet (eclogite-facies) which often have disequilibrium textures. The mafic lenses show a distinct mineralogical zoning related to progressive hydration in which eclogite-facies

Omp + Gar + Kyn assemblages are preserved in the cores and are gradually replaced by amphibolite along the rims. An inclusion (CH 200, Heinrich 1982, 1983) of a pelitic layer in a relatively undeformed mafic lens has preserved corona and pseudomorphic textures indicative of the earlier eclogite-facies metapelite assemblages. The pseudomorphs contain Bio+ Plg + Mus + minor Ksp + Hbl, after the older assemblage Phe + Par + Gar + Qtz + minor Omp (see Heinrich 1982, 1983, Chapter 5). This paragenesis and the textural relationships in the inclusion allowed Heinrich to postulate a generalized whole rock reaction involving dehydration during recrystallization in the amphibolite facies:



Heinrich further proposed that such *dehydration reactions* were directly responsible for the *simultaneous hydration* of the nearby eclogite lenses. The varying degrees of overprinting are explained by differences in reaction rates during amphibolite-facies P,T-conditions. The reactions in the metapelites were relatively fast, possibly because of the presence of intergranular fluid, allowing complete recrystallization; whereas the practically anhydrous mafic rocks reacted slowly and incompletely, with the rates and extent of reaction being dependent upon the supply of water (see also discussion in Section 3.6.1).

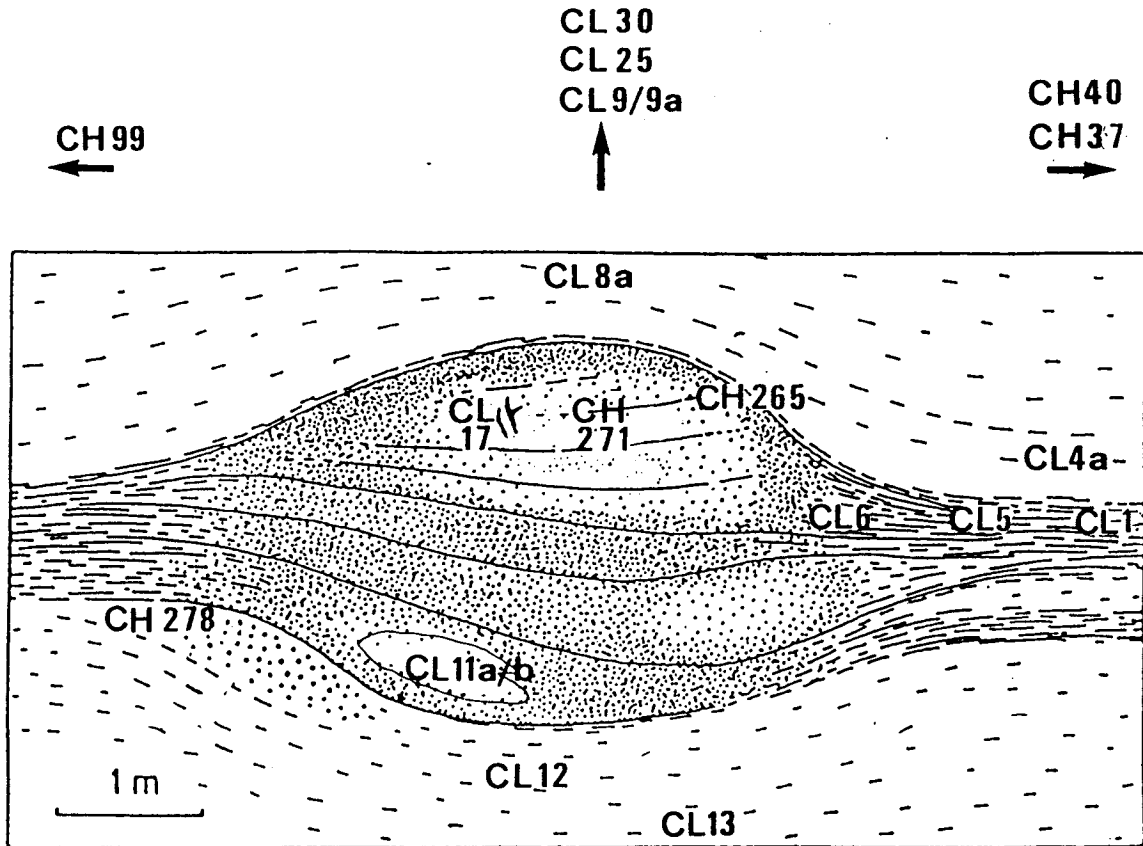
Based on the petrologic models presented by Heinrich, a stable isotope study has been carried out to determine the scales and mechanism of fluid interaction and motion as well to examine the relationship between fluid and deformation and the extent to which isotopic equilibrium is attained in high grade metamorphic rock.

2.3. OUTCROP RELATIONS AND PETROGRAPHY: OUTCROP CH271

(Swiss Map Coordinates: 707 960 / 130 750; see Heinrich 1979, 1982, 1983)

2.3.1. MINERALOGY AND PETROGRAPHY OF MAFIC ROCKS

This outcrop (Fig. 2.3) has been chosen for detailed isotopic studies because it shows the characteristic relationships between the metamorphic mafic and pelitic rocks of the southernmost Adula Nappe. The 3x4 m large mafic lens is located in the kyanite gneiss zone and contains fresh eclogite assemblages in the core and a pronounced mineral banding. The lineation is discordant to the amphibolitized reaction zones and to the schistosity in the surrounding metapelites. Sample numbers of the rocks chosen for isotopic analysis are given in parenthesis. Their relative positions at the outcrop are shown in Fig. 2.3



CH 271	Fresh Eclogite	CL 4a	} Biotite Gneiss
CH 265	Symplectite	CL 25	
CL 17	Qtz-Kyn-Phe Vein	CL 30	
CL 6	Fine-grained Amphibolite	CL 12	} Biotite-Garnet Gneiss
CL 5	} Recrystallized Amphibolite	CL 13	
CL 1		CL 9	
CH 35		CH 278	} Biotite-Garnet Gneiss (with relict Kyanite)
CL 11b	Mafic contact to CL 11a	CL 11a	
CL 8a	} Qtz-Kyn Veins in Metapelite	CH 40	
CL 9a		CH 99	

Fig. 2.3. Sample locations and schematic relations of the mafic lens and surrounding metapelites at outcrop CH 271.

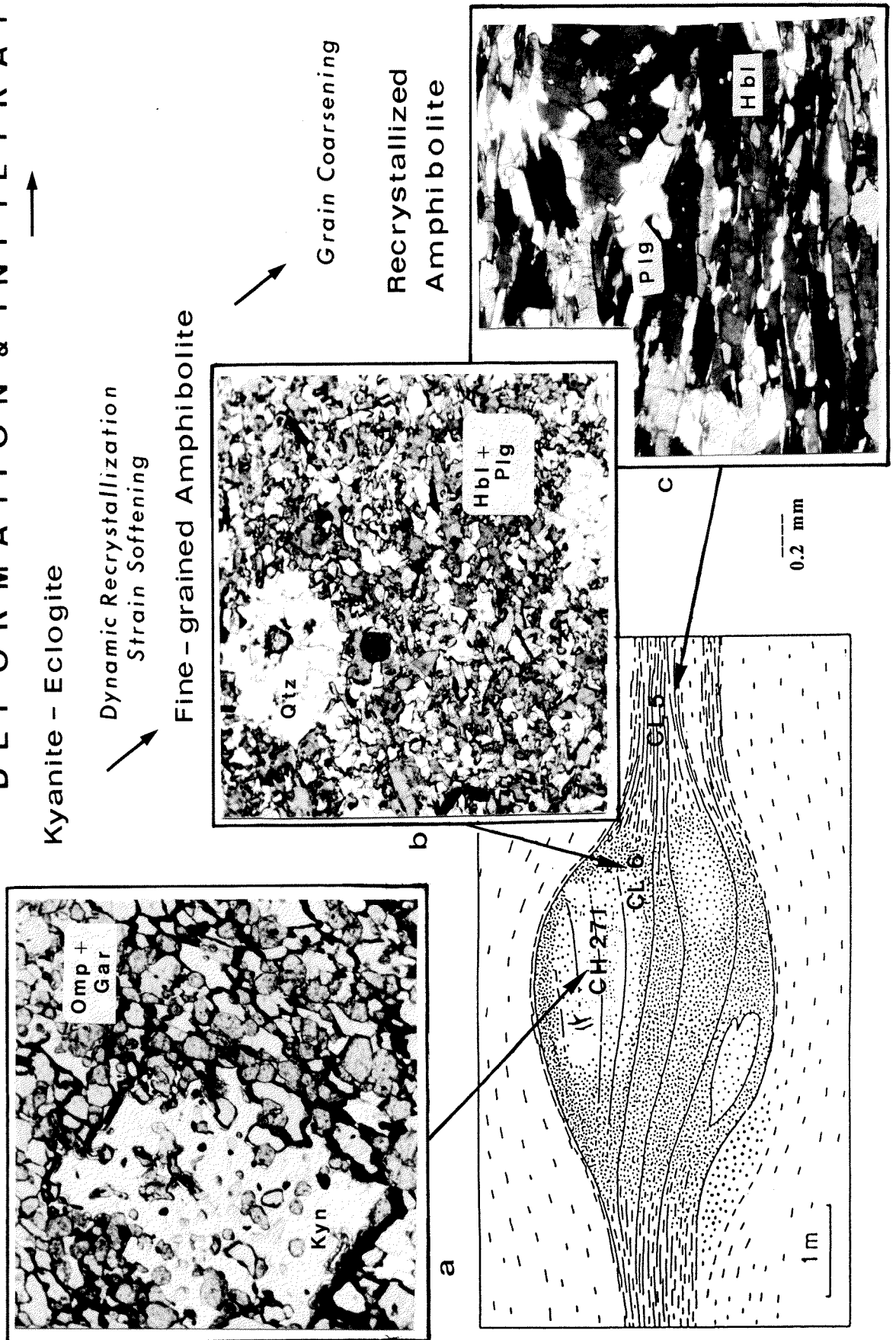
The eclogite core (CH 271) consists of equigranular Omp + Gar + Qtz with poikiloblasts of kyanite and hornblende and minor amounts of ilmenite, rutile, green hornblende and clinozoisite (see Fig. 2.4 a and Heinrich 1983, p. 41). Towards the rim (CH 265) omphacite breaks down and is replaced by a fine-grained symplectite of plagioclase and diopside; garnet is rimmed by green hornblende; relict kyanite is pseudomorphed by fine-grained, zoned aggregates of corundum, plagioclase and biotite. Along the immediate rim of the lens (CL 6) the symplectite assemblages are replaced by fine-grained poikilitic green hornblende, plagioclase and ilmenite. Quartz is minor, often occurring as isolated 1-2 mm elongated pods (Fig. 2.4b), and relict garnet form less than 1 vol % of the rock. A slight lineation is formed by the Hbl + Pl aggregates. The lens has been rotated and forms a more or less sharp contact with completely recrystallized coarser-grained amphibolite (CL 1, CL 5, CH 37). These amphibolites form "tails" on both sides of the lens and are distinguished from those along the rims by their coarser grain size, new growth of sphene, and by the presence of a distinct lineation (Fig. 2.4c). Biotite has grown epitaxially, often discordant to the lineation, as well as together with sphene \pm chlorite in cross-cutting small veins.

2.3.1.1. Deformation / Recrystallization Relations and Mechanism in the Mafic Rocks

The geometric relations of the mafic lens and its amphibolite rim and tails, described in the previous section, resemble porphyroclastic augen structures in mylonitic gneisses (see Simpson and Schmid, 1983; Passchier and Simpson, 1985; Passchier, 1986) although at contrasting scales. On the microstructural scale, quartz porphyroclasts represent rigid bodies in a more ductile environment. Along the rims or mantles of such grains conditions of high stress, and therefore high strain, result in dynamic recrystallization and a reduction in grain size. This reduction in grain size may lead to a strain softening (White et al, 1980), which results in greater deformability and the formation of the tail-structures. The weaker material comprising the tails has a higher rotation rate than the less deformable porphyroclasts. As a result the dynamically recrystallized grains within the tails tend to be oriented parallel to the over-all foliation in the rock, whereas the long axes of the porphyroclasts remain discordant to the foliation.

Fig. 2.4: Schematic deformational and recrystallizational history of a mafic lense at outcrop CH 271 (see text) at the Cima di Gagnone area (Cima Lunga Nappe - Southern Adula). Evolution has been deduced from textural, mineralogical and chemical relations in zoned mafic rocks which occur as isolated lenses and boudinaged layers in semi-pelitic to pelitic schists and gneisses (see also Fig. 2.9).

DEFORMATION & INFILTRATION



The outcrop relations of the mafic rocks to the surrounding strongly foliated schists are directly analogous to quartz porphyroclasts with dynamically recrystallized tails. However, one major inconsistency is immediately noticed, namely that of the grain size of the recrystallized tails. In porphyroclasts with recrystallized tails, there is always a notable reduction in grain size in the tails, whereas the amphibolite tails of the mafic lens at outcrop CH271 is distinctly coarser-grained than the amphibolite which mantles the lens or than the symplectite transition zone towards the core of the lens (see Fig. 2.4). This discrepancy between the grain size predicted by a similar deformation mechanism and the actual grain size suggests that a subsequent mechanism of grain-coarsening may have acted on the the amphibolite tails, or that the strain softening mechanism is of a different nature, i.e. unrelated to grain-size reduction by dynamic recrystallization.

An alternative mechanism of softening could be reaction-enhanced ductility as discussed by Rubie (1983). Unlike dynamic recrystallization of porphyroclasts, in which the mineral phase in the tails remains the same, the rims and tails of the mafic lens show a change in mineralogy relative to the more rigid core. Heinrich (1978, 1983), has shown that the amphibolitisation of eclogite occurred via a very fine-grained symplectite transition phase. The rheological behaviour of the small grain-size of the plagioclase- and diopside-symplectite may be an analogue to that of the jadeite + quartz + zoisite pseudomorphs after plagioclase discussed by Rubie (1983) from the Mte. Mucrone metagranitoids (see also Chapter 4).

The mechanism of reaction-enhanced ductility, proposed by Rubie (1983), results from the small grain-size of the product phases relative to that of the reacting phases. In such a process of grain-size reduction, the dominant mechanisms of deformation may change from dislocation creep to grain boundary deformation mechanisms of superplasticity and result in the weakening of the material (see Rubie, 1983 p.333 and references there in). A similar mechanism of grain softening may have lead to the greater deformability of the symplectite zones along the rims of the mafic lens, resulting in superplastic behaviour during deformation, and to the formation of the tail structures. Recrystallization to amphibolite and grain coarsening in the tail-areas may have occurred during superplastic deformation, which would eventually change the dominant mechanism of deformation back to dislocation creep (see Rubie, 1982,1983). The deformational behaviour of the core of the mafic boudin may be analogous to that of quartz in the Mte. Mucrone metagranitoids during eclogite-facies metamorphism and deformation (see Rubie 1982, 1983 p. 346, Fig. 7). During ductile shearing the quartz grains remained more competent than the fine-grained jadeite + quartz + zoisite layers, resulting in discontinuous coarser-grained lenses and layers of quartz between superplastically- deformed layers of pyroxene, quartz and white mica.

Deformation can enhance reaction kinetics in several ways (see Brodie and Rutter,

1985). Permeability may increase allowing fluid infiltration into the system (Rutter and Brodie, 1985), which in turn can increase rates of reaction and grain growth by several orders of magnitude (Fyfe et al., 1958 pp. 84-85), Tullis and Yund, 1982). The mineralogical change from relatively anhydrous eclogite in the core of the mafic lens to amphibolite along the rim clearly indicates a certain degree of fluid infiltration in these rocks. It is conceivable that the recrystallized tails could represent regions of low mean stress during deformation with larger P_{H_2O} -gradients resulting in localized areas of higher fluid/rock ratios and an enhancement of grain growth of the hornblende and plagioclase aggregates. This possibility is discussed further in light of isotope data in Chapter 3.

2.3.1.2. Summary of observations and interpretations of the mafic rocks.

At the Cima di Gagnone area (Cima Lunga Nappe), mafic rocks occur as isolated lenses, or in some cases as boudinaged layers, within Kyanite-bearing semi-pelitic to pelitic schists and gneisses (Kyanite Gneiss Zone) and more granitic gneisses (Biotite Augengneiss Zone). Fresh eclogite assemblages of $Omp + Gar + Qtz + Kyn \pm Hbl \pm Zoi \pm Phe$ are often preserved in the cores of the lenses, and grade into fine-grained symplectite ($Dio + Plg$), with fine-grained amphibolite ($Hbl + Plg$) forming along the rims. The fine-grained amphibolite along the rims of the lenses often form sharp contacts to completely recrystallized, coarser grained amphibolites, which make up pronounced "tails" extending up to 20 m into the surrounding pelitic schists. The eclogitic cores of the lenses display a pronounced mineral banding, which has been rotated and is discordant to the lineation in the amphibolite rims and tails.

Heinrich (1983, 1986) has determined a polymetamorphic history, based on petrological and textural studies, for the formation of the distinct mineralogical banding found in these mafic rocks. Transformation during early-Alpine high-pressure metamorphism of pre-Alpine amphibolite, may have occurred by dehydration reactions which produced the kyanite-bearing eclogite assemblages. These nearly anhydrous assemblages were re-hydrated to amphibolite during subsequent exhumation under Tertiary amphibolite-facies metamorphic conditions. Recrystallization of eclogite to amphibolite appears to have occurred through an ultrafine-grained transitional stage of symplectite formation.

In this study, the distinct mineralogical and textural relationships of the mafic lenses and the amphibolite rims and tails have been interpreted as the result of an initial greater deformability and an increase in permeability offered by the fine-grained nature of the transitional stage (i.e. reaction-enhanced ductility and permeability). During the Tertiary amphibolite-facies deformation and recrystallization event, superplastic deformation of the fine-grained symplectite zones resulted in the formation of the tail structures.

Increased permeabilities allowed an access of an external fluid which resulted in grain coarsening and transformation to amphibolite. Greater rock permeabilities or lower mean stress in the "structurally weak" tail regions may have lead to sites of fluid concentration during deformation and enhanced grain growth, resulting in the coarser-grained, well-foliated amphibolite. Post-kinematic fluid activity is evidenced by epitaxial growth of biotite and by sphene \pm chlorite veins in the amphibolite tail regions.

2.3.2. MINERALOGY AND PETROGRAPHY OF PELITIC ROCKS

The country rocks around the lens at outcrop CH 271 are predominantly pelitic schists containing biotite, quartz, and plagioclase with differing modal amounts of garnet, muscovite, K-feldspar, kyanite and staurolite. On the basis of mineralogical and textural criteria two main types of metapelites have been distinguished: kyanite-free biotite schists and kyanite-bearing schists. Both types include rocks which exhibit either equilibrium textures and penetrative deformation or less commonly have disequilibrium textures and evidence for static crystal growth. As before, the sample numbers in parentheses correspond to samples chosen for isotopic analysis.

2.3.2.1. Kyanite-Free Scists: (Equilibrium textures CL 12, CL13, CL 9)

With the exception of irregularly-shaped garnet, the kyanite-free biotite schists show a high degree of textural equilibrium. Quartz and plagioclase (An₁₀₋₂₀) occur as slightly elongated, equigranular grains with straight grain boundaries; unaltered red-brown biotite forms a well-defined schistosity. Muscovite, when present, often occurs in clusters and has grown either parallel to schistosity or only slightly discordant to it. In general, the rocks are strain-free; however a weak crenulation of the mica grains (mainly biotite) and undulatory extinction in quartz may be present (e.g. CL 12).

Two size distributions of garnet are commonly observed: small, inclusion-free grains (0.1-0.5 mm in diameter) and larger, cloudy grains (1-4 mm in diameter). The larger grains contain numerous inclusions in the cores and are overgrown by clear, inclusion-free rims (Fig. 2.5 a). The inclusions are mainly fine-grained mica (muscovite and biotite) and quartz. These garnets have either rounded, isometric shapes and occasionally resorbed textures or are slightly elongated and have grown parallel to the schistosity. The smaller garnet grains are always clear and are similar in composition to the rims of the larger garnets (almandine-rich, see below). These textural and chemical differences (discussed below) suggest that continuous garnet growth or at least two different phases of garnet growth took place in these rocks. Accessory and ore minerals in this rocks include ilmenite, rutile, apatite, zircon \pm sphene \pm clinozoisite.

Fig. 2.5a.
Photomicrograph of equilibrium-textured biotite (Bio)- muscovite (Mus) schist (CL 12a) showing inclusion-rich cores of coarse-grained garnets (Gr1) and clear inclusion-free fine-grained garnets (Gr2).

0.2 mm

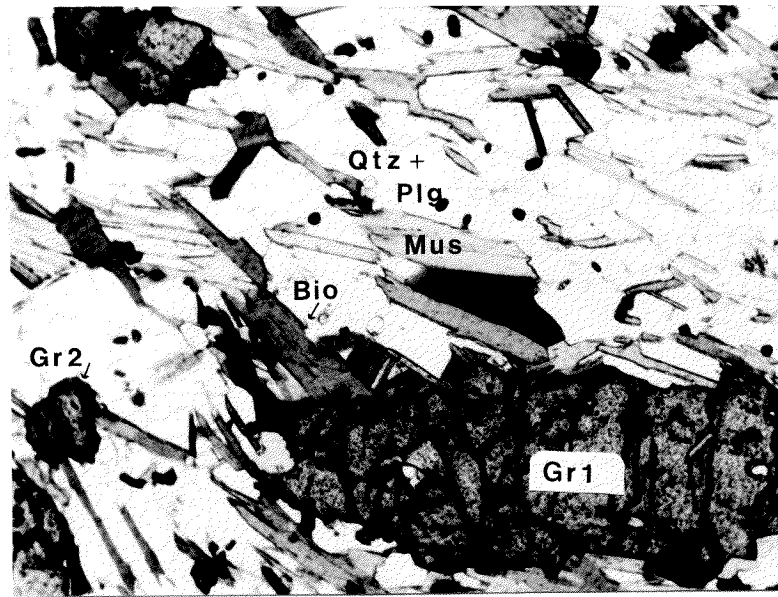


Fig. 2.5b.
Photomicrograph of equilibrium-textured kyanite- (Kyn) bearing biotite-muscovite schist (CH 99) showing recrystallized quartz (Qtz) and plagioclase (Plg) grains and parallelly oriented biotite, muscovite and kyanite grains.

0.2 mm

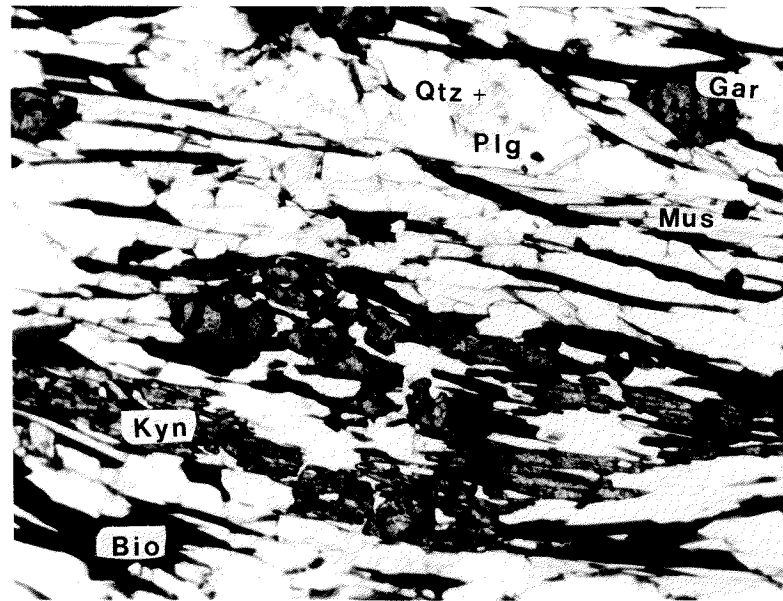
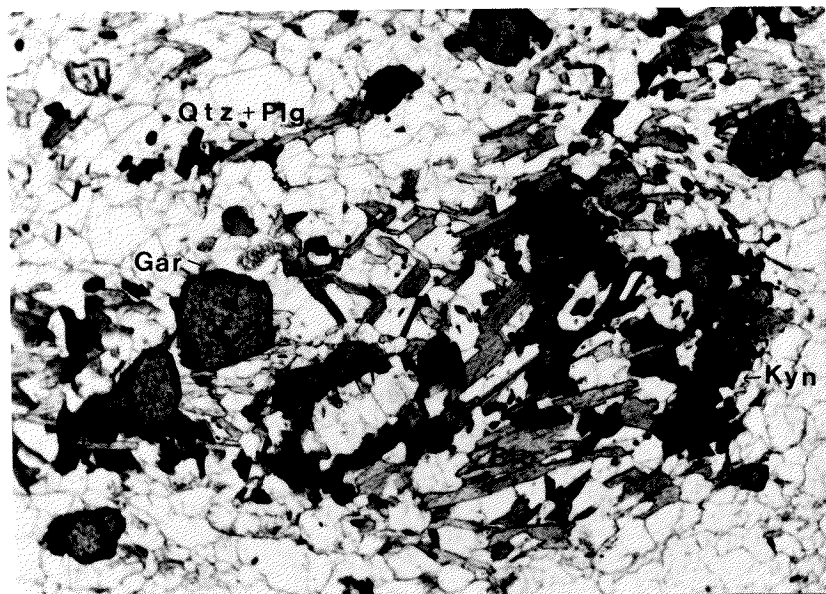


Fig. 2.5c.
Photomicrograph of disequilibrium-textured kyanite-biotite schist. Skeleton-like grains of kyanite represent eclogite-facies relicts and are replaced by fine-grained unoriented aggregates of plagioclase and biotite.

0.2 mm



2.3.2.2. Kyanite-Free Schists: Disequilibrium Textures (CL 4A)

Disequilibrium textures are found in plagioclase-rich rocks (approx 40-50 vol %) that are characterized by a lack of penetrative deformation and by randomly oriented, fine-grained mica grains. The quartz grains have undulatory extinction and deformation bands and often occur as aligned broken pods in discontinuous, sub-parallel layers. The grain boundaries are irregular, and a large variation in grain size is characteristic. Garnets form less than 10 vol % of the rock and occur as small, nearly inclusion-free rounded grains. They are more grossular-rich and slightly spessartine-richer than garnets in the other metapelites in this area (see App.I).

2.3.2.3. Kyanite-Bearing Schists: Equilibrium Textures (CH 40, CH 99)

These rocks exhibit essentially the same equilibrium textures as those without kyanite. They are characterized by an equigranular growth of plagioclase and quartz and a well-developed schistosity defined by alligned mica grains (biotite±muscovite). Kyanite forms up to 1cm long needles which are oriented parallel to schistosity. The grains are always in contact with biotite and plagioclase (see Fig. 2.5b). When present, staurolite (CH 40) occurs as idiomorphic, lath-shaped grains and is nearly always associated with garnet, biotite and plagioclase ± kyanite. As in the other metapelites, two generations of garnet growth can be distinguished in these rocks. Larger garnets are irregularly shaped and have inclusion-rich cores, whereas the smaller grains are idiomorphic and free from inclusions. The compositions are nearly identical to those in the kyanite-free metapelites, and the same zoning patterns from core to rim are found (see below and Fig. 2.6)

2.3.2.4. Kyanite-Bearing Schists: Disequilibrium Textures (CH 278, CL 11a)

Disequilibrium textures in garnet-rich metapelitic rocks which have been described by Heinrich (1983, p. 52), have only been found at the contact to, or as inclusions in, the mafic lens (see sample CH278, Fig. 2.3). They are relatively mica-poor (5-10 vol % biotite) and are characterized by a lack of penetrative deformation (Fig. 2.5 c). Skeleton-like kyanite poikiloblasts often form in clusters with the garnet and are replaced by fine-grained biotite and plagioclase (An_{20-30}) ± staurolite ± quartz. The garnets are often corroded and broken, with inclusions of fine-grained mica and quartz in the cores. The grains show a similar, but less pronounced, chemical zoning as those in the kyanite-free biotite schists, but are slightly less almandine-rich (Fig. 2.6). Staurolite is unoriented and forms lath-shaped, idiomorphic grains which are nearly always associated with biotite at the contact to garnet grains.

In kyanite-free textural domains, biotite and plagioclase form fine-grained aggregates which have a similar texture to the skeleton-like kyanite domains and resemble the pseudomorphs after white mica in sample CH 200 (see Heinrich, 1982, p. 35; 1983, p. 31). A second generation of garnet is indicated by the presence of smaller isometric grains which occur together with randomly oriented biotite and plagioclase. These garnets are undeformed and have few or no inclusions. Their compositions are slightly richer in Fe than the rims of the larger garnets in the kyanite poikiloblast domains. Rutile and ilmenite occur as accessory minerals and are associated with garnet and biotite.

Two size distributions of quartz are observed in these rocks. Larger elongated grains occur in lens-shaped domains which have a subparallel orientation and show undulatory extinction and weak deformation bands. Finer, undeformed quartz grains have straight boundaries with plagioclase and form the matrix of these rocks. At the contact to the mafic lens (sample CL 11A/ CL 11B), the disequilibrium texture in the metapelites is overprinted by epitactic, skeletal growths of green hornblende. Biotite becomes more abundant and kyanite is missing from the paragenesis.

2.3.2.5. Summary of key observations on the pelitic rocks

In contrast to the mafic rocks, the volumetrically more abundant semi-pelitic to pelitic schists and gneisses at the Cima di Gagnone Area contain recrystallized amphibolite-facies mineral assemblages of Bio + Qtz + Plg + Gar \pm Mus \pm Kyn \pm Sta \pm Ksp. The schists and gneisses at outcrop CH 271 (see Fig. 3.2.) are distinguished by varying degrees of textural equilibrium and by differing modal amounts of Kyn, Gar, Mus, Ksp and Sta. In general, the rocks exhibit synkinematic recrystallization. Disequilibrium textures are found in garnet-rich rocks, occurring as inclusions in, or at the contact to the mafic lens (see Fig 2.3). In these rocks skeleton-like kyanite poikiloblasts form in clusters with garnet and are replaced by fine-grained biotite and plagioclase \pm quartz \pm staurolite.

2.3.3. VEINS

Two generations of veins can be identified at outcrop CH 271. Early, eclogite -facies veins and segregations (CL 17) of quartz and phengite with relict kyanite and omphacite (replaced by corundum) occur in the incompletely-overprinted core of the mafic lens (see Fig. 2.3). The quartz is coarse-grained and has undulatory extinction; the phengite forms isometric grains (3-5 mm long) and has macroscopically visible pink alteration rims (made up of a mm-fine mixture of corundum, K-feldspar and biotite; Heinrich, 1983, p. 31).

Coarse-grained, up to 2 cm wide, veins and lenses of quartz (CL 8A, CL 9A) are commonly associated with the kyanite-bearing biotite schists. These veins and segregations contain differing amounts of kyanite (up to 10 cm long), ilmenite and biotite and have invariably been deformed. The kyanite crystals are often bent and are slightly altered to white-mica. They are nearly always oriented parallel to the schistosity in the neighbouring rocks.

Heinrich (1978, p. 7-9) has described complicated, greenschist-facies overprinting in similar veins, but no such relationships were observed at this outcrop. However, late-stage, greenschist-facies veins in the amphibolite tails of the mafic lens are commonly observed. These veins are 2-5 mm wide and cross-cut the well-defined schistosity formed by hornblende and plagioclase. These veins contain fibrous chlorite and sphene.

2.4. MINERAL CHEMISTRY AND CATION-EXCHANGE GEOTHERMOMETRY

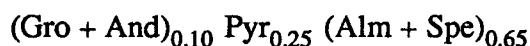
As discussed previously, the pelitic to semi-pelitic rocks comprising the kyanite-gneiss zone at the Cima di Gagnone area have relatively uniform mineralogies, although modal abundances of the coexisting phases vary across individual rock layers. In general, kyanite and coarse-grained garnets represent relicts of the older eclogite-facies assemblages. Amphibolite-facies overprinting of the pelitic rocks is characterized by new growth of biotite and plagioclase \pm muscovite, and is often associated with penetrative deformation resulting in a well-defined mineral foliation.

The compositions of the coexisting mineral phases from representative samples of the various rock types have been determined by electron microprobe analysis. Representative point analyses are given in App. I together with analytical and recalculation procedures.

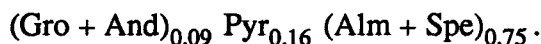
2.4.1. GARNETS

Two size distributions of garnet are generally present in these schists. Coarse grains contain numerous inclusions in the cores and have clear, inclusion-free rims. The smaller garnet grains are inclusion-free and often occur as isometric crystals. The compositions of garnets from representative samples from each of the mineralogical and textural pelitic groups are shown in Fig. 2.6 and are tabulated in App. I. In general a slight depletion in the grossular-component and an enrichment in the almandine component is observed from core to rim in both size distributions. With the exception of sample CL 11a, the finer-grained garnets tend to have more Fe-enriched rims than the rims of the coarse-grained garnets of the same sample (e.g. see samples CL 12, CH

278; Fig. 2.6). Although the garnet compositions vary considerably from core to rim, no systematic zoning patterns could be observed by microprobe point analysis of profiles through the coarse-grained garnets. A general composition of:



corresponds to the cores of the garnets (see App. I), whereas the rims can be characterized by the composition:

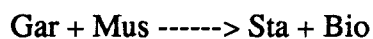


These compositions have been used for GR 1 and GR 2 respectively in the isotope-fractionation models and the whole-rock reactions [3.1] and [3.3], which are discussed in Chapter 3.

With the exception of samples CL 11a and CL 4a, no distinction can be seen between the kyanite-bearing- and the kyanite-free schists, nor between samples of similar mineralogies but varying textures (e.g. see CH 99 and CH 278). However, the Ca-rich garnets of sample CL 4a may reflect the difference in whole rock composition (i.e. more granitic composition), as this sample is mica poor and more plagioclase rich than the others. The garnets in sample CL 11a are anomalous in that they are distinctly more Mg- and Ca-rich. Furthermore, the smaller grains show a compositional zoning becoming more Ca-rich from core to rim. This sample occurs as a pelitic inclusion in the mafic lens. The distinct garnet compositions and zoning may be a result of tectonic mixing during eclogite-facies metamorphism and deformation and/or chemical exchange with the more Mg- and Ca-rich mafic rocks.

These garnets are considerably more Fe-rich than garnets from the kyanite-eclogite core of the mafic lens, as reported by Heinrich (1983, 1986). In addition, the garnets from the mafic rocks show an opposite zoning pattern, whereby the rims are enriched in Mg relative to the cores. This difference in zoning may reflect the differences in prograde vs. retrograde crystallization as discussed below. Similar zoning patterns have been reported by Koons (1982) for garnets from Sesia Zone - type C eclogites (as defined by Coleman et al., 1965).

The increase in Fe-content from core to rim can be related to cation-exchange during the retrograde amphibolite-facies metamorphic event and subsequent cooling. Such Fe-enrichment may be related to the continuous reaction:



as shown in Thompson (1976, p. 413). The textural relationships in the more aluminous schists may correspond to such a reaction.

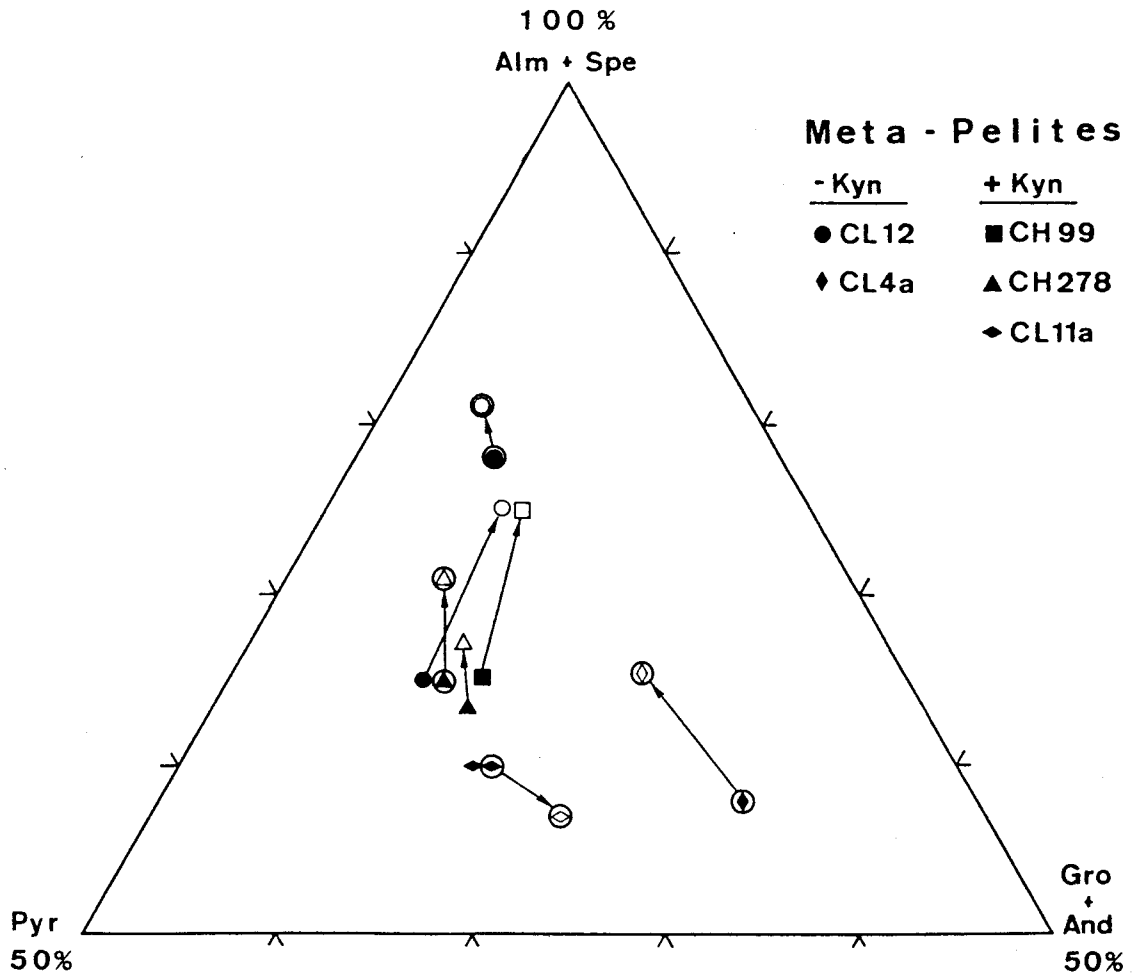


Fig. 2.6. Core (solid symbols) to rim (open symbols) compositional variations (in mole%) between coarse-grained and fine-grained (circled symbols) garnets from the texturally and mineralogically distinct metapelites at the Cima di Gagnone area. Samples CL 4a, CH 278 and CL 11a exhibit disequilibrium textures (see text and Figures 2.5 a-c).

2.4.2. BIOTITES

The biotite compositions of the meta-pelites show more distinct chemical variations among the texturally different rock types. The variations in compositions among the various rock types are shown in AFM-diagrams in Fig. 2.7a. This figure is simply a plot of the molar amounts of Al, Mg and Fe+Mn in biotite, garnet and, when present, staurolite. The compositions are not projected from K-feldspar or muscovite as these minerals are not always present in the rocks; however, these diagrams are not intended for thermodynamic applications. The chemical zoning of garnets coexisting with biotite are easily seen in the analogous CFM-diagrams in Fig. 2.7 b.

The biotite-muscovite schists which have equilibrium textures, have nearly identical garnet and biotite compositions (compare CL 12 and CH 99) despite their slight mineralogical differences (i.e. CL 12 contains no kyanite or staurolite). The biotite compositions from these completely recrystallized rocks are relatively homogeneous with X_{Mg} of approximately 0.50. These are distinctly more Fe- and Al-rich than the fine-grained randomly-oriented biotites in both the mica-poor kyanite schists (CL 11a,b, CH 278) and the plagioclase-rich biotite gneiss (CL 4a), all of which display disequilibrium textures (compare samples CH 278, CL 4a, CL 12). In sample CL 12, biotites occurring as inclusions in the cores of the coarse-grained garnets have similar compositions to those of the disequilibrium kyanite-schists (e.g. sample CL 12 Bio 4, App. I) The biotites in samples containing kyanite (e.g. CH 278, 99) tend to have slightly higher fluorine-contents (up to 0.5 wt %) than the kyanite-free schists.

As with garnet, biotite tends to become more Fe-rich during continuous, retrograde reactions involving aluminosilicates (Kyn, Sil, Sta) and muscovite (see Thompson, 1976). Thus, the more Mg-rich biotite and garnet may represent higher temperatures of crystallization. However, the temperature determined by cation exchange geothermometry for these rock show lower temperature of equilibrium than for the equilibrium texture rocks (see below). Alternatively, the differences in Al- and Mg-contents of the biotites could be a result of bulk compositional variations or of chemical disequilibrium effects during the amphibolite-facies metamorphic and deformational events.

Evidence for chemical disequilibrium can be seen in the AFM- and CFM-plots of sample CL 11a,b (Fig. 2.7 a,b). This Kyn-bearing metapelite occurs as an inclusion in the core of the mafic lens at outcrop CH 271 (see Fig. 2.3). It has a similar texture to sample CH 278, containing kyanite as relict skeleton-like poikiloblasts, which are replaced by fine-grained unoriented aggregates of biotite and plagioclase.

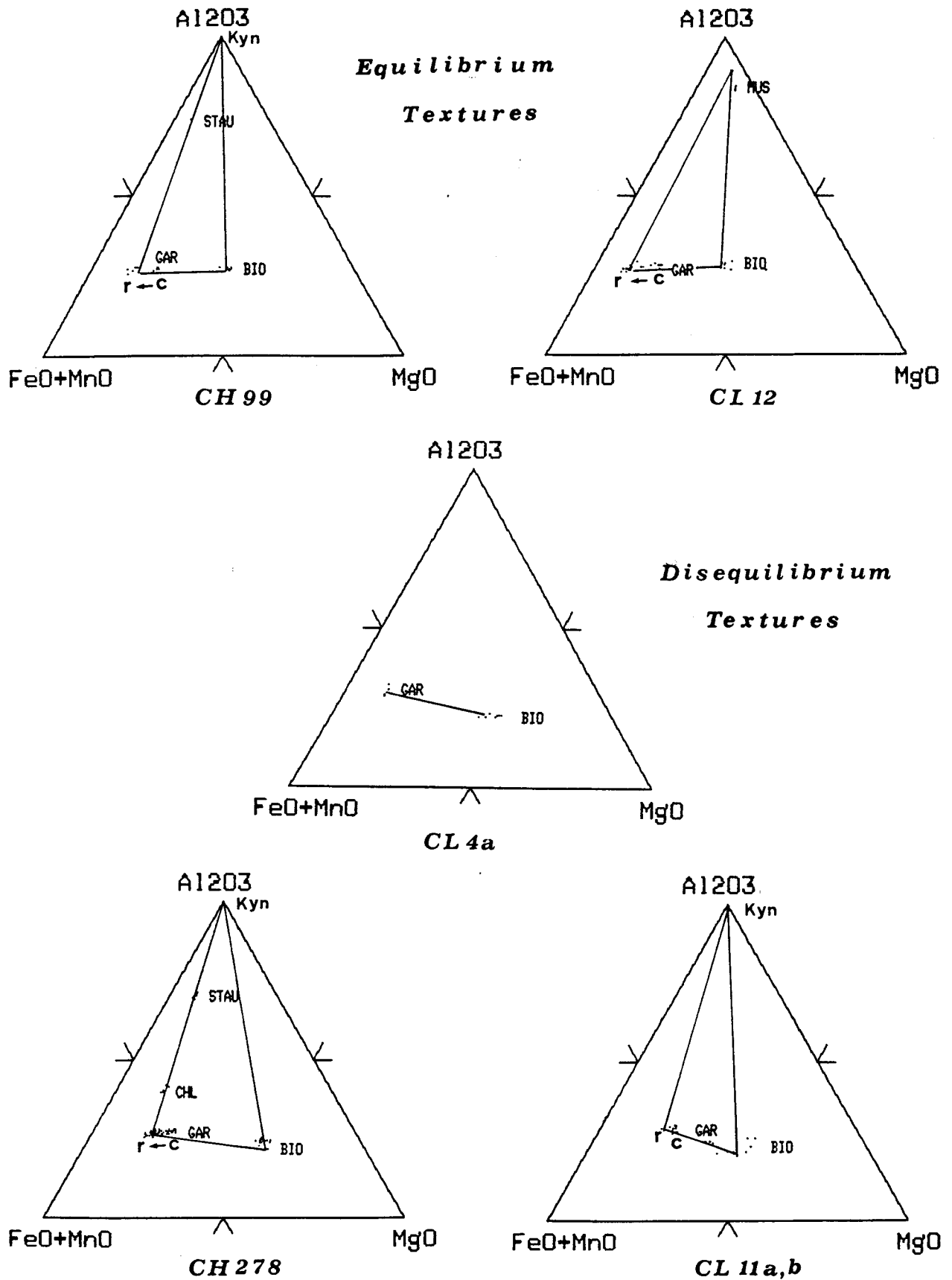


Fig. 2.7a. Al-, Mg- and Fe+Mn-contents (molar %) of coexisting biotite (Bio), Garnet (Gar) and staurolite (Stau) from the Cima di Gagnone area. Compositions have not been projected from any K-bearing phase and are therefore not thermodynamically valid.

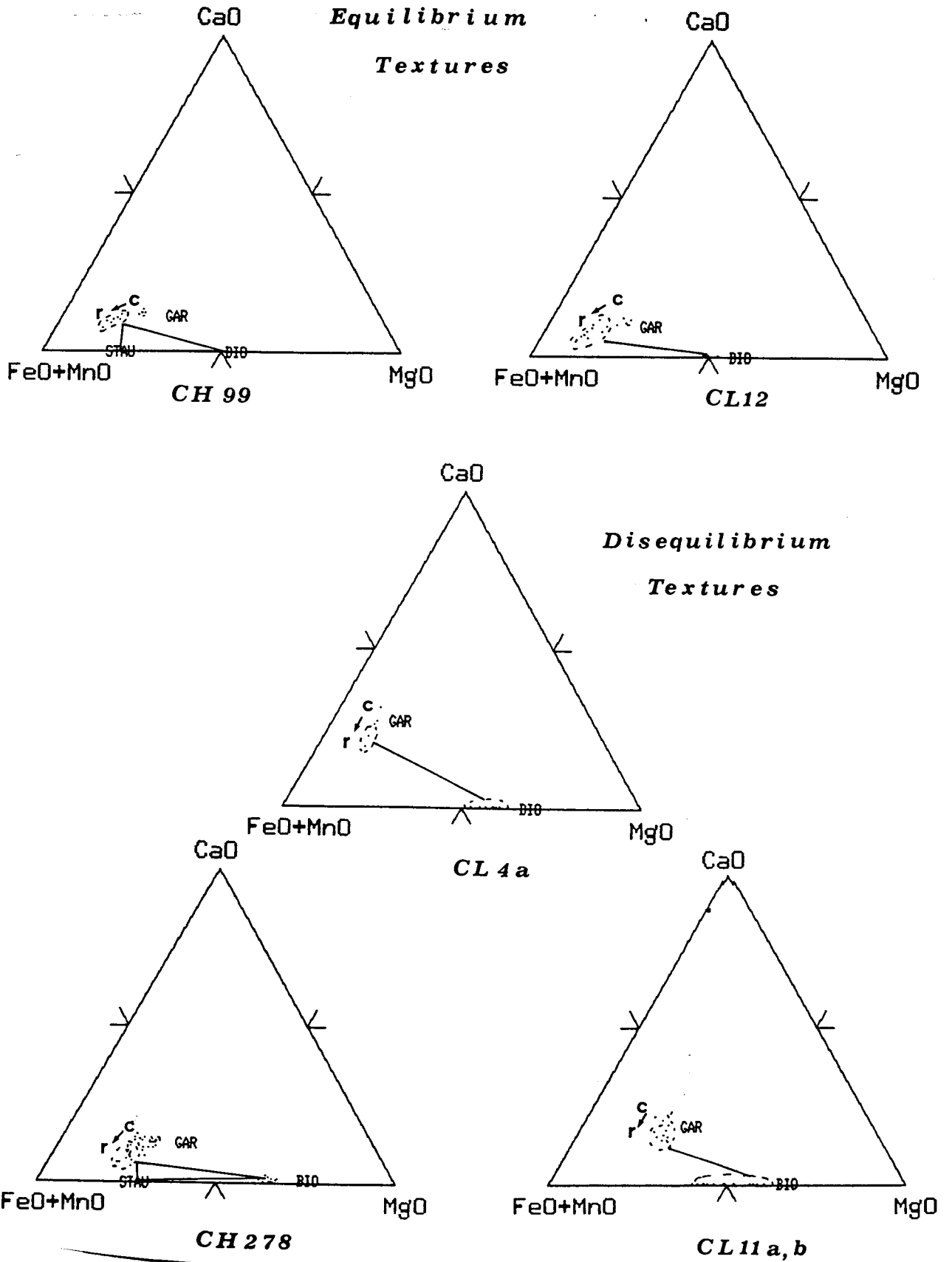


Fig. 2.7b. Ca-, Mg- and Fe+Mn-contents (molar %) of coexisting biotite (Bio), Garnet (Gar) and staurolite (Stau) from the Cima di Gagnone area.

The biotites of sample CL11a,b have heterogeneous compositions which can be divided into three groups according to variations in Al, Si and X_{Mg} (see also App. I). However, a correlation between these chemical differences and textural or spatial characteristics could not be found. The unusual zoning pattern of the garnets in this sample and anomalously high temperature estimated by Fe-Mg-partitioning geothermometry (see below) are further evidence for disequilibrium crystallization conditions.

2.4.3. GARNET-BIOTITE Mg-Fe EXCHANGE THERMOMETRY

Temperatures of Mg-Fe equilibration between garnet and biotite have been calculated for a pressure of 6 Kbar (Adams et al, 1975; Evans and Trommsdorff, 1974; Pfeiffer, 1978, 1981), using the experimentally determined cation-exchange geothermometer of Ferry and Spear (equation 7, 1978), and using the geothermometer of Goldman and Albee (equation 9, 1977) calibrated against $^{18}O / ^{16}O$ -fractionations for quartz-magnetite. These two different geothermometers have been chosen because one is based on experimental calibrations (i.e Ferry and Spear) and the other is based on isotopic fractionations. Values of $\ln K_D$, where $K_D = [(Mg / Fe)_{Gar} / (Mg / Fe)_{Bio}]$, for garnet-biotite pairs were obtained using coexisting garnet-rim and biotite-rim compositions from representative samples from each of the texturally and mineralogically distinct groups. Average values of $\ln K_D$ are shown in Figure 2.8 and are plotted against $10^4 / T$ (°K) and T (°C) obtained from the different calibrations. The $\ln K_D$ -values, which vary from -1.45 to -1.90, would correspond to temperatures ranging from 740 °C (Ferry and Spear calibration) to 450 °C (Goldman and Albee). The "error bars" of Figure 2.8 represent the scatter in data within a single rock sample and simply represent high- and low-values of $\ln K_D$ and temperature respectively. $\ln K_D$ -values ranging from -0.64 to -1.14, not shown in Figure 2.8, were obtained from sample CL 11a,b (disequilibrium-textured Kyn-schist) and correspond to temperatures as high as 1240 °C. These anomalous values substantiate the previous conclusion that chemical equilibrium was not obtained in this sample.

As can be seen temperature estimated by the Goldman and Albee-geothermometer, which corrects for Ca- and Mn- contents in garnet as well as in biotite, are nearly 100°C lower than those calculated for the pressure-dependent geothermometer of Ferry and Spear. These discrepancies in temperatures estimated by the different geothermometers are discussed in the original studies (Goldman and Albee, 1977; Ferry and Spear, 1978; see also Thompson, 1976) and may be an effect of isotopic re-equilibration during cooling or the inaccuracy of the quartz-magnetite calibration of Bottinga and Javoy (1973) (see Goldman and Albee, 1977, p. 762-3). Further problems of the use of

Mg-Fe partitioning between garnet and biotite as a geothermometer are discussed by Essene (1982).

There are many possible explanations for the large scatter in estimated temperatures from the metapelite at the Cima di Gagnone area: errors and uncertainties in the raw microprobe data and the corrected, normalized data; uncertainties in the geothermometric calibrations; unknown effects of Fe^{3+} on the calibrations; and/or chemical disequilibrium effects in the rocks. The slightly higher $\ln K_D$ - values obtained for the kyanite-bearing schists may indicate lower temperatures for mineral reactions involving kyanite and garnet to form staurolite (see Thompson, 1976). However, the large variations in chemical compositions of the mineral phases together with the large scatter in calculated temperatures suggests that chemical equilibrium was not obtained in these rocks. Furthermore, local isotopic disequilibrium in these rocks is indicated by large variations in mineral fractionations and discordant isotopic temperature estimates, which is discussed in detail in Chapter 3.

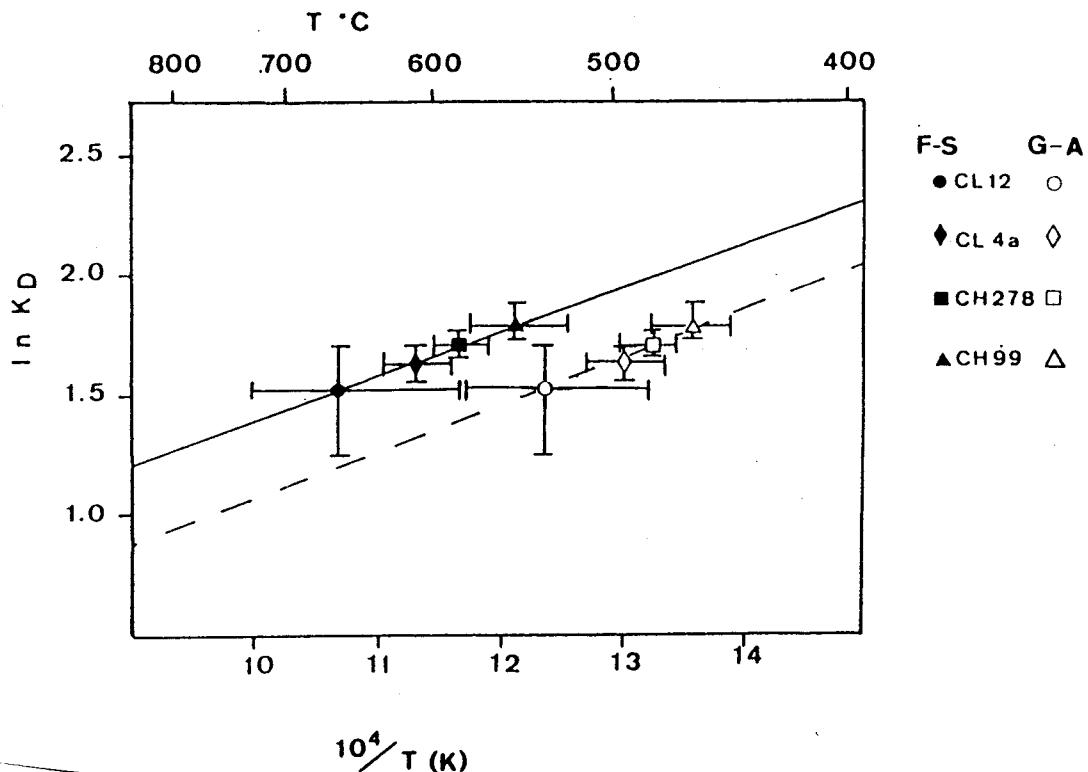


Fig. 2.8. Variations in averaged values of $\ln [(Mg/Fe)_{Gar} / (Mg/Fe)_{Bio}]$ versus $10^4 / T$ ($^{\circ}K$) between the various metapelites at the Cima di Gagnone area. "Error bars" represent the scatter in data within single rock samples indicating high- and low-temperature and $\ln K_D$ -values, respectively. The solid line represents temperatures corresponding to equation 7 of Ferry and Spear (1978) for a pressure of 6 Kbars, and the dashed line represents temperatures corresponding to the pressure-independent equation 9 of Goldman and Albee (1978).

2.4.4. SUMMARY

The contrasting mineralogical and textural characteristics of the mafic and pelitic rocks at the Cima di Gagnone area indicate at least two stages of recrystallization during an Alpine metamorphic evolution. An *Early-Alpine, High pressure metamorphic event* (A1--> E), possibly related to early Cretaceous subduction, is recorded by relict *eclogite-facies* mineral assemblages of *Omp + Gar + Qtz + Kyn*, occurring in the cores of isolated mafic lenses and boudinaged layers within semi-pelitic to pelitic schists and gneisses. Mineral inclusions in the eclogite-facies minerals and consideration of phase relations of the mafic rocks throughout the Adula Nappe suggest that the mafic eclogite assemblages were produced by *dehydration reactions* in pre-Alpine amphibolites (Heinrich 1983,1986). During *subsequent Tertiary exhumation*, deformation and fluid infiltration under *amphibolite-facies* metamorphic conditions (E --> A2) resulted in *re-hydration* and transformation (back) to amphibolite.

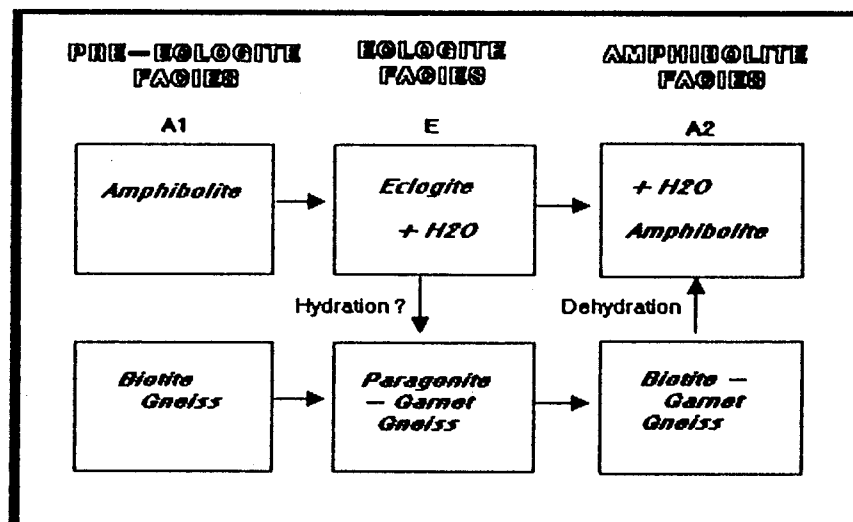


Fig. 2.9. Schematic diagram depicting the metamorphic evolution of the mafic and pelitic rocks at the Cima di Gagnone area.

In contrast to mafic rocks, the *semi-pelitic to pelitic schists and gneisses* exhibit nearly complete *recrystallization* during the later *Tertiary amphibolite-facies metamorphic event* (E --> A2). Based on relict corona textures in an isolated pelitic inclusion in a mafic lens, Heinrich (1982, 1983) proposed that the transformation from *eclogite-facies* mineral assemblages *Qtz + Phe + Par + Gar ± Kyn* to *amphibolite-facies* assemblages *Qtz + Bio + Plg ± Mus* involved *dehydration* reactions. Dehydration reactions in metapelites may have produced and controlled the

water responsible for this later amphibolisation event. The metamorphic evolution of both the metapelites and metabasites of the Cima di Gagnone area of the Cima Lunga Nappe (S. Adula) are summarized in Fig 2.9. On hand from oxygen isotope data, quantitative models and a discussion of fluid-rock evolution of these rocks are presented in Chapter 3.

Amphibolite-facies deformation and syn-kinematic recrystallization in the majority of the metapelites is indicated by a uniform grain-size, straight grain boundaries between quartz and plagioclase, and by a well pronounced schistosity, defined by parallel-oriented mica flakes and kyanite crystals. Varying degrees of chemical homogeneization is indicated by zonation in garnet and inhomogeneous biotite compositions. Geothermometric calculations of cation-exchange between garnet and kyanite, at a pressure of 6 Kbar, yield a large variation in temperature estimates, ranging from 550 to 660 °C for the amphibolite-facies metamorphic event.

CHAPTER 3

STABLE ISOTOPE DATA AND MODELS OF FLUID-ROCK INTERACTION

The major minerals from 16 representative samples and three veins have been separated and analyzed for ^{18}O . The ^{18}O compositions relative to SMOW (standard mean ocean water) are listed in Table 1 and are represented graphically in Fig. 3.1. The relative position (to the mafic lens) of the samples are shown in Fig 2.3.

3.0. SAMPLE PREPARATION AND ANALYTICAL METHODS

Standard heavy liquid and magnetic techniques were used to separate the minerals from crushed hand specimens (2-10 cm thick). All samples were purified by hand picking. Quartz samples were further cleaned by treatment with cold hydrofluoric acid. All samples were ground to $>125\ \mu\text{m}$, with the exception of garnet and kyanite which were ground to ultrafine powders. The purity of the samples was at least 90%.

Extraction was carried out at the Scottish Universities Research and Reactor Center (SURRC) and at the USGS in Menlo Park, California. Oxygen was extracted from the minerals and powders using ClF_3 . The oxygen was converted to CO_2 by reaction with heated carbon, as described by Taylor and Epstein (1962). Oxygen yields of the samples reported in this study were $>90\%$. The isotopic ratios of the minerals and whole rock powders were determined by mass spectrometric analysis and are reported as $\delta^{18}\text{O}$ -values per mill relative to SMOW. The overall reproducibility of the $\delta^{18}\text{O}$ analyses is approximately $\pm 0.2\ \text{‰}$. The δ value for the NBS-28 African sand standard in both laboratories was $9.64\ \text{‰}$.

3.1. OXYGEN ISOTOPE DATA

3.1.1. METABASITES

$\delta^{18}\text{O}_{\text{Qz}}$ from the eclogitic core of the mafic lens (CH 271), quartz segregation veins (CL 17) and symplectite (CH 265) lie in a narrow range from $7.8\ \text{‰}$ to $8.2\ \text{‰}$, with a relatively constant $\delta^{18}\text{O}_{\text{WR}}$ of $5.5\ \text{‰}$. The amphibolites form two distinct groups. The amphibolitized rim (CL 6) has an $\delta^{18}\text{O}_{\text{WR}}$ composition similar to that of the eclogitic core ($5.4\ \text{‰}$); whereas the amphibolite layers which form the tail of the mafic lens

have relatively constant $\delta^{18}\text{O}_{\text{WR}}$ and $\delta^{18}\text{O}_{\text{Plg}}$ compositions of 6.5‰ and 7.9 - 8.4‰, respectively.

3.1.2. METAPELITES

The metapelites form two isotopically distinct groups. Those in the immediate vicinity of the mafic lens (samples CL 4A, CL 11A, CL 11B, CL 12, CL 13, CH 40, CH 278) represent an isotopically "light" group (P1), in which $\delta^{18}\text{O}_{\text{WR}}$ varies between 6.0‰ and 7.6‰. $\delta^{18}\text{O}_{\text{Qz}}$ in this group ranges from 8.6‰ to 9.4‰. In contrast, the metapelites (P2), which are located at least 30 m away from the mafic rocks (samples CL 9, CH 99, CL 25, CL 30) have $\delta^{18}\text{O}_{\text{WR}}$ and $\delta^{18}\text{O}_{\text{Qz}}$ compositions which range from 8.4‰ to 10.2‰ and 10.4‰ and 11.8‰, respectively. In the former group, the isotopic compositions of comparable mineral phases (e.g. Qtz, Gar, Mus, Plg; see Table 2.1 for mineral abbreviations), as well as whole rock ^{18}O -values, only vary by approximately 2‰ from those of the metabasites.

3.1.3. DISCUSSION

Although the compositions of the mafic rocks lie within the range of those known for basalts (e.g. Taylor and Epstein, 1962; Garlick and Epstein, 1967; Gregory and Taylor, 1981; Pineau et al, 1976) and some eclogites (e.g. Javoy, 1971; Vogel and Garlick, 1970; Agrinier et al, 1985; Javoy and Allegre, 1967), the values for the pelitic rocks are depleted in ^{18}O relative to known metasediments of similar metamorphic grade (e.g. Taylor and Epstein 1962a, b; Taylor et al 1963; Garlick and Epstein, 1967; Rye et al, 1976). Early studies of regionally metamorphosed metasediments have shown that ^{18}O of the coexisting mineral phases, and subsequently $\delta^{18}\text{O}_{\text{WR}}$, tend to decrease with increasing grade of metamorphism and approach igneous isotopic compositions (e.g. Silverman, 1951; Taylor and Epstein, 1962a, b; Garlick and Epstein, 1967). For a compilation of the range of $\delta^{18}\text{O}$ -values of various rock types see Graham and Harmon (1983).

The metapelites at the Cima di Gagnone area show even greater depletion in $^{18}\text{O}_{\text{WR}}$ and $\delta^{18}\text{O}_{\text{Qz}}$ than similar rock types in the above studies (see Fig. 3.2). However, the isotopic compositions of the P2-Pelites (CL 9, CH 99, CL 25, PB) are similar to those of isotopically constant pre-Mesozoic rocks from the Central Swiss Alps reported by Hoernes and Friedrichson (1980). In their study Hoernes and Friedrichson (1980, p. 21-22) attribute the depletion in ^{18}O and the large-scale isotopic homogenisation to pervasive interaction with magmatic fluids during a pre-Alpine (Hercynian or older)

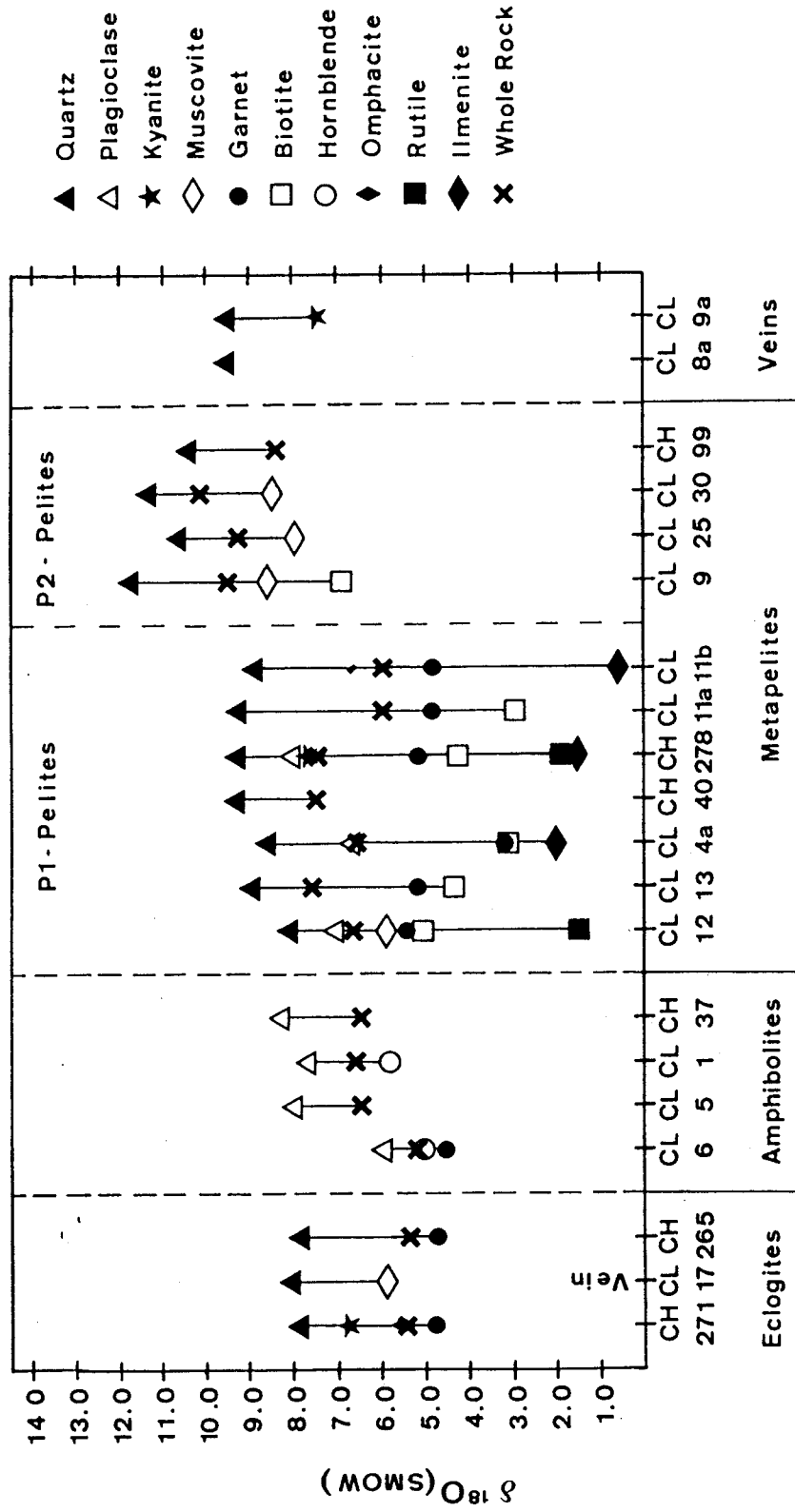


Fig. 3.1: $\delta^{18}\text{O}$ -compositions (relative to SMOW) of the co-existing minerals from the various rock types at the Cima di Gagnone area. P1-pelites represent metapelites in the vicinity of the mafic lens at outcrop CH 271; whereas P2-pelites represent metapelites located at least 30 m away from the mafic rocks. Relative locations of samples are shown in Figure 2.3.

TABLE 3.1

Isotopic compositions of coexisting mineral phases and whole rocks from the Cima di Gagnone area. Mineral modes determined either by point-counting or optical estimation (whole numbers). Sample locations are shown in Fig. 2.3.

Textural and Mineralogical Distinctions:

(a) equilibrium textures - Kyn; (b) disequilibrium textures - Kyn; (c) equilibrium textures + Kyn; (d) disequilibrium textures + Kyn, (e) disequilibrium textures, mafic contact to pelite inclusion (sample Ch278); (f) fresh Kyn-eclogite; (g) symplectite; (h) fine-grained amphibolite; (i) coarse-grained amphibolite

SAMPLE	MINERAL PHASE	$\delta^{18}\text{O}$ (SMOW) ‰	δD (SMOW) ‰	MODAL %	GRAIN-SIZE (mm)
<i>P₁ - METAPELITES</i>					
CL12 (a)	quartz	8.19		25.5	0.14-1.00
	plag. (An ₂₀)	7.25		35.6	0.15-1.00
	biotite	5.20	-62	23.7	0.15-2.00
	muscovite	5.89	-68	6.0	1.00-5.00
	garnet	5.50		10.0	0.10-3.00
	rutile	1.48		1.0	0.50-0.15
	ilmenite			0.1	0.05-0.25
	whole rock	6.70			
CL13 (a)	quartz	9.00		30.2	0.30-3.50
	biotite	4.44		21.5	0.20-5.00
	garnet	5.25		9.8	0.10-3.00
	whole rock	7.57			
CL4a (b)	quartz	8.58		38.4	0.20-3.00
	plag. (An ₃₀)	6.70		46.3	0.50-2.00
	biotite	3.30	-78.5	12.3	0.20-1.50
	garnet	3.34		0.9	0.10-0.50
	rutile			0.2	0.10-0.20
	ilmenite	1.90		1.9	0.10-1.00
	whole rock	6.89			
CH40 (c)	quartz	9.4		35.0	0.50-1.50
	whole rock	7.6			
CH278 (d)	quartz	9.41		35.1	0.15-2.00
	plag. (An ₂₀)	8.13		33.1	0.10-0.50
	kyanite	7.71		1.0	1.00-3.00
	biotite	4.33	-69	14.5	0.10-1.00
	garnet	5.17		14.9	0.10-2.75
	staurolite			0.2	0.05-0.20
	rutile	1.93		0.3	0.05-0.15
	ilmenite	1.66		0.8	0.05-0.20
	whole rock	7.55			
CL11a (d)	quartz	9.31		33.8	0.10-3.00
	biotite	3.03	-67	12.6	0.10-1.00
	garnet	4.81		20.5	0.10-3.00
	whole rock	5.92			

TABLE 3.1 (continued)

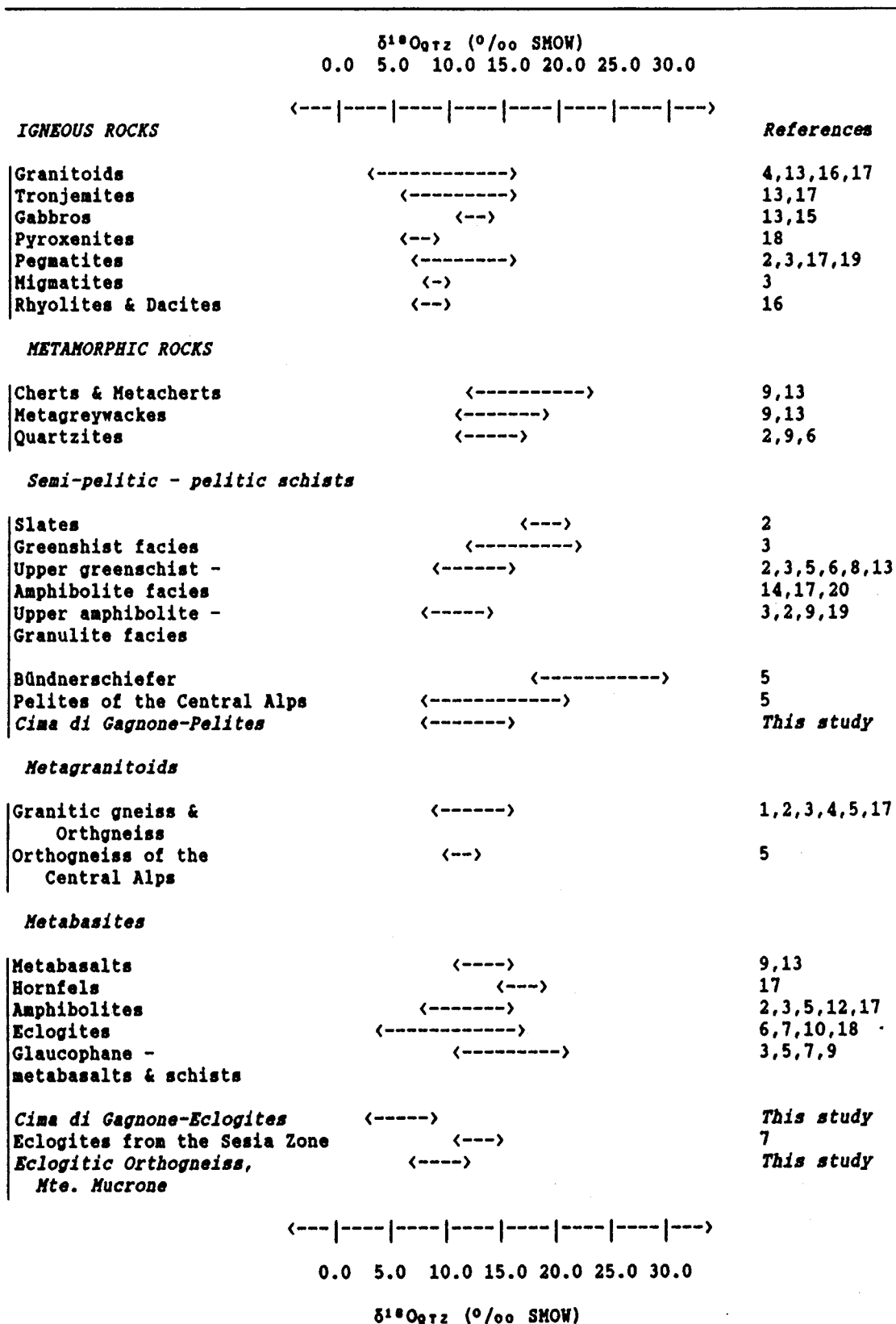
SAMPLE	MINERAL PHASE	$\delta^{18}\text{O}$ (SMOW) ‰	δD (SMOW) ‰	MODAL %	GRAIN SIZE (mm)
P-2 METAPELITES					
CL9 (a)	quartz	11.76		35.0	0.10-2.00
	biotite	6.86		22.0	0.20-3.00
	muscovite	8.56		5.0	0.50-3.50
	garnet	8.24		9.0	0.10-3.50
	whole rock	9.54			
CL25 (a)	quartz	10.61		38.0	0.10-2.50
	biotite			8.0	0.10-2.00
	muscovite	7.85		20.0	0.10-2.00
	whole rock	9.28			
CL30 (a)	quartz	11.35		37.0	0.15-2.20
	biotite			10.0	0.15-3.00
	muscovite	8.50		14.0	0.50-5.00
	whole rock	10.30			
CH99 (c)	quartz	10.40		40.0	0.25-2.00
	whole rock	8.40			
METABASITES					
CH271 (f)	quartz	7.83		10.0	0.10-1.50
	omphacite	5.55		35.0	0.10-1.00
	garnet	4.79		35.0	0.10-1.50
	kyanite	6.76		10.0	0.50-2.50
	whole rock				
CH265 (g)	quartz	7.83		10.0	0.10-1.00
	garnet	4.85		15.0	0.10-1.20
	whole rock	5.43			
CL6 (h)	quartz			5.0	0.10-1.50
	plag (An ₄₀)	6.09		30.0	0.10-0.25
	hornblende	5.08	-60	60.0	0.10-0.50
	garnet	4.65		0.5	0.10-0.25
	whole rock	5.33			
CL5 (i)	plag (An ₃₀)	8.0		40.0	0.50-2.50
	whole rock	6.5			
CL1 (i)	plag (An ₃₀)	7.85		30.0	0.10-1.50
	hornblende	5.73	-74	60.0	0.50-5.00
	biotite			5.0	0.50-2.00
	whole rock	6.56			
CL37 (i)	plag (An ₃₀)	8.40		35.0	0.50-2.50
	whole rock	6.50			
CL11b (e)	quartz	8.98		20.8	0.10-3.00
	garnet	4.82		27.4	0.10-3.50
	ilmenite	0.63		1.6	0.10-0.50
	whole rock	5.95			
	whole rock	5.92			

TABLE 3.1 (continued)

SAMPLE	MINERAL PHASE	$\delta^{18}\text{O}$ (SMOW) o/oo	δD (SMOW) o/oo	MODAL %	GRAIN SIZE (mm)
<i>ECLOGITE-FACIES VEINS</i>					
CL17	quartz	8.17			
	muscovite	5.85	-28		
CL8a	quartz	9.60			
CL9a	quartz	9.61			
	kyanite	7.48			

metamorphic event, and suggest that the isotopic compositions of these rocks were unaffected by subsequent Alpine metamorphism. These conclusions assume that the pre-metamorphic precursor rocks had isotopic compositions similar to marine sediments ($\delta^{18}\text{O}_{\text{Qz}} = 20\text{‰}$). However, if the detrital material in the original sediment were mainly derived from igneous or meta-igneous rocks, their pre-metamorphic isotopic compositions could conceivably have been significantly lower. Interaction with a magmatic fluid phase may also have occurred, but less fluid would be required to produce the homogeneous isotopic compositions of these rocks in the Central Alps. Lower $\delta^{18}\text{O}$ values for greywackes and some shales (avg $\delta^{18}\text{O} = 13\text{‰}$) have been reported by Margaritz and Taylor (1976) from the Franciscan Formation of California. Although no mention is made of the actual source rocks for these sediments, Margaritz and Taylor (1976, p. 221-222) do mention that quartz appears to retain its original isotopic composition and is only slightly more ^{18}O -rich than quartz in average igneous rocks. If the isotopic composition of quartz in the Franciscan Formation represents 'old', unchanged values, their preservation may be indicative of a diffusion-controlled mechanism of isotopic exchange and incomplete re-equilibration during metamorphism. The presence of such preserved values must be taken into consideration in the frequent use of quartz as an isotopic geothermometer.

Large scale interaction with magmatic fluids and/or an igneous-dominated detrital source for the original sediments could be considered for the overall depletion of ^{18}O in the metapelites. However, this would not explain the even greater ^{18}O -depletion observed in the P1-pelitic rocks in direct contact with the mafic lens nor the near isotopic homogenisation between the two different rock types. Assuming that prior to Alpine metamorphism, all the pelitic rocks in the Gagnone area had relatively similar

Fig. 3.2: Variations in $\delta^{18}\text{O}_{\text{Qtz}}$ from various rock types.

Data Sources:

1.Frey et al,1976; 2.Garlick & Epstein,1967; 3.Rye et al,1976; 4.Taylor,1977; 5.Hoernes & Friedrichsen,1980; 6.Matthews & Schliestedt,1984; 7.Desmon & O'Neil,1978; 8.Hoernes & Friedrichson,1978; 9.Taylor & Coleman,1968; 10.Agrinier et al,1985; 11.Schwarz et al,1970; 12.Rumble et al,1982; 13.Magaritz et al,1976; 14.Rumble & Spear,1983; 15.Taylor & Epstein,1962; 16.Taylor,1968; 17.Shieh & Taylor,1970; 18.Vogel & Garlick,1970; 19.Wilson et al,1970; 20.Taylor et al,1963.

chemical and isotopic composition, the subsequent shift in $\delta^{18}\text{O}$ and the approach to isotopic homogenisation indicates further fluid/rock interaction during Alpine metamorphism. In light of the petrological data and conclusions of Heinrich (1986), as well as the spatial relations of the more depleted P1-metapelites, interaction with a locally-derived fluid during dehydration of the mafic rocks under eclogite-facies conditions must be investigated. This possibly is inspected in detail below.

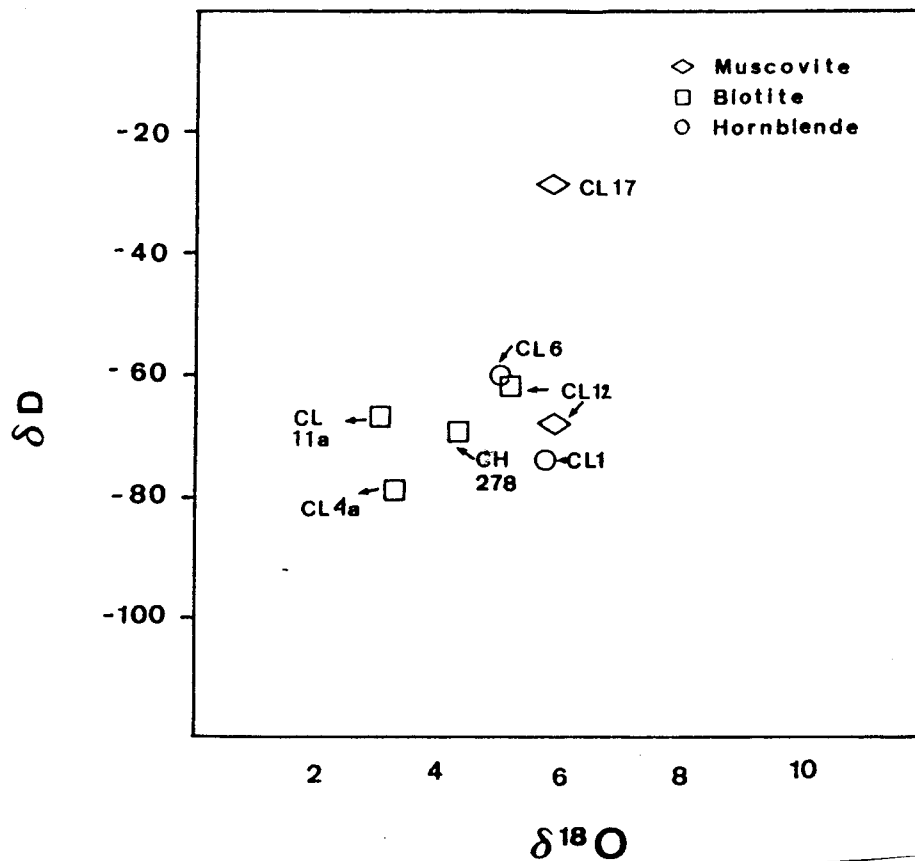


Fig. 3.3. Variation in δD with $\delta^{18}\text{O}$ of coexisting hydrous minerals of the metabasites and metapelites at outcrop CH 271 (see Figure 2.3 for sample locations).

3.2. HYDROGEN ISOTOPE DATA

The hydrogen isotope compositions of biotite, muscovite and hornblende are shown in Table 1 and are plotted against oxygen isotopic compositions in Fig. 3.3. δD (Bio) of the different samples fall within a narrow range from -62‰ to -79‰. The two muscovite samples are considerably different: a δD of -28‰ was obtained for the

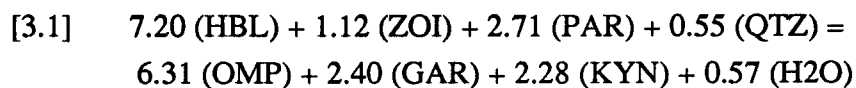
phengite in the eclogite-facies quartz segregation vein (CL17) from the core of the mafic lens, whereas the amphibolite-facies muscovite from sample CL12 shows a δD of -68‰. The muscovite from sample CL12 is anomalous in that it is more enriched in deuterium than the coexisting biotite. However, as discussed below, this rock sample also exhibits discrepancies in oxygen fractionations, which may indicate local isotopic disequilibrium and/or a complex fluid history.

The δD -values from these rocks fall within a range of hydrogen isotope compositions reported from metamorphic rocks from the Western Alps (see e.g. Frey et al. 1976), and are consistent with hydrogen isotope compositions of various hydrous minerals reported from other gneisses in the Central Alps and the Oetztal Alps (Hoernes and Friedrichson, 1978; 1980). Hoernes and Friedrichson concluded that these δD -values of -60 to -65 represent original, pre-Alpine isotopic compositions of biotite and that these data confirm their interpretation that large-scale fluid-rock interaction did not occur during the Alpine metamorphism.

3.3. ECLOGITE-FACIES FLUID-ROCK INTERACTION EVENT (A1-->E)

3.3.1. *A MODEL OF RAYLEIGH DISTILLATION AND DEHYDRATION OF AMPHIBOLITE*

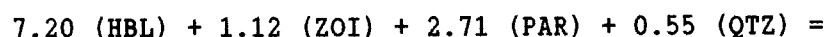
Based on a Rayleigh distillation mechanism of fluid-rock interaction as presented by Rumble (1979, 1982), isotopic fractionation during dehydration of amphibolite has been modelled. The dehydration of amphibolite to form Omp-Gar eclogite (A1-->E; see Fig.3.4) can be described by a simplified reaction, using the mineral compositions shown in Table 3.2:



Oxygen units have been used in this mass balance calculation so that the amount of each mineral is expressed by the number of oxygen atoms it contains, as described by Thompson et al (1982). Since the volume of a silicate is nearly proportional to its number of oxygen atoms, a direct comparison of the relative changes in modal abundances during the reaction is made possible. Somewhat generalized mineral compositions of the phases involved are given in Table 3.2, but these correspond well with actual mineral compositions presented in this study (see Chapter 2) as well as in Heinrich (1983, 1986).

TABLE 3.2

Mineral phase compositions, mineral densities and molecular weights used in reaction [3.1]:



PHASE	NCFMASH-Composition	Molecular Weight (g/mole)	Density (g/cm³)
QTZ	SiO ₂	60.09	2.65
KYN	Al ₂ SiO ₅	162.03	3.55
OMP	Na _{0.5} Ca _{0.5} Al _{0.5} Mg _{0.5} Si ₂ O ₆	208.34	3.33
GAR	Ca _{0.48} Mg _{1.12} Fe _{1.4} Al ₂ Si ₃ O ₁₂	454.88	3.70
ZOI	Ca ₂ Al ₃ Si ₃ O ₁₂ (OH)	454.35	3.30
PAR	NaAl ₃ Si ₃ O ₁₀ (OH) ₂	382.19	2.85
HBL	NaCa _{1.5} Mg _{2.5} FeAl ₃ Si _{6.5} O ₂₂ (OH) ₂	817.74	3.30

Omphacite, garnet and hornblende compositions have been idealized from compositions reported by Heinrich (1983, 1986) for samples from the Adula/Cima Lunga Nappe. Garnet represents a composition similar to that of garnet rims from sample CH271 (Heinrich, 1986 p. 132). The hornblende composition has been generalized from the composition of amphibole in sample Ad 42-9-14 (Heinrich, 1986 p.136).

This reaction does not contradict the petrological observations presented by Heinrich (1983, Ch. 8.3; 1986), but differs from Heinrich's reaction (12) in that garnet occurs in reaction [3.1] above as a product phase. Heinrich (1986, p.144) omitted garnet from the Schreinemakers analysis in order to decrease the number of components necessary to describe the system (combining FeO + MgO), but argues that the main conclusions should not be affected by its omission. However, in order to quantitatively model the modal and isotopic changes occurring during the A1-->E event, all phases which are formed or consumed must be considered. Although garnet may also have been a product of pre-eclogite facies metamorphism, textural and chemical relationships indicate that at least the rims were formed during the A1-->E dehydration event. The actual pre-eclogite evolution of these rocks is difficult to specify since textural relationships have not been preserved and the precursor minerals occur only as relicts in the eclogite-facies minerals (see Heinrich, 1986 p.127-128). A reaction such as [3.1] above is therefore still highly hypothetical, but serves the purpose of illustration.

	PRE-ECLOGITE FACIES	ECLOGITE FACIES	AMPHIBOLITE FACIES
	$(A_1 \rightarrow E)$		$(E \rightarrow A_2)$
	$\delta^{18}O_{WR}$	$\delta^{18}O_{WR}$	$\delta^{18}O_{WR}$
MAFIC ROCKS	5.5‰	5.5‰	5.5-6.5‰
	Hbl Epi Par Qtz ± alb	Omp Gar Qtz Kyn ± hbl ± zoi ± par	Hbl Plg ± gar ± epi ± qtz ± bio ± chl

	DEHYDRATION ----->	HYDRATION ----->	
	Rayleigh Distillation	Infiltration	

	$\delta^{18}O_{WR}$	$\delta^{18}O_{WR}$	$\delta^{18}O_{WR}$
PELITIC ROCKS	? - 9.4‰	6.5-9.4‰	6.5-9.4‰
	? Qtz ? Plg ? Bio ? Mus ? Gar	Qtz Phe Par Gar ± kyn ± stau ?	Qtz Plg Bio Mus ± kyn ± stau ± gar ± ksp

	? HYDRATION ? ----->		DEHYDRATION ----->
	Infiltration ?		Rayleigh Distillation

Fig. 3.4: Summary of mineral assemblages, $\delta^{18}O_{WR}$ -compositions and mechanisms of fluid-rock interaction during the pre-eclogite- to eclogite-facies ($A_1 \rightarrow E$) and eclogite- to amphibolite-facies metamorphism ($E \rightarrow A_2$)

For simplicity and because of their internal consistency, fractionation factors from Bottinga and Javoy (1973) and Javoy (1979) have been chosen for all the mineral phases except for omphacite, which was taken from Matthews et al (1983). The presence of kyanite in the reaction poses a problem in the Rayleigh distillation model as no fractionation data (neither theoretical nor experimental) are available for the aluminosilicates. Few isotopic studies include analyses of kyanite; however, data from this study (see Fig. 3.1 and Table 3.1.), Hoernes and Friedrichsen (1980) and Garlick and Epstein (1967), show that next to quartz, kyanite tends to be more enriched in ^{18}O than the other phases occurring in these rocks (see Table 1.1). In the computations below, the isotopic effects of Rayleigh distillation on the phases in the rock have been calculated

without kyanite. This omission has the effect that the calculated isotopic compositions of the participating phases will be slightly more ^{18}O rich than if kyanite were included, but should not affect the main conclusions.

3.3.1.1. Computation method for Rayleigh Distillation

As mentioned in Chapter 1, Rayleigh distillation is a process by which a fluid phase is internally derived during devolatilization reactions. Once the fluid is produced, it is expelled and does not react with the rock again. The calculation of the isotopic fractionation during the dehydration reaction [3.1] follows the computation scheme presented by Rumble (1982, p. 335-340) and is summarized here for clarity (see also App. IIa). Using the general relationship presented by Craig (1953), Rumble has shown that, to a close approximation, the isotopic composition of the rock is equal to the product of the isotopic composition of each mineral ($\delta^{18}\text{O}_i$) and the atomic fraction of oxygen (X_i) in the mineral i relative to the total amount of oxygen in all the minerals, summed over all of the mineral phases:

$$\delta^{18}\text{O}_{\text{WR}} = \sum_i X_i \delta^{18}\text{O}_i \quad (3.1)$$

Similarly, the isotopic composition of the bulk fluid ($\delta^{18}\text{O}_{\text{Fl}}$) can be described by the product of the isotopic composition of each fluid species ($\delta^{18}\text{O}_f$) and the atomic fraction of oxygen (X_f) in species, f , relative to the total amount of oxygen in all the fluid species, summed over all of the fluid species:

$$\delta^{18}\text{O}_{\text{Fl}} = \sum_f X_f \delta^{18}\text{O}_f \quad (3.2)$$

Since reaction [3.1] involves pure H_2O , equation (3.2) reduces to :

$$\delta^{18}\text{O}_{\text{Fl}} = \delta^{18}\text{O}_{\text{H}_2\text{O}}.$$

Thus, at each increment of the reaction, and before the water is removed from the system, the isotopic composition of the system ($\delta^{18}\text{O}_{\text{Sys}}$) will be expressed by:

$$\delta^{18}\text{O}_{\text{Sys}} = X'_{\text{H}_2\text{O}} \delta^{18}\text{O}_{\text{H}_2\text{O}} + X'_{\text{WR}} \delta^{18}\text{O}_{\text{WR}} \quad (3.3)$$

where $X'_{\text{H}_2\text{O}}$ and X'_{WR} are the atomic fraction of oxygen in the fluid (pure H_2O) and the whole rock, respectively, relative to the total oxygen in the system (*fluid plus minerals*). Since the model reaction is given in O-units, the atomic fraction of oxygen in each of the participating phases (X'_i , $X'_{\text{H}_2\text{O}}$) is directly determined at each increment of the reaction:

$$O_{\text{Sys}} = \sum_i O_i + O_{\text{H}_2\text{O}} \quad (3.4)$$

where O_i and O_{H_2O} are the amount of mineral and water (in O-units), respectively, formed or consumed at each increment of the reaction, thus:

$$X'_i = O_i / O_{\text{Sys}} \quad (3.5a),$$

and

$$X'_{H_2O} = O_{H_2O} / O_{\text{Sys}} \quad (3.5b),$$

where X'_i is the atomic fraction of oxygen in mineral i relative to the *total oxygen* in all of the minerals *and* the fluid. Although O_i changes at each increment of the reaction, O_{H_2O} will remain constant because after each increment of the reaction, the water which forms is removed from the system.

Assuming that quartz (Qtz) equilibrates with each of the phases present (Q-i), the isotopic composition of the individual phases ($\delta^{18}O_i$) in the reaction have been determined using the relationship:

$$\delta^{18}O_i = \delta^{18}O_{\text{Qtz}} - \Delta_{\text{Qtz-i}} \quad (3.6)$$

and recalling that:

$$\Delta_{\text{Qtz-i}} = \delta^{18}O_{\text{Qtz}} - \delta^{18}O_i \approx (1000 \ln \alpha_{\text{Qtz-i}}) \quad (3.7)$$

(see Chapter 1), this relationship can be substituted into equation (3.1) and (3.2) so that:

$$\delta^{18}O_{\text{WR}} = \delta^{18}O_{\text{Qtz}} - \sum_{i \neq Q} X_i \Delta_{\text{Qtz-i}} \quad (3.8)$$

and

$$\delta^{18}O_{H_2O} = \delta^{18}O_{\text{Qtz}} - \Delta_{\text{Qtz-H}_2\text{O}} \quad (3.9).$$

Similarly, using the relationship presented in equation (3.3) the isotopic composition of quartz ($\delta^{18}O_{\text{Qtz}}$) will be given by:

$$\delta^{18}O_{\text{Qtz}} = \delta^{18}O_{\text{Sys}} + \sum_{i \neq Q} X'_i \Delta_{\text{Qtz-i}} + X'_{H_2O} \Delta_{\text{Qtz-H}_2\text{O}} \quad (3.10)$$

where X'_{H_2O} and X'_i are the atomic fraction of oxygen in H_2O and mineral i , respectively, relative to the total oxygen in the system (mineral *plus* fluid).

At this point in the calculation, the water is completely removed from the system and new values for X_i and $\delta^{18}O_{\text{WR}}$ are computed using equation (3.1)

$$\delta^{18}O_{\text{WR}} = \sum_i X_i \delta^{18}O_i \quad (3.1)$$

where X_i is now the atomic fraction of oxygen in mineral i relative to total oxygen in the rock (total minerals *only*). Thus, a full increment of the reaction and isotopic equilibration between the phases is complete and the same procedure is repeated for the next reaction increment. Reiteration continues until one of the reacting phase is exhausted.

3.3.2. RESULTS OF RAYLEIGH DISTILLATION COMPUTATIONS IN METABASITES

In the model mass-balance calculations of reaction [3.1], the progress of the reaction is determined here by a specified amount of omphacite (OMP) formed at each reaction increment, which by mass balance determines the amount of water liberated; both of these will be limited by the porosity of the rock. For basaltic rocks, a porosity of <1% will be assumed. At each increment of the reaction, all phases are allowed to chemically and isotopically equilibrate, after which the increment of H_2O is removed from the system. A large enough number of increments are chosen so that the reaction goes to completion and stops when one of the reacting phases is exhausted. The computer program used to calculate Rayleigh Distillation for reaction [3.1] is given in Appx. IIa.

3.3.2.1 Initial Parameters

The petrological studies of Ch. Heinrich (1983, 1986) have shown that P-T conditions of 600-700°C and 15-25 Kbar can be estimated for the eclogite-facies metamorphism in the Southern Adula Nappe. In the model calculations, an isothermal and isobaric case of 650 °C and 15 Kbar are considered. Inspection of reaction [3.1] shows that this reaction will not be sufficient to produce all the garnet present in the final eclogite (35 vol%). Although garnet does not occur as a reactant as written, its presence in the rock prior to the reaction must be assumed. Furthermore, it is assumed that prior to the A1-->E event, reactions in the rock were essentially water-conserving, as shown by Heinrich (1986). An initial composition of 45% HBL, 8% ZOI, 15% PAR, 19% GAR and 13% QTZ (equivalent to 100 O-units of model amphibolite), and an initial $\delta^{18}O_{WR}$ of 5.5 ‰ have been used.

3.3.2.2 Fluid-Rock Ratios

For every 0.5 O-units of OMP formed, 0.045 O-units (or moles) of H_2O are produced and correspond to 0.08 vol% of the rock (initial volume of the amphibolite is approximately 1060 ccm) at a constant temperature of 650 °C and a pressure of 15 Kbar,

using the Equation of State of Kerrick and Jacobs (1981) to calculate the molar volume of H_2O (see Appendix IIa). Thus, at each increment of the reaction, the instantaneous volumetric fluid to rock ratio (VolFR) will be 7.5×10^{-4} . If we take the mafic lens to be a sphere with a diameter of 4 m, its volume will be 33.5 m^3 , and a total of $2.52 \times 10^{-2} \text{ m}^3$ of water will be produced per increment of reaction.

With a starting composition as stated above, the reaction will stop upon exhaustion of paragonite, whereby a total of 35.6 O-units of OMP will be produced and 3.16 moles of H_2O (or 55.7 ccm) will be released per 100 O-units of rock. The final volume of the rock is approximately 903 ccm, which represents a 14.5% decrease in volume during dehydration and corresponds to nearly a 5% increase in whole rock density (from $\rho_i = 3.22 \text{ g/ccm}$ to $\rho_f = 3.38 \text{ g/ccm}$). This means that between 0.92 and 1.03 moles of H_2O will be released per kilogram of amphibolite that is dehydrated. Thus, a minimum of $5.3 \times 10^{-2} \text{ m}^3 H_2O / \text{m}^3 \text{ rock}$, or a total of $1.8 \text{ m}^3 H_2O$, and a maximum of $6.2 \times 10^{-2} \text{ m}^3 H_2O / \text{m}^3 \text{ rock}$, or a total of $2.1 \text{ m}^3 H_2O$ are produced upon complete dehydration of the 4 m in diameter lens. The mineral densities and molecular weights used in these calculations are given in Table 3.2.

3.3.2.3 Modal Changes and Isotopic Effects of Dehydration and Rayleigh Distillation

The effects of Rayleigh distillation on $\delta^{18}O$ of the whole rock (WR) and the minerals participating in reaction [3.1] are shown in Fig. 3.5 and are tabulated in App.IIa. The horizontal axis represents the progress of the reaction, which is simply the reaction increment, determined by a specified number of O-units of OMP formed during the reaction (see above). The $\delta^{18}O$ compositions of minerals, H_2O and WR are shown on the vertical axis on the top half of the diagram. The relative changes in the modal amounts of the participating phases are shown on the vertical axis on the lower half of the diagram. It can be seen that $\delta^{18}O$ of the coexisting phases and WR decrease by less than 1‰ during the reaction. These results are similar to those described by Rumble (1979,1982) for devolatilization reactions in calc-silicate rocks, and supports his conclusions that devolatilization reactions alone (i.e. no simultaneous infiltration) are not sufficient to produce large shifts in $\delta^{18}O$. This is to be expected as the number of O-atoms which leave the rock as H_2O per increment are nearly negligible (only 0.1% of the entire system) compared to the number of O-atoms which remain behind in the mineral phases.

RAYLEIGH DISTILLATION

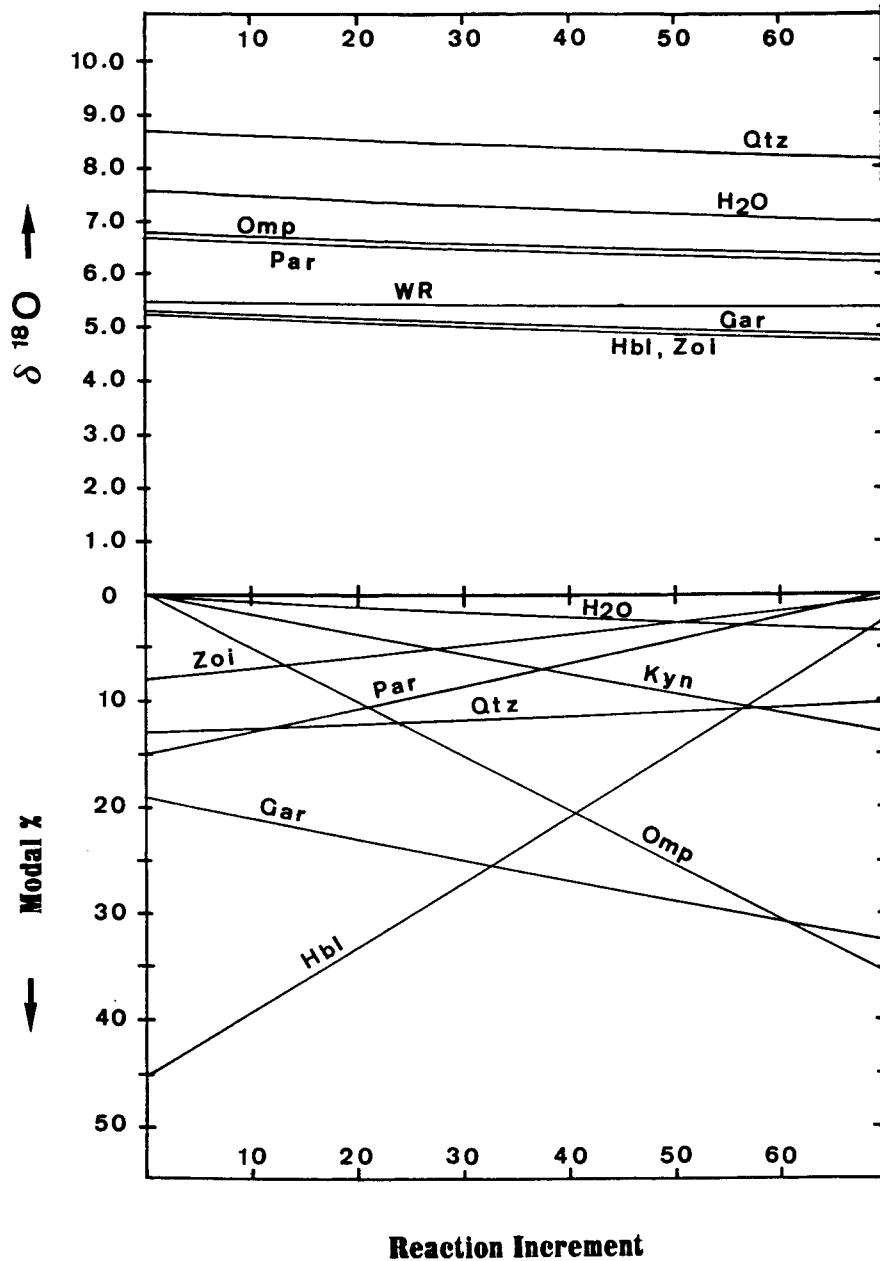
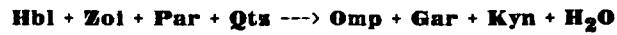
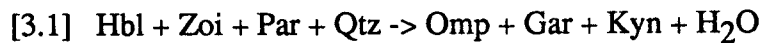


Fig. 3.5: Results of computer modelling (see App. IIa) of Rayleigh Distillation during dehydration of amphibolite to produce eclogite (A1 \rightarrow E) by reaction [3.1] (see text). Mineral compositions, molecular weights and densities are given in Table 3.2. The results are for isothermal and isobaric conditions of 650°C and 15 Kbar. Each reaction increment corresponds to the formation of 0.50 O-units of omphacite and the release of 0.045 O-units of H₂O. See Table 2.1 for an explanation of the abbreviations used.

It should be noted that the starting mineralogical composition of the amphibolite was chosen such that the final calculated modes corresponded roughly to actual modes seen in the rock. This allows a direct comparison between the calculated isotopic compositions of the mineral phases and those measured (compare Fig. 3.5 and Table 3.1, samples CH271, CH265, CL17). The predicted isotopic compositions of the coexisting phases are slightly higher than those measured, but as discussed earlier this is most likely a result of the omission of kyanite in the model calculation.

3.3.2.4 Summary

The dehydration of amphibolite to form kyanite-bearing eclogite (A1 → E) can be described by the simplified reaction



(see also Heinrich, 1986). Based on the incremental computation scheme proposed by Rumble (1979, 1982), the fluid released by this reaction has been modelled by a mechanism of Rayleigh distillation.

Calculations of dehydration and Rayleigh distillation by reaction [3.1] at a pressure of 15 Kbar and a temperature of 650°C have shown that approximately 3.2 moles of H₂O (or 56 cm³) will be released by 100 O-units of rock. This corresponds to approximately 6.2 × 10⁻² m³ of H₂O per m³ of rock, or a total of 2.1 m³ of H₂O upon complete dehydration of a 4 m in diameter lens of model amphibolite. The results of these calculations have shown that Rayleigh distillation of amphibolite produces less than a 0.2‰ depletion in δ¹⁸O_{WR}, and is consistent with model computations by Rumble (1979, 1982) for devolatilization reactions in calc-silicate rocks. The model calculations for reaction [3.1] produce isotopic compositions for coexisting mineral phases which are consistent with those measured (compare Figs. 3.1 and 3.5). For a model amphibolite with an initial isotopic composition of 5.5‰, dehydration and Rayleigh distillation will produce a fluid with an isotopic composition of approximately 7.00 - 7.50‰.

3.3.2.5 Discussion

The Rayleigh distillation model presented above only constrains the source of the fluid phase and the mechanism by which the fluid is produced. The next step is to investigate how this fluid interacts with the surrounding rocks and the scale at which fluid-rock interaction takes place. As yet, no constraints have been put on the mechanism by which the fluid escapes from the rock nor the path which it takes.

At the Cima di Gagnone area there may be evidence for two mechanisms of fluid transport during high pressure metamorphism. If the isotopic compositions of the metapelites adjacent to the mafic lens (P1 pelites) were originally similar to those of the pelites located further away (P2 pelites), then at some point in their metamorphic history they had to have exchanged with either an isotopically light fluid or with an isotopically lighter rock reservoir to obtain the isotopic composition now found. As has been seen with the above example of devolatilization of amphibolite, Rayleigh distillation is not an effective process by which a significant change in isotopic composition in the rock can be reached. Thus, it is reasonable to assume that the later Tertiary amphibolite-facies overprinting of these rocks, which involved dehydration reactions in the pelites, could not have produced the shift from P2 --> P1. Furthermore, it must be assumed that the mineralogical evolution of both P1 and P2 pelites were nearly identical; thus, the only distinction between the two remains their isotopic signatures.

Two contrasting processes of oxygen isotope exchange may be considered to explain the depletion in ^{18}O observed in the pelitic rocks in the near vicinity of the mafic lens: (1) *Fluid-rock* isotopic exchange between a rock and a (flowing?) fluid phase, whereby the fluid may be considered as an 'active' controller of the rock's final isotopic composition; and (2) *Rock-rock* isotopic exchange in which a static pore fluid merely acts as a medium for diffusional oxygen transport between two rocks with initially different isotopic compositions. If the first mechanism is considered, there are at least two possible sources for the fluid responsible for the isotopic shift observed: isotopic exchange with the fluid produced locally during amphibolite dehydration; and/or infiltration of a completely external fluid at some stage in the metamorphic history of these rocks. If the isotopic shift resulted fully or in part by exchange with the fluid produced during eclogite formation, then fluid flow along grain boundaries (i.e. steady state conditions) may be examined as a mechanism of fluid escape. In contrast, the hydrous fluid produced during the A1->E dehydration event may have remained in the system (due to low permeabilities and/or a low $P_{\text{H}_2\text{O}}$ - pressure gradient ?) as a static, grain-boundary film. In this case, the exchange mechanism may have been by oxygen diffusion between the two rock reservoirs, mafic rocks and pelites (i.e. rock-rock interaction), resulting in the $\delta^{18}\text{O}$ -compositions observed in the P1-pelites.

Though irregularly spaced, and not abundant, quartz veins containing eclogite-facies mineralogies in both the metabasites and metapelites suggests that at some point fluid pressure exceeded lithostatic pressure, resulting in fractures and most likely channelized flow (Heinrich, 1986; Walther and Orville, 1982; Wood and Walther, 1986). It is conceivable that as the amphibolites were dehydrating, the permeabilities in both the source rocks and the surrounding metapelites were sufficient to allow fluid flow,

possibly along schistosity, before conditions for fracturing were reached (see Section 1.3 for a discussion of mechanisms of fluid flow).

As discussed by Heinrich (1986 p.150), the water produced by amphibolite dehydration reactions to form eclogite (A1->E) could have been consumed by hydration reactions in the surrounding metapelites. However, nearly all textural and petrological relationships indicative of the metamorphic history of the metapelites prior to the eclogite-->amphibolite-facies transition (E-->A2) have been obliterated. Since the volume of mafic rocks in the Gagnone area is significantly less than the pelitic and granitic rocks, it is unlikely that the amount of fluid produced during the A1-->E event played a major role in the pre-eclogite to eclogite-facies mineralogical evolution of the pelitic and granitic rocks. The possibility that the amount and isotopic composition of this fluid was sufficient to cause local isotopic exchange on the scale of a few meters and the shift seen, is investigated below.

3.3.3. *A MODEL OF ECLOGITE-FACIES FLUID INFILTRATION IN METAPELITES*

In order to test whether the A1-->E dehydration event could have affected the neighbouring metapelites it is first necessary to determine how much water would be required to produce the observed shift in $\delta^{18}\text{O}$ from P2 --> P1. Various models of isotopic exchange as a result of fluid infiltration are discussed in Chapter 1. As a first approximation, an open system, mass balance model of fluid-rock interaction and exchange with a flowing fluid phase will be considered. In such a model the isotopic composition of the infiltrating fluid (in this case pure H_2O) is held constant. Each increment of water makes a single pass through the system and integrated W/R ratios are determined by the equation:

$$W/R = \ln \left[\frac{(\delta_{\text{W}}^{\text{i}} + \Delta - \delta_{\text{R}}^{\text{i}})}{(\delta_{\text{W}}^{\text{i}} - (\delta_{\text{R}}^{\text{f}} - \Delta))} \right] \quad (3.11)$$

(Taylor, 1977); where $\delta_{\text{W}}^{\text{i}}$ and $\delta_{\text{R}}^{\text{i}}$ represent the initial compositions of the water and rock, respectively. Δ is the difference between the final isotopic composition of the rock and the water ($\delta_{\text{R}}^{\text{f}} - \delta_{\text{W}}^{\text{f}}$) and will be a function of the temperature at which isotopic exchange takes place. For rocks of granitic composition, Taylor (1977 p. 524) has shown that δ_{R} at equilibrium is equal to the $\delta^{18}\text{O}$ value of plagioclase (An_{30}), and the δ_{W} in equilibrium with these rocks can be determined by using the feldspar- H_2O geothermometer. However, since these rocks are more pelitic than those discussed by

Taylor (1977), δ^f_w , and thus Δ , have been determined using estimated mineral modes and the relationships:

$$\delta^{18}\text{O}_{\text{WR}} = \delta^{18}\text{O}_{\text{Qtz}} - \sum_{i \neq \text{Qtz}} X_i \Delta_{\text{Qtz}-i} \quad (3.8),$$

$$\delta^{18}\text{O}_{\text{Qtz}} = \delta_{\text{Sys}} + \sum_{i \neq \text{Qtz}} (X'_i \Delta_{\text{Qtz}-i}) + X'_{\text{H}_2\text{O}} \Delta_{\text{Qtz}-\text{H}_2\text{O}} \quad (3.10)$$

and

$$\delta^{18}\text{O}_{\text{Qtz}} - \delta^{18}\text{O}_{\text{H}_2\text{O}} = 4.10 \times 10^6 / T^2 - 3.7 \quad (\text{Bottinga \& Javoy, 1973}) \quad (3.12)$$

For a derivation of equations 3.8 and 3.10 see Chapter 1. $\Delta_{\text{Qtz}-i}$ for each of the minerals has been determined using the theoretically determined fractionation factors of Bottinga and Javoy (1973).

3.3.3.1. Initial Parameters

The modal composition of the final metapelite has been estimated to be 25% PAR, 25% PHE, 15% GAR and 35% QTZ (see below). At a temperature of 650 °C, Δ is -0.39‰.

As discussed previously, the P2-pelites have $\delta^{18}\text{O}$ compositions ranging from 8.4 to 10.2‰, and the P1-pelites range from 6.7 to 7.6‰ (excluding those found as inclusions in the core of the lens); which represents a maximum shift in $\delta^{18}\text{O}$ of -3.5‰ and a minimum shift of -0.8‰ (i.e. enrichment in ^{16}O). Inspection of Fig. 3.5 shows that the isotopic composition of H_2O which is produced during reaction [3.1] varies from approximately 7.5‰ at the beginning of the reaction to 7.0‰ upon exhaustion of paragonite. Thus, the maximum amount of pelite which can be shifted by the dehydrating lens can be determined by taking the minimum shift and the most ^{18}O depleted water (7.0‰) produced by the reaction as an upper limit. In turn, the minimum amount of pelite which can be shifted will be determined by taking the maximum shift and the most ^{18}O enriched water (7.5‰) as a lower limit. The results of such calculations for these limits are presented below.

3.3.3.2 Upper Limit: Maximum amount of P2-->P1 which can be shifted: ($\delta^i_{\text{R}} = 8.4\text{‰} \rightarrow \delta^f_{\text{R}} = 7.6\text{‰}$; $\delta_{\text{H}_2\text{O}} = 7.5\text{‰}$)

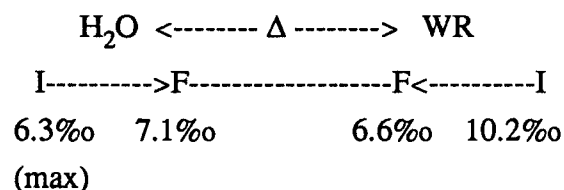
Applying equations 3.8 and 3.10 with the parameters stated above, the minimum amount of water which has passed through the system to produce the -0.8‰ shift from P2-->P1 is 3.4 m³ of H_2O per m³ of rock. As we have seen from the results of

the Rayleigh distillation model presented above, a maximum of 2.1 m^3 of H_2O are produced by complete dehydration of a 2m in radius lens of A1-->E. Thus, the exchange potential of the water produced from a dehydrating lens of this size will only be enough to produce a shift in 0.62 m^3 of pelite.

If we model the lens as a sphere, this corresponds to a 1.2 cm thick rind around the lens (analogous to the peel around an orange). If, however, we assume that a fluid phase tends to follow structural weaknesses, such as schistosity present in the rocks, and assume that the schistosity of the metapelites during eclogite-facies (and deformation?) was roughly parallel to the present schistosity (which now records amphibolite-facies deformation only), we can model the fluid escape path as a cylinder with a radius of 2m, in which the same volume of metabasite occupies the core. In this case the lens will have an exchange potential to shift 2.5 cm of pelite, which is double the amount determined by the spherical model. However, the rocks which show the ^{18}O depletion are located up to 3 m away from the lens. Analogously, in order to produce the -0.8‰ shift at the distances observed, a lens with a radius of 492 m (or $5.0 \times 10^8 \text{ m}^3$ of rock) or a cylinder with a 2 m radius and 492 m long (or $6.2 \times 10^3 \text{ m}^3$) must be dehydrated!

3.3.3.3. Lower limit: minimum amount of P2-->P1 which can be shifted: ($\delta^i_{\text{R}} = 10.2 \text{ ‰}$ --> $\delta^f_{\text{R}} = 6.7 \text{ ‰}$; $\delta_{\text{H}_2\text{O}} = 7.0 \text{ ‰}$)

At a temperature of $650 \text{ }^\circ\text{C}$, the water in equilibrium with samples CL12 and CH278 will be 7.1, which lies completely within the range of the infiltrating fluid (7.5‰ - 7.0‰) and would infer that the rock had exchanged, but not the water, and therefore, defies mass balance assumptions. Inspection of eq. (3.11) above shows that in order to produce the observed shift from P2-->P1, the composition of the interacting fluid must have been 6.3‰ or less. Thus, the water produced by the dehydration reaction could not have been responsible for the shift observed, at least not at a temperature of $650 \text{ }^\circ\text{C}$. This relationship of mass transfer is shown below in the form of the bar graph:



3.3.3.4. Summary and Discussion

The above calculations for both upper and lower limits of fluid rock interaction have shown that a mechanism of isotopic exchange by fluid flow during dehydration of amphibolite to produce eclogite (A1-->E) could not solely be responsible for the shift in $\delta^{18}\text{O}$ seen in the P1-Pelites. In this case, if exchange occurred by such a mechanism, a further fluid phase must have been involved in the isotopic evolution of these rocks. *Assuming* that the P1 isotopic compositions *do not represent original compositions* of the source materials for these rocks, a fluid of $\delta^{18}\text{O}$ of 6.3‰ or less must have exchanged with these rocks in order to produce the isotopic compositions now observed. Exchange with ^{16}O -rich waters is also suggested by the preliminary oxygen isotope data from outcrop Mg163 (see Chapter 2). However, it must be emphasized that various models are possible to explain the ^{16}O -rich rocks at outcrop MG163. The mafic rocks at Mg163 may have exchanged with an external fluid which was more ^{16}O -rich than that indicated for the P1-pelites. Furthermore, there is insignificant evidence to assume that the pre-metamorphic basic rocks as well as the metamorphic histories of all the mafic rocks at the Cima di Gagnone area are identical.

A source of isotopically light fluid could be heated marine water which may have been incorporated into the metamorphic pile during the subduction event which caused the high pressure metamorphism. Pervasive infiltration of sea water to depths of at least 3.5 km has been suggested to have occurred in high-grade metamorphic pelites from the Pyrenees (Wickham and Taylor, 1985). However it has been also suggested that the initial pelite starting compositions for the Pyreneen rocks should have been more quartzofeldspathic than those used by Wickham and Taylor, which would change the need to identify the fluid source as sea water (discussion between R.J. Tracy and J. C. Clemens, communicated to A.B. Thompson, Nov., 1986). Other sources of isotopically light fluids are magmatic waters derived from granitic rocks (Taylor, 1977; 1979), or metamorphic fluids derived from interaction with isotopically light rocks, such as basalts or granites, or possibly even mantle-derived fluids. Interaction with meteoric water is not supported by the hydrogen isotope data on the hydrous minerals in these rocks. The hydrogen isotope data indicate equilibrium with waters which lie within the compositions where the magmatic and metamorphic waters overlap (see e.g. Taylor, 1979 and discussion in Section 5.6). However, the D-enriched muscovite sample from CL17 strongly suggests exchange with marine waters.

The relative position of these isotopically-depleted pelites to the mafic lens suggests that fluid flow may have been enhanced by the structural weakness caused by the contact between the relatively massive, impermeable eclogite and the foliated (more

permeable?) schists. However, unequivocal chemical, mineralogical, and/or structural evidence to support such possibilities has been obliterated by the later amphibolite-facies metamorphic and deformational event. The timing of this infiltration event is also difficult to determine. The results of the models presented below for amphibolite-facies fluid-rock interaction do not indicate exchange with equivalently light fluids, which suggests that fluid exchange occurred *prior* to the amphibolite-facies metamorphic and deformational event, however, there is insignificant data to substantiate this possibility.

An alternative model for the isotopic depletion observed in the P1-pelites is isotopic exchange by a mechanism of oxygen diffusion through a static pore fluid (i.e. rock-rock interaction). Although many isotopic studies present evidence for exchange by a mechanism of fluid flow, in a recent study, Nagy and Parmentier (1982) have shown that narrow equilibrium zones observed between igneous intrusions and metamorphic host rocks in the Santa Rosa Range, Nevada can also be explained by a transport mechanism of self-diffusion of H₂O through a water-rich fluid phase (see also Shieh and Taylor, 1969). Similarly, if the hydrous fluid produced during the A1->E event remained in the system as a thin, static intergranular film, it may have been sufficient to produce diffusive exchange between the mafic and pelitic rocks.

3.4. AMPHIBOLITE FACIES FLUID ROCK INTERACTION EVENT (E-->A2)

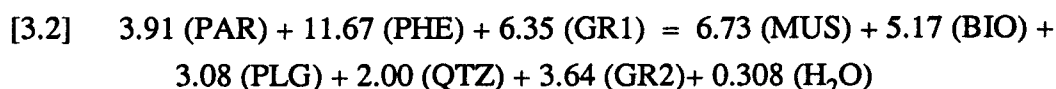
As discussed earlier, the eclogitic rocks of the Adula Nappe have been overprinted by the Tertiary amphibolite-facies regional metamorphic event (E-->A2) which affected a large part of the Central Alps ('Leptontine' Event). Petrographic studies of Heinrich (1982, 1983), Evans and Trommsdorff (1974), and Pfeiffer (1978,1981) as well as cation-exchange geothermometry carried out in this study (see Chapter 2) have shown that the Tertiary regional metamorphism in the Adula Nappe is distinguished from the earlier eclogite-facies metamorphism by a drastic decrease in pressure (in the south of the nappe, from 15-25 kbar (A1-->E) to 6-7 kbar (E-->A2)), with only a minimal decrease in temperature (from >650 °C to 600-650 °C). At the Cima di Gagnone area, this event may be characterized by similar reactions to those of the earlier (prograde) eclogite-facies metamorphism, but can essentially be considered opposite in sign (see Fig. 3.4). Thus, the mechanisms considered for the eclogite-facies event can be applied.

The amphibolites at outcrop CH271 form two isotopically distinct groups (see Fig. 3.1 and Table 3.1). The fine-grained amphibolite (CL6) which occurs along the rim of the lens is isotopically identical to the fresh eclogites in the core. The coarser-grained and more deformed, completely recrystallized amphibolites which make up the tail of

the lens (CL1, CL5, CH37) show an ^{18}O enrichment relative to these rocks. This difference in $\delta^{18}\text{O}$ could be a result of (reaction?) enhanced permeability during deformation allowing a greater amount of H_2O to react with these rocks, which could increase rates of recrystallization and grain growth (see Section 2.3.1.1). Other possibilities are that the isotopic signatures in these rocks reflect original modal variations of pre-amphibolite-facies minerals (such as mineral banding), or contamination due to tectonic mixing with the surrounding pelites. However, the textural relationships in the latter group of rocks indicate that hornblende and plagioclase were completely recrystallized during the E \rightarrow A2 metamorphic and deformational event. In some of the coarser-grained amphibolites, subsequent to recrystallization, further fluid infiltration is indicated by epitaxial growth of biotite and sphene discordant to the pronounced foliation. If the variations in $\delta^{18}\text{O}$ are a result of tectonic mixing, the deformation which caused the mixing as well as chemical homogenization must have occurred prior to complete recrystallisation and grain-coarsening. Furthermore, the isotopic composition of the coarser-grained amphibolites are constant over a distance of 20 meters (compare samples CH37 and CL1), which would require uniform mixing. Although tectonic mixing must be considered as a possibility for the ^{18}O enrichment in the coarser-grained amphibolites, there is no substantial textural or chemical evidence to support this.

3.4.1. A MODEL OF RAYLEIGH DISTILLATION AND DEHYDRATION OF METAPELITES

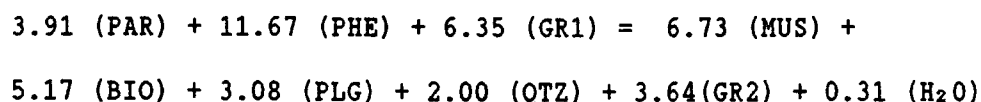
Analogous to the amphibolite dehydration presented above, Rayleigh distillation and oxygen isotope exchange in metapelites have been modelled using the quantitative mass-balance dehydration reaction (see Table 3.3 and abbreviations in Table 2.1):



As above, this reaction is presented in O-units and is similar to Heinrich's reaction (5) (1982, p.35) and corresponds to the replacement textures in metapelites from Trescolmen (Middle Adula Nappe) and Gagnone. Heinrich's reaction (5) is a result of linear combination of simple net transfer reactions in the condensed six-component KCMASH-system (Thompson et al., 1982); whereas reaction [3.2] above has been solved using actual mineral compositions in an eight-component system (KNCFMASH) (see Table 3.3). GR1 and GR2 correspond to the rim-and core-compositions of the garnets in these rocks.

TABLE 3.3

Mineral phase compositions, mineral densities and molecular weights used in reaction [3.2]:



PHASE	KNCFMASH-Composition	Molecular Weight (g/mole)	Density (g/cm³)
QTZ	SiO ₂	60.09	2.65
PLG (An ₂₀)	Na _{0.8} Ca _{0.2} Al _{1.2} Si _{2.8} O ₈	265.43	2.66
GR1	Ca _{0.3} Mg _{0.75} Fe _{1.95} Al ₂ Si ₃ O ₁₂	469.38	4.06
GR2	Ca _{0.27} Mg _{0.48} Fe _{2.25} Al ₂ Si ₃ O ₁₂	580.31	4.13
PAR	NaAl ₃ Si ₃ O ₁₀ (OH) ₂	382.19	2.85
PHE	K _{0.9} Na _{0.1} Mg _{0.32} Fe _{0.15} Al _{2.06} Si _{3.47} O ₁₀ (OH) ₂	400.70	2.85
MUS	K _{0.87} Na _{0.13} Mg _{0.12} Al _{2.76} Si _{3.12} O ₁₀ (OH) ₂	396.02	2.80

Garnet compositions represent averaged compositions of cores (GR1) and of rims (GR2) of the metapelites at outcrop CH271. The phengite composition has been generalized from the composition of sample Ad85 (core) from Trescolmen, reported by Heinrich (1982 p.34). Muscovite and Biotite represent average mica compositions from the meta-pelites and are similar to those of sample CH200 (Heinrich, 1982 p. 34).

3.4.1.1. Initial Parameters

In the model calculations discussed below, an initial rock composition of 25% paragonite (PAR), 25% phengite (PHE), 20% garnet (GR1) and 30% quartz (QTZ), equivalent to 100 O-units of model pelite, has been chosen and is proportionally similar to the modal composition of sample AD 85-1-6 (Heinrich, 1982, p.32). The progress of the reaction and thus the amount of water formed at each increment is determined by a specified amount of muscovite (MUS) and will be limited by the initial modal amount of phengite (see App IIb).

3.4.1.2. Fluid-Rock Ratios

At a constant temperature of 600 °C and a pressure of 5 kbar, 0.05 O-units (or moles) of H₂O are produced for every 1 O-unit of MUS which are formed. This corresponds to 0.09 vol% of the initial rock (initial volume of the model pelite is approximately 1100 ccm) and an instantaneous fluid/rock ratio of $9 \cdot 10^{-4}$. Upon

completion of the reaction, the amount of phengite is exhausted and a total of 0.67 O-units (or 15 ccm) of H₂O are produced per 100 O-units of rock. The change in modal percent of the minerals corresponds to minimal changes in whole rock volume and density (see App. IIb). Thus, approximately $1.3 \times 10^{-2} \text{ m}^3$ of H₂O per m³ of rock, or 2.0 moles of H₂O per Kg of rock, will be released during the reaction. This is similar to the amount of H₂O calculated by Heinrich (1982, p.36) for a slightly different reaction and starting whole rock composition. As stated by Heinrich, the amount of water produced by such a reaction will be sufficient to hydrate all eclogites in the Cima di Gagnone area. He concludes that the differing amount of overprinting in the mafic rocks is a result of slow reaction rates in the mafic rocks compared to relatively fast reaction rates in the metapelites.

3.4.1.3. Modal Changes and Isotopic Effects of Rayleigh Distillation and Dehydration of Metapelites

The mineralogical changes resulting from reaction [3.2] and the effects of Rayleigh distillation on $\delta^{18}\text{O}$ of the whole rock (WR) and the participating phases are shown in Fig. 3.6 and tabulated in App. IIb ($\delta^{18}\text{O}_{\text{WR}}^i = 7.5\%$). The vertical axes are as in Fig. 3.5. The horizontal axis represents the number of reaction increments, corresponding to the progress of the reaction, and have been determined by a specified number of O-units of MUS formed during the reaction. As can be seen in Fig. 3.6, for most of the minerals, the $\delta^{18}\text{O}$ values predicted from the model computations compare well with the actual measured $\delta^{18}\text{O}$ -values of the minerals in the P1-pelites (compare with Fig.3.1 and Table 3.1). However, inspection of the modal amounts predicted by the completion of reaction [3.2] show that this reaction will not be sufficient to produce the relative amounts of mica and feldspar now observed in these rocks (compare Fig. 3.6 with Table 3.1). The largest discrepancy between the calculated modes and those observed in the rocks, is in the amount of plagioclase produced (approximately 7 vol%) as compared to the actual amount present in the rocks (25-35 vol%).

Although the model reaction [3.2] qualitatively corresponds to the replacement textures observed in the rocks of the Adula Nappe, these quantitative results indicate that further reaction(s) must have occurred to produce the modal amounts of minerals now present. However, if we assume that the minerals in the amphibolite-facies metapelites were at least partially produced by a dehydration reaction similar to [3.2], the amount of H₂O produced can be taken as a minimum and the isotopic effects of infiltration into the neighbouring eclogite lens and tail can be investigated.

RAYLEIGH DISTILLATION

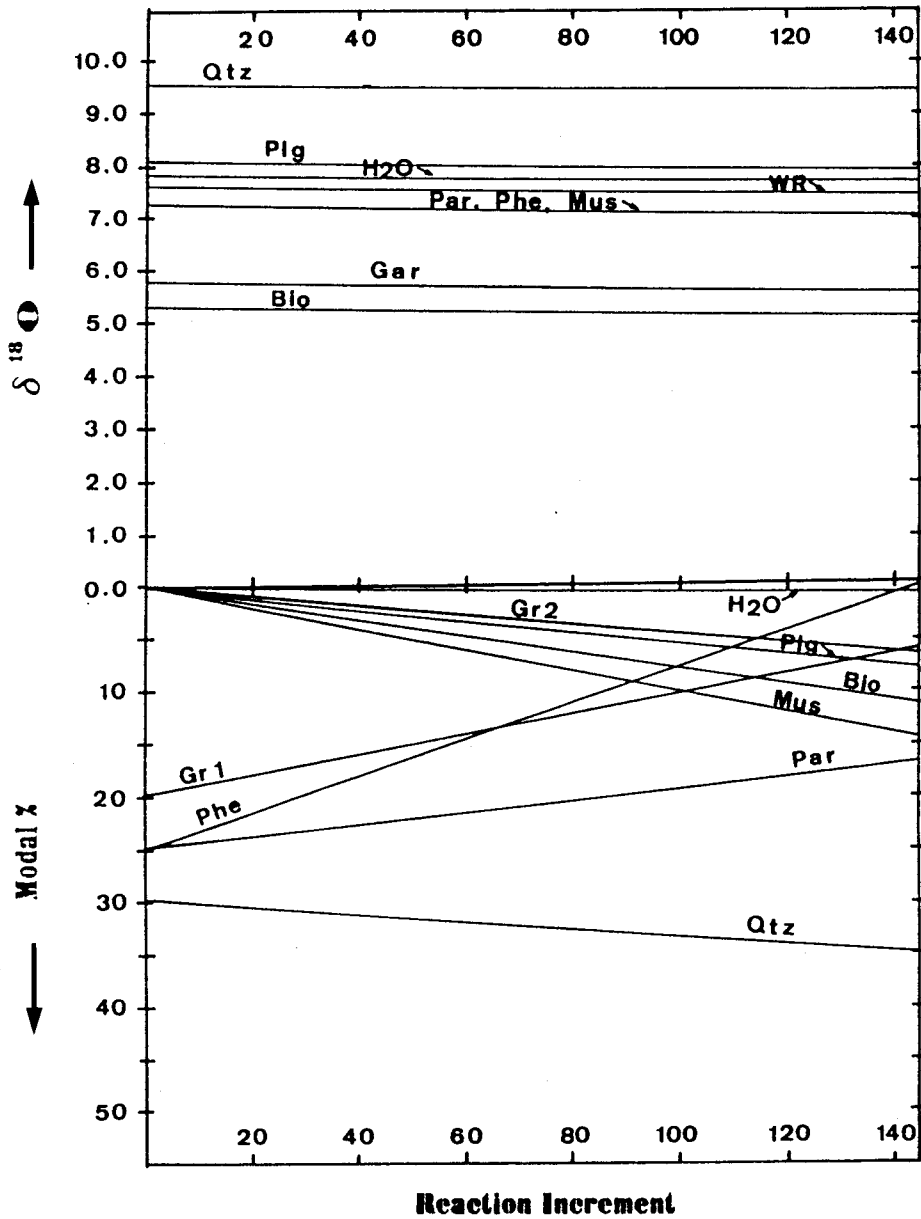
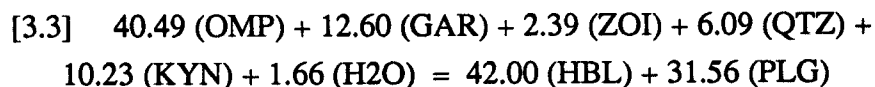


Fig. 3.6:

Results of computer modelling (see App. IIb) of Rayleigh distillation during dehydration of eclogitic metapelites (E \rightarrow A2) under amphibolite-facies isothermal-isobaric conditions of 600°C and 5 Kbar. Mineral compositions, molecular weights and densities are given in Table 3.3. Each increment of reaction corresponds to the formation of 0.10 O-units of muscovite and the release of 0.0016 O-units of H₂O. Abbreviations are defined Table 2.1.

3.4.2. A MODEL OF AMPHIBOLITE-FACIES FLUID INFILTRATION INTO METABASITES

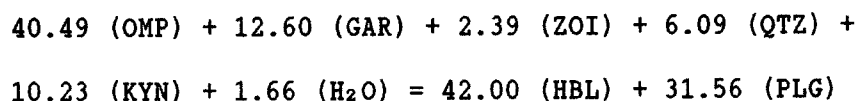
The hydration of kyanite-eclogite to form amphibolite can be described by the whole rock reaction (see Table 3.4):



As in reaction [3.1] actual compositions in the seven-component NCFMASH system have been used, and the reaction is presented in O-units. Infiltration of water produced by the metapelites and isotopic exchange in the eclogites undergoing whole rock reaction [3.3] have been modelled using a similar step-wise procedure as that for Rayleigh distillation.

TABLE 3.4

Mineral phase compositions, mineral densities and molecular weights used in reaction [3.3]:



PHASE	NCFMASH-Composition	Molecular Weight (g/mole)	Density (g/cm ³)
QTZ	SiO ₂	60.09	2.65
PLG	Na _{0.7} Ca _{0.3} Al _{1.3} Si _{2.7} O ₈	276.02	2.70
KYN	Al ₂ SiO ₅	162.03	3.55
OMP	Na _{0.5} Ca _{0.5} Al _{0.5} Mg _{0.5} Si ₂ O ₆	208.34	3.33
GAR	Ca _{0.48} Mg _{1.12} Fe _{1.4} Al ₂ Si ₃ O ₁₂	459.02	3.70
ZOI	Ca ₂ Al ₃ Si ₃ O ₁₂ (OH)	454.35	3.30
PAR	NaAl ₃ Si ₃ O ₁₀ (OH) ₂	382.19	2.85
HBL	Na _{0.35} Ca _{1.75} Mg _{2.6} Fe _{0.9} Al _{2.85} Si _{6.65} O ₂₂ (OH) ₂	841.36	3.10

Omphacite, garnet, paragonite and zoisite compositions are as for reaction [3.1]. Hornblende and plagioclase represent average compositions from sample CL6 along the rim of the mafic lense (see chapter 2).

3.4.2.1 Initial Parameters

An initial whole rock composition of 5% Zoi, 10% Qtz, 35% Omp, 35% Gar, 10% Kyn and 5% Hbl, corresponding to the modal percentage of minerals observed in the kyanite eclogite sample CH271 (see Table 3.1), have been used in the model computations of the amphibolite-facies A1-event. Two cases have been considered: isotopic re-equilibration with water produced by dehydration of the P1-pelites ($\delta_i^{18}\text{O}_{\text{H}_2\text{O}} = 7.7\text{‰}$), and re-equilibration with water produced by the P2-pelites ($\delta_i^{18}\text{O}_{\text{H}_2\text{O}} = 9.6\text{‰}$). In both cases, just enough water is allowed to infiltrate the rock so that reaction [3.3] goes to completion and stops as OMP is exhausted. The results of these computations are shown in Fig. 3.7 and tabulated in App. IIc.

3.4.2.2. Isotopic Effects of Fluid Infiltration and Hydration of Eclogites

The difference in isotopic composition of the infiltrating fluid has no effect on the final WR composition, which remains nearly constant ($\delta_i^{18}\text{O}_{\text{WR}} = 5.5\text{‰}$, $\delta_f^{18}\text{O}_{\text{WR}} = 5.48\text{‰}$; see App. IIb). This is due to the fact that the total amount of O in the H_2O required to hydrate the eclogite is very small compared to the amount of O in the rock (F/R ratio = 1.42×10^{-2}), and its isotopic composition will tend to be buffered by the rock. In order to just hydrate the present amount of amphibolite, 1.1 m^3 of H_2O are required, which corresponds to 78.5 m^3 of dehydrating pelite or a cubic slab with sides 4.3 m long.

Comparison of these results with the measured isotopic compositions of the amphibolites at outcrop CH271 indicates that the fine-grained amphibolites which comprise the rim of the lens represent limited fluid-rock interaction (low F/R ratios, $>0.1:1$), whereby only enough water was able to permeate the rock to cause complete amphibolisation but no isotopic shift. In contrast, the isotopic compositions of the completely recrystallized amphibolites which form the tails of the lens may indicate conditions of greater permeability and greater integrated F/R ratios, resulting in the 1‰ enrichment in ^{18}O of the whole rock. Using equations 3.7, 3.8, 3.9, 3.10, 3.11 and 3.12 from Section 3.3.3 above, for a temperature of 600 °C , it can be shown that a volumetric fluid/rock ratio of 3.1 will be required to produce this shift in ^{18}O . This corresponds to 5720 m^3 of dehydrating pelite or a cubic slab with sides 18 m in length. The possible mechanisms of deformation and recrystallization in forming the rims and tails of the mafic lens have been discussed in Chapter 2. The isotopic evidence presented here is consistent with the suggestion that increased fluid infiltration occurred in the amphibolite tails during deformation (Früh-Green, 1985). The larger influx of fluid may thus have been effective in enhancing the growth rate of the amphibolite and plagioclase aggregates during deformation, resulting in coarser grain sizes.

INFILTRATION & HYDRATION

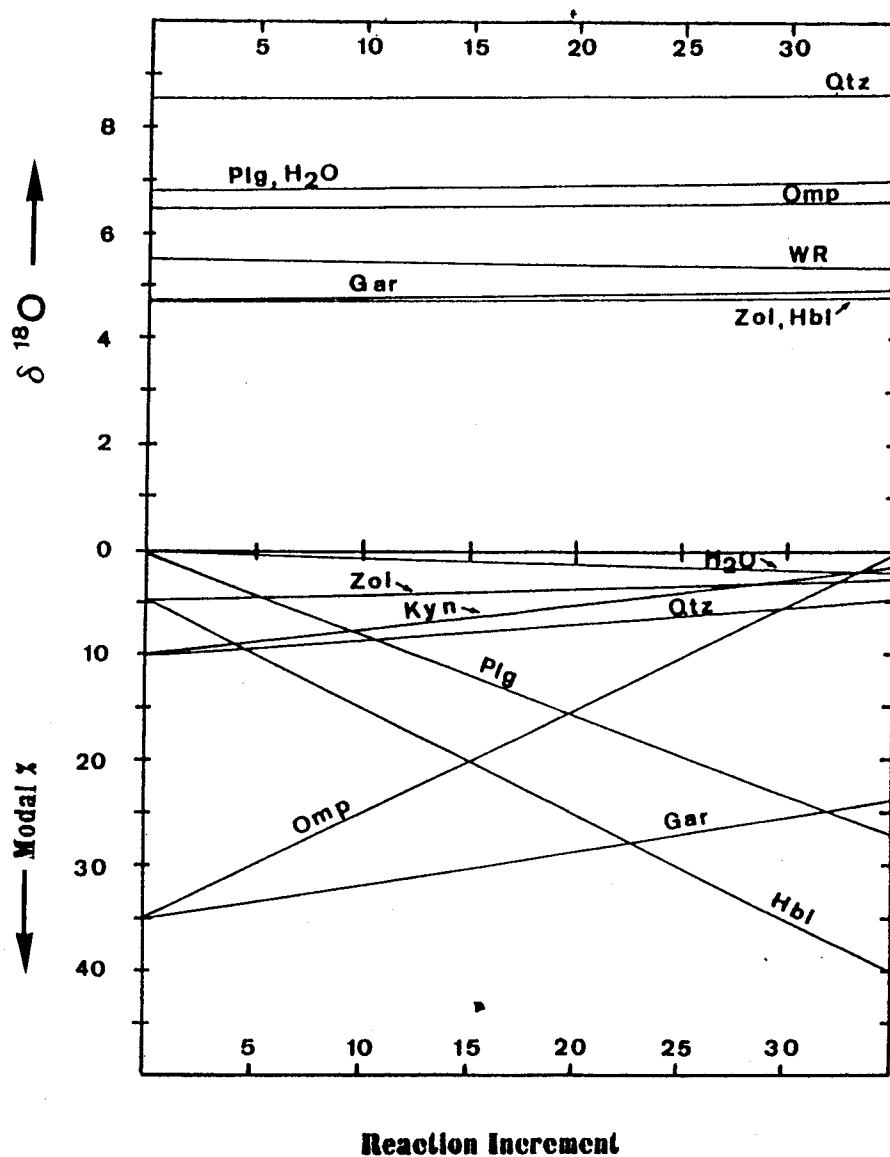


Fig. 3.7: Results of computer modelling (see App. IIc) of fluid infiltration and hydration of kyanite eclogite to form amphibolite (E \rightarrow A2) by reaction [3.3] (see text). Mineral compositions, molecular weights, and densities are given in Table 3.4. The results are for isothermal and isobaric conditions of 600°C and 5 Kbar. Each reaction increment corresponds to 0.04 moles of H₂O or an instantaneous fluid-rock ratio of 8.6×10^{-4} .

3.4.2.3. Summary

Quantitative modelling of step-wise fluid infiltration, hydration and isotopic exchange during amphibolite-facies metamorphism has shown that the fine-grained amphibolites which comprise the rim of the mafic lens at outcrop CH 271 may represent

limited fluid-rock interaction (low F/R ratios, $> 0.1:1$), whereby only enough water was able to permeate the rock to cause complete amphibolitisation but no isotopic shift.

The isotopic shift observed in the recrystallized tails of the mafic lens requires only local interaction with fluids produced by dehydration reactions in the immediately surrounding metapelites. Amphibolite-facies deformation may have been instrumental in increasing permeability of these otherwise impermeable mafic rocks allowing higher F/R ratios and fluid flow. The increased amount of fluid during deformation may have enhanced the growth rates of the hornblende and plagioclase aggregates in the tails of the lens, resulting in the coarse-grained amphibolites and the strong foliation now observed (see also Section 2.3.1.1).

3.5. ATTAINMENT OF OXYGEN ISOTOPE EQUILIBRIUM IN METAMORPHIC ROCKS

The degree to which interlayered rocks have attained isotopic equilibrium has often been used as an indicator for the mechanism and degree of fluid-rock interaction in metamorphic rocks. Rumble and Spear (1983) have also related the degree of oxygen isotope equilibrium to the enhancement of permeability by mechanisms such as fracturing. Any discussion of the attainment of oxygen isotope equilibrium must include both the criteria used to test for equilibrium and the scale at which equilibrium is considered.

In this study, two relative scales of oxygen isotope equilibrium are considered. *Large-scale equilibrium* is used to describe oxygen isotope exchange between heterogeneous rock layers at a distance equal to or greater than the thickness of the layer (cm- to meter scale). On such a scale, equilibrium is assumed if the mineral phases show uniform isotopic compositions despite their original differences prior to metamorphism and deformation. Large scale isotopic exchange and homogenization is often thought to result from pervasive fluid-rock interaction with either a static, intergranular fluid or a fluid flowing through intergranular pores (e.g. Taylor et al, 1963; Garlick and Epstein, 1967; Rumble et al, 1982; Wickham 1985; Hoernes and Friedrichson, 1980; Nagy and Parmentier, 1982).

Local equilibrium is used to describe isotopic exchange and equilibrium between coexisting mineral phases on a millimeter to centimeter scale. Local equilibrium is independent of mineralogical and isotopic heterogeneities in rock types (bulk composition), but will be influenced by diffusional properties of the minerals involved and by changes in temperature. In this study, the principle criteria for determining local isotopic equilibrium are two-fold: 1. Consistencies in temperatures estimated by oxygen isotope fractionation between coexisting mineral pairs; and 2. Constant oxygen isotopic fractionation of mineral pairs from the various rock types, regardless of their

bulk isotopic compositions. Oxygen isotope temperature estimates will depend greatly on the calibration used, and their use as indicators for isotopic equilibrium presents some problems. Use of the existing experimentally-determined fractionation curves between various minerals and water (e.g. Matushisa et al, 1979; Matthews et al, 1980; O'Neil and Taylor, 1967) yield notable variations (see discussion in Graham, 1981) and differ considerably from the theoretically-determined calibration of Bottinga and Javoy (1973) (see Table 3.6).

In earlier studies, isotopic temperatures were thought to represent peak metamorphic conditions, after which all minerals ceased to exchange isotopes. However, Deines (1977) has shown that there is often evidence for retrograde isotopic exchange during cooling of metamorphic rocks, and that evidence of oxygen isotope equilibrium among three or more minerals in metamorphic rocks is rarely found (see also Javoy, 1977). In addition, based on diffusional studies, Graham (1981) has concluded that isotopic equilibrium amongst coexisting minerals in metamorphic rocks will rarely be preserved, except for mineral pairs or triplets with similar diffusional properties, as for example for muscovite and biotite. Furthermore, since oxygen diffusion rates are greatly enhanced by the presence of water, Graham argues that discordant temperature relations may be direct evidence for the presence of a hydrous fluid during cooling of a metamorphic pile. In light of new kinetic data, the effects of diffusion on the oxygen isotope composition of some silicates have been investigated by Giletti (1985). For slowly cooled igneous and metamorphic rocks Giletti concludes that the temperatures acquired by oxygen isotope geothermometry may represent neither maximum metamorphic temperatures nor a single closure temperature at which diffusional exchange ceases, but rather will be a function of grain size, mineral modes, cooling rate of the rock, and will depend on the diffusional properties of the coexisting minerals. Furthermore, Giletti concludes that oxygen isotope fractionations combined with kinetic data may be a useful indicator of the cooling rate of metamorphic rocks. Thus, the use of constant oxygen fractionation temperatures may not be a valid indicator of isotopic equilibrium. However, if constant oxygen isotopic fractionations are observed between similar mineral pairs in rocks with comparable modes and grain sizes, which have experienced identical P-T conditions of metamorphism and cooling rates, it should be reasonable to assume that isotopic equilibrium was preserved. With the same argument, if the cooling rate of a metamorphic pile is known and kinetic data are available for the coexisting mineral pairs, agreement between predicted ^{18}O concentrations and those measured would indicate isotopic equilibrium.

TABLE 3.5**OXYGEN ISOTOPE FRACTIONATIONS**

- A: Biotite-muscovite schists (kyanite-free) with equilibrium textures
 B: Fine-grained, mica schists (\pm kyanite) with disequilibrium textures
 C: Metabasites
 D: Eclogite-facies veins

SAMPLE	ΔQ -PL	ΔQ -MU	ΔQ -BI	ΔQ -GR	ΔQ -RU	ΔQ -IL	ΔQ -KY	ΔQ -OM	Δ PL-HB
A. CL12	2.30	2.30	2.99	2.69	6.71				
CL13			4.56						
CL9		3.20	4.90	3.52					
CL26		2.76							
CL30		2.85							
B. CH278	1.28		5.08	4.24	7.48	7.75	1.70		
CL11a			6.28	4.50					
CL11b				4.16		8.35			
CL4a	1.89		5.29	5.25		6.45			
C. CH271				3.05			1.08	2.29	
CL1									2.12
CL6									1.01
D. CL17		2.32							
CL9a							2.13		

3.5.1. EQUILIBRIUM / DISEQUILIBRIUM RELATIONS IN THE METABASITES

The greater plagioclase-hornblende fractionations in the coarser-grained amphibolites ($\Delta = 2.12\%$, see Tables 3.5 and 3.6.) indicate a lower temperature of reequilibration (605°C) than for the fine-grained amphibolites ($\Delta = 1.01$; $T = 887^\circ\text{C}$). A lower temperature of crystallization in the amphibolite tails is consistent with textural evidence and the arguments presented above for either continual infiltration or a subsequent distinct infiltration event upon cooling (Früh-Green, 1985). The unrealistically high temperature for sample CL 6 may be explained by oxygen diffusional effects as discussed by Giletti (1985). Giletti has shown that for slowly cooled amphibolite, temperatures estimated by Plg-Hbl isotopic fractionations represent neither a single closure temperature nor equilibrium temperatures. Due to slower diffusion rates in hornblende,

TABLE 3.6

Comparison of fractionation temperatures (°C) determined by experimental fractionation data and by theoretical calibrations.

A. Experimental Fractionation Data

SAMPLE	T_{b-PL}	T_{b-MU}	T_{b-BI}	T_{b-RU}	T_{b-IL}	T_{b-OM}	T_{PL-MU}	T_{PL-BI}	T_{PL-RU}	T_{PL-IL}	T_{Gr-BI}^a	T_{Gr-BI}^b
<u>METAPELITES</u>												
CL12	546	474	690	586			393	794	560		663	535
CL13			441									
CH278	421		393	554	539			381	544	537	551	463
CL9		332	409									
CL4a	326		376		621			412		692	610	491
CL11a			311								1098	848
CL11b					508						843	656
CL25		390										
CL30		377										
<u>METABASITES</u>												
CH271						559						
CL17		470										

B. Theoretical Calibrations of Bottinga & Javoy (1973) and Javoy (1977)

SAMPLE	T_{b-PL}	T_{b-MU}	T_{b-BI}	T_{b-GR}	T_{b-IL}	T_{PL-MU}	T_{PL-BI}	T_{PL-GR}	T_{PL-IL}	T_{PL-GR}	T_{Gr-BI}
<u>METAPELITES</u>											
CL12	846	600	741	762		450	700	713			676
CL13			572								
CH278	686		533	551	553		482	485	551		477
CL9		488	546	631							493
CL4a	550		518	468	632		503	416	700		852
CL11a			459	527							310
CL11b				559	523						
CL25		536									
CL30											
<u>METABASITES</u>											
CH271				699							
CL17		595									
CL6							745			887	
CL1										605	

Temperatures (T°C) calculated using the equations:

$$1000 \ln a_{q-H_2O} = 3.34 (10^6 T^{-2}) - 3.31 \text{ (Matsuhisa et al., 1979), (T°K)}$$

$$1000 \ln a_{P1-H_2O} = (2.91 - 0.76\beta) (10^6 T^{-2}) - (3.41 - 0.14\beta), \text{ where } \beta = \text{mole fraction of An (O'Neil and Taylor, 1967)}$$

$$1000 \ln a_{Mn-H_2O} (= 1000 \ln a_{Fe-H_2O}) = 2.38 (10^6 T^{-2}) - 3.89 \text{ (O'Neil and Taylor, 1969)}$$

$$T_{b-BI} \text{ has been calculated using } \Delta_{q-MU} = 0.54 \Delta_{q-BI} \text{ Garlick and Epstein, 1967)}$$

$$1000 \ln a_{q-RU} = 7.23 (10^6 T^{-2}) - 3.08 \text{ (Matthews et al., 1979)}$$

$$T_{b-IL} \text{ has been calculated using } \Delta_{q-IL} = 0.95 \Delta_{q-MU} \text{ (O'Neil and Ghent, 1975) and } 1000 \ln a_{Mn-H_2O} =$$

$$-1.60 (10^6 T^{-2}) - 3.61 \text{ (Anderson et al., 1971)}$$

$$1000 \ln a_{q-OM} = (2.08 - 0.99\beta) (10^6 T^{-2}), \text{ where } \beta = \text{jad-component in pyroxene (Matthews et al., 1983)}$$

T_{Gr-BI}^a : average values of $\ln K_0$ (Mg/Fe)_{Gr-BI} calculated from equation (7) in Ferry and Spear (1978) for a pressure of 6 Kbar.

T_{Gr-BI}^b : average values of $\ln K_0$ calculated from equation (9) in Goldman and Albee (1977).

compared to quartz and plagioclase, Plg-Hbl apparent temperatures will be greater than Qtz-Plg apparent temperatures. A temperature of 600°C for plagioclase-hornblende-recrystallisation lies within the upper limit of the range of temperatures estimated from fractionations between other mineral phases in the metapelites (see below) and from Mg-Fe-exchange between garnet and biotite (Table 3.6). Again, this relatively high temperature of equilibration may be a result of the oxygen-diffusion properties of hornblende and could reflect the difference in closure temperatures between plagioclase, hornblende and the other phases present in the rocks.

A range of temperatures from 470 °C (experimental calibrations) to 700 °C has been determined by oxygen-isotope geothermometry for the coexisting Qtz-Gar-Omp in the fresh eclogite (CH 271) and Qtz-Mus in the eclogitic segregation vein (CL 17) from the center of the mafic lens. This large range in temperature could record a continuous history or be a combined effect of: (1) uncertainties in fractionation calibrations; (2) isotopic disequilibrium and/or diffusional exchange during cooling; and/or (3) retrograde exchange enhanced by a hydrous grain-boundary fluid film upon cooling.

3.5.2. EQUILIBRIUM / DISEQUILIBRIUM RELATIONS IN THE METAPELITES

3.5.2.1. Local Equilibrium

Local equilibrium within single pelitic layers has been evaluated by analysing mineral separates from hand specimens 1-10cm thick. These rocks have been divided into two groups according to their mineralogies and textures. Group A (Table 3.5) represents kyanite-free, biotite-muscovite schists which exhibit 'equilibrium' textures, i.e. the rocks have uniform, recrystallized grain sizes and show pronounced alignment of the micas (see also Chapter 2). Group B represents fine-grained, more aluminous, biotite schists which are distinguished from group A by a lack of muscovite, a presence of kyanite \pm staurolite (except CL 4a) and by 'disequilibrium' textures. The disequilibrium textures are characterized by heterogeneous grain sizes and skeleton-like replacement of kyanite and garnet by unoriented biotite and plagioclase grains. The isotopic fractionations between the various minerals in these rocks show considerable irregularities among the rock types and over distances of less than 10 cm. (see Table 3.5).

In the group B disequilibrium schists, the quartz-ilmenite fractionations ($1000 \ln \alpha_{\text{Qtz-Ilm}}$) vary by nearly 2‰, from 6.45‰ to 8.35‰; whereas $1000 \ln \alpha_{\text{Qtz-Gar}}$ and $1000 \ln \alpha_{\text{Qtz-Bio}}$ show slightly less variations of 1.0‰ and 1.2‰, respectively. These large variations (1-2‰) are also observed in the group A schists. Estimates of metamorphic temperatures based on the measured α -values and using both experimentally determined fractionation factors and the calibrations of Bottinga and

Javoy (1973) and Javoy (1977) are presented in Table 3.6 (see references therein). The isotopic temperatures determined by experimental calibrations are in general 100-200 °C lower than those calculated by the calibrations of Bottinga and Javoy (1973) and Javoy (1977) (with the exception of Qtz-Ilm temperatures which are similar). As with the mineral fractionations, there is a large variation in temperatures, ranging from as low as 326 °C for Qtz-Plg (CL4a) to a maximum of 800 °C for Plg-Bio (sample CL12). These large variations are seen among the different rock-types as well as within single rock samples, as for example CL 4a and CL 12.

In general experimentally-calibrated thermometers yield consistently higher temperatures (470 °C to 700 °C) for the relict eclogite-facies mineral pairs (Qtz-Gar, Qtz-Rut and Qtz-Ilm) than for the amphibolite-facies mineral pairs (Qtz-Mus, Qtz-Bio, Qtz-Plg, Plg-Mus, and Plg-Bio), which range from 311°C to 475 °C. Temperatures determined for quartz-rutile and quartz-ilmenite pairs (experimental calibrations) fall within a narrow range of 540 °C to 620 °C (excluding sample CL 11b). Sample CH 278 is the only one which shows consistent temperature-estimates for more than three mineral pairs; Qtz-Rut, Qtz-Ilm, Plg-Rut and Plg-Ilm fractionations all yield temperatures between 537 °C and 554 °C for both experimental and theoretical calibrations and are consistent with temperatures estimated from Mg-Fe exchange geothermometry (Ferry and Spear- calibration). The distinction between eclogite-facies- and amphibolite-facies mineral pairs is not as evident from temperatures determined by the calibrations of Bottinga and Javoy (1973) and Javoy (1977). Qtz-Gar and Qtz-Ilm temperatures range from 470 °C to 762 °C , whereas Qtz-Plg, Qtz-Bio, Plg-Mus and Plg-Bio temperatures range from 450 °C to 850 °C .Temperatures based on Gar-Bio isotopic fractionations also show inconsistencies with those determined by cation-exchange geothermometry. $T_{\text{Gar-Bio}}$ from samples CH 278 and CL 9 are nearly identical with those determined by the Goldman and Albee Garnet-Biotite Mg-Fe exchange thermometers, whereas $T_{\text{Gar-Bio}}$ from sample CL 12 is similar to that determined by the Ferry and Spear experimental calibration. These variations and temperature trends are easily seen in Figure 3.8, which employs the graphical representation suggested by Javoy et al, 1970.

This graphical method uses $^{18}\text{O}/^{16}\text{O}$ -fractionation data to plot temperatures as a function of $(\Delta_{\text{Qtz-Min}}) - b$ and a ; whereby a and b are constants obtained from the relationship:

$$\Delta_{\text{Qtz-Min}} = a_{\text{Qtz-Min}} (10^6 T^{-2}) + b_{\text{Qtz-Min}}$$

(see also Chapter 1). If the quartz-mineral pairs cease to exchange oxygen isotopes at the same temperature, a plot of $(\Delta_{\text{Qtz-Min}}) - b$ versus a should define a straight line passing through the origin, the slope of which represents the average temperature of equilibration. In Figure 3.8, the constants a and b have been determined from the

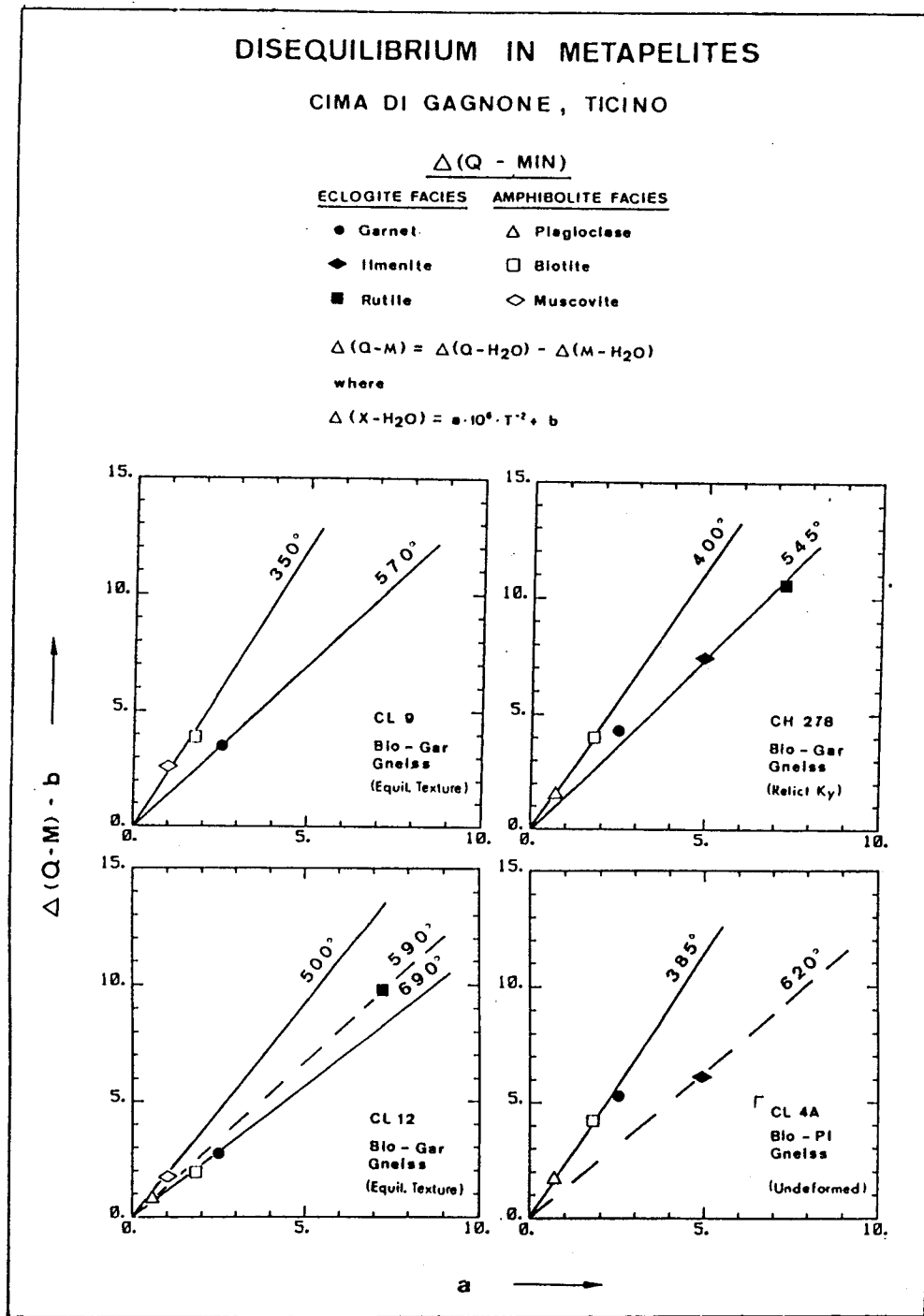


Fig. 3.8:

Graphical representation of the use of $^{18}O/^{16}O$ -fractionations to determine local isotopic equilibrium (after Javoy, 1970). Temperatures have been determined by experimental calibrations (see references in table 6). Isotopic equilibrium is assumed if the fractionation of coexisting mineral phases and quartz (Δ_{Q-Min}) lie on a straight line passing through the origin on a graph whose axes are $(\Delta_{Q-Min}) - b$ and a ; whereby a and b are constants obtained from the relationship:

$$\Delta_{Qtz-Min} = a_{Qtz-Min} (10^6 T^{-2}) + b_{Qtz-Min}$$

and the slope of the line is equal to $10^6 T^{-2}$. Discordant temperature estimates for the metapelites at the Cima di Gagnone area suggest isotopic disequilibrium on a mm- to cm-scale. Lines connecting solid symbols indicate the possible range of isotopic temperatures for the A1 → E event; whereas those connecting open symbols show the possible range of isotopic temperatures for the later E → A2 event (see text).

experimental calibrations listed in Table 3.6. As discussed previously, as well as in Javoy et al (1970), this graphical method of representing isotopic equilibrium relations depends greatly on the accuracy of the calibrations used.

Comparison of variations in mineral fractionations and isotopic-temperature estimates of the metapelites indicates that local equilibrium within single layers was in general not achieved in these rocks. The temperature distributions suggest that garnet, ilmenite and rutile may have retained their eclogite-facies isotopic compositions (A1 -> E), and that significantly lower isotopic temperatures (350-500°C) are indicated for the amphibolite-facies metamorphism than those estimated by cation-exchange geothermometry (460-670°C; see also Evans and Trommsdorff, 1974; Pfeiffer, 1978,1981). Without sufficient kinetic data, it is impossible to determine how much these apparent isotopic temperatures and disequilibrium relations are diffusional effects during cooling. However, samples of comparable grain sizes and mineral modes (e.g. CH 278-CL 11a and CL 12-CL 13) exhibit variabilities which cannot be explained purely by oxygen diffusion upon cooling. These data, however, may indicate the presence of *differing, small amounts* of an *intergranular hydrous fluid*, allowing local (on a mm-scale) $^{18}\text{O}/^{16}\text{O}$ -redistribution between those minerals which are more easily reset to lower temperatures (e.g. plagioclase and mica). These data do not indicate a correlation between the degree of isotopic equilibrium and the degree of recrystallization or deformation observed in these rocks.

3.5.2.2. Large-scale Equilibrium

Large-scale oxygen-isotope equilibrium between the interlayered metapelites and the metabasites can be evaluated by comparison of the isotopic compositions of quartz and plagioclase (see Fig. 3.9). Quartz in the rocks at outcrop CH271 vary from 7.8‰ to 9.4‰; whereas, with the exception of sample CL12, the metapelites show a smaller variation from 8.6‰ to 9.4‰. The eclogite-facies veins in the pelitic rocks show constant $\delta^{18}\text{O}$ -values of 9.6, which indicates near equilibrium with a number of the pelitic samples (compare CH278, CL13, CH40). The quartz segregation vein in the core of the mafic lens also shows near equilibrium values to those in the fresh eclogite and symplectite. As mentioned previously, the rocks in the near vicinity of the mafic lens are isotopically distinct from those located further away, which indicates a lack of equilibrium over distances greater than 30 metres. The data from outcrop CH271, however, indicate that an approach to isotopic homogenization occurred, but complete equilibrium was not achieved. As discussed earlier, this approach to isotopic equilibrium, as well as the relative depletion in ^{18}O observed in the P1-metapelites, may be evidence for fluid-rock interaction on a meter-scale prior to or during the

eclogite-facies metamorphic event (see also Hoernes and Friedrichson, 1980). Alternatively, the near equilibration of the two rock types may provide further evidence for a model of diffusive oxygen isotope exchange between the two oxygen reservoirs, the mafic lens and P1-pelites, in which a static, intergranular fluid phase merely acted as the exchange medium.

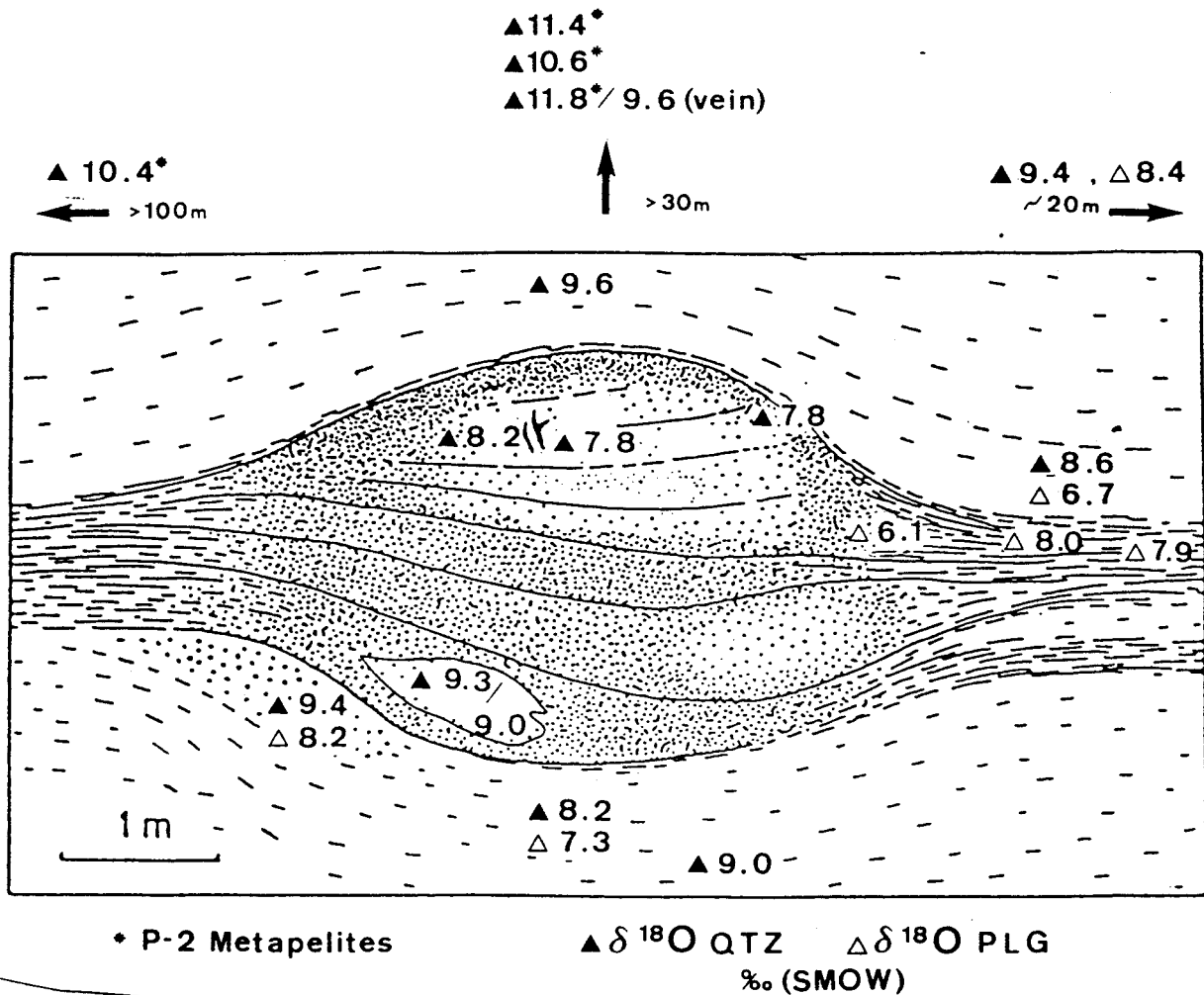


Fig. 3.9:
Comparison of $\delta^{18}\text{O}_{\text{Qtz}}$ - and $\delta^{18}\text{O}_{\text{Plg}}$ of the various rock types at outcrop CH 271 indicates a general lack of large-scale (> 20 m) oxygen isotopic equilibrium. Small variations between P1-pelites (without *) and the mafic rocks suggest an approach to isotopic equilibrium on a meter-scale.

3.6 SUMMARY AND CONCLUSIONS

The isotopic data from the various rocks at the Cima di Gagnone area and the results of the models presented above have shown that:

1. A Rayleigh distillation mechanism of fluid production during dehydration reactions is not sufficient to cause large isotopic shifts in high grade metamorphic rocks. These results are consistent with model computations carried out by Rumble (1979,1982) for devolatilization reactions in calc-silicate rocks. Furthermore, the models of a Rayleigh distillation mechanism of fluid escape during dehydration reactions in both metabasites (eclogite-facies) and metapelites (amphibolite-facies) produce isotopic compositions which are consistent with those measured.
2. Fluid production during eclogite-facies dehydration of amphibolite would not be sufficient to cause the observed isotopic signatures in the surrounding P1-metapelites by a mechanism of fluid flow. This conclusion is based on the assumption that the P1-metapelites were derived from similar source materials as the P2-pelites and experienced identical metamorphic and deformational histories. If such an evolution is assumed, the isotopic compositions of the P1-pelites indicates that prior to the Tertiary amphibolite-facies event (E-->A2), interaction and exchange with isotopically light fluids could have occurred. Sources of such isotopically light fluids could be heated marine water which may have been incorporated into the metamorphic pile during the subduction event which caused the high pressure metamorphism. A further source could be interaction with magmatic, or mantle-derived fluids, possibly during the Hercynian metamorphism. Interaction with meteoric waters is not supported by hydrogen isotope data from mineral separates in the rocks. The relative position of these ^{18}O -depleted pelites to the mafic inclusions suggests that fluid flow and interaction may have been enhanced by a structural weakness caused by the contact between relatively massive, impermeable eclogite and the foliated (more permeable?) metapelites. However, unequivocal chemical, mineralogical or structural evidence to support such possibilities has been obliterated by the later amphibolite-facies metamorphic and deformational event. Furthermore, the timing of a possible infiltration event cannot be determined with the present data.
3. A mechanism of self-diffusion of H_2O molecules through a static, intergranular hydrous fluid can be considered as an alternative model of oxygen transport and isotopic exchange, producing the observed depletion in ^{18}O of the P1-Pelites. These two models of oxygen isotope exchange may be better constrained if the areal extent of the depleted pelites could be determined more precisely.

4. The various dehydration events which occurred during the metamorphic evolution of the rocks at the Cima di Gagnone area could produce small quantities of water-rich fluid resulting in instantaneous F-R ratios of < 0.001 . Upon full completion of the various reactions less than 0.1 m^3 of water would be produced per m^3 of rock which is dehydrated. These results are consistent with the arguments of Wood and Walther (1986) that phase equilibria and isotopic ratios in pelitic rocks are generally not good indicators of high fluid-rock ratios.
5. Quantitative modelling of step-wise fluid infiltration, hydration and isotopic exchange during amphibolite-facies metamorphism has shown that the fine-grained amphibolites which comprise the rim of the mafic lens at outcrop CH 271 represent limited fluid-rock interaction (low F/R ratios, $> 0.1:1$), whereby only enough water was able to permeate the rock to cause complete amphibolitisation but no isotopic shift.
6. The isotopic shift observed in the recrystallized tails of the mafic lens requires only local interaction with fluids produced by dehydration reactions in the immediately surrounding metapelites. Amphibolite-facies deformation may have been instrumental in increasing permeability of these otherwise impermeable mafic rocks allowing higher F/R ratios and fluid flow. The increased amount of fluid during deformation may have enhanced the growth rates of the hornblende and plagioclase aggregates in the tails of the lens, resulting in the coarse-grained amphibolites and the strong foliation now observed. Hbl-Plg fractionations in the recrystallized amphibolite tails of the lens indicate lower temperatures of isotopic exchange, which together with local biotite and sphene, and in some cases chlorite, grown epitaxially and in discordant veins, suggest that fluid infiltration may have occurred under greenschist-facies P-T conditions during cooling of the metamorphic pile. These local biotite veins indicate the mechanism of escape of this subsequent fluid may have been more by hydraulic fracturing (Wood and Walther, 1982, 1986), rather than by steady state fluid flow.
7. Comparison of the variations in mineral fractionations and isotopic temperatures estimated for the metapelites indicates that local equilibrium within single layers was in general not achieved in these rocks. The temperature distributions suggest that garnet, ilmenite and rutile may have retained their eclogite-facies isotopic compositions. Lower isotopic temperatures are indicated for the amphibolite-facies metamorphism ($350\text{-}500^\circ\text{C}$) than those estimated by cation-exchange geothermometry ($460\text{-}670^\circ\text{C}$). Samples of comparable grain sizes and mineral modes

exhibit variabilities which cannot be explained purely by diffusion and redistribution of oxygen upon cooling. The data may indicate the presence of differing, small amounts of an intergranular hydrous fluid, resulting in local (on a mm-scale) oxygen isotope redistribution between those minerals which are more easily reset to lower temperatures (e.g. plagioclase and mica). There is no correlation between the degree of isotopic equilibrium and the degree of recrystallization and/or deformation observed in the metapelitic rocks.

3.6.1. A PHILOSOPHICAL DISCUSSION OF THE PRODUCTION AND CONSUMPTION OF HYDROUS FLUIDS IN POLY-METAMORPHIC TERRAINS

There is no doubt that the presence of hydrous fluids plays an important role in processes of mass transfer, grain growth and mineral transformation during metamorphism. The literature abounds with examples, packed with key words, such as devolatilization reactions, pervasive fluid flow, the influence of rock permeabilities on fluid flow, deformation-enhanced fluid flow, etc. etc. The processes or mechanisms associated with such 'key words' are all interdependent. It is the result of the combination of such processes which lead to the end product: *mineral assemblages* - which is the petrologists only clue to what *might* have happened. The transformation of one mineral into another is influenced by the kinetics of the various mechanisms involved, let it be diffusive mass transfer by grain boundary sliding or dissolution/precipitation. In turn, the kinetics of nearly all processes of mineral growth and transformation will be greatly influenced by temperature, pressure, deformation and fluid access. But, how much fluid is actually necessary to catalyse mineral reactions or enhance diffusion rates? What quantities of a free fluid phase can a polymetamorphic rock sequence actually produce - and *lose* (leading to fluid flow)? Is fluid flow as ubiquitous as the numerous examples from the literature lead one to believe?

The present study has shown that during the various stages in the polymetamorphic history of the pelitic and mafic rocks at the Cima di Gagnone area, either hydration or dehydration mineral reactions may have taken place. The calculated models have shown that regardless of pressure-temperature conditions and bulk rock chemistries, a total of less than 0.1 m^3 of H_2O may be produced per m^3 of rock that is dehydrated (see also Wood and Walter, 1986). It has also been suggested that as the mafic rocks were dehydrating during eclogite-facies metamorphic conditions, the pelitic rocks may have acted as *sinks* in which the fluid was consumed locally in hydration reactions. The reverse situation is indicated during the subsequent uplift history under amphibolite-facies metamorphic conditions: the metapelites provided the source of fluid production and the mafic rocks acted as sinks. Thus, the metamorphic evolution of

these rocks can be considered to involve *local redistribution* of *small quantities* of hydrous fluid on a scale of *a few (tens of) meters*.

The preservation of eclogite-mineral assemblages in the mafic rocks appears to have been directly dependent on a lack of *penetrative* deformation and limited fluid penetration during the subsequent uplift history. Although 'enough' water would have been provided by even partial dehydration reactions in the neighbouring metapelites, lesser degrees of deformability and permeability, offered by the coarser-grained crystal aggregates of omphacite and garnet, may have been determinant to the accessibility of the hydrous fluid. At the Cima di Gagnone area, the textural and structural evidence to indicate what factors controlled the formation of veins or what factors determined localized fluid flow have been obliterated by the latest amphibolite-facies metamorphic and deformational event. Vein-formation is associated with the eclogite-facies event and may indicate limited permeabilities and short-lived excess fluid pressures. However, deformation controls on such events are no longer recorded in these rocks. Field relations and isotopic data suggest that local steady-state flow may have been more dominant during the subsequent amphibolite-facies event, with only minimal vein formation or renewed local fluid activity along pre-existing veins (as evidenced by retrograde recrystallization of andalusite and biotite in some eclogite-facies kyanite veins).

The contrasting degrees of amphibolite-facies overprinting observed in these rocks may directly reflect the *nucleation rates* and *diffusional properties* of the dominant minerals (see also Heinrich 1982, 1983). The formation of the amphibolite-facies assemblages in the metapelites essentially involved Na-K cation exchange between micas and diffusion of Fe and Mg from garnet; whereas the formation of amphibolite from the nearly anhydrous assemblages of Omp + Gar + Kyn not only involved the addition of water into the system, but would require complete phase transformation and redistribution of most of the major elements. In addition, the presence of an *internally-derived* fluid phase and the abundance of mica in the metapelites may have contributed to an overall greater deformability during the amphibolite-facies metamorphic and deformation event, enhancing diffusive mass transfer and grain growth.

Although the metapelites exhibit recrystallized textures, chemical and isotopic equilibrium was not achieved and/or preserved. Furthermore, there is no direct evidence for pervasive, large-scale chemical or isotopic communication via a fluid phase. The isotopic and mineralogical data indicates localized and limited fluid flow across rock layers during the uplift and cooling history. The isotopic fractionations between some minerals, such as plagioclase and biotite, suggest that small quantities of fluid were present during cooling and may have acted as a diffusion medium for retrograde isotopic exchange. However, the presence of a fluid phase does not necessarily have to mean that fluid flow took place during cooling.

In general, stable isotope geochemistry may *not* be a good indicator for fluid-rock interaction in polymetamorphic pelitic terrains because:

- the dominant fluid species produced during metamorphism are close to chemical and isotopic equilibrium with the metapelites. As the produced fluid passes through overlying pelitic rocks, its chemical and isotopic composition may be buffered and the effects of fluid interaction will be difficult to document.
- The oxygen diffusion rates of the dominant minerals in pelitic rocks, such as plagioclase and biotite, may be greatly influenced by the presence of minute quantities of static intergranular pore fluids, resulting in retrograde exchange upon cooling.
- Minimal isotopic shifts in isotopic compositions will accompany dehydration reactions in pelitic rocks during successive metamorphic events.
- Isotopic mass-balance calculations of fluid-rock ratios give minimum values and are often considerably lower than those calculated on the basis of solubility data (see also Wood and Walther, 1986).
- Chemical, textural and isotopic information and details of previous metamorphic events are often masked by recrystallization and re-equilibration during the last-occurring metamorphic event.
- Although pelitic rocks may produce large volumes of fluid by devolatilization reactions during *initial* prograde metamorphism, there will be a *finite potential* to produce a free fluid phase during subsequent metamorphic events.

High fluid-rock ratios have mainly been well documented in meta-carbonate units (e.g. Ferry, 1983; Rumble et al., 1982). This should not be surprising, as interaction with an external hydrous fluid, for example one generated in an underlying pelitic sequence, would have a substantial effect on the composition of the fluid in equilibrium with the carbonate (see also Wood and Walther, 1986). In such cases, chemical and isotopic signatures as evidence of fluid-rock interaction are more likely to be recorded in the rocks. In contrast to carbonate reactions, fluid-rock interaction in pelitic rocks are often difficult to document. Wood and Walter (1986) have argued that even though pelitic sequences produce small volumes of fluid, as each increment of fluid produced in one rock volume sequentially passes through and reequilibrates with the overlying rock volumes, the actual time-integrated fluid-rock ratios, though not recorded, would approach infinity.

CHAPTER 4

MONTE MUCRONE (SESIA-LANZO ZONE): GENERAL GEOLOGY, PETROGRAPHY AND MICROFABRICS

4.1 BRIEF DESCRIPTION OF THE SESIA-LANZO ZONE.

The Sesia-Lanzo Zone is considered to be a slice of Austroalpine polymetamorphic continental crust (Dal Piaz et al, 1973; Compagnoni, 1977; Compagnoni et al, 1977; Gosso, 1977; Lardeaux, 1981) and is one of the main structural units of the internal western alps. It is bordered along the northwest by the penninic Piedmont Zone and is separated from the Canavese Zone and the Ivrea Zone to the southeast by the Canavese Line (Fig. 4.1). The Sesia-Lanzo Zone consists primarily of paraschists, orthogneisses, metacarbonates and minor ultramafics which show varying degrees of Alpine metamorphism and deformation.

Two Alpine metamorphic events have been recognized: an earlier Eo-Alpine event, producing high pressure - relatively low temperature mineral assemblages, and a subsequent Tertiary greenschist-facies metamorphism.

Various Cretaceous ages have been obtained for the earlier Alpine event and is attributed to underthrusting and subduction (Compagnoni et al, 1977; Koons, 1982; Rubie, 1984; Oberhänsli et al, 1985), whereas the latter greenschist-facies event has been dated at ~ 60 my (Dal Piaz et al, 1972; Hunziker, 1974; Oberhänsli et al, 1985). Based on whole rock isocrons, Oberhänsli et al (1985) set a minimum age of 129 ± 15 my for eclogite-facies transformation. Rb-Sr white mica ages vary between 92 and 69 my.

Peak metamorphic conditions for the eclogite/blueschist-facies metamorphism have been estimated to be in a range of 500-620 °C at minimum pressures of 14-16 Kbar, (Compagnoni, 1977; Desmons and Ghent, 1977; Koons, 1982; Hy, 1984).

4.1.1. TECTONIC UNITS

On the basis of lithology, degree of metamorphism and structural position, earlier workers (e.g. Compagnoni, 1977; Dal Piaz, 1972) have distinguished three major units:

- 1) The Eclogitic Micaschist Complex; (EMS)
- 2) The Gneiss Minuti Complex; (GM) and
- 3) The II Zona Diorito-Kinzigitica (II DK).

The II DK forms an allochthonous upper tectonic element which consists of pre-Alpine amphibolite to granulite facies kinzigites (sillimanite-biotite-garnet gneisses and schists) interlayered with amphibolites and marbles, and minor harzburgites. This unit owes its name to its close lithological similarity to the high grade paragneisses associated with marble and amphibolite (corresponding to "diorites" in the older literature) of the (first) "Zona Diorito-Kinzigitica" of the Ivrea Zone. In general, the pre-Alpine mineral assemblages are extensively preserved and have only locally been overprinted by the Alpine metamorphic events. A sharp mylonitic contact containing eclogite/blueschist-facies assemblages separates the II DK from the underlying complexes (Carraro et al, 1970; Dal Piaz et al, 1971; Lardeaux, 1981; Gosso, 1977). In part of the Sesia Zone an upper tectonic slice of EMS overlays the II DK (Lardeaux, 1981; Gosso, 1977).

Together, the EMS- and the GM-complexes, comprise the tectonically lower element of the Sesia-Lanzo-Zone. This element is distinguished from the upper element by the occurrence of abundant pre-Alpine (late Hercynian) granitic rocks and by more extensive Alpine metamorphism. Both complexes contain similar lithologies and are considered to have identical pre-Alpine metamorphic histories, belonging to a single heterogeneous basement complex. They are distinguished from each other on the basis of differing degrees of Alpine metamorphism.

The EMS-Complex is characterized by the widespread occurrence of Eo-Alpine high pressure - relatively low temperature mineral assemblages (Omp-Gar assemblages) in rocks of quartzofelspathic, carbonaceous, pelitic and basic compositions. Only rare relics of pre-Alpine mineral assemblages are preserved in less deformed areas. The internal part of the EMS-Complex shows only minor retrogression during the subsequent Tertiary metamorphism, whereas towards the contact with the GM-Complex more pervasive overprinting is found. The GM-Complex, as well as the more overprinted portions of the EMS-Complex, are characterized by a decrease in grain size and stable greenschist-facies mineral parageneses. Evidence for the previous eclogite/blueschist facies metamorphism of the GM-Complex in many areas is either lacking or has been obliterated by the later lower-pressure metamorphism.

For a more complete and detailed description of the Sesia-Lanzo zone see Compagnoni et al, 1977; Compagnoni, 1977; Gosso, 1977; Dal Piaz et al, 1972.

4.2. MONTE MUCRONE METAGRANITOIDS

Intensively deformed omphacite- and garnet-bearing orthogneiss of quartz dioritic to granitic compositions (Callegari et al, 1976) are typical of the EMS-Complex in the central Sesia-Lanzo Zone. Sharp and discordant contacts with the surrounding eclogitic

micaschists attest to the intrusive nature and pre-Alpine age of intrusion of these rocks. Swarms of meta-aplite (in part deformed) and minor pegmatite dikes crosscut both the eclogitic micaschists and the omphacite-garnet gneisses.

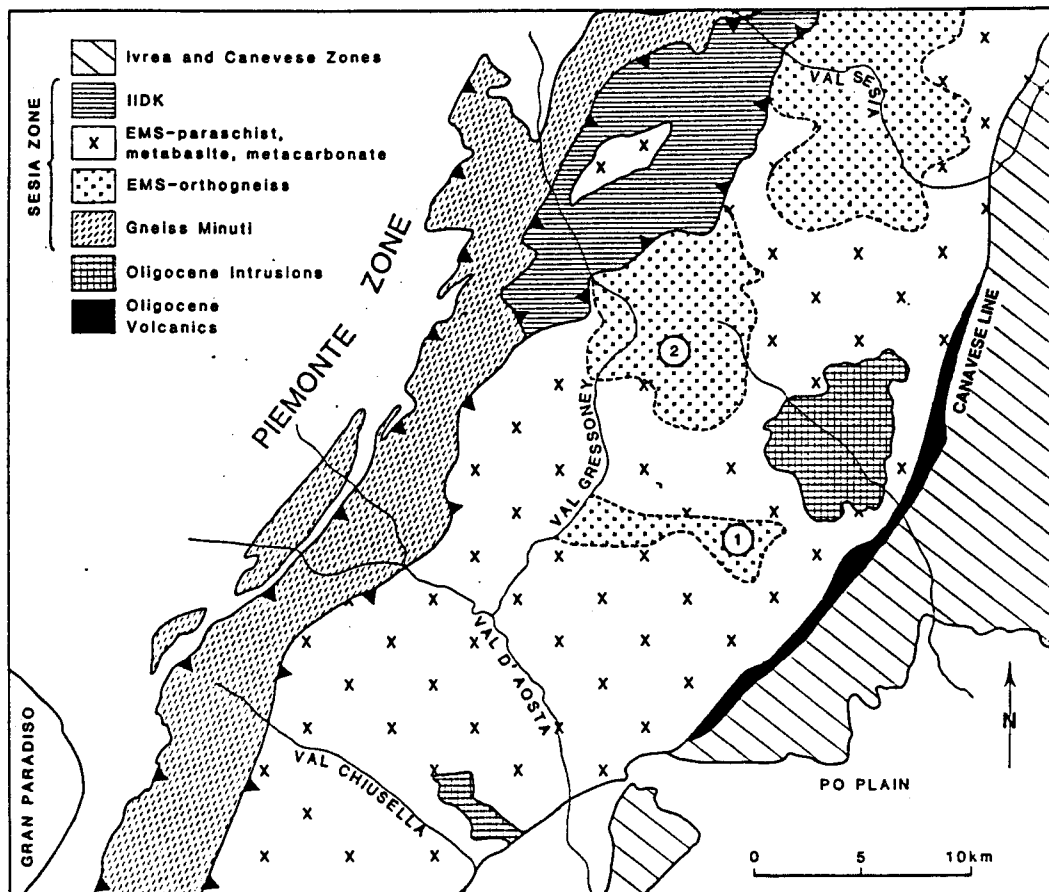


Fig. 4.1: Geologic map of the central Sesia-Lanzo Zone (Northern Italy), showing the three main tectonic units: Seconda Zona Diorito Kinzigitica (IIDK), Eclogitic Micaschist Complex (EMS), and Gneiss Minuti (Campagnoni et al. 1977). Lenses of unfoliated meta-quartz diorite occur within the EMS-orthogneiss zones at Monte Mucrone (1) and Colle della Vecchia (2). *Figure is from Koons et al., in review - modified from Campagnoni et al., 1977.*

4.2.1. GENERAL OVERVIEW

One of the best studied and structurally best-preserved metagranitoid plutons in the central Sesia-Lanzo Zone is found at the Monte Mucrone Area (upper Valle d'Oropa, NW of Biella, Italy). The Mte. Mucrone area is made up of a small granitic stock which intruded into a pelitic sequence, now consisting of omphacite and/or glaucophane-

bearing phengitic micaschists with lenses of glaucophanitic eclogites or glaucophanites. The granitic stock composes the mountain of the Mte. Mucrone and outcrops over an area of approximately 3 km² (see Fig. 4.2). This stock consists of variably deformed pyroxene-garnet orthogneisses, whereby massive portions of un-foliated metagranitic rocks are locally preserved.

Along the contact with the neighbouring eclogitic micaschists, directly south of Lago di Mucrone (Fig. 4.2), the orthogneisses are more quartz-rich and contain less mica than the omphacite-garnet gneisses occurring along the eastern side of Mte. Mucrone. The former rocks are slightly green in colour and are characterized by distinct pods and lenses of quartz, 1mm - 1.2 cm in length, which form a well-defined lineation. These quartz-rich, omphacite-garnet gneisses are cut by meta-aplite dikes.

Along the eastern face of Mte. Mucrone minor enclaves of metagranitic rocks, ranging from quartz diorite to granodiorite compositions, up to 100 m across, have escaped penetrative deformation. These unfoliated rocks are pale grey, medium-grained and have massive, well-preserved igneous textures. In some places mafic inclusions can be found. Primary igneous quartz and biotite are easily recognized macroscopically. The original euhedral plagioclase grains are pseudomorphed by fine-grained aggregates of jadeite + quartz + zoisite, which can only be distinguished microscopically. These breakdown products of plagioclase together with clear corona textures of garnet and phengite around biotite attest to the eclogite/blueschist metamorphism of these rocks.

4.2.1.1. Nomenclature

In previous literature there is some confusion in terminology of these rocks. As mentioned above, the Monte Mucrone metagranitoid stock is *not* composed of one compositionally, homogenous protolith. Although experiencing similar metamorphic and deformational histories, original compositional variations (ranging from granitic to quartz dioritic) are, in part, distinguishable on the basis of texture and feldspar content. The texturally-preserved metagranitoid rocks occurring along the eastern face of Mte. Mucrone (see Fig. 4.2) have been described in general as metagranites s.l. by Compagnoni & Maffeo (1973, p.363). According to their original quartz, K-feldspar, and (inferred) plagioclase contents, Compagnoni & Maffeo define these rocks more explicitly as metagranodiorites in agreement with the terminology presented by Streckeisen (1976).

The metagranodiorites of Compagnoni & Maffeo correspond to the meta-quartz diorites of Koons (1982), Rubie (1984), and Koons et al. (in review), to the 'metagranitoids' or 'metagranites' of Oberhänsli et al. (1985; Samples KAW 987, 988,

GEOLOGICAL MAP OF THE MONTE MUCRONE AREA

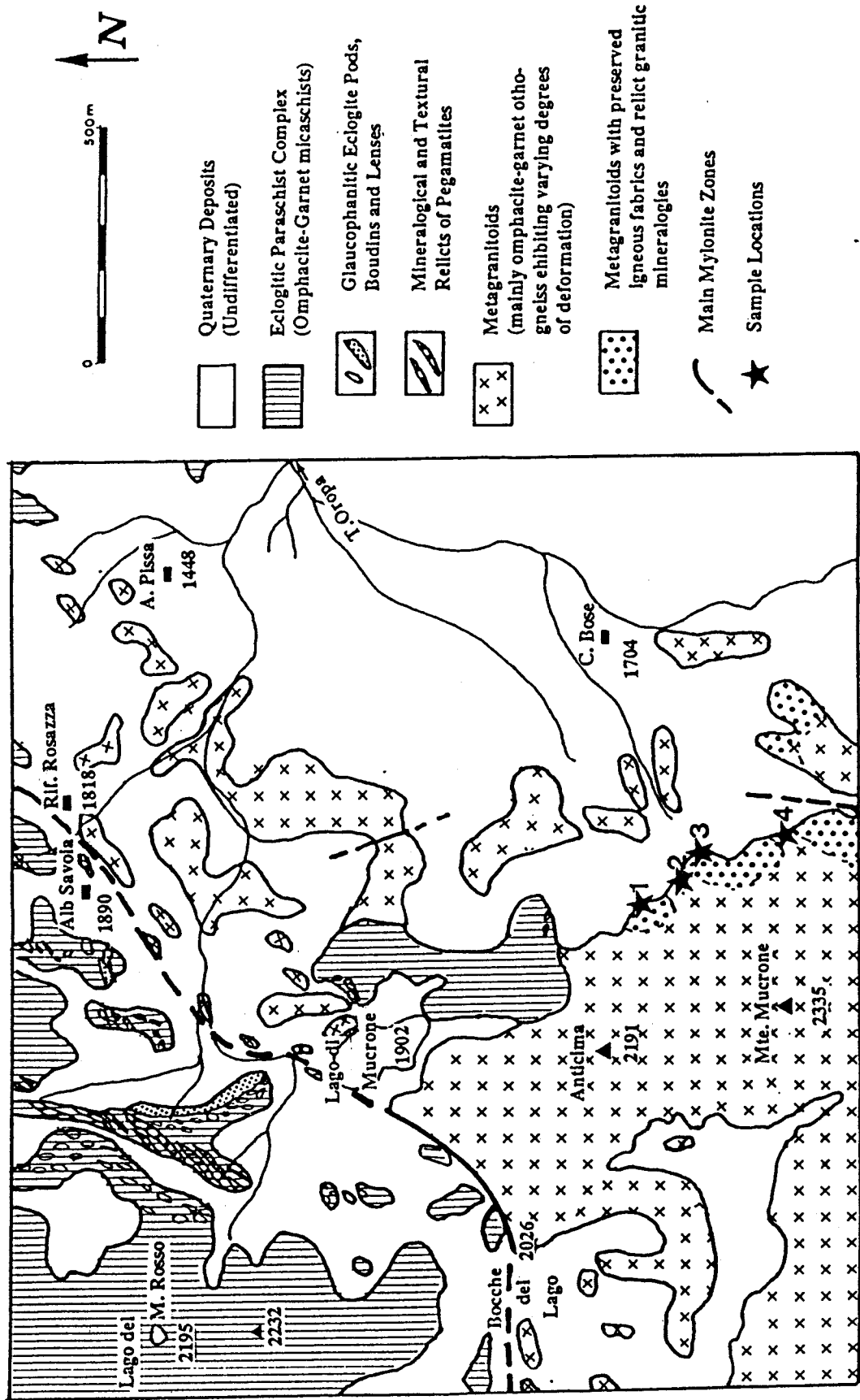


Fig. 4.2: Geological Map of the Mte. Mucrone Area, modified after Hy, 1984, Maffeo and Compagnoni (1973) and Marinotti (1972).
 Location 1: Samples Mu8, Mu9, Mu10, Mu14. Location 2: R185, Location 3: Mu1, Mu2, Mu3, Mu4, Mu5, Mu17, R13/7 Location 4: R82/9 (see Text).

1417, 1421, 1422), as well as to the 'métagranites' of Hy, (1984). The original amount of K-feldspar is difficult to determine in these rocks but appears to make up less than 5 vol % of the unfoliated samples. In the discussions to follow the term meta-quartz diorite will be used in accordance with Koons (1982), Rubie (1984) and Koons et al (in review) for the least deformed, medium- to coarse-grained rocks of approximately quartz dioritic composition (see Chapter 5) which have a well-preserved igneous texture and still contain biotite and minor K-feldspar. Such rocks are rare and can typically be found along the eastern face of Mte. Mucrone (Fig. 4.2).

The deformed and completely transformed eclogite-facies equivalents of the meta-quartz diorites shall be termed here *omphacite-garnet gneiss* (see section 4.6). They contain fine- to medium-grained quartz interlayered with omphacite, garnet, phengite and paragonite, and commonly exhibit a well-defined planar fabric. The term *jadeite-garnet (Jad-Gar) mylonites* is used to describe the intensively deformed metagranitoids which occur in narrow shear zones (see section 4.4) or in distinct mylonitic bands (e.g. sample R81/185, see also Koons et al, in review). The Jad-Gar mylonites are in general recrystallized, but show a lesser degree of chemical homogenization than the omphacite-garnet orthogneisses. Furthermore, the Jad-Gar mylonites contain more jadeitic pyroxenes than the omphacite-garnet orthogneisses, as well as numerous mineral inclusions indicative of earlier stages of transformation. The mylonites in this study are equivalent to the "transition orthogneisses" defined by Koons et al (in review). These highly deformed rocks exhibit variable amounts of overprinting, whereby different phases of recrystallization can be recognized (see section 4.4).

All the omphacite- and garnet-bearing orthogneisses in the Mte. Mucrone area have been classified as orthogneiss by Koons (1982), Rubie (1984), and Koons et al (in review) and simply metagranitoid by Oberhänsli et al (1985), regardless of the slight variations in protolith chemistries. This raises a slight problem in comparing rock types and may lead to inconsistencies in interpretation of the complex metamorphic and deformation histories of these rocks.

In some shear zones, the highly deformed rocks exhibit minimal synkinematic recrystallization (as is characteristic of the Jad-Gar mylonites), but rather contain broken pyroxene and garnet grains which are overgrown by unoriented aggregates of phengitic white mica and quartz. These texturally distinct, deformed rocks are termed '*overprinted eclogitic mylonites*', and are further distinguished from the recrystallized Jad-Gar mylonites on the basis of mineral chemistries. Large variations in textures and mineral chemistries can be observed over very short distances (< five meters), and may attest to the heterogeneous deformation and recrystallization history of this granitic body. The use of the term '*overprinted*' should not be confused with post-eclogite facies deforma-

tion and recrystallization under greenschist facies conditions, which is observed in some shear zones and some deformed rocks from the Mte. Mucrone area (see also Compagnoni and Maffeo, 1973, and Oberhänsli et al, 1982, 1985). The greenschist-facies mylonitic rocks can be distinguished from the overprinted eclogitic mylonites on the basis of quartz microfabrics and the nearly complete replacement of Na-pyroxene by white mica and albite (see Section 4.7).

The present study is concerned primarily with the *eclogite-facies* deformation and metamorphic evolution of these rocks of granodioritic to quartz dioritic compositions occurring on the eastern face of Mte. Mucrone.

4.2.2. PREVIOUS WORK

The transition from relatively undeformed meta-quartz diorite to extensively deformed and recrystallized Na-pyroxene-garnet gneiss which occur over a relatively short distance allows a reconstruction of the complex metamorphic evolution of this area and has been the subject of many detailed studies (e.g. Compagnoni and Maffeo, 1973; Koons, 1982; Oberhänsli et al 1982, 1985; Hy, 1984).

The metamorphic and microstructural evolution of the Mte. Mucrone meta-quartz diorite, together with a discussion of the effects of deformation and disequilibrium on the evolution of these rocks, is presented in detail in Koons, 1982 and Koons et al, in review. Additional geochemical, geochronological and petrographic data is presented in Oberhänsli et al (1985). A detailed structural and petrographic study of the entire Mte. Mucrone area has been carried out by Ch. Hy (1984).

The following sections describe the mineralogical and textural evolution of the meta-quartz diorite during *eclogite-facies* deformation and subsequent recrystallization. As in Chapters 2 and 3, the numbers of the samples investigated in this study are given in parentheses.

4.3. MTE. MUCRONE: UNFOLIATED META-QUARTZ DIORITE.

Along the eastern face of the Mte. Mucrone, relicts of the original igneous meta-quartz diorite are preserved as up to 100m long enclaves or pods within more intensively deformed Na-pyroxene-garnet orthogneisses, which make up the main body of the Mte. Mucrone. The meta-quartz diorites, which have escaped penetrative deformation, exhibit well-preserved igneous textures and contain a relict mineral assemblage of quartz (Qtz) + biotite (Bio) \pm K-feldspar (Ksp) \pm allanite (Aln). The original plagioclase (Plg) is pseudomorphed by very fine-grained aggregates of

Na-pyroxene + zoisite (Zoi) + quartz. The igneous protolith is thought to originally have consisted of 30-40% Qtz + 40-50% Plg ($\approx \text{An}_{20-30}$) + 10-15% Bio \pm Ksp \pm Aln.

The following sections describe the eclogite-facies metamorphic and deformation evolution of the Mte. Mucrone quartz dioritic to granodioritic stock. This evolution is characterized by heterogeneous mineral transformation and high strain deformation. The petrological, phase chemical and textural characteristics associated with this *eclogite-facies metamorphic and deformational evolution only* are presented in Sections 4.3 to 4.6. The most pertinent characteristics of the *subsequent* greenschist facies transformation are discussed in Section 4.7. This study concentrates primarily on the eclogite-facies transformation and any details discussed here should not be confused with the later lower pressure overprinting event associated with exhumation of the Sesia-Lanzo Zone.

4.3.1. MINERALOGY, PETROLOGY AND MINERAL CHEMISTRY

Based on mineralogical and textural differences, Koons (1982), Hy (1984) and Koons et al (in review) have distinguished three distinct textural domains within the meta-quartz diorite (Fig. 4.3). Detailed description of these domains are presented by the above authors and are summarized here for clarity.

Domain I represents original plagioclase grains which are pseudomorphosed by fine-grained Na-pyroxene + zoisite + quartz. Domain II is characterized by corona-replacement textures of phengitic mica (Phe) and Garnet (gar) around primary, incompletely reacted biotite grains. Domain III consists of a fine-grained white mica + quartz \pm sphene, and mainly occurs between the contacts of Plg-pseudomorphs (domain I) and corona-textured biotite (domain II). The remainder of the rock is made up of medium-grained quartz with minor K-feldspar \pm allanite.

4.3.1.1. Na-pyroxene (Pseudomorphing Plagioclase)

The original pseudomorphed grains of plagioclase (0.4-0.8mm in length) in the meta-quartz diorite are undeformed and retain a primary igneous fabric with quartz (Fig. 4.4 a,b). The fine-grained Na-Pyroxene, which pseudomorph the plagioclase, often occur as radiating xenoblastic crystals (20-60 μm dia.) and are intergrown with fine needles ($\sim 15 \mu\text{m}$ long) of zoisite and quartz (both undistinguishable in polarizing microscope; see also Compagnoni and Maffeo, 1973; Rubie, 1983, Fig. 6b and Koons et al, in review). Towards the contacts to biotite (domain II, Koons 1982), the pseudomorphs of plagioclase are often bordered by a 1-3 mm wide rim of fine-grained white mica (domain III, Koons 1982).

Due to the fine-grained nature of Na-pyroxene aggregates, electron microprobe analysis is often difficult (see also Koons, 1982; Koons et al, in review). The jadeite-content of these pyroxenes is relatively constant and ranges from $X_{\text{Jad}} = 0.80-0.93$, whereas the Ca-Tschermak component ($\text{CaAl}_2\text{SiO}_6$) varies from 0.01 to 0.14 (see Table 4.1). In addition, Koons et al (in review, Tab. 1) report a variation in $X_{\text{Mg}} (= \text{Mg}/\text{Mg} + \text{Fe}^{2+})$ from 0.01 to 0.14. The excess alumina and calcium in these analyses may be a result of fine-grained zoisite contamination. Electron microprobe analyses of pyroxenes from this study show the following range in the structural formula of Na-pyroxene (see Table 4.1, compare Koons, 1982):

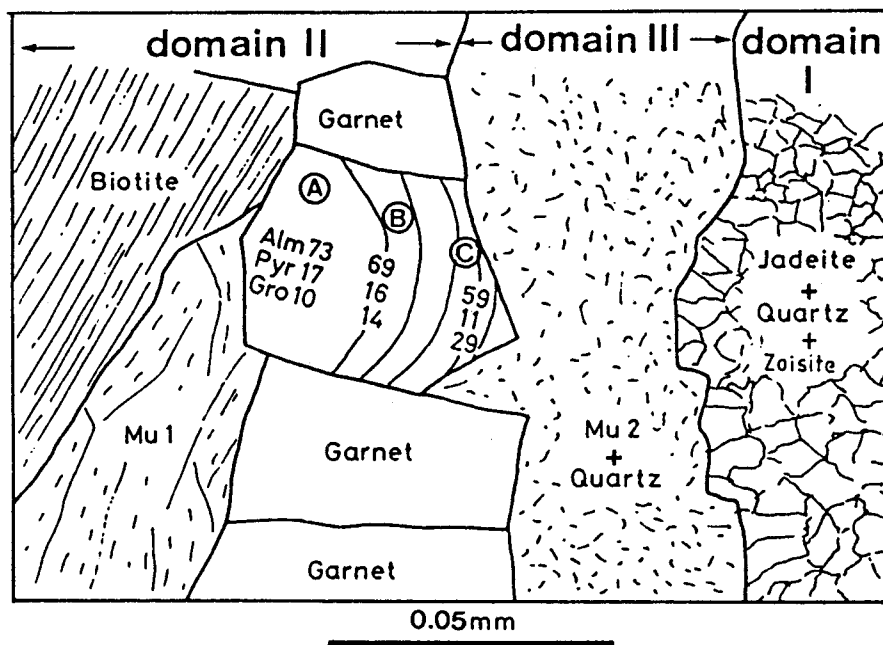


Fig. 4.3: Schematic diagram of the textural relationships between the relict igneous minerals and their replacement products in the meta-quartz diorites (From Koons et al., in review). Domains I, II and III have been defined by Koons (1982) and are based on mineralogical and textural differences (see text). The garnets of Domain II are typically $\approx 50 \mu\text{m}$ in diameter. The characteristic zoning pattern of the garnets is shown as contours of percentage almandine (Alm), pyrope (Pyr) and grossular (Gro); see Table 4.3. Muscovite 1 (Mu1) and Muscovite 2 (Mu2) are as defined by Koons, (1982); see Table 4.2.

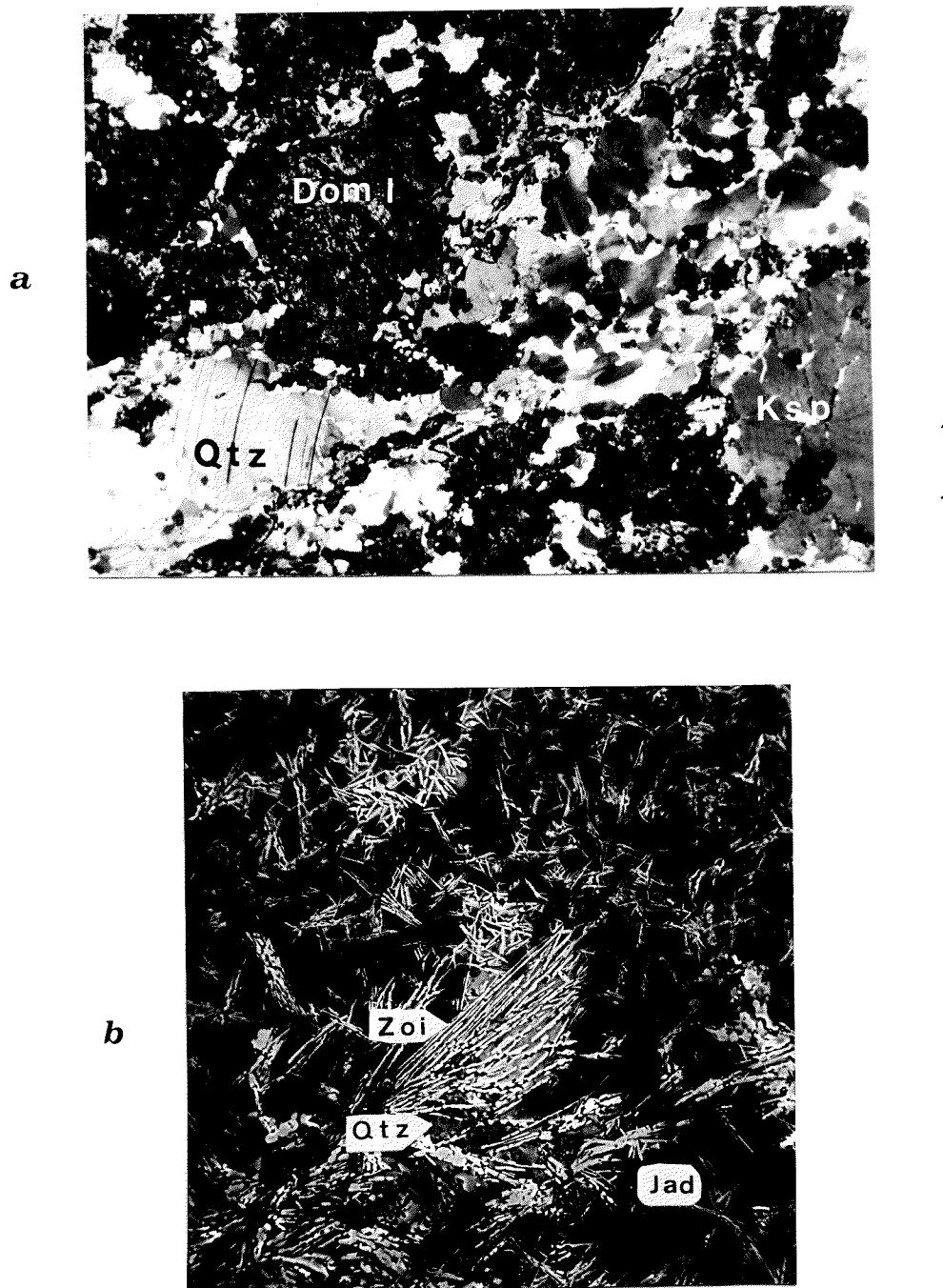
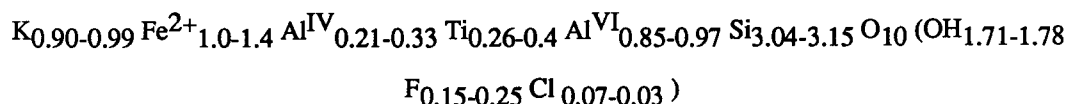


Fig. 4.4: (a) Photomicrograph of meta-quartz diorite showing Domain I (See Fig. 4.3 and text) in which plagioclase is pseudomorphed by fine-grained Jadeite (Jad) + Zoisite (Zoi) + Quartz (Qtz). Scale bar = 1.0 mm
 (b) Photomicrograph of SEM-Backscatter Images of plagioclase pseudomorphs in meta-quartz diorite.

4.3.1.2. Biotite

The biotite content of the meta-quartz diorites varies among individual samples, but in general forms approximately 10 vol% of the rock. Single grains range from 1.0 to 3.5 mm in length and occur as up to 1 cm long aggregates which define a weak foliation in some samples. As mentioned previously, the biotite grains are rimmed by fine-grained phengitic mica (0.2-0.5 mm) and euhedral garnet. No chemical zoning has been found in this study nor by previous workers (e.g Koons, 1982; Hy, 1984; Compagnoni and Maffeo, 1973). The biotites are characterized by a high Ti-content, which leads to a dark red colour in thin section, and contain up to 1 wt % F. Electron microprobe analyses of representative samples from this study show the following range in the structural formula (see Table 4.2):



This range in biotite compositions is slightly more Si-rich and slightly less Mg-rich than the averaged composition reported by Koons (1982) and Koons et al (in review).

4.3.1.3. Garnet

The garnets which rim the biotite grains form euhedral grains 0.01-0.25 mm in diameter and have sharp grain boundaries against adjacent grains. The garnets in the least deformed meta-quartz diorites are characterized by a distinct chemical zoning in which an enrichment in Ca (Gro_{30}) occurs towards the contacts with plagioclase (see Koons, 1982; Hy, 1984 and Fig. 3, Table 3 in Koons et al, in review).

4.3.1.4. Phengitic White Mica

Two chemically distinct white micas (termed here WMI and WMII, corresponding to Muscovite I and II of Koons, 1982 and Koons et al, in review) can be distinguished in the meta-quartz diorites. The micas which form coronas with garnet (Domain II, Koons, 1982) around biotite grains are high in Ti, whereas those which border quartz or plagioclase pseudomorphs (Domain III, Koons, 1982) are higher in alumina and slightly lower in Fe and Mg (Table 4.2, see also Koons, 1982; Hy, 1984; and Koons et al, in review). In some samples, the low Ti-phengitic micas (WM II) form isolate clusters with fine-grained quartz, and may represent replacement of original K-feldspar. Occasionally the replacement of K-feldspar by phengitic white mica is directly observable.

Table 4.1: Representative electron microprobe analyses of pyroxene from the variously deformed and recrystallized metagranitoids at the Mte. Mucrone (See also Appendix III). Analyses are given in weight % oxides.

MTE. MUCRONE METAGRANITOIDS: CLINO-PYROXENES

(UNFOLIATED META-QUARTZ DIORITE) (--- JAD-GAR NYLONITES ---) (OVERPRINTED NYLONITES) (-ORTHOGRNEISS-)

Sample	*MQD	*MQD	JD-GR FEL	M17B	*R185	*R185	MYL C.G.	MYL F.G.	*R191	*R191
S102	58.85	57.06	59.14	59.65	59.98	58.72	58.48	55.74	57.44	55.96
T102	0.00	0.00	0.56	0.02	0.00	0.00	0.02	0.08	0.00	0.00
Al203	24.79	25.43	23.12	21.82	22.08	21.48	22.75	11.19	18.99	12.71
Fe203	0.00	0.00	1.09	0.00	0.00	0.00	0.00	2.98	0.38	0.71
FeO	0.44	0.90	0.48	2.62	3.39	2.17	2.51	4.67	2.51	4.28
MnO	0.00	0.00	0.02	0.00	0.00	0.00	0.02	0.02	0.00	0.00
HgO	0.07	0.26	0.46	0.69	0.62	1.83	0.66	5.93	2.57	6.35
CaO	0.97	2.67	1.07	2.50	1.64	3.59	2.00	11.44	4.63	10.89
Na2O	14.21	12.87	14.78	13.05	13.08	12.45	13.51	7.93	11.69	8.00
K2O	0.04	0.03	0.02	0.05	0.00	0.00	0.07	0.03	0.00	0.00
Total	99.37	99.22	100.73	100.40	100.79	100.24	100.00	100.01	98.21	98.89

CATION DISTRIBUTION

Si	1.9968	1.9500	1.9955	2.0280	2.0311	2.0033	1.9985	1.9969	2.0143	2.0028
Ti	0.0000	0.0000	0.0143	0.0006	0.0000	0.0000	0.0005	0.0022	0.0000	0.0000
Al	0.9913	1.0242	0.9196	0.8743	0.8811	0.8636	0.9161	0.4726	0.7848	0.5361
Fe3	0.0000	0.0000	0.0277	0.0000	0.0000	0.0000	0.0000	0.0802	0.0099	0.0190
Fe2	0.0125	0.0257	0.0134	0.0746	0.0960	0.0619	0.0716	0.1400	0.0736	0.1279
Mn	0.0000	0.0000	0.0006	0.0000	0.0000	0.0000	0.0004	0.0006	0.0000	0.0000
Hg	0.0035	0.0132	0.0231	0.0348	0.0313	0.0931	0.0338	0.3166	0.1344	0.3388
Ca	0.0353	0.0978	0.0385	0.0910	0.0595	0.1312	0.0730	0.4391	0.1739	0.4175
Na	0.9347	0.8527	0.9669	0.8601	0.8587	0.8235	0.8948	0.5510	0.7947	0.5551
K	0.0017	0.0013	0.0007	0.0020	0.0000	0.0000	0.0031	0.0014	0.0000	0.0000

SITE distribution and RATIOS

xHg Fe(II+)	0.221	0.340	0.632	0.318	0.246	0.601	0.321	0.693	0.646	0.726
xHg Fe(tot)	0.221	0.340	0.359	0.318	0.246	0.601	0.321	0.590	0.617	0.697
Al(IV)	0.003	0.050	0.004	0.000	0.000	0.000	0.002	0.003	0.000	0.000
Al(VI)	0.988	0.974	0.915	0.874	0.881	0.864	0.915	0.469	0.785	0.536

ENDMEMBERS

Diopside	0.007	0.016	0.023	0.029	0.015	0.079	0.023	0.303	0.112	0.303
Wollastonite	0.016	0.024	0.018	0.045	0.030	0.066	0.036	0.219	0.087	0.209
Enstatite	0.002	0.007	0.012	0.017	0.016	0.047	0.017	0.158	0.067	0.169
Ferrosilite	0.006	0.013	0.007	0.037	0.048	0.031	0.036	0.070	0.037	0.064
CaAl2SiO6	0.003	0.050	0.000	0.000	0.000	0.000	0.000	0.000	0.000	0.000
Acmite	0.000	0.000	0.028	0.000	0.000	0.000	0.000	0.080	0.010	0.019
Jadeite	0.936	0.854	0.915	0.862	0.859	0.823	0.898	0.469	0.785	0.536

***Samples denoted with * are taken from Koons, Rubie and Frueh-Green (in review)

MTE. MICRON META-QUARTZ DIORITES: BIOTITES

MTE. MUCRONE METAGRANITOIDS: WHITE MICAS

(----- UNFOLIATED META-QUARTZ DIORITE -----) (--- JAD-GAR MTLKITES ---) (---OVERPRINTED ---) (--- ORTHOGNEISS ---)
 MTLKITES ---)

Sample	MOD M1-3	MOD M5	MOD B10	MOD M11	MOD M11	MOD M11	MOD M1-3	MOD M3	MOD M2	JD-GR FEL M17B	WN	*R1B5 WN	*R1B5 MN	MTL F.G P	MTL C.G P	*R89/9 PE	*R191 PRE
S102	38.53	39.14	39.54	49.72	51.59	48.73	47.62	51.23	49.16	50.47	49.98	48.67	49.07	50.11	48.97	49.09	
T102	4.28	6.29	5.42	2.82	2.81	0.15	0.53	0.40	0.64	1.11	0.56	0.56	0.23	1.51	0.41	0.33	
Al203	13.04	13.09	12.54	24.74	26.27	27.33	31.89	28.63	28.89	27.00	31.52	28.68	29.45	25.60	31.34	29.36	
Fe2O3	0.00	0.00	0.00	1.76	2.43	0.00	0.00	2.03	0.39	2.67	1.70	0.00	1.24	1.10	1.40	2.63	
FeO	20.01	15.75	15.12	1.20	0.00	2.56	1.59	0.00	1.40	0.00	0.00	1.26	1.48	1.90	0.00	0.00	
MnO	0.22	0.05	0.04	0.00	0.00	0.00	0.00	0.00	0.00	0.00	0.00	0.00	0.00	0.00	0.00	0.00	
MgO	9.55	10.82	11.80	3.87	3.66	2.42	1.34	3.15	2.48	3.85	2.05	2.20	2.03	3.31	2.26	2.65	
CaO	0.07	0.04	0.00	0.00	0.00	0.06	0.00	0.00	0.00	0.01	0.00	0.00	0.00	0.00	0.00	0.00	
Mg2O	0.06	0.27	0.03	0.12	0.07	0.32	0.23	0.11	0.25	0.23	0.72	0.50	0.18	0.11	1.09	0.96	
K2O	8.98	9.84	10.02	11.04	9.59	11.03	11.20	10.30	10.96	11.15	9.72	10.46	11.07	11.17	9.55	9.27	
F	0.62	0.97	0.00	0.25	0.00	0.23	0.28	0.00	0.61	0.00	0.00	0.12	0.17	0.17	0.00	0.00	
Cl	0.47	0.32	0.00	0.03	0.00	0.05	0.04	0.00	0.07	0.00	0.00	0.00	0.03	0.04	0.00	0.00	
Σ20	3.36	3.25	3.79	4.32	4.59	4.21	4.30	4.57	4.13	4.55	4.59	4.36	4.39	4.34	4.53	4.47	
Total	99.21	99.85	98.30	99.87	101.02	97.09	99.02	100.62	98.99	101.23	100.84	96.69	99.30	99.36	99.55	98.16	

CATIONS calculated on the basis of 7. cations and 12. oxygens

Si	3.0554	3.0996	3.1217	3.3486	3.3664	3.3662	3.2127	3.3594	3.3195	3.3268	3.2637	3.3479	3.3021	3.3871	3.2418	3.2939
Ti	0.2551	0.3736	0.3218	0.1426	0.1379	0.0077	0.0268	0.0197	0.0325	0.0550	0.0275	0.0290	0.0116	0.0766	0.0204	0.0167
Al	1.2188	1.2184	1.1668	1.9636	2.0202	2.2266	2.5559	2.2125	2.2992	2.0977	2.4257	2.3250	2.3359	2.0391	2.4450	2.3217
Fe	1.3270	1.0401	0.9982	0.0694	0.1195	0.0000	0.0000	0.1003	0.0200	0.1424	0.0635	0.0000	0.0630	0.0561	0.0697	0.1027
Mn	0.051	0.0032	0.0027	0.0677	0.0000	0.1480	0.0895	0.0000	0.0790	0.0000	0.0000	0.0000	0.0000	0.1074	0.0000	0.0000
Mg	1.287	1.2741	1.3889	0.0000	0.0000	0.0000	0.0000	0.0000	0.0000	0.0000	0.0000	0.0000	0.0000	0.0000	0.0000	0.0000
Ca	0.0059	0.0033	0.0000	0.3881	0.3560	0.2495	0.1351	0.3079	0.2498	0.3782	0.1996	0.2256	0.2040	0.3337	0.2230	0.2651
K	0.0098	0.0414	0.0046	0.0000	0.0000	0.0000	0.0000	0.0000	0.0000	0.0000	0.0000	0.0000	0.0001	0.0000	0.0000	0.0000
F	0.1567	0.2425	0.0000	0.0161	0.0089	0.0426	0.0304	0.0140	0.0325	0.0290	0.0912	0.0667	0.0236	0.0145	0.1399	0.2419
Cl	0.0638	0.0428	0.0000	0.9485	0.7981	0.9724	0.9635	0.8614	0.9443	0.9375	0.8095	0.9176	0.9499	0.9628	0.8063	0.7933
OB	1.7795	1.7147	2.0000	0.0035	0.0000	0.0062	0.0049	0.0000	0.0084	0.0000	0.0000	0.0000	0.0032	0.0374	0.0000	0.0000
Total	1.9434	2.0000	1.9428	1.9434	2.0000	1.9428	1.9254	2.0000	1.8612	2.0000	2.0000	2.0000	1.9578	2.0000	2.0000	2.0000

Si:Fe distribution and M2:10S

xMg (Fe1+)	0.460	0.551	0.562	0.651	1.000	0.628	0.602	1.000	0.760	1.000	1.000	0.757	0.710	0.756	1.000	1.000
xMg (Fe tot)	0.460	0.551	0.562	0.749	0.628	0.602	0.754	0.716	0.726	0.705	0.757	0.582	0.671	0.762	0.721	0.706
Al(IV)	0.945	0.909	0.878	0.651	0.634	0.632	0.787	0.641	0.680	0.673	0.736	0.652	0.698	0.613	0.758	0.706
Al(VI)	0.274	0.309	0.288	1.312	1.387	1.595	1.749	1.572	1.619	1.424	1.689	1.673	1.638	1.426	1.687	1.616

***Samples denoted with * are taken from Ioccos, Rubie and Frueh-Green (in review).

Table 4.2: Representative electron microprobe analyses of mica from the variously deformed and recrystallized metagranitoids at the Mte. Mucrone (See also Appendix III). Analyses are given in weight % oxides.

MTE. MUCRONE METAGRANITOIDS: GARNETS

Sample	(--UNFOLIATED META-QUARTZ DIORITE--)										(--OVERPRINTED MUCRONES--)										(--OMP-GAR OR THOGEISS--)	
	*HQD A	*HQD B	*HQD C	JD-G3	FELS	17B RIMS	17B CORES	*R185 CORES	*R185 RIMS	RIMS (GarIII)	CORES (GarII)	IDIOM. (GarIII)	VEINS	R191 CORES	R191 RIMS							
SiO2	38.23	38.41	38.66	38.17	38.44	38.28	37.37	37.88	38.36	37.81	37.71	38.18	38.01	38.21								
TiO2	0.09	0.12	0.08	0.14	0.17	0.14	0.05	0.00	0.06	0.22	0.05	0.11	0.05	0.00								
Al2O3	21.21	21.37	21.14	21.75	21.24	21.32	20.95	21.39	21.30	21.06	20.92	21.37	21.57	21.49								
Fe2O3	0.19	0.13	0.65	0.00	0.10	0.11	0.32	0.08	0.51	0.21	0.95	0.08	0.00	0.09								
FeO	31.87	31.06	26.48	27.27	27.39	27.49	25.90	25.88	20.71	26.52	22.05	22.22	25.61	24.79								
MnO	0.71	0.68	0.43	0.44	0.85	1.29	0.33	0.40	0.38	1.18	0.34	0.52	0.40	0.39								
MgO	4.32	3.94	2.85	2.31	1.98	1.86	1.71	2.60	0.71	1.27	0.86	0.54	3.06	2.81								
CaO	3.35	4.78	10.15	10.36	9.79	9.98	12.06	11.21	18.16	11.43	16.60	16.73	10.41	11.87								
K2O	0.03	0.07	0.03	0.01	0.10	0.05	0.00	0.00	0.03	0.05	0.03	0.01	0.03	0.00								
K2O	0.03	0.03	0.04	0.02	0.01	0.01	0.00	0.02	0.01	0.15	0.01	0.01	0.02	0.01								
Total	100.03	100.59	100.52	100.47	100.07	100.53	98.69	99.46	100.23	99.90	99.53	99.78	99.19	99.67								

Sample	CATION DISTRIBUTION													
	S1	T1	Al	Fe3	Fe2	Mn	Mg	Ca	Na	K				
S1	3.0338	3.0273	3.0362	3.0032	3.0460	3.0250	2.9972	2.9993	3.0058	3.0079	2.9868	3.0155	3.0092	3.0090
T1	0.0054	0.0071	0.0047	0.0083	0.0100	0.0083	0.0030	0.0000	0.0036	0.0130	0.0033	0.0063	0.0030	0.0000
Al	1.9836	1.9850	1.9566	2.0173	1.9839	1.9850	1.9802	1.9960	1.9665	1.9745	1.9532	1.9889	2.0125	1.9944
Fe3	0.0111	0.0079	0.0387	0.0000	0.0061	0.0066	0.0196	0.0048	0.0299	0.0125	0.0567	0.0048	0.0000	0.0056
Fe2	2.1150	2.0470	1.7390	1.7944	1.8151	1.8165	1.7369	1.7133	1.3567	1.7641	1.4604	1.4677	1.6954	1.6327
Mn	0.0477	0.0454	0.0286	0.0293	0.0567	0.0863	0.0224	0.0268	0.0254	0.0793	0.0227	0.0346	0.0268	0.0260
Mg	0.5111	0.4630	0.3337	0.2710	0.2340	0.2189	0.2045	0.3069	0.0824	0.1511	0.1011	0.0638	0.3612	0.3299
Ca	0.2848	0.4036	0.8540	0.8730	0.8313	0.8451	1.0362	0.9509	1.5247	0.9744	1.4091	1.4156	0.8855	1.0014
Na	0.0046	0.0107	0.0046	0.0018	0.0156	0.0073	0.0000	0.0000	0.0039	0.0081	0.0053	0.0015	0.0046	0.0000
K	0.0030	0.0030	0.0040	0.0018	0.0012	0.0008	0.0000	0.0020	0.0011	0.0150	0.0015	0.0013	0.0020	0.0010

Sample	ED MEMBERS													
	Grossular	Almandine	Pyrope	Spessartine	Andradite	Other	Other	Other	Other	Other				
Grossular	0.087	0.127	0.266	0.290	0.272	0.275	0.334	0.315	0.492	0.313	0.440	0.469	0.296	0.332
Almandine	0.714	0.690*	0.588	0.604	0.616	0.611	0.579	0.572	0.453	0.593	0.487	0.492	0.570	0.546
Pyrope	0.172	0.156	0.113	0.091	0.079	0.074	0.068	0.102	0.028	0.051	0.034	0.021	0.122	0.110
Spessartine	0.016	0.015	0.010	0.010	0.019	0.029	0.007	0.009	0.008	0.027	0.008	0.012	0.009	0.009
Andradite	0.006	0.004	0.020	0.000	0.003	0.003	0.010	0.002	0.015	0.006	0.028	0.002	0.000	0.003

Table 4.3: Representative electron microprobe analyses of garnet from the variously deformed and recrystallized metagranitoids at the Mte. Mucrone (See also Appendix III). Analyses are given in weight % oxides.

4.3.1.5. Quartz

Two size distributions of quartz can be distinguished in the least-deformed meta-quartz diorites (Fig. 4.5a). Irregularly-shaped cores, up to 2 mm in length, are surrounded by more or less equigranular dynamically recrystallized grains, 0.05-0.5 mm in diameter, typical of core-and-mantle-fabric described by White (1973). The cores have distinct deformation bands and undulatory extinction, whereas the smaller recrystallized grains forming the mantle are relatively strain-free and show no definite preferred orientation of the C-axis. Late-stage cracking may be present in the quartz grains. (see section 4.4.1.4.1. for a further discussion).

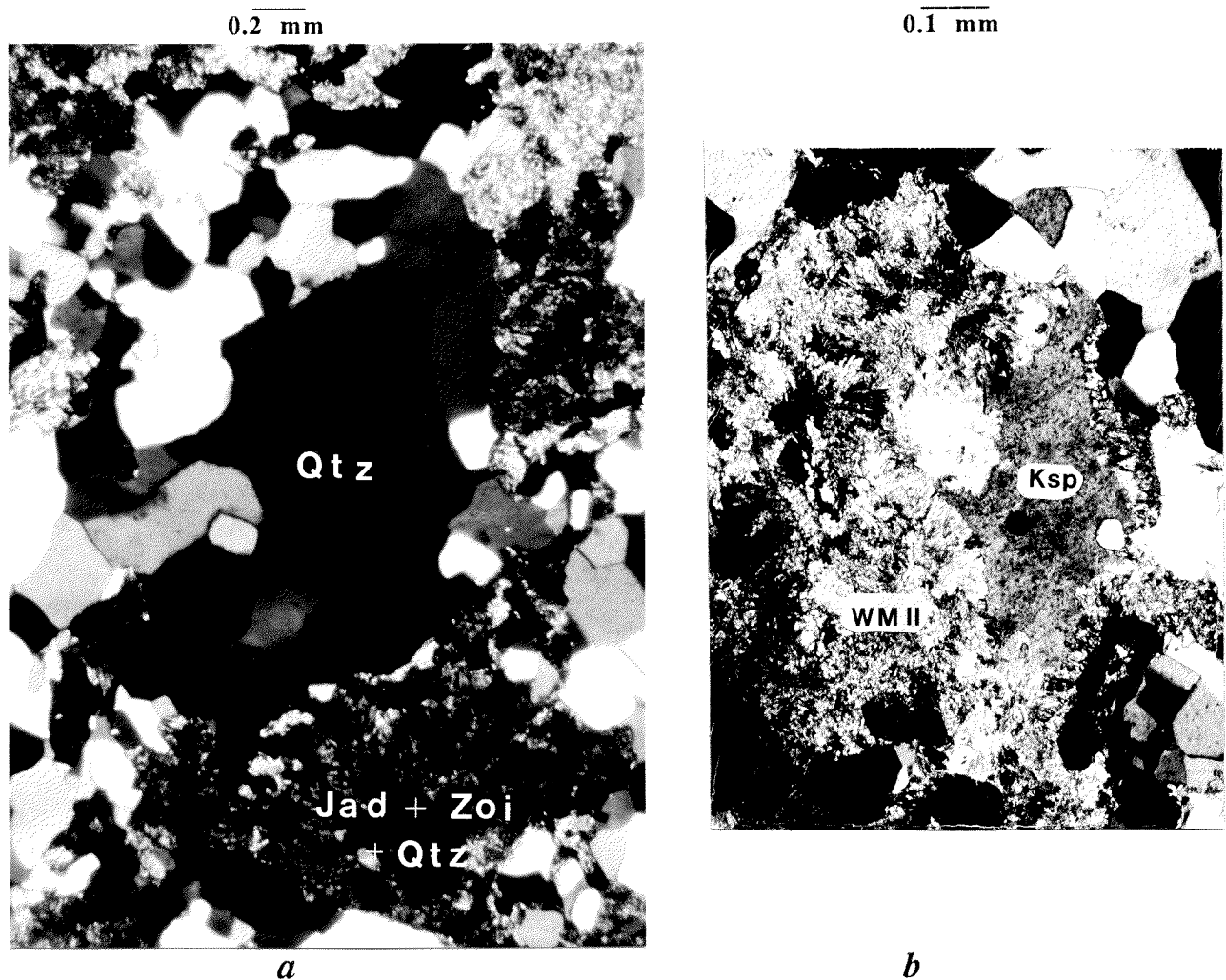


Fig. 4.5: (a) Photomicrograph of quartz in the meta-quartz diorites. Irregularly shaped cores are mantled by equigranular recrystallized, strain-free grains. (b) Photomicrograph of replacement of original igneous K-feldspar by phengite (low Ti variety, see Table 4.2).

4.3.1.6. K-feldspar

The amount of K-feldspar in the original quartz diorite is difficult to estimate, due to the uncertain amount of replacement by phengite and quartz. In the least deformed meta-quartz diorites, K-feldspar occurs as isolated porphyroblasts, up to 2 mm in length, or as small grains (0.5-1.0 mm in length) located between quartz grains and the plagioclase pseudomorphs. As stated above, in some cases, replacement by fine-grained, radiating phengitic mica (low-Ti variety, Mus II of Koons, 1982) can be observed along the edges of K-feldspar (Fig 4.5b, Mu 1-3B). Such replacement textures are always associated with clusters of phengitic mica + quartz defined as Domain II by Koons (1982) and Koons et al (in review). In the samples investigated in this study, relict K-feldspar constitutes less than 3% of the rocks. The grains nearly always exhibit undulatory extinction and often contain a series of phengite-filled parallel cracks through the crystals.

4.3.2. *DEFORMATION AND RETROGRADE OVERPRINTING IN THE META-QUARTZ DIORITES*

Although the meta-quartz diorites have escaped penetrative deformation and have a preserved igneous fabric, deformation is evident by a slight alignment of biotite clusters, by pronounced undulatory extinction and deformation bands in the cores of quartz grains and in relict K-feldspar, and by discontinuous, semi-parallel zones of fine-grained phengitic mica (~ 0.05-0.2 mm wide). Later stage fractures (up to 0.1 mm wide), oriented nearly perpendicular to the weak foliation, are observed in some samples; and in some cases are filled with fine-grained quartz + albite.

In more deformed and recrystallized samples of meta-quartz diorite, retrograde overprinting is characterized by replacement of jadeite by fine-grained, unoriented aggregates of phengitic mica + quartz. Recrystallization after high pressure formation of jadeite + quartz + zoisite after plagioclase is minimal in the meta-quartz diorite samples investigated in this study. However, an increase in the degree of replacement of jadeite by phengite + quartz is observed in samples which are located less than 0.5 meters away from mylonitic shear zones (see below).

4.3.3. *SUMMARY AND DISCUSSION*

The meta-quartz diorites are only preserved as rare isolated pods or lenses in more intensively-deformed Na-pyroxene-garnet orthogneisses. These rocks are characterized by:

- a well-preserved igneous fabric
- a large variation in grain-size
- pseudomorph-textures of jadeite + quartz + zoisite after plagioclase
- corona textures of garnet + phengitic white mica around relict biotite
- a distinct chemical zoning in garnet
- two distinct white mica compositions
- a lack of penetrative Alpine deformation.

The reaction behaviour of the meta-quartz diorite and the effects of non-equilibrium diffusional processes are presented in detail by Koons et al (in review; see also Hy, 1984) and are discussed further in Ch. 5. The pseudomorph textures after plagioclase together with the coronas around biotite represent incomplete breakdown reactions of these two primary igneous mineral phases. The distinct mineralogical and textural domains, as well as the chemical zoning patterns in the garnets and the two compositionally different white micas indicate *limited chemical communication* and incomplete recrystallization during the early stages of the metamorphic evolution of these rocks. The chemical compositions of these product phases seem to be a function of their relative physical positions to the reacting phases and reflect slow diffusion rates during the biotite and plagioclase breakdown reactions. These incomplete reactions during the initial phase of eclogite transformation directly influenced the rheological behaviour of the meta-quartz diorite during subsequent eclogite-facies deformation (see below).

4.4 ECGITIC MYLONITES IN DUCTILE SHEAR ZONES (samples Mu1-1, 1-2, 4-2, Mu 17b, R185, R13/7)

Although the meta-quartz diorites have escaped penetrative deformation, they are commonly cut by numerous shear zones which have produced fine-grained, banded mylonites containing eclogite-facies mineral assemblages (Fig. 4.6). The shear zones vary in length and are up to 30 cm in width. Thin pink veins, 2mm to 1.2 cm in width, containing zoisite, garnet and quartz, are often associated with these zones. These veins are nearly parallel to the mylonite zones and in some cases have been folded by further deformation. A zone of medium- to coarse-grained, undeformed jadeite-garnet orthogneiss (1-5 cm in width) commonly separates the zoisite veins from the mylonite zones.

Macroscopically, the mylonites are characterized by 1.5-4.0 mm thin bands of pyroxene, garnet and white mica which are separated by equally thin, semi-continuous bands of quartz, locally forming cm-long pods and augen-shaped porphyroclasts. Late-stage fractures, up to 3mm wide, occur perpendicular to the foliation formed in the mylonites.

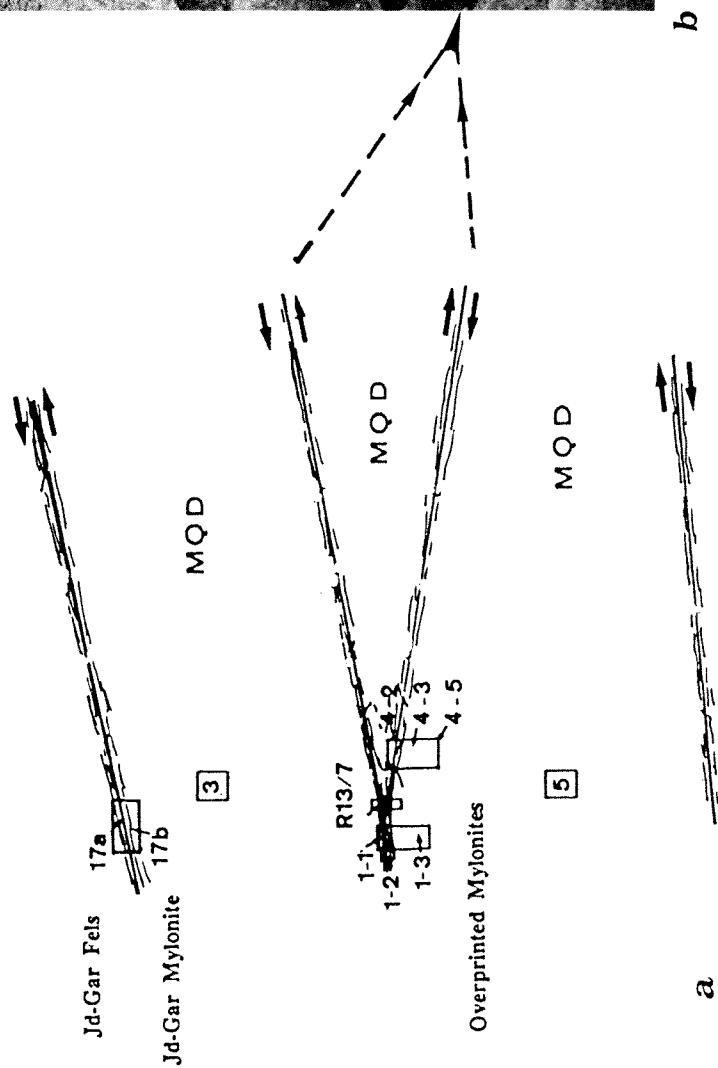


Fig. 4.6: (a) Schematic diagram of sample locations and outcrop relationships of ductile shear zones preserved in relicts of meta-quartz diorite along the eastern face of the Mte. Mucrone. (Scale 1cm ~ 1m). (b) Photograph of the central shear zones shown in (a). Banded mylonites occur in the centers of the shear zones and contain the eclogite mineral assemblage jadeite + quartz + garnet + phengitic white mica. This outcrop corresponds to Location 3 in Fig.4.2. Sample numbers are written in parentheses in the text.

In this study, a series of samples have been collected across a number of eclogitic mylonite zones which occur either as semi-parallel or conjugate shear zones along the eastern face of the Monte Mucrone (see Loc. 3, Fig. 4.2). This outcrop has been chosen for detailed petrographic and oxygen-isotope analysis because the transition from least-deformed meta-quartz diorite to mylonite occurs over a small distance of less than 50 cm. The following discussion describes the transition from most-deformed mylonites in the center of these shear zones to unfoliated meta-quartz diorite.

4.4.1 ECLOGITIC MYLONITES: PETROLOGY, MINERAL CHEMISTRY AND MICROFABRICS

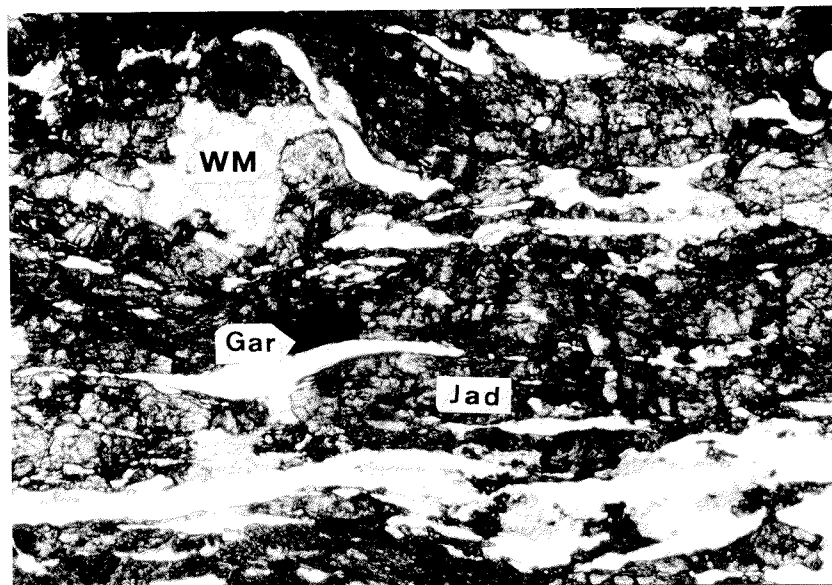
The eclogitic mylonites are easily distinguished from the meta-quartz diorites on the basis of an overall smaller grain-size, a strong planar fabric and mineral banding and a lack of biotite. These rocks contain quartz, Na-pyroxene, phengitic white mica and garnet with minor sphene, rutile, albite, zoisite and rarely relict K-feldspar, allanite and biotite (analyses in Table 4.1, 4.2, 4.3 and App.III).

Microscopically, the mylonites indicate a complex multi-phase crystallization/deformation history. The jadeitic pyroxene + quartz + zoisite aggregates, which pseudomorph plagioclase in the meta-quartz diorites, have been highly strained, producing mm-thin, discontinuous layers (Fig. 4.7). Individual garnet and Na-pyroxene grains are distinctly coarser-grained than those in the less-deformed meta-quartz diorites, and often exhibit post-shearing cracking and replacement by phengite \pm albite. Phengitic white mica is pervasive throughout most rocks, whereby several texturally different generations of mica growth may be distinguished.

In the following discussion, the intensively deformed samples which macroscopically exhibit mylonitic fabrics and contain primary eclogite-facies mineral assemblages with *little or no replacement of pyroxene* are termed *jadeite-garnet (Jad-Gar) mylonites*. Texturally the Jad-Gar mylonites are similar to the *transition orthogneisses* of Koons et al (in review; e.g. sample R185); however some variations in mineral chemistries are observed. Samples which contain phengitic white mica as a replacement product of sodic pyroxene are called *overprinted eclogitic mylonites*. The term "overprinted mylonites" does not necessarily infer large changes in temperature and pressure conditions (see Sect. 5.1.2), but rather describes subsequent recrystallization of the jadeite-garnet mylonite, most likely during eclogite-facies metamorphic conditions. Furthermore, the use of the term 'overprinted' should not be confused with post-eclogitic facies deformation and recrystallization (under greenschist-facies conditions) observed in some shear zones and deformed rocks from the Mte. Mucrone area. The greenschist-facies mylonitic rocks can be distinguished from the overprinted

eclogitic mylonites discussed here on the basis of microfabrics and mineralogies, and is discussed in Sect. 4.7. It should also be emphasized that all of the mylonitic rocks at the Mte. Mucrone area are *macroscopically* nearly identical. The distinction between them (i.e. Jad-Gar mylonite, overprinted eclogitic mylonite and greenschist-facies mylonite) can solely be made on the basis of mineral constituents and phase chemistries.

In general, the mineralogical transition *from* eclogitic mylonite (EML) *to* less-deformed meta-quartz diorite (MQD) takes place more or less gradually over a distance of 3-10 cm; whereas the textural distinction between the two rock types occurs abruptly over distances of 1 cm or less. The transition EML- \rightarrow MQD is characterized by an *overall* coarser grain-size, by a less pronounced parallel fabric of the pyroxene, garnet and white mica grains, and by an increase in the amount of relict biotite and allanite.



0.2 mm

Fig. 4.7: Photomicrograph showing the result of deformation and eclogite-facies recrystallization in the jadeite-garnet mylonites (sample Mu 17b). See Tables 4.1, 4.2, and 4.3 for mineral compositions

4.4.1.1. Na-pyroxene

Although there is an *overall* grain-size reduction in the eclogitic mylonites (compared to the less deformed MQD), the pyroxene grains in the shear zones are distinctly coarser-grained than those in the meta-quartz diorite (up to 0.5 mm) and form mm-thin, highly deformed, discontinuous layers (Fig. 4.7). Replacement by white mica + quartz (\pm albite) is common, whereby the pyroxenes are preserved as isolated grains, together with garnet, in the centers of unoriented white mica \pm albite clusters, in which the individual grain boundaries are often difficult to distinguish. In the overprinted eclogitic mylonites the pyroxene grains are often broken, exhibit undulatory extinction, and/or occur as imbricated grains (Fig. 4.8). New growth of fibrous pyroxene (or less commonly white mica + quartz) is found between the cracks of the deformed grains.

Fine-grained zoisite is often associated with the cracked and deformed pyroxene layers. Individual zoisite grains are rarely larger than 0.01 mm in length and occur in bands of single-grain thickness, which are either parallel to the main foliation or follow the pyroxene grain boundaries. In areas of extensive replacement of jadeitic pyroxene by phengite, the fine-grained zoisite crystals often preserve the shapes of the original, deformed pyroxene grains (see also Fig. 4.9).

Application of SEM-backscatter techniques shows that in some pyroxenes, fine needles ($\sim 10 \mu\text{m}$ long) of zoisite are randomly oriented throughout the grains and resemble the textures formed by jadeite + zoisite + quartz as plagioclase-pseudomorphs in the less deformed meta-quartz diorites. In other grains, zoisite occurs as stubby crystals which are oriented in semi-parallel bands through the pyroxene grains or as bands around the outside of the pyroxenes (white grains in Fig. 4.9 a,b). Further inclusions in pyroxenes include irregularly-shaped "blebs" of quartz and very rarely white mica. Qualitative EDS-analyses indicate that the texturally-different zoisites contain minor amounts of Fe; however a compositional distinction between the two could not be made.

A second generation of fine-grained, nearly idiomorphic, clear Na-pyroxene occurs as 0.5-0.1 mm wide rims along contacts between quartz and garnet or between quartz and phengite-replaced pyroxene domains, as well as in isolated "pockets" within the deformed and recrystallized quartz bands. These pyroxenes can be distinguished from the coarser, deformed pyroxenes by their smaller grain-size, by their inclusion-free nature and by a distinct grass-green weakly pleochroic colour (Fig. 4.10).

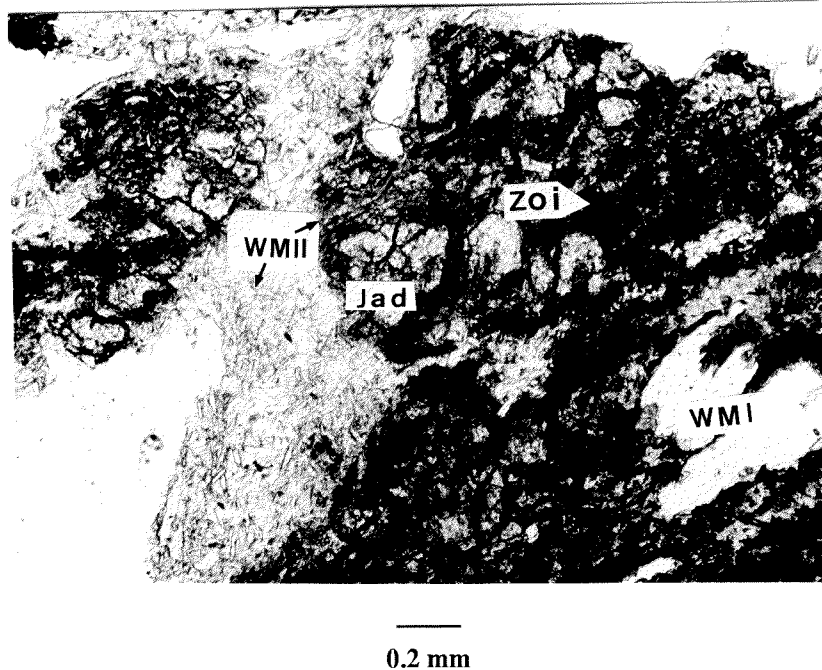


Fig. 4.8: Photomicrograph of cracked jadeitic pyroxene grains (Jad) in the overprinted mylonites, surrounded by fine-grained aggregates of zoisite and phengitic white mica (WMII) with deformed relicts of the high-Ti white mica (WMI). See also Fig. 4.9a.

Microscopic analysis of samples collected across different shear zones in the same area shows a large variation in the amount of replacement of Na-pyroxene by phengitic white mica. In the Jad-Gar mylonites (e.g. Mu 17b), the pyroxenes show little replacement and occur as elongate grains often with garnet, in semi-parallel layers (0.1-1 mm wide) between recrystallized quartz (Fig. 4.7 & 4.18a). These less-overprinted samples are further distinguished by a lack of the texturally-distinct, second generation of pyroxene and by less pronounced, fine-grained zoisite layers. SEM-backscatter analysis of these pyroxene layers in the jd-gar mylonites indicates a greater degree of recrystallization and only minor amounts of stubby zoisite inclusions (Fig. 4.9b). Quartz is more commonly found as inclusions in these pyroxenes. Sample Mu 17b (for sample locations, see Fig. 4.6) collected in this study, is texturally and mineralogically similar to the *transition orthogneiss* sample R81/185 of Koons et al (in review).

Away from the shear zones, the pyroxenes form less distinct mineral bands and gradually occur as isolated clusters, in which the shapes of the original, igneous plagioclase grains become more apparent. In profiles of samples which show overprinting in the mylonites, static replacement of pyroxene by white mica can be followed into less deformed areas of meta-quartz diorite in which the original igneous fabric is preserved (20-30 cm from the centers of the mylonite zones). The second generation of fine-grained undeformed pyroxene are also found in the meta-quartz diorite samples located near the shear zones.

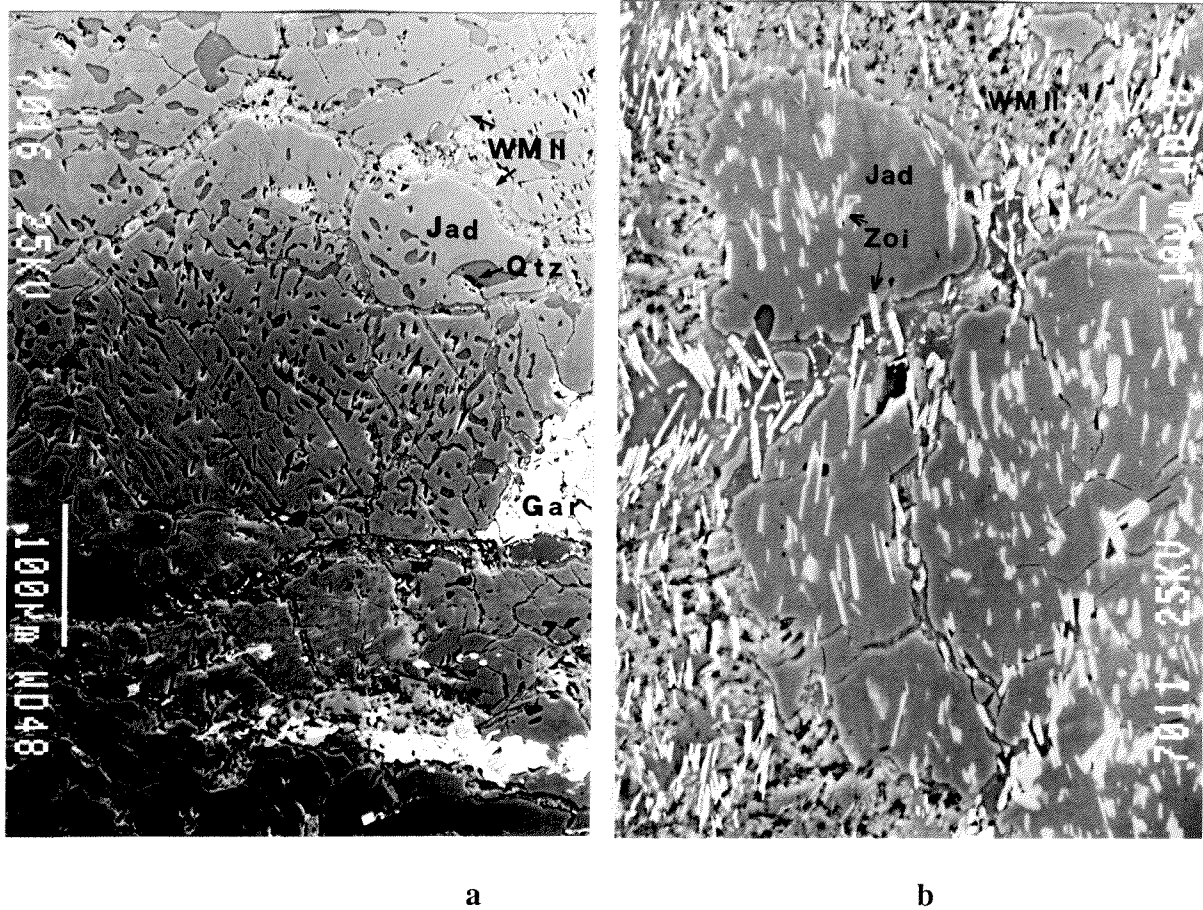


Fig. 4.9: SEM Backscatter Images: Comparison of jadeitic pyroxene microfabrics in (a) the jadeite-garnet mylonites (sample Mu 17b, see also Fig. 4.7) to those in (b) the overprinted mylonites. Quartz (darker grey) is the primary inclusion mineral in the jadeite-garnet mylonites; whereas zoisite (white) occurs as inclusions in- and surrounding the pyroxene layers (lighter grey tones) in the overprinted samples.

4.4.1.1.1 Pyroxene chemistry

As with the meta-quartz diorites, electron microprobe analysis of the Na-pyroxenes is made difficult due to the fine-grained inclusions of zoisite + quartz and due to the retrograde replacement by phengite + quartz \pm albite. The compositions of the coarser-grained pyroxenes in both the Jad-Gar mylonites and the overprinted mylonites are similar to those in the less deformed meta-quartz diorites (Fig. 4.11). The jadeite-content (Jad) lies within a range $X_{\text{Jad}} = 0.80-1.0$; whereas X_{Mg} ($= \text{Mg}/(\text{Mg} + \text{Fe}^{2+})$) ranges from 0.0 to 0.60 (Table 4.1 and App.IV a).

The acmite- (Acm) and Ca-Tschermak's (CaTs)-contents of these jadeitic pyroxenes are generally 0.0; however some rim compositions in grains which have a lower Jad-component are enriched in the Tschermak's (Ts) molecule (CaAlSiAlO_6) up to 0.13. Other than these variations in some samples, no distinct zoning could be found in the pyroxenes.

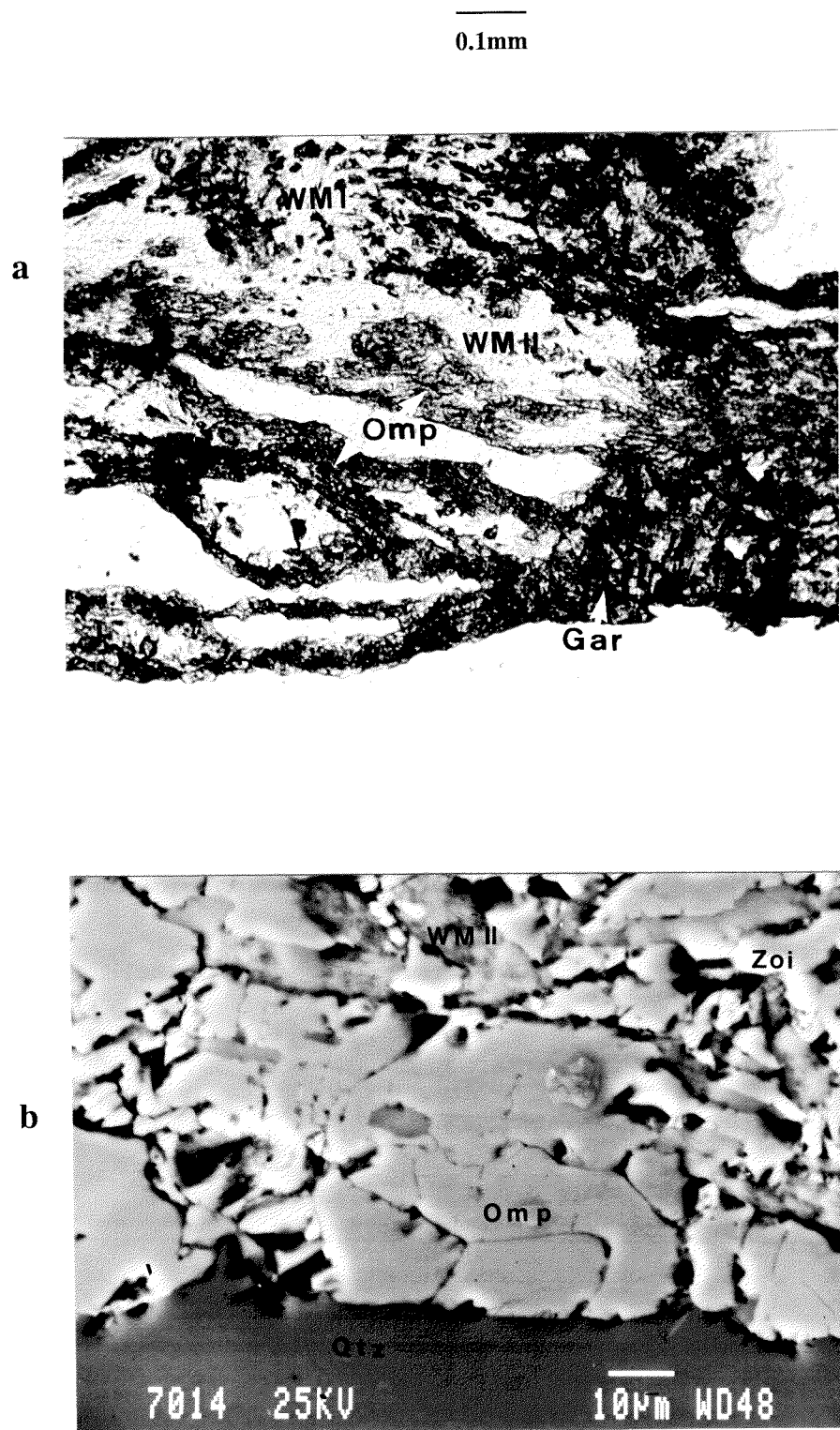


Fig. 4.10: Photomicrograph of post-kinematic omphacite growth in the overprinted eclogitic mylonites (sample Mu1-1a) as seen in thin section (a) and EMS Backscatter Images (b).

The normalized microprobe data have been obtained using the computer program NORM written by P. Ulmer (ETH-Zuerich), which normalizes the cations to a total of six oxygens and is based on the normalization scheme proposed by Lindsey and Anderson (1982). Al^{IV} is calculated on the basis that $\text{Si} + \text{Al}^{\text{IV}} = 2$ and $\text{Fe}^{3+} = \text{Al}^{\text{IV}} + \text{Na} - \text{Al}^{\text{VI}} - 2*\text{Ti}$. In the samples investigated in this study, the acmite component ($\text{NaFeSi}_2\text{O}_6$) is equal to Fe^{3+} and the jadeite component ($\text{NaAlSi}_2\text{O}_6$) is equal to the remaining Na or Al^{VI} , whichever is smaller. Diopside (Dio) is the pure $\text{CaMgSi}_2\text{O}_6$ endmember. Fig. 4.11a utilizes the discrimination diagram of Essene & Fyfe (1967), whereby augite is equal to the wollastonite- (Wo) + enstatite- (En) + Ferrosilite- (Fs) + CaTs-components. In Fig. 4.11b, X_{Jad} is equal to $\text{Jad}/(\text{Jad} + \text{Acm} + \text{Dio})$. The normalized analyses often show an excess of Si and Ca, which may be a result of contamination by zoisite or may be an effect of the fact that pure SiO_2 was used as a silica standard. Another possibility is that sodium may be lost during the analysis, which would lead to an apparent excess of silica.

The jadeitic pyroxenes, which clearly exhibit signs of deformation and represent the high-pressure breakdown of plagioclase (solid circles in Fig. 4.11), are chemically distinct from the undeformed, fine-grained clear green pyroxenes (open circles in Fig. 4.11) which occur at the contacts to quartz. The undeformed, fine-grained pyroxenes are omphacitic and are characterized by a depletion in Na and Al, with an increase in Ca-, Mg-, and Fe-contents (see Table 4.1, Fig. 4.11a and App. IVa). The jadeite-contents are relatively constant with X_{Jad} ranging from 0.48 to 0.61; whereas the acmite- and diopside molecules range from 0.03 to 0.14 and 0.25 to 0.35, respectively.

4.4.1.1.2. Textural evolution of Na-Pyroxene

The textural evolution of pyroxene during eclogite-facies deformation and subsequent overprinting is depicted schematically in Fig. 4.12. This evolution can be described as two dominant phases with various interstages of deformation and recrystallization, all of which most likely represent a more or less continuous deformation and/or recrystallization history during the exhumation of the Mte. Mucrone meta-granitoids. An earlier, *high-strain deformation phase* resulted in the local formation of mylonite in narrow zones. A *post-deformational recrystallization phase* (\pm infiltration) is characterized by static new growth of white mica + quartz \pm albite as breakdown products of jadeitic pyroxene. The degree to which deformation and recrystallization during these, most-likely more or less continuous, events and the intermediate stages are recorded in the rocks varies drastically over distances of less than one meter, and may represent very local variations in chemical gradients.

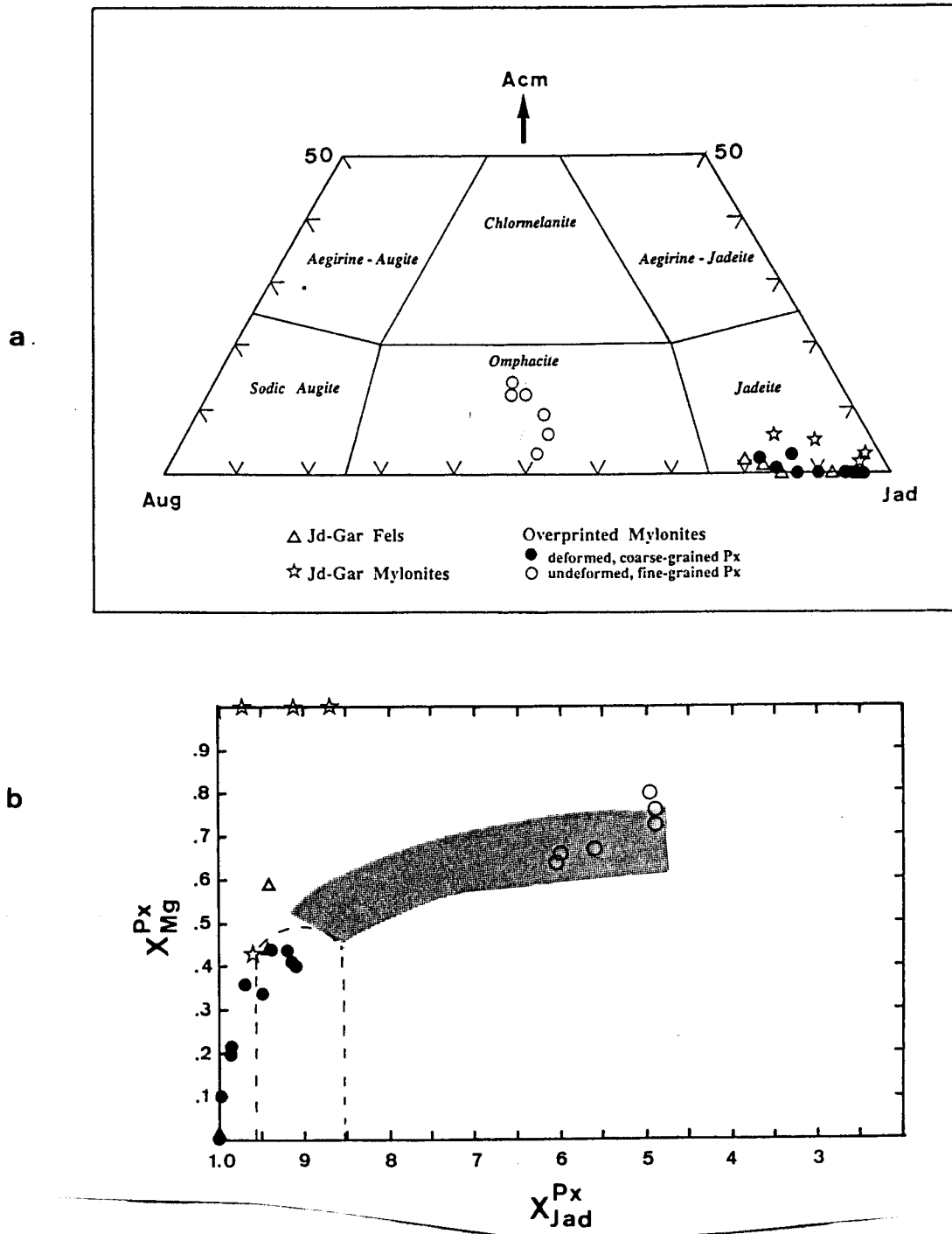


Fig. 4.11:

- (a) Discrimination diagram (Essene and Fyfe, 1967) for pyroxenes from the completely transformed and/or deformed rocks at the eastern face of the Mte. Mucrone. Acmite (Acm) = $\text{NaFeSi}_2\text{O}_6$, Jadeite (Jad) = $\text{NaAlSi}_2\text{O}_6$, and Augite (Aug) = $\text{Wo} + \text{En} + \text{Fs} + \text{CaTs}$; see text for calculation procedure.
- (b) Compositions of pyroxenes from the completely transformed and/or deformed rocks plotted as $X_{\text{Mg}}^{\text{Px}}$ (= $\text{Mg}/(\text{Mg} + \text{Fe}^{2+})$) against jadeite content ($X_{\text{Jad}}^{\text{Px}} = \text{Jad}/(\text{Jad} + \text{Dio} + \text{Acm})$). The region outlined by broken lines represents compositional variations of pyroxenes in the unfoliated meta-quartz diorites; whereas the shaded region represents the compositional transition of pyroxenes from *transitional* orthogneiss to omphacite-garnet orthogneiss presented by Koons, (1982) and Koons et al. (in review).

The rheological behaviour of the fine-grained jadeite + zoisite + quartz aggregates (breakdown products of plagioclase) during the eclogite-facies superplastic* deformation event is discussed in detail by Rubie (1983) and has become a commonly-cited example of reaction-enhanced ductility (e.g. Brodie and Rutter, 1986).

Reaction-enhanced ductility as a mechanism which facilitates deformation of rocks has been discussed in section 2.3.1.1. This mechanism can essentially be thought of as an increase in the ductile behaviour of a rock due to the greater deformability of fine-grained products which form during a mineral reaction. This mechanism is considered to be an alternative mechanism to grain-size reduction as a result of dynamic recrystallization of mineral phases (e.g. quartz) in regions of high strain (see e.g. White, 1976; White and Knipe, 1978; White et al, 1980; Schmid, 1976; Schmid et al, 1977; Etheridge and Wilkie, 1979).

In the shear zones discussed above, the jadeite + quartz + zoisite aggregates have been deformed superplastically. During high strain deformation, the jadeite + quartz + zoisite aggregates appear to have been more ductile than the medium-grained quartz layers. In high strain environments, quartz generally deforms more readily, whereas minerals such as plagioclase, garnet and pyroxene tend to behave more rigidly (e.g. Tullis et al, 1973; Tullis and Yund, 1977; White et al, 1980). In contrast to this "normal" behaviour of quartz relative to other minerals, Rubie (1983) has suggested that the fine-grained nature of the jadeite + quartz + zoisite aggregates prior to deformation enabled them to deform superplastically by a mechanism of grain boundary sliding of pyroxene (rather than a mechanism of dislocation creep common in coarser-grained materials).

An alternative explanation (to the one of Rubie's) is that recrystallization and deformation of the pyroxene grains was preceded by dynamic recrystallization of quartz, which after reaching a certain grain-size, resulted in a change in the *relative* competences of the main phases, quartz and pyroxene. At the point at which dynamic recrystallization in quartz stopped, the fine-grain pyroxene aggregates may have begun to deform superplastically.

The pyroxenes in the mylonites are now coarser-grained than those in the meta-quartz diorites. This suggests that the high-strain deformation of pyroxene was accompanied by grain coarsening. Rubie (1983 p. 333-334) has suggested that as the pyroxene grains grew and became too large to deform by a mechanism of grain boundary sliding, the strain was taken up by superplastic deformation in quartz and the

* In this study the term *superplasticity* is used in the broadest possible sense to describe super-ductile behaviour during deformation. *No mechanism* of deformation or recrystallization is implied (in contrast to the study by Rubie, 1983).

deformation mechanism in pyroxene changed to one of dislocation creep. However, as is discussed in Sect. 4.4.1.4, the quartz fabric characteristic of the Mte. Mucrone rocks is not interpreted as being deformed superplastically. The pod and lens texture of the quartz in these rocks suggest rather rigid behaviour of quartz (i.e. they had already experienced dynamic recrystallization) at the time that the pyroxene grains deformed superplastically (pers. comm. S. Schmid). The cracked and imbricate nature of the pyroxene grains associated with discontinuous layers often observed in the overprinted eclogitic mylonites may reflect limited ductile behaviour (i.e. more brittle behaviour) of the pyroxene grains and may imply local differences in the deformation mechanism.

In the overprinted mylonites, a second phase of recrystallization is characterized by a lack of deformation and by the instability of jadeitic pyroxene. The static growth of white mica, quartz as replacements products of jadeitic pyroxene, accompanied by new growth of omphacitic pyroxene, as well as annealing textures in quartz (see section 4.4.1.4.1 below) are considered to be effects of this post-deformational phase in the evolution of these rocks. As is discussed in more detail below, this second phase may indicate lower pressure conditions and/or a change in Na- and/or H₂O-activity.

A reduction in grain-size and/or an increase in the number and spacing of fractures may enhance the permeability of a rock (e.g. Brace, 1968,1972,1980; Morrow et al, 1981), and thus promote the introduction and mobility of a fluid (usually hydrous) phase (e.g. Sibson, 1977). Widespread retrogression and hydration associated with many shear zones is often considered evidence for an increase in permeability, whereby the highly localized shear zones act as channelways for the transport of volatiles (Beach and Fyfe, 1972; Fyfe et al, 1970; Kerrick et al, 1980, 1984; Sibson, 1981, among others). Shear zones are particularly useful for deformation/recrystallization studies because both undeformed and deformed, as well as untransformed and transformed rocks are available. In some cases there is direct evidence for syntectonic hydration in prograde shear zones, but it is not always clear whether hydro-fracturing causes crack formation and propagation or whether fluid is able to infiltrate into the zones of higher permeability created by shearing.

The possibility that the increase in modal amount of white mica, associated with the the post-deformational recrystallization phase, is a result of fluid infiltration is discussed in the light of hydrogen- and oxygen isotope data in Chapter 5. The textural and chemical distinction between the pre- and post-deformational micas suggest that if fluid infiltration took place, this activity may have been post-peak metamorphic conditions, whereby the mylonite zones provided pathways for fluid migration (Früh-Green, 1985).

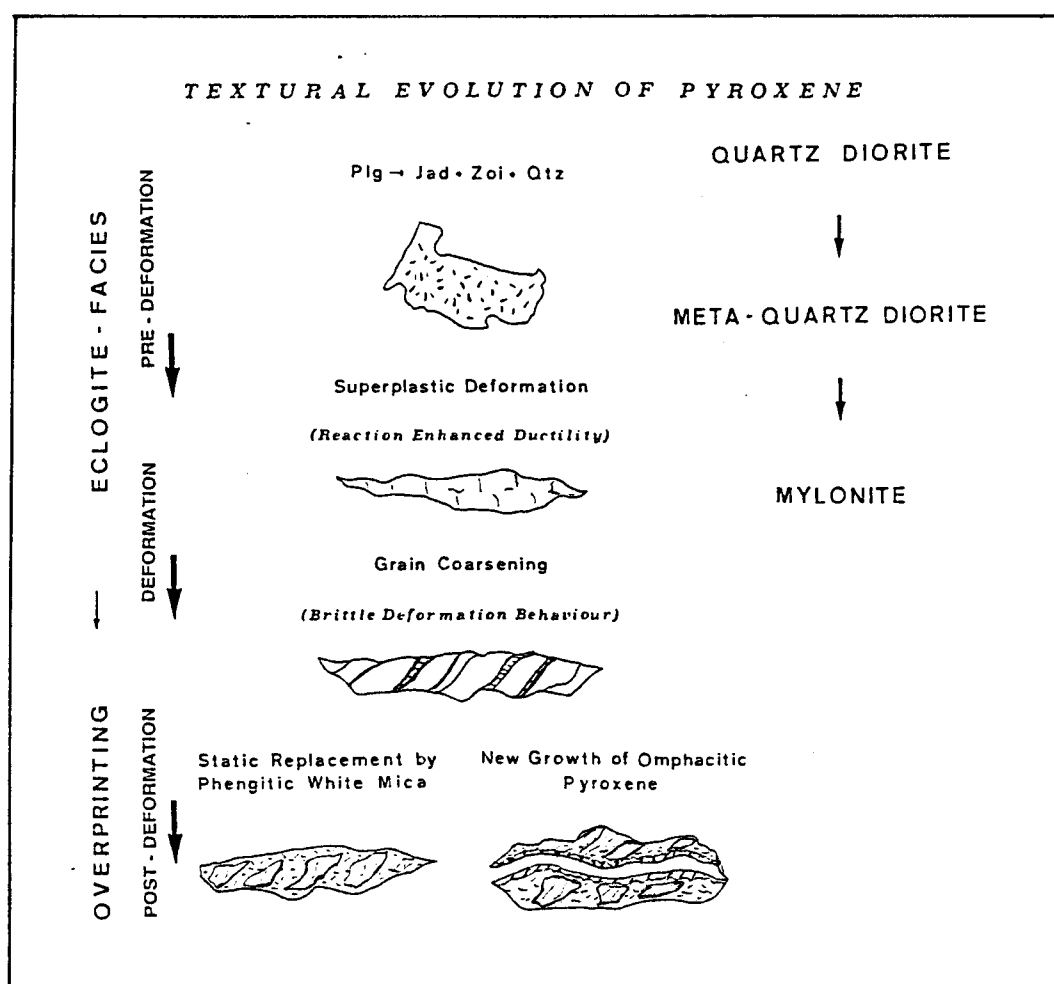


Fig. 4.12: Schematic diagram of the textural and chemical evolution of pyroxene from samples collected along the eastern face of Mte. Mucrone.

4.4.1.2 Garnet

In general, garnet forms irregularly-shaped, often elongate single grains or aggregates, which are aligned in more or less parallel bands and are associated with phengitic white mica. The cores are inclusion-rich, giving the grains a dusty, dark appearance in thin section, whereas the rims are inclusion-free and clear. Several minerals can be distinguished as inclusions in garnet, which include fine-grained sphene, various zosite minerals (including allanite), phengite, quartz, rutile, ilmenite, biotite and apatite. The fine-grained sphene and zosite grains are aligned parallel to the main foliation and form pronounced trails across the garnet grains, often extending out into the surrounding phengite aggregates (Fig. 4.13). In some cases, garnets which contain such inclusion trails have been rotated, resulting in a folded appearance of the inclusion trails.

Less commonly fine-grained phengite occurs as inclusions at the edges of the garnets or between cracked garnets grains. These fine-grained phengites are distinct from larger (up to 0.01mm long) idiomorphic phengite flakes which occur as isolated inclusions in grains that contain the sphene and zoisite inclusion trails. These coarser-grained phengites may be relicts of the phengitic mica associated with garnet which form the coronas around biotite in the less deformed meta-quartz diorites.

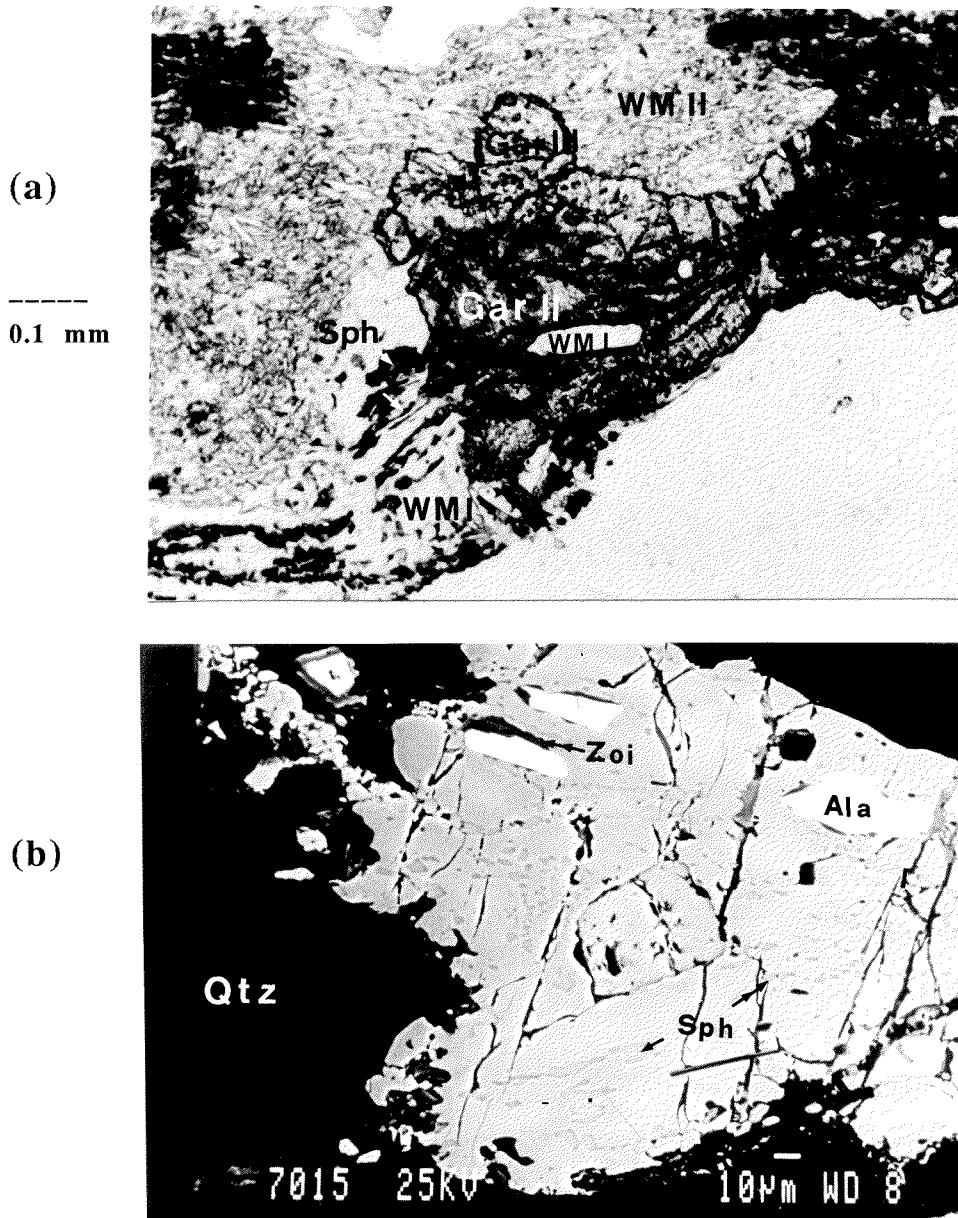
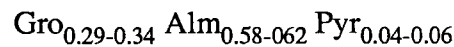


Fig. 4.13: (a) Photomicrograph of garnet from the overprinted mylonites. The cores (Gar II, see text and Figs. 4.14 & 4.15) partially retain the chemical zoning observed in the meta-quartz diorites (see Table 4.3) and are inclusion-rich, containing numerous mineral phases which include sphene (Sph), rutile, ilmenite, biotite, phengite, zoisite (Zoi), allanite (Ala) and quartz. The clear rims (Gar III) are inclusion poor and have similar compositions to isolated idiomorphic garnet grains associated with unoriented phengitic mica (WMII). (b) EMS Backscatter Images of parallel inclusions in garnet grains from the overprinted mylonites.

In the overprinted mylonites, a second generation of post-kinematic garnet growth is indicated by isolated, relatively inclusion-free nearly idiomorphic grains which occur in mica-rich domains (Fig. 4.13). As discussed below, these garnets have similar compositions to the clear rims of the more abundant inclusion-rich garnets. These texturally-different garnets are missing in the jadeite-garnet mylonite samples.

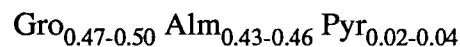
4.4.1.2.1. Garnet chemistry

The garnets in both the Jad-Gar mylonites and the overprinted eclogitic mylonites are characterized by relatively Mg-poor compositions (Table 4.3, Fig. 4.14, and App. IVc). The garnets in the Jad-Gar mylonites have homogeneous compositions; whereas a chemical zoning, associated with an increase in grossular component, is observed from core to rim in garnets from the overprinted mylonites. In general, the inclusion-rich garnet cores (termed here Gar II) in the overprinted mylonites have relatively constant compositions and are similar to those in the Jad-Gar mylonites; both garnets lie in the range of:



These compositions are similar to the Ca-rich areas in the garnets which border the plagioclase pseudomorphs in the meta-quartz diorite (see Koons, 1982; Hy, 1984) and correspond to the core compositions of the transitional orthogneiss sample R81/185 in Koons et al (in review). Incomplete homogenization of the garnet core compositions is evident in some grains from the overprinted mylonites in which the distinct zoning, characteristic in the less deformed rocks, is still preserved (see sample Mu1-2, App. IVc). The garnets in the overprinted mylonites (circles in Fig. 4.14) are distinguished from those in the Jad-Gar mylonites (triangles in Fig. 4.14) by chemically-distinct rims and by the post-deformational growth of idiomorphic inclusion-free garnet. The following discussion deals solely with these characteristically distinct garnets in the overprinted mylonites.

The inclusion-free rims of the garnets, as well as isolated inclusion-poor isometric garnet grains in mica-rich layers (termed here Gar III), are distinguished by a decrease in Mg- and Fe-contents with an increase in Ca-content (Fig. 4.14). In general, the rim compositions lie within the range:



In some elongate garnet grains, this Ca-enrichment is not always present. Instead the grains show relatively homogeneous compositions which correspond to those in the cores, as discussed above. Some garnet grains exhibit asymmetric Ca-enrichment towards the rims, whereby the contacts towards coarser grained white mica aggregates

show relatively constant, high Fe-contents ($X_{\text{Alm}} \approx 0.70$) in contrast to the contacts towards white mica-replaced pyroxene domains, which are enriched in Ca. The compositions of the Ca-enriched rims and the isolated, inclusion-poor grains in fine-grained mica domains are identical to those of the garnets which coexist with zoisite in the pink veins associated with these shear zones (see Secti.4.5.1.2. below and App.III).

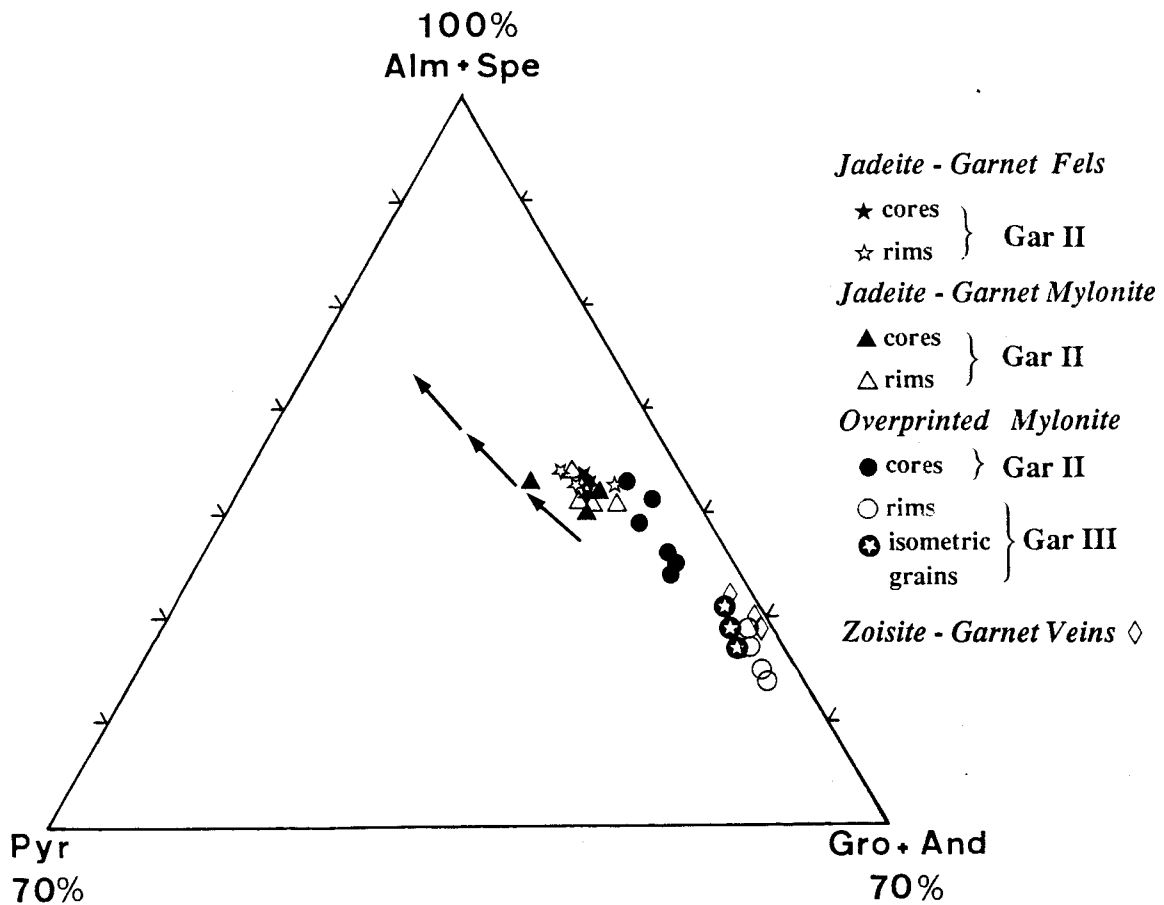


Fig. 4.14:

Compositions of garnets in the completely transformed and/or deformed rocks at the eastern face of Mte. Mucrone plotted in terms of almandine + spessartine (Alm + Spe), pyrope (Pyr) and grossular + andradite (Gro + And) components. The arrows represent the rim-to-rim compositional variations in single-grains of garnets from the meta-quartz diorites (as shown in Fig. 4.3), whereby the more Pyr- and Alm-rich compositions are found towards contacts to biotite.

4.4.1.2.2. Chemical and textural evolution of garnet

The chemical and textural evolution of garnet in the mylonites is shown schematically in Fig. 4.16. As garnet is a relatively undeformable mineral, the textural and chemical characteristics of these garnets are a good monitor of the crystallization history of the Mte. Mucrone metagranitoids. The garnet evolution is distinguished by an overall lack of chemical homogenization and by at least two phases of grain growth.

The *eclogite-facies formation* of garnet and white mica as coronas around biotite (Growth phase I) has been discussed in section 4.3.1.3. Their formation is characterized by a pronounced asymmetrical chemical zoning in which an enrichment in Ca, relative to Fe, occurs towards the contacts to quartz, low-Ti white mica II and jadeite-pseudomorphs after plagioclase.

Although the textural relation to biotite was destroyed during *superplastic deformation and mylonite formation*, relict biotite and phengite are preserved as inclusions. During this deformation phase, garnet became coarser-grained (Garnet Growth Phase II) and was aligned in more or less parallel bands. Chemical homogenization produced garnet compositions similar to the Ca-rich compositions in the meta-quartz diorites; however some garnets retain the distinct chemical zoning characteristic of the meta-quartz diorites. Complete breakdown of biotite during mylonite formation is recorded by the fine-grained sphene inclusions which are oriented parallel to the main foliation (Fig. 4.13 a,b). The calcium-enriched rims around inclusion-rich garnet cores, as well as the isolated calcium-rich isometric garnets, indicate further *post-deformational* garnet growth (Growth Phase III). This phase of garnet growth may have been simultaneous with vein formation, as indicated by the similarities in compositions between the Ca-rich garnets and those which occur together with zoisite in the veins. The calcium-enrichment may be due to local changes in Mg- and Fe-activities during the formation of the omphacitic pyroxenes.

4.4.1.3. White Mica

Two size distributions of white mica can be distinguished in the mylonites. Coarser-grained aggregates or single white mica grains (WMI), up to 0.3mm in width and 0.8mm long, occur in garnet-rich layers, often between quartz layers, and commonly exhibit undulatory extinction or kink-bands. Very fine-grained white mica (WMII), approximately 0.1-0.25mm long, form aggregates which occur either in distinct layers and define the foliation or as more or less unoriented clusters together with fine-grained quartz \pm albite. The latter occurrence of white mica II is commonly associated with the replacement of Na-pyroxene (see Fig. 4.8, 4.9b).

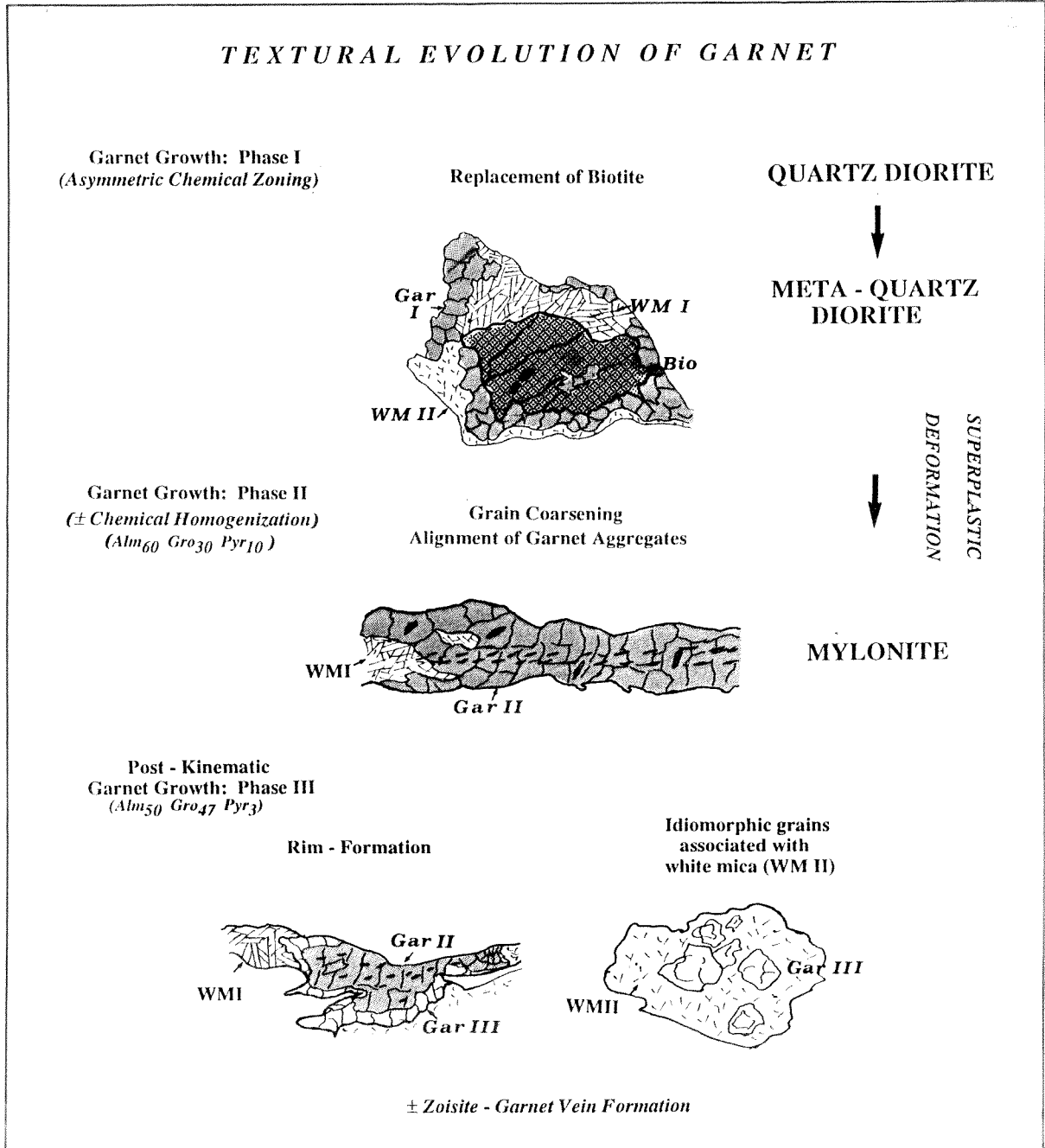
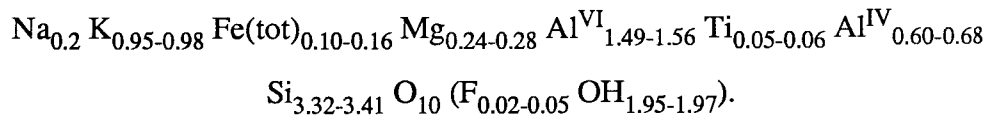


Fig. 4.16: Schematic diagram of the textural and chemical evolution of garnet from samples collected along the eastern face of Mte. Mucrone. Garnets (Gar) I, II, and III correspond to progressive Ca-enrichment and represent distinct compositions as a result of multiple phases of growth during the evolution of these rocks.

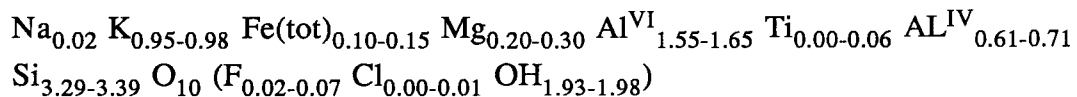
4.4.1.3.1. White Mica chemistry

The texturally different white micas can be distinguished chemically on the basis of Ti-, Fe- and Mg-contents (Fig. 4.16). The coarser-grained, deformed micas (WMI) are phengitic and contain up to 1.5 wt % Ti. These micas often show an enrichment in Fe and less commonly in Mg, relative to the fine-grained white mica II (see Fig. 4.16 and Table 4.2). $X_{Mg} (tot) (= Mg/(Mg + Fe_{tot}))$ is relatively constant, with a value of 0.66 ± 0.03 . As is true for all the white micas investigated in this study, fluctuations in Al and Si are often observed within the same rock samples as well as in the same textural domains. The chemical compositions of the coarse-grained white mica I lie in the range:



Although these micas are not as Ti- and Mg-rich as those in the coronas around biotite in the meta-quartz diorites, the deformed nature and the textural association with the inclusion-rich garnets, indicate that these micas represent the earlier breakdown products of biotite.

The fine-grained phengitic micas (WMII) which occur together with quartz \pm albite in isolated clusters or as replacement products in direct contact with Na-pyroxene have relatively constant compositions (see Table 4.2 and App.IVb). $X_{Mg(tot)}$ varies only slightly from 0.57 to 0.64. Although the mica compositions may be slightly variable, no distinct zonation could be determined. The structural formula of these phengites show the following range in composition:



This compositional range lies within the phengite mica compositions from domain III in the meta-quartz diorite (see above and Mu 2 Koons, 1982; Hy, 1984; Koons et al, in review) and are similar to the mica compositions in the transitional orthogneisses and orthogneisses reported by Koons et al, in review. As in these previous studies, no paragonitic mica could be found in the mylonites.

4.4.1.3.2. Textural evolution of the white mica

The coarser-grained, Ti-rich white mica I in the mylonites represent relicts of the biotite-breakdown reaction which were deformed and aligned parallel to the main foliation during the *high-strain deformation phases*.. The random orientation of the

fine-grained white mica II as a replacement product of jadeitic pyroxene indicate *post-deformational growth* under conditions of higher K- and/or H_2O -activities (see Chapter 5 and Fig. 5.3). Comparison of the textures and chemical compositions of these micas with those in the meta-quartz diorites suggests that these white micas may in general represent post-shearing replacement products.

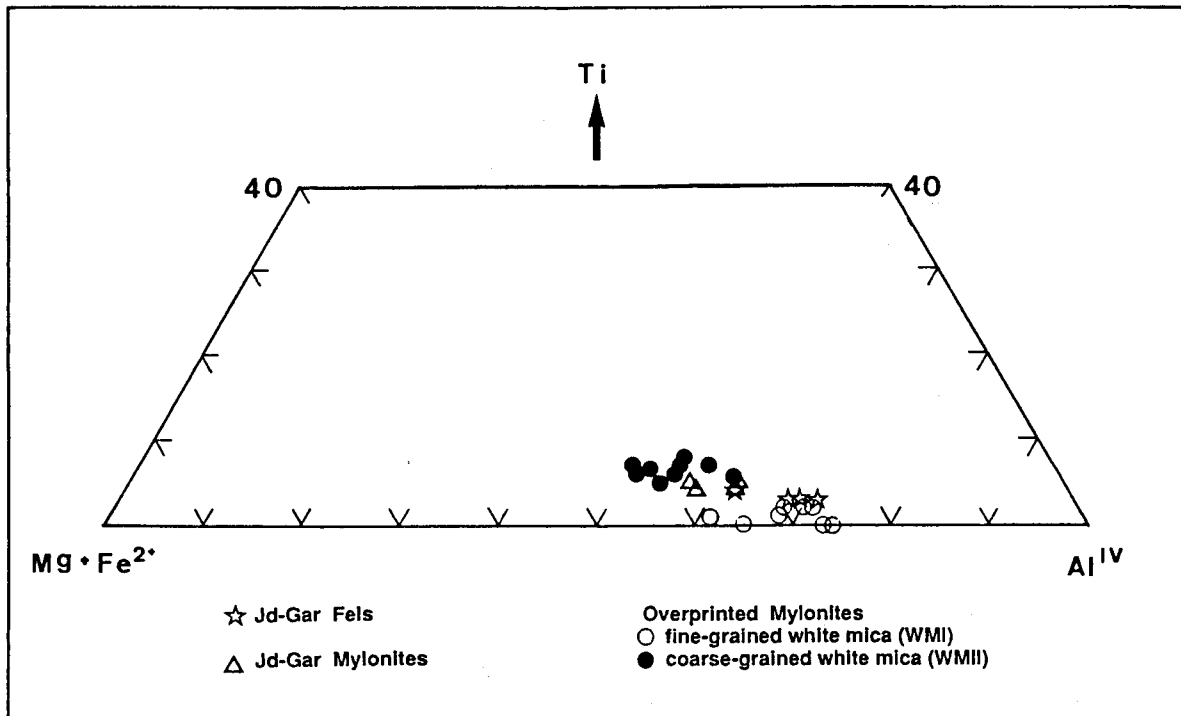


Fig. 4.16: Cation-variations in white mica from the completely transformed and/or deformed rocks at the eastern face of Mte. Mucrone.

4.4.1.4. Quartz

Quartz makes up approximately 30-35 vol% of the mylonites and occurs in 0.5-3 mm thin semi-continuous bands parallel to the main foliation. Locally quartz forms up to 4mm thick lenses and pods. In general, the quartz grains are inclusion-free and show well-crystallized dynamically recrystallized textures. The equigranular, recrystallized grains (0.05-0.5mm in diameter) have polygonal shapes with more or less straight grain boundaries (Fig. 4.17 a).

The quartz grains in the mylonites are distinguished from those in the less deformed meta-quartz diorites by the completely recrystallized fabric and a more uniform grain size of the recrystallized grains, and by ribbon-like tails which can be traced away from the

cores of the quartz aggregates the full width of a thin section (Fig. 4.17b). The recrystallized grains exhibit undulatory extinction and weak deformation bands. Signs of preferred orientation, although irregularly across quartz layers, can be observed with the use of a gypsum plate. (compare Figs. 4.5 a and 4.17 a).

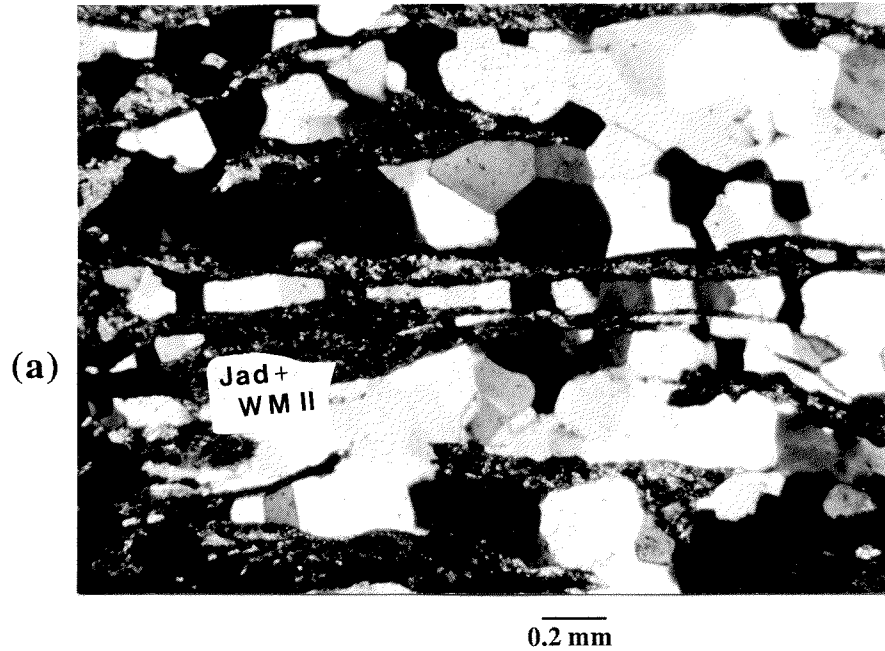
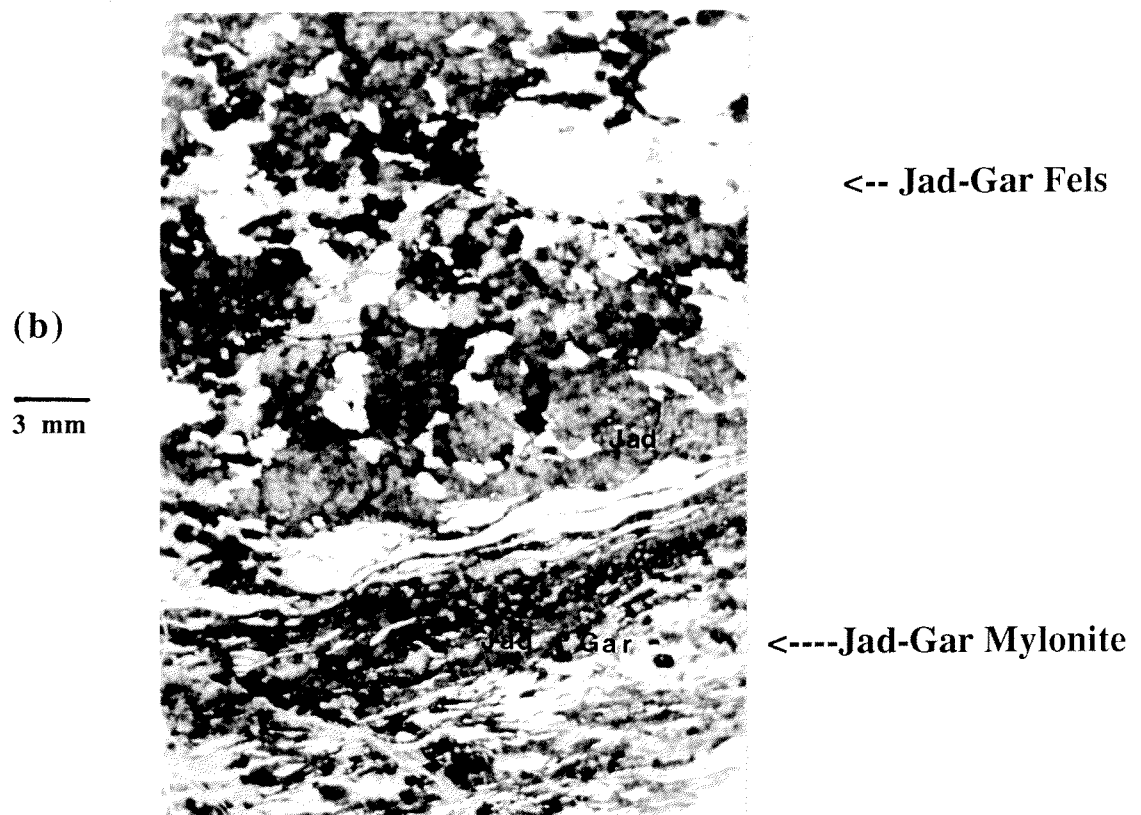


Fig. 4.17:

- (a) Photomicrograph of microfabric of recrystallized quartz grains in the mylonites.
 (b) Overall change in grain-shape of quartz from less deformed Jad-Gar Fels (Sample Mu 17a) to Jad-Gar mylonite (Sample Mu17b).



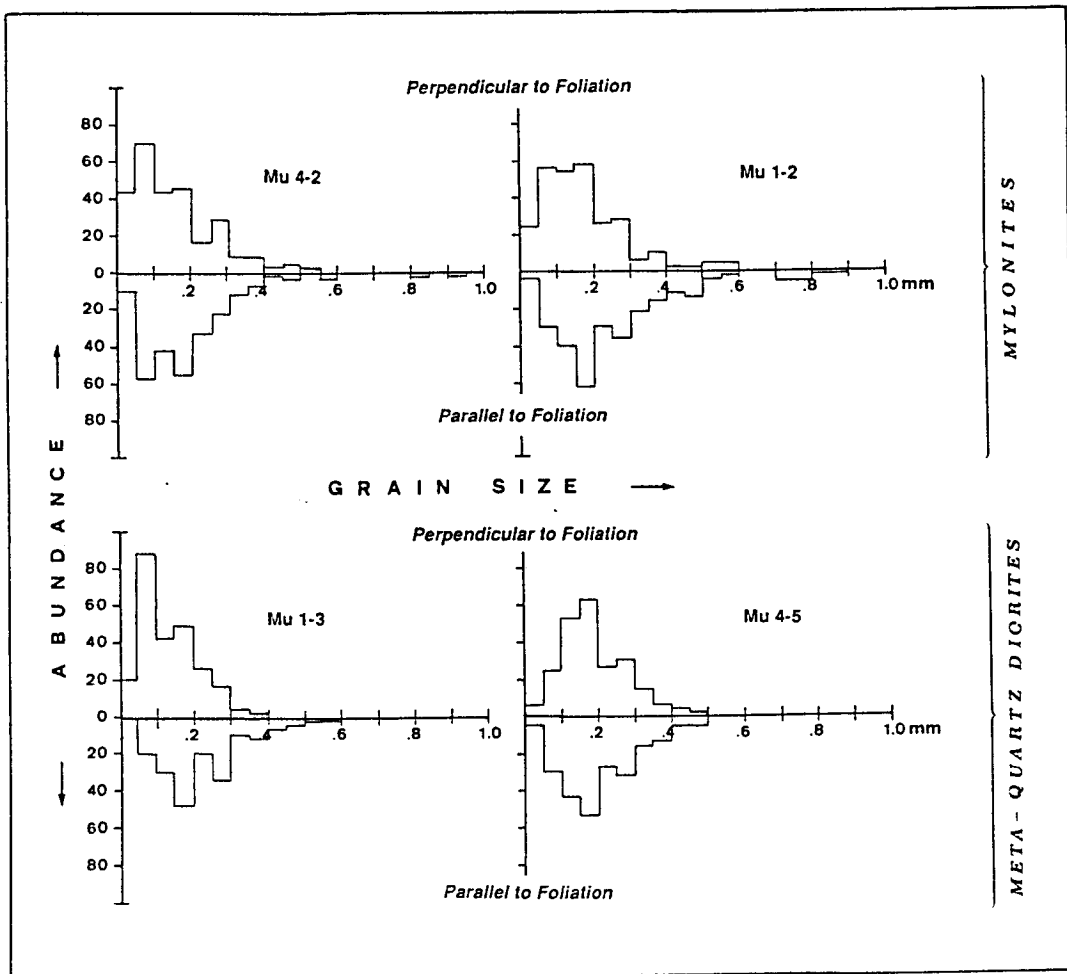


Fig. 4.18:

Grain-size variations of recrystallized quartz grains in meta-quartz diorites and mylonites. The grain-sizes of approximately 300 recrystallized grains were measured perpendicular to and parallel to the main foliation (only weakly present in the meta-quartz diorite samples). The grain-sizes (horizontal axes) are plotted against the number of grains (vertical axes).

4.4.1.4.1. Quartz Microfabrics

A statistical analysis of the *recrystallized quartz* in the eclogitic mylonites and meta-quartz diorites was made by measuring the long and the short axes of the recrystallized grains (i.e. parallel to and perpendicular to the foliation of the mylonites) and by determining the abundance and variations in the grain-sizes. The grain-size distribution of the recrystallized grains in the mylonites and meta-quartz diorites are presented as histograms in Fig. 4.18. In both rock types, the recrystallized quartz grains range from 0.05 to 0.6 mm, and occasionally up to 0.9mm long parallel to the foliation in the

mylonites. Although the two rock types differ greatly in the amount of deformation and degree of mineral transformation, no distinction can be made in the sizes of the recrystallized quartz grains. In both rock types 65-68% of the grains are 0.1-0.2 mm in diameter. This similarity in the morphologies of the recrystallized quartz is interpreted as a result of dynamic recrystallization, occurring contemporaneously during early stages of deformation and at the onset of shearing. Weak deformation (and thus incomplete recrystallization) occurred in the country rocks (i.e. the meta-quartz diorites) as high-strain deformation was concentrated along the shear zones.

In contrast to the recrystallized grains, the *overall* shapes and dimensions of the quartz aggregates represent original igneous quartz that has undergone recrystallization and deformation, and are distinctly different in the two rock types. The quartz aggregates in the meta-quartz diorites have irregular, rounded shapes, which are up to 5 mm in diameter and are randomly distributed in the least deformed rocks. In the highly deformed rocks, the quartz form augen-shaped pods and lenses (rarely more than 1 mm thick) and have pronounced, thin tails which are up to 2 cm long (Fig. 4.18b). This difference in the recrystallized grains and overall grain shapes between the two rock types is interpreted as a reflection of the degree of deformation affecting the two rock types. In the shear zones, as dynamic recrystallization and grain growth of the quartz proceeded, the quartz began to behave more rigidly and became less deformable, at which time the pyroxene aggregates started to deform. Further deformation of quartz is reflected in the formation of isolated quartz pods and quartz lenses with recrystallized tails.

4.4.2. SUMMARY AND DISCUSSION

4.4.2.1 Jadeite-Garnet Mylonites

The Jad-Gar mylonites (samples M17b, R185) are distinguished from the unfoliated meta-quartz diorites by a well-defined foliation, more homogeneous phase compositions, coarser grain-size of pyroxene, garnet and phengite, and by a lack of biotite. As discussed previously, before the onset of the high strain deformation event, the plagioclase breakdown reaction had gone to completion, producing fine-grained aggregates of $Jad + Zoi + Qtz$. At the onset of mylonite formation, quartz began to recrystallize up to the point that the recrystallized quartz aggregates were more competent than the fine-grained pyroxene aggregates resulting in superplastic deformation of the pyroxene in the shear zones. The present coarser grain-size of garnet and jadeite and the deformed nature of the quartz layers indicate that grain-coarsening accompanied deformation and resulted in a *relative* change in the deformation behaviours of the two dominant minerals jadeite and quartz. This coarser grain-size as well as the

homogeneous compositions of garnet and phengite in these un-overprinted samples suggest that deformation (and possibly simultaneous fluid infiltration) may have influenced both the rates of grain growth and the diffusion kinetics which lead to partial chemical homogenization and to the completion of the biotite breakdown reaction (see Chapter 5 and Koons et al., in review).

The evolution of these Jad-Gar mylonites is analogous to that of the *transition orthogneiss* described by Koons et al. (in review). These authors suggest that although deformed and homogeneous in composition, the sodic pyroxenes in the transition orthogneiss do not represent equilibrium chemical compositions. Koons et al. argue that the omphacite-garnet orthogneisses at the Mte. Mucrone evolved from transition orthogneiss by further deformation, resulting in more diopsidic pyroxene compositions (see Section 4.6.2). This possibility is discussed further in light of whole rock chemical data and stable isotope data in Chapter 5.

4.4.2.2 Overprinted Mylonites

Several mineralogical and textural characteristics distinguish the overprinted mylonites from the primary jadeite-garnet mylonites. Although the main eclogite-facies high strain deformation event produced superplastically deformed layers of pyroxene and quartz, subsequent deformation and grain coarsening did not result in homogeneous chemical compositions of the coexisting phases in the overprinted mylonites upon complete breakdown of biotite. The heterogeneous compositions of garnet and phengite reflect the disequilibrium conditions during the eclogite-facies formation of the meta-quartz diorite. Further disequilibrium crystallization is indicated by post-kinematic growth of omphacitic pyroxene and more grossular-rich garnet (Gar III, see Figs. 4.13 & 4.15). The diopside component in pyroxene and the grossular component in garnet may be related to consumption of zoisite during completion of the biotite breakdown reaction. A detailed discussion of the reaction history of these rocks is presented in Ch. 5.

The replacement of jadeitic pyroxene by phengitic white mica II (WMII) + quartz \pm albite further distinguishes the overprinted mylonites from the Jad-Gar mylonites. The amount of albite associated with this replacement is minor and could only be determined by electron microprobe analysis. The timing of the replacement of jadeite remains uncertain due to the difficulties in microscopically determining the textural and modal relationships of the fine-grained aggregates of quartz \pm albite associated with WMII. The replacement of jadeite by phengitic white mica need not be related to a pronounced decrease in pressure, but rather may be due to changes in the chemical activities of K and H₂O in local domains during eclogite-facies metamorphic P-T conditions (see Chapter 5 and Koons 1982, 1986).

Reaction kinetics may be enhanced during deformation in several ways, one of which is to allow water to infiltrate into a previously dry system (see Brodie and Rutter, 1985 and Rutter and Brodie, 1985). There is evidence for possible infiltration by at least small quantities of hydrous fluid during and/or after the main superplastic deformation event. Whole rock chemical data suggest that the deformed rocks derived from eclogite-facies metamorphism of quartz diorite are slightly enriched in H₂O. The enrichment in H₂O can also be related to shifts in isotopic compositions (see Chapter 5 and Früh-Green, 1985). The extent of replacement of jadeite by phengitic white mica may be related to hydration or localized redistribution of water within the rock. In addition, the zoisite + garnet veins associated with the shear zones presumably represent formation from a fluid phase under conditions of high fluid pressure (see Section 4.5 below).

The mineralogical and textural variations observed in the deformed rocks may correspond to different times of recrystallization and/or fluid infiltration relative to deformation during eclogite-facies metamorphism. The jadeite-garnet mylonites may represent syn-deformational recrystallization with the absence any external fluid phase. Post-kinematic fluid infiltration or local changes in H₂O-activity may have produced the distinct chemical characteristics found in the overprinted mylonites, whereas syndeformational infiltration may have been responsible for the formation of paragonite and near equilibrium mineral assemblages in the omphacite-garnet orthogneisses (see Section 4.6). These variations and the evidence for fluid infiltration is discussed further in light of whole rock geochemical and stable isotope data in Chapter 5.

Compagnoni and Maffeo (1973) and Oberhänsli et al. (1985) attribute the replacement of jadeite to a *post-omphacite stage* in the evolution of the Mte. Mucrone metagranitoids (see Section 4.2.2.2). However, the textural characteristics described by the above authors are different than those in the rocks investigated in the present study. Oberhänsli et al. (1985) describe the formation of albite-epidote gneiss by further deformation and hydration of glaucophane micaschist. As stated previously, the amount of albite in the overprinted mylonites is minor and no glaucophane has been observed in these rocks (see also Koons, 1982 and Koons et al., in review).

4.5 VEINS ASSOCIATED WITH THE DUCTILE SHEAR ZONES

The eclogitic mylonite zones discussed above are commonly associated with pink veins, 2.0 mm to 1.2 cm in width. These veins, containing zoisite, garnet (giving the pink colour), quartz and occasionally omphacitic pyroxene and phengitic white mica, are oriented nearly parallel to the mylonite zones and in some cases have been folded by a subsequent deformation. In most cases a zone of medium- to coarse-grained

unfoliated jadeite-garnet fels (1-5 cm in width) separate the zoisite veins from the mylonite zones (see Fig. 4.19). The veins cross-cut a weak foliation present in the jadeite-garnet fels, and in some cases exhibit growth textures indicative of post-kinematic formation (see Fig. 4.20a).

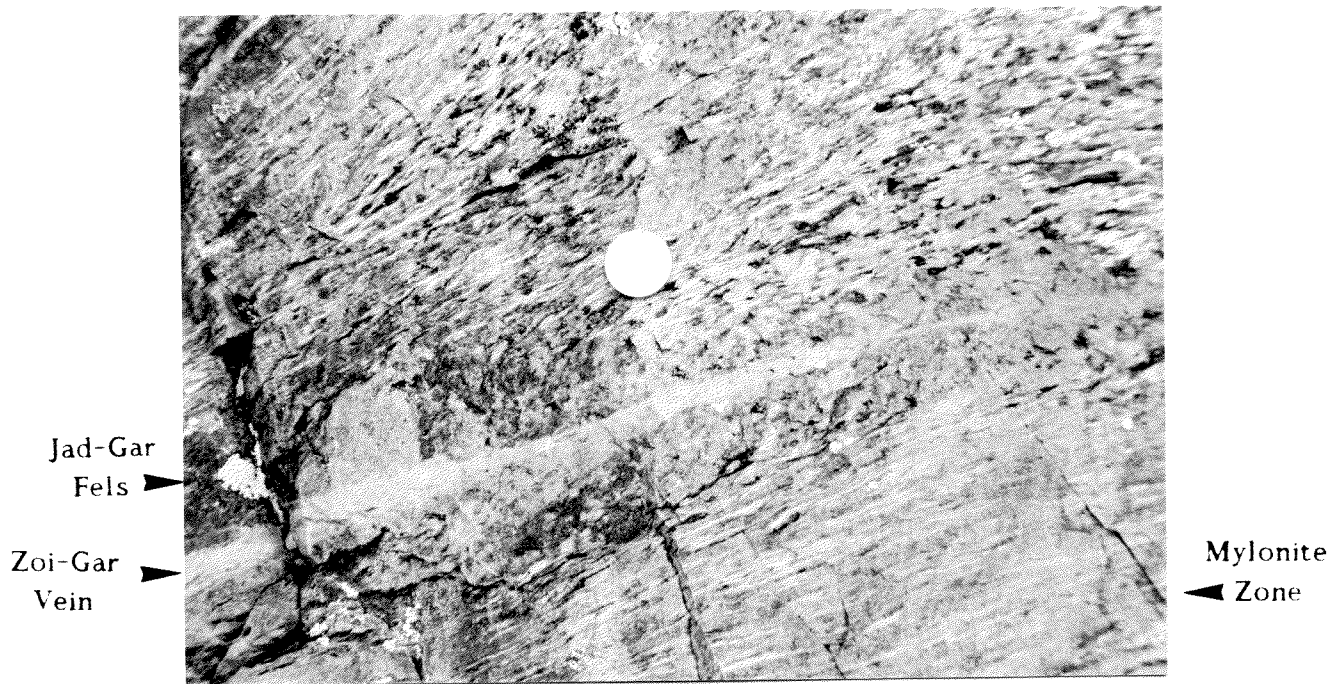


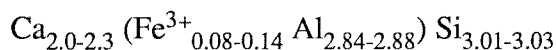
Fig. 4.19: Outcrop relationships (Location 3, Fig. 4.2,) between zoisite-garnet veins and mylonite zones. An approximately 1-5 cm zone of relatively unfoliated rock (Jad-Gar Fels, corresponding to sample Mu17a discussed in text) typically separates the veins from the mylonite zones.

4.5.1. VEIN PETROLOGY, MINERAL CHEMISTRY AND MICRO-FABRICS

4.5.1.1 Zoisite

Zoisite is the dominant mineral in these veins and occurs as radiating, needle-like crystals with anhedral garnet in the interstices (Fig.4.20b). Individual grains are up to 2.0 mm long. They exhibit parallel extinction and characteristically have blue anomalous birefringence.

Electron microprobe analysis yielded relatively homogeneous compositions, which vary only slightly in Fe³⁺- and Al-contents (see App. III). Fe³⁺ (calculated) varies between 1.46 and 2.22 wt% and corresponds to variations in the zoisite structural formula of:

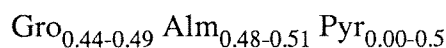


No zoning could be determined by point analyses along profiles through the individual zoisite grains.

4.5.1.2. Garnet

Garnet occurs as amorphous grains (0.1-0.3 mm in diameter) between the undeformed zoisite needles, so that the grain boundaries are often difficult to discern (see Fig. 21b). In general the grains are clear and show no evidence for multiphase growth.

The compositions are homogeneous and correspond to the Ca-rich rim-compositions of the garnets in the mylonites (see Section 4.4.1.2.1. and Fig.4.15). The compositions of these garnets lie within the range (see Table 4.3 and App. III):



These garnet compositions are distinct from the more Fe-rich garnets in the jadeite-garnet gneissic wallrocks (see below).

4.5.1.3 Quartz

The volumetric amount of quartz in the veins varies in different samples. In general quartz occurs as fine, amorphous grains (0.01-0.2 mm in diameter) between the zoisite needles or as up to 3 mm long "pods" in the centers of the veins. In some samples it is difficult to distinguish actual vein quartz from wallrock-quartz which may have physically been incorporated into the the vein during vein-formation. This is especially true of quartz aggregates associated with bright green omphacitic pyroxenes (see Fig. 4.20b).

In general the quartz, zoisite and garnet aggregates are undeformed and represent static growth. However weak undulatory extinction is occasionally present in some of the larger quartz grains.

4.5.1.4. Na-Pyroxene

In some samples, (e.g. R 13/1) isometric, grass-green pyroxene grains (0.3 - 1.0 mm in diameter) occur together with - and as inclusions in quartz in the center of the zoisite veins. Qualitative EDS-analyses indicate an omphacitic composition. The textural occurrence of these pyroxenes is similar to the fine-grained pyroxenes in the mylonites,

which have been interpreted as a second generation of Na-pyroxene growth during post-shearing, eclogite-facies conditions (see Section 4.4.1.1.). Minor amounts of white mica are associated with these pyroxenes in the veins. EMS-Backscatter analysis shows that these omphacitic pyroxenes contain very fine-grained quartz inclusions (5-15 μm in diameter, see Fig. 4.20b).

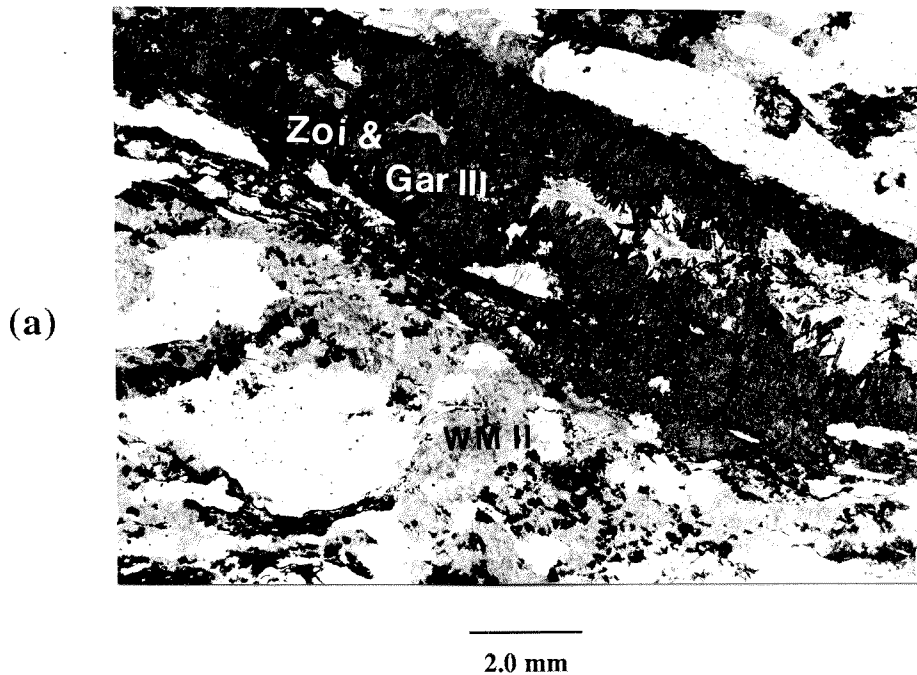
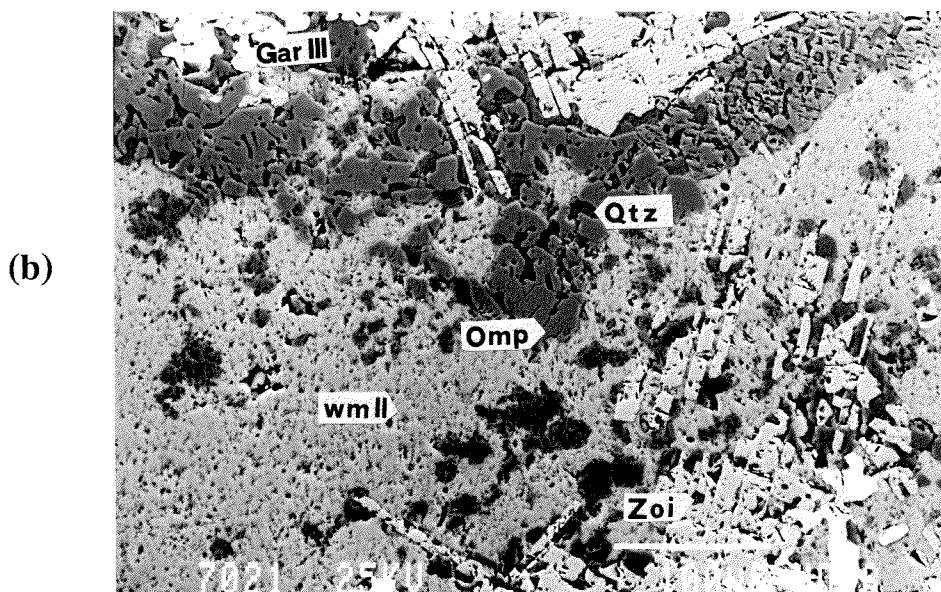


Fig. 4.20:

- (a) Photomicrograph of zoisite-garnet vein in the centers of the mylonite zones. A zone of relatively unfoliated jadeite-garnet fels (Jad-Gar Fels). The vein cross-cuts a weak lineation defined by slightly elongated quartz grains. No signs of deformation can be seen in these veins.
- (b) SEM-Backscatter Images of zoisite (Zoi, light grey)-garnet (Gar, bright white) veins, showing relationship to omphacitic pyroxene (Omp, medium-dark grey) and phengitic white mica (WMII, medium-light grey). The darkest grey mineral in the omphacite grains is quartz (Qtz).



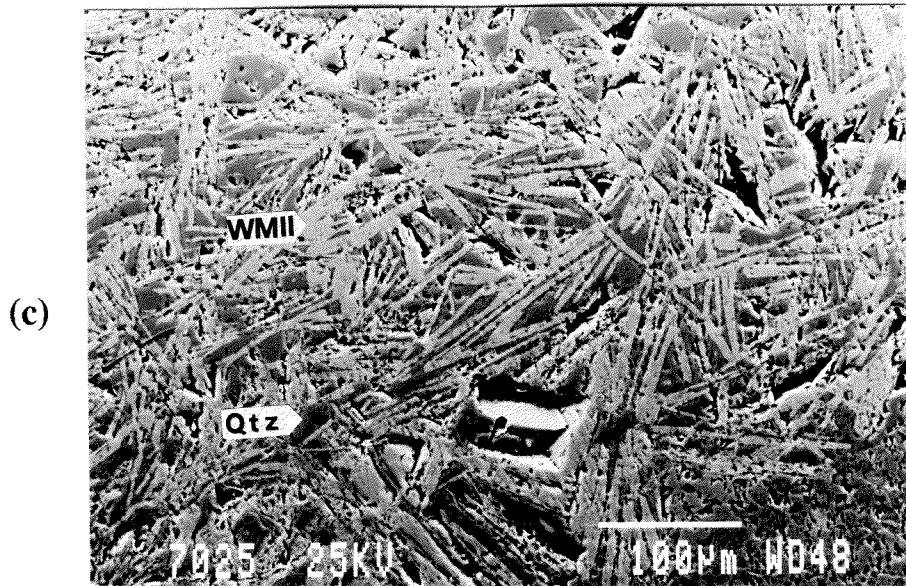


Fig. 4.20:
 (c) SEM-Backscatter Images of relatively unfoliated jadeite-garnet fels in direct contact with the zoisite-garnet veins (Fig. 4.21a,b) in the centers of the mylonite zones. Photograph shows randomly oriented clusters of phengite (WMII, light grey) and quartz (Qtz, dark grey) as replacement of K-feldspar.

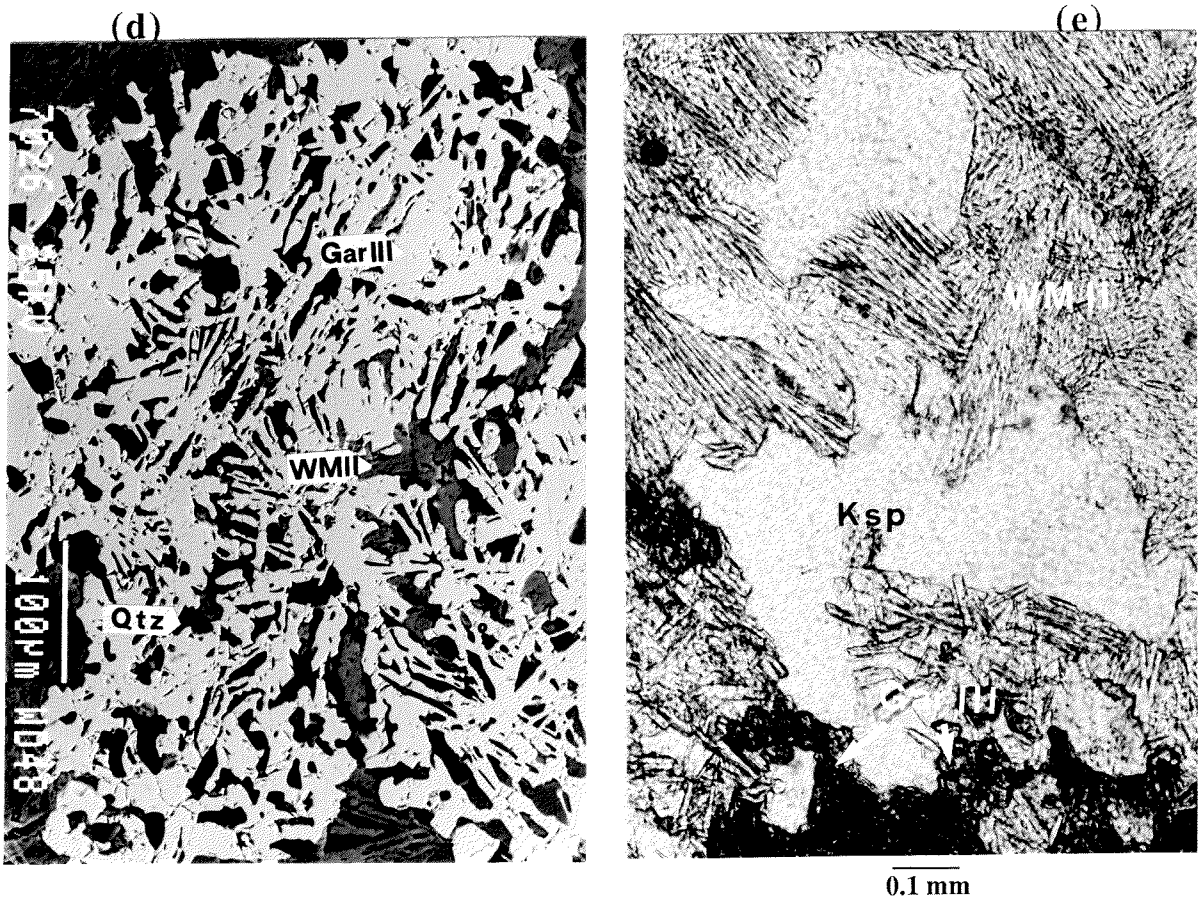


Fig. 4.20:
 (d) SEM-Backscatter Images of relatively unfoliated jadeite-garnet fels in direct contact with the zoisite-garnet veins (Fig. 4.21a,b) in the centers of the mylonite zones. Photograph shows replacement of K-feldspar by garnet (GarIII, bright white), phengite (WMII, grey), and quartz (Qtz, dark grey).
 (e) Photomicrograph of K-feldspar replaced by WMII in overprinted jadeite-garnet fels (sample R13/1).

4.5.2 WALLROCK PETROLOGY, MINERAL CHEMISTRY AND MICROFABRIC

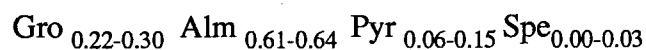
Characteristic of the rocks in direct contact with the zoisite veins is a distinct unfoliated, massive nature which resembles the overall fabric in the meta-quartz diorites. In contrast to the meta-quartz diorites (discussed in Section 4.3), these rocks have been completely transformed and now contain the *eclogite-facies* mineral assemblage quartz + jadeite + garnet + phengite with minor sphene and zoisite. These unfoliated rocks (jadeite-garnet fels) form bands, 2-8 cm wide, between the zoisite veins and mylonitic orthogneiss in shear zones.

4.5.2.1. Jadeite-Garnet Fels

As discussed previously, the zoisite veins nearly always form abrupt contacts to unfoliated and unretrograde jadeite-garnet fels (Mu17a, Mu17b; see Fig. 4.20). The unfoliated fels grades into mylonite (in a 3 cm wide shear zone) over a distance of 5 cm. Essentially no retrograde replacement of pyroxene by white mica is seen in either the deformed nor in the unfoliated rocks. The overall primary igneous texture is preserved in the unfoliated rocks, however the distinct breakdown textures in the plagioclase- and biotite-domains are no longer present. More or less undeformed aggregates of idiomorphic garnet (~0.5 mm in diameter) and white mica occur in distinct domains which represent the complete replacement of biotite. Na-pyroxene, as replacement products of the original plagioclase, form individual idiomorphic grains and are coarser-grained than those in the meta-quartz diorites. The phengitic white micas exhibit a uniform grain size and occur either in distinct domains with garnet or as isolated clusters within the pyroxene aggregates. Quartz shows the typical recrystallized fabric and a uniform grain-size as discussed in Sect. 4.4.1.4.

4.5.2.1.1 Garnet Chemistry

In contrast to the meta-quartz diorites and the mylonites described in Section 4.4, these not-overprinted wallrocks are characterized by relatively homogeneous compositions of both eclogite-facies minerals, jadeite and garnet. No distinct variations in compositions (see Tables 4.1-4.3 and App. III) could be found between the garnets in the unfoliated rocks (e.g. sample Mu17a) and those in the mylonite in the shear zone (e.g. sample Mu17b). The chemical zoning pattern in garnet, characteristic of the meta-quartz diorites, is completely absent in both the unfoliated and foliated rocks, and lie within the following range:



A very slight Ca-enrichment is observed in some of the cores of the garnet grains in the mylonites and corresponds to the average composition of garnet in the unfoliated jadeite-garnet fels (Gro_{29} , Alm_{62} , Pyr_9). These garnet compositions are distinctly more Fe-rich than those in the veins and correspond to both the core-compositions of the chemically-zoned garnets of the more-overprinted mylonites (see Sec. 4.4.1.2.1) and the Ca-rich areas in the garnets which border the plagioclase pseudomorphs in the meta-quartz diorites.

4.5.2.1.2 Pyroxene Chemistry

No chemical zonation in pyroxenes in the foliated nor in the unfoliated wallrocks could be found. In both rock types, the pyroxenes are jadeite-rich, but in the mylonites a slight decrease in X_{Jad} is seen. The pyroxenes in the unfoliated rocks range from Jad_{87} to Jad_{95} , while those in the mylonites range from Jad_{82} to Jad_{87} . SEM-Backscatter analysis showed that fine-grained quartz and minor zoisite occur as inclusions in pyroxene and that the amount of zoisite is distinctly less than in the more-overprinted mylonites (see Sect. 4.4.1.1).

4.5.2.1.3 Mica Chemistry

As with garnet and pyroxene, the white micas in both these unfoliated and mylonitic wallrocks have relatively constant composition. The major element-compositions of these micas lie within a range which is intermediate to the white mica compositions of WM1 and WM2 in the deformed and unfoliated rocks discussed previously (Sect. 4.3 and 4.4). However, a relative enrichment in F-content (see Table 4.2 and App. III) is observed. This relative F-enrichment can be directly related to the completion of the biotite breakdown reaction.

4.5.2.1.4. Discussion

Macroscopically, the unfoliated jadeite-garnet fels are nearly indistinguishable from the meta-quartz diorites. However, microscopically, these rocks show an absence of biotite and contain coarser-grained pyroxene, garnet and phengite grains than the incompletely transformed equivalents. The relatively homogeneous chemical compositions of the coexisting phases in these unfoliated wallrocks suggests that, relative to that indicated in the meta-quartz diorites, a greater degree of diffusive mass transfer and chemical communication, resulting in completion of the plagioclase- and biotite-breakdown reactions, occurred in these areas. The possibility that these zones may represent 'old' fluid pathways, resulting in complete transformation and 'grain hardening', is discussed in light of XRF bulk rock geochemical and stable isotope data in Chapter 5.

The presence of such '*early reaction zones*' may have been determinant to the formation of the mylonite zones (see Section 5.5.6 and Fig. 5.12).

4.5.2.2 Overprinted Jadeite-Garnet Fels

The amount of overprinting in the wallrocks is highly variable in the samples collected in this study. Some samples (e.g. R13/1, 83/1) exhibit considerable replacement of pyroxene by low -Ti phengite (WMII) and garnet, and are associated with new growth of omphacitic pyroxene (See Fig.4.20 c,d). This replacement is similar to that in the mylonites discussed in Section 4.4; however, the micas are coarser-grained (up to 1.5 mm long) and occur in irregular patches, rather than in distinct bands. This difference in texture is primarily a result of the unfoliated nature of the rock. In the overprinted eclogitic mylonites, randomly-oriented phengite flakes, commonly associated with the Ca-rich Gar III, occur as replacement products of jadeitic pyroxene (and in some cases K-feldspar, see Fig. 4.20e), in distinct zones which follow the foliation formed during high-strain deformation. Quartz in the veins has identical recrystallized fabrics as those in the wallrocks (see Section 4.4.1.4), and may represent physically incorporated portions of the recrystallized wallrock during vein formation.

In these overprinted samples, the chronological relationship between vein formation and phengite growth is difficult to determine. The growth of phengite is often associated with a greater modal amount of relict K-feldspar. The randomly-oriented replacement textures of white mica in the wallrocks, as well as the radiating fabric of the zoisite + garnet + quartz grains in the veins, indicates growth during strain-free conditions. The variabilities in the modal amounts of white mica in the wallrocks and the modal variations in the vein assemblages may represent simultaneous crystallization during a single infiltration event in which local variations in H₂O-, Na- and K-activities were present (see also Section 5.5.6 and Fig. 5.12).

4.5.3 SUMMARY AND DISCUSSION

The zoisite-garnet veins, associated with the mylonite zones in the Mte. Mucrone metagranitoids, are characterized by a lack of deformation and by uniform chemical compositions of the coexisting mineral phases. A narrow band of unfoliated jadeite-garnet fels commonly separates these veins from the mylonite zones. These unfoliated jadeite-garnet fels exhibit contrasting degrees of chemical homogenization and overprinting. Vein-formation as well as replacement of pyroxene by phengitic white mica are related to a strain-free recrystallization and infiltration phase in the evolution of the Mte. Mucrone metagranitoids. The relative timing of infiltration relative to deformation may have critical to the development of both the jadeite-garnet fels and to

the concentration of high-strain deformation along these zones. The significance of the veins and the characteristic wall rocks is discussed further in Section 5.5.4. and 5.5.6.

4.6 COMPLETELY RECRYSTALLIZED OMPHACITE-GARNET ORTHOGNEISS

A large part of the central Sesia Zone is composed of medium-grained, well-foliated orthogneiss consisting primarily of quartz + Na-pyroxene + garnet + phengite + paragonite. These completely recrystallized orthogneisses make up a large part of the Mte. Mucrone. The Na-pyroxene-garnet orthogneisses are distinguished from the metaquartz-diorites and the mylonites on the basis of a relatively uniform grain size, and by the presence of paragonite as part of the stable mineral assemblage (Fig.4.21).

The textural and mineralogical evolution of these orthogneisses is discussed in detail by Koons (1982) and Koons et al. (in review), who suggest that they evolved through a transitional orthogneiss-phase (similar to that of the Jad-Gar mylonites) by further deformation (see also Oberhänsli et al. 1985). In this study, samples R82/9 and R191 from Koons et al. (in review) are compared chemically and isotopically (see Chapter 5) to the meta-quartz diorites and mylonitic orthogneisses. Only the essential textural and mineralogical characteristics of these rocks are summarized below; for a more detailed discussion of the evolution of these rocks refer to the above publications.

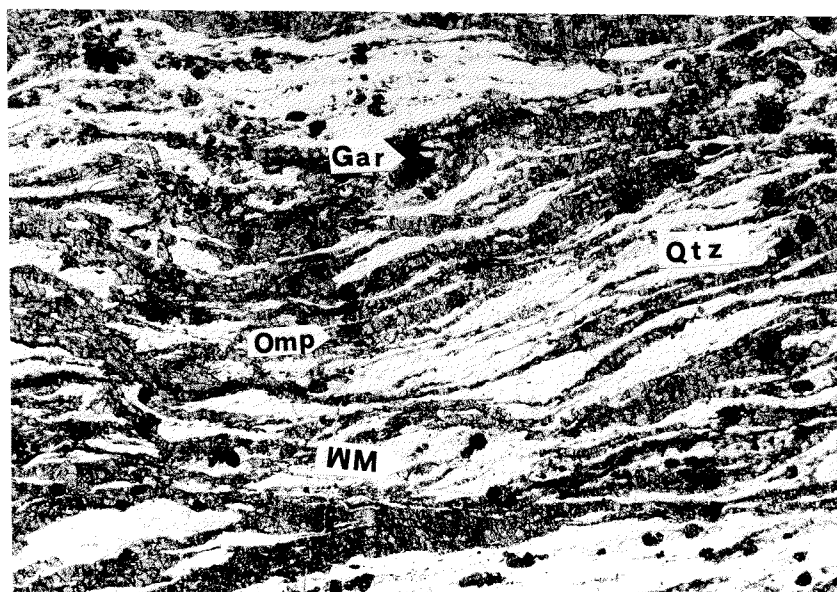
4.6.1. MINERALOGY, PETROLOGY AND PHASE CHEMISTRY (Samples R 82/9, R 191)

These two samples are texturally similar (although coarser-grained) to the Jad-Gar mylonites discussed in Section 4.4. Sodic pyroxene occurs as medium-to coarse-grained, elongate (2-4 mm long) grains in distinct semi-parallel, discontinuous layers (Fig.4.22). Deformation of the pyroxene layers is characterized by undulatory extinction and cracking of individual lath-like grains. The pyroxene compositions are variable and range from $Jad > 80$ to Jad_{50} (Table 4.1; shaded region in Fig. 4.11b). Koons (1982) reports irregular zoning patterns in the pyroxene grains, in which more jadeitic compositions occur in the cores and are surrounded by omphacitic rims. This pattern is the reverse of that found in other rocks of quartzofeldspathic composition from the same region.

Garnet occurs either as euhedral grains (0.5 - 0.8 mm in diameter) in distinct layers or as irregularly-shaped, elongate aggregates. Fine-grained sphene and zoisite form parallelly-oriented inclusion trails through the grains, as described in the mylonites (see Section 4.4.1.2). The garnets exhibit irregular zonation patterns and are compositionally similar to the cores of the garnets in the mylonites (Table 4.3). Koons (1982) and Koons et al. (in review) interpret the irregular grain boundaries of the garnet grains as

evidence for partial resorption associated with omphacite-formation. The presence of Ca-rich garnets, as found as rims and as idiomorphic grains (Gar III) in the overprinted mylonites, has not been reported in these orthogneisses.

A large modal percentage of white mica (phengitic white mica and paragonite), and especially the presence of paragonite, distinguish these completely recrystallized orthogneisses from the meta-quartz diorites and the mylonites. Both micas are medium- to coarse-grained (up to 2 mm long) and have a preferred orientation which defines the main foliation. The paragonite compositions are similar to those found in other Sesia Zone assemblages (Koons, 1982). The phengitic white mica are compositionally similar to the low-Ti micas (WM2) in the meta-quartz diorites and in the mylonites (see Table 4.2).



3.0 mm

Fig. 4.21: Photomicrograph of completely recrystallized omphacite-garnet orthogneiss from the Mte. Mucrone area. Omphacitic pyroxene (Omp) form continuous to semi-continuous layers and are separated by deformed layers of quartz (Qtz) and two species of white mica (WM), phengite and paragonite.

4.6.2 CRYSTALLIZATION AND REACTION HISTORY

The omphacite-garnet orthogneisses are distinguished from the mylonites by an *overall* coarser grain-size and by a well-pronounced foliation of *all* mineral phases (including phengite and paragonite). With the exception of paragonite, the mineral phases in the orthogneiss are chemically similar to those in the jad-gar mylonites (sample M17b, R185). Three main differences between the overprinted mylonites and the omp-gar orthogneisses are recognized:

- The overprinted mylonites contain two texturally distinct pyroxene and garnet phases.
- The Ca-rich garnets (Gar III), characteristic of the overprinted mylonites, are missing in the orthogneisses.
- The growth of omphacitic pyroxene, phengite and paragonite was syn-deformational during orthogneiss formation.

Koons (1982) and Koons et al. (in review) argue that the omphacite-garnet orthogneisses evolved from meta-quartz diorite through a transitional orthogneiss stage in which subsequent deformation caused microstructural reworking, grain coarsening, and an approach to equilibrium mineral assemblages which destroyed all evidence of the earlier superplastic deformation event. The formation of omphacite and paragonite (Par) may be related to a hydration reaction involving jadeite and garnet.

Undulose extinction and the formation of sub-grains in the pyroxenes in these orthogneisses suggests that intracrystalline deformation involved the movement of dislocations. Such a process may have increased the rates of intracrystalline diffusion and acted as a catalyst for omphacite- and paragonite-forming reactions, and would require addition of water either as an external fluid phase or by local redistribution of water within the rock (Früh-Green, 1985; see also Chapter 5).

The formation of omphacite, characteristic of these orthogneisses, has been interpreted by Oberhässli et al. (1982, 1985) as a result of equilibrium recrystallization of pyroxene under conditions of decreasing pressure. Koons (1982) argues that the buffering capacity of the stable mineral assemblages will differ depending on whether or not amphibole is present in the rocks. Contrary to the conventionally accepted interpretation that jadeite represents the high pressure side of a reaction, in the absence of amphibole continuous reactions involving jadeite-exchange may favour more omphacitic pyroxene compositions with increasing pressure (see also Koons, 1986).

As an alternative to an equilibrium reaction history, Koons (1982) and Koons et al. (in review) argue that the orthogneiss represents deformation and recrystallization of meta-quartz diorite, whereby the disequilibrium characteristics of the meta-quartz diorites were inherited during recrystallization. Jadeite-formation was originally a result of limited chemical communication between small domains. Due to the deformation during the main shearing event, greater chemical communication and increased diffusion rates resulted in a change in the effective bulk composition and an approach towards partial equilibrium within new and larger domains.

The above authors argue that the *initial deformation (shearing) event* which produced transition orthogneiss (analogous to the Jad-Gar mylonites in this study) did not produce equilibrium pyroxene compositions. This lack of equilibrium is ascribed to slow intra- and intercrystalline diffusion rates. Diffusion may have been impeded by a deformation mechanism of grain boundary sliding. A change in deformation

mechanism, involving the movement of dislocations during *further* deformation, caused pyroxene to readjust to a new and more mafic effective bulk composition and to become more omphacitic. Although garnet is assumed to be involved in the formation of omphacite and paragonite, zoning profiles in the garnet grains do not indicate readjustment during omphacite-formation. Fe-Mg exchange equilibrium between pyroxene and garnet cannot be assumed in these rocks (for a contrasting interpretation see Oberhänsli et al., 1985).

The time at which deformation took place was probably crucial to the mineralogical evolution of the metagranitoids at the Mte. Mucrone. Koons et al. (in review) suggest that if penetrative deformation had occurred prior to the eclogite-facies breakdown reactions of plagioclase and biotite, a state of equilibrium may have been approached during the complex metamorphism of these rocks. The rheological properties of the primary quartz diorite may have been such that the rock was highly resistant to deformation during the early stages of metamorphism and became more deformable after the formation of the fine-grain plagioclase pseudomorphs (reaction enhanced ductility). Koons et al. (in review) further suggest that a lack of grain boundary fluid and as a result slow intercrystalline diffusion may have been crucial factors in the disequilibrium history of these rocks.

In general, the mineralogical and textural evidence presented in this study is in agreement with the interpretation of a disequilibrium reaction history in the formation of the deformed rocks at the Mte. Mucrone as presented by Koons (1982) and Koons et al. (in review). However, several points were not considered by the above authors. The slight variations in bulk chemical compositions between the transition orthogneiss and the omphacite-garnet gneisses (see Table 5.2 in Chapter 5 and Table 4 in Koons et al., in review) are considered by Koons et al. (in review) to have no effect on the mineralogical evolution of the orthogneiss. The influence of K-feldspar in reactions involving the formation of phengitic white mica have not been investigated. Furthermore, the relative timing of possible fluid infiltration and deformation has not been investigated.

As discussed in Section 4.4.2, the deformed rocks at the Mte. Mucrone are characterized by heterogeneous deformation and by differing phases of syn- and post-kinematic recrystallization, which occur over very small distances of less than one meter. The mineralogical differences between the various metagranitic rock samples discussed in this study are summarized in Fig. 4.22. The evidence presented in this study suggests that not only can the evolution of these rocks be attributed to a disequilibrium reaction history as a result of slow diffusion rates and limited chemical communication, but also may be a result of very local variations in chemical activities of Na, K, and H₂O and may be directly related to the presence or absence of limited amounts

of a hydrous fluid phase during deformation (see Chapter 5 and Früh-Green, 1985).

	Meta-Quartz Diorite	Jad-Gar Mylonite	Overprinted Mylonite	Omp-Gar Orthogneiss
Recrystallization				
Pre - Kinematik	_____	_____	_____	_____
Syn - Kinematik	_____	_____	_____	_____
Post- Kinematik	_____	_____	_____	_____
Main Mineral Phases:				
Original Quartz Diorite				
Plagioclase	_____	_____	_____	_____
K-Feldspar	_____	_____	_____	_____
Biotite	_____	_____	_____	_____
Quartz	_____	_____	_____	_____
Allanite	_____	_____	_____	_____
Jadelite	_____	_____	_____	_____
Omphacite	_____	_____	_____	_____
Zoisite	--- ? ---	_____	_____	_____
Garnet I	_____	---	_____	_____
Garnet II	_____	---	_____	_____
Garnet III	_____	_____	_____	_____
Phengite (WMI)	_____	_____	_____	_____
Phengite (WMI)	_____	_____	_____	_____
Paragonite	_____	_____	_____	_____
Sphene	--- ? ---	_____	_____	_____

Fig. 4.22: Summary of the eclogite-facies mineralogical evolution of the metagranitoids at the Mte. Mucrone area.

4.7. GREENSCHIST-FACIES DEFORMATION AND RECRYSTALLIZATION

Post-eclogite-facies recrystallization of the Mte. Mucrone metagranitoids is marked by complete replacement of Na-pyroxene by white mica and albite, the appearance of epidote and, in some cases, new growth of pale-green biotite and minor calcite (see also Campagnoni and Maffeo (1974) and Oberhaensli et al., 1985). Campagnoni and Maffeo (1974) and Oberhaensli et al. (1985) also report that these retrograde phases are associated with the presence of chloromelanitic pyroxene and green amphibole, rimming glaucophane. Oberhaensli et al. (1985) describe the occurrence of aegerine-augitic pyroxene in retrograde samples exhibiting deformation (see Fig. 9, in Oberhänsli et al., 1985). These minerals, typical of the greenschist-facies overprinting during uplift

(Oberhaensli et al., 1985), are in general finer-grained than those in the eclogitic mylonites and orthogneisses discussed in the previous sections.

Ductile deformation, resulting in distinct mylonite zones, also occurred during subsequent uplift under greenschist-facies conditions. Macroscopically these shear zones are indistinguishable from the eclogite-facies mylonite zone (Fig. 4.23). As with the eclogitic mylonites, these shear zones are commonly found together with zoisite-garnet veins, which are separated from the mylonites by coarse-grained unfoliated zones as discussed above.

Microscopically, these retrograde shear zones are easily distinguished from the eclogitic mylonites. The zones consist of superplastically deformed layers (0.1 - 0.3mm thick) of white mica, epidote, garnet and relict pyroxene, alternating with equally thin intensively-deformed layers of quartz (Fig. 4.24a). Relict Na-pyroxene grains occur as imbricated isolated grains in mica-rich layers or form boudinaged layers oriented parallel to schistosity. The centers of these mylonite zones are characterized by the formation of second order shear bands (Fig. 4.24a, see also Simpson, 1981). The occurrence of such second order shear bands are essentially missing in the older eclogite-facies mylonites.

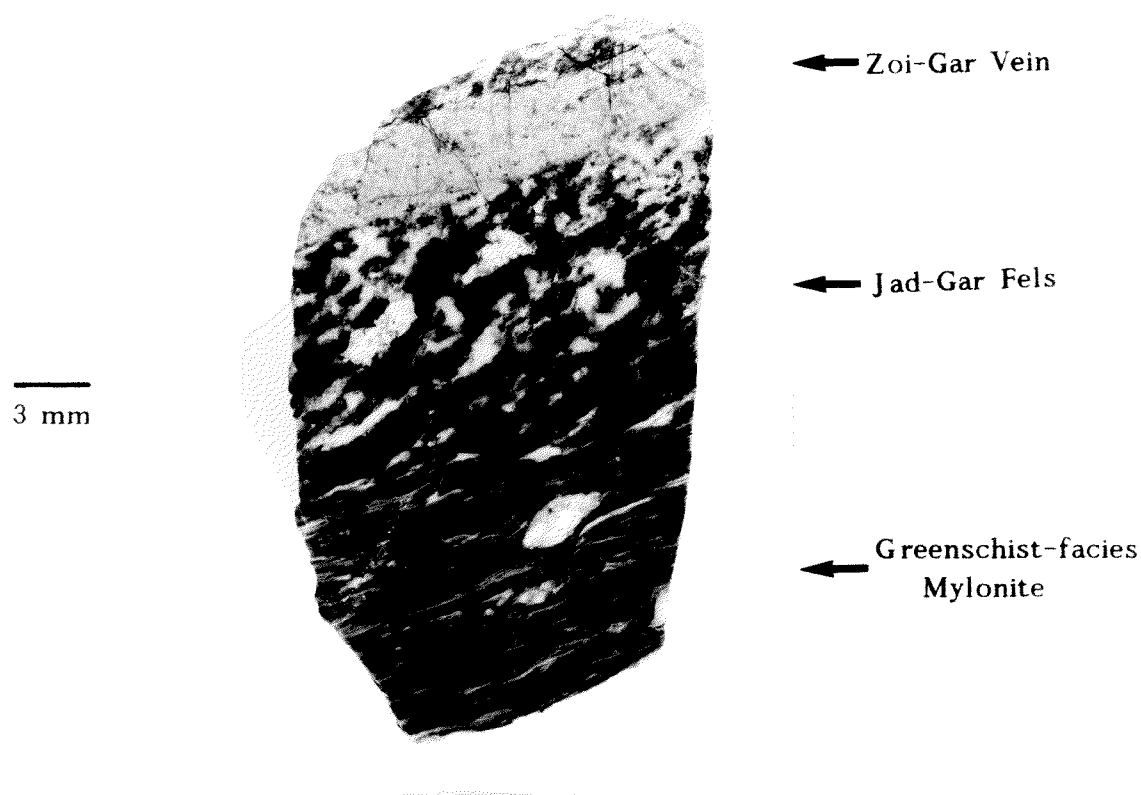


Fig. 4.23: Hand specimen of greenschist-facies mylonite. Macroscopically, these shear zones are indistinguishable from those formed under eclogite-facies conditions (Sample 83/1).

K-feldspar porphyroclasts are common, and are mantled by fine-grained dynamically recrystallized grains. The recrystallized grains are commonly rotated and form thin tail structures. According to the terminology presented by Simpson (1981), Simpson and Schmid (1983), and Passchier and Simpson (1985), the K-feldspar porphyroclasts have σ -shapes (e.g. samples 83/1-3, Mu 8-1; see Fig. 4.24b). In Fig. 4.24c, fine-grained epidote and green pyroxene (aegerine-augite?) grains form rims and tails around relict allanite. These grains have been rotated, with deflection of the epidote and pyroxene tails, resulting in δ -shapes (Passchier, 1982; Passchier and Simpson, 1985). According to Passchier and Simpson (1985), both σ - and δ -type porphyroclasts are common in mylonite zones on a micrometer to centimeter scale, and have been reported for feldspar in ultramylonites and mylonites of quartzofeldspathic compositions from the Pyrenees, Grenville Province in Canada, and from thrust faults in California.

The quartz fabrics in these shear zones are distinct from those in the eclogitic mylonites discussed previously. In contrast to the coarse-grained, recrystallized grains with equilibrated grain boundaries in the eclogitic mylonites, quartz in these retrograde shear zones occur as elongate and imbricated grains, forming 0.1 to 0.5mm thick bands, and exhibit pronounced deformation bands, undulatory extinction, and sutured grain boundaries (see Fig. 4.24d). Away from the immediate mylonite zones, lower strain conditions are marked by undulatory extinction, weaker deformation bands and sutured grain boundaries, whereby the old grains are still evident.

The presence of these texturally-distinct shear zones, indicative of lower pressure and temperature conditions (Schmid, personal communication, compare also Simpson, 1984), suggests that multiple deformation events occurred throughout the exhumation history of the Mte. Mucrone granitic body (see also Oberhassli et al., 1985). The close association of some of these zones with the zoisite-garnet veins suggests that the presence of the veins may have acted as strain 'localizers' during greenschist-facies deformation (see also Section 5.5). High strain conditions during uplift may also have been concentrated along earlier mylonite zones (although textural evidence to support this is scarce).

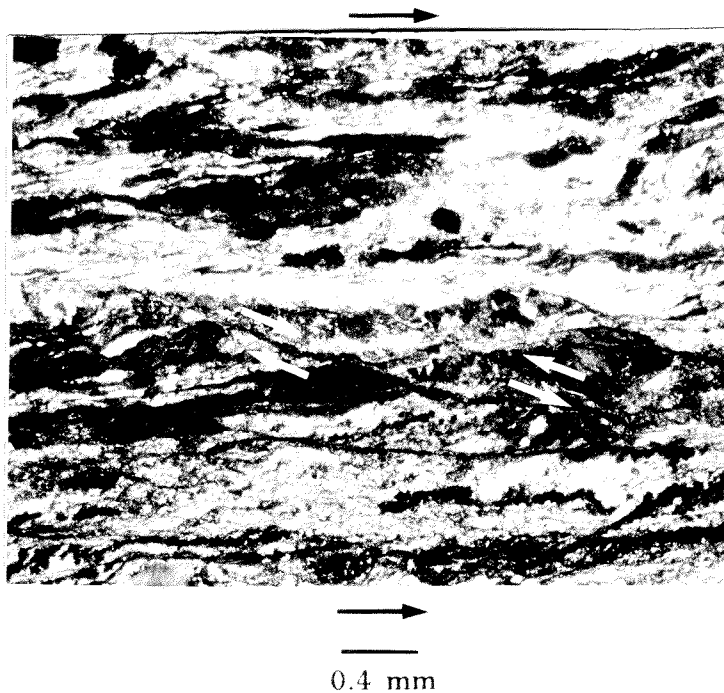


Fig. 4.24

(a): Photomicrograph showing the general of microfabric of the greenschist-facies mylonites. Relict bands of Na-pyroxene have been disrupted and form imbricate and boundinage layers. Second order shear bands depicted by the arrows indicate a dextral sense of shear (relative to the plane of the page).

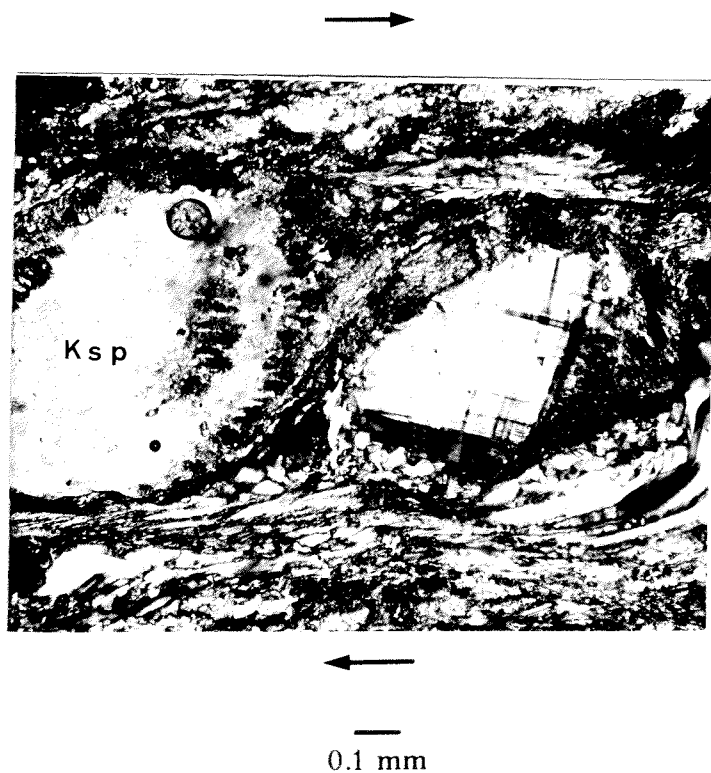


Fig. 4.24

(b): Photomicrograph showing K- feldspar σ - porphyroclasts, with recrystallized rims and tails of fine-grained epidote and feldspar. A dextral sense of shear (relative to the plane of the page) is indicated by the deflection of the tails as a result of deformation.

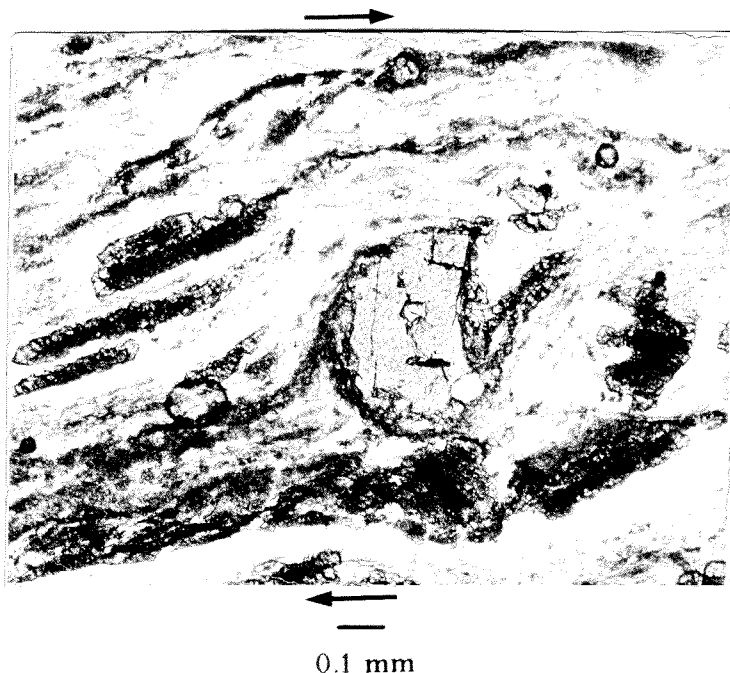


Fig. 4.24

(c): Photomicrograph of allanite porphyroblast in the greenschist-facies mylonites. Fine-grained epidote and pyroxene form rims and tails which have been deflected during deformation, resulting a characteristic δ -shape. As with K-feldspar porphyroblast, a dextral sense of shear (relative to the plane of the page) is indicate.



Fig. 4.24

(d): Photomicrograph of quartz micro-fabric of the greenschist-facies mylonites. Quartz is characterized by pronounced deformation bands, sutured grain boundaries and imbricated subgrains. In some cases deformation of previously annealed grains are evident.

CHAPTER 5

MONTE MUCRONE METAGRANITOIDS: ECLOGITE-FACIES GEOCHEMICAL AND REACTION HISTORY

The Mte. Mucrone metagranitoids are characterized by heterogeneous deformation histories and by varying degrees of eclogite-facies recrystallization. Changes in mineralogies and mineral chemistries, as well as multiple phases of mineral growth distinguish the deformed rocks from the unfoliated relicts of the original igneous protolith. The mineralogical and textural characteristics of these metagranitoids may be the result of two different possible reaction histories: (1) continuous recrystallization during decreasing pressure and/or temperature conditions; or (2) incomplete disequilibrium recrystallization and limited chemical communication, due to slow diffusion and growth rates, under relatively constant pressure-temperature conditions. In this chapter, these two possibilities are investigated in light of bulk rock geochemical and stable isotope data as well as thermodynamical considerations of possible reactions. Furthermore, the relationship between deformation and recrystallization and the evidence for infiltration of an external fluid phase are discussed.

5.1. POSSIBLE REACTIONS IN THE MONTE MUCRONE METAGRANITOIDS

Each of the rock types described in Chapter 4 is, at least in part, characterized by distinct mineralogical domains and heterogeneous mineral compositions. The pseudomorph textures after plagioclase together with coronas around biotite in, for example, the unfoliated meta-quartz diorites represent breakdown reactions of these two primary igneous phases. Little information is actually available on the state of complexing of migrating components (see also Fisher, 1983; Koons, 1981); therefore, in order to simplify the description of these breakdown reactions, end-member compositions have been used, and diffusing components are referred to as oxides. Because of the uncertainties in volume changes as well as the difficulties in determining the diffusing components, precise reactions which lead to the observed textures can not be written. The following discussion is thus only a qualitative description of the reaction behaviour of the meta-quartz diorite and is intended to demonstrate the lack of chemical equilibrium. Chemical equilibrium is not necessarily implied. An explanation of the abbreviations is given in Table 5.1 and the thermodynamic data used in the calculation of the end-member reactions are taken from the University of British Columbia (UBC)-database and is presented in App. IV. The reaction curves in Fig. 5.1 and 5.2 have been calculated with the computer program PTX, written by E. Perkins (ETH-Zuerich).

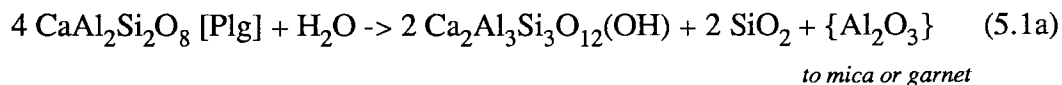
TABLE 5.1: Abbreviations for the phases and components used in the reactions discussed in the text and shown in Fig. 5.1

<i>Phase</i>		<i>Component</i>		<i>Composition</i>
Biotite	[Bio]	phlogopite annite	(Phl) (Ann)	$\text{KMg}_3\text{AlSi}_3\text{O}_{10}(\text{OH})_2$ $\text{KFe}_3\text{AlSi}_3\text{O}_{10}(\text{OH})_2$
Plagioclase	[Plg]	anorthite albite	(An) (Ab)	$\text{CaAl}_2\text{Si}_2\text{O}_8$ $\text{NaAlSi}_3\text{O}_8$
K-Feldspar	[Ksp]	K-feldspar	(Ksp)	KAlSi_3O_8
White-mica	[WM]	muscovite paragonite	(Mus) (Par)	$\text{KAl}_2\text{AlSi}_3\text{O}_{10}(\text{OH})_2$ $\text{NaAl}_2\text{AlSi}_3\text{O}_{10}(\text{OH})_2$
Garnet	[Gar]	grossular almandine pyrope	(Gro) (Alm) (Pyr)	$\text{Ca}_3\text{Al}_2\text{Si}_3\text{O}_{12}$ $\text{Fe}_3\text{Al}_2\text{Si}_3\text{O}_{12}$ $\text{Mg}_3\text{Al}_2\text{Si}_3\text{O}_{12}$
Clinopyroxene	[Cpx]	jadeite diopside Ca- Tschermarks	(Jad) (Dio) (CaTs)	$\text{NaAlSi}_2\text{O}_6$ $\text{CaMgSi}_2\text{O}_6$ $\text{CaAlSi}_2\text{O}_6$
Zoisite	[Zoi]	zoisite	(Zoi)	$\text{Ca}_2\text{Al}_3\text{Si}_3\text{O}_{12}(\text{OH})$

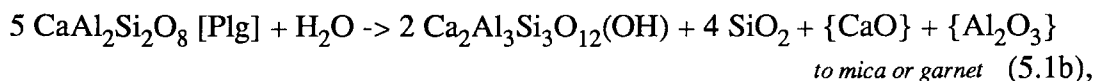
5.1.1. POSSIBLE REACTIONS IN THE UNFOLIATED META-QUARTZ DIORITES

The reaction behaviour of the meta-quartz diorite and the effects of non-equilibrium diffusional processes are discussed in detail by Koons et al. (in review) and Hy (1984). For clarity, the most pertinent aspects of the petrochemical evolution of these rocks are presented here.

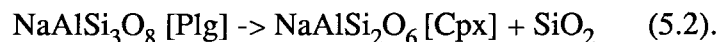
The higher pressure assemblage of jadeite, zoisite and quartz found in Domain I (see Fig. 4.3) as breakdown products of plagioclase could have been formed by the reactions:



or with limited H₂O activity,



and



Phase relationships suggest that with rising pressure, continuous reactions in plagioclase may produce more albitic feldspar until reaction 5.2 is reached (Green and Ringwood, 1968; Koons and Thompson, 1984). However, no direct mineralogical

evidence has been preserved in these rocks which would indicate whether the plagioclase became progressively more albitic before crossing the equilibrium boundary for reaction 5.2 or remained metastable at the original igneous composition until reaction 5.2 was significantly overstepped. In either case, the breakdown of the anorthite component in the original igneous plagioclase served as a source of CaO and Al_2O_3 for the formation of both zoisite in domain I and grossular component in garnet in domain II.

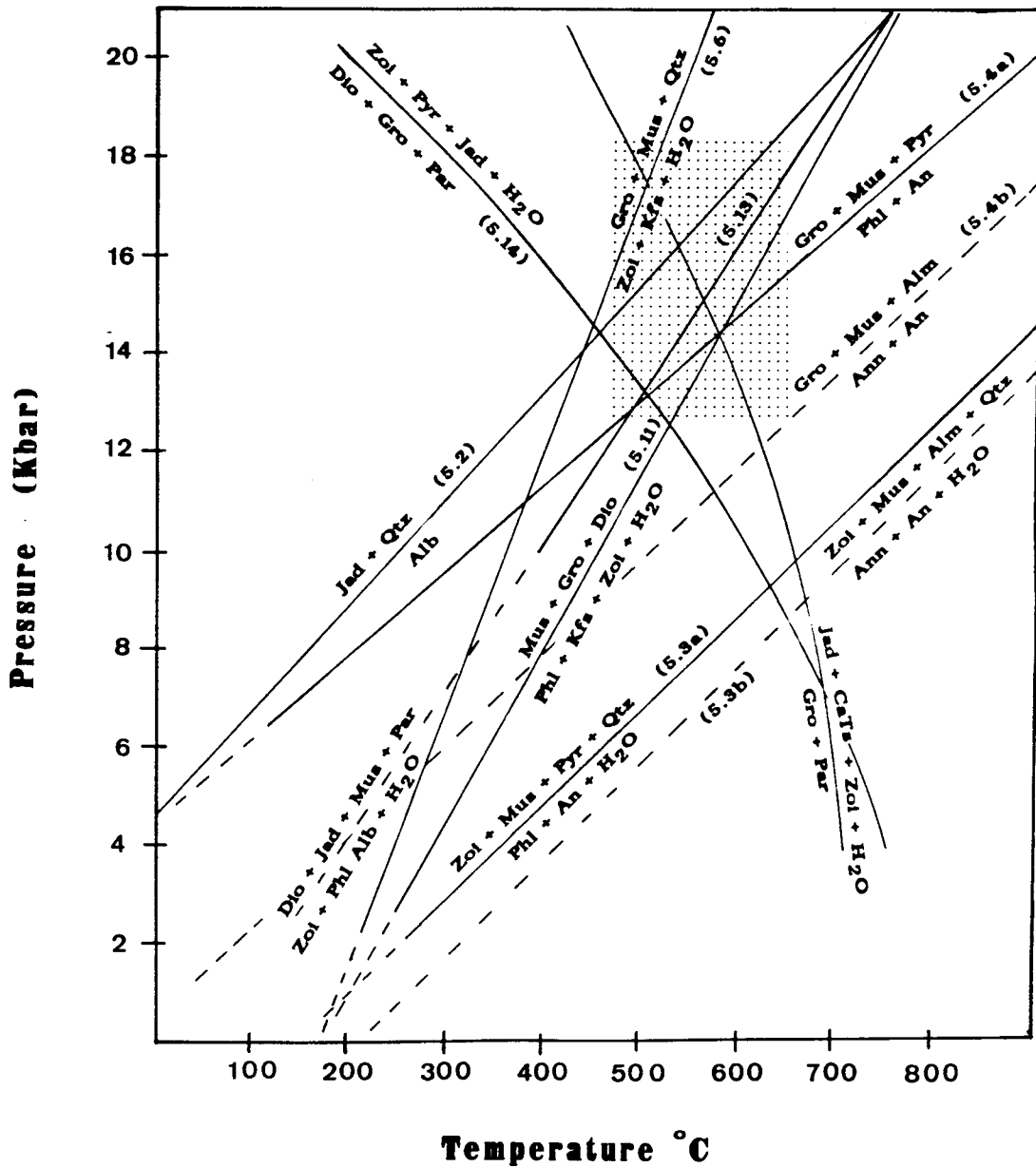
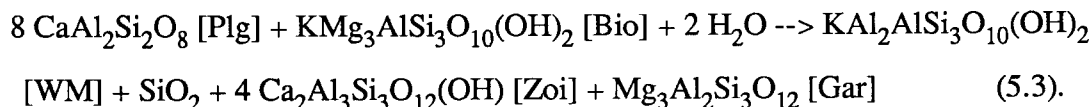


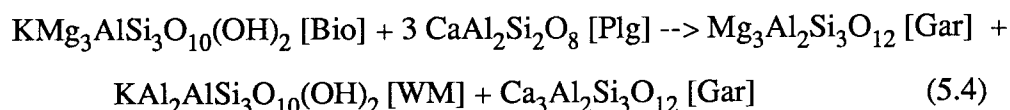
Fig. 5.1: Pressure-temperature diagram of reactions discussed in the text. Stippled regions represent the range of temperatures determined by cation-exchange geothermometry and oxygen isotope data for the surrounding eclogitic micaschists (see Table 5.4. and Section 5.3.). Data source: University of British Columbia, Canada (see Appendix IV). Reaction curves have been calculated by the computer program PTX, written by E. Perkins (ETH Zürich).

As a first approximation, the corona textures around biotite in domain II and the formation of zoisite in domain I can be described by an end-member hydration reaction in the KCMASH- system:



In this and other cases, solid solutions, for example FeMg-1 in biotite and garnet, can be included through the incorporation of the appropriate exchange equilibria and activity coefficients. Reaction 5.3 could have occurred early in the reaction history during rapid pressure increase associated with the early Alpine collision event (Rubie, 1983, Oberhänsli et al., 1985) (see Fig. 5.1). Both reactions 5.1 and 5.3 will be controlled by the availability of H₂O; with limited activity of H₂O, the anorthite component in plagioclase could have remained stable until pressure and temperature conditions of albite instability.

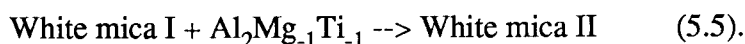
With increasing temperature and pressure (see Fig. 5.1), and/or in the absence of a hydrous fluid phase, the water-conserving reaction:



may have been significant in the formation of the meta-quartz diorites. For P-T paths that involve pressure increases greater than temperature increases (e.g. rapid burial), thermodynamic considerations (Fig. 5.1) indicate that reaction 5.4 will take place before the albite breakdown reaction (5.2). This equilibrium curve will be displaced to lower pressures with increasing activity of the annite component in biotite (Rxn. 5.4b, dashed lines in Fig. 5.1).

The distinct corona textures of white mica and garnet around the incompletely reacted biotite grains, as well as the inhomogeneous chemical compositions of these product phases (see Section 4.3.1), may be attributed to diffusion-controlled processes during transformation of the original quartz diorite (Fisher, 1977). The high Ti-content in the white micas directly in contact with biotite, as well as the depletion in grossular component towards biotite, suggest that the breakdown of biotite was directly influenced by diffusion of CaO and Al₂O₃ from the plagioclase domains to the biotite domains. The compositions of the product phases were evidently controlled by their position of growth relative to the chemical potential gradients of the diffusing species.

The chemical distinction between the white mica compositions of domains II and III may be a result of continuous reactions, such as



Rutile may have formed by such a reaction or the displaced Ti may have reacted with diffusing CaO and Al₂O₃ to produce the sphene observed in domain III.

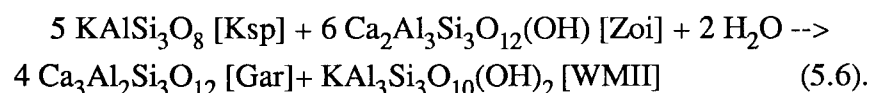
The lack of chemical homogeneity of the mineral phases and the incompleteness of the biotite breakdown reaction may either be due to an absence of intergranular fluid and consequently slow transport of the diffusing species between the mineralogical domains (Tracy and McLellan, 1985), or be a result of cessation of CaO and Al₂O₃ production during the plagioclase breakdown reaction. Consideration of the stability fields of the above reactions indicates that the reaction history recorded in the meta-quartz diorite took place during prograde metamorphic conditions of increasing pressure and temperature (see Fig. 5.1).

5.1.2. POSSIBLE REACTIONS IN THE MYLONITES

The mylonites are distinguished from the unfoliated meta-quartz diorites by a well-defined foliation, more homogeneous phase compositions, coarser grain-sizes of pyroxene, garnet and phengite, and by a lack of biotite. As discussed in Chapter 4, before the onset of the high strain deformation event, the transformation of plagioclase, possibly by reactions 5.1 and 5.2, had gone to completion, producing the fine-grained aggregates of jadeite + zoisite + quartz. At the onset of deformation, these fine-grained products deformed superplastically at which time quartz appears to have remained less deformable. Grain-coarsening may have accompanied deformation, resulting in a relative change in the deformation behaviours of the two dominant minerals jadeite and quartz (see Rubie, 1983 and Section 4.4.1.1.2).

5.1.2.1. Jadeite-Garnet Mylonites

In the un-overprinted jadeite-garnet mylonite samples, the coarser grain-sizes (compared to those in the meta-quartz diorites) and more homogeneous compositions of pyroxene, garnet and phengite (see Figs. 4.11, 4.14 and 4.16) suggest that deformation influenced both the rates of grain growth and the diffusion kinetics which lead to chemical homogenization and to the completion of the biotite breakdown reaction 5.4 (see also Koons et al., in review). The decrease in the K-feldspar content and in the amount of zoisite present as inclusions in the jadeite grains (see Fig. 4.9) suggests that biotite breakdown was accompanied by zoisite consumption, which can be described by the reaction



Inspection of Fig. 5.1 and Fig. 5.2 shows that in the presence of jadeite, reaction 5.6 requires temperatures greater than 420 °C and pressures above 13 Kbar. With increasing activity of the almandine component in garnet, this reaction curve will be

displaced to higher temperatures as shown by the dashed lines in Fig. 5.2. Furthermore, such a reaction requires either an external source of an hydrous fluid or localized redistribution of water within the rock. Deformation may not only have increased the size of the equilibrium domains in these rocks, but may also have enhanced the permeabilities, allowing infiltration of water into the system. Experimental studies on rock deformation have shown that the addition of even small traces of H_2O to a previously dry system can increase reaction rates and grain growth by several orders of magnitude (Fyfe et al. 1958; Tullis and Yund, 1982; see also discussion by Rubie and Thompson, 1985 and references therein).

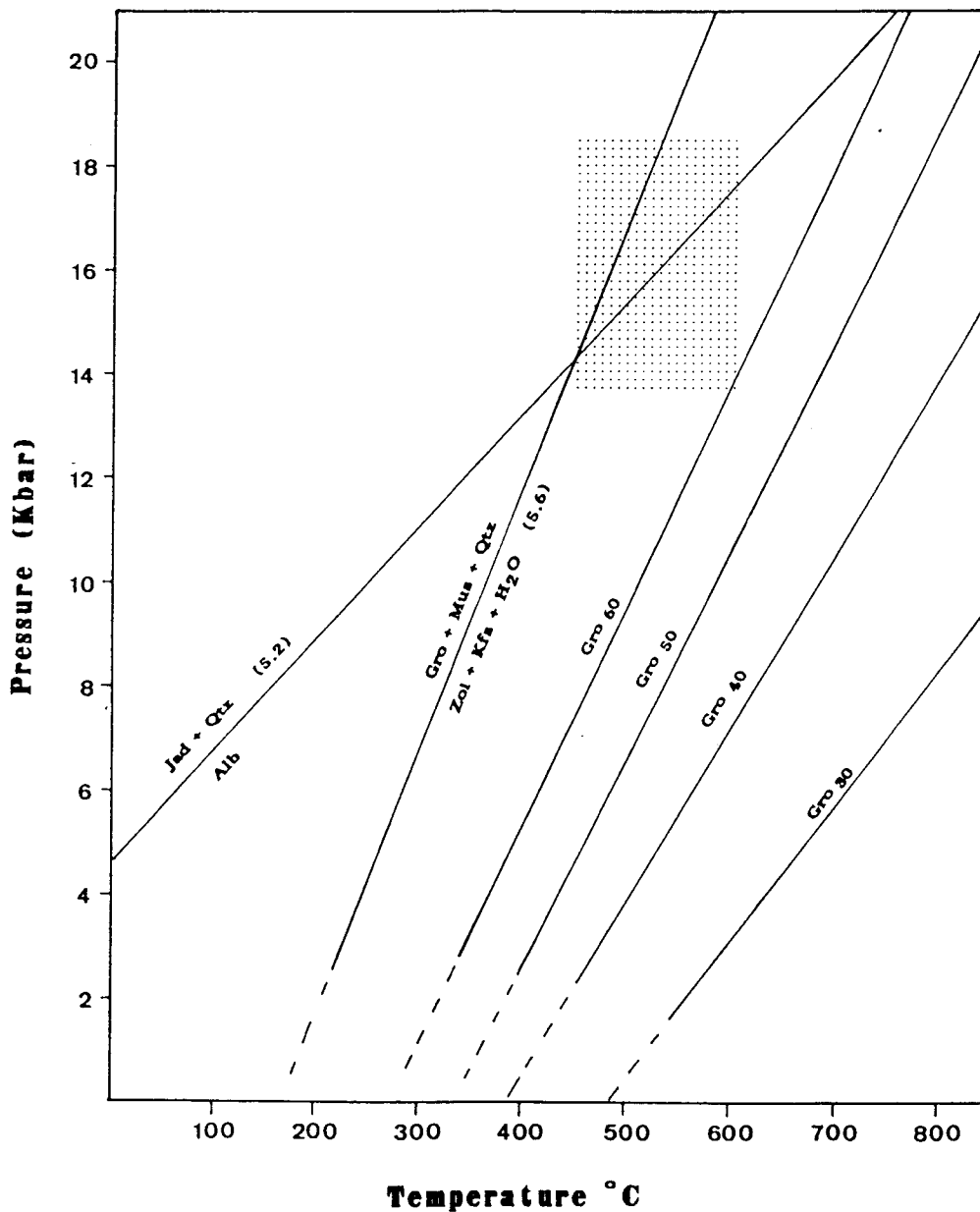
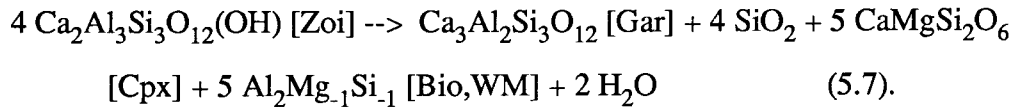


Fig. 5.2: Pressure-temperature diagram of reactions 5.2 and 5.6. (see text), showing the placement of the isopleths for reaction 5.6. with decreasing activity of grossular (Gro) component in Gar. Stippled area and data source are as in Fig. 5.1.

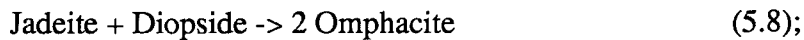
5.1.2.2 Overprinted Mylonites

As discussed in Section 4.4.2, several mineralogical and textural characteristics distinguish the overprinted mylonites from the primary jadeite-garnet mylonites. Although the main eclogite-facies high strain deformation event produced superplastically deformed layers of pyroxene and quartz, subsequent deformation and grain coarsening did not result in homogeneous chemical compositions of the coexisting phases in the overprinted mylonites upon completion of the biotite breakdown reaction 5.4. The heterogeneous compositions of garnet and phengite (see Figs. 4.14 & 4.16 and Tables 4.2 & 4.3) reflect the disequilibrium conditions during the eclogite-facies formation of the meta-quartz diorite. Further disequilibrium is indicated by post-kinematic growth of omphacitic pyroxene and more grossular-rich garnet (Gar III, see Fig. 4.14).

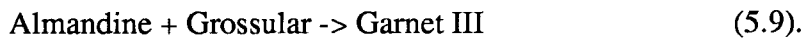
The increase in the diopside component and the grossular component in these two phases indicates Ca-Mg-exchange and may be related to zoisite consumption during a continuous reaction:



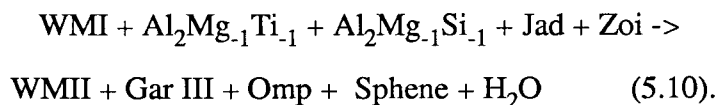
The Tschermarks-component could have been produced either by the complete breakdown of biotite by reaction 5.4 and/or by the transformation of white mica I to white mica II by reaction 5.5, so that:



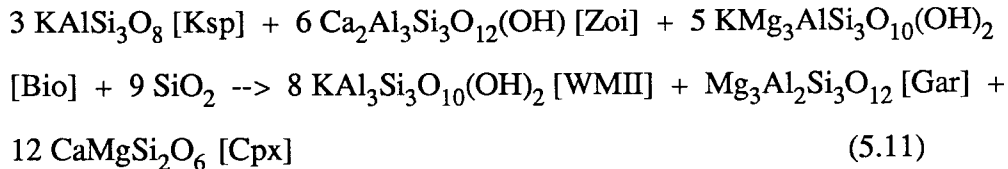
and



The replacement of jadeitic pyroxene by phengitic white mica II (WMII) + quartz further distinguishes the overprinted mylonites from the Jad-Gar mylonites. In the absence of K-feldspar, white-mica II may have been formed by the biotite breakdown reaction 5.4, coupled with TiO_2 -diffusion to produce sphene. Thus, the formation of the characteristic phases in the overprinted mylonites can be described by a generalized reaction involving the transformation of WMI:



Relicts of K-feldspar replaced by phengitic white mica and quartz, and associated with textural domains rich in grossular-rich Gar III (see Figs. 4.20 c,d, & e), suggest that reaction 5.6 may have been, at least in part, important in the formation of WMII and Gar III (see Fig. 5.1 & 5.2). In the presence of biotite, a water-conserving reaction similar to:



would also explain the replacement of K-feldspar observed in some of the overprinted mylonites rocks and may provide an additional source of potassium for the formation of phengite.

The replacement of jadeite by phengitic white mica need not be related to a pronounced decrease in pressure, but alternatively could be due to local changes in the chemical activities of K and H₂O in local domains during eclogite-facies metamorphic P-T conditions. Theoretical K-, Na- and H₂O-activity diagrams, balanced on alumina (constructed by J. Ganguin, ETH-Zürich, work in preparation), for the phases jadeite, paragonite, kyanite and K-feldspar under constant eclogite-facies pressure-temperature conditions (i.e. P > 14 Kbar and T > 500 °C) are shown in Figs. 5.3 a,b.

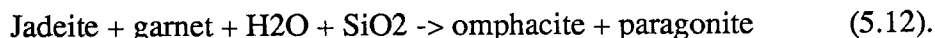
The initial activities of sodium (μ_{Na}) and potassium (μ_{K}) prior to the main shearing event, are represented by the solid star in Fig. 5.3a, in which K-feldspar, jadeite and muscovite coexist, and is analogous to that in the H₂O- ($\mu_{\text{H}_2\text{O}}$) vs. K-activity diagram in Fig. 5.3b. A decrease in the activities of one or more of these elements, as represented by the arrows in these diagrams, would decrease the stability of K-feldspar, whereby only jadeite and phengite would coexist. The diagrams, although schematic, clearly show the ranges of fluid compositions that could have been responsible for possible metasomatic changes (see Section 5.2 below).

5.1.3. *POSSIBLE REACTIONS IN THE OMPHACITE-GARNET ORTHOGNEISSES*

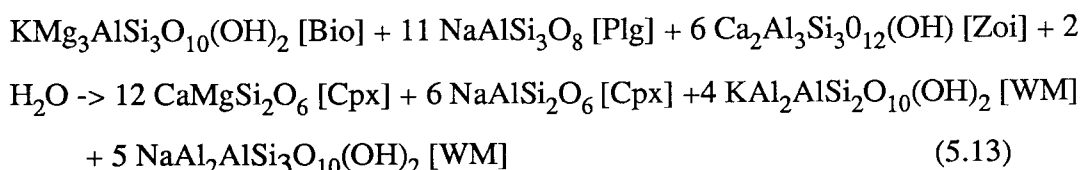
Omphacite-garnet orthogneiss comprises the largest volume of the metagranitoids at the Mte. Mucrone and represents complete recrystallization during eclogite-facies metamorphism of the original quartz dioritic body. These strongly foliated rocks are distinguished from the mylonites by an overall coarser grain-size, more omphacitic pyroxene compositions (see Fig. 4.11), and by the presence of paragonite as part of the stable mineral assemblage. As discussed in Sect. 4.6, jadeite-rich domains in the cores of the pyroxene grains and irregular zoning patterns in garnet suggest that the Omp-Gar orthogneisses evolved from meta-quartz diorite through similar stages of recrystallization as those observed in the mylonites. Further deformation resulted in coarser grain-sizes and a parallel alignment of all the mineral phases, whereby all evidence of the initial superplastic deformation was destroyed. Syn-kinematic grain growth, accompanied by changes in the mineral compositions, may indicate that both

the diffusion kinetics and grain growth rates were enhanced by deformation, resulting in an approach to equilibrium mineral assemblages.

The formation of omphacite and paragonite, characteristic of these orthogneisses, may be related to a reaction involving garnet, as proposed by Koons et al. (in review, Rxn 7):

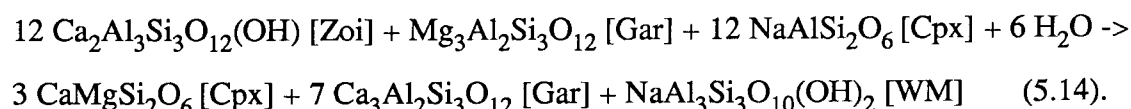


However, the omphacite component in pyroxene (Cpx) may also be related to zoisite-consumption as in the continuous reaction 5.8. As seen in Rxn 5.12, paragonite-formation requires the presence of a hydrous phase. If a hydrous fluid was present during the early stages of deformation and recrystallization, the reaction



could have produced an assemblage with omphacitic pyroxene and paragonite at the onset of the eclogite-facies metamorphic event (see also Koons et al., in review).

As discussed previously, the jadeite-rich domains in the cores of the pyroxene grains as well as irregular zoning patterns in garnet and the presence of only one phengitic mica phase suggests that the completely recrystallized orthogneiss initially underwent the same phases of recrystallization as those recorded in the mylonites. Thus, if an external hydrous fluid were present during the deformation phase which produced the orthogneisses, both the diopside-component in pyroxene and paragonite may have been formed by a reaction such as



Inspection of Fig. 5.1 shows that the stability boundary for reaction 5.14 lies at pressures less than 15 Kbar for temperatures greater than 500 °C. With increasing activity of the almandine component in garnet reaction 5.14 will be displaced to higher temperatures.

Whole rock geochemical and oxygen isotope data (see Section 5.2 below) indicate that the formation of mylonite involved a certain degree of hydration and is related to a general loss of alumina and/or potassium. The distinction between the mylonite and orthogneiss mineralogies and microfabrics may simply be a function of the *timing and duration* of infiltration of an external hydrous fluid phase *relative* to deformation. As can be seen in Fig. 5.1, if deformation, accompanied by fluid infiltration, occurred subsequent to the albite-breakdown reaction (5.2) and before complete consumption of biotite, without significant changes in pressure and temperature, the equilibrium

boundary for reaction 5.13 would have sufficiently been overstepped such that omphacitic pyroxene and paragonite could have been a part of the stable mineral assemblage.

Examination of the activity diagrams in Fig. 5.3 indicates that at constant pressure and temperature (above the Alb \rightarrow Jad + Qtz reaction boundary), a decrease in the chemical potentials of Na and K, to compositions denoted by the open stars, would lead to the stable mineral assemblage jadeite + paragonite + muscovite.

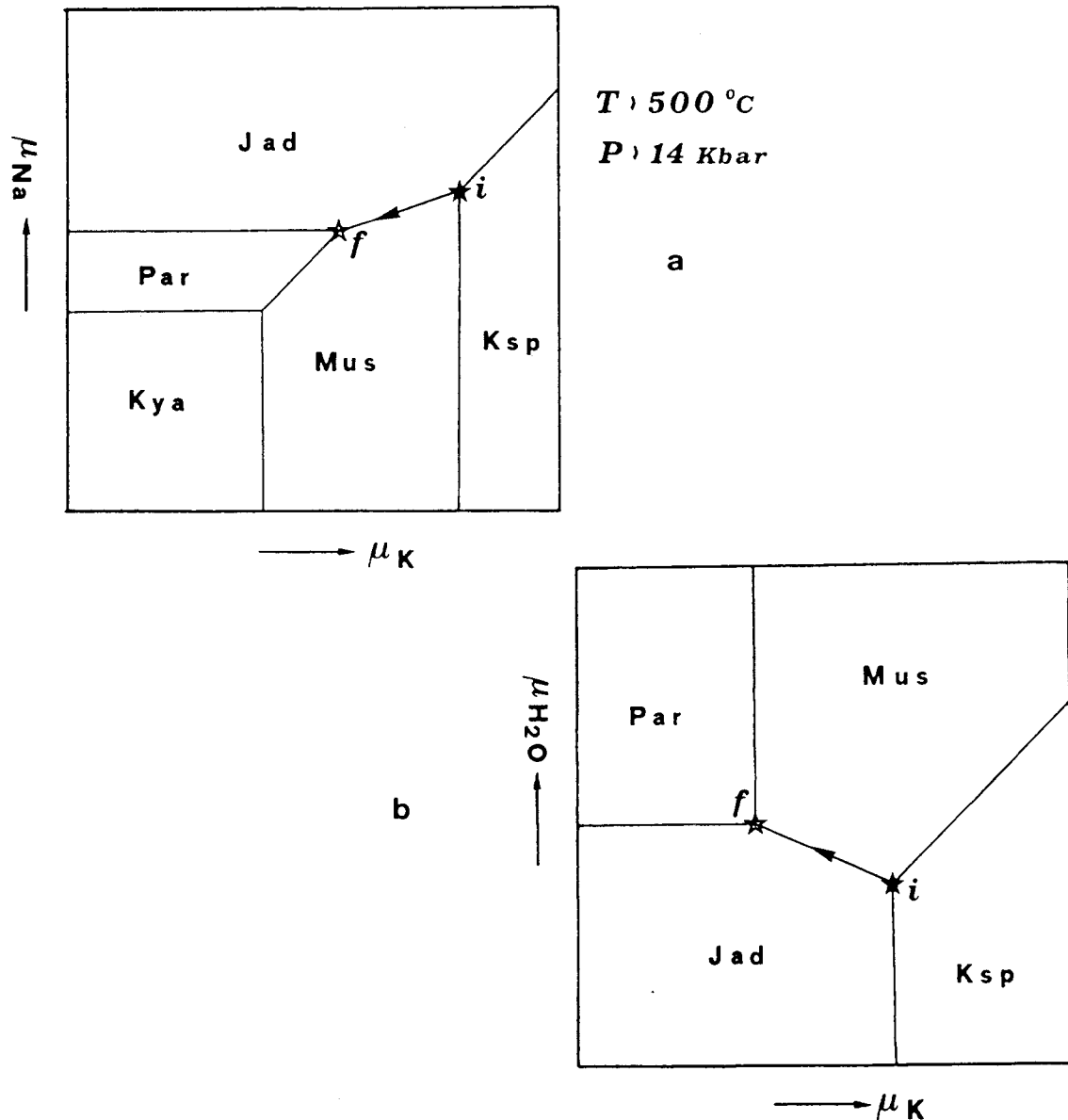


Fig. 5.3.

Schematic μ - μ diagram showing the possible changes in chemical potentials of Na-, K-, and H_2O associated with the transformation of meta-quartz diorite (initial composition, i , depicted by the solid stars) to omphacite-garnet ortho-gneiss (final composition, f , depicted by the open stars). Possible ranges in fluid compositions in equilibrium with the mylonites are shown by the arrows. *Diagram constructed by J. Ganguin, work in progress, ETH Zürich.*

5.2 BULK ROCK AND STABLE ISOTOPE GEOCHEMISTRY OF THE MTE. MUCRONE METAGRANITOIDS

XRF bulk chemical analyses of the samples investigated in this study are shown in Table 5.2 (see also Oberhaensli et al., 1985). The oxygen and hydrogen isotope compositions are presented in Table 5.3 and are shown graphically in Fig. 5.4. Due to the fine-grained and strongly intergrown nature of most of the mineral phases, only the isotopic compositions of quartz separates (see Section 3.0 for separation techniques) and bulk rock could be determined for many of the samples.

5.2.1. *BULK ROCK AND STABLE ISOTOPE GEOCHEMISTRY OF THE UNFOLIATED META-QUARTZ DIORITES*

The least deformed meta-quartz diorites have relatively constant chemical compositions and show only slight variations in SiO_2 - and Al_2O_3 -contents (see also Oberhänsli et al., 1985). The oxygen isotope compositions of quartz and whole rock are also constant, ranging from 10.4‰ to 10.8‰ and 9.2‰ to 9.3‰, respectively (relative to SMOW, see Sections 1.2.1 and 3.0.1 for terminologies and separation techniques). These isotopic values lie within the range known for normal granitic rocks (Taylor, 1977).

5.2.2. *BULK ROCK AND STABLE ISOTOPE GEOCHEMISTRY OF THE JADEITE- GARNET MYLONITES*

In order to compare bulk rock chemical analyses of metamorphosed rocks, some control on the changes in volume is necessary. Some studies normalize the data by assuming that elements such as alumina and titanium remain immobile during metamorphism. However, this method may be unsatisfactory when considering high pressure rocks. In this study the graphical method of Gresens (1967) has been employed, which takes into consideration changes in volume associated with the transformation of the metagranitoids. Whole rock densities, given in Table 5.3, have been determined from rock powder by a pycnometer method (under vacuum), based on the principle described by Hutchinson (1974). The graphical method of Gresens allows determination of weight percent gain or loss of the chemical elements between two rock compositions (plotted on the vertical axis; see for example Fig. 5.5) with regard to changes in volume of the two rocks (plotted as a volume factor on the horizontal axis). The volume factor is determined by equation 14 in Gresens (1967 p. 50). In an isochemical system with no change in volume, comparison of two rock samples should yield a graph in which all the lines intersect at a point of 0.0 weight % gain and a

Table 5.2: Representative XRF whole rock chemical analyses of Monte Muchrone metagranitoids.

Sample Nr.	13/3	R81/186	R81/189	13/1X	13/1Y	13/7	R82/5	R81/185	R81/191	R81/191	R82/9	
	← META-QUARTZ DIORITE →							← JAD-GAR →				
	FELS							ORTHOGRANITE				
Weight %												
SiO2	67.42	67.09	68.91	69.81	68.63	68.13	71.17	68.10	67.56	68.50	63.66	
TiO2	0.51	0.49	0.40	0.44	0.44	0.44	0.37	0.48	0.51	0.51	0.70	
Al2O3	16.41	16.49	15.73	15.07	15.57	15.93	15.14	15.97	15.56	15.26	17.88	
Fe2O3	3.40	3.55	2.80	2.45	2.40	2.75	2.35	0.95	1.16	0.72	0.96	
FeO	0.05	0.05	0.04	0.05	0.05	0.05	0.04	2.90	3.15	3.45	3.65	
MnO	1.01	1.03	0.75	0.86	0.87	0.83	0.72	0.04	0.07	0.07	0.06	
MgO	4.02	3.68	3.10	2.72	3.08	3.21	3.34	0.93	1.53	1.44	1.51	
CaO	3.19	3.55	3.45	2.99	3.43	3.28	3.43	3.73	4.38	4.16	4.54	
Na2O	2.60	2.73	3.21	3.30	3.27	2.75	1.65	3.55	3.64	3.37	3.67	
K2O	0.18	0.15	0.14	0.13	0.13	0.13	0.08	1.85	0.98	1.00	1.46	
P2O5	0.85	0.84	0.83	1.19	1.29	1.47	1.00	0.14	0.15	0.15	0.22	
H2O+	0.12	0.12	0.08	0.06	0.10	0.18	0.14	1.18	1.16	1.51	1.53	
CO2	0.00	0.00	0.00	0.00	0.00	0.00	0.00	0.13	0.04	0.02	0.02	
CR2O3	0.00	0.00	0.00	0.00	0.00	0.00	0.00	0.00	0.00	0.00	0.00	
NiO	0.00	0.00	0.00	0.00	0.00	0.00	0.00	0.00	0.00	0.00	0.00	
TOTAL	99.95	99.90	99.71	99.94	100.27	99.90	99.89	99.95	99.89	100.16	99.86	

ppm :	← JAD-GAR →											
	ORTHOGRANITE											
ppm :												
BA	849	823	767	1026	989	981	388	670	335	336	485	
DA	868	847	784	1054	1012	997	386	666	323	319	453	
RB	87	106	102	109	106	81	73	55	26	29	47	
SR	223	239	196	155	188	224	339	375	206	217	461	
PB	12	19	8	9	23	8	8	15	8	8	24	
TH	<5	<5	<5	<5	<5	<5	<5	5	<5	<5	<5	
U	<1	<1	<1	<1	<1	<1	<1	<1	<1	<1	<1	
NB	<3	<3	<3	<3	<3	<3	<3	3	<3	<3	<3	
LA	56	36	27	42	33	38	<15	61	31	25	49	
CE	84	54	44	70	73	71	30	114	65	68	100	
ND	38	31	18	27	26	22	10	49	36	28	36	
Y	14	8	3	17	17	9	4	14	11	12	15	
ZR	199	160	146	167	186	171	163	202	142	145	172	
V	117	140	95	59	67	70	28	44	56	56	<10	
CR	<10	<10	<10	<10	<10	10	<10	<10	14	<10	11	
NI	<3	<3	<3	<3	<3	<3	<3	<3	<3	<3	<3	
CO	23	22	22	17	18	16	17	14	20	16	18	
CU	<4	<4	<4	<4	<4	<4	<4	<4	<4	<4	<4	
ZN	56	70	58	53	51	56	37	58	63	61	81	
GA	14	14	13	11	12	14	12	16	14	13	18	
SC	9	10	6	8	7	7	4	7	5	4	6	
S	<20	<20	<20	<20	<20	<20	<20	<20	<20	<20	<20	
TOTAL	2649	2579	2289	2824	2808	2775	1499	2368	1355	1337	1976	

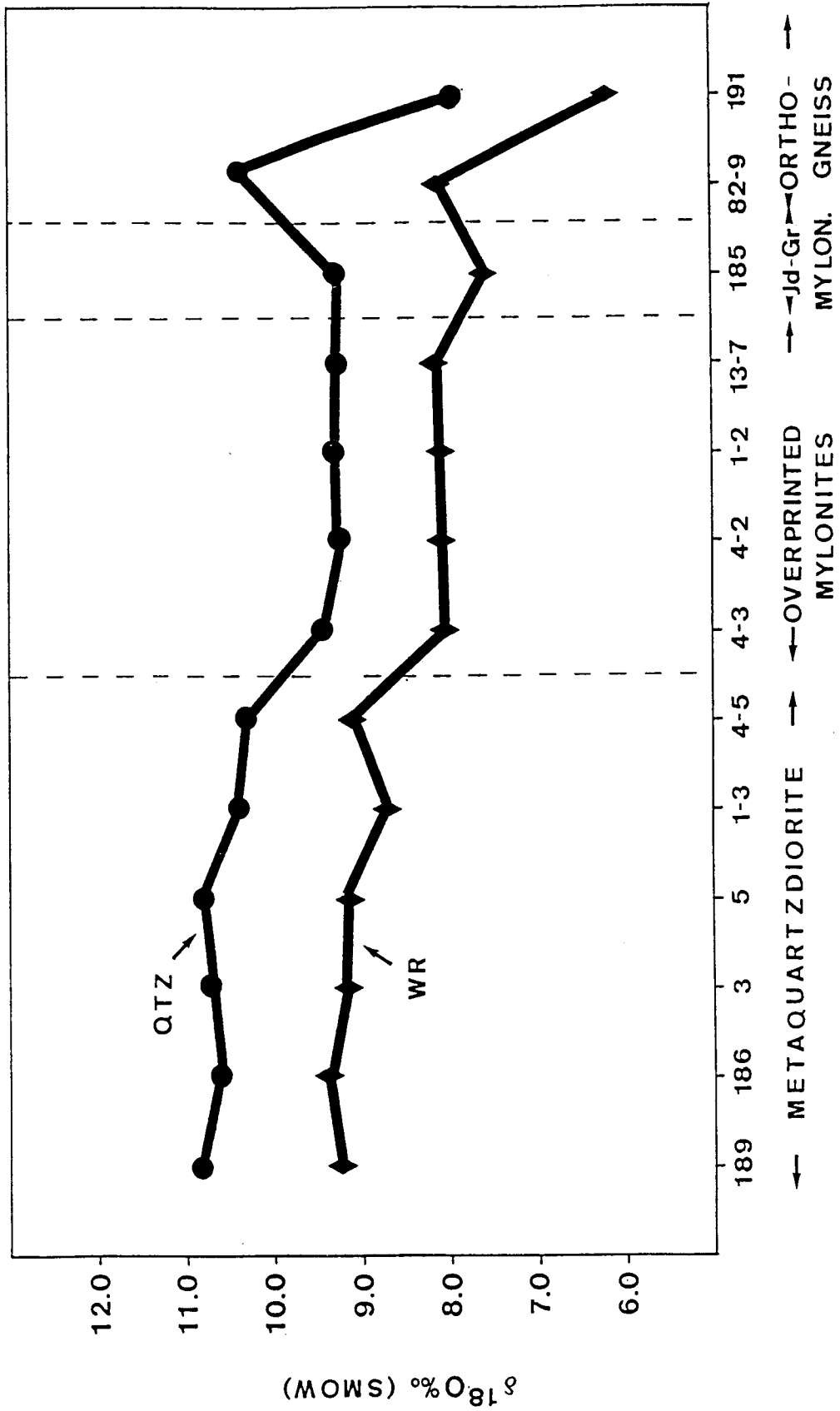


Fig 5.4: Variations in the oxygen isotope compositions between the variously transformed metagranitoids at the Mtc. Mucrone (Italy).

volume factor of 1.0. The diagrams in this study have been constructed using a computer program written by R. Panozzo (ETH, Zuerich) which is based on the original publication of Gresens (1967).

Using the graphical method of Gresens, the bulk rock chemical data of the jadeite-garnet mylonites (sample R185, Table 5.2) is compared with that of the unfoliated meta-quartz diorites (sample R186) in Fig. 5.5. It can be seen that with constant silica (stippled line a in Fig. 5.5), a slight decrease in volume is associated with the transformation from meta-quartz diorite to jadeite-garnet mylonite. However, if alumina is assumed to have remained constant (stippled line b in Fig. 5.5), a slight increase in volume would have accompanied the eclogite-facies deformation and transformation to jadeite-garnet mylonite. With constant silica, the amounts of MgO, CaO, TiO₂, and Na₂O remained constant, whereas the transformation resulted in a change in the oxidation state of iron and is associated with a loss of alumina and potassium and a gain in H₂O. With constant alumina, in addition to an increase in H₂O, a very slight increase in Na and Ca and 4.0 wt% gain in Si is indicated.

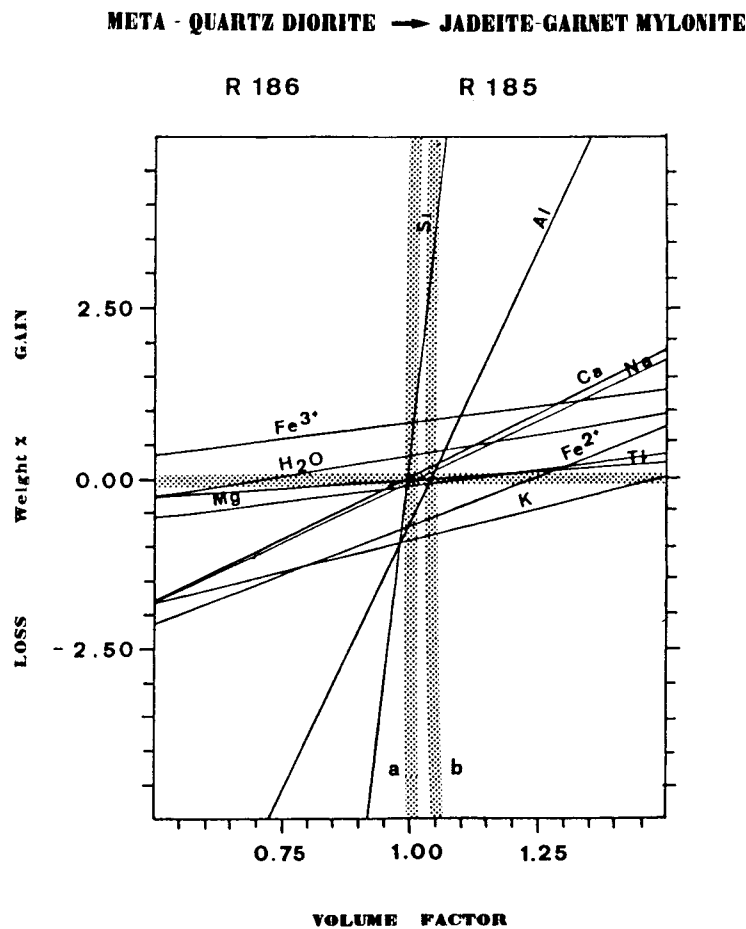


Fig. 5.5: Comparison of XRF bulk chemical analyses (see Table 5.2.) between incompletely transformed meta-quartz diorite (R186) and Jad-Gar mylonite, using the graphical method described by Gresens (1967). If constant silica is assumed (stippled line a), with a slight decrease in volume, the transformation resulted in a change in the oxidation state of iron and a loss of alumina and potassium, with a gain in H₂O. If alumina is assumed to be constant (stippled line b), a metasomatic input of Na, Ca, and Si is indicated.

Table 5.3: Oxygen and hydrogen isotopic compositions, modal percentages and whole rock densities for the Mte. Mucrone Metagranitoids

		$\delta^{18}\text{O}_{(\text{SMOW})}$	$\delta\text{D}_{(\text{SMOW})}$	Modal %	Density
<u>Meta-Quartz Diorites</u>					
Mu 3	quartz	10.42		46	
	biotite	6.58		6	
	'plagioclase' (*)			37	
	white-mica			5	
	garnet			3	
	K-feldspar			3	
	Whole rock	9.21			2.82
Mu 5	quartz	10.81		34	
	biotite	6.00		5	
	'plagioclase' (*)			45	
	white-mica			7	
	garnet			5	
	K-feldspar			4	
	Whole rock	9.15			2.84
Mu 1-3	quartz	10.40		34	
	biotite			2	
	'plagioclase' (*)			44	
	white-mica			12	
	garnet			6	
	K-feldspar			2	
	Whole rock	9.16			2.78
Mu 4-5	quartz	10.26		40	
	biotite			2	
	'plagioclase' (*)			39	
	white-mica			12	
	garnet			5	
	K-feldspar			2	
	Whole rock	8.75			2.82
R189	quartz	10.83		50	
	biotite	6.64		2	
	'plagioclase' (*)	9.00		33	
	white-mica			7	
	garnet			5	
	K-feldspar			3	
	Whole rock	9.33	-77		2.84
R186	quartz	10.47		38	
	biotite	5.80		5	
	'plagioclase' (*)			42	
	white-mica			6	
	garnet			5	
	K-feldspar			4	
	Whole rock	9.30	-66		2.82
<u>Jadeite-Garnet Fels</u>					
R82/5	quartz	10.80			
	jadeite (Jad 85-90)	8.45			
	Whole rock	9.12	-73		2.82

(*) Isotopic compositions and modal percentage of original plagioclase grains pseudomorphed by fine-grained aggregates of jadeite + zoisite + quartz

Table 5.3
(continued): Oxygen and hydrogen isotopic compositions, modal percentages and whole rock densities for the Mte. Mucrone Metagranitoids

		$\delta^{18}\text{O}_{(\text{SMOW})}$	$\delta\text{D}_{(\text{SMOW})}$	Modal %	Density
<u>Mylonites</u>					
R185	quartz	9.40		38	
	clinopyroxene (Jad ₈₈)	6.66		29 ^(b)	
	white-mica	6.57		19	
	garnet	5.06		13	
	spheue + rutile			1	
	K-feldspar			< 1	
	Whole rock	7.50	-62		2.84
Mu 1-2	quartz	9.30		40	
	clinopyroxene (Jad ₈₈)	7.05		30 ^(b)	
	white-mica			20	
	garnet	5.53		8	
	spheue + rutile			1	
	K-feldspar			< 1	
	Whole rock	8.11			2.80
Mu 4-2	quartz	9.26		35	
	clinopyroxene (Jad ₈₈)			29 ^(b)	
	white-mica			24	
	garnet			10	
	spheue + rutile			1	
	K-feldspar			< 1	
	Whole rock	8.10			2.76
Mu 4-3 (c)	quartz	9.45		41	
	clinopyroxene (Jad ₈₈)			25 ^(b)	
	white-mica			21	
	garnet			11	
	spheue + rutile			1	
	K-feldspar			< 1	
	Whole rock	8.10			2.75
R 13/7	quartz	9.50		41	
	clinopyroxene (Jad ₈₈)	6.67		23 ^(b)	
	white-mica	7.27		29	
	garnet	5.04		7	
	spheue + rutile			1	
	K-feldspar			< 1	
	Whole rock	8.21	-65		2.74
<u>Veins</u>					
R13/7V	quartz	9.75			
	garnet	5.24			
R13/1	quartz	9.72			
M83/1	quartz	9.64			

(b) Modal percent of clinopyroxene include fine-grained zoisite. Jad - component used to calculate Q-Cpx temperatures shown in Table 5.4.

(c) Sample Mu 4-3 is transitional between mylonite and meta-quartz diorite. See Fig. 4.7.

Table 5.3
(continued): Oxygen and hydrogen isotopic compositions, modal percentages and whole rock densities for the Mte. Mucrone Metagranitoids

<i>Orthogneiss</i>		$\delta^{18}\text{O}_{(\text{SMOW})}$	$\delta\text{D}_{(\text{SMOW})}$	Modal %	Density
R 82/9	quartz	10.24		38	
	clinopyroxene (Jad ₅₅)	7.41		27	
	white-mica: phengite	7.47		20	
	paragonite				
	garnet	6.00		12	
	sphene + rutile			1	
	zoisite			2	
	Whole rock	8.16	-61		2.84
R 191	quartz	7.92		40	
	clinopyroxene (Jad ₅₅)	5.12		23	
	white-mica: phengite	5.15		26	
	paragonite	5.75			
	garnet	4.79		8	
	sphene + rutile			1	
	zoisite			2	
	Whole rock	6.08	-60		2.84

It should be noted that the amount of H₂O in the bulk chemical analyses is a calculated value, determined by the loss on ignition and corrected for Fe-oxidation and measured amount of CO₂. As discussed in Chapter 4, biotite in the meta-quartz diorites contain up to 1 wt% chlorine and fluorine. Thus, the calculated weight % H₂O in these analyses represents a combined value of the volatile elements H₂O, Cl and F. However, the actual percentage of the latter two elements remains relatively small in comparison to the percentage of H₂O.

The isotopic compositions of quartz in the jadeite-garnet mylonite sample R185 is 9.4‰ and lies within the range defined by the overprinted mylonites (see Table 5.3 and Fig. 5.4). Comparison with the isotopic compositions of quartz in the unfoliated meta-quartz diorites shows that quartz in the mylonites are depleted in ¹⁸O by at least 1‰. The whole rock isotopic composition of the jadeite-garnet mylonite (sample R185) exhibits nearly a 2‰ depletion in ¹⁸O to a value of 7.5‰ (SMOW). This is a greater depletion than that indicated for the overprinted mylonites (see below and Fig. 5.4).

5.2.3. BULK ROCK AND STABLE ISOTOPE GEOCHEMISTRY OF THE OVERPRINTED MYLONITES

Application of the graphical method of Gresens (1967) indicates that deformation and transformation from meta-quartz diorite (sample R186) to overprinted mylonite (sample R13/7) resulted in a slight increase in volume (Fig. 5.6). Similar to the jadeite-garnet mylonites, deformation and transformation resulted in a change in the oxidation state of iron, possibly a loss of alumina, and a gain in H₂O. In contrast to the jadeite-garnet mylonites, the overprinted samples also show a slight depletion in calcium and sodium and a conservation of potassium, relative to the less deformed meta-quartz diorites. If alumina is assumed to be constant, an increase in silica is also indicated, as discussed above.

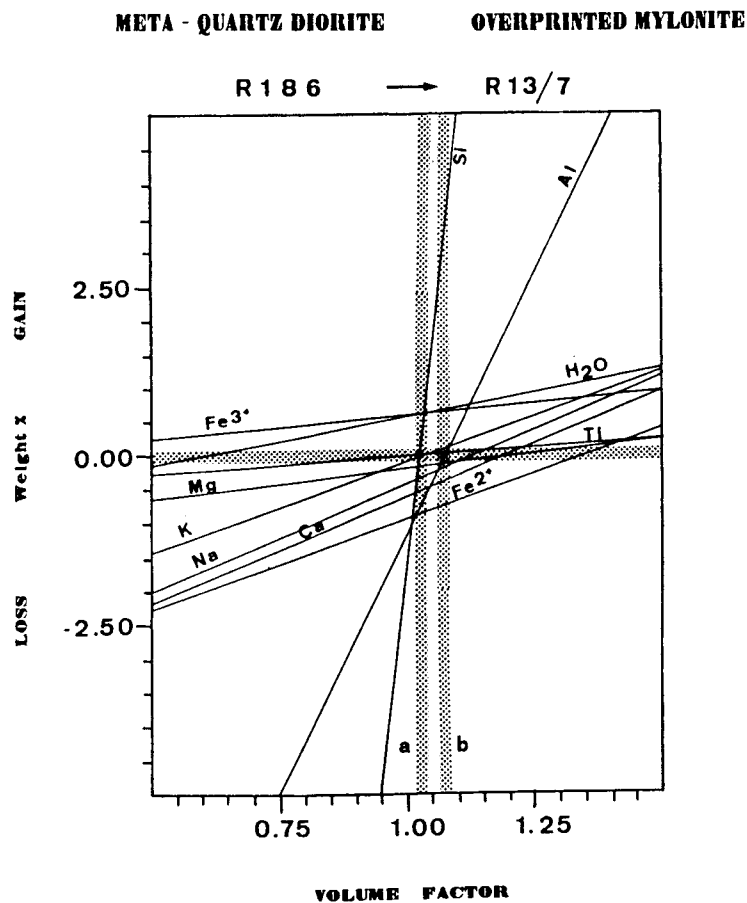
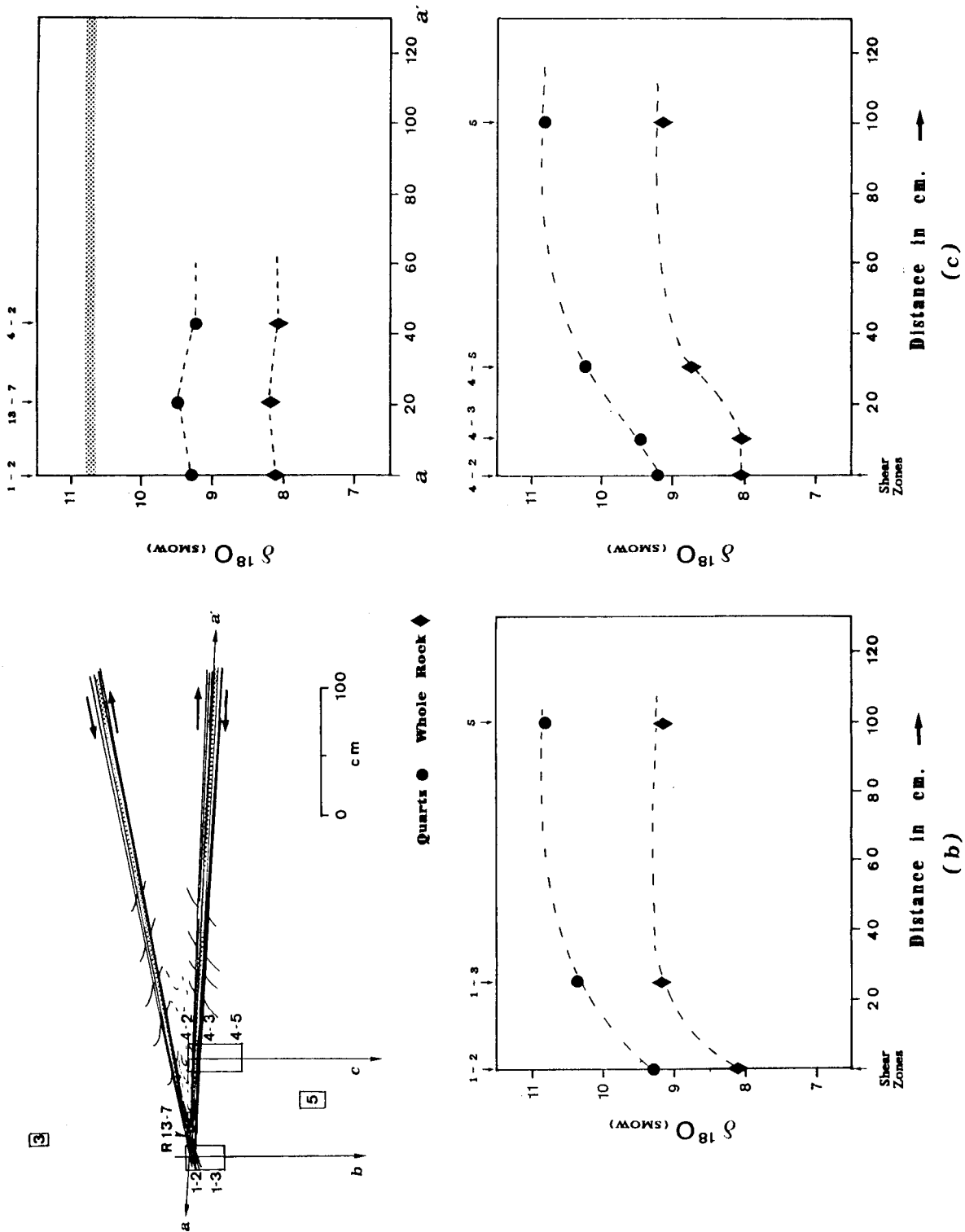


Fig 5.6. Comparison of XRF bulk chemical analyses (see Table 5.2.) between incompletely transformed meta-quartz diorite (R186) and overprinted mylonite (R 13/7), using the graphical method described by Gresens (1967). If silica is assumed to be constant (stippled line a), deformation and transformation resulted in a change in the oxidation state of iron, a gain in H₂O and a possible loss of Al. If alumina is assumed to be constant, (stippled line b), an increase in Si may also be indicated.

Fig. 5.7: $\delta^{18}\text{O}_{\text{Qtz}}$ and $\delta^{18}\text{O}_{\text{WR}}$ plotted as a function of distance away from the center of the shear zones in profile (b) and (c) and along the shear zones in profile a-a'. A depletion in $\delta^{18}\text{O}$ relative to the incompletely transformed meta-quartz diorites (isotopic composition shown as stippled line in (a)) is observed in the mylonites, and is restricted to the immediate deformation zones (profile b and c). Relatively constant isotopic compositions along profile a-a' suggests that fluid flow and isotopic exchange was concentrated in the centers of the zones with a diffusive infiltration front perpendicular to the centers of the mylonite zones (profiles b and c).



Detailed sampling for isotopic analysis was made across the shear zones (shown in Fig. 4.6), which consist of overprinted mylonites and are associated with the post-kinematic zoisite-garnet veins. $\delta^{18}\text{O}_{\text{Qtz}}$ and $\delta^{18}\text{O}_{\text{WR}}$ from these samples are compared with the other rock types in Fig. 5.4 and Table 5.3, and are plotted as a function of distance, both *away* from the centers of the shear zones in Fig. 5.7 b,c and *along* the zones in Fig. 5.7a.

The oxygen isotopic compositions of quartz in the overprinted samples are similar to those of the jadeite-garnet mylonites and range from 9.2‰ to 9.5‰. However, the bulk rock oxygen isotopic compositions are more ^{18}O -rich than the jadeite-garnet mylonites, and fall within a narrow range of 8.1‰ to 8.2‰. As can clearly be seen from Figs. 5.7b and 5.7c, the depletion in $\delta^{18}\text{O}_{\text{Qtz}}$ and $\delta^{18}\text{O}_{\text{WR}}$ is restricted to the immediate deformation zone, whereas the primary igneous values are retained in samples located only 30cm from the centers of the shear zones (e.g samples Mu 1-3 and Mu 4-5). Although a very slight increase in $\delta^{18}\text{O}_{\text{Qtz}}$ is observed in the profile along the shear zones in the direction of the zoisite-garnet veins (Fig. 5.7c), its significance can not be determined due to the error of $\pm 0.2\%$ inherent in the isotopic analyses. The isotopic compositions of the quartz in the zoisite-garnet veins (9.65 \pm 0.2‰) indicates isotopic equilibrium with the deformed rocks.

The relatively constant isotopic compositions seen the profile in Fig. 5.7a suggests that isotopic exchange, as a result of fluid infiltration, was concentrated along the centers of the shear zones. Fluid flow may have been controlled by the foliation present in the mylonites. The profiles shown in Figs. 5.7b & c suggest that a diffusive infiltration front penetrated the mylonites perpendicular to the centers of the shear zones (see also Brodie and Rutter, 1985; Rutter and Brodie, 1985; and Baumgartner and Rumble, 1986, in review). Textural evidence suggests that the fluid infiltration event responsible for the shift in $\delta^{18}\text{O}$ occurred subsequent to the high-strain deformation event which produced the mylonites (see also Sections 5.5 and 5.6 and Figs. 5.12 and 5.15).

5.2.4. BULK ROCK AND STABLE ISOTOPE GEOCHEMISTRY OF THE COMPLETELY RECRYSTALLIZED OMPHACITE-GARNET ORTHOGNEISSES

Comparison of the bulk rock geochemical data with the graphical method of Gresens (1967) indicates that the recrystallization of Jad-Gar mylonite (sample R185) to form Omp-Gar orthogneiss (sample R191) would have taken place with constant volume and involved an approximately 1 weight % loss of alumina and potassium (see Fig. 5.8a). In comparison to the meta-quartz diorite (sample R186), transformation to orthogneiss resulted in a net weight loss of nearly 2% K and Al (see Fig. 5.8b). As in the other deformed samples, deformation and transformation to orthogneiss resulted in a change in the oxidation state of iron and a slight increase in H_2O (approximately 0.5 wt%).

Furthermore, the orthogneiss samples are enriched in calcium and magnesium relative to the mylonites and the unfoliated meta-quartz diorites. Although some variations are seen in the bulk rock compositions of the meta-quartz diorites, the Mg-, Ca- and K-contents are relatively constant, and are distinctly less magnesium- and calcium-rich than the orthogneisses investigated in this study.

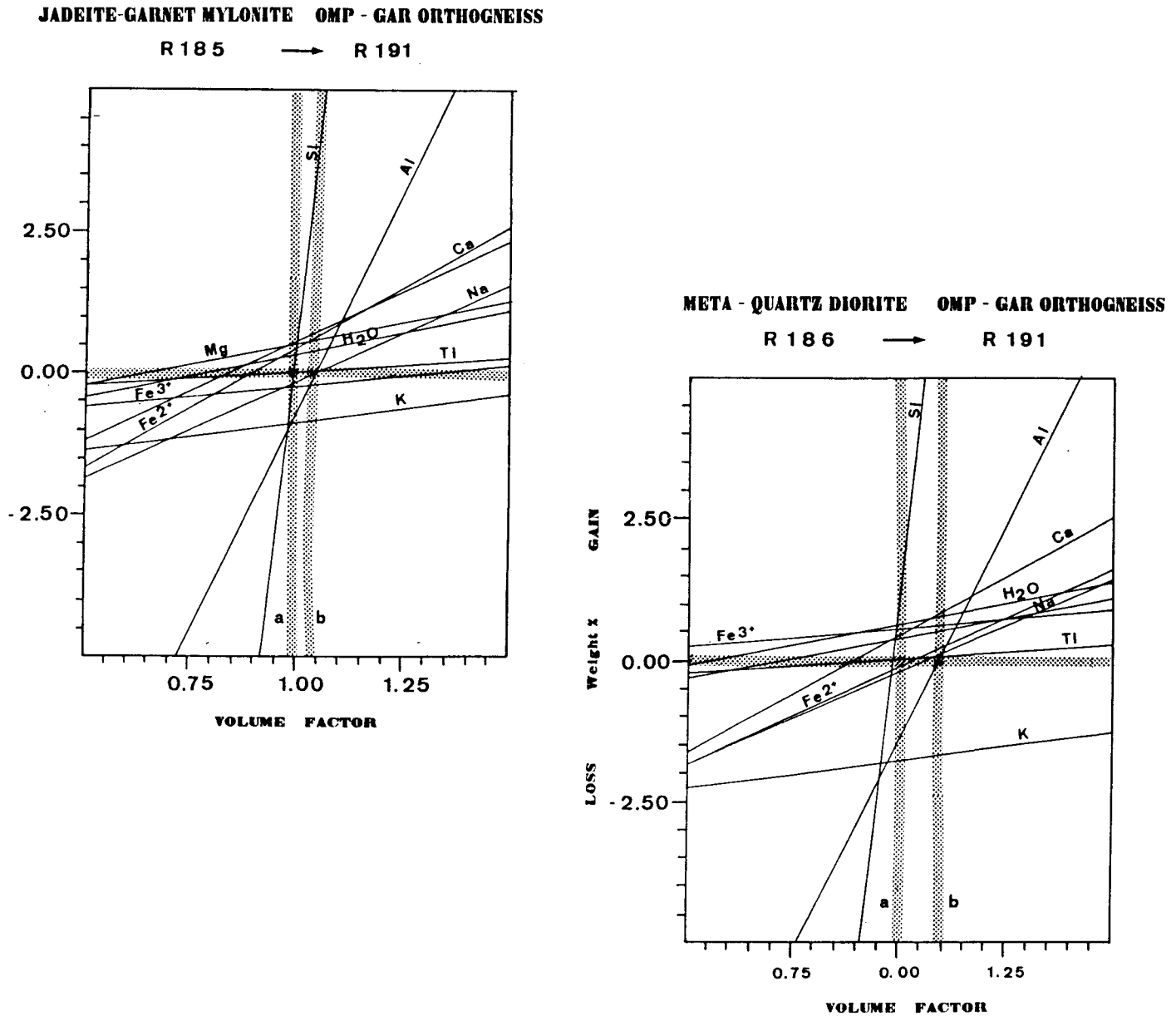


Fig. 5.8:

(a) Comparison of XRF bulk chemical analyses (see Table 5.2) between Jad-Gar mylonite and completely recrystallized Omp-Gar orthogneiss. Stippled lines a, for constant silica, and b, for constant alumina, show the relative changes in volume and respective gains or loss associated with the transformation. Figure (b) shows the total loss and gain of the major elements associated with the deformation and recrystallization of incompletely transformed meta-quartz diorite to form Omp-Gar orthogneiss (compare also Figs. 5.5 and 5.6).

The possibility cannot be ruled out that the apparent change in Mg- and Ca-contents in the Omp-Gar orthogneisses may only represent original differences in the meta-granitoids before metamorphism. A slightly more basic (or Mg-rich) composition could have been the determining factor as to whether or not omphacite and/or paragonite formed during eclogite-facies metamorphism. However, samples of omphacite-garnet gneiss investigated by Oberhänsli et al. (1985, Table I) do not show a significant change in Mg- and/or Ca-contents (see also Koons et. al., in review). In contrast to the samples investigated in the present study, the above authors do not report the presence of paragonite in their completely recrystallized omphacite-garnet-phengite gneisses (see samples KAW 989 and KAW 1419, Table I in Oberhänsli et al. 1985).

The whole rock geochemical data substantiates the interpretation of Figs. 5.3a,b that changes in the chemical potentials of sodium, potassium and/or H₂O could result in paragonite as part of the stable mineral assemblage. If the differences in mineral parageneses between the paragonite-bearing orthogneisses and the mylonites represent original variations in bulk rock chemistries, the initial compositions during the primary shearing event may have been located either on the jadeite-muscovite boundary, represented by the arrow in the activity diagrams in Figs. 5.3a and 5.3b or at the triple point denoted by the open star. In the latter case, paragonite may have been present from the beginning of the high pressure metamorphic event. Although slightly different initial bulk rock chemistries may have influenced the formation of omphacite and/or paragonite in the completely recrystallized orthogneisses, the chemical characteristics of the coexisting mineral phases may still record similar deformation and recrystallization histories as those in the meta-quartz diorites and mylonites.

Oxygen isotope data of the Omp-Gar orthogneisses show considerable differences between the two samples investigated in this study (samples R82/9 and R191 in Table 5.3 and Fig 5.4). Comparison with the unfoliated meta-quartz diorites shows that quartz in sample R82/9 retains the original igneous value of 10.24‰, whereas the $\delta^{18}\text{O}_{\text{WR}}$ shows the same depletion in ¹⁸O as that seen in the mylonites. Sample R191 exhibits a considerable depletion in ¹⁸O of bulk rock and quartz, compared to both the meta-quartz diorites and the mylonites.

The difference in $\delta^{18}\text{O}_{\text{Qtz}}$ between the two orthogneiss samples may be related to the degree of recrystallization which occurred in these samples. Sample R82/9 has a distinct quartz fabric which is characterized by pronounced deformation bands and undulatory extinction with sutured grain-boundaries and numerous fine-grained subgrains (5-20 micron in dia.). The characteristic recrystallized quartz fabric observed in the other samples (see Section 4.4.1.4.1 and Fig. 4.17a) is completely absent in sample R82/9. The distinct quartz microfabric in sample R82/9 is most likely the result of *subsequent* deformation which destroyed an equilibrated fabric.

5.3. PRESSURE - TEMPERATURE CONSIDERATIONS FOR THE ECLOGITE - FACIES METAMORPHISM OF THE MONTE MUCRONE METAGRANITOIDS

Various temperature and pressure estimates for the eclogite-facies metamorphic event at the Mte. Mucrone area are available from the literature. A summary of these data, as well as temperature estimates based on oxygen isotope fractionations of coexisting minerals investigated in this study, are presented in Table 5.4.

5.3.1. PRESSURE ESTIMATES

Pressure estimates, ranging from 13 to 16 Kbars, were obtained for the surrounding eclogitic micaschists at the Mte. Mucrone area by Hy (1984). These estimates were determined by independent temperature estimates and the geobarometer of Holland (1980), which is based on experimental determination of the $Ab \rightarrow Jad + Qtz$ reaction boundary. Lower pressures, ranging from 11 to 13Kbar, have been determined by the same geobarometer by Oberhaensli et al. (1985) for the metagranitic rocks at the Mte. Mucrone. However, the exact rock types (i.e. mineral assemblages and stage of transformation) for which these estimates have been made are not given in the study by Oberhaensli et al. (1985). A different approach was taken by Koons (1982). By considering variations along pressure-sensitive exchange vectors in pyroxenes and amphiboles, Koons (1982) calculated a set of isopleths for the reaction: $paragonite + omphacite \rightarrow glaucophane + zoisite + jadeite + H_2O$. The pressure estimates derived from these isopleths (see Fig. 5.12 and 5.13 in Koons, 1982) and combined with geothermometric calculations range from 17.5 to 18.5 Kbar for rocks of mafic composition from the eclogitic mica schist complex.

5.3.2 CATION-EXCHANGE GEOTHERMOMETRY

Based on various cation-exchange geothermometers (see Table 5.4), temperatures ranging from 550 to 650 °C have been determined for the eclogite-facies metamorphism of the surrounding mica schists at the Mucrone area (Koons, 1982 and Hy, 1984). A large scatter in the data for the metagranitoids was found by Oberhaensli et al. (1985) with temperatures ranging from 400 to 600 °C. As stated previously, it is difficult to determine the significance (with relation to deformation/recrystallization) of the estimates by Oberhaensli et al., as no rock descriptions have been given for the samples for which these temperature estimates have been made. Furthermore, the previous discussion has shown that the deformational and recrystallization history of the Mte. Mucrone metagranitoids is characterized by general disequilibrium relationships and incomplete reactions. The large scatter in temperature estimates presented by Oberhaensli et al. (1985) may reflect this lack of equilibrium.

5.3.3. OXYGEN ISOTOPE FRACTIONATION GEOTHERMOMETRY

A narrow range of temperatures from 530 to 580 °C have been determined by Desmons and O'Neil (1978) and are based on oxygen isotope fractionations between quartz and rutile (Δ_{Q-R}) and between quartz and phengite (Δ_{Q-M}) in the neighbouring eclogite mica schists at the Mte. Mucorne - Mte. Camino area. These estimates are in general agreement with the results of Koons (1982) and Hy (1984) based on cation exchange geothermometry. As stated in Section 5.2, due to the fine-grained and intergrown nature of the coexisting phases, pure mineral separates were difficult to obtain for many of the samples investigated in this study. The oxygen isotope compositions for coexisting phases in a few samples are given in Table 5.3. See Section 3.1 for a discussion of the sample preparation and analytical methods.

Oxygen isotope temperature estimates will depend greatly on the calibration used (Fig.5.9, see also Section 3.5). Temperature estimates based on (1) experimental calibrations for quartz-muscovite fractionations, Δ_{Q-M} (Δ_{Q-H_2O} determined by Matsuhisa et al., 1979; Δ_{M-H_2O} determined by O'Neil and Taylor, 1969); (2) experimental calibrations for quartz-sodic pyroxene (Δ_{Q-Cpx}) fractionations (Matthews et al., 1983); and (3) theoretical calibrations of Bottinga and Javoy (1973) and Javoy (1977) for Δ_{Q-M} and quartz-garnet (Δ_{Q-G}) are presented in Table 5.4. The temperatures estimated from these calibrations vary considerably from 380 to 600 °C (see Fig. 5.9).

Experimentally-calibrated oxygen-isotope thermometers for various mineral-water pairs (e.g. Clayton et al., 1972; Matsuhisa et., 1979; O'Neil and Taylor, 1967 for Δ_{Q-H_2O} and Δ_{Fsp-H_2O}) yield notable variations in temperatures, depending on which calibration is used (see discussion in Graham, 1981), and in general give consistently lower temperature estimates than those determined by the theoretically-calibrated thermometers of Bottinga and Javoy (1973) and Javoy (1977) (see also discussion in Section 3.5). Such variations can clearly be seen for Δ_{Q-M} temperature estimates in Table 5.4 and Fig. 5.9. The least amount of scatter in estimated temperatures is found for quartz-garnet pairs, determined by the theoretical calibrations of Bottinga and Javoy (1973), and yield temperatures ranging from 530 to 600 °C for the mylonites. Such temperatures are consistent with those estimated by Desmons and O'Neil (1978) for quartz-rutile and quartz-phengite pairs in the neighbouring mica schists.

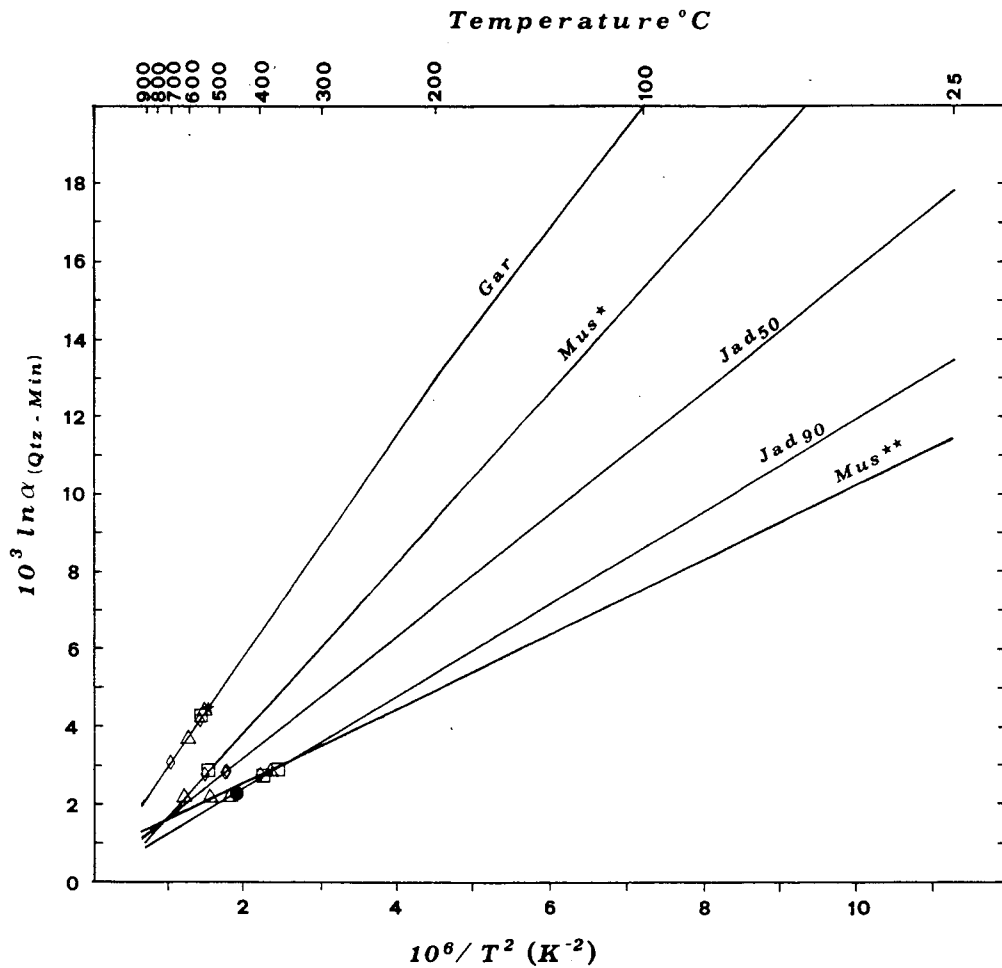


Fig. 5.9:

Fractionation factors between quartz and the minerals: garnet, muscovite, and pyroxene, used to estimate isotopic temperatures shown in Table 5.4. The curves for quartz-garnet and quartz-muscovite (Mus*) correspond to the theoretical fractionation factors of Javoy, 1977. Jad_{90} and Jad_{50} have been determined by Matthews et al., 1983; and Mus** corresponds to the experimentally calibrated curves for muscovite- H_2O (O'Neil and Taylor, 1969) and quartz- H_2O (Matsuhisa et al., 1979; see also App.V). Note the large variation between estimated temperatures for the quartz-muscovite pairs determined by the theoretical (*) calibrations and the experimental (**) calibrations.

TABLE 5.4: Pressure-temperature estimates from eclogitic assemblages from rocks from the Mte. Mucrone - Mte. Camino Area

Cation-Exchange Geothermometry and Geobarometry

Study	T°C ^c	T°C ^d	T°C ^e	P (Kbar)
<u>Koons, 1982</u>				
Glaucophanitic Mica Schists	590-620			17.5-18.5 ^a
<u>Hy, 1984</u>				
(1) Jad- and Glaucophane-bearing Mica Schists		610-640		11.0-14.0 ^b
(1) Chloitoid-bearing Mica Schists		550-650		
<u>Oberhänsli et al., 1985</u>				
Metagranitoids (undifferentiated)	429-625		435-564	11.0-14.0 ^b

Oxygen Isotope Fractionation Geothermometry (°C)

	T ^f _{q-r}	T ^g _{q-phe}	T ^h _{q-phe}	T ⁱ _{q-gar}	T ^j _{q-cpx}
<u>Desmon and O'Neil, 1978</u>					
(1) Glaucophanitic mica schists	550	530			
(2) Eclogites	565-570	570-580			
<u>Früh-Green, this study</u>					
Jad-Gar Fels	R82/5				472
Jad-Gar Mylonites	R185	528	380	541	397
Overprinted Mylonites	R13/7	608	490	530	380
	Mu1-2			601	454
Zoisite-Garnet Veins	R13/7V			526	
Omp-Gar Orthogneiss	R82/9	535	390	551	402
	R191	535	390	686	470

(a) Pressure estimates based on X_{Jad} and thermodynamic calculations of the reaction $\text{Par} + \text{Omp} \rightarrow \text{Gla} + \text{Zoi} + \text{Jad} + \text{H}_2\text{O}$

(b) Geobarometer for the reaction $\text{Ab} \rightarrow \text{Qtz} + \text{Jad}$ (Holland, 1980)

Cation - exchange geothermometry:

Gar-Cpx pairs: (c) (Ellis and Green, 1979) (e) (Räheim and Green, 1979)

Gar-Phe pairs: (d) (Green and Helmann, 1982)

Oxygen isotope fractionations:

(f) quartz-rutile (Addy and Garlick, 1974)

(g) quartz-muscovite (*phengite*) (Bottinga and Javoy 1973)

(h) quartz-muscovite (*phengite*) ($\Delta_{\text{Q-H}_2\text{O}}$, Matsuhisa et al., 1979;

$\Delta_{\text{Mu-H}_2\text{O}}$, O'Neil & Taylor, 1969)

(i) quartz-garnet (Bottinga and Javoy 1973)

(j) quartz-clinopyroxene (Matthews et al., 1983)

5.4. MECHANISMS OF OXYGEN ISOTOPE EXCHANGE

5.4.1. A DISCUSSION

Isotope exchange during mineral-fluid interaction can occur by diffusion or by means of surface reaction mechanisms which involve solution-precipitation or chemical reaction with the formation of a new phase (e.g. Cole et al. 1983; Matthews et al., 1983; Giletti, 1985; Cole and Ohmoto, 1986 - see also Section 1.2.3). Rates of isotopic exchange, regardless of the mechanisms, will depend primarily on temperature, total surface area (i.e. grain dimensions), and fluid (or volatile)/solid ratios. Water pressure and crystal anisotropy may have a pronounced effect on rates of isotopic exchange through diffusion. Based on published data from isotopic exchange experiments which showed evidence for a surface-controlled reaction mechanism of isotopic exchange, Cole et al. (1983) and Cole and Ohmoto (1986) calculated oxygen isotope exchange rates for many of the rock-forming minerals. Their results indicate a systematic order of increasing activation energies:

carbonates < sulfates < silicates.

Oxygen isotope exchange rates increase significantly with increasing temperature, and for temperatures above 300 °C, the relative order of the rate of oxygen isotope exchange (in units of moles of O / m² / sec) is:

Ba-Sr carbonates > barite > K/Na-feldspars > Ca sulfate ≈ Ca- Mg carbonates >
quartz ≥ kaolinite > paragonite > pyroxene

(see Figs. 10 & 11 in Cole and Ohmoto, 1986). Cole and Ohmoto (1986) point out that these trends in isotope exchange rates are similar to the order of rates of nucleation or precipitation.

According to Cole and Ohmoto (1986), the best evidence for chemical reaction in natural systems is the presence of new phases as alteration products of old minerals. In some cases, no signs of alteration can be observed in thin section, yet the minerals have exchanged isotopes (e.g. Forester and Taylor, 1977, Giletti, 1985). Both diffusion-controlled isotopic exchange and solution-precipitation recrystallization mechanisms could lead to isotopic readjustment without significant change in microfabrics or chemical compositions (Giletti, 1985).

Few experimental studies in stable isotope geochemistry have actually been aimed at determination of the mechanisms of oxygen isotope exchange. Even fewer experiments are designed to measure diffusional exchange rates (e.g. Giletti et al. 1978). However, with recent improvements in ion microprobe techniques more data is becoming available on oxygen isotope diffusion rates for the more common silicate minerals (e.g. Giletti et al., 1978; Matthews et al., 1983; Giletti, 1985). As discussed by Giletti (1985), isotope

diffusional data combined with fractionation data may provide valuable information on the cooling rates of metamorphic rocks. A compilation of experimental data on oxygen and hydrogen diffusion is given by Cole and Ohmoto (Fig. 12, 1986). The relative order of rates of oxygen diffusion in mineral-fluid systems is:

feldspar > quartz \geq phlogopite > amphibole > magnetite

(Cole and Ohmoto, 1986).

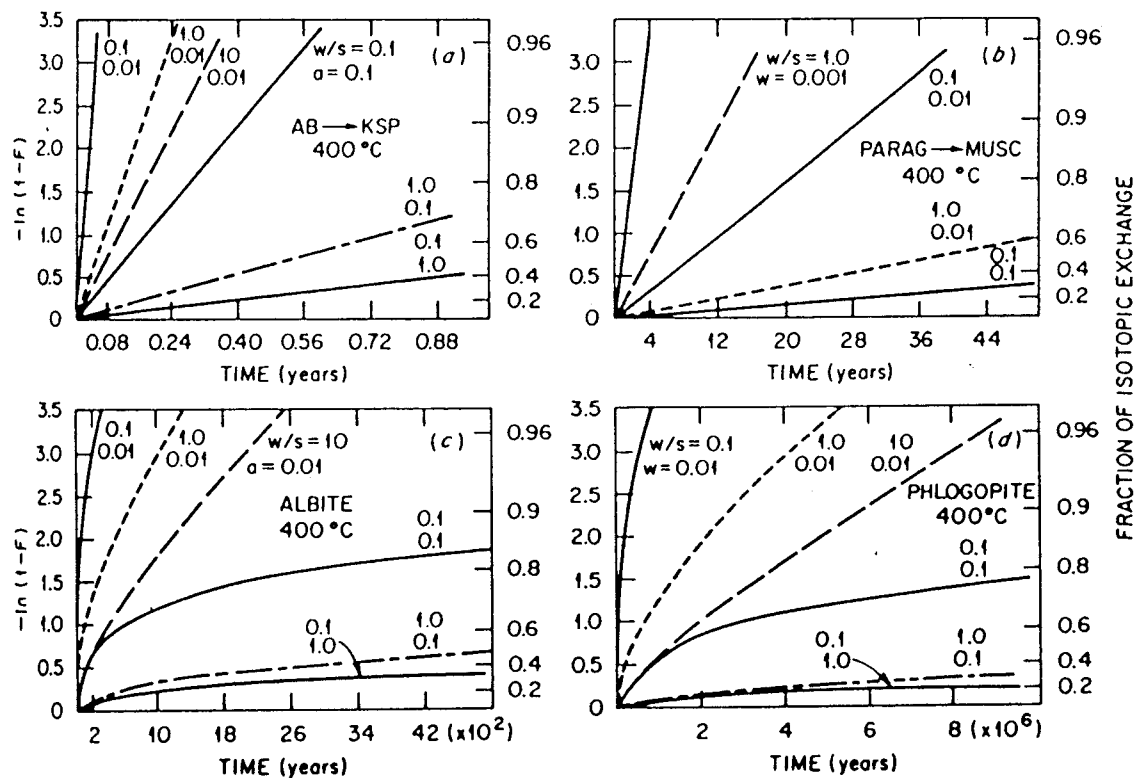


Fig. 5.10.

Comparison of Surface-reaction (a,b) and diffusion models (c,d) of oxygen isotopic exchange in feldspar-fluid and mica-fluid systems at a temperature of 400 °C (from Cole and Ohmoto, 1986). The fraction of oxygen isotopic exchange, represented as $\ln(1-F)$ is plotted against time for various fluid to solid mass ratios (W/S). Rate constants for the transformation of Alb \rightarrow Ksp and Par \rightarrow Musc are from Cole et al (1983). Diffusion coefficients used to calculate the models in figures (c,d) are from Giletti et al (1978) and Giletti and Anderson (1975). Grain size (a = grain radius for feldspar and W = plate thickness for mica) is represented by the bottom number on each curve. For more detail see Cole and Ohmoto, 1986).

Model calculations by Cole et al. (1983), using rates of isotopic exchange data for feldspars and micas, show that under the same conditions (i.e. temperature, grain-size, fluid/mineral ratios), diffusion-controlled rates of isotopic exchange are several orders of magnitude slower than those for surface reactions (see Fig. 5.10). For example, at a temperature of 400 °C and a fluid/mineral mass ratio of 1.0, a 0.1 cm in diameter grain

of albite altered to K-feldspar (surface-controlled exchange mechanism) attains 40% exchange in 0.88 years, compared to 4200 years for diffusional isotopic exchange in albite under the same conditions. Furthermore, these authors have shown that the exchange time will decrease with decreasing fluid/mineral mass ratios, which is explained as a result of the fact that the solid does not need to shift as far in composition (see Fig. 5.10).

Cole et al. (1983) conclude that oxygen isotope exchange occurs primarily through surface reaction mechanisms when the fluids and minerals are out of chemical equilibrium, and through diffusion once chemical equilibrium has been attained.

5.4.2. OXYGEN ISOTOPE EXCHANGE MECHANISMS IN THE FORMATION OF THE MTE. MUCRONE METAGRANITOIDS

The bulk rock chemical data, presented in Section 5.2 above, indicates that the evolution of the Mte. Mucrone mylonites from meta-quartz diorite may have involved metasomatic alteration with a wt% loss of Al and Fe²⁺ (and in some cases K, Na and Ca), and a gain in Fe³⁺ and H₂O. The previous discussion has shown that in mineral/fluid systems, in which initial disequilibrium conditions prevail (i.e. fluid is initially out of chemical equilibrium with the mineral phases), as is indicated for the Mte. Mucrone mylonites, surface-controlled mechanisms of oxygen isotope exchange will dominate. Chemical transformation as the dominant mechanism of isotopic exchange in mylonite formation, resulting in the observed depletion in ¹⁸O relative to the unfoliated meta- quartz diorites, is further substantiated by the textural characteristics in the mylonites. The un-overprinted Jad-Gar mylonites exhibit recrystallization textures and an approach to chemical equilibrium. The alteration of deformed jadeitic pyroxene by phengitic white mica and the replacement of K-feldspar by garnet + phengite + quartz in the overprinted mylonites suggests recrystallization during a post-shearing infiltration event.

Consistencies in the isotopic compositions of the mineral phases measured in these texturally-different mylonites suggests that isotopic re-equilibration occurred through the same exchange mechanism(s) and with a relatively constant isotopic and chemical composition of the infiltrating fluid. The textural distinctions between the mylonites may be attributed to differences in the relative timing of deformation, fluid infiltration, and recrystallization.

Surface-controlled reactions may have been the dominant mechanism of oxygen isotope exchange during the initial stages of fluid infiltration and recrystallization; however, the discordancies in the temperature estimates (see Table 5.4 and Fig. 5.9) from the different mineral pairs suggests that subsequent oxygen diffusion during

cooling may have occurred in these rocks. As discussed above, Cole et al. (1983) conclude that diffusive isotope exchange may occur after chemical equilibrium between fluid and solid has been attained. Although the discordant temperature estimates for the deformed rocks at the Mte. Mucrone may represent *actual* recrystallization temperatures, the effects of diffusional exchange upon cooling must be considered.

Recent studies have shown that there is often evidence for retrograde isotopic exchange during cooling of metamorphic rocks, and evidence of oxygen isotope equilibrium among three or more minerals is rarely found (e.g. Deines, 1977; Javoy, 1977; Graham, 1981; Giletti, 1985; see also Section 3.5 in this study). Based on diffusion studies, Graham (1981) suggests that discordant temperature relations may be direct evidence for the presence of a hydrous fluid during cooling of a metamorphic pile. For slowly cooled igneous and metamorphic rocks, Giletti (1985) concludes that the temperatures acquired by oxygen isotope geothermometry may represent neither maximum metamorphic crystallization temperatures nor a single closure temperature at which diffusion exchange ceases, but rather will be a function of grain size, mineral modes, cooling rates, and will depend on the diffusional properties of the coexisting minerals. For example, for rocks consisting of hornblende, plagioclase and quartz, Giletti (1985) has shown that the order in which oxygen diffusion essentially ceases to be recorded is:

$$\text{hornblende} \geq \text{quartz} \geq \text{plagioclase},$$

and discordant temperatures decreasing in the same relative order would be expected.

A comparison of the relative order of diffusive exchange rates with those for surface reaction mechanisms (see above) suggests that for the Mte. Mucone Metagranitoids, the relative order of rates of oxygen diffusion may be:

$$\text{garnet} < \text{pyroxene} < \text{white mica} < \text{quartz},$$

thus, the relative order of decreasing temperature estimates may be:

$$T_{\text{Q-Gar}} > T_{\text{Q-Cpx}} > T_{\text{Q-Phe}}$$

As discussed previously, isotopic temperature estimates depend greatly on the calibration used. The above order of decreasing estimated temperature (i.e. 686 - 470 - 390 °C) is only observed in omphacite-garnet orthogneiss sample R191, if one considers the quartz-phengite (Q-Phe) temperature of 390 °C, determined by the experimental calibration of O'Neil and Taylor (1969). In the other samples, $T_{\text{Q-Mus}}$ and $T_{\text{Q-Cpx}}$ appear to be in the "wrong" order or give concordant temperature estimates (again, depending on which calibration is considered for Q-Phe).

This apparent discrepancy between the predicted order of recorded temperature and that determined may only be a reflection of the calibrations used to determine temperature, or could be an effect of the presence of a hydrous grain-boundary film and

the relative *diffusion paths* in the two minerals phengite and clinopyroxene upon cooling. In general, diffusion in minerals occurs by volume diffusion through regions of good crystal structure and by a variety of diffusion mechanisms, whereby atoms and molecules move along the 'easiest' path available. Easy diffusion paths may be along surface or line defects in crystals, such as along grain boundaries, dislocations, or fast diffusion directions on free surfaces (Manning, 1974). In the same way, volume diffusion mechanisms in crystals generally depends on the presence of point defects, such as vacancies or interstitial atoms (Lasaga, 1981; Cole and Ohmoto, 1986). A schematic diagram of possible volume diffusion paths is shown in Fig. 5.11 (taken from Cole and Ohmoto, 1986, originally from Manning, 1974).

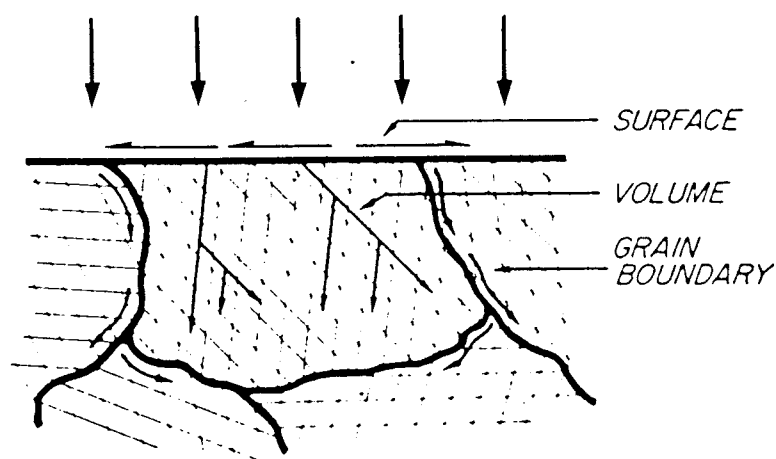


Fig. 5.11.

Schematic illustration of the possible paths of volume diffusion, surface diffusion and grain boundary diffusion (taken from Cole and Ohmoto, 1986- after Manning, 1974). Diffusion in minerals generally occurs by volume diffusion through areas of good crystal structure and by other diffusion mechanisms along short-circuit paths of easy diffusion.

The presence of a large number of dislocations in the pyroxene grains may have resulted in a greater diffusivity of oxygen, relative to phengite, so that diffusive oxygen exchange between quartz, pyroxene and phengite continued upon cooling. However, studies by Yund and Tullis (1980) and Yund et al. (1981) on oxygen diffusion rates in albite indicate that a high dislocation density ($5 \times 10^9 \text{ cm}^{-2}$) only results in approximately one order of magnitude increase in the rate of oxygen diffusion. Their studies indicate that simultaneous high shear stress would be necessary to produce significant increases in reaction rates. Without sufficient diffusion data on sodium pyroxene and muscovite it is difficult to say whether the presence of a high density of dislocations or crystal defects would greatly effect the diffusion rates in pyroxene and lead to greater oxygen diffusivity relative to phengitic white mica.

In conclusion, the textural, chemical and isotopic data of the deformed rocks at the Mte. Mucrone suggest that oxygen isotope exchange occurred through a mechanism of recrystallization driven by initial disequilibrium between the mineral phases and an infiltrating fluid. As chemical equilibrium was achieved between fluid and minerals, oxygen exchange through a diffusion mechanism prevailed. Discordant oxygen isotope fractionation temperatures may indicate the presence of an interstitial grain-boundary film during the cooling history of these rocks.

5.5. DISCUSSION: THE ROLE OF HYDROUS FLUIDS IN THE MINERALOGICAL AND DEFORMATIONAL HISTORY OF THE MTE. MUCRONE METAGRANITOIDS

5.5.1. STABLE ISOTOPE CONSTRAINTS

As discussed above, the WR- and Qtz-isotopic compositions of the deformed Mte. Mucrone metagranitoids which contain eclogite- facies mineral assemblages are depleted in ^{18}O relative to the unfoliated and less transformed equivalents. In a *closed system* and assuming a uniform ^{18}O composition of the original igneous protolith, the partitioning of ^{18}O between phases will change with change in temperature and modal content, but the overall ^{18}O -budget of the rock should remain constant (see Section 1.2.4). Because quartz tends to be the most ^{18}O -rich mineral in a rock, a depletion in $\delta^{18}\text{O}$ can result from an increase in the modal percentage of quartz during recrystallization but will not affect the whole rock ^{18}O -composition.

The modal amount of quartz in the Mte. Mucrone metagranitoids is difficult to determine precisely due to its pervasive occurrence as fine-grained inclusions in pyroxene and garnet; however, modal percentages determined by point-counting (Table 5.3) indicate a relatively constant percentage of quartz in both the unfoliated and foliated rocks. Inspection of Figs. 5.5, 5.6 and 5.8 also indicates that the weight percent of SiO_2 remained constant with relatively small changes in volume during mylonite and orthogneiss formation. The element loss and gain indicated by Figs. 5.5, 5.6 and 5.8, as well as the depletion in $^{18}\text{O}_{\text{WR}}$ of the mylonites and orthogneisses, indicates that deformation and the resulting recrystallization of these rocks cannot be viewed as a closed system.

In an *open system*, a depletion in $^{18}\text{O}_{\text{WR}}$ could be caused either by devolatilization reactions in which an escaping fluid is enriched in ^{18}O , or by fluid influx whereby a more ^{16}O -enriched fluid equilibrates with the rock, depleting it in ^{18}O (see Section 1.2.4). There is no evidence that devolatilisation reactions took place during the main shearing event. Instead, comparison of the bulk rock chemical data indicates that an increase in H_2O is associated with the deformed rocks. The possibility of hydration is

further substantiated by the inferred mineral reactions (Section 5.1 - 5.1.3), in which H₂O is absorbed (e.g. reactions 5.1 and 5.6).

5.5.2. META-QUARTZ DIORITE FORMATION

The textural relationships and the distinct chemical characteristics of the mineral phases in the unfoliated meta-quartz diorite, as well as the constant bulk rock chemical and stable isotope compositions, strongly suggests the recrystallization history of the Mte. Mucrone metagranitoids was essentially anhydrous up to eclogite-facies pressure-temperature conditions of albite instability and jadeite formation. As discussed previously, the corona textures around biotite and the distinct chemical zoning in garnet in the unfoliated meta-quartz diorites suggests that the mechanism of transformation of biotite was controlled by diffusion of calcium and alumina from the plagioclase domains (see also Koons et al., in review). The degree of transformation and the preservation of the primary igneous fabric and mineral phases may have been directly controlled by a lack of penetrative deformation and/or the paucity of an intergranular hydrous fluid (see also Rubie and Thompson, 1985 and references therein).

The inter-relationship between deformation and metamorphism and the role of fluids in the various processes involved has received considerable attention in past years. Theoretical considerations and experimental studies of mineral transformation have shown that reaction pathways, as well as the mechanisms and kinetics of mineral reactions and grain growth may change significantly in the presence of a hydrous fluid phase and/or with increases in shear stress (e.g. Fisher, 1970; Yund and Tullis, 1980; Tullis and Yund, 1982; Wood and Walther, 1983; see also discussion by Rubie and Thompson, 1985). Fundamental to any such study is the problem of the 'chicken and the egg': Does an increase in rock permeability, as a result of grain-size reduction during metamorphic reactions or as a response to stress gradients, or by dilation due to crack propagation, allow fluid access into a previously tight rock; or does a rise in fluid pressure result in initial weakening and fracturing of the rock, catalysing mineral reactions and enhancing deformation mechanisms?

In this study, the textural, chemical and isotopic differences between the intensively deformed rocks and their unfoliated equivalents can be attributed to processes of deformation and fluid-rock interaction subsequent to the initial stage of jadeite crystallization. But, which occurred first: deformation or infiltration; and how were they interrelated? The following section addresses these fundamental questions, and the significance of the timing of these two processes on the metamorphic evolution is discussed.

5.5.3. FLUID INFILTRATION AND MYLONITE FORMATION

As discussed in Section 4.4.2 an initial high strain deformation event, subsequent to albite instability and jadeite formation during eclogite-facies pressure-temperature conditions, produced superplastic deformation of the fine-grained jadeite + zoisite + quartz aggregates (relating to the *transitional orthogneiss stage* of Koons et al.).

5.5.3.1 Jadeite-Garnet Mylonites

The homogeneous chemistries of the mineral phases in the deformed layers in the *jadeite-garnet mylonites* suggest that deformation enhanced the diffusive mass transfer processes between the coexisting mineral phases and led to completion of the biotite breakdown reaction (5.4 and/or 5.11; Fig. 5.1). An increase in fluid activity may have catalysed reaction 5.6 leading to the decrease in the modal percentage of K-feldspar in these rocks and the disappearance of zoisite as inclusions in pyroxene (see Fig. 4.9) observed in these highly deformed rocks. The well-defined foliation of the resulting mineral assemblage of Jad + Qtz + Gar + Phe, together with the slight increase in water-content and the shift in $\delta^{18}\text{O}_{\text{WR}}$, suggests that fluid infiltration and recrystallization was simultaneous with deformation.

5.5.3.2. Overprinted Mylonites (e.g. Location 3, Fig. 4.2)

In contrast to the homogeneous jadeite-garnet mylonites, the distinct heterogeneous chemical compositions of garnet and phengite, as well as the numerous mineral inclusions in garnet and the preservation of zoisite as inclusions in jadeite in the *overprinted mylonites*, suggests that the high strain deformation resulting in the shear zones shown in Fig. 4.6 occurred under nearly anhydrous conditions with limited diffusive mass transfer. The static growth of omphacite, grossular-rich garnet (GarIII) and Ti-poor phengite (WMII), and the replacement of K-feldspar (see Fig. 4.5b) in these overprinted mylonites indicates *post-kinematic phase of infiltration*, which may have catalysed reactions 5.6 and/or 5.11. Comparison with the nearly complete chemical homogenization in the jadeite-garnet mylonites, the preservation of the distinct zonation in the overprinted mylonites suggests that the presence of a fluid phase was determinant in the approach to chemical re-equilibration. Thus, superplastic deformation alone may have not been sufficient to enhance the degree of diffusive mass transfer between the mineralogical domains.

Infiltration of an external fluid phase in the mylonites is substantiated by the shift in oxygen isotope compositions (Früh-Green, 1985). Comparison of the isotopic compositions of quartz in the veins with those of the mylonites indicate isotopic

equilibration with an isotopically similar fluid. Examination of the oxygen isotope profiles in Fig. 5.7a,b shows that infiltration and the associated shift in $\delta^{18}\text{O}$ is restricted to the immediate deformation zones and may reflect *fluid flow along* the shear zones and *diffusive infiltration* perpendicular to the shear zones (see also Brodie and Rutter, 1985; Rutter and Brodie, 1985; and Baumgartner and Rumble, 1986). Theoretical considerations by Rutter and Brodie (1985) have shown that permeation of volatiles *along* shear zones can be between 10 and 100 times more effective than *across* them.

The textural characteristics of the overprinted mylonites in these shear zones point to a post-kinematic timing of the infiltration event leading to reaction 5.6, which, together with the bulk rock geochemical data, strongly suggests that the initial stages of deformation increased the permeabilities such that the shear zones acted as channelways for the localized flow of an external fluid (see also Brace, 1980; Walter and Orville, 1982; Etheridge et al., 1983; Brodie and Rutter, 1985; and Rutter and Brodie, 1985). Similarities in the garnet compositions in the zoisite-garnet veins with those of garnet III in the overprinted mylonites (see Fig. 4.14), as well as concordant oxygen isotope temperature estimates for quartz-garnet pairs (see Table 5.4, samples 13/1 and 13/7) suggest that the formation of the veins occurred at similar pressures and temperatures under low strain conditions and equilibrated with a fluid of chemically and isotopically constant composition. The loss of calcium, alumina and Fe^{2+} in the overprinted mylonites, as indicated in Fig. 5.6, may be related to the formation of the zoisite-garnet veins associated with this post-kinematic infiltration phase.

5.5.4. FLUID INFILTRATION AND VEIN FORMATION

As discussed in Sect. 4.5, the zoisite-garnet veins are nearly always separated from the mylonite zones by narrow bands of unfoliated jadeite-garnet fels (see Fig. 4.19). The formation of these nearly undeformed bands of rock, relative to the timing of deformation and fluid infiltration in the neighbouring shear zones, remains problematic. Although these jadeite-garnet fels retain the original igneous fabric, they are distinguished from the texturally-similar meta-quartz diorites by complete recrystallization and coarser grain-sizes of pyroxene, garnet and phengite and by a lack of biotite. As discussed above, an access of a hydrous fluid appears to have been crucial to the processes of mass transfer and grain growth which led to the completion of the biotite breakdown reaction and an approach to chemical homogenization. One possibility may be that an early phase of fluid infiltration occurred *prior* to the high strain deformation event and caused the observed transformation. An excess in fluid pressure may have resulted in hydrofracturing and the formation of the zoisite-garnet veins; or an initial fault

or crack formed during the early stages of deformation and lower stress conditions, and acted as fluid escape pathway. If fluid flow was concentrated along these zones, the unfoliated jadeite-garnet fels may represent reaction zones during an early infiltration phase.

If vein formation and transformation of meta-quartz diorite to jadeite-garnet fels occurred prior to deformation, the resultant grain coarsening may have acted as a 'hardening mechanism', whereby the transformed reaction zones and veins remained rigid and undeformable, in an analogous way to garnet porphyroblasts, during the entire deformation history of the surrounding rocks. The presence of such undeformable domains may have been determinant to the development of the shear zones. Local stress gradients could have resulted in high strain deformation which was concentrated in narrow zones on either side of the rigid domains with no signs of deformation being recorded in either the transformed reaction zones or the veins.

An alternative, but unlikely, explanation may be that vein formation is, in general, attributed to the same relative (post-kinematic) timing of a single infiltration phase as that indicated in the overprinted mylonites located only centimeters away. Limited permeabilities in the mylonite zones may have resulted in an excess of fluid pressure during infiltration and led to brittle failure and fracturing into the adjacent rocks, which for some reason had remained undeformed during the shearing event. In some cases, alteration of the unfoliated wall rock adjacent to the zoisite veins is observed (e.g. sample 13/1, Fig. 4.2). This suggests that vein formation occurred subsequent to the formation of the reaction zones. However, this would not explain the presence of the relatively undeformed zone which is nearly always associated with the shear zones along the eastern face of the Mte. Mucrone. In addition, there is no textural or mineralogical evidence to suggest that the jadeite-garnet fels went through the superplastic deformation stage and then were later recrystallized. In addition, the textural characteristics along the contacts between the veins and the wall rocks, discussed in Section 4.5.1, clearly indicate that the veins grew under low-strain conditions and cross-cut a weak foliation in the jadeite-garnet fels. The loss of calcium, alumina and Fe^{2+} in the overprinted mylonites, as indicated in Fig. 5.6, may be related to the formation of the zoisite-garnet veins associated with the post-kinematic infiltration phase observed in the overprinted mylonites.

In a recent study on the nucleation of ductile shear zones in California and Spain, Segall and Simpson (1985) have shown that dilatant fracturing may precede the localization of ductile shear deformation. In some cases, the shear zones occur parallel to mineralized fractures, across which no shear deformation is observed, and in which completely undeformed mineral assemblages are observed. In the same area, other

zones contain deformed mineral fillings and offset strain markers. Segall and Simpson (1985) have argued that the presence of dynamically recrystallized mineral fillings in microcracks associated with the shear zones demonstrate that fracturing predated the ductile deformation. The formation of the undeformed jadeite-garnet fels, associated with the zoisite veins at the Mte. Mucrone, may have occurred in a similar way to the shear zones investigated by Segall and Simpson.

5.5.5. FLUID INFILTRATION AND OMPHACITE-GARNET ORTHOGNEISS FORMATION

As discussed previously, the omphacite-garnet orthogneisses may have evolved from meta-quartz diorite through similar stages of transformation as those recorded in the mylonites (see also Koons (1982) and Koons et al. (in review)). Subsequent deformation may have caused microstructural reworking, grain coarsening, and an approach to equilibrium mineral assemblages which destroyed all evidence of the earlier superplastic deformation event. Consideration of phase relations as well as the changes in both isotopic and bulk rock chemical compositions indicates that the mineralogical evolution of these rocks may have been greatly influenced by the presence of an external hydrous fluid, whereby complete homogenization of the mineral phases was not achieved.

The formation of the orthogneisses has been interpreted by Oberhänsli et al. (1982, 1985) as a result of *equilibrium recrystallization* during conditions of decreasing temperatures with variable amounts of fluid infiltration along shear zones. As an *alternative* to an equilibrium reaction history, Koons (1982) and Koons et al. (in review) argue that the orthogneiss represents deformation and recrystallization of meta-quartz diorite, whereby the disequilibrium characteristics of the meta-quartz diorites were inherited during recrystallization. Jadeite-formation may have originally been a result of limited chemical communication between small domains. Due to the deformation during the main shearing event, greater chemical communication and increased diffusion rates may have resulted in a change in the effective bulk composition and an approach towards partial equilibrium within new and larger domains.

Both the bulk rock geochemical data and the shift in oxygen isotope compositions of the Omp-Gar orthogneisses, as well as the need for water to make the various mineral reactions proceed, indicate interaction with a hydrous fluid. The *relative duration* and *timing* between deformation and infiltration may have been crucial to the mineralogical evolution of these rocks. The above model for the formation of the overprinted mylonites in the shear zones at Location 3 (see Fig. 4.2) along the eastern face of the Mte. Mucrone suggests that anhydrous deformation would not be sufficient to enhance

diffusion rates between mineral domains and produce homogenization of mineral compositions. If deformation were synchronous with fluid infiltration and both occurred subsequent to overstepping the $\text{Ab} \rightarrow \text{Jad} + \text{Qtz}$ reaction boundary (Rxn 5.2, see Fig. 5.1) but before complete consumption of biotite, the reaction boundaries for the formation of omphacitic pyroxene and paragonite (e.g. Rxn 5.11, see Fig. 5.1) may have been sufficiently overstepped to produce the assemblages observed in the orthogneisses (see also discussions in Rubie and Thompson, 1985 and Ridley, 1985).

5.5.6. A MODEL OF FLUID-ROCK INTERACTION DURING THE EVOLUTION OF THE MTE. MUCRONE DUCTILE SHEAR ZONES

Based on the textural, chemical and isotopic characteristics of the deformation zones discussed above (and in Section 4.4), a model for the deformation/infiltration history during the formation of the shear zones, shown in Fig. 4.6, is presented below and shown schematically in Fig. 5.12.

1. Subsequent to jadeite formation and incomplete biotite reaction, an initial phase of deformation caused the formation of isolated cracks or faults (in some cases conjugate fractures) in the relatively undeformable and incompletely transformed meta-quartz diorites. There is no evidence that dehydration reactions occurred in the early stages of eclogite-facies recrystallization of the metagranitoids (see also section 5.6 below), resulting in an initial build up of locally-derived fluid; therefore it will be assumed that initial crack-formation occurred under anhydrous conditions.
2. As a result of the initial brittle failure, the permeability of the system was increased and allowed the infiltration of an external initial pulse of fluid into the system (Infiltration Phase I). Fluid flow was concentrated along this permeable zone in the otherwise impermeable meta-quartz diorites. Perpendicular to the direction of fluid flow, diffusion of water along grain boundaries in the wallrocks, envisioned as a diffusive infiltration front, catalysed mineral reactions and resulted in the formation of a 1-5 cm wide reaction zone. A mechanism such as dissolution/reprecipitation along the diffusive infiltration front could have caused a relative homogenization of phase compositions and formation of a coarse-grained crystal aggregates of jadeite + garnet + quartz + phengite. This recrystallization process, termed here *fluid-induced reaction hardening*, resulted in a relative change in the deformability of the reaction zone, and can be thought of as a counterpart to mechanisms of reaction-enhanced ductility.

3. Subsequent to this initial pulse of fluid activity, either a second phase of deformation occurred or there was continual build up of stress in the rock body to the point of failure and superplastic deformation. During this subsequent stage of deformation, the coarse-grained reaction zones behaved as rigid blocks and superplastic deformation was concentrated on both sides. Continual (or renewed), localized fluid accompanied deformation in some zones and resulted in an approach to chemical and textural equilibrium. In other zones, in which the initial pulse of fluid activity ceased, deformation catalysed mineral reactions but the absence of a synkinematic fluid phase limited diffusive mass transfer and resulted in the preservation of primary chemical zonation in the eclogite-facies mineral phases. As grain coarsening progressed in response to increased superplastic deformation, the deformation mechanism in the pyroxene and garnet eventually changed and may have limited the duration of the ductile deformation event.
4. After deformation ceased, a further pulse of fluid permeated the system (Infiltration Phase II) and was localized along some of the more permeable zones created by the ductile deformation phase. The localized fluid activity resulted in overprinting in the mylonites, characterized by replacement of jadeite by phengitic white mica, the growth of grossular-rich garnet (Gar III) and the formation of omphacite in isolated domains. In some cases, the initial fluid pathways, marked by the reaction zones, were reactivated and resulted in zoisite-garnet vein formation and various degrees of overprinting in the reaction zones.

The sequential deformation/infiltration evolution proposed by this model may have occurred at constant pressure and temperature and constant fluid composition, as indicated by similarities in mineral chemistries, textures and oxygen isotope signatures between the overprinted mylonites and the zoisite-garnet veins. However, examination of other samples, not discussed in detail in this study (see Section 4.7), point to repeated high-strain deformation events and possibly multiple pulses of fluid infiltration throughout the uplift history of the Mte. Mucrone Metagranitoids (see Maffeo and Compagnoni, 1973; Oberhaensli et al. 1985). In mylonite samples which clearly exhibit greenschist-facies high-strain deformation (see Section 4.7), identical relationships as those discussed above for the eclogite-facies deformation/infiltration events can be observed between veins, reaction zones and mylonite zones. This suggests that high-strain deformation during uplift and exhumation of the Mte. Mucrone granitoid body may have been concentrated along the 'older' reaction zones, possibly even reactivating previous eclogite-facies deformation zones.

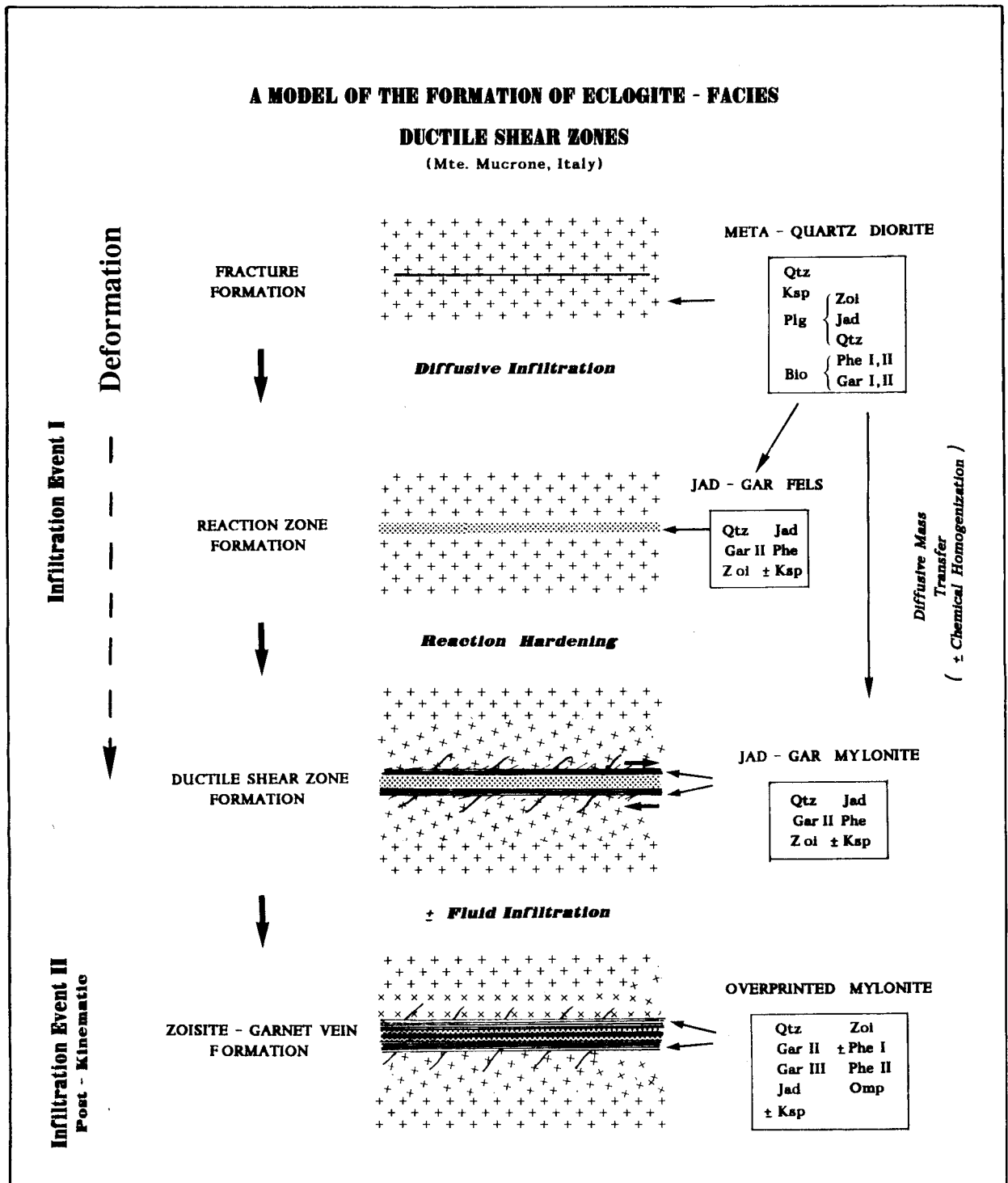


Fig. 5.12: Hypothetical model for the eclogite-facies of the mylonite zones from Location 3 (Fig. 4.2) along the eastern face of Mte. Mucrone. This model is based on field evidence, textural characteristics, phase chemistry and oxygen isotope compositions.

5.6 SOURCE AND AMOUNT OF EXTERNAL FLUID

In open systems of fluid-rock interaction, shifts in ^{18}O away from the original isotopic composition will primarily be controlled by the difference between the *initial* compositions of the rock ($\delta^{18}\text{O}_R$) and the fluid phase ($\delta^{18}\text{O}_{\text{Fl}}$) which either enters or leaves the system, and by the total amount of oxygen in the initial fluid (X_{Fl}^i) relative to the total amount of oxygen in the rock (X_{WR}^i), i.e. the fluid to rock ratios (Fl/R), (see also Sections 1.2.4 and 1.2.5). Various models of isotopic exchange as a result of fluid infiltration are discussed in Chapter 1.

As a first approximation, an open system, mass balance model of fluid-rock interaction will be considered for the infiltration event which produced the overprinted mylonites. In such a model the isotopic composition of the infiltrating fluid (in this case pure H_2O is assumed) is held constant. Each increment of H_2O makes a single pass through the system and integrated W/R ratios are determined by the equation:

$$W/R = \ln [(\delta_w^i + \Delta - \delta_R^i) / (\delta_w^i - (\delta_R^f - \Delta))] \quad (\text{Eq. 5.1})$$

(Taylor, 1977), where δ_w^i and δ_R^i represent the initial compositions of the water and rock, respectively, Δ is the difference between the final isotopic composition of the rock and the water ($\delta_R^f - \delta_w^f$) and will be a function of the temperature at which isotopic exchange takes place. For rocks of granitic composition, Taylor (1977, p.524) has shown that δ_R at equilibrium is equal to the $\delta^{18}\text{O}$ value of plagioclase (An_{30}), and the δ_w in equilibrium with these rocks can be determined by using a feldspar- H_2O oxygen isotope geothermometer (e.g. $\Delta \approx 2.68 (10/T^2) - 3.53$; O'Neil and Taylor 1967). The W/R values defined by equation 5.1 are based on the ratios of water oxygen to rock oxygen.

As can be seen from the above equation, in an open system of isotopic fluid-rock interaction, there will be three unknowns: (1) the temperature of equilibration; (2) the initial isotopic composition of the infiltrating water; and (3) the amount of fluid relative to the rock, i.e. the water to rock (W/R) ratio. Taylor's single pass - open system model of fluid infiltration has been applied for the overprinted mylonites in the shear zones shown in Fig. 4.6, the results of which are presented graphically in Fig. 5.13. Assuming a constant temperature of 500 °C, W/R-ratios have been calculated for various initial oxygen isotope compositions of infiltrating fluid.

The isotopic composition of the fluid will be limited by the value of fluid in equilibrium with the mylonites at 500 °C, which is equal to 7.20‰, shown as the dashed line in Fig. 5.13. With increasingly lighter values for δ_{Fl}^i , the W/R decreases from a value of 2.3 close to the equilibrium value to less than 0.5 at a composition of 4.0‰. The values of >7.00‰ calculated in Fig. 5.13 indicate that the shift in ^{18}O from original igneous isotopic compositions required interaction with a relatively ^{16}O -rich (i.e. isotopically light) hydrous fluid.

Fluid Infiltration

Open System - Single Pass

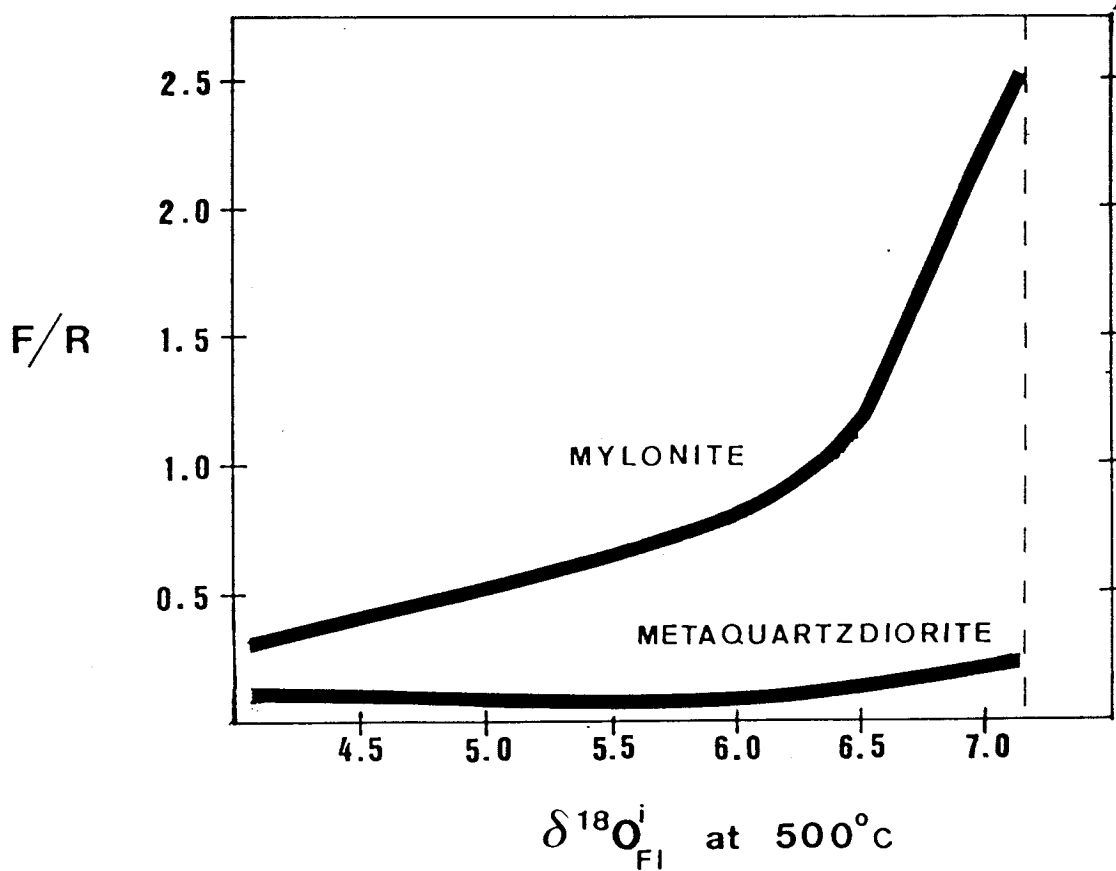


Fig. 5.13:

Fluid to rock ratios (F/R) for a temperature of 500 °C are shown for various isotopic compositions of infiltrating fluid which could have produced the shift in ^{18}O observed in the overprinted mylonites (Location 3, Fig. 4.2 and Fig. 4.6). An open system - single pass isotope mass-balance model, proposed by Taylor (1977) has been applied (see Eq. 5.1 in text). Both curves have been calculated for an initial WR-isotopic composition of 9.40‰, which corresponds to the most ^{18}O -rich meta-quartz diorite sample. For the mylonite curve, the composition of sample Mu 1-2 (See Fig. 5.6) has been used as the final WR-isotopic composition (= 8.10‰). For the meta-quartz diorite curve, the final WR-composition is equal to 9.10‰ and corresponds to the meta-quartz diorite sample Mu 1-3.

Most stable isotope studies apply mineral-water fractionation data to calculate metamorphic water compositions because they can not, in general, be measured directly. Calculated metamorphic water compositions cover a wide spectrum of values from $\approx +3$ to $+20\text{‰}$ (see Fig. 5.14). Waters evolved from sedimentary rocks generally lie within the 'heavy' end of this range; whereas waters in equilibrium with mafic rocks generally correspond to the more ^{16}O -rich end (see summary and discussion by Sheppard, 1986). Primary magmatic waters are considered to cover a narrower range of values from $\approx +5$ to $+10\text{‰}$ (Sheppard et al., 1969). Present-day meteoric waters have H- and O-isotope compositions which vary in a very systematic way (see Fig. 5.14), such that a meteoric water line could be defined. In general, the oxygen isotope composition of meteoric waters lie within a range of 0 to -20‰ , with H-isotope compositions ranging from 0 to $\approx -150\text{‰}$ (Esptein and Mayeda, 1953; Friedman, 1953; Craig, 1961; Friedman et al., 1964; Sheppard, 1986 and references therein).

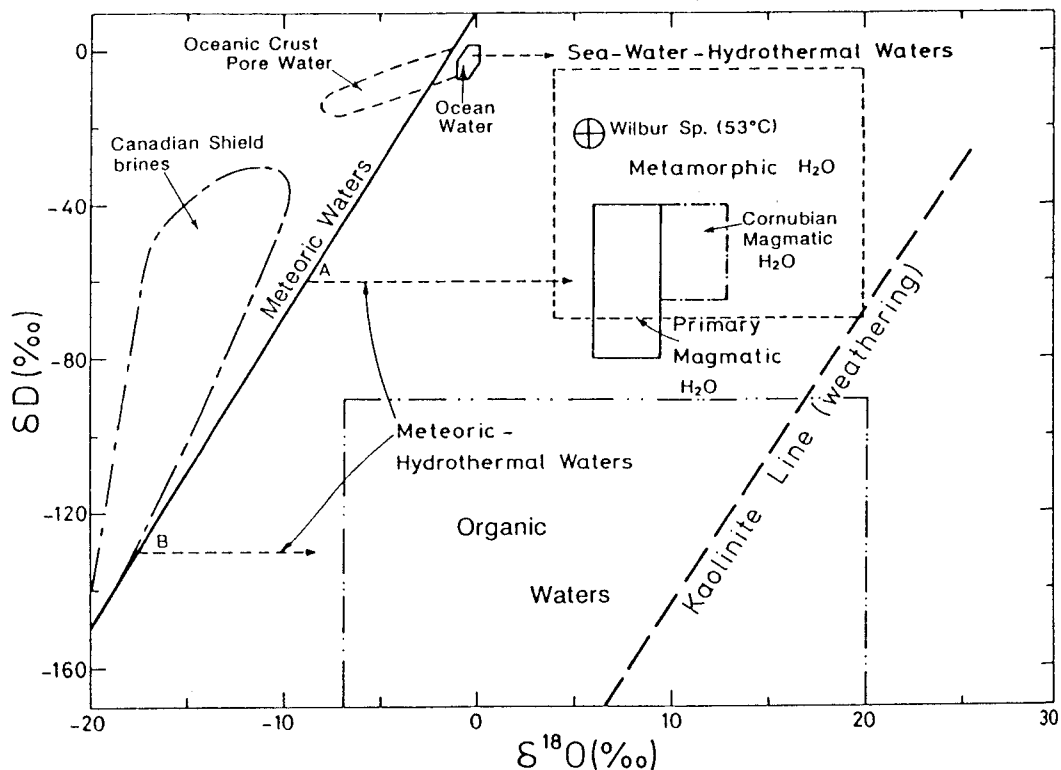


Fig 5.14. Variations in isotopic compositions for seawaters, meteoric waters, primary magmatic waters, metamorphic waters, and organic waters (taken from Sheppard, 1986 - see references and discussion therein). Shifts in ^{18}O due to water-rock interaction and exchange in hydrothermal systems are shown for seawaters and meteoric waters of initial compositions A and B.

Hydrogen isotopic compositions of the Mte. Mucrone metagranitoids investigated in this study range from -66‰ to -72‰ (Table 5.3) and fall within a normal range for both magmatic and metamorphic waters. Thus, the possibility that the shift in ^{18}O represents limited exchange with meteoric water can be ruled out. Comparison of these results with the isotopic study of Desmons & O'Neil (1978) for the neighbouring eclogitic mica schists indicates that there is no evidence to suggest that an extremely ^{16}O -rich fluid (i.e. meteoric water) was involved in the metamorphism of the rocks at the Mte. Mucrone - Mte. Camino area. $\delta^{18}\text{O}_{\text{Qtz}}$ of the eclogitic rocks from the Mte. Mucrone - Mte. Camino area investigated by Desmons & O'Neil range from 10.8‰ to 12.0‰, and lie within the same range defined by other samples from the eastern Sesia zone.

The similarities in $\delta^{18}\text{O}$ between rock types, together with uniform δD -values and a regular order of ^{18}O -enrichment amongst coexisting mineral phases led Desmons & O'Neil to conclude that a relatively pervasive metamorphic fluid enabled isotopic communication between the mafic and pelitic country rocks. However, the difference between the isotopic compositions of the coexisting phases recorded in the metagranitoids (e.g. $\delta^{18}\text{O}_{\text{Qtz}}$ 8.00‰ - 10.8‰) suggests that if a pervasive fluid were present in the surrounding country rocks, infiltration and isotopic communication with the granitic rocks was limited.

Calculated values of $\delta^{18}\text{O}$ of water in equilibrium with rutile at the equilibrium temperature of 570 °C (temperature determined by Desmons and O'Neil on the basis of the fractionation curve of Addy and Garlick, 1974) range from 9.16 to 10.33 for the three Mucrone samples presented in the study of Desmons and O'Neil. This would suggest that the exchange with an isotopically light water with a composition of >7.00‰ was restricted to the metagranitic rocks. However, the exact locations of the samples investigated by Desmons and O'Neil are not given. Furthermore, three samples can not be considered representative of an entire area and can not be used as evidence to rule out the possibility that the fluid which infiltrated the metagranitoids was not derived from metamorphic reactions in the neighbouring pelitic rocks (compare results from the Adula Nappe presented in Chapter 3).

At least two major phases of eclogite-facies deformation and recrystallization have been distinguished in the neighbouring mica schists (Hy, 1984). The mineralogical changes and consideration of phase relations indicate that both hydration (in glaucophane- and chloritoid-bearing mica schists) and dehydration reactions (in kyanite-bearing mica schists) were involved in the eclogite-facies transformation of the high temperature-low pressure kinsingitic rocks (Hy, 1984). The relatively ^{18}O -rich compositions of the eclogitic schists at the Mucrone area, compared to other known Type C-eclogite terrains (Vogel and Garlick, 1970, Agrinier et al., 1985; this study

Chapter 3 and Fig. 3.2) may reflect the isotopic compositions of the original amphibolite-facies parascists, and suggests that the fluid was internally-produced and buffered isotopically by the isotopic composition of the existing rocks (Desmons and O'Neil, 1978). There is no evidence to indicate that significant quantities of external fluid (i.e. fluid not derived from the existing rocks) was involved in the eclogite-facies metamorphism of the mica schists or the metagranitoids (see also Desmons and O'Neil, 1978). *Dehydration reactions in the surrounding pelitic rocks* may, thus, have provided the source of fluid involved in the eclogite-facies formation of the mylonites and orthogneisses. Limited supplies of such fluid and/or low permeabilities of the granitic rocks may have directly influenced the degree of recrystallization and the approach to chemical equilibrium. More detailed sampling and isotopic analysis in the neighbouring eclogitic schists could possibly provide a better constraint on the source of the fluid involved in the metamorphism of the metagranitic rocks and could yield more information of the actual degree of chemical and isotopic communication between the different rock units (compare results in Chapter 3 from the Adula Nappe).

Marine water, incorporated into the tectonic pile during subduction and underthrusting, may be considered as another possible source for the ^{16}O -rich fluid involved in the evolution of the Mte. Mucrone metagranitoids (see Fig. 5. 14). However, there is little, or no, chemical and isotopic evidence to support this possibility.

Comparison of the geochemical data as well as the microstructural and mineralogical evolution determined in this study with the results of Desmons and O'Neil, indicates that the isotopic composition of the infiltrating hydrous fluid was just slightly out of equilibrium with the original quartz diorite and was channelized along deformation zones. Thus, considering the constraints presented above, a value of 6.0‰ for the initial isotopic composition of the infiltrating hydrous fluid and a constant temperature of 500 °C have been assumed in order to determine the change in water to rock ratios (W/R) as a function of distance away from the shear zones. The results of calculations using these assumptions and equation 5.1 above are presented in Fig. 5.15.

Due to the nature of equation 5.1, the W/R-ratios are directly related to whole rock ^{18}O -compositions, resulting in similar shapes of the curves. The values decrease from 0.75 directly in the shear zones to 0.2 just 30cm away. Thus, with an infiltrating fluid with an initial isotopic composition of 6.00‰ at a constant temperature of 500 °C, only 75 oxygen units of water would be required per 100 oxygen units of rock to produce the shift in ^{18}O observed in the mylonites. Since a typical granitic rock contains only approximately 45-50 wt% oxygen, compared to 89 wt% oxygen in water, the water/rock ratio in weight units is approximately equal to 0.5 W/R (Taylor, 1977). This means that for every kilogram of meta-quartz diorite, 375 grams of water would be

required to produce the observed isotopic signature. Comparison of this value with the bulk rock geochemical data for the mylonites presented in Figs. 5.5 and 5.6 and Table 5.2 indicates an 0.5 wt% enrichment in H_2O in the overprinted mylonites relative to the unfoliated meta-quartz diorites, which suggests that nearly 100 times as much water may have passed through the centers of the shear zones as that taken up in hydration reactions.

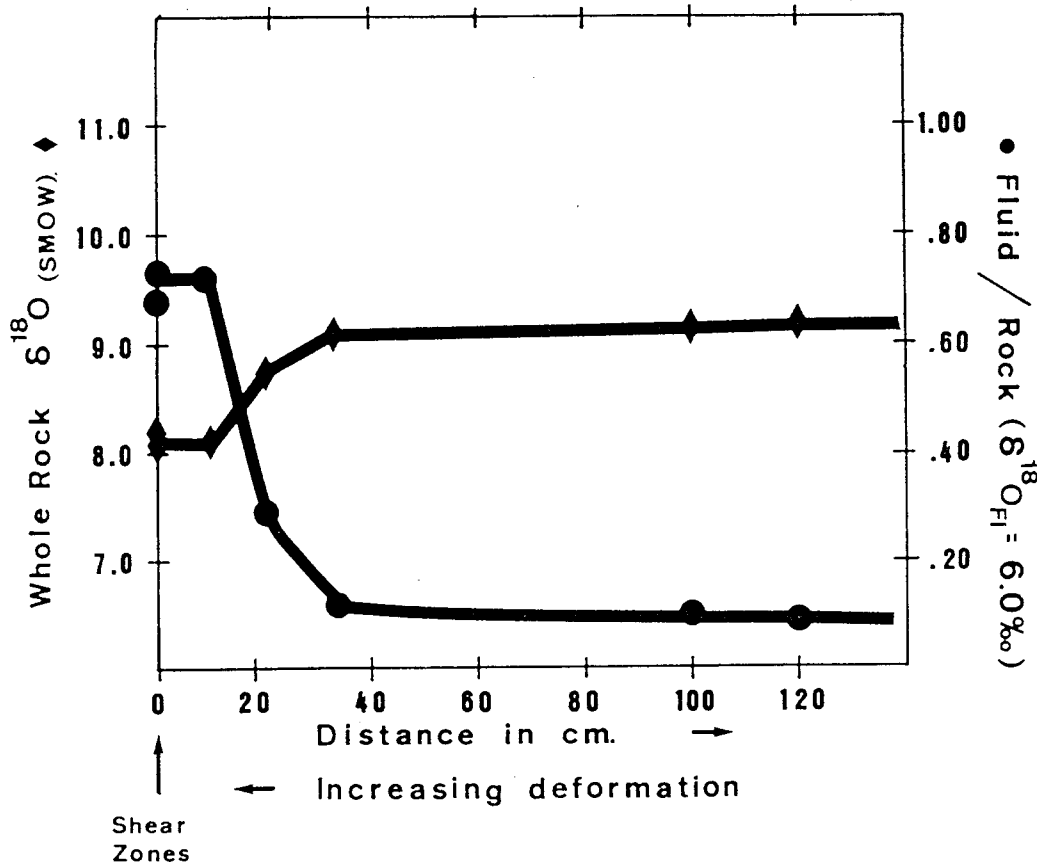


Fig. 5.15:

Calculated F/R ratios (from Eq. 5.1) are plotted as a function of distance away for the centers of the shear zones (for samples Mu 1-2, 1-3, 4-2, 4-3, 4-5; shown in Fig. 5.7), for a temperature of 500 °C and an initial infiltrating fluid of 6.00‰. This diagram combines the two profiles b & c, shown in Fig. 5.7. This figure suggests that fluid flow may have been concentrated in the centers of the mylonite zones, shown here as F/R ratio of 0.75, with diffusive infiltration occurring perpendicular to the flow direction. Textural evidence suggests that an infiltration event may have occurred subsequent to the formation of the mylonite zones (see Fig. 5.12). Fluid flow may have been controlled by the foliation present in the mylonites and may be associated with the zoisite-garnet vein formation.

It must be emphasized that fluid/rock ratios, attained from open system mass-balance models of isotopic exchange, will always represent minimum values, and are often considerably lower than those estimated from solubility data (see e.g. Wood and Walther, 1986). A further limitation has been pointed out by Baumgartner and Rumble (1986): such isotopic mass-balance calculations do not allow an insight into the evolution of fluid-rock systems through space and time. Wood and Walther (1986) have shown that, in contrast to fluid/rock ratios calculated from oxygen isotope data, the use of solubility data for quartz indicates high fluid/rock ratios of 6:1 in pelitic sequences which actually produce small volumes of hydrous fluid. In addition, these authors have suggested that Cl- and F-activity gradients recorded in micas may yield useful information about fluid/rock ratios. The calculations of Wood and Walther (1986, p. 104) suggest that fluid/rock ratios necessary to eliminate activity gradients in mica will depend on the Na/K ratios in the infiltrating fluid. If the fluid is K-rich, resulting in the addition of K to the system, fluid/rock ratios on the order of 3:1 may be required to re-equilibrate the mica. On the other hand, if an addition of Na and a depletion of K accompanies fluid infiltration (as in the case of the eclogitic mylonites and omphacite-garnet orthogneisses), cation exchange requires fluid/rock ratios of only approximately 0.3:1.

More information about the scales of fluid-rock interaction during the evolution of the Mte. Mucrone metagranitoid could possibly be obtained by more detailed sampling along profiles parallel to, as well as perpendicular to, the veins and the associated ductile shear zones. In addition, application of solubility data for zoisite and garnet, as well as the consideration of Na/K ratios in micas, could be combined with stable isotope data to more accurately limit the volume of fluid involved in the evolution of these rocks.

5.7. SUMMARY AND CONCLUSIONS

The petrological, geochemical and microstructural data presented in this study indicate large variations in the degree of eclogite-facies recrystallization and deformation recorded in the Mte. Mucrone metagranitoids. At least two *main phases of eclogite-facies recrystallization* are evident in these rocks and can be directly related to the *timing and degree of deformation*. An *initial pre-kinematic Jadeite Phase* resulted in the formation of fine-grained aggregates of jadeite + quartz + zoisite as pseudomorphs after the primary igneous plagioclase. Plagioclase breakdown reactions may have accompanied or have been subsequent to biotite breakdown reactions which produced garnet and phengitic white-mica. The progress of biotite breakdown may have been limited by the supply of alumina and calcium from plagioclase domains, as is indicated by the chemically distinct corona textures of garnet and phengitic white-mica around biotite in the meta-quartz diorites. Incomplete reaction, resulting in the corona textures,

may have been due to slow diffusion rates and/or a paucity of intergranular fluid during the initial stages of eclogite-facies metamorphism (see also Koons, 1982; Hy, 1984; and Koons et al., in review).

An *initial high strain deformation stage* resulted in dynamically recrystallized quartz grains and superplastically-deformed pyroxene layers, grain coarsening and partial chemical homogenization. Enlargement of equilibrium domains may have resulted in the completion of the biotite reaction and produced the assemblage jadeite + garnet + phengite + quartz, characteristic of the mylonitic rocks. Bulk rock geochemical and stable isotope data indicate that infiltration of an external hydrous fluid phase is associated with deformation and recrystallization in the jadeite-garnet mylonites. Local changes in the activities of sodium, potassium and H₂O could have produced the assemblages observed in the deformed rocks.

The *duration* and *timing* of fluid infiltration relative to *high strain deformation* appears to have been crucial to the mineralogical evolution of the Mte. Mucrone granitoids, resulting in the chemical and microstructural differences recorded in these rocks. A model has been presented for the formation of the ductile shear zones at the Mte. Mucrone. It has been suggested that subsequent to the formation of fine-grained aggregates of Jad + Zoi + Qtz, as pseudomorphs after igneous plagioclase, an initial stage of fluid infiltration occurred along fractures or faults, catalysing diffusive mass transfer and grain growth rates and resulting in the formation of coarser-grained, 1-5 cm wide, reaction zones. Fluid-induced reaction and grain coarsening may have acted as a hardening mechanism and resulted in the concentration of subsequent high strain deformation, and the formation of the mylonites, along these zones.

The jadeite-garnet mylonites, characterized by nearly homogeneous phase compositions and coarser grain-sizes of jadeite, garnet and phengite (relative to the unfoliated meta-quartz diorites), may represent syn-deformational recrystallization and limited fluid infiltration. Preserved chemical zoning in garnet, heterogeneous mica compositions, and inclusion-rich pyroxene grains in some mylonite samples (i.e. in overprinted mylonites) indicates local anhydrous deformation, whereby localized post-kinematic infiltration along these deformation zones resulted in new growth of omphacitic pyroxene and a second generation of more grossular-rich garnet. Limited permeabilities in the mylonite zones may have resulted in an excess of fluid pressure during infiltration and led to fracturing into less deformed wallrocks and the formation of the zoisite-garnet veins.

Complete recrystallization and formation of omphacite-garnet orthogneiss may have resulted from progressive syn-kinematic infiltration and longer deformation periods. The presence of omphacite and paragonite, characteristic of the orthogneiss, may be due to original variations in bulk rock chemistries and/or may be related to a decrease in Na-, K- and H₂O-activities during deformation and fluid infiltration.

The microfabrics of the deformed rocks, combined with stable isotope and bulk rock geochemical data, suggest that fluid infiltration may not have been continuous but rather occurred in pulses and was channelized along zones of increased permeabilities due to high strain deformation. High-strain deformation continued during exhumation and may have been accompanied by further pulses of fluid activity.

Rudimentary, isotopic mass-balance modelling of the infiltration event suggests that the hydrous fluid was ^{16}O -rich and may have been *produced locally* by dehydration reactions in the neighbouring metapelitic and metabasic rocks. However, comparison with the isotopic study of Desmons and O'Neil (1978) indicates a lack of large-scale isotopic exchange between the granitic rocks and the neighbouring eclogitic mica schist complex. Minimum fluid to rock ratios, based on depletions in ^{18}O in the deformed rocks, have been estimated to range from approximately 1.0 to 0.75 for equilibration with fluids with isotopic compositions of 6.0 to 6.5‰ and at a temperature of 500 °C. Stable isotope profiles perpendicular to the ductile shear zones indicate a decrease in W/R-ratios to values of less than 0.1 at distances of approximately 30 cm.

The evidence for metasomatic alteration, associated with deformation and formation of the mylonites and Omp-Gar orthogneisses, suggests that isotopic exchange occurred through a surface-controlled mechanism of chemical transformation and was driven by disequilibrium relationships between metagranitoid and the infiltrating fluid. Discordant calculated isotopic temperatures, as well as apparent discrepancies between a predicted order of recorded temperature and that determined may reflect the presence of intergranular, static fluid, resulting in diffusive oxygen exchange between quartz, phengite and Na-pyroxene upon cooling.

The results of this study suggest that under eclogite-facies metamorphic conditions, diffusion and growth rates may be extremely slow in nearly anhydrous rocks, and may directly hinder complete reaction and recrystallization. Both deformation and an external fluid appear to be determining factors in the metamorphic evolution of the Mte. Mucrone granitic body. However, an access of limited amounts of hydrous fluid appears to have been determinant to the attainment of chemical homogenization of garnet and pyroxene.

The rheological properties of the primary quartz diorite may have been such that the rock was highly resistant to deformation during the early stages of metamorphism and became more deformable after the formation of the fine-grained plagioclase pseudomorphs (reaction enhanced ductility). At the onset of eclogite-facies metamorphism, a paucity of grain boundary fluid, and as a result slow intercrystalline diffusion, caused local chemical and textural domains and an overall state of disequilibrium. High strain deformation may have enhanced intra- and intercrystalline diffusion rates and may have increased permeabilities such as to allow infiltration of an external hydrous fluid into the previously dry system.

CHAPTER 6

GENERAL SUMMARY AND CONCLUSIONS

The scales and mechanisms of fluid-rock interaction during high-pressure metamorphism and subsequent uplift histories of two areas of continental crust have been investigated in this study. Based on petrological, isotopic and microstructural data of mafic and pelitic rocks at the Cima di Gagnone area of the Cima Lunga Nappe (southern Switzerland), it has been shown that small quantities of hydrous fluid may have been produced during dehydration reactions. Fluid release can be modelled by a mechanism of Rayleigh distillation, whereby the escaping fluid may only have travelled short distances of a few (tens of) meters before being consumed in hydration reactions in neighbouring rocks.

The results of models for the various hydration/dehydration events at the Cima di Gagnone area suggest that local variations in bulk rock compositions in interlayered metasedimentary sequences may be sensitive to the access of an external fluid, catalyzing hydration reactions, and thus, creating important "sinks" for fluid intake. Such alternating hydration and dehydration reactions in interlayered rocks may provide a mechanism in which fluid flow may be limited during metamorphism. The capacity for polymetamorphic pelitic sequences to produce a free fluid phase may be limited. Although great volumes of hydrous fluid and large shifts in isotopic compositions may be associated with initial dewatering of pelitic rock sequences, stable isotope geochemical methods may not be good indicators of fluid-rock interaction during high-grade metamorphism of polymetamorphic metapelites.

Oxygen isotope data from both areas of study indicate a depletion in $\delta^{18}\text{O}$ during eclogite-facies metamorphism, which may have resulted from infiltration of limited quantities of hydrous low- ^{18}O fluids. Magmatic waters or hydrous fluids derived from the metamorphism of igneous rocks may be considered as source for such fluids. However, the possibility that the common occurrence of low- ^{18}O eclogites may be related to the incorporation and trapping of marine water during subduction processes should be investigated more closely. Detailed hydrogen isotope studies in areas exhibiting ^{18}O -depletion may provide a mean of identifying marine water-components in metamorphic fluids.

The isotope fractionations between multiple mineral pairs from the high-grade mafic, pelitic and granitic metamorphic rocks investigated in this study have shown that isotopic equilibrium is rarely attained. Furthermore, retrograde exchange upon cooling may be indicated by discordant isotopic temperature estimates. Diffusive exchange mechanisms of oxygen isotope upon cooling may be important for mineral pairs such as

mica and feldspar. No correlation has been found between textural equilibrium, recrystallization and the degree to which isotopic equilibrium is attained.

Detailed studies along eclogite-facies ductile shear zones at the Mte. Mucrone indicate that high-strain deformation was crucial to processes of diffusive mass transport and the completion of mineral reactions. However, chemical homogenization may have required the access of an external source of fluid. A model for the formation of the shear zones has been presented. Prior to the main ductile deformation event, fracturing in the otherwise impermeable and nearly anhydrous metagranitic rocks may have increased permeabilities, allowing penetration of an external hydrous fluid. Fluid-induced enhancement of diffusive mass transfer may have resulted in the formation of narrow, coarse-grained reaction zones, and may provide an example of reaction hardening. The presence of such "hard", undeformable zones may have resulted in a concentration of strain during the subsequent ductile deformation event. A major infiltration event, associated with zoisite-vein formation followed high-strain deformation. Comparison with other isotopic studies in the Mte. Mucrone are suggests localised, rather than pervasive flow, channalized along shear zones and possibly reactivated, "old" fluid pathways.

Suggestions for Future Work

The problem of identifying "fluid-producers" and "fluid-aquifers" during regional metamorphic processes has only been touched upon in this study. In most petrological and isotopic studies of fluid-rock interaction (-this study being no exception), a generalized whole-rock reaction is presented and it is assumed that such a reaction is applicable to the entire metamorphic sequence of rock. However, the possibility that thinly-layered metamorphic sequences may undergo simultaneous hydration and dehydration reactions during the same metamorphic event could be investigated in more detail. Polymetamorphic terrains, however, should be avoided as important information is often masked by multiple phase of recrystallization and/or deformation.

Preliminary data from a large ultramafic and mafic layer in metagranitic to metapelitic rocks (outcrop Mg163) at the Cima di Gagnone area indicates extremely ^{18}O -depleted whole rock compositions (2.5 - 3.5‰). Further isotopic data, especially hydrogen isotope compositions may yield valuable information about the source of the ^{16}O -rich fluids which could have caused such depletions. A detailed petrographic basis and geochemical data on possible fluid compositions are available for this area.

The study at the Mte. Mucrone have left many open questions. The relationship between fluid activity in the metagranitic rocks and possible dehydration reactions in

surrounding pelitic rocks remains uncertain. In addition, the extent to which isotopic homogenization has been achieved in this area can not be determined by existing data. The model proposed for the formation of the ductile shear zones could be further tested by more detailed sampling in a direction parallel to the shear zones.

Variations in isotopic fractionations between coexisting mineral pairs in interlayered rocks, as well as discordant temperature estimates, indicated in this study, may represent effects of variations in diffusion properties and isotope exchange mechanisms. The retention of "old" compositions during subsequent metamorphic events has direct implications for the use of stable isotopes in geothermometric studies. As more diffusion data becomes available, some of the uncertainties in interpreting stable isotope data may be clarified. The combination of diffusion data and stable isotope data may provide valuable information about the cooling and uplift histories of metamorphic rocks.

REFERENCES

- Addy, S.K. and Garlick, G.D. (1974): Oxygen isotope fractionation between rutile and water. *Contrib. Mineral. Petrol.* 45, 119-121.
- Agrinier, P., Javoy, M., Smith, D.C. and Pineau, F. (1985): Carbon and Oxygen isotopes in eclogites, amphibolites, veins and marbles from the Western Gneiss Region, Norway. *Chem. Geol. (Isotope Geoscience Section)*, 52, 145-162.
- Anderson, A.T. (1967): The dimensions of oxygen isotopic equilibrium attainment during prograde metamorphism. *J. Geology*, 75, 323-332.
- Anderson A.T., Klayton R.N. and Mayeda T.K. (1971): Oxygen isotope thermometry of mafic igneous rocks. *J. Geol.* 79, 715-729.
- Anderson T.F. and Kaspar R.B. (1975): Oxygen self-diffusion in albite under hydrothermal conditions. *EOS Trans. Am. Geophys. Union* 56, 495.
- Baertschi P. and Silvermann S.R. (1951): The determination of relative abundances of the oxygen isotopes in silicate rocks. *Geochim. Cosmochim. Acta.* 17, 317-328.
- Baumgartner, L.P. and Bucher-Nurminen, K. (1986a): Fluid pathways around a cooling pluton in deformed wall-rock South-West Adamello, Italy. In review.
- Baumgartner, L.P. and Rumble, D. III (1986b): Transport of stable isotope; 1: Development of a kinetic continuum theory for stable isotope transport. In review.
- Baumgartner, L.P. (1986c): Transport of stable isotope; 2: Transport of oxygen and carbon isotopes in the contact aureole of the Tertiary Adamello intrusive complex. In review.
- Beach A. (1976): The interrelation of fluid transport, deformation and geochemistry and heat flow in early Proterozoic shear zones in the Lewisian complex. *Phil. Trans. Roy. Soc. London A* 280, 529-604.
- Beach A. (1977): Vein arrays, hydraulic fracture and pressure solution structures in a deformed flysch sequence. *Tectonophysics* 40, 201-225.
- Beach A. (1980): Retrogressive metamorphic processes in shear zones with special reference to the Lewisian Complex. *J. Struct. Geol.* 2, 257-263.
- Beach, A. and Fyfe, W.S. (1972): Fluid transport and shear zones at Scourie Sutherland: evidence of overthrusting? *Contrib. Mineral. Petrol.* 36, 175-180.
- Bell T.H. and Etheridge M.A. (1976): The deformation and recrystallization of quartz in a mylonite zone, Central Australia. *Tectonophysics* 32, 235-267.
- Behner E.C. (1978): Slaty cleavage and related strain in Martinsbourg slate, Delaware Water Gap, New Jersey. *Am. J. Sci.* 278, 1-13.
- Bigeleisen, J. and Mayer, M.G. (1947): Calculations of equilibrium constants for isotopic exchange reactions. *J. Chem. Phys.* 15, 261.
- Blattner P. (1975): Oxygen isotope composition of fissure grown quartz, adularia and calcite from Broadlands geothermal field, New Zealand. *Science* 275, 785-800.
- Blattner P. and Bird G.W. (1974): Oxygen isotope fractionation between quartz and K-feldspar at 600 C. *Earth. Plan. Lett.* 23, 21-27.
- Bottinga, Y and Javoy, M. (1973): Comments on oxygen isotope geothermobarometry. *Earth Plan. Sci. Letters* , 20, 250-265.
- Bottinga, Y and Javoy, M. (1975): Oxygen isotope partitioning among the minerals in igneous and metamorphic rocks. *Rev. Geophys. Space Phys.*, 13, 401-418.
- Borradaile G.J. Bayly M.B. and Powell C. (1982): Atlas of deformational and metamorphic rock fabrics. Springer Verlag, Berlin, 551 p.
- Boullier A.M. and Gueguen Y (1975): SP-mylonites: origin of some mylonites by superplastic flow. *Contr. Mineral. Petrol.* 50, 93-104.
- Brace W.F. (1968): The mechanical effects of pore pressure on the fracturing of rocks In: Baer and Norris (eds) *Research in tectonics. Geol. Surv. of Canada Paper* 68/52, 113-142.
- Brace W.F. (1980): Permeability of crystalline and argillaceous rocks. *Int. J. Rock Mech. Min. Sci.* 17, 241-251.
- Brace W.F., Walsh J.B. and Frangos W.T. (1968): Permeability of granite under high pressure. *J. Geophys. Res.* 73, 2225-2236.

- Brodie K.H. and Rutter E.H. (1985): On the relationship between deformation and metamorphism, with special reference to the behaviour of basic rocks. In: Thompson A.B. and Rubie D.C. (eds): *Metamorphic reactions, kinetics, textures and deformation Advances in Physical Geochemistry Vol. 4.*, 138-179.
- Callegari, E., Compagnoni, R., Dal Piaz, G.V., Frisatto, V., Gosso, G. e Lombardo, B. (1976): Nuovi affioramenti di metagranitoidi nella zona Sesia-Lanzo. *Rend. Soc. It. Min. Petr.*, 32, 97-111.
- Clayton R.N. (1981): Isotopic Thermometry. In: Newton R.C. et al. (Ed): *Thermodynamics of minerals and melts.*
- Clayton, R.N. and Epstein, S. (1961): The use of oxygen isotopes in high temperature geological thermometry. *J. Geology*, 69, 447-452.
- Clayton, R.N. and Mayeda, T.K. (1963): The use of bromine pentafluoride in the extraction of oxygen from oxides and silicates for isotopic analysis. *Geochim. Cosmochim. Acta.* 27, 43-50.
- Clayton, R.N., O'Neil, J.R. and Mayeda, T.K. (1972): Oxygen isotope exchange between quartz and water. *J. Geophys. res.*, 77, 3057-3067.
- Clayton R.N. and Steiner A. (1975): Oxygen isotope studies of geothermal systems at Wairakei, New Zealand. *Geochim. Cosmochim. Acta* 39, 1179-1186.
- Codoni, A. (1981): *Geologia e petrografia della regione del Pizzo di Claro.* Diss ETH Zürich.
- Cole, D.R., Ohmoto, H. and Lasaga, A.C. (1983): Isotopic exchange in mineral-fluid systems. I: Theoretical evaluation of oxygen isotopic exchange accompanying surface reactions and diffusion. *Geochim. Cosmochim. Acta*, 47, 1681-1693.
- Cole D.R. and Ohmoto H. (1986): Kinetics of isotopic exchange at elevated temperatures and pressures In: Valley J.W., Taylor H.P and O'Neil J.R (eds): *Stable isotopes in high temperature geological processes.* *Rev in Mineralogy Vol. 16, Am. Mineral. Soc.*, 41-90.
- Coleman, M.L., Sheppard, T.J., Durham, J.J, Rouse, J.E. and Moore, G.R. (1982): Reduction of water with zinc for hydrogen isotope determination. *Anal. Chem.*, 54, 993-995.
- Coleman R.G., Lee D.E. Beatty L.B. and Brannock W.W. (1965): Eclogites and eclogites: their differences and similarities. *Bull. Geol. Soc. Am.* 76, 483-508.
- Compagnoni, R. (1977): The Sesia-Lanzo Zone: high pressure-low temperature metamorphism in the austroalpine continental margin. *Rend. Soc. It. Min. Petr.* 33 (1), 335-374.
- Compagnoni, R., Dal Piaz, G.V., Hunziker, J.C., Gosso, G., Lombardo, B. and Williams, P. (1977): The Sesia-Lanzo Zone, a slice of continental crust with high pressure-low temperature assemblages in the Western Italian Alps. *Rend. Soc. It. Min. Petr.* 33, 281-334.
- Compagnoni, R. and Maffeo, B. (1973): Jadeite-bearing metagranitoids s.l. and related rocks in the Mte. Mucrone area (Sesia-Lanzo Zone, Western Italian Alps). *S.M.P.M.* 53, 355-378.
- Craig, H. (1953): The geochemistry of the stable carbon isotopes. *Geochim. Cosmochim. Acta* 3, 53
- Craig, H. (1961): Isotopic variations in meteoric waters. *Science* 133, 10702-1703.
- Dal Piaz, G.V., Gosso, G e Martinotti, G. (1971): La II zona diorito-kinzigitica tra la val Sesia e la valle d' Ayas (Alpi occidentali). *Mem. Soc. Geol. It.*, 10, 257-276
- Dal Piaz, G.V., Hunziker, J.C. and Martinotti, G. (1972): La zona Sesia-Lanzo e l'evoluzione tettono-metamorfica delle Alpi nordoccidentali interne. *Mem. Soc. Geol. It.*, 11, 433-460.
- Dal Piaz, G.V., Hunziker, J.C. and Martinotti, G. (1973): Excursion to the Sesia Zone of the Schweizerische Mineralogische und Petrographische Gesellschaft. *S.M.P.M.* 53, 477-490.
- Deines, P. (1977): On the oxygen isotope distribution among triplets in igneous and metamorphic rocks. *Geochim. Cosmochim. Acta* 41, 1709-1730.

- Desmons, J. and O'Neil, J.R. (1978): Oxygen and hydrogen isotope compositions of eclogites and associated rocks from the Eastern Sesia Zone (Western Alps, Italy). *Contrib. Mineral. Petrol.*, 67, 79-85.
- Devereux I. (1968): Oxygen isotope ratios of mineral from the regionally metamorphosed schists of Otago, New Zealand. *N.Z. J. Sci.* 11, 526-548.
- Downs, W.F., Touyinhthiphonexay, Y. and Deines, P. (1981): A direct determination of the oxygen isotope fractionation between quartz and magnetite at 600 °C and 800 °C and 5 Kbar. *Geochim. Cosmochim. Acta*, 45, 2065-2072.
- Emiliani, C (1955): Pleistocene temperatures. *J. Geol.* 63, 538
- Epstein, S. and Mayeda, T.K. (1953): Variation of ^{18}O content of waters from natural sources. *Geochim. Cosmochim. Acta* 4, 213-224.
- Eslinger E.V. and Savin S.M. (1973): Mineralogy and oxygen isotope geochemistry of the hydrothermally altered rocks of the Ohaki Broadlands, New Zealand. *Am. J. Sci.* 273: 240-267.
- Essene E.J. (1982): Geologic thermometry and barometry. In Ferry (ed), *Reviews in Mineralogy* 109, 153-206.
- Etheridge M.A. and Wilkie J.C. (1979): Grain size reduction, grain boundary sliding and flow strength of mylonites. *Tectonophysics* 58, 159-178.
- Etheridge, M.A., Wall, V.J. and Vernon, R.H. (1983): The role of the fluid phase during regional metamorphism and deformation. *J. Met. Geol.* 1, 205-226.
- Etheridge, M.A., Wall, V.J., Cox, S.F. and Vernon, R.H. (1983): High fluid pressures during regional metamorphism and deformation - implications for mass transport and deformation mechanisms. *J. Geophys. res.* ??
- Evans, B.W. and Trommsdorff, V. (1974): Stability of enstatite + talc, and CO_2 -metasomatism of peridotite, Val d' Efra, Lepontine Alps. *Am. J. Sci.* 274, 274-296.
- Evans, B.W. and Trommsdorff, V. (1978): Petrogenesis of garnet-lherzolite, Cima di Gagnone, Lepontine Alps. *Earth Plan. Sci. Letters* 40, 333-348.
- Evans, B.W. and Trommsdorff, V. and Richter, W. (1979): Petrology of an eclogite-metarodingite suite at Cima di Gagnone, Ticino, Switzerland. *Am. Min.* 64, 15-31.
- Evans, B.W. and Trommsdorff, V. and Goles, G. (1981): Geochemistry of high-grade eclogites and metarodingites from the Central Alps. *Contrib. Mineral. Petrol.* 76, 301-311.
- Ferry, J.M. (1976a): Metamorphism of calcareous sediments in the Waterville-Vassalboro area, south-central Maine: mineral reactions and graphical analysis. *Am. J. Sci.* 276, 274-296
- Ferry, J.M. (1976b): P, T, f_{CO_2} , $f_{\text{H}_2\text{O}}$ during metamorphism of calcareous sediments in the Waterville-vassalboro area, south-central Maine. *Contrib. Mineral. Petrol.* 57, 119-143.
- Ferry, J.M. (1978): Fluid interaction between granite and sediment during metamorphism, south-central Maine. *Am. J. Sci.* 278, 1025-1056.
- Ferry, J.M. (1979): A map of chemical potential differences within an outcrop. *Am. Min.* 64, 966-985.
- Ferry, J.M. (1980): A comparative study of geothermometers and geobarometers in pelite schists from south-central Maine. *Am. Min.* 65, 720-732.
- Ferry, J.M. (1980): A case study of the amount and distribution of heat and fluid during metamorphism. *Contrib. Mineral. Petrol.* 71, 373-385.
- Ferry, J.M. (1982): Mineral reactions and element migration during metamorphism of calcareous sediments from the Vassalboro formation, Central Maine. *Am. Min.* 67,
- Ferry, J.M. (1983): Regional metamorphism in the Vassalboro Formation south-central Maine, USA: a case study of the role of fluid in metamorphic petrogenesis. *J. Geol. Soc. London* 140, 551-576.
- Ferry, J.M. (1984): A biotite isograd in south-central Maine: mineral reactions, fluid transfer and heat transfer. *J. Petrology* 25, 871-893.

- Ferry, J.M. (1986): Reaction progress: A monitor of fluid-rock interaction during metamorphic and hydrothermal events. In Walther J.V and Wood B.J (eds): fluid-rock interactions during metamorphism. *Advances in physical chemistry* 5,, 69-88.
- Ferry J. M. and Spear F.S (1978): Experimental calibration of the partitioning of Fe and Mg between biotite and garnet. *Contr. Min. Petrol.* 66, 113-117.
- Ferry, J.M. and Burt D.M. (1982): Characterization of metamorphic fluid compositions through mineral equilibria. in: *Reviews in mineralogy*, volume 10, Min. Soc of Am., 207-263.
- Fisher G.W. (1978): Rate laws in metamorphism. *Geochim. Cosmochim. Acta* 42, 1035-1050.
- Frey, M., Hunziker, J.C., Frank, W., Bocquet, J., Dal Piaz, G.V., Jäger, E. and Niggli, E. (1974): Alpine metamorphism of the alps. A review. *S.M.P.M.* 54, 247-290.
- Frey, M., Hunziker, J.C., O' Neil, J.R. and Schwander, H.W. (1976): Equilibrium-disequilibrium relations in the Monte Rosa granite, western Alps: petrological, Rb-Sr and stable isotope data. *Contrib. Mineral. Petrol.* 55, p.147-149.
- Frey, M., Bucher, K. and Mullis, J. (1980): Alpine metamorphism along the geotraverse Basel-Chiasso - A review. *Eclogae Geol. Helv.* 73, 527-546.
- Friedman, I. and O' Neil, J.R. (1977): Compilation of stable isotope fractionation factors of geological interest. *U.S.G.S. Prof. Pap.* 440-kk.
- Früh-Green, G. and Thompson A.B. (1985): Stable isotope indications of fluid motion in the amphibolisation of eclogites in the adula nappe. (Abstract). *Terra Cognita* 5 (2-3), 336.
- Früh-Green, G. (1986): Stable isotope indications of fluid movement in ductile shear zones during eclogite facies metamorphism. *EOS*, V66, No. 46, 1126-1127.
- Forester, R.W. and Taylor H.P. (1977): $^{18}\text{O}/^{16}\text{O}$, D/H and $^{13}\text{C}/^{12}\text{C}$ studies of the Tertiary igneous complex of Skye, Scotland. *Am. J. Sci.* 277, 136-177
- Fyfe, W.S., Price, N.J. and Thompson, A.B. (1978): *Fluids in the earth's crust.* Elsevier, Amsterdam.
- Garlick, G. D. (1966): Oxygen isotope fractionation in igneous rocks. *Earth Plan. Sci. Letters* 1, 361-368
- Garlick, G.D. and Epstein, S. (1967): Oxygen isotope ratios in coexisting minerals of regionally metamorphosed rocks. *Geochim. Cosmochim. Acta* 31, 181-214.
- Garlick, G.D., Mac Gregor I.D. and Vogel D.E. (1971): Oxygen isotope ratios in eclogites from kimberlites. *Science* 171, 1025-1027.
- Giletti, B.G. (1985): The nature of oxygen transport within minerals in the presence of hydrothermal water and the role of diffusion. *Chem. Geol.* 53, 197-206.
- Giletti, B.G. (1986): Diffusion effects on oxygen isotope temperatures of slowly cooled igneous and metamorphic rocks. *Earth Plan. Sci. Lett.* 77, 218-228.
- Giletti, B.G. and Anderson T.F. (1975): Studies in diffusion II: Oxygen in phlogopite mica. *Earth. Plan. Sci. Lett.* 28, 225-223.
- Giletti, B.G., Semet M.P. and Yund, R.A. (1978): Studies in diffusion. III: oxygen in feldspars: an ion microprobe determination. *Geochim. Cosmochim. Acta* 42, 45-57.
- Giletti, B.G. and Nagy K.L. (1981): Grain boundary diffusion of oxygen along lamellar boundaries in perthitic feldspars (Abstr), *Trans. Am. Geophys. Union* 62, 428.
- Giletti, B.G. and Yund R.A. (1984): Oxygen diffusion in quartz. *J. Geophys. Res.* 89, 4039-4046.
- Goldman, D.S. and Albee A.L. (1977): Correlation of Mg/Fe partitioning between garnet and biotite with $^{18}\text{O}/^{16}\text{O}$ partitioning between quartz and magnetite. *Am. J. Sci.* 277, 750-767.
- Gosso, G. (1977): Metamorphic evolution and fold history in the eclogitic micaschists of the upper Gussoney Valley (Sesia-Lanzo zone, Western Alps). *Rend. Soc. It. Min. Petr.*, 33 (1), 389-407.

- Graham, C.M. (1981): Experimental hydrogen isotopic studies III: Diffusion of hydrogen in hydrous minerals, and stable isotope exchange in metamorphic rocks. *Contrib. Mineral. Petrol.*, 216-228.
- Graham, C.M., Sheppard, S.M.F. and Heaton, T.H.E. (1980): Experimental hydrogen isotope studies, I: systematics of hydrogen isotope fractionation in the system epidote-H₂O, zoisite-H₂O, and AlO(OH)-H₂O. *Geochim. Cosmochim. Acta* 44, 353-364.
- Graham, C.M., Greig, K.M., Sheppard, S.M.F. and Turi, B. (1983): Genesis and mobility of the H₂O-CO₂ fluid phase during regional greenschist and epidote amphibolite facies metamorphism: a petrological and stable isotope study in the Scottish Dalradian. *J. Geol. Soc. Lond.*, 140, 577-599.
- Greenwood, H.J. (1961): Buffering of pore fluids by metamorphic reactions. *Am. J. Sci.*, 275, 573-593.
- Greenwood, H.J. (1962): Metamorphic reactions involving two volatile components. *Carnegie Inst. Wash. Year Book* 61, 82-85.
- Greenwood, H.J. (1967): Mineral equilibria in the system MgO-SiO₂-H₂O-CO₂. In: Abelson P.H. (Ed) *Researchs in geochemistry, II*. John Wiley and Sons N.Y. pp. 542-549.
- Greenwood, H.J. (1975): Thermodynamically valid projections of extensive phase relationships. *AM. Mineral.*, 60, 1-8.
- Gregory, R.T. and Taylor, H.P. Jr (1981): An oxygen isotope profile in a section of Cretaceous oceanic crust, Samail ophiolite, Oman: evidence for ¹⁸O buffering of the oceans by deep (5Km) seawater-hydrothermal circulation at mid-ocean-ridges. *J. Geophys. Res.* 86 (B4), 2737-2755.
- Gresens, R.L. (1966): Composition volume relationships of metasomatism. *Chem. Geol.* 2, 47-65.
- Hamza, M.S. and Epstein S. (1980): Oxygen isotopic fractionation between oxygen of different sites in hydroxyl-bearing silicate minerals. *Geochim. Cosmochim. Acta* 44, 173-182
- Hänny, R., Grauert, B., Soptrajanova, G. (1975): Paleozoic migmatites affected by high-grade tertiary metamorphism in the Central Alps (Valle Bodengo, Italy). A geochronological study. *Contrib. Mineral. Petrol.* 51, 173-196.
- Heaton, T.H.E. and Sheppard S.M.F. (1977): Hydrogen and oxygen isotope evidence for seswater hydrothermal alteration and ore deposition, Troodos Complex, Cyprus. *Geol Soc. London Spec. Paper* 7, 42-57.
- Heinrich, C.A. (1978): *Metamorphose und Strukturen der Cima Lunga-Serie: I C. di Gagnone-Val Motto*. Diploma thesis ETH zürich.
- Heinrich, C.A. (1982): Kyanite-eclogite to amphibolite facies evolution of hydrous mafic and pelitic rocks, Adula Nappe, Central Alps. *Contrib. Mineral. Petrol.* 81, 30-38.
- Heinrich, C.A. (1983): *Die regionale Hochdruckmetamorphose der Adula Decke, Zentralalpen, Schweiz*. Diss. ETH Zürich.
- Heinrich, C.A. (1986): Eclogite facies regional metamorphism of hydrous mafic mafic rocks in the central alpine Adula nappe. *J. of Petrology* 27, part 1, 123-154.
- Helgeson, H.C. (1968): Evaluation of irreversible reactions in geochemical processes involving minerals and aqueous solutions I. Thermodynamic relations. *Geochim. Cosmochim. Acta.* 32, 853-877.
- Helgeson H.C., Brown T.H., Nigrini A and Jones T.A (1979): Calculation of mass transfer in geochemical processes involving aqueous solutions. *Geochim. Cosmochim. Acta* 34, 569-592.
- Hoernes, S. and Friedrichsen, H. (1974): Oxygen isotope studies on metamorphic rocks of the Western Hohe Tauern area (Austria). *S.M.P.M.* 54, 769-788.
- Hoernes, S. and Friedrichsen, H. (1978): Oxygen isotope studies on the polymetamorphic area of the Northern Oetztal, Stubai Alps (Tyrol). *Contr. Mineral. Petrol.* 67, 305-315.

- Hoernes, S. and Friedrichsen, H. (1980): Oxygen and hydrogen isotopic compositions of alpine and pre-alpine minerals of the Swiss Central Alps. *Contrib. Mineral. Petrol.*, 72, 19-32.
- Holland, T.J.B. (1979): High water activity in the generation of high pressure kyanite eclogites of the Tauern Window, Austria. *J. Geology* 87/1, 1-27.
- Holland, H.D. and Malini S.D. (1979): The solubility and occurrence of non-ore minerals. In: Barnes H.L. (ed): *Geochemistry of hydrothermal deposits* Wiley N.Y. P. 461-508.
- Hunziker, J.C. (1974): Rb-Sr and K-Ar age determination and the alpine tectonic history of the Western Alps. *Mem. degli Istituti di Geologia e Mineralogia dell' Università di Padova*, Vol. XI, 54 p.
- Hurford, A.J. and Hunziker, J.C. (1985): Alpine cooling history of the Monte Mucreone eclogites (Sesia-Lanzo zone: fission track evidence. *Schweiz. Mineral. Petrogr. Mitt.* 65, 325-334.
- Hotchinson, C.S. (1974): *Laboratory handbook of petrographic techniques*. Wiley and Sons.
- Hy, Ch (1984): *Metamorphisme polyphase et évolution tectonique dans la croûte continentale écoligite: les séries granitiques et pelitiques du Monte Mucreone, (zone Sesia-Lanzo, Alpes Italiennes)*. *Mem. Sc. Terre Univ. Curie, Paris* N° 84-51, 199 p.
- Jaeger, E., Niggli, E. and Wenk, E. (1967): Rb-Sr Altersbestimmungen an Glimmern der Zentralalpen. *Beitr. Geol. Karte Schweiz* NF 134.
- Jaeger, E., Hunziker, J.C., Grauert, B. and Grünenfelder, M. (1969): *Geochronology of phanerozoic orogenic belts. Guide book, field trips, Switzerland*, Unpublished.
- Javoy, M. (1971): Composition isotopique de l'oxygène dans les roches écoligites. *C. R. Acad. Sci. Paris*, 273, 2414-2417.
- Javoy, M. (1977): Stable isotopes and geothermometry. *J. Geol. Soc.* 133, 609-636.
- Javoy, M. et al (1970): Graphical method for examination of $^{18}\text{O}/^{16}\text{O}$ fractionations in silicate rocks. *Earth Plan. Sci. Letters*, 10, 12-16.
- Javoy, M. and Allègre, C.J. (1967): Étude de la composition $^{18}\text{O}/^{16}\text{O}$ de quelques écoligites. *Consequences pétrologiques et géophysiques*. *Bull. Soc. Geol. Fr.* 9, 800-808.
- Kerrick, R., Beckinsale, R.D. and Durham, J. J (1977): The transition between deformation regimes dominated by intercrystalline creep evaluated by oxygen isotope thermometry. *Tectonophysics*, 38, 241-257.
- Kerrick, R., Allison, I., Barnett, R.L., Moss, S. and Starkey, J. (1980): Microstructural and chemical transformations accompanying deformation of granite in a shear zone at Miéville, Switzerland; with implications for stress corrosion cracking and superplastic flow. *Contrib. Mineral. Petrol.* 73, 221-242.
- Kerrick, R., La Tour, T.E. and Willmore, L. (1984): Fluid participation in deep fault zones: evidence from geological, geochemical and $^{18}\text{O}/^{16}\text{O}$ relations. *J. Geophys. res.*, 89, N° B6, 4331-4343.
- Kieffer, S.W. (1982): Thermodynamics and lattice vibration of minerals: Application to phase equilibria, isotopic fractionation and high-pressure thermodynamic properties. *Rew. of Geophys. and Space Phys.* 20, 827-849.
- Koons, P.O. (1981): A study of natural and experimental metasomatic assemblage in an ultramafic-quartzofeldspathic system from the Haast Schist. *New Zealand. Contrib. Mineral. Petrol.* 78, 189-195.
- Koons, P.O. (1982): An investigation of experimental and natural assemblages from the Sesia Zone, Western Alps, Italy. *Unpubl. Dr. Sc. Nat. Thesis, Eth, Zürich*.
- Koons, P.O. (1986): Relative geobarometry from high pressure rocks of quartzofeldspathic composition from the Sesia zone, Western Alps, Italy. *Contrib. Mineral. Petrol.* (in press).
- Koons, P.O. and Thompson, A.B. (1985): Non mafic rocks in the greenschist, blueschist and eclogite facies. *Chem. Geol.* 50, 3-30.

- Koons, P.O., Rubie, D. and Früh-Green, G. (in review) The effect of disequilibrium and deformation on the mineralogical evolution of quartz diorite during metamorphism in the eclogite facies. *J. of Petrol.*
- Kreulen, R. (1980): CO₂-rich fluids during regional metamorphism on Naxos (Grece): carbon isotopes and fluid inclusions. *Am. J. Sci.* 286, 745-771.
- Lambert, S.J. and Epstein, S. (1980): Stable isotope investigations of an active geothermal system in Valles Calderas, New Mexico. *J. Volc. Geotherm. Res.* 8, 111-129.
- Lardeaux, J.M. (1981): Evolution tectono-métamorphique de la zone nord du massif de Sesia-Lanzo (Alpes occidentales): un exemple d'éclogitisation de croûte continentale. Thèse 3eme Cycle., Paris IV.
- Lattanzi, P., Rye, D.M. and Rice, J.M. (1980): Behavior of ¹³C and ¹⁸O in carbonates during contact metamorphism at Maryville, Montana: implications for isotope systematics in impure dolomitic limestones. *Am. J. Sci.*, 280, 890-906.
- Manning, J.R. (1968): Diffusion kinetics for atoms in crystals. Van Norstrand Co., Princeton, 257 pp.
- Manning, J.R. (1974): Diffusion kinetics and mechanisms in simple crystals. In: Hoffman et al (eds) *Geochemical transports and kinetics.*, Carnegie Inst. Washington Publ. 634, 3-13.
- Margaritz, M. and Taylor, H.P. (1976): O, H and C-isotope studies of the Franciscan Formation. *Geochim. Cosmochim. Acta*, 40, 215-234.
- Matsuhisa, Y, Goldsmith, J.R. and Clayton, R.N. (1979): Oxygen isotopic fractionation in the system quartz-albite-anorthite-water. *Geochim. Cosmochim. Acta*, 43, 1131-1140.
- Matthews, A. (1979): Oxygen isotope fractionation between rutile and water and geothermometry of metamorphic eclogites. *Min. Mag.* , 43, 405-413.
- Matthews, A. and Kolodny, Y. (1978) Oxygen isotope fractionation in decarbonation metamorphism: the mottled zone event. *Earth and Plan. Sci. Letters* 39, 179-192.
- Matthews, A., Goldsmith, J.R. and Clayton, R.N. (1980): ¹⁸O/¹⁶O and ¹⁷O/¹⁶O fractionation studies on Ca-Mg silicate minerals. *Trans. Am. Geophys. Union* 61: 403 (Abstract).
- Matthews, A., Goldsmith, J.R. and Clayton, R.N. (1983): On the mechanisms and kinetics of oxygen isotope exchange in quartz and feldspars at elevated temperatures and pressures. *GSA Bull.*, 94, 393-412.
- Matthews, A. et al (1983): Oxygen isotope fractionation involving pyroxenes: the calibrations of mineral pair geothermometers. *Geochim. Cosmochim. Acta*, 47, 631-644.
- Matthews, A. et al (1983): Oxygen isotope fractionation between zoisite and water *Geochim. Cosmochim. Acta* 47, 645-654.
- Mühlenbachs, K. and Clayton, R.N. (1971) Oxygen isotope studies of fresh and weathered submarine basalts. *Can. J. Earth Sci.*, 9, 172-184.
- Mühlenbachs, K. and Clayton, R.N. (1972): Oxygen isotope geochemistry of submarine greenstones. *Can. J. Earth Sci.*, 9, 471-478.
- Mühlenbachs, K and Kushiro I. (1974): Oxygen isotopic exchange and equilibrium of silicates with CO₂ or O₂. *Carnegie Inst. Wash. Yearbook* 73, 232-236.
- Mühlenbachs, K. and Clayton, R.N. (1976): Oxygen isotopic composition of the oceanic crust and its beaving on seawater. *J. Geophys. res.* 81, 4365-4369.
- Nagy, K.L. and Parmentier, E.M. (1982): Oxygen isotope exchange at an igneous contact. *Earth Plan. Sci. Letters* 59, 1-10.
- Norris, R.J. and Henley, R.W. (1976): Dewatering of a metamorphic pile. *Geol.*, 4, 333-336.
- Norton, D. and Knapp (1977): Transport phenomena in hydrothermal systems: the nature of porosity. *Am. J. Sci.* 277, 913-936.
- Norton, D. and Knight, J. (1977): Transport phenomena in hydrothermal systems: cooling plutons. *Am. J. Sci.*, 277, 937-981.

- Norton, D. and Taylor, H.P. (1979): Quantitative simulation of hydrothermal systems of crystallising magmas on the basis of transport theory and oxygen isotope data: Skaergaard intrusion. *J. Petrology*, 20, 421-486.
- Oberhänsli, R., Hunziker, J.C., Martinotti, G. and Stern, W.B. (1982): Mucronites: an example of Eo-Alpine eclogitisation of Permian granitoids, Italy. *Terra Cognita*, 2, 325.
- Oberhänsli, R., Hunziker, J.C., Martinotti, G. and Stern, W.B. (1985): Monte Mucrone: an example of Eo-Alpine eclogitisation of Permian granitoids, Sesia-Lanzo Zone (western Alps). *Chem. Geol. (Isotope geoscience section)* 52, 165-184.
- Ohmoto H. and Kerrick D (1977): Devolatilisation equilibria in graphic systems. *Am.J. Sci.*, 1013-1044.
- O' Neil, J.R. (1979): Stable isotope geochemistry. *Rew. Geophys. Space Phys.* 17, 839-850.
- O' Neil, J.R. (1986): Theoretical and experimental aspects of isotopic fractionation. In: Valley J.W., Taylor H.P and O'Neil J.R (eds): *Stable isotopes in high temperature geological processes. Rew in Mineralogy Vol. 16*, Am. Mineral. Soc., 1-40.
- O' Neil, J.R. and Taylor, H.P. (1967): The oxygen isotope and cation exchange chemistry of feldspars. *Am. Min.* 52, 1414-1437.
- O' Neil, J.R., Clayton R.N. and Mayeda T.K. (1969): Oxygen isotope fractionation in divalent metal carbonates. *J. Chem. Phys.* 51, 5547-5558.
- O' Neil, J.R. and Taylor, H.P. (1969): Oxygen isotope equilibrium between muscovite and water. *J. Geophys. res.*, 74, 6012-6022.
- O' Neil, J.R. and Ghent E.D. (1975): Stable isotope study of coexisting metamorphic minerals from the Esplanade Range, British Columbia. *Bull. Geol. Soc. Am.* 86-1078-1712.
- O' Neil, J.R. and Kharaka, Y. (1976): Hydrogen and oxygen isotope exchange reactions between clay minerals and water. *Geochim. Cosmochim. Acta* 40, 241-246.
- Passchier, C.W. and Simpson C. (1985): Porphyroclast systems as kinematic indicators. Personal preprint.
- Pfeifer, H. R. (1978): Hydrothermal alpine metamorphism in metaperidotite rocks of the Cima Lunga Zone, Valle Verzasca, Switzerland. *S.M.P.M.* 58, 400-405.
- Pfeifer, H.R. (1981): A model for fluids in metamorphosed ultramafic rocks. 3. Mass transfer under amphibolite conditions in olivine-enstatite rock of the Central Alps, Switzerland. *Bull. Mineral.* 104, 834-847.
- Pineau, F., Javoi, M., Hawkins, J.W. and Craig, H. (1976): Oxygen isotope variations in marginal basins and ocean-ridge basalts. *Earth Plan. Sci. Letters* 28, 299-307.
- Poirier, J.P. Bouchez, J.L. and Jonas, J.J. (1979): A dynamic model for aseismic ductile shear zones. *Earth and Plan. Sci. Letters.* 43, 441-453.
- Ramsay, J.G. (1967): *Folding and fracturing of rocks*. Mac Graw Hill, N.Y. 568 pp.
- Ramsay, J.G. (1980): The crack seal mechanism of rock deformation. *Nature* 248, 139-139.
- Richet, P., Bottinga Y. and Javoy, M. (1977): A review of hydrogen, carbon, nitrogen, oxygen, sulphur and chlorine stable isotope fractionation among gaseous molecules. *Ann. Rew. Earth and Plan. Sci.* 5, 65-110.
- Ridley, J. The effect of reaction enthalpy on the progress of a metamorphic reaction. In Thompson A.B. and Rubie D.C. (eds): *Metamorphic reactions, kinetics, textures and deformation Advances in Physical Geochemistry Vol. 4.*, 80-95.
- Ridley, J. and Dixon, J.E. (1984): Reaction pathways during the progressive deformation of a blueschist metabasite: the role of chemical disequilibrium and restricted range equilibrium. *J. Metam. Geol.* 2, 115-128.

- Ridley, J. and Thompson, A.B. (1986): The role of mineral kinetics in the development of metamorphic microtextures. In: Walther J.V. and Wood B.J. (eds): Fluid-rock interactions during metamorphism. *Advances in Physical Geochemistry Vol 5*, Springer Verlag N.Y.
- Roedder, E. (ed) (1984): Fluid inclusions. *Reviews in Mineralogy 12*. Mineral. Soc. Am.
- Rubie, D.C. (1983): Reaction-enhanced ductility: the role of solid-solid univariant reaction in deformation of the crust and mantle. *Tectonophysics 96*, 331-352.
- Rubie, D. C. (1984): A thermal-tectonic model for high-pressure metamorphism and deformation in the Sesia Zone, Western Alps. *J. Geol.* 92, 21-36.
- Rubie, D.C (1986): The catalysis of mineral reactions by water and restrictions on the presence of aqueous fluid during metamorphism. *Min. Mag.* 50, 399-415.
- Rubie, D.C. and Thompson A.B. (1985): Kinetics of metamorphic reactions at elevated temperatures and pressures: an appraisal of available experimental data In: Thompson A.B. and Rubie D.C. (eds): *Metamorphic reactions, kinetics, textures and deformation Advances in Physical Geochemistry Vol. 4.*, 27-79.
- Rumble, D (1978)... Mineralogy and oxygen isotopic geochemistry of the Clough Formation, Black Mtn. West N.H., USA. *J. Petrol.* 19, 317-340.
- Rumble, D. (1979): O-isotope fractionation during regional metamorphism. *Annual Report of the Director, Geophysical Laboratory, Carnegie Inst. of Wa.; Yearbook 79*, 328-332.
- Rumble, D. (1982): Stable isotope fractionation during metamorphic devolatilisation reactions. In: *Reviews in Mineralogy- Vol 10*. Chapter 8. Mineralogical Society of America.
- Rumble, D. and Hoering T.C. (1980): O-isotope fractionation during regional metamorphism. *Annual Report of the Director, Geophysical Laboratory, Carnegie Inst. of Wa.; Yearbook 80*, 363-370.
- Rumble, D., Ferry, F.M., Hoerring, T.C. and Boucot, A.J. (1982): Fluid flow during metamorphism at the Beaver Brook fossil locality, New Hampshire. *Am. J. Sci.* 282, 886-919.
- Rumble, D. III and Spear, F. (1983): Oxygen isotope equilibrium and permeability enhancement during regional metamorphism. *J. Geol. Soc. London* 140, 619-628.
- Rutter, E.H. (1976): The kinetics of rock deformation by pressure solution. *Phil. Trans. R. Soc. London* 283A, 203-219.
- Rutter, E.H. (1983): Pressure solution in nature, theory and experiment. *J. Geol. Soc. London* 140, 725-740.
- Rutter, E.H. and Brodie, K.H (1985): The permeation of water into hydrating shear zones. In: Thompson, A.B. and Rubie, D.C. (eds): *Metamorphic reactions, kinetics, textures and deformation Advances in Physical Geochemistry Vol. 4.*, 242-250.
- Rye, R.O., Schilling, D.M., Rye, D.M. and Jansen, L.B.H. (1967): Carbon, hydrogen and oxygen isotope studies of the regional metamorphic complex at Naxos, Greece. *Geochim. Cosmochim. Acta* 40, 1031-1049.
- Savin, S.M. and Epstein, S. (1970): The oxygen and hydrogen isotope geochemistry of clay minerals. *Geochim. Cosmochim. Acta* 34, 25-42.
- Savin, S.M. and Epstein, S. (1970): The oxygen and hydrogen isotope geochemistry of ocean sediments and shales. *Geochim. Cosmochim. Acta* 34, 43-64.
- Schläpfer, E. (1978): *Metamorphose und Strukturen der Cima Lunga-Serie: Lago d' Efra-Val Gagnone*. Diploma thesis ETH zürich.
- Schmid, S.M. (1982): Microfabric studies as indicators of deformation mechanisms and flow laws operative in mountain building. In Hsü K.J. (Ed): *Mountain building processes.*, Academic Press.
- Schwarcz, H.P., Clayton, R.N. and Mayeda, T.K. (1970): Oxygen isotopic studies of calcareous and pelitic metamorphic rocks, New England. *Bull. Geol. Soc. Am.* 81, 2299-2316.

- Segall, P. and Simpson, C. (1986): Nucleation of ductile shear zones on dilatant fractures. *Geology*.
- Sheppard, S.M.F. (1977): Identification of the origin of ore-forming solutions by the use of stable isotopes. In: *Volcanic processes in ore genesis*. Institute of Mining and Metallurgy and Geol. Soc. London. p. 25-41.
- Sheppard, S.M.F. (1981): Stable isotope geochemistry of fluids. In: Rickard D.T. and Wichman F.E. (Ed): *Chemistry and geochemistry of solutions at high temperatures and pressures*. *Phys. Chem. Earth* 13/14, 419-445.
- Sheppard S.M.F. (1986): Characterisation and isotopic variation in natural waters. In: Valley J.W., Taylor H.P and O'Neil J.R (eds): *Stable isotopes in high temperature geological processes*. *Rev in Mineralogy* Vol. 16, Am. Mineral. Soc., 165-184.
- Sheppard, S.M.F., Nielson, R.L. and Taylor, H.P. (1969): Oxygen and hydrogen isotope ratios of clay minerals from Porphyry copper deposits. *Econom. Geol.* 64, 755-780.
- Sheppard, S.M.F. and Epstein, S. (1970): D/H and $^{18}\text{O}/^{16}\text{O}$ ratios of minerals of possible mantle or lower crust origin. *Earth Plan. Sci. Letters* 9, 232-239.
- Shieh, Y.N and Taylor, H.P. (1969): Oxygen and carbon isotope studies of contact metamorphism of carbonate rocks. *J. Petrol.* 10, 307 p.
- Shieh, Y.N. and Schwarcz, H.P. (1974): Oxygen isotope studies of granite and migmatite, Greenville Province of Ontario, Canada. *Geochim. Cosmochim. Acta* 38, 21-45.
- Sibson, R.H. (1981): Fluid flow accompanying faulting: field evidence and models. In: Simpson, D.W. and Richards, *Earthquake Prediction: An international review*. Maurice Ewing Ser. AGU Washington D.C., Vol 4, 593-604.
- Sibson, R.H. (1983): Continental fault structure and the shallow earthquake source. *J. Soc. Geol. London* 140, 741-767.
- Silverman, R.R. (1951): The isotope geology of oxygen. *Geochim. Cosmochim. Acta.*, 2, 26-42.
- Simpson, C. (1980): Some criteria to determine the sense of movement in sheared rocks. (manuscript).
- Simpson, C. (1982): Strain and shape fabric variations associated with ductile shear zones. *J. Struct. Geol.* 5, 61-72.
- Simpson, C. (1984): Borrego Springs-Santa Rosa mylonite zone: A late Cretaceous west-directed thrust in southern California. *Geology* 12, 8-11.
- Simpson, C. (1985): Deformation of granitic rocks across the brittle-ductile transition. *J. Struct. Geol.* 7, 503-511.
- Simpson, C., Carreras, J. and Losantos, M. (1982): Inhomogeneous deformation in roses granodiorite, N.E. Spain. *Acta Geol. Hispanica* 17, 219-226.
- Smith, B.M. and Giletti, B.J. (1979). The nature of fluids near a granite-limestone contact, Isle of Skye, NW Scotland. *Trans. Am. Geophys. Union*, 60, 417.
- Spooner, E.T.C., Beckinsale, R.D., Fyfe, W.S. and Smewing, J.D. (1974): ^{18}O enriched ophiolitic metabasic rocks from E. Liguria (Italy), Pindos (Greece) and Troodos (Cyprus). *Contrib. Mineral. Petrol.* 47, 41-62.
- Stäubli, J. (1978): *Metamorphose und Strukturen der Cima Lunga-Serie: II Val d' Agro*. Diploma thesis ETH zürich.
- Stern, M.J. et al (1968): Temperature dependence of isotope effects. *J. Chem Phys.* 48, 2909.
- Streckeisen, A. (1976): To each plutonic rock its proper name. *Earth Sci. Rev.*, 12, 1-33.
- Suzuoki, T. and Epstein, S. (1976): Hydrogen isotope fractionation between OH-bearing minerals and water. *Geochim. Cosmochim. Acta* 40, 1229-1240.
- Taylor, H.P. (1967): Oxygen isotope studies of hydrothermal mineral deposits. In: Barnes, H.L. (Ed) *Geochemistry of Hydrothermal ore deposits*. Holt, Rinehart and Winston Inc. New York. p. 109-142.
- Taylor, H.P. (1968): The oxygen isotope geochemistry of igneous rocks. *Contrib. Mineral. Petrol.* 19, 1-71.

- Taylor, H.P. Jr. (1971): Oxygen isotope evidence for large scale interaction between ground water and Tertiary granodioritic intrusives, W. Cascades Range. *J. Geophys. Res.* 76, 7855-7874.
- Taylor, H.P. Jr. (1977): Water/rock interactions and the origin of H₂O in granitic batholiths. *J. Geol. Soc. London.* 133, 509-558.
- Taylor, H.P. (1979): Oxygen and hydrogen isotope relationships in hydrothermal mineral deposits. In . Barnes, Ed., *Geochemistry of hydrothermal ore deposits*, 2nd ed. p. 236-277.
- Taylor, H.P. and Epstein, S. (1962): Relation between ¹⁸O/¹⁶O ratios in coexisting minerals of igneous and metamorphic rocks.
 1. Principles and experimental results. *Geol. Soc. Amer. Bull.* 73, 461.
 2. Application to petrologic problems. *Geol. Soc. Amer. Bull.* 73, 675.
- Taylor, H.P., Albee, A.L. and Epstein, S. (1963): ¹⁸O/¹⁶O ratios of coexisting minerals in three assemblages of kyanite-zone pelitic schists. *J. Geology* 71, 513-522.
- Taylor, H.P. and Coleman, R.G. (1968): ¹⁸O/¹⁶O ratios of coexisting minerals in glaucophane-bearing metamorphic rocks. *Geol. Soc. Am. Bull.* V. 79, 1727-1756.
- Taylor, H.P. Jr, and Forester, R.W. (1979): An oxygen and hydrogen isotope study of the Skaergaard intrusion and its country rocks. A description of 55 my. old fossil hydrothermal system. *J. Petrol.* 20, 355-419.
- Thompson, A.B. and England, P.C. (1984): Pressure-temperature-time paths of regional metamorphism. II some petrological constraints from mineral assemblages in metamorphic rocks. *J. Petrol* 25, 929-955.
- Thompson, A.B. and Rubie, D.C. (eds)(1985): *Metamorphic reactions, kinetics, textures and deformation Advances in Physical Geochemistry Vol. 4.*, 277 p.
- Thompson, J.B., Laird, J. and Thompson, A.B. (1982): Reaction in amphibolite, greenschist and blueschists. *J. Petrol.* 23, 1-27.
- Tracy, R.J., Rye, D.M., Hewitt, D.A. and Schiffries, C.M. (1983): Petrologic and stable-isotopic studies of fluid-rock interactions, South-Central Connecticut: I. The role of infiltration in producing reaction assemblages in impure marbles. *Am. J. Sci.* 283-A, 589-616.
- Trommsdorff, V. (1980): Excursion to Corte di Cima-Val Agro-Lavertzezzo. In Trümpy, Ed., *Geology of Switzerland - Part 2: A guidebook.* stop 28, p. 313. Wepf, Basel.
- Trommsdorff, V., Evans, B.W. and Richter, W. (1975): Eklogit/Rodingit-Übergänge in Ultramafititen der Cima Lunga Serie. *S.M.P.M.* 55, 572-574.
- Truesdell, H. (1974): Oxygen isotope activities and concentrations in aqueous salt solutions at elevated temperatures. *Earth plan. Sci. Lett.* 23, 386-396.
- Tullis, J.A. and Yund, R.A. (1977): Experimental deformation of dry aWesterly granite. *J. Geophys. Res.* 82, 5705-5718.
- Tullis, J.A, Shelton, G.L. and Yund, R.A. (1979): Pressure dependences of rock strength: implications for rock weakening. *Bull. Mineral.* 102, 110-114.
- Tullis, J.A and Yund, R.A. (1980): Hydrolic weakening of experimentally deformed Westerly granite and Hale albite rock. *J. Struct. Geol.* 2, 439-451.
- Tullis, J.A and Yund, R.A. (1982): Grain growth kinetics of quartz and calcite aggregates. *J. Geol.* 90, 301-318.
- Urey, H.C. (1947): The thermodynamic properties of isotopic substances. *J. Chem. Soc.*, 562-581.
- Vernon, R.H. (1977): Relationships between microstructures and metamorphic assemblages. *Tectonophysics* 39, 43-52.
- Vogel, D.E. and Garlick, G.D. (1970): Oxygen isotope ratios in metamorphic eclogites. *Contrb. Mineral. Petrol.* 28, 183-191.
- Valley, J.W., Taylor, H.P and O'Neil, J.R (eds) (1986): *Stable isotopes in high temperature geological processes.* Rew in *Mineralogy Vol. 16*, Am. Mineral. Soc. 570p.

- Walther, J.V and Helgeson, H.C (1980): Description and interpretation of metasomatic phase relations at high pressure and temperatures: 1 Equilibrium activities of ionic species in nonideal mixtures of CO₂ and H₂O. *Am. J. Sci.* 280, 575-606.
- Walther, J.V. and Orville, P.M. (1982) Volatile production and transport in regional metamorphism. *Contrib. Mineral. Petrol.* 79, 252-257.
- Walther, J.V. and Wood, B.J. (eds) (1986): Fluid-rock interactions during metamorphism. *Advances in Physical Geochemistry Vol 5*, Springer Verlag N.Y.
- Walther, J.V. and Wood, B.J. (1986): Mineral-fluid reaction rates. In: Walther, J.V. and Wood, B.J. (eds): Fluid-rock interactions during metamorphism. *Advances in Physical Geochemistry Vol 5*, Springer Verlag N.Y.
- Wood, B.J. and Graham, C.M. (1986): Infiltration of aqueous fluid and high fluid/rock ratios during greenschist facies metamorphism: a discussion. *J. Petrol.*, 27, 751-761.
- Wood, B.J. and Walther, J.V. (1986): Fluid flow during metamorphism and its implications for fluid-rock ratios. In: Walther J.V. and Wood B.J. (eds) Fluid-rock interactions during metamorphism. *Advances in Physical Geochemistry Vol 5*, Springer Verlag N.Y.
- Wenner, D.B. and Taylor, H.P. (1971): Temperatures of serpentinisation of ultramafic rocks based on ¹⁸O/¹⁶O fractionation between coexisting serpentine and magnetite. *Contrib. Mineral. Petrol.* 32, 165-185.
- Wenner, D.B. and Taylor, H.P. (1973): Oxygen and hydrogen isotope studies of the serpentinisation of ultramafic rocks in oceanic environments and continental ophiolite complexes. *Am. J. Sci.* 273, 207-239.
- White S. (1976): The effect of strain on the microstructures, fabrics and deformation mechanisms in quartzites. *Phil. Trans. R. Soc. London, A* 283, 69-86.
- White, S.H. and Knipe, R.J. (1978): Transformation and reaction enhanced ductility in rocks. *J. Geol. Soc. London* 135, 513-516.
- Wilson, A.F., Green, D.C. and Davidson, L.R. (1970): The use of oxygen isotope geothermometry on the granulites and related intrusives, Musgrave Range, Central Australia. *Contr. Mineral. Petrol.* 27, 166-178.
- Yardley, B.W.D. (1977): The nature and significance of the mechanism of sillimanite growth in the Connemara schists, Ireland. *Contrib. Mineral. Petrol.* 65, 53-58.
- Yardley, B.W.D. (1983): Heat of reaction- the key to metamorphic kinetics? (Abstract) *J. Geol. Soc. London* 140, 162.
- Yardley, B.W.D. (1986): Fluid migration in the connemara schists, Ireland. In: Walther J.V. and Wood B.J. (eds): Fluid-rock interactions during metamorphism. *Advances in Physical Geochemistry Vol 5*, Springer Verlag N.Y.
- Yund, R.A. (1983): Diffusion in feldspars. In: Ribbe P.H. (Ed) *Feldspar Mineralogy. Rev. In Mineralogy*, 2. Mineral. Soc. America. 203-222.
- Yund, R.A. and Anderson, T.F. (1974): Oxygen isotope exchange between potassium feldspar and KCl solution. In: A.W. Hoffmann, B.J. Giletti, H.S. Yoder Jr., R.A. Yund (eds) *Geochemical transport and kinetics*, pp. 99-105. Washington DC: carnegie inst. Washington Yearb. Publ. 643.
- Yund, R.A. and Anderson, T.F. (1978): The effect of fluid pressure on oxygen isotope exchange between feldspar and water. *Geochim. Cosmochim. Acta* 42, 235-239.
- Yund, R.A. and Tullis, J. (1980) : The effect water, pressure and strain on Al/Si order-disorder kinetics in feldspar. *Contrib. Mineral. Petrol.* 72, 297-302.
- Yund, R.A. , Smith, B.M. and Tullis, J. (1981): Dislocation assisted diffusion of oxygen in albite. *Phys. Chem. Minerals* 7, 185-189.
- Zingg, A. (1978): *Metamorphose und Strukturen der Cima Lunga-Serie: III Val d' Efra.* Diploma thesis ETH zürich.

**Electron Microprobe Analyses of Garnet from Metapelites at the
Cima di Gagnone Area. Samples exhibit equilibrium textures.
Analyses are given in weight % oxides.**

FINE GRAINS
 <----- CORES -----> <----- RIMS ----->
 23 26 39 45 40 42 46
 CL12 GR10 CL12 GR11 CL12 GR12 CL12 GR15 CL12 GR13 CL12 GR14 CL12 GR16
 Sample
 Coexisting BIO 6 BIO 8 BIO 11
 Biotite Sample

Sample	5	16	48	50	6	17	19	51
SiO2	38.31	38.24	37.53	38.89	37.92	37.00	37.13	37.91
TiO2	0.00	0.12	0.00	0.14	0.00	0.00	0.00	0.00
Al2O3	21.50	21.86	21.66	22.30	21.19	21.14	21.08	22.27
Fe2O3	1.14	0.00	0.00	0.00	0.00	0.32	0.00	0.00
FeO	27.72	29.24	29.33	27.88	30.98	32.29	31.79	30.59
MnO	1.34	1.03	2.28	1.66	1.86	2.24	2.69	1.40
MgO	7.03	5.81	5.15	6.62	3.82	4.16	3.56	4.18
CaO	3.60	3.48	3.23	3.66	3.42	2.05	2.34	4.10
Na2O	0.03	0.03	0.00	0.03	0.00	0.00	0.04	0.04
K2O	0.00	0.00	0.00	0.00	0.02	0.00	0.00	0.00
Total	100.67	99.82	99.18	101.18	99.21	99.21	98.61	100.49

CATIONS assuming stoichiometry and charge balance

	5	16	48	50	6	17	19	51
Si	2.9696	3.0031	2.9826	2.9958	3.0407	2.9764	3.0091	2.9847
Ti	0.0000	0.0074	0.0000	0.0082	0.0000	0.0000	0.0000	0.0000
Al	1.9638	2.0235	2.0290	2.0246	2.0027	2.0043	2.0133	2.0659
Fe3	0.0667	0.0000	0.0000	0.0000	0.0000	0.0193	0.0000	0.0000
Fe2	1.7969	1.9200	1.9491	1.7957	2.0775	2.1721	2.1544	2.0139
Mn	0.0877	0.0686	0.1534	0.1086	0.1264	0.1526	0.1845	0.0936
Mg	0.8118	0.6798	0.6106	0.7601	0.4571	0.4983	0.4302	0.4900
Ca	0.2991	0.2929	0.2754	0.3019	0.2940	0.1770	0.2028	0.3457
Na	0.0045	0.0047	0.0000	0.0051	0.0000	0.0000	0.0057	0.0062
K	0.0000	0.0000	0.0000	0.0000	0.0017	0.0000	0.0000	0.0000
Grossular	0.066	0.094	0.092	0.097	0.099	0.049	0.068	0.117
Almandine	0.600	0.647	0.652	0.604	0.703	0.724	0.725	0.684
Pyrope	0.271	0.229	0.204	0.256	0.155	0.166	0.145	0.166
Spessartine	0.029	0.023	0.051	0.037	0.043	0.051	0.062	0.032
Andradite	0.033	0.000	0.000	0.000	0.000	0.010	0.000	0.000
Ti-Al Garnet	0.000	0.001	0.000	0.002	0.000	0.000	0.000	0.000
Na-Ti Garnet	0.000	0.005	0.000	0.005	0.000	0.000	0.000	0.000

ENDMEMBERS

CATIONS assuming stoichiometry and charge balance

	23	26	39	45	40	42	46
Si	2.9706	2.9706	3.0241	3.0202	3.0527	2.9666	3.0198
Ti	0.0000	0.0114	0.0000	0.0000	0.0091	0.0000	0.0000
Al	2.0702	1.9851	1.9292	2.0217	2.0177	2.0635	2.0303
Fe3	0.0000	0.0329	0.0708	0.0000	0.0000	0.0000	0.0000
Fe2	2.1285	2.2372	2.1558	2.1844	2.1955	2.2025	2.1643
Mn	0.1551	0.2072	0.1594	0.1390	0.2034	0.2145	0.1842
Mg	0.4460	0.3898	0.4500	0.4410	0.3809	0.3885	0.4108
Ca	0.2255	0.1625	0.2010	0.1938	0.1340	0.1581	0.1858
Na	0.0041	0.0034	0.0079	0.0000	0.0068	0.0064	0.0048
K	0.0000	0.0000	0.0017	0.0000	0.0000	0.0000	0.0000
Grossular	0.076	0.031	0.032	0.066	0.040	0.053	0.063
Almandine	0.720	0.746	0.727	0.738	0.752	0.743	0.735
Pyrope	0.151	0.130	0.152	0.149	0.130	0.131	0.139
Spessartine	0.053	0.069	0.054	0.047	0.070	0.072	0.063
Andradite	0.000	0.016	0.036	0.000	0.000	0.000	0.000
Ti-Al Garnet	0.000	0.004	0.000	0.000	0.001	0.000	0.000
Na-Ti Garnet	0.000	0.003	0.000	0.000	0.007	0.000	0.000

ENDMEMBERS

CL12 GRAPHTS
 表表表表表表表表表表

Electron Microprobe Analyses of Garnet from Metapelites at the
Cima di Gagnone Area. Analyses are given in weight % oxides.

Equilibrium Textures

Disequilibrium Textures

CH99 GARNETS

CL4A GARNETS

<----- CORE -----> <----- RIMS ----->

<----- CORE -----> <----- RIMS ----->

Sample	42	43	56	64	38	39	41	63	39	43	44	40	45
CH99 GR5B CH99 GR5C CH99 GR6E CH99 GR8 CH99 GR4D CH99 GR4E CH99 GR5A CH99 GR7	CH99 GR5B CH99 GR5C CH99 GR6E CH99 GR8 CH99 GR4D CH99 GR4E CH99 GR5A CH99 GR7	CL4A GR1	CL4A GR4	CL4A GR4	CL4A GR4	CL4A GR4	CL4A GR2	CL4A GR5	CL4A GR4	CL4A GR4	CL4A GR4	CL4A GR2	CL4A GR5
Coexisting	BID 9						BID 9					BID 5	BID 7
Biotite Sample													
SiO2	38.30	38.65	39.11	38.36	37.62	39.22	39.02	37.41	38.45	39.13	38.99	38.43	38.66
TiO2	0.00	0.00	0.00	0.00	0.00	0.04	0.00	0.00	0.00	0.00	0.00	0.00	0.00
Al2O3	20.04	21.51	21.45	20.65	20.13	21.07	21.31	20.83	20.68	21.11	20.67	20.77	20.47
Fe2O3	1.90	0.00	0.62	1.17	1.40	0.93	0.28	0.62	1.01	0.87	1.59	1.10	1.25
FeO	29.89	30.37	28.72	30.45	27.23	28.26	31.14	31.28	24.02	24.16	24.39	25.12	24.56
MnO	3.74	2.49	0.77	1.99	1.46	0.59	3.93	2.77	2.34	1.30	2.81	3.79	4.51
MgO	3.39	3.91	5.67	4.25	5.26	5.84	3.24	3.72	3.13	2.91	3.22	3.25	3.34
CaO	3.36	3.67	4.67	3.55	3.95	4.29	2.56	3.17	9.53	11.03	9.43	7.82	6.68
Na2O	0.00	0.00	0.00	0.00	0.05	0.00	0.00	0.00	0.00	0.00	0.00	0.03	0.00
K2O	0.01	0.03	0.00	0.00	0.41	0.02	0.03	0.01	0.00	0.01	0.00	0.00	0.02
Total	100.62	100.63	101.01	100.43	97.51	100.25	101.51	99.81	99.16	100.53	101.10	100.32	99.49

CATIONS assuming stoichiometry and charge balance

CATIONS assuming stoichiometry and charge balance

Si	Ti	Al	Fe3	Fe2	Mn	Mg	Ca	Na	K
3.0592	0.0000	1.8860	0.1140	1.9959	0.2529	0.4036	0.2873	0.0000	0.0012
3.0524	0.0000	2.0017	0.0000	2.0058	0.1667	0.4600	0.3102	0.0000	0.0032
3.0383	0.0000	1.9640	0.0360	1.8656	0.0506	0.6566	0.3888	0.0000	0.0000
3.0421	0.0000	1.9303	0.0697	2.0191	0.1339	0.5028	0.3020	0.0000	0.0000
3.0368	0.0000	1.9147	0.0853	1.8381	0.0997	0.6335	0.3412	0.0082	0.0426
3.0690	0.0023	1.9432	0.0545	1.8495	0.0394	0.4811	0.3594	0.0000	0.0015
3.0809	0.0000	1.9832	0.0168	2.0558	0.2630	0.3813	0.2164	0.0000	0.0027
2.9966	0.0000	1.9660	0.0374	2.0952	0.1878	0.4437	0.2718	0.0000	0.0015
3.0512	0.0000	1.9487	0.0513	1.5824	0.0863	0.3396	0.9258	0.0000	0.0014
3.0512	0.0000	1.9066	0.0934	1.5959	0.1863	0.3758	0.7908	0.0000	0.0000
3.0368	0.0000	1.9345	0.0655	1.6391	0.2536	0.3832	0.6621	0.0047	0.0000
3.0850	0.0000	1.9249	0.0751	1.6391	0.3047	0.3980	0.5715	0.0000	0.0018

ENDMEMBERS

ENDMEMBERS

Grossular	Almandine	Pyrope	Spessartine	Andradite	Ti-Al Garnet
0.040	0.679	0.137	0.086	0.058	0.000
0.105	0.682	0.156	0.057	0.000	0.000
0.113	0.630	0.222	0.017	0.018	0.000
0.067	0.683	0.170	0.045	0.035	0.000
0.073	0.631	0.217	0.034	0.044	0.000
0.094	0.631	0.233	0.013	0.028	0.001
0.066	0.705	0.131	0.090	0.009	0.000
0.072	0.699	0.148	0.063	0.019	0.000
0.289	0.539	0.116	0.029	0.026	0.048
0.245	0.544	0.126	0.054	0.031	0.033
0.221	0.541	0.127	0.063	0.048	0.033
0.191	0.561	0.130	0.086	0.033	0.039
0.158	0.563	0.137	0.105	0.039	0.039

**Electron Microprobe Analyses of Garnet from Metapelites at the
Cima di Gagnone Area. Samples exhibit disequilibrium textures.
Analyses are given in weight % oxides.**

CZ78 GARNETS

Sample Coexisting Biotite Sample	C O A R S E G R A I N S										F I N E G R A I N S									
	4	7	11	17	30	5	8	12	18	29	9	19	22	79	74	78	80	81		
	C278 GR1	C278 GR4	C278 GR8	C278 GR10	C278 GR17	C278 GR2	C278 GR5	C278 GR9	C278 GR11	C278 GR16	C278 GR6	C278 GR12	C278 GR13	C278 GR25	C278 GR22	C278 GR24	C278 GR26	C278 GR27		
SiO2	39.40	38.68	39.05	39.90	39.85	38.59	38.96	39.47	38.40	38.90	39.36	40.17	39.21	38.70	38.77	38.53	38.53	38.24		
TiO2	0.00	0.54	0.00	0.00	0.00	0.00	0.00	0.00	0.00	0.00	0.00	0.00	0.00	0.05	0.06	0.00	0.06	0.05		
Al2O3	21.01	20.95	21.09	21.38	20.06	21.34	20.38	21.46	20.48	21.09	21.41	21.22	21.53	20.76	21.38	21.11	21.98	21.73		
Fe2O3	1.39	0.70	0.95	0.94	2.44	0.55	1.72	0.61	1.63	1.15	0.62	1.21	0.72	1.56	0.66	0.88	0.00	0.35		
FeO	26.43	28.82	26.72	26.57	25.77	30.90	29.62	28.84	29.76	28.80	28.46	25.76	28.25	30.45	30.81	32.34	32.26	30.44		
MnO	0.53	0.95	0.59	0.72	0.88	0.88	0.99	0.53	1.13	0.86	0.62	0.31	1.19	1.22	1.25	1.46	1.32	1.21		
MgO	6.98	6.36	6.18	7.05	5.96	5.60	5.15	5.23	5.67	5.84	6.21	7.15	5.36	5.89	5.39	4.99	4.83	5.62		
CaO	4.67	3.55	5.25	4.17	5.05	2.92	3.46	4.95	3.18	4.42	3.89	4.69	5.52	2.82	3.32	2.21	2.22	3.36		
Mg2O	0.02	0.00	0.00	0.00	0.00	0.03	0.00	0.05	0.00	0.00	0.00	0.05	0.00	0.00	0.00	0.00	0.00	0.00		
K2O	0.00	0.00	0.00	0.00	0.00	0.00	0.00	0.00	0.00	0.00	0.00	0.00	0.00	0.02	0.02	0.02	0.04	0.02		
Total	100.43	100.55	99.83	100.73	100.02	100.81	100.28	101.15	100.26	101.05	100.58	100.54	101.78	101.46	101.65	101.54	101.23	101.02		
	C O A R S E G R A I N S										F I N E G R A I N S									
	C O R E S										C O R E S									
	R I M S										R I M S									
	B I O 1										B I O 21									
	B I O 1										B I O 23									
	C O R E S										C O R E S									
	R I M S										R I M S									
	B I O 1										B I O 21									
	B I O 1										B I O 23									
	C O R E S										C O R E S									
	R I M S										R I M S									
	B I O 1										B I O 21									
	B I O 1										B I O 23									
	C O R E S										C O R E S									
	R I M S										R I M S									
	B I O 1										B I O 21									
	B I O 1										B I O 23									
	C O R E S										C O R E S									
	R I M S										R I M S									
	B I O 1										B I O 21									
	B I O 1										B I O 23									
	C O R E S										C O R E S									
	R I M S										R I M S									
	B I O 1										B I O 21									
	B I O 1										B I O 23									
	C O R E S										C O R E S									
	R I M S										R I M S									
	B I O 1										B I O 21									
	B I O 1										B I O 23									
	C O R E S										C O R E S									
	R I M S										R I M S									
	B I O 1										B I O 21									
	B I O 1										B I O 23									
	C O R E S										C O R E S									
	R I M S										R I M S									
	B I O 1										B I O 21									
	B I O 1										B I O 23									
	C O R E S										C O R E S									
	R I M S										R I M S									
	B I O 1										B I O 21									
	B I O 1										B I O 23									
	C O R E S										C O R E S									
	R I M S										R I M S									
	B I O 1										B I O 21									
	B I O 1										B I O 23									
	C O R E S										C O R E S									
	R I M S										R I M S									
	B I O 1										B I O 21									
	B I O 1										B I O 23									
	C O R E S										C O R E S									
	R I M S										R I M S									
	B I O 1										B I O 21									
	B I O 1										B I O 23									
	C O R E S										C O R E S									
	R I M S										R I M S									
	B I O 1										B I O 21									
	B I O 1										B I O 23									
	C O R E S										C O R E S									
	R I M S										R I M S									
	B I O 1										B I O 21									
	B I O 1										B I O 23									
	C O R E S										C O R E S									
	R I M S										R I M S									
	B I O 1										B I O 21									
	B I O 1										B I O 23									
	C O R E S										C O R E S									
	R I M S										R I M S									
	B I O 1										B I O 21									
	B I O 1										B I O 23									
	C O R E S										C O R E S									
	R I M S										R I M S									
	B I O 1										B I O 21									
	B I O 1										B I O 23									
	C O R E S										C O R E S									
	R I M S										R I M S									
	B I O 1										B I O 21									
	B I O 1										B I O 23									
	C O R E S										C O R E S									
	R I M S										R I M S									
	B I O 1										B I O 21									
	B I O 1										B I O 23									
	C O R E S										C O R E S									
	R I M S										R I M S									
	B I O 1										B I O 21									
	B I O 1										B I O 23									
	C O R E S										C O R E S									
	R I M S										R I M S									
	B I O 1										B I O 21									
	B I O 1										B I O 23									
	C O R E S										C O R E S									
	R I M S										R I M S									
	B I O 1										B I O 21									
	B I O 1										B I O 23									
	C O R E S										C O R E S									
	R I M S										R I M S									
	B I O 1										B I O 21									
	B I O 1										B I O 23									
	C O R E S										C O R E S									
	R I M S										R I M S									
	B I O 1										B I O 21									
	B I O 1										B I O 23									
	C O R E S										C O R E S									
	R I M S										R I M S									
	B I O 1										B I O 21									
	B I O 1										B I O 23									
	C O R E S										C O R E S									
	R I M S										R I M S									
	B I O 1										B I O 21									
	B I O 1										B I O 23									
	C O R E S										C O R E S									
	R I M S										R I M S									
	B I O 1										B I O 21									
	B I O 1										B I O 23									
	C O R E S										C O R E S									
	R I M S										R I M S									
	B I O 1										B I O 21									
	B I O 1										B I O 23									
	C O R E S										C O R E S									
	R I M S										R I M S									
	B I O 1										B I O 21									
	B I O 1										B I O 23									
	C O R E S										C O R E S									
	R I M S										R I M S									
	B I O 1										B I O 21									
	B I O 1										B I O 23									
	C O R E S										C O R E S									
	R I M S										R I M S									
	B I O 1										B I O 21									
	B I O 1										B I O 23									
	C O R E S										C O R E S									
	R I M S										R I M S									
	B I O 1										B I O 21									
	B I O 1										B I O 23									
	C O R E S										C O R E S									
	R I M S										R I M S									
	B I O 1										B I O 21									
	B I O 1										B I O 23									
	C O R E S										C O R E S									
	R I M S										R I M S									
	B I O 1										B I O 21									
	B I O 1										B I O 23									
	C O R E S										C O R E S									
	R I M S										R I M S									
	B I O 1										B I O 21									
	B I O 1										B I O 23									
	C O R E S										C O R E S									
	R I M S										R I M S									
	B I O 1										B I O 21									
	B I O 1										B I O 23									
	C O R E S										C O R E S									
	R I M S										R I M S									
	B I O 1										B I O 21									
	B I O 1										B I O 23									
	C O R E S										C O R E S									
	R I M S										R I M S									
	B I O 1										B I O 21									
	B I O 1										B I O 23									
	C O R E S										C O R E S									
	R I M S										R I M S									
	B I O 1										B I O 21									
	B I O 1										B I O 23									
	C O R E S										C O R E S									
	R I M S										R I M S									
	B I O 1										B I O 21									
	B I O 1										B I O 23									
	C O R E S										C O R E S									
	R I M S										R I M S									
	B I O 1										B I O 21									
	B I O 1										B I O 23									
	C O R E S										C O R E S									
	R I M S										R I M S									
	B I O 1										B I O 21									
	B I O 1										B I O 23									
	C O R E S										C O R E S									
	R I M S										R I M S									
	B I O 1										B I O 21									
	B I O 1										B I O 23									
	C O R E S										C O R E S									
	R I M S										R I M S									
	B I O 1										B I O 21									
	B I O 1										B I O 23									
	C O R E S										C O R E S									
	R I M S										R I M S									
	B I O 1										B I O 21									
	B I O 1										B I O 23									
	C O R E S										C O R E S									
	R I M S										R I M S									
	B I O 1										B I O 21									
	B I O 1										B I O 23									
	C O R E S										C O R E S									
	R I M S										R I M S									
	B I O 1										B I O 21									
	B I O 1										B I O 23									
	C O R E S										C O R E S									
	R I M S										R I M S									
	B I O 1										B I O 21									
	B I O 1										B I O 23									
	C O R E S										C O R E S									
	R I M S										R I M S									
	B I O 1										B I O 21									
	B I O 1										B I O 23									
	C O R E S										C O R E S									
	R I M S										R I M S									
	B I O 1										B I O 21									
	B I O 1										B I O 23									
	C O R E S										C O R E S									
	R I M S										R I M S									
	B I O 1										B I O 21									
	B I O 1										B I O 23									
	C O R E S										C O R E S									
	R I M S										R I M S									
	B I O 1										B I O 21									
	B I O 1										B I O 23									
	C O R E S										C O R E S									
	R I M S										R I M S									
	B I O 1										B I O 21									
	B I O 1										B I O 23									
	C O R E S										C O R E S									
	R I M S										R I M S									
	B I O 1										B I O 21									
	B I O 1										B I O 23									
	C O R E S										C O R E S									
	R I M S										R I M S									
	B I O 1										B I O 21									
	B I O 1										B I O 23									
	C O R E S										C O R E S									
	R I M S										R I M S									
	B I O 1										B I O 21									
	B I O 1										B I O 23									
	C O R E S										C O R E S									
	R I M S																			

**Electron Microprobe Analyses of Garnet from Metapelites at the
Cima di Gagnone Area. Samples exhibit disequilibrium textures.
Analyses are given in weight % oxides.**

CL11A GARNETS

C O A R S E G R A I N S

(--- C O R E S ---) <----- R I M S ----->

Sample	4	7	6	23	25
Coexisting	11A GAR1	11A GAR4	11A GAR3	11A GAR8	11A GAR9
Biotite Sample	B10 4	B10 9			

SiO2	38.98	38.92	38.87	38.62	38.57
TiO2	0.00	0.00	0.00	0.00	0.00
Al2O3	21.88	21.96	21.37	21.89	22.15
Fe2O3	0.17	0.30	0.72	0.17	0.00
FeO	25.74	26.89	25.95	26.98	27.27
MnO	0.71	0.62	0.64	0.67	0.77
MgO	6.23	6.67	6.32	6.84	6.27
CaO	6.87	5.67	6.21	5.04	5.03
Na2O	0.00	0.00	0.00	0.00	0.00
K2O	0.00	0.00	0.00	0.00	0.00
Total	100.58	101.03	100.07	100.20	100.06

CATIONS assuming stoichiometry and charge balance

Si	3.0082	2.9924	3.0216	2.9917	2.9999
Ti	0.0000	0.0000	0.0000	0.0000	0.0000
Al	1.9899	1.9900	1.9581	1.9982	2.0302
Fe3	0.0101	0.0176	0.0419	0.0100	0.0000
Fe2	1.6609	1.7286	1.6868	1.7475	1.7733
Mn	0.0461	0.0401	0.0423	0.0439	0.0506
Mg	0.7169	0.7643	0.7321	0.7902	0.7267
Ca	0.5679	0.4670	0.5171	0.4184	0.4191
Na	0.0000	0.0000	0.0000	0.0000	0.0000
K	0.0000	0.0000	0.0000	0.0000	0.0000

ENDMEMBERS

Grossular	0.185	0.147	0.153	0.134	0.141
Almandine	0.555	0.576	0.566	0.583	0.597
Pyrope	0.240	0.255	0.246	0.263	0.245
Spessartine	0.015	0.013	0.014	0.015	0.017
Andradite	0.005	0.009	0.021	0.005	0.000

CL11A & F GARNETS

F I N E G R A I N S

<--- C O R E S ---> <----- R I M S -----> <----- C O R E S -----> <----- R I M S ----->

Sample	11A GAR6	11A GAR11	11A GAR7	11A GAR10	11A GAR12	11A GAR13	11A GAR15	11A GAR18	11A GAR14	11A GAR17
SiO2	39.28	38.60	38.41	38.50	38.97	39.00	38.50	38.10	38.77	38.32
TiO2	0.00	0.15	0.00	0.00	0.00	0.00	0.00	0.00	0.00	0.00
Al2O3	22.00	21.44	21.47	21.49	22.00	21.72	22.63	22.10	21.42	21.38
Fe2O3	0.12	0.88	0.15	0.66	0.15	0.05	0.22	0.29	0.80	1.03
FeO	28.09	26.69	27.18	24.35	24.44	26.55	26.07	24.97	24.91	26.16
MnO	0.61	0.73	0.89	0.63	0.59	0.66	0.69	0.67	0.62	0.86
MgO	5.88	6.38	5.35	5.94	5.95	6.60	5.57	5.92	5.86	4.93
CaO	5.56	5.83	5.93	8.26	8.53	4.97	7.56	7.79	8.10	8.00
Na2O	0.02	0.05	0.00	0.00	0.03	0.00	0.00	0.00	0.00	0.03
K2O	0.00	0.00	0.00	0.00	0.00	0.00	0.00	0.00	0.00	0.00
Total	101.55	100.75	99.39	99.82	100.66	99.55	100.63	99.85	100.48	100.71

CATIONS assuming stoichiometry and charge balance

Si	3.0199	2.9855	3.0231	2.9925	2.9972	3.0420	2.9762	2.9598	3.0000	2.9802
Ti	0.0000	0.0089	0.0000	0.0000	0.0000	0.0000	0.0000	0.0000	0.0000	0.0000
Al	1.9932	1.9544	1.9911	1.9688	1.9941	1.9949	2.0088	2.0231	1.9535	1.9597
Fe3	0.0068	0.0512	0.0089	0.0387	0.0067	0.0031	0.0130	0.0172	0.0455	0.0601
Fe2	1.8055	1.7265	1.7888	1.5826	1.5717	1.7316	1.6862	1.6219	1.6119	1.7008
Mn	0.0399	0.0476	0.0576	0.0416	0.0387	0.0434	0.0454	0.0443	0.0408	0.0567
Mg	0.6734	0.7356	0.6283	0.6880	0.6822	0.7677	0.6420	0.6858	0.6756	0.5717
Ca	0.4577	0.4834	0.5003	0.6877	0.7029	0.4153	0.6263	0.6479	0.6718	0.6661
Na	0.0037	0.0068	0.0000	0.0000	0.0045	0.0000	0.0000	0.0000	0.0000	0.0047
K	0.0000	0.0000	0.0000	0.0000	0.0000	0.0000	0.0000	0.0000	0.0000	0.0000

ENDMEMBERS

Grossular	0.150	0.130	0.164	0.210	0.230	0.139	0.202	0.207	0.201	0.192
Almandine	0.607	0.576	0.601	0.538	0.525	0.585	0.562	0.541	0.537	0.568
Pyrope	0.226	0.245	0.211	0.229	0.228	0.260	0.214	0.229	0.225	0.191
Spessartine	0.013	0.016	0.020	0.014	0.013	0.015	0.015	0.015	0.014	0.019
Andradite	0.003	0.026	0.004	0.019	0.004	0.002	0.007	0.009	0.023	0.030

**Electron Microprobe Analyses of Biotite from Metapelites at the
Cima di Gagnone Area. Samples exhibit equilibrium textures.
Analyses are given in weight % oxides.**

CH99 BIOTITES *****		CH99 B15 CH99 B16 CH99 B19 CH99 B110 CH99 B111 CH99 B112 GAR 5A, 5B		53		59		CL12 BIOTITES *****		12 B101 12 B103 12 B104 12 B106 12 B108 12 B1013 GAR 3 GAR 4 GAR 5 GAR 10 GAR 11					
Sample	Coexisting Garnet Samples	31	36	47	50	53	59	Sample	Coexisting Garnet Sample	7	9	12	24	27	52
SiO2		35.84	36.01	37.13	35.21	35.92	36.14	SiO2		35.62	36.04	36.75	35.88	36.48	35.84
TiO2		2.14	2.00	1.79	1.76	1.74	2.13	TiO2		2.09	3.12	2.38	2.63	2.81	2.38
Al2O3		19.42	19.07	19.38	19.47	19.40	18.81	Al2O3		18.99	18.56	18.88	19.99	19.41	19.77
FeO		17.41	17.64	17.75	18.41	17.35	17.17	FeO		18.14	17.25	12.80	17.66	17.85	18.62
MnO		0.16	0.18	0.20	0.18	0.18	0.15	MnO		0.00	0.00	0.00	0.00	0.00	0.00
MgO		10.60	11.01	10.77	10.05	10.89	10.92	MgO		10.05	10.61	13.61	9.94	9.87	9.78
CaO		0.00	0.00	0.00	0.00	0.00	0.00	CaO		0.03	0.00	0.00	0.03	0.05	0.07
Mg2O		0.16	0.31	0.21	0.20	0.25	0.30	Mg2O		0.27	0.27	0.43	0.33	0.38	0.32
K2O		9.03	9.00	9.08	8.52	8.99	8.83	K2O		9.00	8.79	8.97	8.93	8.59	8.74
F		0.55	0.36	0.47	0.36	0.25	0.31	F		0.00	0.21	0.21	0.26	0.00	0.16
Cl		0.02	0.03	0.02	0.03	0.02	0.03	Cl		0.04	0.03	0.00	0.02	0.02	0.03
H2O		3.62	3.73	3.72	3.67	3.77	3.73	H2O		3.83	3.76	3.83	3.77	3.89	3.82
Total		98.94	99.34	100.52	97.86	98.76	98.51	Total		98.07	98.63	97.87	99.44	99.36	99.53
Si		2.7620	2.7603	2.8136	2.7381	2.7634	2.7899	Si		2.7786	2.7879	2.8030	2.7596	2.8025	2.7545
Ti		0.1238	0.1154	0.1018	0.1027	0.1009	0.1237	Ti		0.1228	0.1814	0.1367	0.1524	0.1624	0.1378
Al		1.7639	1.7233	1.7304	1.7842	1.7586	1.7112	Al		1.7461	1.6920	1.6969	1.8121	1.7577	1.7902
Fe2		1.1217	1.1311	1.1250	1.1971	1.1165	1.1085	Fe2		1.1833	1.1156	0.8160	1.1356	1.1464	1.1966
Mn		0.0104	0.0114	0.0127	0.0121	0.0117	0.0095	Mn		0.0000	0.0000	0.0000	0.0000	0.0000	0.0000
Mg		1.2181	1.2585	1.2165	1.1658	1.2490	1.2572	Mg		1.1691	1.2232	1.5476	1.1403	1.1309	1.1209
Ca		0.0000	0.0000	0.0000	0.0000	0.0000	0.0000	Ca		0.0028	0.0000	0.0000	0.0025	0.0039	0.0055
Na		0.0243	0.0461	0.0307	0.0303	0.0366	0.0451	Na		0.0410	0.0400	0.0638	0.0488	0.0559	0.0479
K		0.8875	0.8803	0.8770	0.8447	0.8823	0.8691	K		0.8956	0.8670	0.8726	0.8759	0.8419	0.8562
F		0.1347	0.0875	0.1130	0.0894	0.0606	0.0749	F		0.0000	0.0523	0.0518	0.0643	0.0000	0.0379
Cl		0.0027	0.0037	0.0031	0.0037	0.0028	0.0038	Cl		0.0049	0.0036	0.0000	0.0024	0.0030	0.0042
OH		1.8626	1.9089	1.8838	1.9069	1.9366	1.9212	OH		1.9951	1.9441	1.9482	1.9333	1.9970	1.9580
		SITE distribution and RATIOS						SITE distribution and RATIOS							
xMg (FeII+)		0.521	0.527	0.520	0.493	0.528	0.531	xMg (Fe tot)		0.497	0.523	0.655	0.501	0.497	0.484
xMg (Fe tot)		0.521	0.527	0.520	0.493	0.528	0.531	Al(IV)		1.221	1.212	1.197	1.240	1.197	1.245
Al(IV)		1.238	1.240	1.186	1.262	1.237	1.210	Al(VI)		0.525	0.480	0.500	0.572	0.560	0.545
Al(VI)		0.526	0.484	0.544	0.522	0.522	0.501								

CATIONS calculated on the basis of 7, cations and 12, oxygens

CATIONS calculated on the basis of 7, cations and 12, oxygens

**Electron Microprobe Analyses of Biotite from Metapelites at the
Cima di Gagnone Area. Samples exhibit disequilibrium textures.
Analyses are given in weight % oxides.**

CL4A BIOTITES

Sample	33	34	37	42	46
Coexisting Garnet Sample	4A B101	4A B102	4A B104	4A B106	4A B107
	GAR 5				
SiO2	38.14	38.56	37.27	37.12	36.95
TiO2	2.38	3.04	2.65	2.80	2.14
Al2O3	16.28	16.06	16.11	15.79	16.37
FeO	15.88	16.00	15.22	17.55	16.36
MnO	0.21	0.28	0.19	0.20	0.39
MgO	13.06	12.87	13.31	12.24	12.28
CaO	0.02	0.02	0.05	0.06	0.08
Na2O	0.21	0.15	0.13	0.15	0.12
K2O	9.27	9.10	9.20	9.02	9.09
F	0.00	0.00	0.00	0.00	0.00
Cl	0.05	0.05	0.05	0.06	0.05
H2O	3.93	3.95	3.88	3.88	3.85
Total	99.43	100.08	98.06	98.85	97.68

CH278 BIOTITES

Sample	52	67	68	69	72
	C278 B111	C278 B117	C278 B118	C278 B119	C278 B120
SiO2	37.33	38.25	37.11	38.28	37.04
TiO2	1.65	1.48	1.59	1.64	1.55
Al2O3	19.31	17.05	17.82	18.55	18.47
FeO	13.83	15.20	14.64	13.53	14.19
MnO	0.04	0.06	0.00	0.04	0.04
MgO	14.38	14.55	14.63	14.93	14.68
CaO	0.00	0.00	0.00	0.00	0.00
Na2O	0.62	0.42	0.57	0.51	0.57
K2O	8.28	7.73	8.06	7.85	8.12
F	0.39	0.39	0.48	0.41	0.56
Cl	0.00	0.04	0.02	0.02	0.02
H2O	3.85	3.82	3.76	3.86	3.74
Total	99.67	98.98	98.66	99.63	98.98

CATIONS calculated on the basis of 7. cations and 12. oxygens

Si	2.9005	2.9157	2.8678	2.8578	2.8688
Ti	0.1360	0.1726	0.1533	0.1621	0.1246
Al	1.4591	1.4312	1.4611	1.4327	1.4980
Fe2	1.0101	1.0115	0.9794	1.1297	1.0618
Mn	0.0137	0.0181	0.0121	0.0131	0.0259
Mg	1.4806	1.4509	1.5265	1.4046	1.4208
Ca	0.0015	0.0013	0.0041	0.0049	0.0067
Na	0.0316	0.0223	0.0191	0.0220	0.0181
K	0.8993	0.8776	0.9026	0.8858	0.9001
F	0.0000	0.0000	0.0000	0.0000	0.0000
Cl	0.0061	0.0061	0.0062	0.0081	0.0068
OH	1.9939	1.9939	1.9938	1.9919	1.9932
xMg (FeII+)	0.594	0.589	0.609	0.554	0.572
xMg (Fe tot)	0.594	0.589	0.609	0.554	0.572
Al(IV)	1.099	1.084	1.132	1.142	1.131
Al(VI)	0.360	0.347	0.329	0.290	0.367

SITE distribution and RATIOS

CATIONS calculated on the basis of 7. cations and 12. oxygens

Si	2.7692	2.8514	2.7823	2.8213	2.7658
Ti	0.0918	0.0827	0.0898	0.0907	0.0871
Al	1.6884	1.4977	1.5746	1.6109	1.6254
Fe2	0.8576	0.9474	0.9178	0.8339	0.8857
Mn	0.0027	0.0038	0.0000	0.0028	0.0023
Mg	1.5903	1.6170	1.6355	1.6403	1.6337
Ca	0.0000	0.0000	0.0000	0.0000	0.0000
Na	0.0890	0.0606	0.0822	0.0735	0.0820
K	0.7830	0.7345	0.7703	0.7380	0.7728
F	0.0917	0.0922	0.1144	0.0962	0.1331
Cl	0.0000	0.0052	0.0019	0.0031	0.0031
OH	1.9083	1.9026	1.8837	1.9007	1.8638
xMg (Fe tot)	0.650	0.631	0.641	0.663	0.648
Al(IV)	1.231	1.149	1.218	1.179	1.234
Al(VI)	0.458	0.349	0.357	0.432	0.391

SITE distribution and RATIOS

Electron Microprobe Analyses of *Biotite* from Metapelites at the Cima di Gagnone Area. Samples exhibit *disequilibrium textures*. Analyses are given in weight % oxides.

CL11a,b BIOTITES

	9	22	21	34	14	31	13	41
Sample	CL11A B11	CL11A B1B	CL11A B17	CL11A B11	CL11A B14	CL11A B11	CL11A B11	CL11B B11
Coexisting Garnet Samples					GAR 8			
SiO ₂	33.78	33.18	34.83	35.14	36.14	36.13	36.31	36.63
TiO ₂	2.90	3.38	3.58	3.21	3.05	3.24	3.05	2.56
Al ₂ O ₃	17.70	17.78	18.82	18.55	15.50	15.51	15.91	15.60
FeO	21.28	21.82	15.89	14.78	19.76	19.24	19.31	17.23
MnO	0.23	0.25	0.12	0.13	0.13	0.24	0.20	0.25
MgO	9.21	8.83	12.09	12.76	10.98	10.51	11.89	12.69
CaO	0.15	0.13	0.12	0.13	0.11	0.11	0.16	0.14
Na ₂ O	0.06	0.05	0.15	0.12	0.05	0.32	0.05	0.15
K ₂ O	8.99	8.52	9.06	9.43	8.84	8.49	9.04	9.05
F	0.00	0.00	0.25	0.38	0.17	0.00	0.27	0.22
Cl	0.03	0.03	0.03	0.00	0.05	0.02	0.03	0.03
H ₂ O	3.78	3.77	3.77	3.71	3.74	3.80	3.78	3.76
Total	98.11	97.74	98.71	98.36	98.54	97.61	99.99	98.30

CATIONS calculated on the basis of 7. cations and 12. oxygens

Si	2.6705	2.6301	2.6763	2.7053	2.8203	2.8477	2.7813	2.8348
Ti	0.1723	0.2015	0.2069	0.1861	0.1791	0.1921	0.1754	0.1488
Al	1.6496	1.6608	1.7037	1.6831	1.4256	1.4408	1.4365	1.4224
Fe ₂	1.4069	1.4465	1.0207	0.9518	1.2895	1.2684	1.2364	1.1145
Mn	0.0155	0.0171	0.0080	0.0086	0.0083	0.0161	0.0131	0.0161
Mg	1.0853	1.0440	1.3843	1.4652	1.2771	1.2348	1.3574	1.4634
Ca	0.0123	0.0109	0.0097	0.0108	0.0096	0.0090	0.0134	0.0116
Na	0.0097	0.0070	0.0221	0.0186	0.0069	0.0483	0.0080	0.0227
K	0.9069	0.8611	0.8876	0.9263	0.8800	0.8536	0.8826	0.8926
F	0.0000	0.0000	0.0603	0.0916	0.0428	0.0000	0.0651	0.0544
Cl	0.0044	0.0036	0.0037	0.0000	0.0071	0.0030	0.0035	0.0040
OH	1.9956	1.9964	1.9360	1.9084	1.9501	1.9970	1.9314	1.9416

SITE distribution and RATIOS

xMg (FeTot)	0.435	0.419	0.576	0.606	0.498	0.493	0.523	0.568
Al(IV)	1.329	1.370	1.324	1.295	1.180	1.152	1.219	1.165
Al(VI)	0.320	0.291	0.380	0.388	0.246	0.289	0.218	0.257

APPENDIX IIA: Computer Program used to calculate Rayleigh Distillation
and Isotope Exchange in Metabasites

C
C
C

PROGRAM NUDIST

C
C

C Version AMP IV: Dehydration of Hbl + Epi + Par / equilibrium model
C (With Kyn and Gar)
C This version modified by Eric Reusser and Gretchen Frueh
C from and original by Doug Rumble III.

C
C

Declarations and definitions

C
C

INTEGER N
PARAMETER (N = 200)

C

REAL DOQZ(N), DOHBL(N), DOEPI(N), DOGAR(N), DOPAR(N),
. DOOMP(N), DOH2O(N), DOWR(0:N), DKYN, MKYN, MTOT,
. T, WRI, MHL, MEPI, MGAR, MPAR, MQZ, MH2O, MOMP,
. DOMP, DPAR, DEPI, DGAR, DHBL, DQZ, DH2O, WTKYN,
. XOMP, XHBL, XEPI, XGAR, XPAR, XQZ, XH2O, OSYS,
. AQHBL, AQPAP, AQGAR, AQEPI, AQH2O, AQOMP, D18QZ,
. D18HB, D18PA, D18EP, D18GR, D18OM, D18WA, DENKYN,
. DENHBL, DENEPI, DENGAR, DENPAR, DENQZ, DENOMP, P,
. WTHBL, WTEPI, WTGR2, WTGR1, WTPAR, WTQZ, WTOMP,
. NQZ, NHBL, NEPI, NPAR, NGAR, NOMP, NH2O, VWRI,
. DENWRI, DENWR, DENCH, IVFR, TOTH2O, VOLCH, MIN,
. MAX, VOLH2O, MINH2O, MAXH2O, TOTMIN,
. TOTMAX, VWR, VOLPER
INTEGER INC, I, J

C

CHARACTER*40 FNAME

C

DATA DENHBL, DENEPI, DENGAR, DENPAR, DENQZ, DENOMP, DENKYN/ 3.30,
. 3.30, 3.70, 2.85, 2.65, 3.33, 3.55/

C

DATA WTHBL, WTEPI, WTGR2, WTPAR, WTQZ, WTOMP, WTKYN, WTGR1/
. 817.74, 454.35, 454.88, 382.19, 60.09, 208.34, 162.03,
. 455.98/

C

C WTGR2 avg of actual WTS for GR1 and GR2

C

DATA P /15000./

C

DATA MHL, MEPI, MPAR, MQZ/ 50., 15., 15., 20./

C

C

C Start of program

C

C VAX

OPEN (UNIT = 7, FILE = 'SYSS\$OUTPUT', STATUS = 'NEW')
OPEN (UNIT = 5, FILE = 'SYSS\$INPUT', STATUS = 'NEW')

C CDC

OPEN (UNIT = 7, FILE = 'OUTPUT', STATUS = 'NEW')
OPEN (UNIT = 5, FILE = 'INPUT', STATUS = 'NEW')

C PDP

C OPEN (UNIT = 7, FILE = 'TT:', STATUS = 'NEW')

II-A-2

```

C      OPEN ( UNIT = 5, FILE = 'TT:', STATUS = 'NEW' )
C
      OPEN ( UNIT = 2, FILE = 'INZEST.INP', STATUS = 'NEW' )
      WRITE (7, 10)
10  FORMAT (//10X, '**** Program NUDIST Version AMP III ****',
.        // 5X, 'This program computes Rayleigh distillation of ',
.        'O-18 for amphibolites',
.        // 5X, 'Type output file name')
      READ (5, '(A)') FNAME
      OPEN ( UNIT = 1, FILE = FNAME, STATUS = 'NEW' )
      WRITE (7, *) 'Type number of increments [INTEGER]'
      READ (5, *) INC
      WRITE (7, *) 'Type initial whole rock O-18 [REAL]'
      READ (5, *) WRI
      WRITE (7, *) 'Type initial modes of HBL, EPI, PAR, QTZ,',
.        'GAR [REAL]'
      READ (5, *) MHBL, MEPI, MPAR, MQZ, MGAR
      WRITE (7, *) 'Type amount of OMP formed at each increment [REAL]'
      READ (5, *) DOMP
      WRITE (7, *) 'Type initial temperature [deg C] [REAL]'
      READ (5, *) T
      WRITE (1, 20) T, INC, DOMP, MHBL, MEPI, MPAR, MQZ, MGAR
20  FORMAT (' **** Program NUDIST Version AMP III ****',
.        // ' This program computes Rayleigh distillation of',
.        ' O-18 for the reaction'///' 7.200(HBL) + 1.118(EPI)',
.        ' + 2.712(PAR) + 0.546(QTZ) = '/' 6.312(OMP) + 2.400(GAR)',
.        ' + 2.275(KYN) + 0.569(H2O)'///' At a constant temperature',
.        ' of ',F5.0,' deg C'///' Number of reaction increments = ',
.        I3/' Amount of OMP formed at each increment = ',F6.2/
.        ' Initial modes: HBL = ',F6.2,' EPI = ',F6.2,
.        ' PAR = ',F6.2,' QTZ = ',F6.2,' GAR = ',F6.2)
C-----
C Coefficients are in O-units
C-----
C Start calculation
C -----
C Calculate alpha's,
C HBL, PAR = MUS, QZ, GAR ref JAVOY, 1977
C OMP ref MATTHEWS; EPI ref RUMBLE (program)
C
      T = T + 273.15
      AQHBL = 3.15E6 / T**2 - 0.3
      AQEPI = 3.148E6 / T**2 - 0.3
      AQPAR = 2.20E6 / T**2 - 0.6
      AQGAR = 2.88E6 / T**2
      AQH2O = 4.10E6 / T**2 - 3.7
      AQOMP = 1.585E6 / T**2
C
C
      DHBL = DOMP * (7.200 / 6.312)
      DEPI = DOMP * (1.118 / 6.312)
      DGAR = DOMP * (2.400 / 6.312)
      DPAR = DOMP * (2.712 / 6.312)
      DQZ = DOMP * (0.546 / 6.312)
      DH2O = DOMP * (0.569 / 6.312)
      DKYN = DOMP * (2.275 / 6.312)
C
C Loop around increment
C
      DOWR(0) = WRI

```

MOMP = 0.
 MH2O = 0.
 MKYN = 0.

C
 C-----
 C
 C
 C

Volume of whole rock

VWRI = MHBL*WTHBL/(24.*DENHBL) + MGAR*WTGR1/(12.*DENGAR) +
 . MEPI*WTEPI/(13.*DENEPI) + MOMP*WTOMP/(6.*DENOMP) +
 . MQZ*WTQZ/(2.*DENQZ) + MPAR*WTPAR/(12.*DENPAR) +
 . MKYN*WTKYN/(5.*DENKYN)

C

VOLH2O = VH2O(P,T)
 VOLH2O = VOLH2O*DH2O
 VOLPER = VOLH2O*100./VWRI
 IVFR = VOLH2O/VWRI
 TOTH2O = IVFR * 33.5
 DENWRI = MHBL*DENHBL + MEPI*DENEPI + MGAR*DENGAR + MQZ*DENQZ +
 . MOMP*DENOMP + MPAR*DENPAR + MKYN*DENKYN
 DENWRI = DENWRI / 100

C

WRITE (1,25) DH2O, P, T, VH2O(P,T), VOLH2O, VOLPER, VWRI
 25 FORMAT (' The amount of H2O formed at each increment = ',F7.4,
 . ' moles or O-units/' ' The molar volume of H2O at ',F7.0,
 . ' bar and',F7.0,' K =',F7.4,' ccm/mole'/' ' The amount of',
 . ' H2O formed at each increment = ',F7.4,' ccm'/' ' This',
 . ' corresponds to', F7.2,' vol% of the initial whole rock',
 . '/ ' The volume of the initial whole rock = ', F7.2,' ccm')
 WRITE (1, 26) DENWRI, IVFR, TOTH2O
 26 FORMAT (' The density of the initial rock = ',F7.2,' g/ccm'/'
 . ' The instantaneous FR-ratio at each increment = ',F7.5,/
 . ' The TOTAL amount of H2O produced by a boudin 4m in',
 . ' diameter at'/' each increment of the reaction =',
 . F7.4,' ccm'//)

C

C-----

C

WRITE (1, 30) MHBL, MEPI, MPAR, MQZ, MOMP, MGAR, MKYN, MH2O
 30 FORMAT (' Amount of phases at each increment'/'/' INC HBL',
 . ' EPI PAR QZ OMP GAR',
 . ' KYN H2O'/'/' 0',8(1X,F8.2))

C

DO 1 I = 1, INC
 MHBL = MHBL - DHBL
 MEPI = MEPI - DEPI
 MPAR = MPAR - DPAR
 MQZ = MQZ - DQZ
 IF (MHBL.GE. 0. .AND. MEPI.GE. 0. .AND. MPAR.GE. 0.
 . .AND. MQZ.GE. 0.) THEN
 MOMP = MOMP + DOMP
 MGAR = MGAR + DGAR
 MKYN = MKYN + DKYN
 MH2O = MH2O + DH2O
 MTOT = MHBL + MEPI + MPAR + MQZ + MOMP + MGAR + MKYN
 MHBL = MHBL*100/MTOT
 MEPI = MEPI*100/MTOT
 MPAR = MPAR*100/MTOT
 MOMP = MOMP*100/MTOT
 MGAR = MGAR*100/MTOT

```

MKYN = MKYN*100/MTOT
MQZ = MQZ*100/MTOT
WRITE (1, 40) I, MHBL, MEPI, MPAR, MQZ, MOMP, MGAR, MKYN, MH2O
40 FORMAT (1X,I3,8(1X,F8.2))

```

C
C
C

RE-CALCULATE MODES OF ROCKS WITHOUT KYANITE

```

MTOT = MHBL + MEPI + MPAR + MQZ + MOMP + MGAR + MH2O
NHBL = MHBL*100/MTOT
NEPI = MEPI*100/MTOT
NPAR = MPAR*100/MTOT
NOMP = MOMP*100/MTOT
NGAR = MGAR*100/MTOT
NH2O = DH2O*100/MTOT
OSYS = NHBL + NEPI + NPAR + NQZ + NOMP + NGAR + NH2O
XHBL = NHBL / OSYS
XEPI = NEPI / OSYS
XPAR = NPAR / OSYS
XQZ = NQZ / OSYS
XOMP = NOMP / OSYS
XGAR = NGAR / OSYS
XH2O = NH2O / OSYS

```

C

```

D18QZ = XHBL*AQHBL + XEPI*AQEPI + XGAR*AQGAR +
        XPAR*AQPAR + XOMP*AQOMP
D18QZ = WRI + D18QZ + XH2O * AQH2O
D18HB = D18QZ - AQHBL
D18EP = D18QZ - AQEPI
D18PA = D18QZ - AQPAR
D18GR = D18QZ - AQGAR
D18OM = D18QZ - AQOMP
D18WA = D18QZ - AQH2O
DOQZ(I) = D18QZ
DOHBL(I) = D18HB
DOEPI(I) = D18EP
DOGAR(I) = D18GR
DOOMP(I) = D18OM
DOPAR(I) = D18PA
DOH2O(I) = D18WA
WRITE (2, *) DOH2O(I)

```

C

```

OSYS = NHBL + NEPI + NGAR + NOMP + NPAR + NQZ
XHBL = NHBL / OSYS
XEPI = NEPI / OSYS
XGAR = NGAR / OSYS
XPAR = NPAR / OSYS
XOMP = NOMP / OSYS
XQZ = NQZ / OSYS

```

C

```

WRI = D18HB*XHBL + D18EP*XEPI + D18GR*XGAR + D18OM*XOMP
      + D18PA*XPAR + D18QZ*XQZ
DOWR(I) = WRI
J = I

```

ELSE

```

IF ( MHBL .LT. 0. ) THEN
  WRITE (7, *) 'No HBL left'
  WRITE (1, 80)

```

```

80 FORMAT (/' The reaction has stopped because there is no HBL left')
END IF
IF ( MEPI .LT. 0. ) THEN

```

```

        WRITE (7, *) 'No EPI left'
        WRITE (1, 84)
84  FORMAT (/ ' The reaction has stopped because there is no EPI left')
      END IF
        IF ( MPAR .LT. 0. ) THEN
          WRITE (7, *) 'No PAR left'
          WRITE (1, 85)
85  FORMAT (/ ' The reaction has stopped because there is no PAR left')
      END IF
        IF ( MQZ .LT. 0. ) THEN
          WRITE (7, *) 'No QTZ left'
          WRITE (1, 90)
90  FORMAT (/ ' The reaction has stopped because there is no QTZ left')
      END IF
      GO TO 2
    END IF
1  CONTINUE
   WRITE (7, *) 'Reaction is finished'

```

C

C

C

C

2

.

.

C

Volume of whole rock

```

VWR = MHLB*WTHBL/(24.*DENHBL) + MGAR*WTGR2/(12.*DENGAR) +
.  MEPI*WTEPI/(13.*DENEPI) + MOMP*WTOMP/(6.*DENOMP) +
.  MQZ*WTQZ/(2.*DENQZ) + MPAR*WTPAR/(12.*DENPAR)

```

```

VOLH2O = VH2O(P,T)

```

```

VOLH2O = VOLH2O*MH2O

```

```

VOLPER = VOLH2O*100./VWR

```

```

DENWR = MHLB*DENHBL + MEPI*DENEPI + MGAR*DENGAR + MQZ*DENQZ +
.  MOMP*DENOMP + MPAR*DENPAR + MKYN*DENKYN

```

```

DENWR = DENWR / 100

```

```

MIN = (MH2O*1000)/(VWR * DENWR)

```

```

MAX = (MH2O*1000)/(VWRI * DENWRI)

```

```

VOLCH = 100 - (100*VWR / VWRI)

```

```

DENCH = (DENWR*100 / DENWRI) - 100

```

```

MINH2O = VOLH2O / VWRI

```

```

MAXH2O = VOLH2O / VWR

```

```

TOTMIN = MINH2O * 33.5

```

```

TOTMAX = MAXH2O * 33.5

```

C

```

WRITE (1,44) MH2O, DENWR

```

```

44  FORMAT (/,' The total amount of H2O =',F7.4,' moles',/
.  ' The final density of the WR =',F7.2,' g/ccm')

```

C

```

WRITE (1, 45) VWR, VOLCH, DENCH, VOLH2O, VOLPER, MAXH2O, TOTMAX

```

```

45  FORMAT (' The final volume of the whole rock = ', F7.2, ' ccm',/
.  ' This represents a',F7.2,' % change in volume',/,
.  ' and corresponds to a',F7.2,' % change in density',/
.  ' The final volume of the total amount of H2O produced =',
.  F7.4,' ccm'/' This corresponds to',F7.3,' vol% H2O',/
.  ' The MAXIMUM amount of H2O produced =',F7.4,' m3 H2O/m3',
.  /,' or a total of',F7.4,' m3 H2O')

```

```

WRITE (1, 46) MINH2O, TOTMIN, MIN, MAX

```

```

46  FORMAT (' The MINIMUM amount of H2O produced =',F7.4,' m3 H2O/m3',
.  /,' or a total of',F7.4,' m3 H2O',/, ' Between ',F7.4,
.  ' and',F7.4,' moles of H2O will be released per Kg rock')

```

```

WRITE (1, 50) DOWR(0)

```

```

50  FORMAT (// ' Delta 0-18 of phases at each increment'//
.  ' INC   WR   HBL   EPI   PAR   QZ   OMP',

```

IIA - 6

```

.      '      GAR      H2O'//'  0  ',F6.2)
DO 3 I = 1, J
  type *, dowl(i)
  WRITE (1, 60) I, DOWR(I), DOHBL(I), DOEPI(I), DOPAR(I),
.      DOQZ(I), DOOMP(I), DOGAR(I), DOH2O(I)

```

C

```

3 CONTINUE
60 FORMAT (1X,I3,8(2X,F6.2))

```

C

```

STOP
END

```

C

C*****

C

```

REAL FUNCTION VH2O (P,T)

```

C

C*****

C

```

C Subroutine to compute molar volumes of H2O
C using the equation of state of Kerrick & Jacobs (1981).
C Solution is performed by the method of NEWTON-RAPHSON.

```

ER 9/84

C

C*****

C

```

C Output :      V      Molar volume / ccm

```

C

```

C Input  :      P      Pressure / bar
C          T      Absolute temperature / Kelvin

```

C

```

C          R      Gas constant ( = 83.143 ccm....)

```

C

```

C          B      Covolume (Repulsive parameter)

```

C

```

C          C,D,E  Temperature dependent coefficient of the
C                  Kerrick-Jacobs expansion of the attractive param.
C                  a(T,V) = C(T) + D(T)/V + E(T)/V**2

```

C

C*****

C

```

C Declarations

```

C

```

REAL V,P,T,V0,R,B,C,D,E,T12,RT,Y,CY,PREP,PATT,DPREP,DPATT,EPS,
.      T2

```

C

```

C      Y      Hardsphere term B/(4*V)

```

C

```

C      CY     Complement of Y: 1. - Y

```

C

```

C      PREP   Pressure due to repulsive intermolecular forces

```

C

```

C      PATT   Pressure due to attractive intermolecular forces

```

C

```

C      DPREP, DPATT  Differential of PREP resp. PATT

```

C

```

C      EPS    Absolute accuracy of the molar volume

```

C

C*****

C

```

C PURE H2O

```

C

```

EPS = 0.01
T2 = T**2
R = 83.143
B=29.
C=(290.78-0.30276*T+1.4774E-4*T2)*1.E6
D=(-8374.+19.437*T-8.148E-3*T2)*1.E6
E=(76600.-133.9*T+0.1071*T2)*1.E6

```

II A - 7

```

V0=15.
IF (P.LT.1000.) V0=22.5
IF (P.GE.210..AND.P.LT.600..AND.TC.GE.550.) V0=75.
IF (P.GE.210..AND.P.LT.600..AND.TC.LT.550.) V0=35.
IF (P.GE.210..AND.P.LT.600..AND.TC.LT.400.) V0=20.
IF (P.GE.100..AND.P.LT.210..AND.TC.LT.400.) V0=15.
IF (P.GE.100..AND.P.LT.210..AND.TC.GE.400.) V0=100.
IF (P.LT.100.) V0=500.
IF (P.LT.5.) V0=7000.

```

C

```

T12 = SQRT (T)
RT = R * T

```

C

C Iteration loop to approximate molar volume

C

```

1  Y = 0.25 * B / V0
   CY = 1. - Y

```

C

```

PREP = RT * (1. + Y*(1. + Y*CY)) / (V0 * CY**3)
PATT = (C + (D + E/V0)/V0) / (T12 * V0 * (V0+B))
DPREP = (2. * (RT * (CY-Y**2)/(V0*CY**3) - PREP)/CY - PREP)/V0
DPATT = -(PATT*(2.*V0+B) + (D+2.*E/V0)/(T12*V0**2)) / (V0*(V0+B))

```

C

C Newton - Raphson approximation

C

```

V = V0 - (PREP - PATT - P)/(DPREP - DPATT)

```

C

C If molar volume is enough accurate RETURN, else next iteration step

C

```

IF (ABS (V-V0) .LT. EPS) GO TO 2
V0 = V
GO TO 1

```

C

C *** End of subroutine VSOLVE

C

```

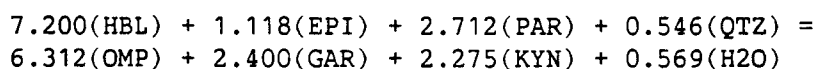
2  VH2O = V
   END

```

 *APPENDIX IIA: Calculated Results of NUDIST program for Rayleigh *****
 * Distillation of Metabasites (Corresponds to Fig. 3.5)*****

**** Program NUDIST Version AMP III ****

This program computes Rayleigh distillation of O-18 for the reaction



At a constant temperature of 650. deg C

Number of reaction increments = 100
 Amount of OMP formed at each increment = 0.50
 Initial moles: HBL = 45.00 EPI = 8.00 PAR = 15.00 QTZ = 13.00 GAR = 19.00
 The amount of H2O formed at each increment = 0.0451 moles or O-units
 The molar volume of H2O at 15000. bar and 923.K = 17.6478 ccm/mole
 The amount of H2O formed at each increment = 0.7954 ccm
 This corresponds to 0.08 vol% of the initial whole rock
 The volume of the initial whole rock = 1059.50 ccm
 The density of the initial rock = 3.22 g/ccm
 The instantaneous FR-ratio at each increment = 0.00075
 The TOTAL amount of H2O produced by a boudin 4m in diameter at each increment of the reaction = 0.0252 ccm

Amount of phases at each increment

INC	HBL	EPI	PAR	QZ	OMP	GAR	KYN	H2O
0	45.00	8.00	15.00	13.00	0.00	19.00	0.00	0.00
1	44.45	7.92	14.79	12.96	0.50	19.20	0.18	0.05
10	39.49	7.15	12.92	12.63	5.01	20.99	1.81	0.45
20	33.96	6.30	10.82	12.25	10.05	23.00	3.62	0.90
30	28.40	5.44	8.72	11.88	15.11	25.01	5.45	1.35
40	22.81	4.57	6.61	11.50	20.19	27.04	7.28	1.80
50	17.20	3.71	4.48	11.12	25.30	29.07	9.12	2.25
60	11.57	2.84	2.35	10.74	30.43	31.11	10.97	2.70
70	5.90	1.96	0.21	10.35	35.59	33.16	12.83	3.16

The reaction has stopped because there is no PAR left

The total amount of H2O = 3.1551 moles
 The final density of the WR = 3.38 g/ccm
 The final volume of the whole rock = 905.62 ccm
 This represents a 14.52 % change in volume
 and corresponds to a 4.78 % change in density
 The final volume of the total amount of H2O produced = 55.6806 ccm
 This corresponds to 6.148 vol% H2O
 The MAXIMUM amount of H2O produced = 0.0615 m3 H2O/m3
 or a total of 2.0597 m3 H2O
 The MINIMUM amount of H2O produced = 0.0526 m3 H2O/m3
 or a total of 1.7606 m3 H2O
 Between 1.0313 and 0.9237 moles of H2O will be released per Kg rock

IIA-9

Delta 0-18 of phases at each increment

INC	WR	HBL	EPI	PAR	QZ	OMP	GAR	H2O
0	5.50							
1	5.50	5.25	5.25	6.66	8.64	6.78	5.26	7.53
10	5.49	5.18	5.18	6.60	8.58	6.72	5.20	7.47
20	5.48	5.11	5.11	6.52	8.51	6.65	5.13	7.39
30	5.47	5.03	5.04	6.45	8.43	6.57	5.05	7.32
40	5.46	4.96	4.96	6.37	8.35	6.49	4.97	7.24
50	5.45	4.88	4.88	6.29	8.27	6.41	4.89	7.16
60	5.44	4.79	4.80	6.21	8.19	6.33	4.81	7.08
70	5.43	4.71	4.71	6.12	8.10	6.24	4.72	6.99

APPENDIX IIB Computer Program used to calculate Rayleigh Distillation
and Isotopic Exchange in Metapelites

```
C
C
C PROGRAM NUDIST
C-----
C
C Version PET I: Dehydration and isotopic exchange in metapelites
C (Modified by Eric Reusser and Gretchen Frueh from an
C original version by Doug Rumble III; last updated
C Nov. 5, 1986)
C-----
C Declarations and definitions
C-----
C
C INTEGER N
C PARAMETER ( N = 200 )
C
C REAL DOQZ(N), DOPHE(N), DOGAR(N), DOPAR(N), DOMUS(N),
C . DOH2O(N), DOWR(0:N), DOBIO(N), DOPLG(N), MBIO,
C . T, WRI, MPHE, MGAR, MPAR, MQZ, MH2O, DH2O, MMUS,
C . MPLG, DPAR, DPHE, DGAR, DQZ, DMUS, DBIO, XMUS,
C . XPHE, XGAR, XPAR, XQZ, XH2O, OSYS, XBIO, XPLG,
C . AQPAR, AQGAR, AQH2O, AQPLG, AQBIO, D18QZ, D18BI,
C . D18PH, D18PA, D18GR, D18WA, D18MU, D18PL, IVFR,
C . DENPHE, DENGR1, DENPAR, DENQZ, DENBIO, DENPLG,
C . DENMUS, WTPHE, WTGR1, WTPAR, WTQZ, WTBIO, WTPLG,
C . WTMUS, P, DENWRI, DENWR, VWRI, VWR, DENCH, MTOT,
C . VOLCH, MIN, MAX, VOLH2O, MINH2O, MAXH2O, VOLPER,
C . DENGR2, WTGR2, MGR1, MGR2, DGR1, DGR2, D18QZT,
C . NPAR, NPHE, NMUS, NBIO, NPLG, NGAR, NQZ, NH2O
C INTEGER INC, I, J
C
C CHARACTER*40 FNAME, INPUT
C
C DATA DENPHE, DENGR1, DENPAR, DENQZ, DENMUS, DENBIO, DENPLG, DENGR2/
C . 2.85, 4.06, 2.85, 2.65, 2.80, 3.0, 2.66, 4.13/
C
C DATA WTGR1, WTPAR, WTQZ, WTPHE, WTMUS, WTBIO, WTPLG, WTGR2/
C . 469.38, 382.19, 60.09, 400.70, 396.02, 457.60, 265.43,
C . 580.31/
C DATA P / 5000./
C
C DATA MPAR, MPHE, MGR1, MQZ/ 15., 30., 20., 35./
C-----
C Start of program
C-----
C VAX
C OPEN ( UNIT = 7, FILE = 'SYSS$OUTPUT', STATUS = 'NEW' )
C OPEN ( UNIT = 5, FILE = 'SYSS$INPUT', STATUS = 'NEW' )
C CDC
C OPEN ( UNIT = 7, FILE = 'OUTPUT', STATUS = 'NEW' )
C OPEN ( UNIT = 5, FILE = 'INPUT', STATUS = 'NEW' )
C PDP
C OPEN ( UNIT = 7, FILE = 'TT:', STATUS = 'NEW' )
C OPEN ( UNIT = 5, FILE = 'TT:', STATUS = 'NEW' )
C
C WRITE (7, 10)
10 FORMAT (//10X, '**** Program NUDIST Version PET I ****',
```

```

.      // 2X, 'This program computes dehydration and isotopic ',
.      'exchange of O-18 in metapelites',
.      // 5X, 'Type output file name')
READ   (5, '(A)')  FNAME
OPEN   ( UNIT = 1, FILE = FNAME, STATUS = 'NEW' )
WRITE  (7, *) 'Type initial whole rock O-18 [REAL]'
READ   (5, *)  WRI
WRITE  (7, *) 'Type initial temperature [deg C] [REAL]'
READ   (5, *)  T
WRITE  (7, *) 'Type number of increments [INTEGER]'
READ   (5, *)  INC
WRITE  (7, *) 'Type amount of MUS formed at each increment[REAL]'
READ   (5, *)  DMUS
WRITE  (7, *) 'Type initial modes of PAR, PHE, GR1, QZ [REAL]'
READ   (5, *)  MPAR, MPHE, MGR1, MQZ
WRITE  (1, 20) T, MPAR, MPHE, MGR1, MQZ, INC, DMUS
20  FORMAT (' **** Program NUDIST Version PET I ****',
.          // ' This program computes dehydration and isotopic',
.          ' exchange of O-18 '/' in metapelites for the reaction:',
.          // ' 3.914 (PAR) + 11.674 (PHE) + 6.352 (GR1) =',
.          ' 6.729 (MUS) + '/' 5.169 (BIO) + 3.075 (PLG) + ',
.          ' 2.000 (QZ) +3.641 (GR2) + 0.308 (H2O)'//,
.          ' At a constant temperature of ', F5.0, ' deg C'//,
.          ' Mineral modes: PAR = ', F6.2, ' PHE = ', F6.2,
.          ' GR1 = ', F6.2, ' QTZ = ', F6.2, /
.          ' Number of reaction increments = ', I3, '/', ' Amount of MUS',
.          ' formed at each increment = ', F6.2, '/', ' Plagioclase',
.          ' composition = An 20')
C -----
C The equation above is recalculated using actual mineral compositions,
C but based on the dehydration reaction of HEINRICH, 1982, p.35
C Coefficients are in O-units
C -----
C Start calculation
C -----
C Calculate alpha's,
C   PAR = MUS, QZ, GAR, BIO, PLG ref JAVOY, 1977
C   PLG = Ab80,
C
C   T = T + 273.15
C   AQPAR = 2.20E6 / T**2 - 0.6
C   AQGAR = 2.88E6 / T**2
C   AQH2O = 4.10E6 / T**2 - 3.7
C   AQBIO = 3.69E6 / T**2 - 0.6
C   AQPLG = 1.078E6 / T**2
C
C   DPAR = DMUS * (3.914 / 6.729)
C   DPHE = DMUS * (11.674 / 6.729)
C   DGR1 = DMUS * (6.352 / 6.729)
C   DBIO = DMUS * (5.169 / 6.729)
C   DPLG = DMUS * (3.075 / 6.729)
C   DQZ  = DMUS * (2.000 / 6.729)
C   DGR2 = DMUS * (3.641 / 6.729)
C   DH2O = DMUS * (0.308 / 6.729)
C
C Loop around increment
C
C   DOWR(0) = WRI
C   MMUS = 0.
C   MBIO = 0.

```

```

MPLG = 0.
MH2O = 0.
MGR2 = 0.
MGAR = MGR1 + MGR2

```

```

C-----
C
C   Volume of whole rock
C
VWRI = MGR1*WTGR1/(12.*DENGR1) + MQZ*WTQZ/(2.*DENQZ) +
.   MPAR*WTPAR/(12.*DENPAR) + MPHE*WTPHE/(12.*DENPHE) +
.   MBIO*WTBIO/(12.*DENBIO) + MPLG*WTPLG/(8.*DENPLG) +
.   MMUS*WTMUS/(12.*DENMUS) + MGR2*WRGR2/(12.*DENGR2)
C
VOLH2O = VH2O(P,T)
VOLH2O = VOLH2O*DH2O
VOLPER = VOLH2O*100./VWRI
IVFR   = VOLH2O/VWRI
DENWRI = MPAR*DENPAR + MPHE*DENPHE + MGR1*DENGR1 + MQZ*DENQZ +
.   MPLG*DENPLG + MBIO*DENBIO + MMUS*DENMUS + MGR2*DENGR2
DENWRI = DENWRI / 100
C
WRITE (1,25) DH2O, P, T, VH2O(P,T), VOLH2O, VOLPER, IVFR, VWRI
25  FORMAT (' The amount of H2O formed at each increment = ',
.         F7.4,' moles or O-units'/' The molar volume of H2O at',
.         F7.0,' bar and',F7.0,'K = ',F7.4,' ccm/mole'/' The',
.         ' amount of H2O formed at each increment = ',F7.4,' ccm'/',
.         ' This corresponds to', F7.2,' vol% of the initial whole',
.         ' rock'/' and a F/R ratio of ',F7.4,':1'/',
.         '/' The volume of the initial whole rock = ', F7.2,'ccm')
C
WRITE (1, 26) DENWRI
26  FORMAT (' The density of the initial rock =',F7.2,' g/ccm'//)
C
C-----
WRITE (1, 30) MPAR, MPHE, MGR1, MGR2, MQZ, MMUS, MBIO, MPLG, MH2O
30  FORMAT (' Amount of phases at each increment'/' INC   PAR',
.         '   PHE   GR1   GR2   QZ   MUS   BIO',
.         '   PLG   H2O'/'   0',9(F8.2))
C-----
C
DO 1 I = 1, INC
  MPAR = MPAR - DPAR
  MPHE = MPHE - DPHE
  MGR1 = MGR1 - DGR1
  IF ( MPAR.GE. 0. .AND. MPHE.GE. 0. .AND. MGR1.GE. 0.
.     .AND. MQZ.GE. 0. ) THEN
    MMUS = MMUS + DMUS
    MBIO = MBIO + DBIO
    MPLG = MPLG + DPLG
    MQZ  = MQZ  + DQZ
    MGR2 = MGR2 + DGR2
    MH2O = MH2O + DH2O
    MGAR = MGR1 + MGR2
  MTOT = MPAR + MPHE + MGAR + MQZ + MBIO + MMUS + MPLG
  MPAR = (MPAR*100.)/MTOT
  MPHE = (MPHE*100)/MTOT
  MGAR = (MGAR*100)/MTOT
  MBIO = (MBIO*100)/MTOT
  MMUS = (MMUS*100)/MTOT
  MPLG = (MPLG*100)/MTOT

```

$$MQZ = (MQZ*100)/MTOT$$

$$MGR2 = (MGR2*100)/MTOT$$

C
C
C

WRITE (1, 40) I,MPAR,MPHE,MGR1, MGR2, MQZ, MMUS, MBIO, MPLG, MH2O
40 FORMAT (1X,I3,9(F8.2))

C
C
C
C

Calculate delta 0-18 of system

$$MTOT = MPAR + MPHE + MGAR + MQZ + MBIO + MMUS + MPLG + MH2O$$

$$NPAR = (MPAR*100) / MTOT$$

$$NPHE = (MPHE*100) / MTOT$$

$$NGAR = (MGAR*100) / MTOT$$

$$NBIO = (MBIO*100) / MTOT$$

$$NMUS = (MMUS*100) / MTOT$$

$$NPLG = (MPLG*100) / MTOT$$

$$NQZ = (MQZ*100) / MTOT$$

$$NH2O = (MH2O*100) / MTOT$$

C

$$OSYS = NPAR + NPHE + NQZ + NGAR + NH2O + NMUS + NBIO \\ + NPLG$$

$$XPAR = NPAR / OSYS$$

$$XQZ = NQZ / OSYS$$

$$XPHE = NPHE / OSYS$$

$$XGAR = NGAR / OSYS$$

$$XPLG = NPLG / OSYS$$

$$XH2O = NH2O / OSYS$$

$$XBIO = NBIO / OSYS$$

$$XMUS = NMUS / OSYS$$

C
C
C

Rock reequilibrates with increment of water

$$D18QZT = XGAR*AQGAR + XPHE*AQPAR + XPAR*AQPAR \\ + XMUS*AQPAR + XBIO*AQBIO + XPLG*AQPLG$$

$$D18QZ = WRI + D18QZT + XH2O*AQH2O$$

$$D18PA = D18QZ - AQPAR$$

$$D18PH = D18QZ - AQPAR$$

$$D18GR = D18QZ - AQGAR$$

$$D18MU = D18QZ - AQPAR$$

$$D18BI = D18QZ - AQBIO$$

$$D18PL = D18QZ - AQPLG$$

$$D18WA = D18QZ - AQH2O$$

$$DOQZ(I) = D18QZ$$

$$DOPAR(I) = D18PA$$

$$DOPHE(I) = D18PH$$

$$DOGAR(I) = D18GR$$

$$DOBIO(I) = D18BI$$

$$DOPLG(I) = D18PL$$

$$DOMUS(I) = D18MU$$

$$DOH2O(I) = D18WA$$

C
C
C
C

At this point the increment of water is removed from the system and
a new Delta 0-18 for the whole rock is calculated

$$OSYS = NPAR + NPHE + NGAR + NBIO + NPLG + NQZ + NMUS$$

$$XGAR = NGAR / OSYS$$

$$XPAR = NPAR / OSYS$$

$$XPHE = NPHE / OSYS$$

$$XQZ = NQZ / OSYS$$

```

        XBIO = NBIO / OSYS
        XMUS = NMUS / OSYS
        XPLG = NPLG / OSYS
C
        WRI = D18GR*XGAR + D18PH*XPHE + D18PA*XPAP + D18QZ*XQZ
          + D18BI*XBIO + D18MU*XMUS + D18PL*XPLG
        DOWR(I) = WRI
        J = I
    ELSE
        IF ( MPAR .LT. 0. ) THEN
            WRITE (7, *) 'No PAR left'
            WRITE (1, 80)
80 FORMAT (/ ' The reaction has stopped because there is no PAR left' )
        END IF
        IF ( MPHE .LT. 0. ) THEN
            WRITE (7, *) 'No PHE left'
            WRITE (1, 84)
84 FORMAT (/ ' The reaction has stopped because there is no PHE left' )
        END IF
        IF ( MGR1 .LT. 0. ) THEN
            WRITE (7, *) 'No GR1 left'
            WRITE (1, 85)
85 FORMAT (/ ' The reaction has stopped because there is no GR1 left' )
        END IF
        GO TO 2
    END IF
1 CONTINUE
  WRITE (7, *) 'Reaction is finished'
-----
C
C
C   Volume of whole rock
C
2   VWR = MPAR*WTPAR/(12.*DENPAR) + MGR1*WTGR1/(12.*DENGR1) +
    .   MPHE*WTPHE/(12.*DENPHE) + MBIO*WTBIO/(12.*DENBIO) +
    .   MQZ*WTQZ/(2.*DENQZ) + MPLG*WTPLG/(8.*DENPLG) +
    .   MMUS*WTMUS/(12.*DENMUS) + MGR2*WTGR2/(12.*DENGR2)
C
  VOLH2O = VH2O(P,T)
  VOLH2O = VOLH2O*MH2O
  VOLPER = VOLH2O*100./VWR
C
  DENWR = MPAR*DENPAR + MPHE*DENPHE + MGR1*DENGR1 + MQZ*DENQZ +
    .   MPLG*DENPLG + MBIO*DENBIO + MMUS*DENMUS + MGR2*DENGR2
  DENWR = DENWR / 100
  MIN = (MH2O*1000)/(VWR * DENWR)
  MAX = (MH2O*1000)/(VWRI * DENWRI)
  VOLCH = 100 - (100*VWR / VWRI)
  DENCH = 100 - (DENWR*100 / DENWRI)
  MINH2O = VOLH2O / VWRI
  MAXH2O = VOLH2O / VWR
  WRITE (1,44) MH2O, DENWR
44 FORMAT (/, ' The total amount of H2O = ',F7.4,' moles',/,
    .   ' The final density of the WR = ',F7.2,' g/ccm')
C
  WRITE (1, 45) VWR, VOLCH, DENCH, VOLH2O, VOLPER, MAXH2O
45 FORMAT ( ' The final volume of the whole rock = ', F7.2, ' ccm',/,
    .   ' This represents a',F7.2,' % change in volume',/,
    .   ' and corresponds to a',F7.2,' % change in density',/,
    .   ' The final volume of the total amount of H2O produced = ',
    .   F7.4,' ccm'/' This corresponds to',F7.3,' vol% H2O',/

```


C PURE H2O

C

```

EPS = 0.01
T2 = T**2
R = 83.143
B=29.
C=(290.78-0.30276*T+1.4774E-4*T2)*1.E6
D=(-8374.+19.437*T-8.148E-3*T2)*1.E6
E=(76600.-133.9*T+0.1071*T2)*1.E6
V0=15.
IF (P.LT.1000.) V0=22.5
IF (P.GE.210..AND.P.LT.600..AND.TC.GE.550.) V0=75.
IF (P.GE.210..AND.P.LT.600..AND.TC.LT.550.) V0=35.
IF (P.GE.210..AND.P.LT.600..AND.TC.LT.400.) V0=20.
IF (P.GE.100..AND.P.LT.210..AND.TC.LT.400.) V0=15.
IF (P.GE.100..AND.P.LT.210..AND.TC.GE.400.) V0=100.
IF (P.LT.100.) V0=500.
IF (P.LT.5.) V0=7000.

```

C

```

T12 = SQRT (T)
RT = R * T

```

C

C Iteration loop to approximate molar volume

C

```

1   Y = 0.25 * B / V0
    CY = 1. - Y

```

C

```

PREP = RT * (1. + Y*(1. + Y*CY)) / (V0 * CY**3)
PATT = (C + (D + E/V0)/V0) / (T12 * V0 * (V0+B))
DPREP = (2. * (RT * (CY-Y**2)/(V0*CY**3) - PREP)/CY - PREP)/V0
DPATT = -(PATT*(2.*V0+B) + (D+2.*E/V0)/(T12*V0**2)) / (V0*(V0+B))

```

C

C Newton - Raphson approximation

C

```

V = V0 - (PREP - PATT - P)/(DPREP - DPATT)

```

C

C If molar volume is enough accurate RETURN, else next iteration step

C

```

IF (ABS (V-V0) .LT. EPS) GO TO 2
V0 = V
GO TO 1

```

C

C *** End of subroutine VSOLVE

C

```

2   VH2O = V
    END

```

 *APPENDIX IIB: Calculated Results of NUDIST program for Rayleigh *****
 * Distillation of Metapelites (Corresponds to Fig. 3.6) *****

**** Program NUDIST Version PET I ****

This program computes dehydration and isotopic exchange of O-18
 in metapelites for the reaction:

3.914 (PAR) + 11.674 (PHE) + 6.352 (GR1) = 6.729 (MUS) +
 5.169 (BIO) + 3.075 (PLG) + 2.000 (QZ) + 3.641 (GR2) + 0.308 (H2O)

At a constant temperature of 600. deg C

Mineral modes: PAR = 25.00 PHE = 25.00 GR1 = 20.00 QTZ = 30.00
 Number of reaction increments =200
 Amount of MUS formed at each increment = 0.10
 Plagioclase composition = An 20
 The amount of H2O formed at each increment = 0.0046 moles or O-units
 The molar volume of H2O at 5000. bar and 873.K = 22.3622 ccm/mole
 The amount of H2O formed at each increment = 0.1024 ccm
 This corresponds to 0.01 vol% of the initial whole rock
 and a F/R ratio of 0.0001:1

The volume of the initial whole rock = 1105.10ccm
 The density of the initial rock = 3.03 g/ccm

Amount of phases at each increment

INC	PAR	PHE	GR1	GR2	QZ	MUS	BIO	PLG	H2O
0	25.00	25.00	20.00	0.00	30.00	0.00	0.00	0.00	0.00
1	24.95	24.83	19.91	0.05	30.04	0.10	0.08	0.05	0.00
10	24.48	23.32	19.06	0.54	30.37	1.00	0.77	0.46	0.05
20	23.96	21.64	18.11	1.08	30.74	2.01	1.54	0.92	0.09
30	23.43	19.96	17.17	1.62	31.11	3.01	2.31	1.38	0.14
40	22.91	18.27	16.22	2.16	31.49	4.02	3.09	1.84	0.18
50	22.38	16.58	15.28	2.71	31.86	5.03	3.86	2.30	0.23
60	21.85	14.88	14.34	3.25	32.23	6.04	4.64	2.76	0.27
70	21.32	13.18	13.39	3.79	32.61	7.06	5.42	3.23	0.32
80	20.79	11.47	12.45	4.33	32.98	8.08	6.21	3.69	0.37
90	20.25	9.76	11.50	4.87	33.36	9.10	6.99	4.16	0.41
100	19.72	8.05	10.56	5.41	33.74	10.12	7.77	4.63	0.46
110	19.18	6.33	9.62	5.95	34.11	11.15	8.56	5.09	0.50
120	18.65	4.61	8.67	6.49	34.49	12.17	9.35	5.56	0.55
130	18.11	2.88	7.73	7.03	34.87	13.20	10.14	6.03	0.60
140	17.57	1.15	6.78	7.58	35.25	14.24	10.93	6.51	0.64
146	17.24	0.11	6.22	7.90	35.47	14.86	11.41	6.79	0.67

The reaction has stopped because there is no PHE left

The total amount of H2O = 0.6683 moles
 The final density of the WR = 2.94 g/ccm
 The final volume of the whole rock = 1149.77 ccm
 This represents a -4.04 % change in volume
 and corresponds to a 2.98 % change in density
 The final volume of the total amount of H2O produced =14.9440 ccm

IIB-9

This corresponds to 1.300 vol% H₂O

The MAXIMUM amount of H₂O produced = 0.0130 m³ H₂O/m³

The MINIMUM amount of H₂O produced = 0.0135 m³ H₂O/m³

Between 0.1976 and 0.1994 moles of H₂O will be released per Kg rock

Delta 0-18 of phases at each increment

INC	WR	PAR	PHE	GAR	QZ	MUS	BIO	PLG	H ₂ O
0	7.50								
1	7.50	7.11	7.11	5.62	9.40	7.11	5.16	7.98	7.72
10	7.50	7.11	7.11	5.62	9.39	7.11	5.15	7.98	7.72
20	7.50	7.11	7.11	5.61	9.39	7.11	5.15	7.98	7.71
30	7.50	7.10	7.10	5.61	9.39	7.10	5.15	7.97	7.71
40	7.50	7.10	7.10	5.61	9.38	7.10	5.14	7.97	7.71
50	7.50	7.10	7.10	5.60	9.38	7.10	5.14	7.97	7.70
60	7.50	7.09	7.09	5.60	9.38	7.09	5.14	7.96	7.70
70	7.50	7.09	7.09	5.60	9.37	7.09	5.13	7.96	7.70
80	7.50	7.08	7.08	5.59	9.37	7.08	5.13	7.96	7.69
90	7.50	7.08	7.08	5.59	9.37	7.08	5.13	7.95	7.69
100	7.50	7.08	7.08	5.59	9.36	7.08	5.12	7.95	7.69
110	7.50	7.07	7.07	5.58	9.36	7.07	5.12	7.95	7.68
120	7.50	7.07	7.07	5.58	9.36	7.07	5.12	7.94	7.68
130	7.50	7.07	7.07	5.58	9.35	7.07	5.11	7.94	7.68
140	7.50	7.06	7.06	5.57	9.35	7.06	5.11	7.94	7.67
146	7.50	7.06	7.06	5.57	9.35	7.06	5.11	7.93	7.67

APPENDIX IIC: Computer Program used to calculate isotopic exchange during
infiltration of metabasites

```
C
C-----
C
C      PROGRAM INZEST
C-----
C
C Version AMP I: Hydration of OMP + GAR + QTZ + EPI + KY /
C               to form Hbl + Plg / equilibrium model
C               (updated last 10.11.86)
C               written by G. Frueh, based on the step-wise calculation
C               method presented by D. Rumble III (1982)
C-----
C Declarations and definitions
C-----
C
C      INTEGER N
C      PARAMETER ( N = 200 )
C
C      REAL      DOQZ(N), DOHBL(N), DOEPI(N), DOGAR(N), DOPLG(N), MHB,
C      .         DOOMP(N), DOH2O(N), DOWR(0:N), DKYN, MKYN, MTOT, WTHB,
C      .         T, WRI, MHBL, MEPI, MGAR, MPLG, MQZ, MH2O, MOMP, DENHB,
C      .         DOMP, DPLG, DEPI, DGAR, DHBL, DQZ, DH2O, WTKYN, H2OI,
C      .         XOMP, XHBL, XEPI, XGAR, XPLG, XQZ, XH2O, OSYS,
C      .         AQHBL, AQPLG, AQGAR, AQEPI, AQH2O, AQOMP, D18QZ,
C      .         D18HB, D18PL, D18EP, D18GR, D18OM, D18WA, DENKYN,
C      .         DENHBL, DENEPI, DENGAR, DENPLG, DENQZ, DENOMP, P,
C      .         WTHBL, WTEPI, WTGAR, WTPLG, WTQZ, WTOMP,
C      .         NQZ, NHBL, NEPI, NPLG, NGAR, NOMP, NH2O, VWRI,
C      .         DENWRI, DENWR, DENCH, IVFR, TOTH2O, VOLCH, MIN,
C      .         MAX, VOLH2O, MINH2O, MAXH2O, TOTMIN,
C      .         TOTMAX, VWR, VOLPER
C      INTEGER INC, I, J
C
C      CHARACTER*40 FNAME
C
C      DATA DENHBL, DENEPI, DENGAR, DENPLG, DENQZ, DENOMP, DENKYN, DENHB/ 3.10,
C      .         3.30, 3.70, 2.70, 2.65, 3.33, 3.55, 3.30/
C
C      DATA WTHBL, WTEPI, WTGAR, WTPLG, WTQZ, WTOMP, WTKYN, WTHB/
C      .         841.36, 454.35, 454.88, 276.02, 60.09, 208.34, 162.03,
C      .         817.74/
C
C WTHB and DENHB refer to old hornblende (eclogite facies)
C See REACT output for mineral compositions
C
C      DATA P / 5000./
C
C      DATA MOMP, MEPI, MGAR, MQZ, MKYN, MHB/ 35., 5., 35., 10., 10., 5./
C
C      DATA WRI/ 5.5/
C-----
C Start of program
C-----
C VAX
C      OPEN ( UNIT = 7, FILE = 'SYS$OUTPUT', STATUS = 'NEW' )
C      OPEN ( UNIT = 5, FILE = 'SYS$INPUT', STATUS = 'NEW' )
C CDC
C      OPEN ( UNIT = 7, FILE = 'OUTPUT', STATUS = 'NEW' )
```

```

C      OPEN ( UNIT = 5, FILE = 'INPUT', STATUS = 'NEW' )
C      PDP
C      OPEN ( UNIT = 7, FILE = 'TT:', STATUS = 'NEW' )
C      OPEN ( UNIT = 5, FILE = 'TT:', STATUS = 'NEW' )
C
C      WRITE (7, 10)
10  FORMAT (//10X, '**** Program INZESTKY VERSION I ****',
.         // 5X, 'This program computes hydration of and isotopic',
.         ' exchange in eclogites',
.         // 5X, 'Type output file name')
      READ (5, '(A)') FNAME
      OPEN ( UNIT = 1, FILE = FNAME, STATUS = 'NEW' )
      WRITE (7, *) 'Type number of increments [INTEGER]'
      READ (5, *) INC
C      WRITE (7, *) 'Type initial whole rock O-18 [REAL]'
C      READ (5, *) WRI
C      WRITE (7, *) 'Type initial modes of HBL, EPI, PAR, QTZ,',
C      ' GAR [REAL]'
C      READ (5, *) MHL, MEPI, MPAR, MQZ, MGAR
      WRITE (7, *) 'Type amount of H2O infiltrated at each increment',
.         ' [REAL]'
      READ (5, *) DH2O
      WRITE (7, *) ' Type Delta O-18 of infiltrating water'
      READ (5, *) H2OI
      WRITE (7, *) 'Type initial temperature [deg C] [REAL]'
      READ (5, *) T
      WRITE (1, 20) T, INC, H2OI, DOMP, MGAR, MQZ, MEPI,
.         MKYN, MHB
20  FORMAT (' **** Program INZESTKY Version I ****',
.         // ' This program computes infiltration and isotopic',
.         ' exchange for the reaction'// ' 10.225(KYN) + 2.392(EPI)',
.         ' + 6.092 (QTZ) + 40.488 (OMP) + 12.60 (GAR) '/,
.         ' + 1.658 (H2O) = 42.00 (HBL) + 31.560 (PLG)'//,
.         ' At a constant temperature of ', F5.0, ' deg C'//,
.         ' Number of reaction increments = ', I3/,
.         ' The initial delta O-18 of H2O = ', F6.2/,
.         ' Initial modes: OMP = ', F5.2, ' GAR = ', F5.2,
.         ' QTZ = ', F5.2, ' EPI = ', F5.2, ' KYN = ', F5.2, /,
.         ' HBL = ', F5.2)
C-----
C      Coefficients are in O-units
C-----
C      Start calculation
C-----
C      Calculate alpha's,
C      HBL, PAR = MUS, QZ, GAR ref JAVOY, 1977
C      OMP ref MATTHEWS; EPI ref RUMBLE (program)
C      Anorthite component in PLG = 0.3
C
      T = T + 273.15
      AQHBL = 3.15E6 / T**2 - 0.3
      AQEPI = 3.148E6 / T**2 - 0.3
      AQPLG = 1.282E6 / T**2
      AQGAR = 2.88E6 / T**2
      AQH2O = 4.10E6 / T**2 - 3.7
      AQOMP = 1.585E6 / T**2
C
C
      DHBL = DH2O * (42.00 / 1.658)
      DEPI = DH2O * (2.392 / 1.658)

```

```

DGAR = DH2O * (12.60 / 1.658)
DPLG = DH2O * (31.56 / 1.658)
DQZ  = DH2O * (6.092 / 1.658)
DKYN = DH2O * (10.225 / 1.658)
DOMP = DH2O * (40.488 / 1.658)

```

C

C Loop around increment

C

```

DOWR(0) = WRI
MHLB = 0.
MH2O = 0.
MPLG = 0.
MHLB = MHB + MHLB

```

C

C-----

C

C

C

Volume of whole rock

```

VWRI = MHLB*WTHB/(24.*DENHB) + MGAR*WTGAR/(12.*DENGAR) +
.     MEPI*WTEPI/(13.*DENEPI) + MOMP*WTOMP/(6.*DENOMP) +
.     MQZ*WTQZ/(2.*DENQZ) + MPLG*WTPLG/(12.*DENPLG) +
.     MKYN*WTKYN/(5.*DENKYN)

```

C

```

VOLH2O = VH2O(P,T)
VOLH2O = VOLH2O*DH2O
VOLPER = VOLH2O*100./VWRI
IVFR   = VOLH2O/VWRI
TOTH2O = IVFR * 33.5
DENWRI = MHLB*DENHB + MEPI*DENEPI + MGAR*DENGAR + MQZ*DENQZ +
.       MOMP*DENOMP + MPLG*DENPLG + MKYN*DENKYN
DENWRI = DENWRI / 100

```

C

```

WRITE (1,25) DH2O, P, T, VH2O(P,T), VOLH2O, VOLPER, VWRI
25 FORMAT (' The amount of H2O infiltrating at each increment = ',
.         F7.4,' moles or O-units'/' The molar volume of H2O at',
.         F7.0,' bar and',F7.0,'K =',F7.4,'ccm/mole'/,
.         ' The amount of H2O infiltrating at each increment =',
.         F7.4,' ccm'/' This',
.         ' corresponds to', F7.2,' vol% of the initial whole rock',
.         '/' The volume of the initial whole rock = ', F7.2,' ccm')
WRITE (1, 26) DENWRI, IVFR, TOTH2O
26 FORMAT (' The density of the initial rock =',F7.2,' g/ccm'/,
.         ' The instantaneous FR-ratio at each increment =',F7.5,/
.         ' The TOTAL amount of H2O needed at each increment for',
.         '/' the entire amount of mafic rocks =',F7.4,' ccm'//)

```

C

C-----

C

```

WRITE (1, 30) MEPI, MQZ, MOMP, MGAR, MKYN, MHLB, MPLG, MH2O
30 FORMAT (' Amount of phases at each increment'/'/' INC     EPI',
.         '      QTZ      OMP      GAR      KYN      HBL',
.         '      PLG      H2O'/'/' 0',8(1X,F8.2))

```

C

```

DO 1 I = 1, INC
  MTOT = MHLB + MEPI + MPLG + MQZ + MOMP + MGAR + MKYN + DH2O
  MHLB = MHLB*100/MTOT
  MEPI = MEPI*100/MTOT
  MPLG = MPLG*100/MTOT
  MOMP = MOMP*100/MTOT
  MGAR = MGAR*100/MTOT

```

IIC-4

```

MKYN = MKYN*100/MTOT
MQZ = MQZ*100/MTOT
MEPI = MEPI - DEPI
MQZ = MQZ - DQZ
MOMP = MOMP - DOMP
MGAR = MGAR - DGAR
MKYN = MKYN - DKYN
IF ( MOMP.GE. 0. .AND. MEPI.GE. 0. .AND. MGAR.GE. 0.
    .AND. MQZ.GE. 0. .AND. MKYN.GE. 0.) THEN
    MHBL = MHBL + DHBL
    MPLG = MPLG + DPLG
    MH2O = MH2O + DH2O

```

```

WRITE (1, 40) I, MEPI, MQZ, MOMP, MGAR, MKYN, MHBL, MPLG, MH2O
40 FORMAT (1X, I3, 8(1X, F8.2))

```

C

C RE-CALCULATE MODES OF ROCKS WITHOUT KYANITE

C

```

MTOT = MHBL + MEPI + MPLG + MQZ + MOMP + MGAR + MH2O
NHBL = MHBL*100/MTOT
NEPI = MEPI*100/MTOT
NPLG = MPLG*100/MTOT
NOMP = MOMP*100/MTOT
NGAR = MGAR*100/MTOT
NH2O = DH2O*100/MTOT
OSYS = NHBL + NEPI + NPLG + NQZ + NOMP + NGAR + NH2O
XHBL = NHBL / OSYS
XEPI = NEPI / OSYS
XPLG = NPLG / OSYS
XQZ = NQZ / OSYS
XOMP = NOMP / OSYS
XGAR = NGAR / OSYS
XH2O = NH2O / OSYS

```

C

```

D18QZ = XHBL*AQHBL + XEPI*AQEPI + XGAR*AQGAR +
        XPLG*AQPLG + XOMP*AQOMP
D18QZ = WRI + D18QZ + XH2O * AQH2O
D18HB = D18QZ - AQHBL
D18EP = D18QZ - AQEPI
D18PL = D18QZ - AQPLG
D18GR = D18QZ - AQGAR
D18OM = D18QZ - AQOMP
D18WA = D18QZ - AQH2O
DOQZ(I) = D18QZ
DOHBL(I) = D18HB
DOEPI(I) = D18EP
DOGAR(I) = D18GR
DOOMP(I) = D18OM
DOPLG(I) = D18PL
DOH2O(I) = D18WA
WRITE (2, *) DOH2O(I)

```

C

C

```

OSYS = NHBL + NEPI + NGAR + NOMP + NPLG + NQZ
XHBL = NHBL / OSYS
XEPI = NEPI / OSYS
XGAR = NGAR / OSYS
XPLG = NPLG / OSYS
XOMP = NOMP / OSYS
XQZ = NQZ / OSYS

```

C

```

WRI = D18HB*XHBL + D18EP*XEPI + D18GR*XGAR + D18OM*XOMP

```

```

      + D18PL*XPLG + D18QZ*XQZ
      DOWR(I) = WRI
      J = I
    ELSE
      IF ( MOMP .LT. 0. ) THEN
        WRITE (7, *) 'No OMP left'
        WRITE (1, 80)
80 FORMAT (/ ' The reaction has stopped because there is no OMP left')
      END IF
      IF ( MEPI .LT. 0. ) THEN
        WRITE (7, *) 'No EPI left'
        WRITE (1, 84)
84 FORMAT (/ ' The reaction has stopped because there is no EPI left')
      END IF
      IF ( MGAR .LT. 0. ) THEN
        WRITE (7, *) 'No GAR left'
        WRITE (1, 85)
85 FORMAT (/ ' The reaction has stopped because there is no GAR left')
      END IF
      IF ( MQZ .LT. 0. ) THEN
        WRITE (7, *) 'No QTZ left'
        WRITE (1, 90)
90 FORMAT (/ ' The reaction has stopped because there is no QTZ left')
      END IF
      IF ( MKYN .LT. 0. ) THEN
        WRITE (7, *) 'No KYN left'
        WRITE (1, 95)
95 FORMAT (/ ' The reaction has stopped because there is no KYN left')
      END IF
      GO TO 2
    END IF
1 CONTINUE
  WRITE (7, *) 'Reaction is finished'

```

C

C

C

C

2

.

.

C

Volume of whole rock

```

VWR = MHBL*WTHBL/(24.*DENHBL) + MGAR*WTGAR/(12.*DENGAR) +
      MEPI*WTEPI/(13.*DENEPI) + MOMP*WTOMP/(6.*DENOMP) +
      MQZ*WTQZ/(2.*DENQZ) + MPLG*WTPLG/(12.*DENPLG)

```

VOLH2O = VH2O(P,T)

VOLH2O = VOLH2O*MH2O

VOLPER = VOLH2O*100./VWR

DENWR = MHBL*DENHBL + MEPI*DENEPI + MGAR*DENGAR + MQZ*DENQZ +

MOMP*DENOMP + MPLG*DENPLG + MKYN*DENKYN

DENWR = DENWR / 100

MIN = (MH2O*1000)/(VWR * DENWR)

MAX = (MH2O*1000)/(VWRI * DENWRI)

VOLCH = 100 - (100*VWR / VWRI)

DENCH = (DENWR*100 / DENWRI) - 100

MINH2O = VOLH2O / VWRI

MAXH2O = VOLH2O / VWR

TOTMIN = MINH2O * 33.5

TOTMAX = MAXH2O * 33.5

C

WRITE (1,44) MH2O, DENWR

```

44 FORMAT (/, ' The total amount of H2O needed to hydrate 100 O-units',
      . ' of rock =' ,F7.4, ' moles'/,
      . ' The final density of the WR =' ,F7.2, ' g/ccm')

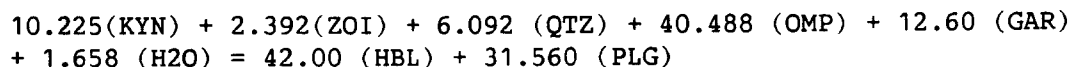
```


IIC - 8

 *APPENDIX IIC: Calculated Results of INZESTKY program for Rayleigh *****
 * Distillation of Metapelites *****

**** Program INZESTKY Version I ****

This program computes infiltration and isotopic exchange for the reaction



At a constant temperature of 600. deg C

Number of reaction increments = 100

The initial delta O-18 of H2O = 7.70

Initial modes: OMP = 35.00 GAR = 35.00 QTZ = 10.00 ZOI = 5.00 KYN = 10.00
 HBL = 5.00

The amount of H2O infiltrating at each increment = 0.0400 moles or O-units

The molar volume of H2O at 5000. bar and 873.K = 22.3622ccm/mole

The amount of H2O infiltrating at each increment = 0.8945 ccm

This corresponds to 0.09 vol% of the initial whole rock

The volume of the initial whole rock = 1036.04 ccm

The density of the initial rock = 3.41 g/ccm

The instantaneous FR-ratio at each increment = 0.00086

The TOTAL amount of H2O needed at each increment for

the entire amount of mafic rocks = 0.0289 ccm

Amount of phases at each increment

INC	ZOI	QTZ	OMP	GAR	KYN	HBL	PLG	H2O
0	5.00	10.00	35.00	35.00	10.00	5.00	0.00	0.00
1	4.94	9.85	34.01	34.68	9.75	6.01	0.76	0.04
5	4.70	9.24	30.05	33.41	8.75	10.05	3.80	0.20
10	4.40	8.49	25.10	31.82	7.50	15.09	7.60	0.40
15	4.11	7.74	20.17	30.23	6.25	20.12	11.39	0.60
20	3.81	6.99	15.25	28.65	5.00	25.14	15.17	0.80
25	3.51	6.24	10.34	27.07	3.76	30.15	18.94	1.00
30	3.22	5.49	5.43	25.49	2.52	35.15	22.70	1.20
35	2.92	4.75	0.54	23.92	1.28	40.14	26.46	1.40

The reaction has stopped because there is no OMP left

The total amount of H2O needed to hydrate 100 O-units of rock = 1.4000 moles

The final density of the WR = 3.07 g/ccm

The final volume of the whole rock = 1000.92 ccm

This represents a 3.39 % change in volume

and corresponds to a -10.00 % change in density

The final volume of the total amount of H2O needed

to hydrate the boudin and its tails (33.51 ccm) = 31.3071 ccm

This corresponds to 3.128 vol% H2O

The MAXIMUM amount of H2O needed = 0.0313 m3 H2O/m3

or a total of 1.0478 m3 H2O

The MINIMUM amount of H2O needed = 0.0302 m3 H2O/m3

or a total of 1.0123 m3 H2O

Between 0.4557 and 0.3962 moles of H2O will be required per Kg rock that is hydrated.

IIC - 7

```

C      Y      Hardsphere term B/(4*V)
C      CY     Complement of Y: 1. - Y
C      PREP   Pressure due to repulsive intermolecular forces
C      PATT   Pressure due to attractive intermolecular forces
C      DPREP, DPATT Differential of PREP resp. PATT
C      EPS    Absolute accuracy of the molar volume
C
C*****
C
C PURE H2O
C
      EPS = 0.01
      T2 = T**2
      R = 83.143
      B=29.
      C=(290.78-0.30276*T+1.4774E-4*T2)*1.E6
      D=(-8374.+19.437*T-8.148E-3*T2)*1.E6
      E=(76600.-133.9*T+0.1071*T2)*1.E6
      V0=15.
      IF (P.LT.1000.) V0=22.5
      IF (P.GE.210..AND.P.LT.600..AND.TC.GE.550.) V0=75.
      IF (P.GE.210..AND.P.LT.600..AND.TC.LT.550.) V0=35.
      IF (P.GE.210..AND.P.LT.600..AND.TC.LT.400.) V0=20.
      IF (P.GE.100..AND.P.LT.210..AND.TC.LT.400.) V0=15.
      IF (P.GE.100..AND.P.LT.210..AND.TC.GE.400.) V0=100.
      IF (P.LT.100.) V0=500.
      IF (P.LT.5.) V0=7000.
C
      T12 = SQRT (T)
      RT = R * T
C
C Iteration loop to approximate molar volume
C
1     Y = 0.25 * B / V0
      CY = 1. - Y
C
      PREP = RT * (1. + Y*(1. + Y*CY)) / (V0 * CY**3)
      PATT = (C + (D + E/V0)/V0) / (T12 * V0 * (V0+B))
      DPREP = (2. * (RT * (CY-Y**2)/(V0*CY**3) - PREP)/CY - PREP)/V0
      DPATT = -(PATT*(2.*V0+B) + (D+2.*E/V0)/(T12*V0**2)) / (V0*(V0+B))
C
C Newton - Raphson approximation
C
      V = V0 - (PREP - PATT - P)/(DPREP - DPATT)
C
C If molar volume is enough accurate RETURN, else next iteration step
C
      IF (ABS (V-V0) .LT. EPS) GO TO 2
      V0 = V
      GO TO 1
C
C *** End of subroutine VSOLVE
C
2     VH2O = V
      END

```

IIC - 9

Delta 0-18 of phases at each increment

INC	WR	OMP	GAR	ZOI	QZ	HBL	PLG	H2O
0	5.50							
1	5.50	6.47	4.77	4.72	8.55	4.71	6.86	6.87
5	5.50	6.49	4.79	4.74	8.56	4.73	6.88	6.89
10	5.49	6.51	4.81	4.76	8.59	4.75	6.90	6.91
15	5.49	6.53	4.83	4.78	8.61	4.78	6.93	6.93
20	5.49	6.55	4.85	4.80	8.63	4.79	6.94	6.95
25	5.48	6.57	4.87	4.82	8.64	4.81	6.96	6.97
30	5.48	6.58	4.88	4.83	8.66	4.83	6.98	6.98
35	5.48	6.60	4.90	4.85	8.68	4.85	7.00	7.00

IIC-10

```

*****
*APPENDIX IIC: Calculated Results of INZESTKY program for Rayleigh      *****
*           Distillation of Metapelites (Corresponds to Fig. 3.7:      *****
*           Composition of Infiltration water = 7.70‰)                  *****
*****
**** Program INZESTKY Version I ****
  
```

This program computes infiltration and isotopic exchange for the reaction

10.225(KYN) + 2.392(ZOI) + 6.092 (QTZ) + 40.488 (OMP) + 12.60 (GAR)
 + 1.658 (H2O) = 42.00 (HBL) + 31.560 (PLG)

At a constant temperature of 600. deg C

Number of reaction increments = 200

The initial delta O-18 of H2O = 7.70

Initial modes: OMP = 35.00 GAR = 35.00 QTZ = 10.00 ZOI = 5.00 KYN =10.00
 HBL = 5.00

The amount of H2O infiltrating at each increment = 0.0400 moles or O-units

The molar volume of H2O at 5000. bar and 873.K =22.3622ccm/mole

The amount of H2O infiltrating at each increment = 0.8945 ccm

This corresponds to 0.09 vol% of the initial whole rock

The volume of the initial whole rock = 1036.04 ccm

The density of the initial rock = 3.41 g/ccm

The instantaneous FR-ratio at each increment =0.00086

The TOTAL amount of H2O needed at each increment for

the entire amount of mafic rocks = 0.0289 ccm

Amount of phases at each increment

INC	ZOI	QTZ	OMP	GAR	KYN	HBL	PLG	H2O
0	5.00	10.00	35.00	35.00	10.00	5.00	0.00	0.00
1	4.94	9.85	34.01	34.68	9.75	6.01	0.76	0.04
5	4.70	9.24	30.05	33.41	8.75	10.05	3.80	0.20
10	4.40	8.49	25.10	31.82	7.50	15.09	7.60	0.40
15	4.11	7.74	20.17	30.23	6.25	20.12	11.39	0.60
20	3.81	6.99	15.25	28.65	5.00	25.14	15.17	0.80
25	3.51	6.24	10.34	27.07	3.76	30.15	18.94	1.00
30	3.22	5.49	5.43	25.49	2.52	35.15	22.70	1.20
35	2.92	4.75	0.54	23.92	1.28	40.14	26.46	1.40

The reaction has stopped because there is no OMP left

The total amount of H2O needed to hydrate 100 O-units of rock = 1.4000 moles

The final density of the WR = 3.07 g/ccm

The final volume of the whole rock = 1000.92 ccm

This represents a 3.39 % change in volume

and corresponds to a -10.00 % change in density

The final volume of the total amount of H2O needed

to hydrate the boudin and its tails (33.51 ccm) =31.3071 ccm

This corresponds to 3.128 vol% H2O

The MAXIMUM amount of H2O needed = 0.0313 m3 H2O/m3

or a total of 1.0478 m3 H2O

The MINIMUM amount of H2O needed = 0.0302 m3 H2O/m3

or a total of 1.0123 m3 H2O

Between 0.4557 and 0.3962 moles of H2O will be required per Kg rock
 that is hydrated.

IIC-11

Delta 0-18 of phases at each increment

INC	WR	OMP	GAR	ZOI	QZ	HBL	PLG	H2O
0	6.50							
1	6.50	7.47	5.77	5.72	9.55	5.71	7.86	7.87
5	6.50	7.49	5.79	5.74	9.56	5.73	7.88	7.89
10	6.49	7.51	5.81	5.76	9.59	5.75	7.90	7.91
15	6.49	7.53	5.83	5.78	9.61	5.78	7.93	7.93
20	6.49	7.55	5.85	5.80	9.63	5.79	7.94	7.95
25	6.48	7.57	5.87	5.82	9.64	5.81	7.96	7.97
30	6.48	7.58	5.88	5.83	9.66	5.83	7.98	7.98
35	6.48	7.60	5.90	5.85	9.68	5.85	8.00	8.00

Pyroxene Analyses from the Mte. Mucrone Area

Samples from Location 3, Fig. 4.2 and are shown in composition diagrams in Fig. 4.12 a,b. (Analyses are given in weight % oxides)

Jadeite - Garnet Fels

Sample	100 M17A PX5	101 M17A PX6	102 M17A PX7	105 M17A PX10
SiO ₂	59.59	60.34	57.51	59.10
TiO ₂	0.07	0.04	0.06	0.05
Al ₂ O ₃	24.07	23.97	21.61	22.84
Fe ₂ O ₃	1.34	0.66	2.37	1.87
FeO	0.22	0.00	0.00	0.00
MnO	0.04	0.04	0.00	0.00
MgO	0.09	0.08	1.22	0.44
CaO	0.62	0.49	1.96	1.19
Na ₂ O	15.12	15.23	13.88	14.90
K ₂ O	0.02	0.03	0.01	0.00
Total	101.19	100.88	98.63	100.39

CATIONS assuming stoichiometry and charge balance

Si	1.9970	2.0190	1.9903	2.0017
Al	0.9508	0.9453	0.8812	0.9118
Fe ₃	0.0339	0.0166	0.0617	0.0476
Fe ₂	0.0062	0.0000	0.0000	0.0000
Mg	0.0047	0.0037	0.0632	0.0224
Ca	0.0222	0.0177	0.0726	0.0432
Na	0.9820	0.9877	0.9314	0.9782

SITE distribution and RATIOS

xMg Fe(tot)	0.104	0.184	0.506	0.320
Al(IV)	0.003	0.000	0.010	0.000
Al(VI)	0.948	0.945	0.871	0.912

ENDMEMBERS

Diopside	0.008	0.014	0.070	0.043
Wollastonite	0.010	0.009	0.035	0.022
Enstatite	0.002	0.002	0.032	0.011
Acmite	0.034	0.017	0.062	0.048
Jadeite	0.948	0.945	0.870	0.912

Jadeite-Garnet Mylonites

Sample	17 M17B PX8A	42 M17B PX11	43 M17B PX12	44 M17B PX13	46 M17B PX13	47 M17B PX13
SiO ₂	59.69	59.75	59.49	60.05	58.75	60.18
TiO ₂	0.05	0.00	0.08	0.00	0.00	0.00
Al ₂ O ₃	22.98	20.40	20.66	22.31	20.87	23.72
Fe ₂ O ₃	0.00	0.89	0.00	0.00	0.31	0.00
FeO	2.18	1.90	3.20	2.65	2.55	2.17
MgO	0.00	1.52	1.40	0.00	1.20	0.00
CaO	1.86	3.51	3.43	1.77	3.21	1.22
Na ₂ O	13.00	12.75	12.36	13.55	12.81	13.83
K ₂ O	0.13	0.00	0.15	0.00	0.00	0.00
Total	99.89	100.71	100.77	100.32	99.71	101.11

CATIONS assuming stoichiometry and charge balance

Si	2.0283	2.0307	2.0266	2.0382	2.0198	2.0193
Ti	0.0012	0.0000	0.0022	0.0000	0.0000	0.0000
Al	0.9202	0.8171	0.8292	0.8923	0.8457	0.9380
Fe ₃	0.0000	0.0228	0.0000	0.0000	0.0081	0.0000
Fe ₂	0.0619	0.0541	0.0911	0.0751	0.0733	0.0610
Mg	0.0000	0.0768	0.0711	0.0000	0.0615	0.0000
Ca	0.0678	0.1277	0.1251	0.0642	0.1182	0.0437
Na	0.8564	0.8399	0.8163	0.8915	0.8538	0.8995
K	0.0057	0.0000	0.0065	0.0000	0.0000	0.0000

SITE distribution and RATIOS

xMg Fe(tot)	0.000	0.500	0.438	0.000	0.430	0.000
Al(IV)	0.000	0.000	0.000	0.000	0.000	0.000
Al(VI)	0.920	0.817	0.829	0.892	0.846	0.938

ENDMEMBERS

Diopside	0.000	0.075	0.055	0.000	0.054	0.000
Wollastonite	0.034	0.064	0.063	0.032	0.059	0.022
Enstatite	0.000	0.038	0.036	0.000	0.031	0.000
Ferrosilite	0.031	0.027	0.046	0.038	0.037	0.031
Acmite	0.000	0.023	0.000	0.000	0.008	0.000
Jadeite	0.862	0.817	0.823	0.892	0.846	0.899

Pyroxene Analyses from Overprinted Mylonites - Mte. Muconre Area

Samples from Location 3, Fig. 4.2 and are shown in composition diagrams in

Fig. 4.12 a,b. (Analyses are given in weight % oxides)

Sample	COARSE-GRAINED PYROXENES													FINE-GRAINED (UNDEFORMED) PYROXENES												
	13 M1-1 P19	42 M1-1 P19	75 M1-1 P19	76 M1-1 P19	83 M1-1 P19	86 M1-2 P18B	87 M1-2 P18E	92 M1-2 P19A	93 M1-2 P19B	133 M1-2 P12B	61 M1-2 P16	74 M1-2 P18	45 M1-2 P11	52 M1-2 P12	54 M1-2 P13	55 M1-2 P14	56 M1-2 P15	57 M1-2 P16	103 M1-2 P11							
SiO2	58.62	57.50	57.50	57.19	58.54	59.20	58.97	58.39	59.63	58.27	59.48	58.24	55.19	56.18	54.98	56.60	55.11	55.42	56.67							
TiO2	0.03	0.08	0.08	0.04	0.00	0.00	0.00	0.00	0.00	0.00	0.00	0.00	0.12	0.12	0.08	0.12	0.06	0.08	0.00							
Al2O3	22.49	20.19	21.47	21.56	21.74	22.10	23.91	24.87	25.03	21.24	25.61	22.85	11.15	10.08	10.96	10.97	11.64	11.52	12.00							
Fe2O3	0.00	0.64	0.00	0.00	1.05	0.00	0.00	0.00	0.00	0.58	0.00	0.00	4.52	4.47	5.34	2.54	1.17	3.24	2.35							
FeO	3.22	3.26	4.55	2.84	2.20	2.53	1.47	0.97	0.87	2.27	1.34	1.98	2.93	3.57	3.96	4.06	5.73	4.78	5.18							
MnO	0.04	0.00	0.04	0.05	0.00	0.00	0.00	0.00	0.00	0.00	0.03	0.03	0.00	0.00	0.06	0.03	0.00	0.04	0.00							
MgO	0.45	1.42	1.42	0.81	0.89	0.95	0.22	0.06	0.00	0.99	0.08	0.17	6.35	6.40	5.65	6.39	5.65	5.33	5.72							
CaO	1.41	3.30	2.07	3.66	2.27	2.42	1.03	1.72	0.84	2.77	0.47	1.20	11.29	11.89	11.63	11.50	11.55	11.44	10.78							
Mn2O	13.53	12.58	12.60	12.74	13.63	13.25	14.26	13.81	14.47	13.13	14.58	13.83	8.06	7.95	7.93	7.74	7.58	8.05	8.21							
K2O	0.02	0.15	0.43	0.01	0.00	0.02	0.01	0.05	0.03	0.00	0.05	0.06	0.01	0.00	0.04	0.02	0.05	0.06	0.02							
Total	99.81	99.13	100.15	98.89	100.32	100.47	99.87	99.87	100.89	99.24	101.64	98.35	99.62	100.66	100.64	99.98	98.54	99.96	100.94							

CATIONS assuming stoichiometry and charge balance

Si	2.01	1.99	1.99	1.99	2.00	2.01	2.00	1.98	2.00	2.01	1.98	2.01	1.98	2.00	1.97	2.02	2.00	1.99	2.00
Al	0.91	0.83	0.88	0.88	0.88	0.89	0.96	0.99	0.99	0.86	1.00	0.93	0.47	0.42	0.46	0.46	0.50	0.49	0.50
Fe3	0.00	0.02	0.00	0.00	0.03	0.00	0.00	0.00	0.00	0.01	0.00	0.00	0.12	0.12	0.14	0.07	0.03	0.09	0.06
Fe2	0.09	0.09	0.13	0.08	0.06	0.07	0.04	0.03	0.02	0.07	0.04	0.06	0.09	0.11	0.12	0.12	0.17	0.14	0.15
Mg	0.02	0.07	0.07	0.04	0.05	0.05	0.01	0.00	0.00	0.05	0.00	0.01	0.34	0.34	0.30	0.34	0.31	0.29	0.30
Ca	0.05	0.12	0.08	0.14	0.08	0.08	0.04	0.06	0.03	0.10	0.02	0.04	0.43	0.45	0.45	0.44	0.45	0.44	0.41
Na	0.90	0.85	0.84	0.86	0.90	0.87	0.94	0.91	0.94	0.88	0.94	0.93	0.56	0.55	0.55	0.53	0.53	0.56	0.56
K	0.00	0.01	0.02	0.00	0.00	0.00	0.00	0.00	0.00	0.00	0.00	0.00							

SITE distribution and RATIOS

xMg Fe(tot)	0.20	0.40	0.36	0.34	0.34	0.40	0.21	0.10	0.00	0.40	0.10	0.13	0.62	0.60	0.53	0.64	0.60	0.55	0.58
Al(IV)	0.00	0.00	0.01	0.01	0.00	0.00	0.00	0.02	0.00	0.00	0.02	0.00	0.02	0.00	0.03	0.00	0.00	0.01	0.00
Al(VI)	0.91	0.83	0.86	0.87	0.88	0.89	0.96	0.98	0.98	0.86	0.99	0.93	0.45	0.42	0.43	0.46	0.50	0.48	0.50

ENDMEMBERS

Diopside	0.01	0.05	0.03	0.04	0.04	0.03	0.01	0.00	0.00	0.05	0.00	0.01	0.33	0.35	0.30	0.32	0.29	0.29	0.27
Wollastonite	0.03	0.06	0.04	0.06	0.04	0.04	0.02	0.02	0.01	0.05	0.00	0.13	0.21	0.23	0.21	0.22	0.22	0.22	0.20
Enstatite	0.01	0.04	0.04	0.02	0.02	0.01	0.01	0.00	0.00	0.02	0.00	0.00	0.04	0.05	0.06	0.06	0.09	0.07	0.15
Ferrosillite	0.05	0.07	0.04	0.04	0.03	0.04	0.02	0.01	0.01	0.03	0.02	0.01	0.01	0.00	0.02	0.00	0.00	0.00	0.08
CaAl2SiO6	0.00	0.00	0.00	0.01	0.00	0.00	0.00	0.02	0.00	0.00	0.02	0.04	0.12	0.12	0.14	0.07	0.03	0.09	0.06
Acaite	0.00	0.00	0.00	0.00	0.03	0.00	0.00	0.00	0.00	0.01	0.00	0.00	0.44	0.42	0.41	0.46	0.50	0.48	0.50
Jadeite	0.90	0.83	0.86	0.86	0.88	0.87	0.94	0.91	0.94	0.86	0.94	0.66							

Garnet Analyses from *Overprinted Mylonites* - Mte. Mucrone Area

Samples from Location 3, Fig. 4.2 and are shown in composition diagrams in Fig. 4.15a,b. (Analyses are given in weight % oxides)

Sample	CORES										INCLUSION-POOR ISOMETRIC GRAINS				
	19	65	66	67	76	25	45	46	61	71	28	29	30	32	33
	MI-1 GR1	MI-1 GR13	MI-2 GR3C	MI-2 GR3D	MI-2 GR3L	MI-1 GR3	MI-1 GR5	MI-1 GR6	MI-1 GR10	MI-2 GR3H	MI-2 GR2A	MI-2 GR2B	MI-2 GR2C	MI-2 GR2D	MI-2 GR2E
SiO2	38.76	38.06	38.63	38.72	38.67	37.89	38.21	37.38	37.39	37.79	38.77	37.69	37.20	37.84	37.80
TiO2	0.09	0.00	0.00	0.00	0.04	0.14	0.18	0.33	0.20	0.31	0.04	0.06	0.06	0.00	0.04
Al2O3	21.55	20.77	21.37	21.31	21.20	20.32	20.82	21.06	20.71	20.65	21.64	21.17	20.69	21.39	20.61
Fe2O3	0.21	1.15	0.59	0.36	0.82	1.14	0.46	0.29	0.60	0.57	0.18	0.79	1.45	0.51	1.11
FeO	21.00	20.80	20.01	21.40	21.11	25.71	25.34	25.86	26.68	26.99	22.54	22.59	21.60	22.69	21.45
MnO	0.37	0.65	0.30	0.42	0.34	0.96	0.54	0.43	2.13	1.52	0.28	0.35	0.49	0.25	0.32
MgO	0.74	0.58	0.76	0.59	0.78	1.14	1.44	1.22	1.08	1.57	0.99	0.75	0.68	0.85	1.01
CaO	17.85	17.89	18.77	17.08	17.86	11.95	11.67	12.74	10.85	10.14	16.49	16.42	16.93	16.39	16.79
Na2O	0.00	0.00	0.02	0.00	0.00	0.00	0.03	0.08	0.05	0.07	0.00	0.04	0.00	0.03	0.00
K2O	0.01	0.00	0.00	0.00	0.00	0.03	0.37	0.00	0.00	0.00	0.01	0.00	0.00	0.00	0.00
Total	100.58	99.90	100.46	99.88	100.82	99.28	99.06	99.38	99.68	99.61	100.94	99.85	99.11	99.95	99.14

Sample	CORES										INCLUSION-POOR ISOMETRIC GRAINS				
	19	65	66	67	76	25	45	46	61	71	28	29	30	32	33
	MI-1 GR1	MI-1 GR13	MI-2 GR3C	MI-2 GR3D	MI-2 GR3L	MI-1 GR3	MI-1 GR5	MI-1 GR6	MI-1 GR10	MI-2 GR3H	MI-2 GR2A	MI-2 GR2B	MI-2 GR2C	MI-2 GR2D	MI-2 GR2E
Si	3.0252	3.0033	3.0140	3.0510	3.0169	3.0420	3.0555	2.9826	2.9961	3.0242	3.0205	2.9780	2.9659	2.9825	3.0042
Ti	0.0054	0.0000	0.0000	0.0000	0.0025	0.0087	0.0107	0.0200	0.0118	0.0186	0.0022	0.0034	0.0035	0.0000	0.0025
Al	1.9821	1.9318	1.9651	1.9784	1.9492	1.9225	1.9615	1.9802	1.9560	1.9470	1.9871	1.9714	1.9435	1.9872	1.9308
Fe3	0.0125	0.0682	0.0349	0.0216	0.0483	0.0688	0.0278	0.0171	0.0361	0.0344	0.0108	0.0472	0.0872	0.0303	0.0667
Fe2	1.3709	1.3723	1.3051	1.4099	1.3772	1.7257	1.6944	1.7250	1.7873	1.8060	1.4683	1.4929	1.4400	1.4953	1.4255
Mn	0.0244	0.0433	0.0201	0.0283	0.0224	0.0654	0.0368	0.0289	0.1444	0.1028	0.0188	0.0233	0.0330	0.0165	0.0215
Mg	0.0859	0.0685	0.0884	0.0694	0.0910	0.1361	0.1717	0.1451	0.1286	0.1871	0.1148	0.0879	0.0808	0.0996	0.1192
Ca	1.4925	1.5126	1.5691	1.4414	1.4925	1.0279	0.9995	1.0890	0.9313	0.8696	1.3763	1.3902	1.4461	1.3837	1.4297
Na	0.0000	0.0000	0.0033	0.0000	0.0000	0.0000	0.0041	0.0120	0.0083	0.0102	0.0000	0.0057	0.0000	0.0049	0.0000
K	0.0011	0.0000	0.0000	0.0000	0.0000	0.0028	0.0381	0.0000	0.0000	0.0000	0.0014	0.0000	0.0000	0.0000	0.0000
Total	100.58	99.90	100.46	99.88	100.82	99.28	99.06	99.38	99.68	99.61	100.94	99.85	99.11	99.95	99.14

Sample	CORES										INCLUSION-POOR ISOMETRIC GRAINS				
	19	65	66	67	76	25	45	46	61	71	28	29	30	32	33
	MI-1 GR1	MI-1 GR13	MI-2 GR3C	MI-2 GR3D	MI-2 GR3L	MI-1 GR3	MI-1 GR5	MI-1 GR6	MI-1 GR10	MI-2 GR3H	MI-2 GR2A	MI-2 GR2B	MI-2 GR2C	MI-2 GR2D	MI-2 GR2E
Grossular	0.493	0.471	0.509	0.478	0.475	0.308	0.323	0.342	0.285	0.264	0.456	0.438	0.437	0.447	0.443
Almandine	0.461	0.458	0.438	0.478	0.462	0.584	0.583	0.575	0.596	0.607	0.493	0.498	0.480	0.499	0.476
Pyrope	0.029	0.023	0.030	0.024	0.031	0.046	0.059	0.048	0.043	0.063	0.039	0.029	0.027	0.033	0.040
Spessartine	0.008	0.014	0.007	0.010	0.008	0.022	0.013	0.010	0.048	0.035	0.006	0.008	0.011	0.005	0.007
Andradite	0.006	0.034	0.018	0.011	0.024	0.035	0.014	0.009	0.018	0.017	0.005	0.024	0.044	0.015	0.033

CATIONS assuming stoichiometry and charge balance

ENDMEMBERS *****

Garnet and Zoisite Analyses from *Jadeite-Garnet Fels and Veins* -
Mte. Mucrone Area

Samples from Location 3, Fig. 4.2 and are shown graphically in Fig. 4.15 a,b.

GARNET *****																								
	VEINS				RIMS				CORES															
Sample	85		86		88		89		92		106		109		113		117		110		112		136	
	M17A	GR1	M17A	GR2	M17A	GR3	M17A	GR4	M17A	GR5	M17A	GR6	M17A	GR7	M17A	GR6E	M17A	GR7	M17A	GR6C	M17A	GR6D	M17A	GR9
SiO2	38.28		38.74		38.03		37.44		38.27		38.28		38.17		38.31		38.49		38.19		38.41		38.03	
TiO2	0.06		0.12		0.05		0.12		0.12		0.14		0.18		0.07		0.06		0.09		0.12		0.32	
Al2O3	22.12		21.07		21.47		21.46		20.83		21.45		22.17		21.52		22.36		21.09		21.76		21.94	
Fe2O3	0.00		0.57		0.35		0.45		0.79		0.00		0.00		0.06		0.00		0.96		0.20		0.00	
FeO	21.21		22.53		26.04		22.22		21.60		27.30		27.17		28.24		26.56		27.85		27.37		28.12	
MnO	0.51		0.58		0.75		0.52		0.46		0.14		0.33		0.94		0.25		0.35		0.71		0.37	
HgO	0.53		0.55		0.91		0.89		0.19		2.34		2.22		2.23		1.77		2.19		2.23		3.17	
CaO	17.19		16.01		13.45		16.27		17.45		10.42		10.71		9.55		11.30		10.66		10.96		8.89	
Na2O	0.00		0.00		0.00		0.04		0.00		0.03		0.00		0.05		0.00		0.00		0.00		0.00	
K2O	0.03		0.00		0.01		0.02		0.00		0.03		0.01		0.02		0.00		0.02		0.01		0.04	
Total	99.93		100.17		101.06		99.45		99.71		100.12		100.95		101.00		100.80		101.40		101.77		100.88	

CATIONS assuming stoichiometry and charge balance

Si	3.0083	3.0565	2.9885	2.9638	3.0334	3.0212	2.9873	3.0085	3.0173	2.9915	2.9873	2.9753
Ti	0.0036	0.0069	0.0029	0.0074	0.0073	0.0081	0.0104	0.0042	0.0038	0.0052	0.0069	0.0190
Al	2.0484	1.9593	1.9878	2.0018	1.9458	1.9954	2.0447	1.9921	2.0652	1.9467	1.9943	2.0225
Fe3	0.0000	0.0338	0.0208	0.0270	0.0469	0.0000	0.0000	0.0036	0.0000	0.0567	0.0115	0.0000
Fe2	1.3939	1.4862	1.7106	1.4712	1.4314	1.8016	1.7782	1.8547	1.7409	1.8243	1.7797	1.8395
Mn	0.0341	0.0385	0.0499	0.0350	0.0308	0.0091	0.0216	0.0622	0.0166	0.0229	0.0471	0.0243
Hg	0.0621	0.0651	0.1062	0.1053	0.0225	0.2750	0.2590	0.2617	0.2073	0.2563	0.2591	0.3703
Ca	1.4469	1.3536	1.1321	1.3803	1.4819	0.8815	0.8977	0.8036	0.9490	0.8949	0.9129	0.7453
Na	0.0000	0.0000	0.0000	0.0060	0.0000	0.0052	0.0000	0.0076	0.0000	0.0000	0.0000	0.0000
K	0.0028	0.0000	0.0012	0.0024	0.0000	0.0028	0.0011	0.0017	0.0000	0.0017	0.0012	0.0038

ENDMEMBERS

Grossular	0.491	0.439	0.366	0.442	0.472	0.292	0.298	0.264	0.324	0.268	0.295	0.241
Almandine	0.475	0.505	0.570	0.491	0.483	0.606	0.601	0.621	0.597	0.608	0.593	0.617
Pyrope	0.021	0.022	0.035	0.035	0.008	0.093	0.088	0.088	0.071	0.085	0.086	0.124
Spessartine	0.012	0.013	0.017	0.012	0.010	0.003	0.007	0.021	0.006	0.008	0.016	0.008
Andradite	0.000	0.017	0.010	0.013	0.024	0.000	0.000	0.002	0.000	0.028	0.006	0.000

ZOISITE IN VEINS

Sample	82		84		87		98	
	M17A	ZO1	M17A	ZO3	M17A	ZO4	M17A	ZO7
SiO2	39.25		39.94		39.68		39.89	
TiO2	0.05		0.05		0.04		0.05	
Al2O3	32.01		31.85		31.78		31.55	
Fe2O3	2.22		1.32		2.43		2.14	
FeO	0.00		0.12		0.01		0.00	
CaO	24.46		24.93		24.74		25.20	
Cl	0.04		0.00		0.00		0.00	
H2O	1.95		1.97		1.98		1.98	
Total	99.98		100.19		100.66		100.82	

CATIONS calculated on the basis of 8. cations and 13. oxygens

Si	2.9938	3.0336	3.0085	3.0185
Al	2.8769	2.8511	2.8399	2.8136
Fe3	0.1275	0.0757	0.1389	0.1218
Fe2	0.0000	0.0077	0.0007	0.0000
Ca	1.9988	2.0289	2.0099	2.0431
Cl	0.0048	0.0000	0.0000	0.0000
OH	0.9952	1.0000	1.0000	1.0000

**Biotite and White Mica Analyses from Unfoliated Metagranitoids
Mte. Mucrone Area**

(Analyses are given in weight % oxides)

Meta-Quartz Diorites

RELICT BIOTITES

Sample	WHITE MICA I -----) (---WHITE MICA II---)											
	10	35	103	115	8	9	28	37	89	113	24	90
	MI-3 BI01	MI-3 BI05	MUCS BI01	MUCS BI02	MI-3 PBE1	MI-3 PBE2	MI-3 PBE5	MI-3 PBE9	MUC3 PBE5	MUC5 PBE2	MI-3 PBE4	MUC3 PBE6
SiO2	38.58	38.49	38.69	39.60	50.63	49.81	49.63	50.45	48.47	49.40	48.73	47.62
TiO2	4.21	4.35	6.77	5.82	1.94	2.48	3.41	2.36	2.65	3.72	0.15	0.53-
Al2O3	11.56	13.04	13.56	12.63	23.16	23.56	22.69	23.87	24.68	24.30	27.33	31.89
Fe2O3	0.00	0.00	0.00	0.00	0.00	0.00	0.37	2.93	0.00	0.00	0.00	0.00
FeO	20.29	19.73	15.89	15.61	2.61	2.48	2.69	0.81	2.04	2.82	2.56	1.59
MnO	0.24	0.21	0.00	0.10	0.00	0.00	0.00	0.00	0.00	0.00	0.00	0.00
HgO	9.56	9.54	10.86	10.79	4.07	3.78	4.23	4.11	3.56	3.36	2.42	1.34
CaO	0.10	0.04	0.02	0.06	0.13	0.08	0.09	0.10	0.11	0.17	0.32	0.23
Na2O	0.09	0.04	0.14	0.13	11.33	11.22	10.96	10.94	11.16	10.82	11.03	11.20
K2O	9.42	8.54	9.85	9.83	0.33	0.30	0.32	0.27	0.20	0.12	0.23	0.28
F	0.60	0.65	1.01	0.93	0.05	0.06	0.04	0.00	0.07	0.00	0.05	0.04
Cl	0.50	0.45	0.22	0.42	4.21	4.20	4.22	4.33	4.21	4.35	4.21	4.30
H2O	3.30	3.34	3.29	3.22								
Total	98.46	98.41	100.29	99.14	98.46	98.05	98.99	100.19	97.15	99.07	97.09	99.02

CATIONS calculated on the basis of 7. cations and 12. oxygens

Si	3.1114	3.0608	3.0350	3.1470	3.4668	3.4294	3.3926	3.3873	3.3598	3.3609	3.3682	3.2127
Ti	0.2551	0.2601	0.3991	0.3478	0.0997	0.1282	0.1754	0.1192	0.1382	0.1903	0.0077	0.0268
Al	1.0989	1.2224	1.2535	1.1828	1.8685	1.9116	1.8279	1.8885	2.0161	1.9480	2.2266	2.5359
Fe2	1.3687	1.3121	1.0424	1.0377	0.0000	0.0000	0.0189	0.1480	0.0000	0.0000	0.0000	0.0000
Hn	0.0166	0.0138	0.0000	0.0064	0.1496	0.1426	0.1540	0.0457	0.1181	0.1604	0.1480	0.0895
Hg	1.1492	1.1308	1.2700	1.2783	0.0000	0.0000	0.0000	0.0000	0.0000	0.0000	0.0000	0.0000
Ca	0.0090	0.0030	0.0016	0.0051	0.4154	0.3883	0.4311	0.4113	0.3678	0.3405	0.2495	0.1351
Na	0.0140	0.0059	0.0207	0.0206	0.0000	0.0071	0.0247	0.0000	0.0000	0.0020	0.0042	0.0000
K	0.9689	0.8662	0.9854	0.9964	0.9896	0.9848	0.9556	0.9369	0.9861	0.9229	0.9724	0.9635
F	0.1527	0.1636	0.2510	0.2338	0.0720	0.0647	0.0688	0.0578	0.0445	0.0260	0.0510	0.0597
Cl	0.0690	0.0605	0.0287	0.0571	0.0053	0.0067	0.0043	0.0000	0.0081	0.0000	0.0062	0.0049
OH	1.7783	1.7759	1.7202	1.7091	1.9227	1.9287	1.9268	1.9422	1.9475	1.9740	1.9428	1.9354

SITE distribution and RATIOS

xHg (Fe tot)	0.456	0.463	0.549	0.552	0.735	0.731	0.737	0.900	0.757	0.680	0.628	0.602
Al(IV)	0.889	0.999	0.965	0.853	0.735	0.731	0.714	0.680	0.757	0.680	0.628	0.602
Al(VI)	0.210	0.283	0.289	0.330	0.533	0.571	0.607	0.613	0.640	0.639	0.632	0.787
Al(VI)					1.335	1.341	1.221	1.276	1.376	1.309	1.595	1.749

Jadeite - Garnet Fels

Sample	WHITE MICA I -----) (---WHITE MICA II---)						
	108	114	115	123	127	MI7A PH2	MI7A PH7
	MI7A PH2	MI7A PH3	MI7A PH4	MI7A PH7	MI7A PH7E	MI7A PH7E	MI7A PH7E
SiO2	50.13	48.38	49.07	49.52	48.67		
TiO2	0.74	0.64	0.68	0.59	0.54		
Al2O3	28.49	29.61	29.62	29.71	30.03		
Fe2O3	0.26	0.93	1.15	1.70	1.05		
FeO	1.54	1.07	0.55	0.28	0.63		
MnO	0.00	0.00	0.00	0.00	0.00		
HgO	2.74	2.39	2.52	2.49	2.27		
CaO	0.00	0.00	0.00	0.00	0.00		
Na2O	0.22	0.28	0.25	0.23	0.25		
K2O	11.09	11.23	10.97	10.72	10.81		
F	0.83	0.56	0.66	0.49	0.51		
Cl	0.08	0.06	0.07	0.08	0.07		
H2O	4.07	4.16	4.15	4.25	4.19		
Total	100.19	99.32	99.79	100.07	99.04		

CATIONS calculated on the basis of 6. cations and 12. oxygens

Si	3.3482	3.2649	3.2841	3.2939	3.2749
Ti	0.0374	0.0325	0.0344	0.0294	0.0276
Al	2.2422	2.3544	2.3360	2.3291	2.3809
Fe3	0.0131	0.0473	0.0581	0.0850	0.0533
Fe2	0.0859	0.0605	0.0362	0.0158	0.0356
Hg	0.2731	0.2404	0.2511	0.2468	0.2277
Na	0.0287	0.0369	0.0329	0.0297	0.0331
K	0.9447	0.9666	0.9360	0.9095	0.9277
F	0.1744	0.1190	0.1400	0.1035	0.1096
Cl	0.0090	0.0072	0.0077	0.0086	0.0081
OH	1.8166	1.8738	1.8523	1.8879	1.8823

SITE distribution and RATIOS

xHg (Fe tot)	0.734	0.690	0.727	0.710	0.719
Al(IV)	0.652	0.735	0.716	0.706	0.725
Al(VI)	1.590	1.619	1.620	1.623	1.656

White Mica Analyses from Jadeite-Garnet Mylonites -
Mte Mucrone Area.

Samples from Location 3, Fig. 4.2 and are shown graphically in Fig. 4.17a,b. (Analyses are given in weight % oxides)

PHENGITIC WHITE MICAS

Sample	58 M17B PH4	59 M17B PH5	60 M17B PH6	61 M17B PH7	64 M17B PH8
SiO ₂	48.79	51.23	50.41	51.13	50.79
TiO ₂	1.02	1.04	1.00	1.00	1.04
Al ₂ O ₃	24.91	27.39	27.85	26.80	28.06
Fe ₂ O ₃	5.25	0.18	2.38	0.99	2.04
FeO	0.00	1.58	0.00	1.58	0.00
MgO	5.07	3.37	3.90	3.23	3.67
NiO	0.05	0.00	0.00	0.00	0.00
CaO	0.02	0.01	0.00	0.00	0.00
Na ₂ O	0.20	0.26	0.22	0.23	0.22
K ₂ O	11.12	11.21	11.26	11.00	11.17
H ₂ O	4.52	4.53	4.57	4.51	4.58
Total	100.95	100.79	101.60	100.49	101.55

CATIONS calculated on the basis of 6. cations and 12. oxygens

Si	3.2359	3.3867	3.3021	3.3955	3.3253
Ti	0.0508	0.0517	0.0493	0.0499	0.0510
Al	1.9474	2.1338	2.1501	2.0973	2.1650
Fe ₃	0.2618	0.0087	0.1175	0.0497	0.1003
Fe ₂	0.0000	0.0873	0.0000	0.0880	0.0000
Mg	0.5015	0.3318	0.3811	0.3195	0.3584
Ca	0.0017	0.0009	0.0000	0.0000	0.0000
Na	0.0256	0.0337	0.0280	0.0300	0.0277
K	0.9409	0.9451	0.9405	0.9320	0.9323
OH	2.0000	2.0000	2.0000	2.0000	2.0000

SITE distribution and RATIOS

xMg (Fe tot)	0.657	0.776	0.764	0.699	0.781
Al(IV)	0.764	0.613	0.698	0.604	0.675
Al(VI)	1.183	1.520	1.452	1.493	1.490

White Mica Analyses from Overprinted Mylonites - Mte. Muconre Area
 Samples from Location 3, Fig. 4.2 and are shown graphically in Fig. 4.17 a,b.

COARSE-GRAINED PHEGITES (Left side) FINE - GRAINED PHEGITES (Right side)

Sample	72	23	24	25	58	59	61	98	99	100	101	Sample	67	68	69	71	136	137	25	77	96
	MU4-2 PH4	MI-2 PH1A	MI-2 PH1B	MI-2 PH1C	MI-2 PH3	MI-2 PH4	MI-2 PH6	MI-2 PH13	MI-2 PH14	MI-2 PH15	MI-2 PH16	MI-1 PH6	MI-1 PH7	MI-1 PH8	MI-1 PH9	MI-2 PH5	MI-2 PH6	MI-2 PH8	MI-2 PH7	MI-2 PH11	
SI02	50.31	50.19	49.83	50.25	49.14	50.08	50.01	50.76	50.10	50.59	49.90	SI02	50.33	49.39	49.50	49.61	49.02	49.35	48.82	48.95	49.98
TI02	1.10	1.58	1.19	1.56	1.85	1.79	1.65	1.51	1.52	1.41	1.42	TI02	0.25	0.38	0.37	0.41	0.00	0.00	0.29	0.25	0.21
Al203	26.12	24.98	24.96	24.81	25.46	26.16	26.27	24.44	25.82	25.37	27.18	Al203	28.01	30.06	30.15	29.30	28.73	28.04	30.21	29.30	29.11
Fe203	0.19	0.83	2.04	0.00	1.41	0.80	0.66	1.67	2.94	0.00	1.77	Fe203	0.00	1.21	1.33	0.69	1.63	1.25	0.83	1.62	1.62
FeO	2.81	2.21	1.63	2.66	1.97	2.16	2.28	1.01	0.23	2.64	1.14	FeO	2.60	1.14	1.15	1.66	1.29	1.97	1.89	1.44	1.44
MnO	0.00	0.00	0.00	0.00	0.00	0.00	0.00	0.00	0.00	0.00	0.00	MnO	0.00	0.00	0.00	0.00	0.00	0.00	0.00	0.00	0.00
MgO	2.81	3.39	3.37	3.34	3.26	3.22	3.06	3.95	3.75	3.30	2.98	MgO	2.25	2.19	2.09	2.13	2.32	2.30	1.98	1.93	2.33
CaO	0.00	0.00	0.00	0.00	0.00	0.00	0.00	0.00	0.00	0.00	0.00	CaO	0.00	0.00	0.00	0.00	0.00	0.00	0.00	0.00	0.00
Na2O	0.10	0.10	0.15	0.10	0.14	0.10	0.10	0.09	0.13	0.09	0.11	Na2O	0.13	0.16	0.14	0.16	0.18	0.17	0.14	0.15	0.42
K2O	11.19	11.15	11.04	11.16	11.32	11.45	11.34	10.81	11.04	11.36	11.00	K2O	11.16	11.27	11.19	10.99	11.17	11.24	11.02	11.13	10.94
F	0.23	0.23	0.27	0.21	0.16	0.25	0.14	0.27	0.18	0.00	0.00	F	0.10	0.10	0.16	0.11	0.19	0.10	0.16	0.00	0.00
Cl	0.05	0.04	0.05	0.05	0.04	0.02	0.04	0.07	0.04	0.04	0.03	Cl	0.03	0.04	0.03	0.03	0.05	0.00	0.01	0.03	0.02
H2O	4.30	4.29	4.26	4.28	4.31	4.34	4.38	4.28	4.38	4.42	4.47	H2O	4.39	4.45	4.43	4.41	4.32	4.37	4.40	4.43	4.51
Total	99.22	98.99	98.78	98.40	99.06	100.38	99.93	98.84	100.14	99.20	100.00	Total	99.25	100.38	100.54	99.52	98.94	98.78	99.77	98.89	100.60

CATIONS calculated on the basis of 6. cations and 12. oxygens

CATIONS calculated on the basis of 6. cations and 12. oxygens

	SI	TI	Al	Fe3	Fe2	Hg	Na	K	F	Cl	OH		SI	TI	Al	Fe3	Fe2	Hg	Na	K	F	Cl	OH	
SI	3.4072	3.4089	3.3952	3.4312	3.3467	3.3591	3.3648	3.4343	3.3523	3.4234	3.3370	SI	3.3911	3.2847	3.2862	3.3246	3.3177	3.3490	3.2652	3.3094	3.3190			
TI	0.0560	0.0809	0.0608	0.0946	0.0767	0.0715	0.0835	0.0767	0.0764	0.0714	0.0714	TI	0.0126	0.0188	0.0183	0.0208	0.0000	0.0000	0.0144	0.0126	0.0107			
Al	2.0845	1.9991	2.0044	1.9969	2.0432	2.0673	2.0830	1.9490	2.0361	2.0230	2.1416	Al	2.2236	2.3556	2.3585	2.3141	2.2914	2.2429	2.3814	2.3341	2.2785			
Fe3	0.0098	0.0422	0.1046	0.0000	0.0724	0.0403	0.0336	0.0849	0.1480	0.0000	0.0890	Fe3	0.0000	0.0607	0.0667	0.0347	0.0832	0.0636	0.1006	0.0422	0.0808			
Fe2	0.1593	0.1253	0.0929	0.1518	0.1123	0.1209	0.1283	0.0572	0.0129	0.1492	0.0637	Fe2	0.1467	0.0633	0.0636	0.0931	0.0733	0.1120	0.0406	0.1067	0.0802			
Hg	0.2832	0.3436	0.3421	0.3399	0.3307	0.3219	0.3069	0.3980	0.3742	0.3328	0.2973	Hg	0.1467	0.0633	0.0636	0.0931	0.0733	0.1120	0.0406	0.1067	0.0802			
Na	0.0134	0.0138	0.0194	0.0191	0.0188	0.0136	0.0136	0.0113	0.0167	0.0116	0.0147	Na	0.0168	0.0216	0.0207	0.0212	0.0234	0.0233	0.1978	0.1949	0.2308			
K	0.9659	0.9654	0.9597	0.9715	0.9828	0.9797	0.9733	0.9329	0.9417	0.9806	0.9379	K	0.9587	0.9561	0.9472	0.9392	0.9638	0.9727	0.9483	0.9598	0.9546			
F	0.0489	0.0484	0.0575	0.0444	0.0353	0.0296	0.0353	0.0571	0.0382	0.0000	0.0000	F	0.0204	0.0201	0.0331	0.0243	0.0416	0.0205	0.0341	0.0000	0.0000			
Cl	0.0059	0.0051	0.0058	0.0052	0.0042	0.0022	0.0043	0.0077	0.0050	0.0043	0.0029	Cl	0.0034	0.0042	0.0037	0.0038	0.0059	0.0000	0.0015	0.0029	0.0027			
OH	1.9451	1.9465	1.9367	1.9504	1.9606	1.9453	1.9662	1.9352	1.9568	1.9957	1.9971	OH	1.9761	1.9756	1.9632	1.9719	1.9525	1.9795	1.9644	1.9971	1.9973			

SITE distribution and RATIOS

SITE distribution and RATIOS

	XHg (FeII+)	XHg (Fe tot)	Al(IV)	Al(VI)
XHg (FeII+)	0.640	0.733	0.786	0.691
XHg (Fe tot)	0.626	0.672	0.634	0.691
Al(IV)	0.593	0.591	0.605	0.569
Al(VI)	1.492	1.408	1.400	1.428
				1.390
				1.426
				1.448
				1.383
				1.388
				1.446
				1.479
				1.615
				1.640
				1.645
				1.639
				1.609
				1.592
				1.647
				1.644
				1.597

APPENDIX IV: SUMMARY OF THERMODYNAMIC DATA USED IN CHAPTER 5
(University of British Columbia Data Base)

STANDARD STATE PROPERTIES

Solid Phases

	ENTHALPY (J)	ENTROPY (J)	VOLUME (CM ³)
Albite	-3934448.0	207.412	100.250
Almandine	-5268416.0	340.021	115.110
Anorthite	-4228102.0	200.439	100.750
Annite	-5166998.0	413.658	154.300
Diopside	-3201898.0	142.500	66.179
Grossular	-6632395.0	255.000	125.300
Jadeite	-3023838.0	133.869	60.400
K-feldspar	-3972462.0	214.051	108.870
Muscovite	-5981249.0	288.300	140.757
Paragonite	-5941532.0	277.969	132.469
Phlogopite	-6213900.0	335.600	149.920
Pyrope	-6288710.0	267.270	113.181
α -Quartz	- 910699.0	41.259	22.688
Ca-Al Pyroxene	-3297295.0	141.225	63.560
Zoisite	-6890028.0	295.438	135.750

Gas phases

H ₂ O	- 241816.0	188.720	*
------------------	------------	---------	---

* Volumetric properties of water calculated using Kerrick and Jacobs Redlich-Kwong Equation of State

Figures 5.1 and 5.2 were calculated with this data set by means of the computer program PTX, written by E. Perkins (ETH - Zürich)

Appendix V: Oxygen Isotope Fractionation Factors

A. Experimentally - determined Fractionation Factors

Mineral	$1000 \ln \alpha =$	Reference
Qtz - H ₂ O	3.34 ($10^6 T^{-2}$) - 3.31	Matsuhisa et al., 1979
Qtz - H ₂ O (200 - 500 °C)	3.38 ($10^6 T^{-2}$) - 2.90	Clayton et al., 1972
Qtz - H ₂ O (500 - 700 °C)	2.51 ($10^6 T^{-2}$) - 1.96	Clayton et al., 1972
Alb - H ₂ O Ksp - H ₂ O	2.39 ($10^6 T^{-2}$) - 2.51	Matsuhisa et al., 1979
Ksp - H ₂ O (350 - 800 °C)	2.91 ($10^6 T^{-2}$) - 3.41	O'Neil & Taylor, 1967
Ano - H ₂ O (500 - 800 °C)	2.15 ($10^6 T^{-2}$) - 3.82	O'Neil & Taylor, 1967
Plg - H ₂ O (500 - 800 °C)	(2.91 - 0.76β)($10^6 T^{-2}$) - (3.41 - 0.14β)	" β = An-comp.
Mus - H ₂ O (400 - 650 °C)	2.38 ($10^6 T^{-2}$) - 3.89	O'Neil & Taylor, 1969
Rut - H ₂ O (575 - 775 °C)	-4.10 ($10^6 T^{-2}$) + 0.96	Addy & Garlick, 1974
Rut - H ₂ O (500 - 700 °C)	-(4.72 ± 0.40) ($10^6 T^{-2}$) + 1.62 ± 0.53	Matthews et al., 1979
Calcite - H ₂ O (0 - 800 °C)	2.78 ($10^6 T^{-2}$) - 3.39	O'Neil et al., 1969
Mag - H ₂ O (700 - 800 °C)	-1.60 ($10^6 T^{-2}$) - 3.61	Anderson et al., 1971
Qtz - Na-Cpx	(2.08 - 0.99β) ($10^6 T^{-2}$)	Matthews et al., 1983 β = Jad - component
Δ Qtz - Mus =	0.54 Δ Qtz - Bio	Garlick & Epstein, 1967
Δ Qtz - Ilm =	0.95 Δ Qtz - Mag	O'Neil & Ghent, 1975

B. Theoretical Fractionation Factors, Javoy (1977)

	$1000 \ln \alpha_{Qtz - Min} = A + B (10^6 T^{-2})$	
	A	B
Feldspar	0	0.97 + 1.04β
Pyroxene	0	2.75
Olivine	0	3.91
Muscovite	- 0.60	2.20
Amphibole	- 0.30	3.15
Biotite	- 0.60	3.69
Ilmenite	0	5.29
Manetite	0	5.57
Garnet	0	2.88
Chlorite } Serpentine }	- 1.63	5.44

β = An - component

ABSTRACT

published in: EOS, 1985, Vol. 66, No. 46, p. 1126-1127

Stable Isotope Indications of Fluid Involvement
in Ductile Shear Zones During Eclogite Facies
Metamorphism

GRETCHEN FRUEH-GREEN (Inst Min Petro ETH Zentrum
CH-8092 Zürich Switzerland)
(Sponsor: Alan B Thompson)

At Mte. Mucrone (Sesia Zone, Western Alps, Italy) a quartz diorite intrusion was intensely deformed and transformed to orthogneiss (now containing Qtz, Phen, Gar, Omp) during prograde, early-alpine metamorphism in the eclogite facies. Stable isotope analyses at various points across ductile shear zones within less deformed meta-quartz diorite (with relic Ksp + Bio) show a 3% depletion in ^{18}O , suggesting introduction of an external fluid during shearing; a fact not otherwise evident from petrographic observation. A correlation may be seen between the amount of fluid involved and the degree of deformation and recrystallisation. Qtz-Gar, Qtz-Omp, and Qtz-Phen ^{18}O -fractionations yield concordant temperatures of 500-550°C for the deformation event; these are consistent with estimates based on mineral equilibria. Calculated ^{18}O values of the fluid in equilibrium with quartz in the plastically deformed rocks are 6.50-6.90‰.

Comparison with other isotopic studies in the Mte. Mucrone area suggests localised rather than pervasive flow of the peak metamorphic fluids, possibly channelled along shear zones.

X16

**STABLE ISOTOPE INDICATIONS OF FLUID MOTION
IN THE AMPHIBOLISATION OF ECLOGITES IN THE
ADULA NAPPE**

G. FRUEH-GREEN and A.B. THOMPSON

Erdwissenschaften, ETH-Zürich, CH-8092 Zürich, Switzerland.

O- and H- isotope compositions of co-existing minerals indicate that two phases of fluid infiltration affected eclogite boudins of the Adula Nappe, Switzerland. No isotopic change occurred during the hydration of "dry" eclogites (Cmp+Gar+Kya+Qtz) to fine-grained amphibolite (Phase I). This indicates low Fluid/Rock ratios or that any fluid was almost in isotopic equilibrium with the rock. The hydration of eclogite to symplectite (Hbl+Dio+Plg) and amphibolite occurred at the same time as dehydration of muscovite in the enclosing metapelites (now containing Qtz+Plg+Bio+Gar). Phase II is accompanied by grain coarsening, progressive deformation and new growth of biotite in the amphibolite. Isotopic compositions suggest that Fluid/Rock ratios were greater than in Phase I or that the isotopic composition of the fluid changed. Scattered isotopic compositions of the enclosing metapelites indicate no homogenous isotopic re-equilibration or pervasive fluid phase during amphibolisation of the eclogite boudins but may yield information about Fluid/Rock interaction during the older eclogite facies metamorphism of both mafic and pelitic compositions.

CURRICULUM VITAE

I, Gretchen Lieuana Früh-Green, the daughter of Donald Eugene Green and Margaret Ann Maurer-Green, was born on June 5th, 1956 in Pocatello, Idaho. After attending 12 years of primary and secondary school in San Francisco and Sunnyvale, California, I entered the University of California at Santa Barbara (UCSB) in 1975 and started my studies in geology. During the four years of study at UCSB, I worked part-time for the United States Geological Survey in Ventura, California and as a laboratory assistant under Prof. Michael Fuller. I obtained a Bachelor of Arts degree in geology in June, 1979, after which I came to Switzerland and spent eight months learning "German" in Canton Appenzell. In April, 1980, I entered the University of Zürich and completed the diplom in petrography in July, 1982, at which time I married Rudolf Früh, from Heiden AR. Since August, 1982, I have worked as a teaching and research assistant, while completing my doctoral thesis, in the Institute of Mineralogy and Petrography at the ETH, under Professor Alan B. Thompson. Since May, 1981, I have also taught English part-time at the Schweizerische Technische Fachschule in Winterthur.